High palaeolatitude record of Late Maastrichtian – Early Danian climate change, Seymour Island, Antarctica

Submitted by Peter Alan Frost to the University of Exeter
as a thesis for the degree of
Doctor of Philosophy in Earth Resources
in February 2017

I certify that all material in this thesis which is not my own work has been identified and that no material has previously been submitted and approved for the award of a degree by this or any other University.

Abstract

The Latest Cretaceous period was characterised by global cooling, superimposed on this pattern of climate change were perturbations in global climate. In high palaeolatitude settings in the Southern Hemisphere short term glacial episodes may have occurred through the latest Cretaceous. The extensive sedimentary succession within the James Ross Basin, Antarctica, provided an opportunity to test the possibility of late Cretaceous glaciation in particular through the succession exposed on Seymour Island. A high resolution oxygen and carbon stable isotope record through the Late Maastrichtian – Early Danian was generated by analysing diagenetically unaltered aragonite nacre shell material from a molluscan fauna collected from the López de Bertodano Fm., part of the Marambio Group present on Seymour Island, Antarctica. The Marambio Group forms an extensive 1100 m thick Late Maastrichtian section that crops out over ~70 km^2 of the southernmost part of the island. Coverage of stable isotope data for the measured stratigraphy was good with 213 screened analyses that included data from within 1 m of the K-Pg boundary located at 1029 m above datum, determined from the first occurrence of the dinoflagellate cyst *Senegalinium obscurum*.

Stable isotope data (‰ VPDB) for primary aragonite from bivalves, cephalopods and gastropods exhibited screened stable isotope data ranges of -0.06 to +2.05‰ for $\delta^{18}O$ and -7.54 to +3.7‰ for $\delta^{13}C$. Data showed that at individual stratigraphic levels the range in measured $\delta^{18}O$ exhibited significant variability. Benthic specimens provided the majority of the stable isotope data, bivalves exhibited the widest range of $\delta^{18}O$ and $\delta^{13}C$ values. Data show that individual specimens from the same genus can exhibit significant variability for $\delta^{18}O$ and $\delta^{13}C$ and that analysis of single samples at discrete stratigraphic levels may provide an erroneous interpretation of climate change. Higher oxygen isotope values were seen mid-section and complement previous records of periods of cooler climate identified from palynology, clumped isotopes and sea level. Palaeotemperatures were calculated for $\delta^{18}O$ values for a seawater composition of SMOW = -1.0‰, representing an ice free ocean, 6 to 14°C for bivalves, 9 to 12°C for gastropods and 9 to 15°C for cephalopods. Temperatures indicated relatively stable benthic temperatures (~10°C) with a cooling phase that commenced at ~450 m (~69.5 Ma) with the coolest temperatures developed at ~630 m (~69 Ma). Cooling trends showed a good correlation with the position of seawater lowstands. Thereafter temperatures recovered towards the K-Pg boundary before a cooling trend developed that closely correlated with the PaDa1 lowstand. Acceptance of Deccan Traps volcanism as a causal mechanism for the limited degree of observed warming close to the K-Pg event was limited by a lack of suitable specimens.

Table of Contents

Figures

Tables

1 Introduction

Study of palaeoclimate change provides a valuable tool towards an understanding of current and potential future climate change, highly topical given the overwhelming evidence that the Earth is currently experiencing climate change due to anthropogenic factors (Hay, 2011). The Cretaceous experienced what has been described as a 'greenhouse' climate (Hallam 1985; Brentnall *et al*., 2005), a term also used to describe a possible future climate scenario for the Earth (Hay, 2011). The importance of the polar regions for climate sensitivity have been well documented (Goody, 1980; Manabe and Stouffer, 1980; Florindo *et al*., 2003). The analysis of carbon and oxygen stable isotopes and the interpretation of marine palaeotemperatures from the Latest Maastrichtian of the James Ross Basin within this study provides a data set that is of value to present day climate scientists working on the modelling of both late Cretaceous palaeoclimates and predicted future climate change during the remainder of the 21st and subsequent centuries. In addition the news in 2013 that atmospheric CO_2 levels had reached a mean concentration of 400 ppm at the monitoring station situated on Mauna Lau, Hawaii (Tans and Keeling, 2015) makes data sets as presented in this thesis of wider significance. This atmospheric CO_2 value represents an increase of 1.43 x pre-industrial CO_2 levels (Ethridge *et al*., 1996; Hunter *et al*., 2013).

The Cretaceous period was characterised by extreme warmth during the mid Cretaceous followed by global climatic cooling during the late Cretaceous (Hallam, 1985; Brentnall *et al*., 2005; Gallagher *et al*., 2008). Superimposed on this overall pattern of climate change were shorter-term perturbations in global climate, particularly in the latest Cretaceous (see Miller *et al*., 1999, 2003, 2004, 2005a,b; Gallagher *et al*., 2008; Kominz *et al*., 2008; Flogel *et al*., 2011). In high palaeolatitude settings in the Southern Hemisphere palaeoclimate modelling (Sellwood and Valdes, 2005; Flogel *et al*., 2011) and data derived from palynology (Thorn *et al*., 2007, 2008; Bowman *et al*., 2013) and palaeoenvironmental data (Tobin *et al*., 2012; Tobin and Ward, 2015; Little *et al*., 2015; Petersen *et al*., 2016) suggested that short term glacial episodes may have occurred through the latest Cretaceous; these episodes appear to be reflected within the record of short term changes in global sea level (see Miller *et al*., 1999, 2003, 2005a,b). The presence of glauconite within the succession may either represent the presence of deeper water or reflect a reduction in the sediment supply (McRae, 1972) for the James Ross Basin sourced from the Trinity Peninsula (Macellari, 1984, 1988). The extensive sedimentary succession within the James Ross Basin, Antarctica provides an opportunity to test the possibility of late Cretaceous glaciation in particular

through the succession exposed on Seymour Island (Crame *et al*., 2004; Thorn *et al*., 2007, 2008; Tobin *et al*., 2012; Bowman *et al*., 2013; Tobin and Ward, 2015; Petersen *et al*., 2016). The succession is locally richly fossiliferous with good preservation of primary skeletal carbonates, in particular aragonite nacre from a molluscan fauna. Previously published research from this area provide a broad picture of climate change based upon the stable isotope geochemistry of skeletal carbonates, but these data only provide a broad framework. Advances in the understanding of the regional stratigraphy (Crame *et al*., 2004; Witts *et al*., 2015) and updated age models (Tobin *et al*., 2012, Petersen *et al*., 2016), along with new analytical facilities, provide the opportunity to develop a more robust and high-resolution geochemical record of climate change.

In particular this project:

1. Provides a high resolution carbon and oxygen stable isotope record for the late Cretaceous and early Paleogene of the James Ross Basin.
2. Provides a high resolution Strontium Isotope Stratigraphy record for the latest Maastrichtian and earliest Danian of the James Ross Basin.

The Earth's climate is in a real sense defined by conditions at the poles (Goody, 1980; Manabe and Stouffer, 1980). Changes in the equator to pole thermal gradient that represent an important control on atmospheric and oceanic circulation are expressed principally as variations in polar temperatures (Spicer and Parrish, 1990a,b). Significant ice forms most easily in polar regions and thus climate at the poles is a major determinant of global sea level; a number of authors have reviewed the impact of Antarctic ice sheets on global eustacy (see Miller *et al*., 1999, 2003, 2005a,b; Haq, 2014). A polar continental ice sheet cannot form unless there is land near the pole and such a landmass reduces the efficiency of oceanic heat transport and provides a site for the accumulation of snow, both of which lead to cooling (Spicer and Parrish, 1990a). Seasonality of temperature is expressed most strongly at the poles and must have maintained a powerful effect on the distribution and productivity of global biota (Goody, 1980; Manabe and Stouffer, 1980; Florindo *et al*., 2003). The Antarctic region has both in the past and at the present day exerted a significant effect on global climates. These effects influenced sea level, atmospheric composition and dynamics and patterns of ocean circulation (Goody, 1980; Manabe and Stouffer, 1980; Miller *et al*., 1999; Florindo *et al*., 2003; Miller *et al*., 2003, 2005a,b). A greater understanding of the palaeoclimate of this region and the Antarctic cryosphere is crucial to a broader understanding of the global climates and palaeoceanography at all scales (Florindo *et al*., 2003). Particular attention has been paid to climate processes in polar regions, in recognition of their importance to global climate and understanding the boundary conditions for the formation of ice. Many of the processes involved are inadequately

understood, partly because the models and data are poorly constrained (Spicer and Parrish, 1990a,b and references therein).

A high resolution oxygen and carbon stable isotope record through the latest Maastrichtian – earliest Danian was generated using diagenetically unaltered aragonite nacre shell material from a molluscan fauna collected from the López de Bertodano Formation, an extensive 1100 m thick late Maastrichtian section from Seymour Island, Antarctica. The exceptionally well exposed K-Pg boundary sequence on Seymour Island offers the opportunity to further investigate the palaeoenvironmental and biotic change at this critical period of Earth history (Crame *et al*., 2004). The macrofossils exhibit a good state of preservation, specimens selected for stable isotope analysis all retained primary shell material comprised of aragonite nacre. For the purposes of this study no planned stable isotope analyses were carried out for specimens exhibiting a calcite shell mineralogy. This decision was taken because the studied section is dominated by macrofossils with preserved aragonite nacre; calcitic macrofossils are relatively rare, and those taxa which are present (e.g. the serpulid *Rotularia*) have shells which are sensitive to diagenetic over-prints (see Chapter 3). In addition, if isotopic data from calcitic shells with potentially differing levels of diagenetic alteration (see Chapter 3) were analysed then this would introduce uncertainty into the stable isotope data set.

Overall coverage of data for the measured stratigraphic section was good, with 247 specimens screened for diagenetic alteration and subsequent stable isotope analyses that included data from within 1 m of the K-Pg boundary, which was at a position of 1029 m above datum as determined by palynology, namely the first appearance of the dinoflagellate cyst *Senegalinium obscurum* (Bowman *et al*., 2012). Multiple analyses at discrete stratigraphic levels enabled the comparison of stable isotope data from both benthic and pelagic macrofossils at corresponding stratigraphic levels to be investigated, to test for the potential for water stratification in the James Ross Basin. In addition the $\delta^{18}O$ data for nektonic cephalopods might reflect ontogenetic change related to the stage of life (see Chapter 4; Lukeneder *et al*., 2010).

Following a successful application for NERC funding a limited number of specimens were also sampled in preparation for $^{87}Sr/^{86}Sr$ isotopic analysis to enable the incorporation of absolute ages into the measured stratigraphy through the application of strontium isotope stratigraphy using the LOWESS version 3 age look up tables (McArthur *et al*., 2001). A number of previous studies have generated spot $^{87}Sr/^{86}Sr$ ages within the López de Bertodano Fm. (McArthur *et al*., 1998, 2000, 2001; Crame *et al*., 2004; Petersen *et al*., 2016) but these were insufficient to provide a regular dating of the sediments within the Cretaceous sequence on Seymour Island. Available age

data were incorporated into the age model employed in this study, which included the addition of magnetostratigraphy, biostratigraphy and limited strontium isotope stratigraphy (see Figure 1-5; McArthur *et al*., 1998, 2000, 2001; Crame *et al*., 2004; Tobin *et al*., 2012; Witts *et al*., 2015). Note that whilst Petersen *et al*. (2016) reported on the analysis of spot $^{87}Sr/^{86}Sr$ ages none of these data were incorporated into their age model.

Analysis of $^{87}Sr/^{86}Sr$ ratios were carried out at the NERC Isotope Geosciences Laboratory, Kingsley Dunham Centre and involved individual, duplicate and in certain cases triplicate analyses of shell material from selected specimens, (see Chapter 5 for a discussion of the strontium isotope stratigraphy methodology and data interpretation). Petersen *et al*. (2016) included $^{87}Sr/^{86}Sr$ data which are compared with corresponding data from this study and further discussed in Chapter 5.

1.1 History of exploration and previous research

The Antarctic Peninsula is the most northerly part of the continent and reaches above the Antarctic Circle experiences the mildest climate and on the north side is the least icebound during the summer and therefore the most accessible. When Norwegian Captain, Carl Anton Larsen landed from his ship, the *Jason*, on Seymour Island, he returned with maps of the territory and fossils of long-extinct species. Interestingly, Larsen's trip aboard the *Jason* was significantly more successful than his Swedish Antarctic Expedition between 1901 and 1903. During that trip, his ship, the *Antarctic*, was crushed and sunk by icebergs and he and his crew were forced to weather fourteen months on Snow Hill Island, surviving on penguins and seals.

Since Larsen's voyage on the *Jason*, Seymour Island has been the subject of continuing research in a number of fields including **palaeontology** (for example Hall, 1977; Jerzmańska, 1991; Aguirre-Urreta, 1995; Aronson and Blake, 2001; Feldmann *et al*., 2003; Jeffrey and William, 2003; Stilwell and Zinsmeister, 2003; Cantrill and Poole, 2005; Carrie *et al*., 2005; Emig and Bitner, 2005; Schweitzer *et al*., 2005; Beu, 2009; Acosta Hospitaleche *et al*., 2012; Acosta Hospitaleche and Reguero, 2014; Acosta Hospitaleche and Gelf, 2015; Witts *et al*., 2015; Petersen *et al*., 2016; Witts *et al*., 2016), **palaeoenvironmental** (for example Gaździcki *et al*., 1992; McArthur *et al*., 1998; Pirrie *et al*., 1998; Dingle and Lavelle, 2000; Javier *et al*., 2001; Dutton *et al*., 2002, 2007; Ivany *et al*., 2008; Svojtka *et al*., 2009; Tobin *et al*., 2012; de Souza *et al*., 2014; Little *et al*., 2015; Tobin and Ward, 2015; Petersen *et al*., 2016), **palaeoclimate** (Pirrie *et al*., 1998; Dutton *et al*., 2002, 2007; Gaździcki *et al*., 1992; Ivany *et al*., 2008; Tobin *et al*., 2012; Bowman *et al*., 2013, 2014; Tobin and Ward, 2015; Petersen *et al*., 2016), **sedimentological and structural studies** (for example Valle *et al*., 1992;

Marenssi *et al*., 2002; Borzotta and Trombotto, 2004; Eduardo *et al*., 2008; Maestro *et al*., 2008; Olivero *et al*., 2008; Pirrie *et al*., 2009; Svojtka *et al*., 2009; Johnson *et al*., 2011; de Souza *et al*., 2014).

1.2 Geographical and geological setting

Seymour Island, referred to as 'Isla Vicecomodoro Marambio' in Argentine literature, is located towards the north eastern end of the Antarctic Peninsula at a latitude of 64°15' S and longitude 56°45' W (Figure 1-1). The location of Seymour Island in relation to the north-eastern section of the Antarctic Peninsula and in particular the Trinity Peninsula is shown in Figure 1-2(a).

Figure 1-1. Geographic location of Seymour Island in the Antarctic Peninsula region. After http://www.eoearth.org/article/Antarctic_Peninsula, 2013.

The Larsen Basin forms a distinct sub-basin of the larger Weddell Basin (MacDonald *et al*., 1988; Pirrie *et al*., 1991) with an approximate area of 2 x 10^5 km^2, a mean depth of fill of 5 km and an approximate volume of 1 x 10^6 km^3. The Maastrichtian section on Seymour Island has a stratigraphic thickness of ~1100 m and a number of authors have reported estimated basin infill rates of ~270, 175 and 100 to 200 m/Ma^{-1} (McArthur *et al*., 1988; Dutton *et al*., 2007; Tobin *et al*., 2012).

The James Ross Basin, a smaller sub-basin of the Larsen Basin, comprises the most continuous and complete Cretaceous – Paleogene (K-Pg) sequence in the Austral Realm (Macellari, 1986; Crame *et al*., 2004; Tobin *et al*., 2012; Witts *et al*., 2015). During the Late Cretaceous the James Ross Basin was located to the east of an active

volcanic island arc now represented by the Trinity Peninsula (Figure 1-2; MacDonald *et al*., 1988; Pirrie *et al*., 1991). A coastal plain and shoreline trended approximately NNE - SSW and major rivers transported siliciclastic sediments offshore with material sourced from the peninsula (Zinsmeister, 1982; Macellari, 1988; Pirrie, 1989; Hathway, 2000; Crame *et al*., 2004; Olivero *et al*., 2008). Seymour Island exhibits the youngest part of the stratigraphic sequence forming the Seymour Island Group and represents marine deposits sourced from the back arc. The basin deposits span the Early Cretaceous to the Early Paleogene in age and comprise three principal lithostratigraphic groups, the Gustav Group (Aptian – Coniacian), Marambio Group (Santonian – Danian) and Seymour Island Group (Paleocene – Eocene) (Crame *et al*., 1991; Pirrie *et al*., 1997; Hathway, 2000; Crame *et al*., 2004; Crame *et al*., 2006; Olivero, 2012).

A view of the López de Bertadano Fm. on Seymour Island facing the Weddel Sea is presented in Figure 1-2(b). The locations of stratigraphic sections that were sampled during the fieldwork programme are presented in Figure 1-2(c). Macellari (1988) defined the location of informal geological boundaries identified as units 1 to 10. Note that a number of the boundaries were later re-classified as undifferentiated (units 4-9), see also the stratigraphy detailed in Figure 1-3 (Crame *et al*., 2004).

Samples analysed in this study were collected from the López de Bertodano Fm.. This forms the upper part of the ~3000 m thick Marambio Group (Olivero, 2012) and crops out over ~70 km^2 of southern Seymour Island, neighbouring Snow Hill Island and southern and northern James Ross Island, Vega Island and Humps Island (Figure 1-2(a); Pirrie *et al*., 1997; Crame *et al*., 2004; Olivero *et al*., 2008; Bowman *et al*., 2012). The James Ross Basin has been tectonically stable over the last 80 Ma with a gentle regional dip of 8 to 10° to the southeast (MacDonald *et al*., 1988; Pirrie *et al*., 1991; Crame *et al*., 2004; Tobin *et al*., 2012). Crame *et al*. (1991) noted the occurrence of major NE – SW trending faults of an unknown age that result in repetition of the stratigraphy on northern and southern James Ross Island. No other major faults cut the upper Cretaceous, the only possible exception being the similar trending Quebrada Largo valley on Seymour Island (Crame *et al*., 1991). The presence of well preserved macrofossils with abundant aragonite nacre indicated only shallow burial (1 to 2 km) and associated low temperature diagenesis (~30 to <60°C) (Svojtka *et al*., 2009; Tobin *et al*., 2012).

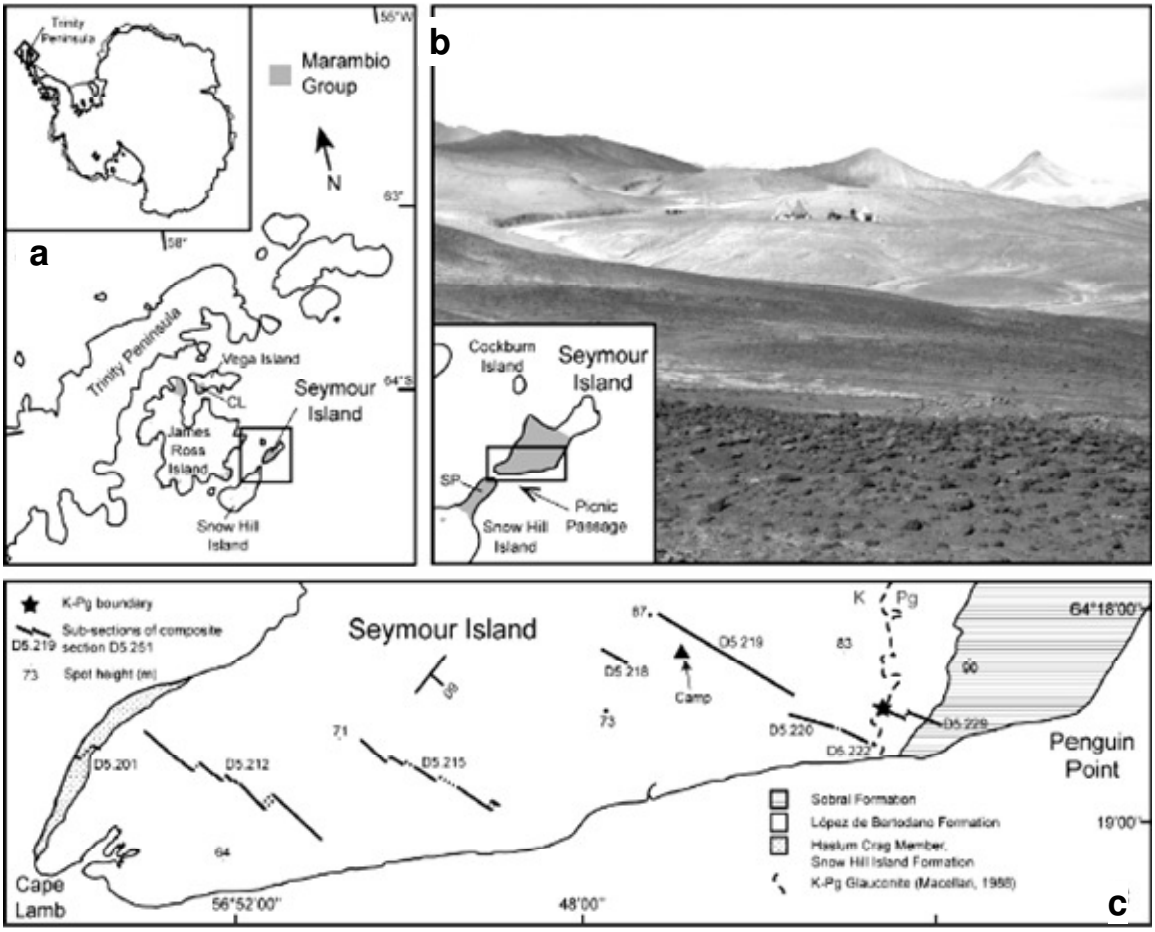

Figure 1-2. Locality maps of the area studied and location of measured sections. a) Location of Seymour Island, James Ross Basin, Antarctic Peninsula. b) Field photograph of the landscape of the López de Bertodano Fm. exposed on Seymour Island, looking south-eastwards towards the Weddell Sea, field camp provides scale. The inset map shows Seymour Island and adjacent islands; SP — Spath Peninsula. c) Enlarged map of the southern end of Seymour Island to illustrate the geology and location of identified measured sections, the K-Pg boundary occurs within a distinctive glauconite-rich interval traceable along strike. Diagrams (a and c) and field photograph (b) after Bowman *et al*., 2012).

The data presented in Table 1-1 are derived from GSSP (Gradstein *et al*., 2012) and define the key magnetochron tie points and ages together with the K-Pg position within the measured stratigraphy. The upper Maastrichtian - lower Danian interval as determined by biostratigraphy (Thorn *et al*., 2009; Bowman *et al*., 2012, 2014) and magnetostratigraphy (Tobin *et al*., 2012) forms part of the Marambio Group and is represented by the López de Bertodano Fm. which is uncomformably overlain by the Sobral Fm. of Paleocene age, see Figure 1-3. Seymour Island is the highest palaeolatitude K–Pg boundary section in the southern hemisphere with a similar palaeolatitude (62°S) to the current latitude (64°17′S) based upon plate tectonic reconstruction (Torsvik *et al*., 2008). This location makes it ideal for examining climate change associated with the K–Pg boundary because polar amplification produces larger and more detectable temperature changes at higher latitudes (Goody, 1980; Manabe and Stouffer, 1980; Pirrie *et al*., 1995; Holland and Bitz, 2003).

Table 1-1. Magnetochron tie points, key ages derived from GSSP (Gradstein *et al*., 2012) and positions within the measured stratigraphy of the López de Bertodano Fm..

Magnetochron Tie Points	Age (Ma)	Stratigraphic Height (m)
29R - 29N	65.688	1088
K-Pg boundary	66.043	1029
30N - 29R	66.398	953
30R - 30N	68.196	771
31N - 30R	68.369	753
31R - 31N	69.269	565
31N - 32R	71.449	140

The expanded stratigraphic section generally shows continuous sedimentation, the presence of glauconite rich horizons suggests periods of episodic sedimentation (see Figure 1-3; McRae, 1972; Tobin *et al*., 2012). The section also exhibits an abundance of well preserved macrofossils. Many with outstanding preservational characteristics that include rare primary aragonite nacre and low magnesium calcite shell mineralogy together with an undeformed three-dimensional shape (Tobin *et al*., 2012). The preservation in the fossil record of primary biogenic aragonite from a molluscan fauna is rare (Wendt, 1977; Jordan *et al*., 2015) because metastable aragonite is readily recrystallised to LMC by low temperature alteration (~30°C to >60°C) (Svojtka *et al*., 2009) and through the development of diagenetic cements resulting from fluid flow; with alteration indicated by changes in the trace element geochemistry. The presence of primary aragonite nacre provided an initial guide for the selection of geochemical samples with minimal levels of mineralogical or diagenetic alteration (Tobin *et al*., 2012).

The K–Pg boundary has been located between units 9 and 10 of the upper López de Bertodano Fm. through various means in the past and is currently defined by the first occurrence of Paleogene dinoflagellate cysts that are associated with an iridium enhancement (Elliot *et al*., 1994; Bowman *et al*., 2009, 2012). Global correlation of the late Cretaceous on Seymour Island has been hampered by the increasing endemism of macrofossils and microfossils in the Maastrichtian and an absence of any absolute age control from ash layers (Macellari, 1988; Olivero and Medina, 2000; Bowman *et al*., 2012; Tobin *et al*., 2012; Tobin and Ward, 2015).

Whilst some age constraints from Sr isotope ratios on molluscan carbonate have been reported from the lower units of the López de Bertodano Fm. no such age constraints were reported from the upper units that approach and cross the K–Pg boundary until limited strontium isotope stratigraphy provided further age data for the succession (McArthur *et al*., 1998, 2000; Petersen *et al*., 2016).

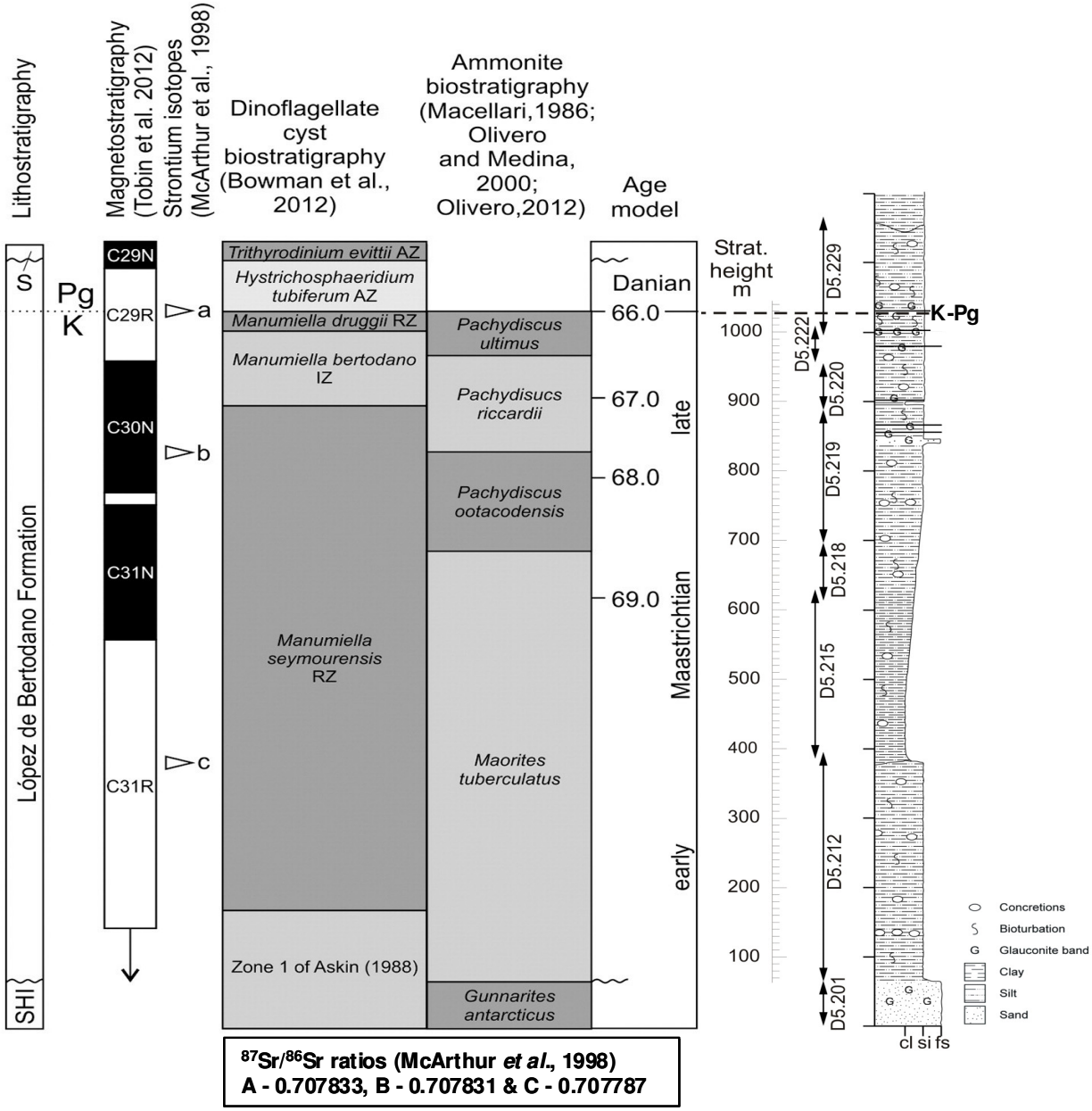

Figure 1-3. Lithostratigraphy and sedimentology of the measured section from the Latest Maastrichtian – Earliest Danian, Seymour Island, Antarctica correlated with magnetostratigraphy (Tobin *et al*., 2012). K-Pg and Maastrichtian ages defined from GSSP (Gradstein *et al*., 2012), $^{87}Sr/^{86}Sr$ dates (McArthur *et al*., 1998; Crame *et al*., 2004). Diagram modified from Witts *et al*. (2015). Sedimentology log measured by Francis and Thorn, pers. comm. (2008). Based upon GSSP and $^{87}Sr/^{86}Sr$ data the lower 310 m of the section has a sedimentation rate of ~113 m/Ma^{-1}, whilst the section from 310 m – 1029 m (K-Pg) has a corresponding rate of ~200 m/Ma^{-1}. An estimated average rate of basin infill based upon these two rates is ~160 m/Ma^{-1}. The base of the Maastrichtian is defined by an age of 72.05 Ma (Gradstein *et al*., 2012).

Note that Petersen *et al*. (2016) did not include any age correlation with the LOWESS Smoothed Global Strontium Isotope Curve (McArthur *et al*., 1998, 2001). Magnetostratigraphy was introduced by Tobin *et al*. (2012) and included into the age model, see Figure 1-3.

In an attempt to constrain the absolute age of the youngest units from the succession a number of specimens were selected for $^{87}Sr/^{86}Sr$ isotopic measurements. Discussion

of the methodology employed, the significance of the data generated and correlation of those data with the Latest Maastrichtian section of the Late Cretaceous Strontium Isotope Stratigraphy (SIS) curve will be covered in Chapter 5 (see also McArthur *et al*., 1998, 2001). Previous Sr isotope analyses were carried out on macrofossil specimens, principally molluscan, collected from Seymour Island some of which data were subsequently incorporated into the LOWESS Smoothed Global Strontium Isotope Curve (McArthur *et al*., 1998, 2001).

1.3 Sedimentology

An 1100 m thick section through the Latest Maastrichtian, López de Bertodano Fm., which comprises the southern and central areas of Seymour Island, was measured, logged and sampled (Francis and Thorn, pers. comm., 2008) at stratigraphic intervals between 0.25 and 2 m (see Figures 1-2 and 1-3). The deposition of 1100 m of sediment in approximately 6 million years indicates a rapid sedimentation rate (~183 m/Ma^{-1}), at times perhaps reaching a figure of ~270 m/Ma^{-1} a fourfold increase over the rate of the equivalent Stevns Klint section from Denmark (McArthur *et al*., 1998; Thorn *et al*., 2008). Based upon the measured thickness and with a stated sampling separation of 0.25 to 2 m between identified stations suggested an idealised temporal resolution of ~20 ka for the section. Alternative estimated basin infill rates of 175 and 100 to 200 m/Ma^{-1} have also been reported (Dutton *et al*., 2007; Tobin *et al*., 2012). Based upon GSSP and $^{87}Sr/^{86}Sr$ data the lower 310 m of the section has a sedimentation rate of ~113 m/Ma^{-1} whilst the section from 310 m – 1029 m (K-Pg) has a corresponding rate of ~200 m/Ma^{-1}. An estimated average rate of basin infill based upon these two rates is ~160 m/Ma^{-1}.

The sedimentary sequence, sourced from calc-alkaline arc volcanic and plutonic rocks from the Trinity Peninsula (Pirrie *et al*., 1991) has a gentle dip of ~09° SE and principally consists of heavily bioturbated muddy silts and silty muds containing varying amounts of both detrital and authigenic glauconite, see Figure 1-4 which shows a field photograph of the López de Bertodano Fm., Seymour Island, Antarctica looking south-eastwards towards the Weddell Sea. The presence of glauconite at specific levels within the succession suggests that sedimentation was episodic and may reflect a reduction in the supply of sediment into the basin or alternatively the presence of highstands (McRae, 1972). Both possible causes are compatible with the presence of minor ice sheets on the Antarctic continent as discussed by a number of authors, subjects included a eustatic reduction in sea level of 30 to 40 m in the early Maastrichtian with a more pronounced reduction in sea level of 60 m in the late Maastrichtian to Eocene (Miller *et al*., 1999). The development of restricted ephemeral

ice sheets in Antarctica paced by Milankovitch forcing (Miller *et al.*, 2003). A comparison of the timing and duration of lowstands indicated the presence of rapid high amplitude (200 m) eustatic change at a rate of 20 m/ky^{-1} resulting from the development of ice sheets and a low amplitude slower rate of 10 m/ky^{-1} due to dessication and inundation (Miller *et al.*, 2005a; Haq, 2014).

Figure 1-4. Seymour Island, Antarctica, field photograph of the López de Bertodano Fm. looking SE towards the Weddell Sea. (Photograph after Thorn *et al.*, 2009).

Previous authors have described the K-Pg boundary on Seymour Island as being coincident with a significant glauconite rich horizon in association with a fish mortality bed (Macellari, 1988; Zinsmeister *et al.*, 1989; Zinsmeister, 1998). Several glauconite-rich fish teeth/bone horizons have been identified throughout the succession (see Figure 1-3), often topped with fossiliferous 'lags' containing many molluscs and other fossils, that suggest episodic periods of sediment starvation (Crame *et al.*, 2004). Previous authors have also suggested that this upper portion of the succession across the K–Pg boundary represents a regressive phase with a loss of accommodation space (Macellari, 1988; Crame *et al.*, 2004; Olivero, 2012; Tobin *et al.*, 2012). The lithostratigraphy and sedimentology of the López de Bertodano Fm. have previously been described by a number of authors (Macellari, 1988; Crame *et al.*, 1991; Pirrie *et al.*, 1997; Crame *et al.*, 2004; Olivero *et al.*, 2008; Olivero, 2012). Ten numbered informal lithostratigraphic units were defined (Macellari, 1986, 1988), a number of the units have subsequently been re-classified as being undifferentiated (units 4-9) (Crame *et al.*, 2004). Note that Tobin *et al.* (2012) continue to refer to the upper "molluscan units" (units 7–10), which become increasingly fossiliferous through units 9 and 10. In contrast, (Crame *et al.*, 2004) suggested that a slight decrease in grain size above the underlying Haslum Crag Member of the Snow Hill Island Fm. (as noted by Pirrie *et al.*,

1997), together with the poorly fossiliferous nature of this portion of the succession represented deep water shelf conditions. Stratigraphically higher, the mid-upper portion of the formation represents an overall transgression with the establishment of mid to outer shelf facies (Macellari, 1988; Crame *et al*., 2004; Olivero *et al*., 2008; Olivero, 2012).

The base of a prominent series of glauconite horizons ~1000 m above the base of the sequence (Figure 1-3) was interpreted as being equivalent to the 'K–T glauconite' succession described by Zinsmeister (1998) and coincides with a distinct change in both macro and microfossil faunas and floras (Elliot *et al*., 1994; Zinsmeister, 1998; Crame *et al*., 2004; Stilwell *et al*., 2004; Bowman *et al*., 2012; Witts *et al*., 2015). The base of this glauconite-rich interval contains an iridium (Ir) spike and the first appearance of the dinoflagellate cyst *Senegalinium obscurum*, markers used by previous authors to locate the K–Pg boundary on Seymour Island (Elliot *et al*., 1994; Crame *et al*., 2004; Bowman *et al*., 2012). This horizon was also the contact between informal mapping units 'Klb9' and 'Klb10' (Macellari, 1988; Sadler, 1988). Above this the 50 to 70 m thick unit 'Klb10' is made up of brown/grey mudstones and siltstones with scattered concretions and a distinctive macrofossil fauna (Macellari, 1988; Crame *et al*., 2004; Montes *et al*., 2010; Tobin *et al*., 2012; Crame *et al*., 2014; Little *et al*., 2015; Tobin and Ward, 2015; Witts *et al*., 2015; Petersen *et al*., 2016).

Principally comprising siltstones with a larger percentage of sandstones and concretionary layers than the lower units, these upper units are interpreted as transgressive over the lower group, and were deposited in shelf and slope facies at water depths between 100 and 200 m (Macellari, 1988; Olivero, 2012). Although largely homogeneous the succession also contains occasional sandstone beds interspersed with the dominant finer-grained lithologies and discrete layers of early diagenetic concretions, some of which contain well preserved macrofossils (Pirrie and Marshall 1991; Tobin *et al*., 2012). No sedimentological or palaeontological evidence has been reported for any major hiatuses in the López de Bertodano Fm. on Seymour Island (McArthur *et al*., 1998; Crame *et al*., 1999; McArthur *et al*., 2000; Dutton *et al*., 2007; Tobin *et al*., 2012).

1.4 Palaeontology

Macrofossil rich beds are common in the upper parts of the sequence that correspond to the informal units 6-9 (Macellari, 1988) and that were later described as 'undifferentiated' (Crame *et al*., 2004) (Figure 1-3). Based upon the macrofossils available for this study there was a marked reduction in suitable specimens in the lower 300 m section of the stratigraphy. The López de Bertodano Fm. contains a relatively

low diversity but abundant invertebrate and vertebrate macrofauna, a macroflora (calcified fossilised wood), a microfauna (including foraminifera and silicoflagellates) and a microflora (marine and terrestrial palynomorphs) ([Ammonoidea, *Rotularia*] Macellari, 1984, 1986; Witts *et al*., 2015; [Bivalvia] Askin, 1988a; Macellari, 1988; Zinsmeister and Macellari, 1988; Zinsmeister *et al*., 1989a; Little *et al*., 2015; [Nautiloidea] Cichowolski *et al*., 2005; [Palynomorphs] Thorn *et al*., 2008, 2009; Bowman *et al*., 2012). The invertebrate fauna includes ammonites, bivalves, gastropods, echinoids, corals, serpulid worms – *Rotularia*, vertebrate macrofossils included marine reptiles, fish and sharks. Macrofossil specimens and sediment samples were collected at 0.25 to 2 m intervals throughout the sequence, allowing an assessment of changes in marine diversity and community composition through time (Stillwell, 2003; Crame *et al*., 2004; Thorn *et al*., 2008, Witts *et al*., 2015). Many of the molluscan macrofossils retained original aragonite nacre shell material and in most cases exhibited a good state of shell preservation (Figure 1-5). The preservation state of the aragonite nacre indicated that individual specimens had not been subject to significant diagenesis (Tobin *et al*., 2012; Witts *et al*., 2015; Petersen *et al*., 2016). See Chapter 3 for further information regarding the screening and selection of specimens exhibiting minimal evidence of diagenetic features. Many of the best preserved specimens exhibited bright nacreous shell layers with colours more reminiscent of the ‘Mother of Pearl’ from shells of extant molluscs, see Figure 1-5(b, c and d).

Whilst an abundant fauna was recorded from the succession, for the purposes of the stable isotope analysis a key requirement was for a molluscan fauna, namely bivalves, cephalopods and gastropods. A distinct ‘recovery fauna’ (Stilwell, 2003; Crame *et al*., 2004, 2014) was identified in the earliest Paleogene sediments informally identified as ‘Klb10’ (Macellari, 1988), which indicated a domination of deposit feeders over suspension feeders characterised by a sharp increase in gastropod species (Crame *et al*., 2014). First indications are that taxonomic diversity levels recovered relatively quickly across the K-Pg boundary (Stillwell, 2003; Bowman *et al*., 2012) and this feature may stand in marked contrast to localities elsewhere in the world.

A number of authors have published work on Cretaceous stable isotope research based upon the analysis of calcite and aragonite shell material from a molluscan fauna (Pirrie *et al*., 1998; Sial *et al*., 2001; King and Howard, 2005; Steuber and Rauch, 2005; Thomas *et al*., 2005; Steuber and Buhl, 2006; McArthur *et al*., 2007; Prokoph *et al*., 2008; Tripati *et al*., 2010; Passey and Henkes, 2012; Tobin *et al*., 2012; Stevenson *et al*., 2014; Little *et al*., 2015; Tobin and Ward, 2015; Witts *et al*., 2015; Petersen *et al*., 2016). For this study stable isotope analyses focussed on the abundant aragonite

nacre, the presence of which provided an indication of good diagenetic stability (see Chapter 3).

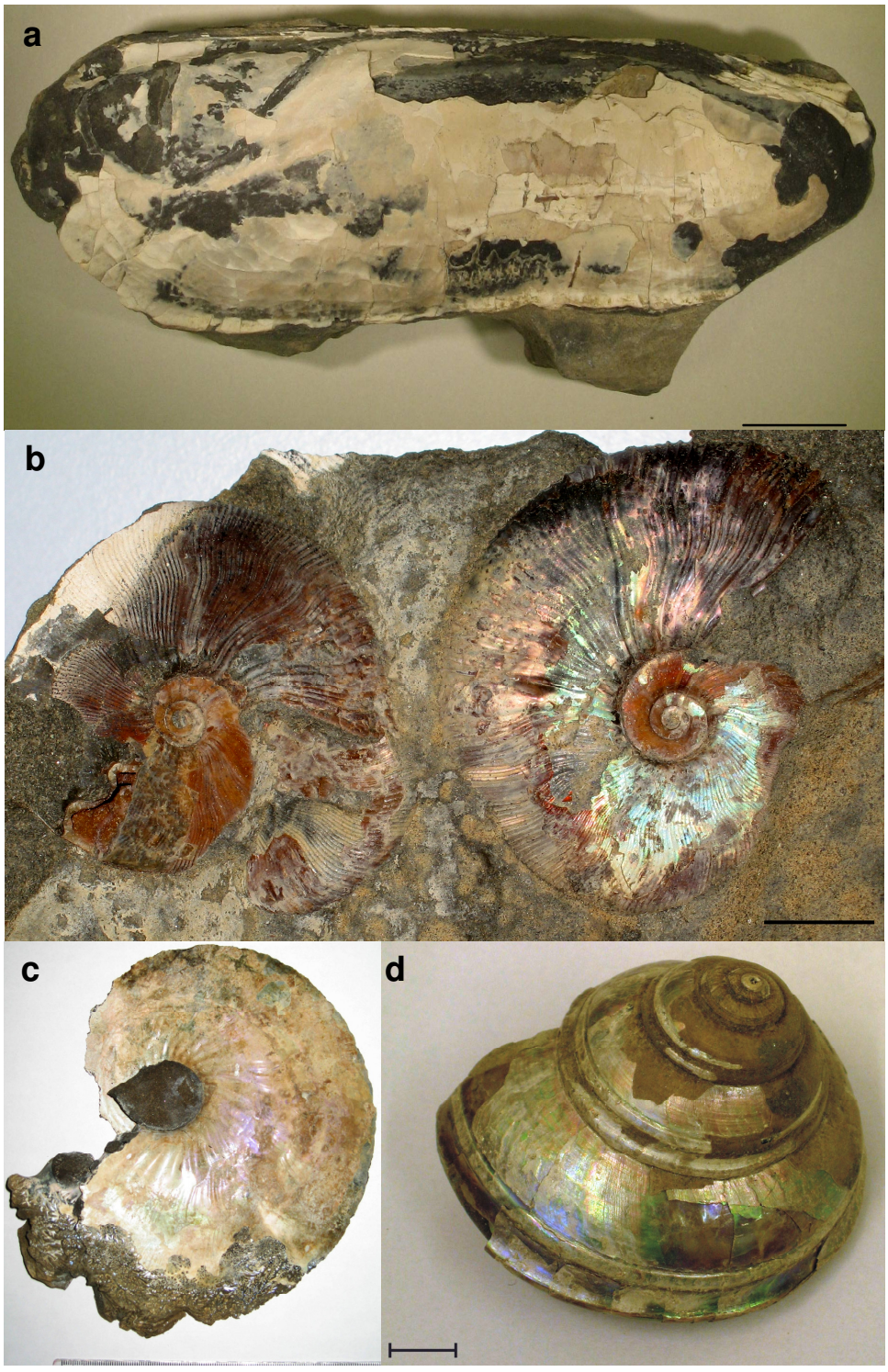

Figure 1-5. Photographs of molluscan specimens from the López de Bertodano Fm., note the presence of well preserved nacreous aragonite shell material in the images. a) Bivalve genus - *Solemya rossiana* an infaunal thiotrophic chemosymbiont involved in the anaerobic oxidation of methane (Little *et al.*, 2015). Specimen Id - D5.215.347.2/M. Scale bar 10 mm. b) Ammonite genus – *Maorites densicostatus* a nektonic carnivore, specimen Id - D5.219.1185.2/G. Scale bar ~20 mm. c) Ammonite genus – *Pachydiscus* a nektonic carnivore. Specimen Id - D5.222.1248.2/K. Field of view ~200 mm. d) Gastropod genus – *Pleurotomaria* an epifaunal scavenger/carnivore, specimen Id - D5.215.216.5/A. Scale bar 10 mm.

The extensive and unbroken thickness of the sequence on Seymour Island makes the late Maastrichtian – earliest Danian section the most important Austral location for palaeoenvironmental investigation of the K-Pg boundary and the associated extinction of marine and terrestrial taxa (Crame *et al*., 2004; Bowman *et al*., 2012; Tobin *et al*., 2012; Little *et al*., 2015; Witts *et al*., 2015; Petersen *et al*., 2016).

Table 1-2 lists a genus level identification of macrofossil specimens selected for analysis, where no genus level identification was possible aragonite nacre shell material was sampled as a source of 'bulk' samples. All selected specimens were analysed for $\delta^{18}O$ and $\delta^{13}C$ stable isotope data and a smaller subset were also analysed for $^{87}Sr/^{86}Sr$ isotope data. Both identified and unidentified samples of shell material were subject to an identical diagenetic screening process (see Chapter 3 and Appendices B, C and D for a detailed discussion). See Appendix G, Table G-1, for the distribution of identified macrofossils within the latest Maastrichtian Seymour Island succession. Note that the table does not represent the full range of identified individual specimens and that for clarity duplicate entries were removed.

Table 1-2. Genus level identification of aragonite nacre bearing macrofossil specimens + aragonite nacre shell material where no genus level identification was possible that were analysed for $\delta^{18}O$ and $\delta^{13}C$ stable isotope data and for a smaller subset $^{87}Sr/^{86}Sr$ stable isotope data. Both identified and unidentified samples of shell material were subject to an identical diagenetic screening process (see Chapter 3 and Appendices B, C and D for a detailed discussion). See Appendix G, Table G-1 for the distribution of identified macrofossils within the latest Maastrichtian Seymour Island succession. Note that the table does not represent the full range of identified individual specimens and that for clarity duplicate entries have been removed.

Genus	**Specimens**	**Type**
Total specimens	213	
Diplomoceras lambi	1	Ammonite
Grossouvrites	1	Ammonite
Maorites	17	Ammonite
Unidentified - Ammonite	9	Ammonite
Eselaevitrigonia	43	Bivalve
Lahillia	1	Bivalve
Nucula	49	Bivalve
Oistotrigonia	28	Bivalve
Pinna	5	Bivalve
Solemya rossiana	3	Bivalve
Unidentified - Bivalve	22	Bivalve
Amberlaya	14	Gastropod
Unidentified - Gastropod	4	Gastropod
Unidentified	10	Unidentified

1.5 Project synopsis

This project will contribute high resolution stable isotope data, interpreted palaeotemperatures and strontium isotope data to a NERC funded research project,

namely AFI 6/28 titled **"Terminal Cretaceous climate change and biotic response in Antarctica"**. The project investigated Latest Cretaceous to Earliest Palaeogene (~72-65.5 Ma) climates in the James Ross Basin, Antarctica. The extensive sedimentary sequence on Seymour Island, James Ross Basin, Antarctic Peninsula provided an opportunity to study the nature of high-latitude climate at the end of the Cretaceous period and in particular to test the hypothesis that the end-greenhouse climate was punctuated by conditions cold enough to allow short-term glacial conditions.

Geological evidence suggested that after the peak Cretaceous greenhouse warmth (~90 Ma) climates cooled considerably during the Maastrichtian (~72-66 Ma) (Brentnall *et al*., 2005). Controversially, it has been argued that cooling was at times so severe that mountainous high latitude regions experienced short-term periods of glaciation, causing sea level changes worldwide (see Spicer and Parrish, 1990a,b; Miller *et al*., 1999, 2003, 2005a,b; Kominz *et al*., 2008; Miller, 2009; Miller *et al*., 2011; Haq, 2014). Miller *et al*. (1999, 2005a) and Miller (2009) proposed that ice sheets in Antarctica during the Late Cretaceous - Eocene reached a maximum of 8 to 12 x 10^6 km^3, a glacioeustatic equivalent of 20 to 30 m that was complemented by lowstand data reported by Haq (2014).

Palaeotemperature evidence for the possible presence of sea ice was reported by Petersen *et al*. (2016) where temperatures derived from clumped isotope analyses indicated low benthic temperatures of ~3 - 5℃ and in some cases sub-zero temperatures. Bowman *et al*. (2013) proposed the development of winter sea ice determined from the palynomorph record of Seymour Island, Antarctica. The authors reported the dominance of the dinoflagellate cyst *Impletosphaeridium clavus* caused by the presence of cysts from dinoflagellate blooms associated with the decay of winter sea ice. They also reported that peaks and lows of *Impletosphaeridium clavus* abundance marked cold temporary stratification of polar waters, interposed with warmer periods when the ocean was well-mixed. Prior to the K-Pg boundary *Impletosphaeridium clavus* decreased dramatically in abundance possibly due to the onset of warming associated with Deccan Traps volcanism. Tobin *et al*. (2012) and Petersen *et al*. (2016) also proposed that there was evidence in the stable isotope record that suggested the presence of warming trends immediately prior to the K-Pg that were linked to warming associated with the onset of the Deccan Traps volcanism. Petersen *et al*. (2016) also stated that the temperature data indicated the presence of 2 separate phases of warming prior to the K-Pg. Kemp *et al*. (2014) reported on MATs from the Late Maastrichtian – Paleocene of Seymour Island, the data demonstrate that MATs from the López de Bertodano and Sobral Formations averaged 12.4 ± 5 ℃

based on MBT′/CBT analyses on terrigenous material. They authors also commented that paleotemperature estimates for this method may be biased toward summer month temperatures.

The proposed presence of ice sheets suggested that short-term glacial climates may have punctuated supposedly stable warm climates (Haq, 2014). Such dramatic environmental change stressed the terrestrial and marine biota and made them particularly susceptible to extinction related to the global environmental catastrophe at the end of the Cretaceous. The youngest part of the sequence on Seymour Island includes the Cretaceous/Paleogene (K-Pg) boundary; however, previous terrestrial palynomorph studies suggested that there was relatively little evidence of any major environmental change affecting the region during this event (Askin and Jacobson, 1996; Bowman *et al*., 2012). It was noted that the extensive Late Cretaceous section on Seymour Island that included the Cretaceous/Paleogene (K-Pg) boundary, was particularly suitable for the investigation of Maastrichtian palaeoenvironmental and climate change prior to the K-Pg event (Crame *et al*., 2004; Tobin *et al*., 2012; Tobin and Ward, 2015; Witts *et al*., 2015; Little *et al*., 2015; Petersen *et al*., 2016).

Whilst both the base and the top of the Maastrichtian stage in Antarctica have been defined using strontium isotope stratigraphy (McArthur *et al*., 1998; Crame *et al*., 2004) the exceptional thickness of the section and the abundance of well preserved palaeontological material provide an opportunity for further high resolution dating within the Latest Maastrichtian stage. Indeed some parts of the Maastrichtian global Strontium Isotope Stratigraphy curve include data derived from the analysis of samples collected from the López de Bertodano Fm. on Seymour Island (McArthur *et al*., 1998 and 2001). The determination of climate trends was enhanced by the relatively high latitude position of the basin (~65° palaeo-south, Lawver *et al*., 1992). Seasonality of temperature is expressed most strongly at the poles and, by extension, has a powerful effect on the distribution and productivity of global biota. Spicer and Parrish (1990a,b) stated that understanding the climate conditions at the poles was a necessary part of understanding the entire global climate system.

During the 2006 Austral field season over 1100 m of the latest Cretaceous and earliest Palaeogene (Maastrichtian-Danian) sedimentary sequence on Seymour Island was measured, logged and sampled (Francis and Thorn pers. comm. 2008). The monotonous sequence of bioturbated muddy siltstones were sourced from the volcanic arc to the west that is represented by the Trinity Peninsula region and were subsequently deposited in a subsiding but rapidly filling marine basin, the James Ross Basin.

The Seymour Island sequence (see Figure 1-2(c) for the location of section lines) was exploited to obtain high resolution records of palaeontological and geochemical signals to:

1. Investigate the nature of latest Cretaceous-early Palaeogene climate change at high Austral palaeolatitudes
2. Test the hypothesis that ice was present at times and to test climate/ice-sheet model simulations
3. Understand the environmental context in which the K-Pg extinctions occurred

Ongoing studies of the fossil faunas, floras (palynology and wood), sediments and glauconite horizons indicate that environmental conditions changed on several scales during this period. The high latitude temperate marine fauna indicates a general shallowing in the depositional environment with periods of low oxygen bottom water conditions. At times the green iron enriched silicate mineral glauconite (McRae, 1972) was able to form, which indicated that sedimentation rates were periodically extremely low (Pirrie *et al.*, 1994; Westermann *et al.*, 2010), possibly due to highstands that may in turn indicate a glacioeustatic control on sea level with the growth and reduction of ice sheets (see Spicer and Parrish, 1990a,b; Miller *et al.*, 1999, 2003, 2005a,b; Kominz *et al.*, 2008; Miller, 2009; Miller *et al.*, 2011; Haq, 2014).

Initial palynomorph studies (Thorn *et al.*, 2009; Bowman *et al.*, 2012) indicated that the K-Pg boundary was marked by a transition in the marine dinoflagellate cyst flora that reflected unstable ocean palaeoecology after the K-Pg catastrophe. Conversely, there was little change in the terrestrial palynology across the K-Pg, with only a gradual increase in angiosperm pollen noted into the Danian (Thorn *et al.*, 2009; Bowman *et al.*, 2012).

Climate simulations for the Maastrichtian using a fully coupled ocean-atmosphere global climate model HadCM3L were performed to understand the global context (Sellwood and Valdes, 2006). Results indicated that a modern Greenland size ice sheet may have been present on East Antarctica with atmospheric CO_2 concentrations equivalent to 4 x pre-industrial level (Sellwood and Valdes, 2006). These results tentatively suggested that bipolar glaciation was possible even during the Late Cretaceous.

1.5.1 Layout of chapters and appendices

The organisation of chapters within this thesis reflects the following structure:

- Chapter 1 provides a general introduction and overview of the research project including details of the primary research aims, the logistics and broad

methodologies employed during the various phases of investigation and analysis of the collected palaeontological specimens and materials.

- Chapter 2 provides a literature review tracing the key achievements in the field of geochemical proxies for palaeothermometry and their application to the study of palaeotemperatures and palaeoenvironmental research and in particular the study and implementation of proxy methods utilising the stable isotopes of carbon and oxygen. Also including the development and application of 'clumped isotope' analysis and the continuing development of organic geochemical proxies such as TEX_{86} and $U_{37}^{k'}$. A synthesis of the current state of knowledge relating to Cretaceous climates and especially of previous research relating to the Maastrichtian/Danian of the James Ross Basin Is also included.
- Chapter 3 provides an introduction and overview of the diagenetic screening methodology employed during the selection and preparation of aragonite samples for analyses. The chapter also discusses the implementation of a screening index consisting of a score-based approach utilising textural, mineralogical and geochemical analysis. A number of different techniques were available that indicated whether shell material had been subject to diagenesis. Results of the diagenetic screening techniques that were specified in Appendices B, C and D determined whether samples were finally selected for inclusion in the stable isotope analyses. Techniques employed included: optical microscopy, carbonate staining, imaging of shell ultrastructure using scanning electron microscopy, cold cathodoluminescence, identification of shell mineralogy utilising X-ray diffraction and semi-quantitative E(nergy) D(ispersive) S(pectrometry) investigation of shell chemistry using scanning electron microscopy and ICP-OES/MS techniques. Finally the chapter presents a brief introduction to the diagenetic screening of the carbon and oxygen stable isotope data with special emphasis placed on the effectiveness of screening low magnesium calcite (LMC) from the overall data set. Further discussion of the selection process that determined whether individual $\delta^{18}O$ and $\delta^{13}C$ stable isotope pairs were considered as being diagenetically least altered and therefore suitable for palaeotemperature determination.
- Chapter 4 provides an introduction and overview of the methodologies used for the analysis of carbon and oxygen stable isotopes from screened aragonitic molluscan shell material. The stable isotope processing carried out at the stable isotope laboratory in the School of Earth and Ocean Sciences, University of Liverpool is described. Plus a further discussion of the significance of the stable isotope and palaeoclimate data generated. Finally the chapter discusses a

comparison of the data from this study with that from recent studies from the Latest Maastrichtian of Seymour Island (Tobin *et al*., 2012; Tobin and Ward, 2015; Little *et al*., 2015; Petersen *et al*., 2016) plus a comparison with published palaeotemperature data from the Boreal realm.

- Chapter 5 describes previous work carried out on marine strontium isotope stratigraphy (SIS) in the James Ross Basin, the adopted methodology, selection and preparation of samples for $^{87}Sr/^{86}Sr$ analysis. Followed by a discussion of the data generated and the nature of the correlation with other published strontium isotope stratigraphy for the Latest Maastrichtian.
- Chapter 6 discusses the findings presented in this thesis document and presents the primary conclusions drawn from this study. Also described is a plan for the writing up of the research and the scope for future research work associated with the project.
- Appendix A describes the selection and identification methodologies for individual specimens
- Appendix B introduces the diagenetic screening adopted to ensure that sample powders submitted for stable isotope analysis were not subject to any substantial diagenetic signature. The SEM imaging of shell microstructure is described and the final digenetic screening data are presented.
- Appendix C describes the XRD data
- Appendix D lists the trace element geochemical data.
- Appendix E lists the stable isotope data
- Appendix F lists the strontium isotope data
- Appendix G lists the palaeontology data
- Appendix H lists the primary analysis data, representing a sub-set of all data held in the main Excel database.

1.5.2 Research Publications

Since the project data set conveniently splits into a number of discrete areas actual results will be published as a series of manuscripts for publication. Topics to be covered include:

1. An overall discussion of the oxygen and carbon stable isotope data and interpreted palaeotemperatures.
2. A discussion of the wide variability seen in the oxygen and carbon stable isotope data at individual stratigraphic levels in comparison with the overall variability seen for the full succession.

3. A discussion of the preservation of molluscan aragonite nacre from Seymour Island.
4. A discussion of the $^{87}Sr/^{86}Sr$ data and how well they correlate with the published global marine Strontium Isotope Stratigraphy curve.

An oral presentation of preliminary findings titled '**Late Maastrichtian stable isotope data, Seymour Island, Antarctica'** was presented at the 8th International Symposium on the Cretaceous System (ISCS) at the University of Plymouth in September 2009. A further poster presentation titled '**Latest Maastrichtian - Earliest Danian stable isotope data, Seymour Island, Antarctica'** describing the stable isotope data from this research was presented at the 11th International Symposium on Antarctic Earth Sciences, University of Edinburgh in July 2011.

2 Late Cretaceous climate of the James Ross Basin

2.1 Introduction

This chapter introduces the nature of the late Cretaceous climate together with a number of related topics that include information about climate modelling and how well the output from models agrees with the geological record. Also discussed are the various palaeoproxies that can be employed to assess the nature of a palaeoclimate using palaeobotany, palynology, glacioeustacy and global sea level as well as the distribution of temperature dependent sediments. The nature and cyclicity of changes to global sea level are discussed with evidence of orbital forcing (Milankovitch) and how some of the other proxies correlate with the presence and influence of changes to insolation. Other geochemical palaeoproxies including trace element and stable isotope data will be discussed in Chapters 3 and 4 respectively.

A key question for the late Maastrichtian climate is whether evidence exists for the development of icesheets and their areal extent on Antarctica together with supporting evidence from other proxies. A number of authors have discussed aspects of the Cretaceous climate (for example Li and Keller, 1999; Craggs, 2005; Hay, 2008; Keller, 2008; Thorn *et al*., 2008; Zakharov *et al*., 2011; Hay and Floegel, 2012; Dennis *et al*., 2013). Study of past climate change provides a valuable tool towards an understanding of current climate change (Hay, 2011). The importance of polar regions for climate sensitivity are well documented (Goody, 1980; Manabe and Stouffer, 1980; Florindo *et al*., 2003). The interpretation of marine palaeotemperatures from the Latest Maastrichtian of the James Ross Basin may be relevant to the modelling of likely future climate change during the remainder of the 21st and subsequent centuries. A slight modification to and an expansion of the ‘Principle of Uniformitarianism’ yields the statement that: *‘The present is the key to the past and the past may indeed be a potential key to the future’*.

The Cretaceous has been described as having experienced a ‘greenhouse’ climate (Hallam, 1985). Whilst this may be true in general evidence exists that the Cretaceous climate regime was not always equable and stable with higher mean temperatures than at present and characterised by a low polar – equatorial latitudinal temperature gradient, (Pirrie and Marshall, 1990; Huber *et al*., 1995; Hay, 2011). A latitudinal temperature range of 14°C was quoted by Huber *et al*. (1995) for the Cretaceous, in contrast to the present day range of 30°C (Veizer and Prokoph, 2015). The possibility that polar ice sheets existed during the Cretaceous was also dismissed as being unlikely (Hallam, 1985). Later research (Alley and Frakes, 2003; Miller *et al*., 2005a;

Spicer and Herman, 2010; Bowman *et al*., 2013; Petersen *et al*., 2016) suggested that polar ice sheets might have existed during the Cretaceous and that if the James Ross Basin developed ice sheets during the late Cretaceous then a reassessment may be required regarding the overall nature of the Cretaceous climate and the extant climate forcing mechanisms. Assumptions concerning the geochemistry, in particular the nature of the $\delta^{18}O_{water}$ value for the Cretaceous seawater, might also require amendment (Price *et al*. 2000; Petersen *et al*., 2016) along with subsequent re-interpretation of palaeotemperatures.

More recent techniques including 'Clumped Isotope', TEX_{86} and U-37(K') offer the opportunity to derive sea water temperatures independent of the $\delta^{18}O_{water}$ composition of the ocean waters. With values for the temperature and the $\delta^{18}O_{Carbonate}$ composition of shell material these techniques also enable the calculation of the original $\delta^{18}O_{water}$ composition of the ocean.

2.2 Climate proxies

Palaeoenvironmental proxies provide a potential window into the palaeoclimatic conditions that existed in the past. This section will discuss the nature and usefulness of a number of proxies, the majority of which require calcite or aragonite but there are a number of proxies now in common use that work on either a molecular basis or on the analysis of fossil wood and leaf characteristics. Evidence for past climates comes from various geological proxies, amongst which the are the distribution of certain distinctive temperature sensitive sedimentary rock types, for example tillites, coals, evaporites, bauxites and laterites (Craggs *et al*., 2012) and the fossils of climate sensitive flora and fauna. Geochemical data also enable an estimation of specific aspects, such as temperature and seasonal patterns of rainfall and weathering. Such evidence shows that the Earth commenced a broadly warming trend, with notable oscillations, as with global sea-level through the Mesozoic. At no time during that era did polar glaciers ever develop on a large scale. Mean global temperatures appear to have reached a maximum in the earlier part of Late Cretaceous times, when it is probable that polar ice was entirely absent at sea level although there was some cooling towards the end of the Cretaceous (Skelton 2003).

Since there is evidence for the presence of ice sheets, however limited in areal extent, during the Cretaceous (see Miller *et al*., 1999, 2003, 2005a,b; Haq, 2014) it follows that a re-evaluation of the $\delta^{18}O_{water}$ of the Cretaceous ocean, influenced in part by the presence or absence of polar ice, must be made. Seawater on Earth, during periods that were free from major icecaps would have been isotopically lighter than at present and a $\delta^{18}O_{water}$ of -1.2‰, (equivalent to -1.0‰, SMOW), has previously been suggested as

appropriate. If small icecaps were present during the early Cretaceous the $\delta^{18}O_{water}$ of a Cretaceous ocean may have been slightly heavier (Price *et al*., 2000). Note that the value of $\delta^{18}O_{water}$ may also reflect more localised variation, for example due to fresh water runoff as proposed by Petersen *et al*. (2016).

Palaeotemperature evidence for the possible presence of sea ice was reported by Petersen *et al*. (2016) where temperatures derived from clumped isotope analyses indicated low benthic temperatures of ~3 - 5°C and in some cases sub-zero temperatures. Bowman *et al*. (2013) proposed the development of winter sea ice determined from the palynomorph record of Seymour Island, Antarctica. The authors reported the dominance of the dinoflagellate cyst *Impletosphaeridium clavus* caused by the presence of cysts from dinoflagellate blooms associated with the decay of winter sea ice. They also reported that peaks and lows of *Impletosphaeridium clavus* abundance marked cold temporary stratification of polar waters, interposed with warmer periods when the ocean was well-mixed. Prior to the K-Pg boundary *Impletosphaeridium clavus* decreased dramatically in abundance possibly due to the onset of warming associated with Deccan Traps volcanism. Tobin *et al*. (2012) and Petersen *et al*. (2016) also proposed that there was evidence in the stable isotope record that suggested the presence of warming trends immediately prior to the K-Pg that were linked to warming associated with the onset of the Deccan Traps volcanism. Petersen *et al*. (2016) also stated that the temperature data indicated the presence of 2 separate phases of warming prior to the K-Pg. Kemp *et al*. (2014) reported on MATs from the Late Maastrichtian – Paleocene of Seymour Island, the data demonstrate that MATs from the López de Bertodano and Sobral Formations averaged 12.4 ± 5 °C based on MBT′/CBT analyses on terrigenous material. The authors also commented that paleotemperature estimates for this method may be biased toward summer month temperatures.

2.2.1 Palaeobotany

Palaeobotanical and palynological evidence indicated that deciduous trees were present at higher latitudes than at the present day (Francis, 1986; Frakes and Francis, 1990; Francis and Poole, 2002; Francis *et al*., 2006, 2008; Thorn *et al*., 2008, 2009; Bowman *et al*., 2012, 2013). Work based on the analysis of tree growth rings clearly showed that climate conditions during the Campanian-Maastrichtian included periods of either intense aridity or freezing. Palaeobotany has furnished substantial evidence that glacial or at least freezing conditions existed at the poles during the late Cretaceous (Bowman *et al*., 2013).

The presence of plant remnants in southern high palaeolatitude environments gave rise to the '*Antarctic climate paradox*' in that despite the present day continent having a freezing climate and a substantial ice cap, some of the most common fossils preserved in its rock record are those of ancient plants (Francis *et al*., 2008). These plant fossils indicate a world with globally warm (Hallam, 1985; Francis *et al*., 2008; Hay, 2011) and generally ice-free climates, with dense vegetation flourishing close to the poles (see Francis, 1986; Frakes and Francis, 1990; Francis and Poole, 2002; Francis *et al*., 2006, 2008; Thorn *et al*., 2008, 2009; Bowman *et al*., 2012, 2013). However, evidence from research into sea level perturbations indicates that the globally warm climate in the southern high palaeolatitudes was punctuated by the development of significant ice sheets (see Miller *et al*., 1999, 2003, 2005a,b). What mechanisms were driving these cool spells during the Late Cretaceous greenhouse climate?

Palaeobotany helps to furnish data about terrestrial climates in high latitudes, the regions on Earth most sensitive to climate change (Goody, 1980; Manabe and Stouffer, 1980; Florindo *et al*., 2003). Although plants of Permian and Triassic age provide a signal of terrestrial climates for the Transantarctic region (Taylor and Taylor, 1990; Francis *et al*., 2008), it was during the Cretaceous that the Antarctic continent reached a position over the South Pole (Lawver *et al*., 1992; Torsvik *et al*., 2008). With intermittent ice cover Cretaceous vegetation flourished at high latitudes, the nature of the terrestrial Antarctic climate during the Cretaceous greenhouse has been illustrated by the substantial record of plant remains including wood, fossil leaves, flowers and pollen (Francis *et al*., 2008). Different patterns of growth rings in fossil wood from the Eromanga Basin, Southern Australia were interpreted as indicating two populations reflecting different climate regimes, the growth rings were well defined in both indicating distinct seasonal climate conditions (Marshall *et al*., 1993). But the ring widths and therefore growth rates were markedly different, these wood data were interpreted as representing seasonal climates with the two populations representing growth in cool upland and warmer lowland climates respectively (Marshall *et al*., 1993).

Spicer and Parrish (1990a,b) described analyses of plant community structure, vegetational and leaf physiognomy and growth rings and vascular systems in wood from the North Slope, Alaska. They showed that qualitative and quantitative data could be combined to define non-marine palaeoclimate parameters with better resolution than those available from sedimentological methods (see Herman and Spicer, 1997; Kennedy *et al*., 2002; Craggs, 2005; Spicer *et al*., 2009; Spicer and Herman, 2010; Tomsich *et al*., 2010).

Application of these techniques to Cretaceous floras from high palaeolatitudes (75º - 85º N) imply a polar light regime similar to that of the present day, plant data suggested

Mean Annual air Temperatures (MATS) ranging from 13ºC to 5ºC in the Coniacian and Maastrichtian (see Spicer and Parrish, 1990a,b; Herman and Spicer, 1997; Craggs, 2005; Spicer and Herman, 2010; Tomsich *et al*., 2010; Craggs *et al*., 2012). Evapotranspirational stresses at sea level were low and precipitation was in most part uniform throughout the growing season in the Cenomanian, with possible seasonal drying occurring by the Maastrichtian. Maastrichtian winter freezing was likely, but periglacial conditions did not exist at sea level (see Spicer and Parrish, 1990a,b). Permanent ice was likely above 1000 m at 85º N in the Maastrichtian. These near-polar data provided critical constraints on global models of Late Cretaceous climates (Spicer and Parrish, 1990a,b). Studies of polar vegetation in Alaska whilst not directly supporting evidence for the development of ice sheets indicated that seasonal climate conditions exhibited MATs well below freezing (see Spicer and Parrish, 1990a,b; Herman and Spicer, 1997; Craggs, 2005; Spicer and Herman, 2010; Tomsich *et al*., 2010). Applying an adiabatic lapse rate of ~6ºC km^{-1} (Strahler and Archibold, 2011) to Antarctica indicated that localised ice sheets may have been present during the Late Maastrichtian, the presence of which were also indicated by evidence of sea level changes (Miller *et al*., 1999, 2003, 2005a; Haq, 2014), proposed development of winter sea ice derived from analysis of palynological data (Bowman *et al*., 2013) and clumped stable isotope data based upon the analysis of of bivalve shell material (Petersen *et al*., 2016).

The presence of montane ice has important consequences for climate modelling. Significant year-round montane ice and seasonal ice at sea level would greatly raise the albedo at these critical high latitudes (Spicer and Parrish, 1990a,b). However, analysis of fossil wood (Francis, 1986; Frakes and Francis, 1990; Francis and Poole, 2002; Francis *et al*., 2006, 2008) and palynology (Thorn *et al*., 2007, 2008; Bowman *et al*., 2012, 2013) from Antarctica indicated that the climate was sufficiently warm for trees to flourish at palaeolatitudes of 59° - 62°S.

2.2.2 Stable isotopes as palaeoclimate proxies

For an overall introduction to the rationale behind the investigation of palaeoclimate proxies and palaeothermometry then perhaps no better description exists than that as stated by Urey (1947) - '*It would be interesting indeed to know not only the mean temperature but also the variations of temperature on an ancient beach… However, too much optimism is not justified, for all the thermometers may be destroyed*'.

Analysis of carbon and oxygen stable isotopes from biogenic carbonate sources has generally been carried out using calcite as the source shell material. However, the paucity of calcite bearing macrofossils from the BAS collection together with a strong

correlation between calcite shell material and excessive diagenetic trace element levels (see Chapter 3 and Appendix D) indicated that there were good reasons in this study for the rejection of calcite for stable isotope analysis. The good preservation of the aragonitic macrofossil specimens collected from Seymour Island, Antarctica have made it possible to carry out a high resolution analysis of carbon and oxygen stable isotopes from aragonite alone. Benefits of this approach included a more straightforward sample selection and screening process and more direct diagenetic checks of the material selected, for a discussion of the diagenetic screening see Chapter 3 and Appendix B for details of the actual diagenetic methodology and analysis together with the data recorded.

Pirrie *et al*. (1993) and Ditchfield *et al*. (1994) presented results of oxygen isotope studies of diagenetically unaltered macrofossils from James Ross Island, Antarctica. Their data suggested that the Late Cretaceous climate was cooler and more variable than previously thought, also that during both the Early and Late Cretaceous polar glaciation may have occurred during a period of 'greenhouse' climate. For example, well constrained stable isotope data from the Albian of Australia suggested relatively cool palaeotemperatures at mid to high palaeolatitudes and supported published Cretaceous marine latitudinal temperature gradients of ~2ºC per 10º of latitude (Pirrie and Marshall 1990). The data provided the first direct evidence using reliable oxygen isotope data for cool climates in the Albian of Australia (Pirrie *et al*., 1993; Ditchfield *et al*., 1994). Li and Keller (1999) quoted two separate latitudinal temperature ranges, determined by whether the temperatures related to warm or cold intervals, with each range divided in two depending upon latitudinal position:

Warm intervals	0.01 – 0.06ºC/1º latitude (low/middle)
	0.15 – 0.29ºC/1º latitude (middle/high)
Cool intervals	0.03ºC/1º latitude (low/middle)
	0.17 – 0.18ºC/1º latitude (middle/high)

Jenkyns *et al*. (2004) reported a latitudinal gradient of ~15ºC for low to high latitudes during the Late Maastrichtian from the Arctic.

A primary requirement for evaluation of palaeotemperature using oxygen isotope ratios is that the biogenic carbonate was precipitated in isotopic equilibrium (Weiner and Dove 2003) with respect to the seawater (Tripati *et al*., 2010). A number of authors have published research which indicated that precipitation of biogenic carbonates in isotopic equilibrium may not always be the norm and that in certain cases temperature proxies may show evidence for biological isotopic fractionation (‘vital effects’) (Shackleton and Opdyke, 1973; Marshall *et al*., 1996; Bemis *et al*., 1998; Tripati *et al*., 2010; Lécuyer *et al*., 2012). The data described in Marshall *et al*. (1996) are particularly

relevant since they deal with an extant fauna from Antarctica. The precipitation of the biogenic carbonate should, ideally, have taken place all year round and over a number of years. If these conditions were met then it was likely that isotopic variations did indeed reflect long-term temperature variability or variability in the isotopic concentration of seawater. However, consider the contrary requirements for ontogenetic sampling, where the intention is to measure the isotopic signals that reflect intra-annual variability that were either seasonal or growth related (see Lukeneder *et al.*, 2010).

The estimation of seawater $\delta^{18}O_{water}$ values for the Cretaceous can be problematic because of uncertainties relating to the presence or absence of polar ice and the possibility of an equator-to-pole change in the isotopic composition of seawater. Superimposed upon this potential variability is the possibility of local isotopically light precipitation or freshwater runoff entering the marine system, which may account for some of the fluctuations of isotopic values (Price *et al.*, 2000; Petersen *et al.*, 2016). A description of proxy techniques that offer an opportunity to dispense with this requirement are discussed in subsequent sections that describe the use of 'Clumped' Stable Isotopes and the TEX_{86} proxy.

2.2.3 Aragonite palaeothermometry

Palaeotemperatures may be calculated using the following aragonite palaeothermometry equation (Grossman and Ku, 1986) modified by Lukeneder *et al.* (2010).

$$T°(C) = 20.6 - 4.34\ (\delta^{18}O_{aragonite} - [\delta^{18}O_{water} - 0.2]), \qquad \text{Eqn (1)}$$

Where the $\delta^{18}O_{aragonite}$ term represents the oxygen isotopic composition of aragonite with respect to the international VPDB standard and the $\delta^{18}O_{water}$ term represents the oxygen isotopic composition of the seawater from which the aragonite was precipitated with respect to the Surface Mean Ocean Water (SMOW) standard. In order to calculate palaeotemperatures a $\delta^{18}O_{water}$ value for the Cretaceous ocean must be quantified with the assigned value influenced by the presence or absence of polar ice. Price *et al.* (2000) suggested the following values for $\delta^{18}O_{water}$:

- $\delta^{18}O_{water}$ = -1.2‰, (equivalent to -1.0‰ SMOW) - No major icecaps and seawater that was isotopically lighter than at present
- $\delta^{18}O_{water}$ = -0.9‰, (equivalent to -0.7‰ SMOW) - Small polar ice sheets were present at altitude and the seawater may have been slightly heavier.
- $\delta^{18}O_{water}$ = -1.5‰, (equivalent to -1.3‰ SMOW) - Freshwater run off.

The ability to calculate a seawater temperature without requiring a value for the $\delta^{18}O_{water}$ also offers the possibility of directly deriving a value for $\delta^{18}O_{water}$ through a

rearrangement of terms in Eqn 1. Thus for a measured 'Clumped Isotope' temperature and corresponding $\delta^{18}O_{aragonite}$ value the derivation of $\delta^{18}O_{water}$ may be calculated from Equation 2.

$$\delta^{18}O_{water} = 1 / 4.34 (T°_{\text{'Clumped Isotope'}} - 20.6) + \delta^{18}O_{aragonite} + 0.2 \qquad \text{Eqn (2)}$$

Petersen *et al*. (2016) discussed the selection of a suitable Late Maastrichtian value for $\delta^{18}O_{water}$ for Seymour Island, Antarctica; the authors suggested that the choice of any single fixed value for $\delta^{18}O_{water}$ might be erroneous especially given the wide variability in their $\delta^{18}O$ data. They suggested that a $\delta^{18}O_{water}$ value of -1.2‰ was restrictive since it failed to represent the true nature of the modified $\delta^{18}O_{water}$ isotopic signature that resulted from surface run off, see Table E-6 for the $\delta^{18}O_{water}$ values derived from their clumped isotope analyses. The adoption of a single fixed $\delta^{18}O_{water}$ value had the effect of significantly reducing the overall range of temperatures at any particular stratigraphic horizon (Petersen *et al*., 2016).

In the absence of temperature data derived from the analysis of either clumped isotope or suitable molecular proxies the value of $\delta^{18}O_{water}$ used will always be an estimate. Thus for a new marine, fluvial or lacustrine temperature proxy a key goal was to dispense with the requirement for a $\delta^{18}O_{water}$ term in the temperature calculation.

2.2.4 Clumped Stable Isotopes

Clumped isotope geochemistry (Ghosh *et al*., 2006; Schauble *et al*., 2006 and Eiler 2007) is concerned with the state of ordering of rare isotopes in natural materials. The technique examined the extent to which rare isotopes (e.g. D, ^{13}C, ^{15}N, ^{18}O) bond with or near each other rather than with the sea of light isotopes in which they swim (Schauble *et al*., 2006). Abundances of isotopic 'clumps' in natural materials are influenced by a wide variety of factors. In most cases, with concentrations that approached (within ca. 1%, relative) the amount expected for a random distribution of isotopes. Deviations from this stochastic distribution resulted from factors that included enhanced thermodynamic stability of heavy-isotope 'clumps' and slower kinetics of reactions requiring the breakage of bonds between heavy isotopes. In carbonates rare heavy isotopes (^{13}C and ^{18}O) occurred in a pool of abundant light isotopes, the proportion of ^{13}C and ^{18}O that were bound to each other within the carbonate mineral lattice was predicted to be temperature dependent based upon principles of statistical thermodynamics (Schauble *et al*., 2006). The equilibrium constant for the following reaction formed the theoretical basis for the carbonate 'clumped isotope' thermometer (Schauble *et al*., 2006):

$$\mathbf{Ca^{12}C^{18}O^{16}O_2 + Ca^{13}C^{16}O_3 \longleftrightarrow Ca^{13}C^{18}O^{16}O_2 + Ca^{12}C^{16}O_3,} \qquad \textbf{(Reaction 1)}$$

The temperature-dependent 'clumping' of heavy isotopes into bonds with each other is driven by subtle vibrational energy differences between isotopologues. Although clumped isotope geochemistry is a relatively young field, it appears that proportions of $^{13}C–^{18}O$ bonds in carbonate minerals are sensitive to their growth temperatures, independent of bulk isotopic composition. Thus, 'clumped isotope' analysis of ancient carbonates can be used as a quantitative palaeothermometer that requires no assumptions about the $\delta^{18}O$ of waters from which carbonates were precipitated. Current analytical methods limit precision of this palaeothermometer to ca. ± 2℃, 1σ (Ghosh *et al*., 2006). This technique has been used to reconstruct marine temperatures across the Phanerozoic, terrestrial ground temperatures across the Cenozoic, thermal histories of aqueously altered meteorites, diagenesis of carbonatites and the development of new 'clumped' isotope techniques, for example the analysis of siderite as a proxy for humid continental environments amongst many other applications (see [**Methodology**] Eiler 2006, 2007; Ghosh *et al*., 2007; Affek *et al*., 2008; Eiler *et al*., 2008, 2010; Bernasconi *et al*., 2011; Eiler 2011; Grauel *et al*., 2013; Eiler *et al*., 2014; Fernandez *et al*., 2014; [**Diagenesis**] Dennis and Schrag 2010; [**Geochemistry**] Ferry *et al*., 2011; [**Palaeoclimate**] Came *et al*., 2007; Snell *et al*., 2007; Affek *et al*., 2008; Huntington *et al*., 2008, 2010; Tripati *et al*., 2010; Csank *et al*., 2011; Dennis *et al*., 2013; Grauel *et al*., 2013; Henkes *et al*., 2013; Fernandez *et al*., 2014; Gothmann *et al*., 2015; Petersen *et al*., 2016; [**Mass extinction**] Brand *et al*., 2012; Petersen *et al*., 2016).

The data presented by Petersen *et al*. (2016) were particularly relevant since they were derived from the analysis of Maastrichtian bivalve specimens from Seymour Island. Petersen *et al*. (2016) also reported on calculated values for $\delta^{18}O_{water}$ (see Table E-6) for their measured stratigraphy that terminated at ~600 m (BAS D5 stratigraphy). Unfortunately this was approximately 300 m above the position of the lowest specimen selected for stable isotope analysis in this study. They concluded that the wide variability in their data was attributable to alteration of the $\delta^{18}O_{water}$ by freshwater run-off with temperatures reflecting changes to the $\delta^{18}O$ ratio of the seawater.

2.2.5 Molecular Proxies

A number of current molecular palaeotemperature proxies do not require the oxygen isotope ratio of the seawater and provide a direct determination of the water temperature.The fundamentals of these methods are the establishment of molecular parameters, compound abundances and carbon, hydrogen, nitrogen and oxygen isotopic contents derived by the analysis of sediment extracts (Schouten *et al*., 2007; Eglinton and Eglinton, 2008). These parameters may then be interpreted as proxy

measures that in turn define the climate conditions operating at the time (Schouten *et al*., 2007; Eglinton and Eglinton, 2008). Environmentally persistent organic molecules derived from either plant remains that provide a measure of terrestrial climatic conditions, e.g. long chain (circa C_{30}) hydrocarbons, alcohols and acids remnants of leaf wax compounds, or marine proxies based upon membrane lipids derived from marine plankton, in particular *Crenarchaeota* (Schouten *et al*., 2007; Eglinton and Eglinton, 2008) that are measures of sea surface temperatures (SST). Marine proxies include UK^{37}, based on the relative abundances of C_{37} alkenones photosynthesised by unicellular algae, members of the Haptophyta and TEX_{86}, based on C_{86} glycerol tetraethers (GDGTs) synthesised by some of the archaeal microbiota, the Crenarchaeota and the methylation index of branched tetraethers/cyclization ratio of branched tetraethers (MBT/CBT) (Hopmans *et al*., 2004; Schouten *et al*., 2007; Eglinton and Eglinton, 2008; Kemp *et al*., 2014). The TEX_{86} parameter has also been shown to be insensitive to salinity or depositional redox conditions (Wuchter *et al*., 2004).

The application of terrestrial (lacustrine, ice cores and terriginous materials) and marine molecular records have proven to be of value as palaeoclimate proxies (Jenkyns *et al*., 2004; Herfort *et al*., 2006; Schouten *et al*., 2007; Kim *et al*., 2008; Mutterlose *et al*., 2010). Although not directly relevant to this study, one major advantage of these molecular proxies is that they are not dependent upon the presence of carbonate fossil material and thus offer an opportunity to provide palaeotemperatures from anoxic mud rich sediments (Jenkyns *et al*., 2004; Schouten *et al*., 2007). The relationship between the TEX_{86} value and temperature (Wuchter *et al*., 2005) is described by the following equation:

$$\mathbf{TEX_{86} = 0.0015 * T + 0.28}$$

Where $T_{(°C)}$ = annual mean Sea Surface Temperature (SST).

Jenkyns *et al*. (2004) reported on the close correlation between a low to high latitude range of ~15°C for the late Maastrichtian from the Arctic, as measured by TEX_{86}, with a similar figure of ~14°C between low and high latitude from the Southern Hemisphere based on $\delta^{18}O$ data derived from planktonic foraminifera (Huber *et al*., 1995). Kemp *et al*. (2014) also report on the record of terrestrial palaeotemperatures from the Late Maastrichtian to Early Palaeogene of Seymour Island derived from sediment samples using the MBT/CBT proxy.

2.2.6 Glacioeustasy

Palaeokarst features from Jamaican Upper Cretaceous limestones in the Guinea Corn Fm. were reported by Miller and Mitchell, (2003), they proposed that the

development of these features represented uplift as opposed to progradation of the shoreline. Two such events were proposed, suggesting that the fall and subsequent rise in sea level represented the waxing and waning of small, but significant, ice caps during the globally warm climate in the southern high palaeolatitudes (see Miller *et al*., 1999, 2003, 2005a). It was proposed that ice sheets in Antarctica during the Late Cretaceous - Eocene reached a maximum of 8-12 x 10^6 km^3, a glacioeustatic equivalent of 20-30 m (Miller *et al*., 2005b; Miller, 2009). Miller *et al*. (2005b) also suggested that ice sheets did not reach the coast and that coastal Antarctica deep waters were relatively warm even whilst there were significant glacioeustatic changes. The authors suggested that ice sheets existed due to peak Milankovitch insolation and were only present for short intervals of time with Antarctica ice free during the Late Cretaceous to middle Eocene. Evidence for the development of lowstands was reported by Haq (2014), 4 events occurred during the Late Maastrichtian and 1 event occurred during the Early Danian. Further evidence for seasonal ice sheets was reported by Bowman *et al*. (2013) based upon palynological studies and by the determination of low to sub-zero benthic seawater temperatures (Petersen *et al*., 2016). There is a need to reconsider whether polar ice sheets did exist on Antarctica during times of a warm climate (Miller *et al*., 2005b).

2.3 Modelling Palaeoclimates

Numerical models that simulate the elements of modern and ancient climates are employed at several institutions worldwide. Each model is different in design and function and thus the results of the same experiment will differ from model to model. The principal tools for modelling palaeoclimate change are climate models, of which the most sophisticated versions are General Circulation Models (GCM) based on the HadCM3 GCM developed at the Hadley Centre for Climate Prediction and Research at the UK Meteorological Office, see Gordon *et al*. (2000), Randall *et al*. (2007) and Hunter *et al*. (2008) for a description of the models, required initial constraints and any design limitations.

2.3.1 General circulation model - HadCM3L

HadCM3L is a version of the HadCM3 model modified to incorporate a lower resolution ocean descriptions of the models can be found in Gordon *et al*. (2000) and Hunter *et al*. (2008), and are summarised below. HadCM3 is a coupled atmosphere–ocean general circulation model (AOGCM) comprising the HadAM3 atmospheric model linked to a fully dynamic ocean model and a sea-ice model. The horizontal resolution of the atmosphere is 2.5° latitude×3.75° longitude, equivalent to a grid spacing of 278 km north–south and 417 km east–west at the equator, reducing to 278 km×295 km at 45°

of latitude. It has 19 vertical layers and a 30 minute time step. A detailed description of HadAM3 can be found in Pope *et al*. (2000). Within the oceanic component, ocean bathymetry may be prescribed, but sea surface temperatures (SSTs) and oceanic heat transport are predicted by the model. In its standard version, the ocean has a horizontal resolution of 1.25°×1.25°. However, to meet the demands of spinning up a deep ocean in the Maastrichtian, a resolution of 2.5°×3.75°, with 20 vertical layers was used. This version of the model is called HadCM3L and it allows longer integrations. A full description of HadCM3 underlining its improvements over earlier versions is given by Gordon *et al*. (2000).

To model the ocean requires knowledge of the heat and fresh water flux at the surface as well as the surface wind stress. For the Cretaceous, these can only be specified from knowledge of the atmosphere based on climate models. An atmospheric model requires the sea surface temperature and thus the only way to completely model the oceans is to couple an atmospheric GCM to an oceanic GCM. An alternative approach is to use a highly simplified ocean model and to specify the horizontal heat transport within the ocean, so called ‘slab’ models. As an alternative sea surface temperatures (SST) may be specified, based on oxygen isotope estimates, since the atmospheric model only requires the sea surface temperature. If the sea surface temperatures are reasonable, then the amount of net incoming solar radiation should balance the net outgoing long wave radiation. Climate proxy data can be used to simulate the Cretaceous climate but boundary conditions are needed for the models, these are either external processes, or those processes, which act on very long time scales.

The value of GCM modelling depends on quantitative data obtained from the geological record in order to either establish realistic boundary conditions or provide tests equal in resolution to the model results. Results from palaeoclimate modelling indicate that the Cretaceous may have experienced glaciation in the southern hemisphere (Sellwood and Valdes, 2006). Spicer and Parrish (1990a) suggest that an increase in grid resolution plus the inclusion of better defined vegetation and ice related albedo together with better constrained temperature parameters would yield more realistic model results. A comprehensive overview of climate modelling is provided by Randall *et al*. (2007). No doubt the quality and accuracy of GCM simulations will increase as more powerful computing facilities become available (e.g. massive parallel architecture systems) and with the growth of model complexity.

The role of palaeogeography (palaeotopography and palaeobathymetry) in defining palaeodrainage conditions for models of surface processes is described by Marwick and Valdes (2004) with reference to the development of a Maastrichtian digital

elevation model (DEM) (see Figure 2-1). Definition of palaeodrainage is a necessary requirement for the HadCM3 climate model.

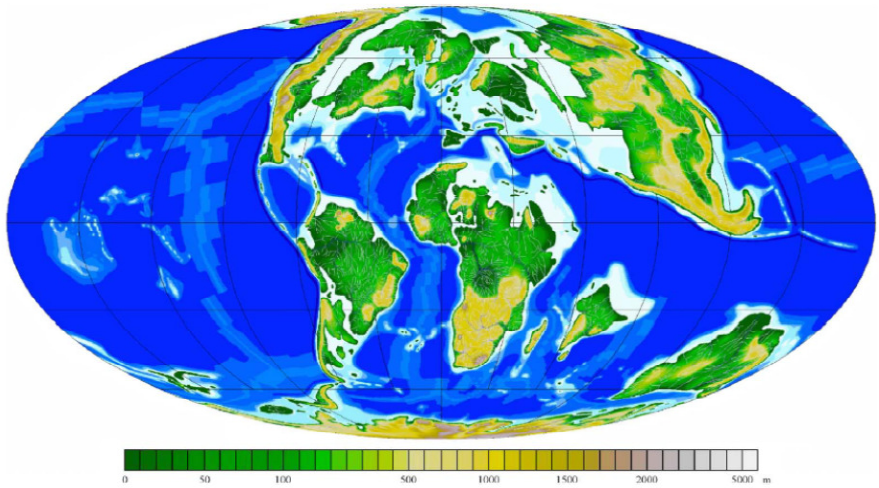

Figure 2-1. Maastrichtian palaeo digital elevation model (DEM). Mollweide projection. After Marwick and Valdes (2004)

2.4 The Austral Cretaceous world

During the Mid-Late Cretaceous the layout and general continental outlines were dissimilar to present day landmasses but by the Early Palaeogene certain continental landmasses had started to form recognisable outlines e.g. Africa, Antarctica, Australia and South America, see Figure 2-2 for a comparison of landmass distribution between the Mid Cretaceous and the Early Palaeogene.

At mid-higher southern palaeolatitudes Gondwana began to break up in the Early Cretaceous with the opening of the South Atlantic suture between South America and Southern Africa. Later in the period, the nascent ocean joined the Central Atlantic, whilst to the north the North Atlantic also began to open up between North America and Western Europe. Hence by the start of the Late Cretaceous, there existed a continuous, although locally constricted, Atlantic Ocean. Likewise, the drift of India and Madagascar from an original position nestled between Africa and Antarctica gave rise to the Indian Ocean during the Cretaceous. In the Southern Hemisphere large parts of southern Gondwana were situated at or near the pole whilst in the Arctic there was a small almost totally enclosed Arctic Ocean. The connections between this northern polar sea and the rest of the world's oceans were shallow and narrow. From time to time these connections widened and shrank, as the sea-level rose and fell, but at all times deep-water connections were absent. This had profound implications for ocean circulation and the poleward transport of heat and global climate (Skelton, 2003).

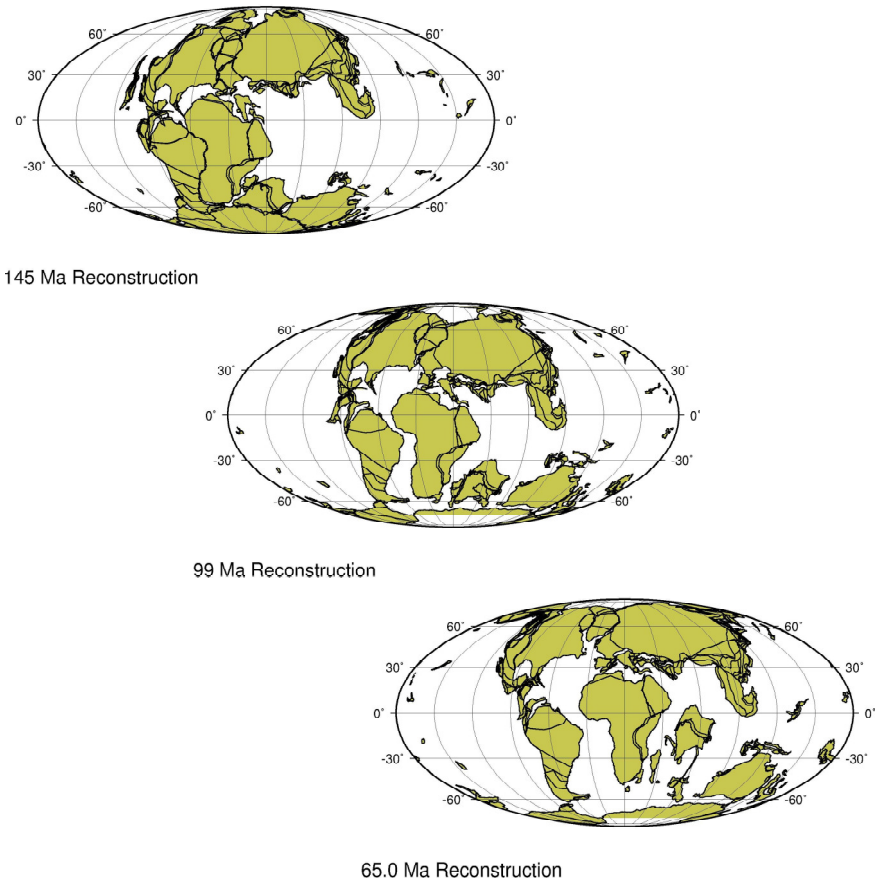

Figure 2-2. Early to Late Cretaceous landmass distribution. After ODSN Plate Tectonic Reconstruction Service (2012)

2.4.1 Global Sea-Level

Sea-level underwent both long and short term oscillations, according to changes in the capacity of and hence displacement of water from, the ocean basins and as a result of glacioeustatic changes (see Miller *et al*., 1999, 2003, 2005b; Kominz *et al*., 2008; Miller, 2009; Miller *et al*., 2011; Haq, 2014). The main variable controlling basin capacity was the total volume of mid-ocean ridges. As oceans opened and closed, the cumulative length of mid-ocean ridges increased or decreased. Moreover, given the constant proportional rate of subsidence of cooling oceanic crust as it moves away from a ridge, changes in the rate of seafloor spreading affected the relative widths of mid-ocean ridges, such that more rapid spreading created relatively wider profiles (Skelton, 2003).

Continental break-up thereafter gave birth to new oceans, each with their own mid-ocean ridge systems. These mid-ocean ridges cumulatively displaced more and more water, thus leading to higher sea levels. Despite several pronounced oscillations of global sea-level (probably largely related to changes in sea-floor spreading rates together with the sub/duction of the Palaeotethys ridge system), an overall long-term rise ensued during the Mesozoic, reaching a peak in the Late Cretaceous.

The Late Cretaceous eustatic maximum was associated with the expansion of seas across large areas of the continents (Skelton 2003), it has been well established that global sea levels throughout much of the Mesozoic were generally higher than at present (Haq, 2014). The apparent absence of major ice caps accounts for some of this eustatic rise (by comparison with the present), but absence of ice and the thermal expansion of water can only contribute around 100 m or so to the rise. In addition, high rates of sea floor spreading (on average 75% greater than at present) will have led, it is assumed, to the elevation of oceanic ridges and the displacement of ocean waters over what were, for most of the time interval, relatively subdued or subsident continental masses (Skelton *et al*., 2003; Sellwod *et al*., 2006). However, Haq (2014) also highlighted the presence of a number of Late Maastrichtian and Early Danian lowstands that exhibited characteristics of medium amplitude events with a 25 – 75 m reduction in sea level.

2.5 Maastrichtian climate of the James Ross Basin

Study of palaeoenvironmental proxies for the latest Cretaceous to the early Danian have described data derived from analysis of flora and fauna together with associated geochemical data. The use of data derived from flora has special importance since it offers an indication of the terrestrial environment, of particular importance in attempting to predict or model the likelihood of ice sheets. Palaeobotanical and palynological evidence from Antarctica indicated that deciduous trees were present at higher latitudes than at the present day (Francis, 1986; Frakes and Francis, 1990; Francis and Poole, 2002; Francis *et al*., 2006, 2008; Thorn *et al*., 2008, 2009; Bowman *et al*., 2012, 2013). Palaeobotany has furnished substantial evidence that glacial or at least freezing conditions existed at the poles during the late Cretaceous (Spicer *et al*., 2010; Bowman *et al*., 2013). Some of the most common fossils preserved in the Antarctic rock record are those of ancient plants (Francis *et al*., 2008). These plant fossils indicate a world with a globally warm (Francis *et al*., 2008; Hay, 2011) and generally ice-free climate, with dense vegetation flourishing close to the poles (see Francis, 1986; Frakes and Francis, 1990; Francis and Poole, 2002; Francis *et al*., 2006, 2008; Thorn *et al*., 2008, 2009; Bowman *et al*., 2012, 2013).

Evidence from research into sea level perturbations indicated that the globally warm climate in the Austral high palaeolatitudes was punctuated by the development of significant ice sheets (10×10^6 km^3, equivalent to a glacioeustatic rise and fall of 20-30 m) (Miller *et al*., 1999, 2005a; Haq, 2014) and other research utilising stable isotope studies, palynology, palaeobotany and climate modelling also indicated that whilst the

overall climate was warm there were distinct cooling trends present prior to the K-Pg boundary.

Climate patterns from a number of global locations indicated an Antarctic record of cooling during the Late Cretaceous and across the K-Pg boundary (Frakes *et al*., 1992; Dennis *et al*., 2013). Late Cretaceous warmth was also determined from analysis of floras from the Arctic. Mean Annual air Temperatures (MAT) from fossil angiosperm leaf assemblages from Cretaceous high latitude sites in Alaska (~75°N) (Spicer *et al*., 2010) provides MAT estimates for a cooling phase in the Maastrichtian. The palynology and floral record in the Gippsland Basin, SE Australia at palaeolatitude 60°S, a comparable position to that of the James Ross Basin, shows evidence of variable climate conditions during the Late Maastrichtian based upon variations in the taxa forming the tree canopy (Gallagher *et al*., 2008). Oxygen isotope data were sparse and relatively light during the latest Cretaceous suggesting Southern Hemisphere bottom water temperatures of around 8°C (Gallagher *et al*., 2008). Floral data from this interval confirm that cool to temperate conditions prevailed in the southern high latitudes, oxygen isotope data also show a similar variability to the floral data in this interval reflecting a temperature control (Gallagher *et al*., 2008). This wet/temperate to drier/temperate climate variability in the Late Cretaceous succession matches Milankovitch frequencies and correlates to global oxygen isotope events and sea level estimates (Gallagher *et al*., 2008). Data suggest that regional climate variability in Gippsland in the latest Cretaceous was controlled by Milankovitch forcing (Gallagher *et al*., 2008). Key elements of their estimate include a strong 400 ky eccentricity frequency that according to Laskar *et al*. (2004) was one of the most stable frequencies in the orbital solution for the last 100 Ma.

The 71.5 Ma oxygen isotope excursion and sea level minima of Miller *et al*. (2004) correlated with an interval of longer term insolation stability in the Laskar *et al*. (2004) orbital solution. A correlation exists for 67 to 66 Ma, suggesting an association between orbital insolation stability/minima and temperature or ice volume (Gallagher *et al*., 2008). The correlation of minima prediction with sequence boundaries on the New Jersey margin suggests that ephemeral ice sheets with 100 ky durations may have existed in Antarctica during times of orbital insolation minima in the Late Cretaceous or were caused by another unknown mechanism (Miller *et al*., 1999, 2005a). To account for apparent relatively high marine temperatures and an Antarctic temperate flora, Miller *et al*. (1999, 2005a) suggested that these small ice caps did not reach the sea and that these drier and wetter periods were related to the waxing and waning of ice sheets. The Late Cretaceous climate variability (Gallagher *et al*., 2008) fits within the global picture as the climate evolved from an equable Cretaceous greenhouse world to

the Late Cretaceous– Eocene greenhouse world in which significant, but ephemeral, ice sheets occurred (Miller *et al*., 2005a,b; Kominz *et al*., 2008; Miller, 2009; Miller *et al*., 2011; Haq, 2014). This pattern follows the oxygen isotope data indicating widespread global cooling near the end of the Cretaceous.

Ocean temperature records from outside the Antarctic Peninsula region also reflect Late Cretaceous warmth. Climate cooling across the K-Pg boundary and into the Early Palaeocene is also now apparent globally (e.g. Barrera and Savin, 1999). Although there are no records of glacial sediments of this age, the presence of ice sheets has been proposed to account for large and rapid sea level drops during the Maastrichtian in the USA (Miller *et al*., 2005b, 2011; Haq, 2014). Oxygen isotope records from foraminifera from Site 690 at 65°S indicated that deep water temperatures would have been about 5°C, with implications that ice sheets may have been present at higher latitudes (Miller *et al*., 2005b).

Climate data determined from palynology (Bowman *et al*., 2013), sediments and geochemical indicators (Tobin *et al*., 2012, Kemp *et al*., 2014; Tobin and Ward, 2015; Little *et al*., 2015; Petersen *et al*., 2016) for the Antarctic Peninsula region show a distinct pattern of warming and cooling through the Late Cretaceous into the early Palaeogene (Francis and Poole, 2002; Poole *et al*., 2005). The climate cooled during the Maastrichtian and cold wet and possibly seasonal environments prevailed with low MATs estimated from angiosperm wood (7°C). At higher latitudes, as a result of the adiabatic lapse rate MATs below freezing may have allowed the formation of ice sheets, especially at higher elevations (Francis and Poole, 2002; Poole *et al*., 2005).

2.5.1 Antarctic Maastrichtian climate modelling

Results from an Antarctic Maastrichtian simulation using an atmosphere model with prescribed sea surface temperatures based upon provisional results from a fully coupled atmosphere–ocean (HadCM3L) were presented in Sellwood and Valdes (2006). See Figure 2-3 for an indication of temperature and precipitation data generated by the simulation. The model predicted that Antarctica was cool (≤ 0°C) over much of the continent throughout the Austral winter with warming commencing in the Austral spring with temperatures that may have exceeded 24°C. The Antarctic Peninsula exhibited a similar overall pattern but with a more moderate temperature range, maximum temperatures may have exceeded 16°C. The model predicted that Antarctica was a dry continent but in balance with respect to evaporation and precipitation, with much of the winter precipitation as snow (Sellwood and Valdes, 2006).

A further evaluation of the results from a HadCM3L modelling of the latest Cretaceous was reported by Craggs *et al*. (2012), the study was based upon the presence of sediments sensitive to climatic conditions (e.g. Peat/coal, bauxites and laterites). The authors reported that whilst there was a good correlation between mid to low latitudes with the geological record there was a serious cold bias at high latitudes and in continental interiors; They concluded that even newer climate models still produced results which were incompatible with the geological data (Craggs *et al*., 2012).

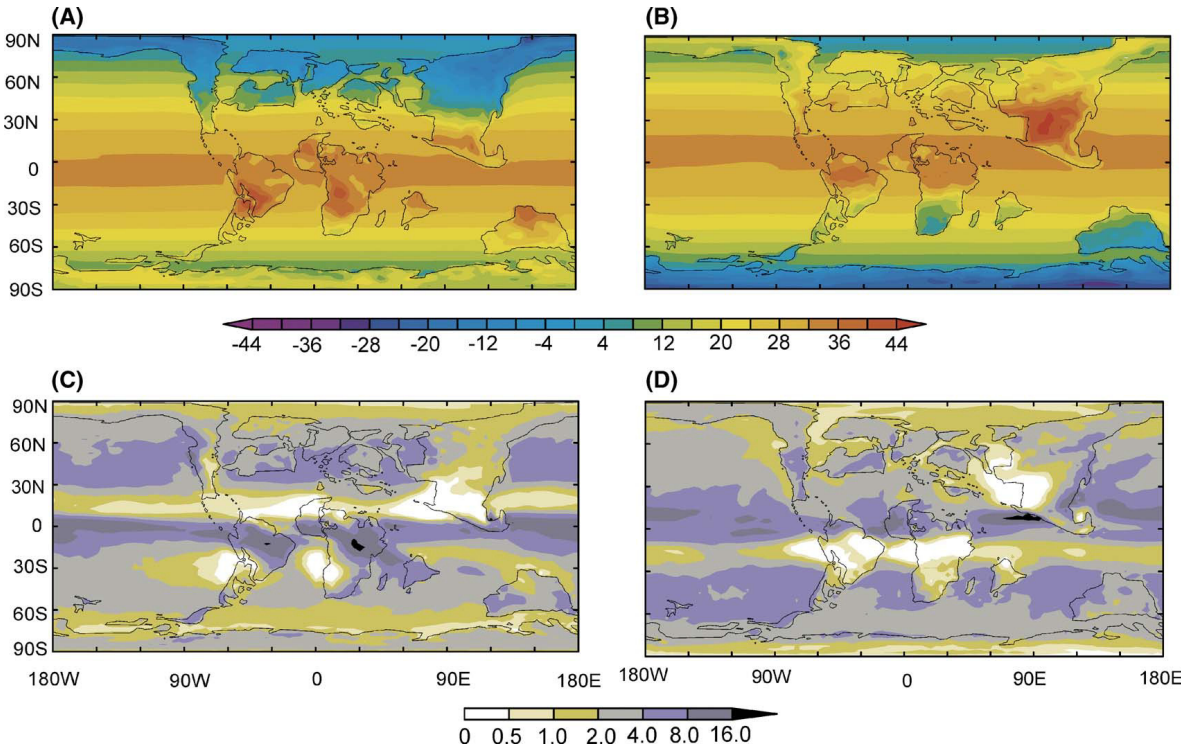

Figure 2-3. (A, B) Model simulated, mean seasonal temperatures for the Late Cretaceous for (A) December–January–February season and (B) June–July–August season. Units are in ℃ and the contour interval is every 4℃. (C and D) Model simulated, mean seasonal precipitation for the Late Cretaceous (C) December–January–February season and (D) June–July–August season. Units are in mm/day and contour interval is irregular. Diagram after Sellwood and Valdes, 2006.

3 Cretaceous aragonite preservation in Antarctica

3.1 Synopsis/Summary

This chapter presents an overview of biogenic aragonite preservation through geological time and in particular during the late Cretaceous of Antarctica. It provides a summary of previous studies in which primary aragonite was recorded and analysed from skeletal carbonates and the corresponding importance for palaeoclimate studies offered by primary aragonite. Details of the taxa selected for analysis are presented together with the analytical methods adopted for the diagenetic screening employed during the selection and preparation of samples prior to running stable isotope analyses. The suitability of the individual diagenetic screening methodologies are described and an overall assessment and scoring made of the quality of the selected specimens. Whilst all carbonates are suitable for stable isotope analysis the intended outcome of the screening process was to identify the least altered specimens that retained an original palaeoclimate signal. It was anticipated that a further phase of the selection and screening process would take place after the measurement and correlation of oxygen and carbon stable isotopes from the diagenetically unaltered aragonite nacre shell material selected. The final stage of the selection procedure will be further expanded in Appendix D, section D.5.

3.2 Aragonite preservation through geological time

Aragonite is the metastable polymorph of calcium carbonate and is less commonly preserved in the macrofossil record than calcite. Where preserved it represents a crucial link to the original biogenic shell material. Where present in the fossil record and depending on the vagaries of diagenesis it may offer an opportunity to observe the preserved geochemical characteristics, including carbon and oxygen stable isotope data, of the original shell material as secreted by the organism. For the molluscan specimens collected from Seymour Island these geochemical data also provide an indication of the marine conditions prevailing at the time the organism was growing. Wendt (1977) stated that aragonite preservation in macrofossils decreased with increasing age in the geological record; the presence of any biogenic aragonite in fossil specimens must be considered both important and fortunate (Jordan *et al*., 2015).

A number of authors have published studies concerning the occurrence of Palaeozoic molluscan macrofossils with intact preserved aragonite from the middle Pennsylvanian (Late Carboniferous) Buckhorn Asphalt Quarry (Wendt, 1977; Brand, 1989; Seuß *et al*., 2009; Seuss *et al*., 2012). Brand (1989) describes the geochemical characteristics of the diagenetic aragonite to calcite alteration of molluscs whilst

(Wendt, 1977; Seuß *et al*., 2009; Seuss *et al*., 2012) describe the nature of the fauna and review the Palaeozoic fossil Lagerstätte with aragonite preserved by the presence of a bituminous coating around the macrofossils. Shell material exhibited good preservation of ultrastructures and also included evidence of microboring (Seuss *et al*., 2012). Unusually for a Palaeozoic invertebrate fauna there were approximately 160 species dominated by molluscs, perhaps suggesting that dissolution of aragonite shell material may generate a major bias towards calcite in the fossil record (Seuss *et al*., 2012). Rogala *et al*. (2010) discussed the diagenesis of macrofossil shell material, including aragonite, from the early Permian Darlington (Sakmarian) and Berriedale (Artinskian) Limestones (Lower Parmeener Supergroup) from high latitude environments now exposed in Tasmania.

Many authors have published research describing the diagenesis, geochemistry and stable isotope record in molluscan aragonite shell material (e.g. Morrison and Brand, 1988; Brand, 1989, 1991; Marshall *et al*., 1996; Rexfort and Mutterlose, 2006; Foster *et al*., 2008; Sayani *et al*., 2011; Collins, 2012; Griffiths *et al*., 2013; Petersen *et al*., 2016; Witts *et al*., 2016). Morrison and Brand (1988) described the diagenesis and chemostratigraphy of upper Cretaceous molluscs from the Canadian interior seaway whilst Brand (1991) described the impact of diagenesis on biogenic aragonite and low Mg calcite (LMC) with regard to strontium isotopes. Marshall *et al*. (1996) discussed the carbon and oxygen stable isotope composition of skeletal carbonates, including both aragonite and calcite, from extant Antarctic marine invertebrates; oxygen isotopic values exhibited a considerable overall range from +0.8 to +3.8‰ and within individual specimens of the same species by +0.3 to +2.0‰. These data indicated that the shell material might reflect inequilibrium precipitation and the authors suggested that the variability of the isotopic data might reflect some 'vital effect' of a particular taxon or indeed that from an individual specimen (Marshall *et al*., 1996). Rexfort and Mutterlose (2006) discussed a high resolution record of stable isotope data ($\delta^{18}O$ and $\delta^{13}C$) from cuttlebones of extant specimens of *Sepia officinalis*; the study investigated whether ontogenetic variations of the isotope signature were discernible and their data suggested that the oxygen isotope composition was in isotopic equilibrium with the surrounding seawater and reflects ambient temperature. Migration and seasonal temperature changes were visible in the acquired data set. The carbon isotope signature showed signs of biofractionation and no direct correlation to the oxygen signature as far as ontogeny and ecology were concerned. Foster *et al*. (2008) assessed the potential of Mg/Ca ratios in an extant bivalve (*Arctica islandica*) for use as a climate proxy. LA-ICPMS analysis of the shell material indicated that there was no correlation between seasonal Mg/Ca variability and seawater temperature. They also

reported that X-ray Absorption Near Edge Spectroscopy (XANES) indicated that the Mg did not substitute into aragonite but was possibly hosted by an inorganic phase. Sayani *et al*. (2011) described the geochemical effects of post-depositional diagenesis on skeletal carbonates from modern and young fossil corals. Whilst Griffiths *et al*. (2013) evaluated the effect of diagenetic cements on element/Ca ratios, used in palaeoenvironmental reconstruction, in aragonitic Early Miocene (~16 Ma) Caribbean corals. LA–ICPMS analyses indicated significant differences in Sr/Ca, Mg/Ca, B/Ca, Ba/Ca and U/Ca in aragonite and calcite cements compared to primary skeletal aragonite and increased Sr/Ca and decreased Mg/Ca ratios were found in aragonite cements compared to skeletal aragonite, these trends were reversed for calcite cements. Ullmann *et al*. (2013) discussed the significance of covariance between Sr and Mn as a tool for assessing the scale of diagenesis that had affected the skeletal carbonate. The authors reported that as diagenesis progresses the level of Mn increases whilst Sr level decreases. A laboratory study of trace elements in an extant aragonite bivalves suggested that incorporation of Mg and Sr into the aragonite were subject to control by the organism (a 'vital effect') and did not fully reflect any environmental control (Poulain *et al*., 2014).

Based on the above review of previous research it is apparent that the presence of aragonite which is subject to calcitisation as a result of pore fluid diagenesis or thermal alteration is extremely important for geochemical and palaeoenvironmental research. This is due in part to the rarity of well preserved molluscan macrofossil aragonite specimens in the geological record. The good preservation of the molluscan shell material from the James Ross Basin and in particular from the López de Bertadano Fm. of Seymour Island illustrates the value of aragonite as the shell mineralogy of choice for this study. In the remainder of this chapter the diagenetic screening process will be described and discussed. The nature of the molluscan shell material encountered will be assessed and the final selected specimens that will form the nucleus of the carbon and oxygen stable isotope and strontium isotope analyses will be further discussed in Chapters 4 and 5.

3.2.1 Diagenesis of skeletal carbonates

The two diagenetic realms in which porosity modifications (e.g., dissolution and cementation) take place are the marine and meteoric environments. Modern shallow-marine environments are particularly susceptible to porosity destruction by cementation due to high levels of supersaturation of marine waters relative to metastable carbonate minerals. Under normal marine conditions the aragonite compensation depth lies at ~1.75 km but below this level a decreasing saturation with depth can lead to

development of secondary porosity by dissolution of aragonite (Boggs 2009). Given the extensive range of aragonite preservation within the James Ross Basin it it is apparent that the basin was shallower than the aragonite compensation depth.

3.2.2 X-ray Diffraction (XRD) analysis

It has been shown that shell material identified as pure aragonite can exhibit evidence for diagenetic alteration of molluscan shell material (e.g. Cochran *et al*., 2003; Wierzbowski and Joachimski, 2007; Cochran *et al*., 2010; Wierzbowski and Rogov, 2011). A further indication of other diagenetic characteristics that might have affected an individual specimen was determined by analysing the powdered shell material by X-ray diffraction (XRD) for a semi-quantitative indication of the primary shell mineralogy. There were 28 specimens for which no XRD profiles were generated and in the absence of other diagenetic data these specimens were deemed unsuitable for palaeotemperature determination. See Appendix B, Table B-3 for full details of the overall results from the comparative diagenetic screening.

Prior to stable isotope analysis each powder sample was analysed for major mineralogical phases using a Siemens D5000 X-ray Diffractometer. In semi-quantitative mode the equipment provided a detection limit of ~5%, mineral phases present below that level could not be reported with confidence. Principal minerals of interest were aragonite, calcite (including both HMC and LMC), dolomite and gypsum – a common Antarctic surface weathering product (Bain, 1990; de Souza *et al*., 2014). Samples were also investigated for the presence of other mineral phases, e.g. pyrite – present at a microscopic level as framboids, (see Figure B-5(c), and oxyhydroxides of Fe and Mn.

Initially the X-ray Diffractometer was run with a 2θ range of 2-70 but it was noted that for aragonite significant peaks did not appear until 2θ reached a value of ~25. As a result the 2θ range was reduced to 20-70 with a corresponding reduction in run time. Data shown in Table 3-1 give the operational parameters used for the XRD analyses.

The standard profiles (Figures 3-1 and 3-2) illustrate the primary mineral phases expected within the samples (refer to Table B-3 for details of the XRD screening results and scoring applied). Restricting the operating 2θ range to 20 – 70 did not add a significant uncertainty to the XRD screening of the specimens, the only possible exception was for gypsum where the primary peak appears at 2θ = 11.67 and thus would not be apparent within the restricted 2θ range. However, there was also a strong secondary peak for gypsum present at 2θ = 20.78 and which more significantly was not subject to overlaps from other observed mineral phases.

Table 3-1. Operational parameters for the Siemens D5000 X-ray Diffractometer adopted during analysis of carbonate shell material.

Estimated scan time	41 mins
Scan mode	Continous scan
Start position (2θ)	20
Increment	0.02
No of steps	2500
Time per step (s)	1
Synchronous rotation	On
Generator voltage	40 kV
Generator current	30 mA
Radiation	Cu(kα)

Sample powders prepared for stable isotope analysis were sub-sampled for XRD analysis, although in certain cases where the volume of sample was small the entire sample was used. Sample powders rarely exceeded 1 g and in the majority of cases the mass of available powder was between 35 - 300 mg.As a result the sample powders were analysed, recovered and subsequently reanalysed for major and trace element geochemistry, stable isotope and in selected cases strontium isotope analyses. Steps were taken to ensure that any cross-contamination was reduced to a minimum whilst handling the specimen powders. Semi-quantitative XRD analysis was completed for each powder sample prior to the assessment of the suitability of the material for stable isotope analysis. This methodology had the benefit of speed and provided a reliable indication of the mineral phases present subject to the concentration of a mineral phase exceeding the instrument detection limit (5% in semi-quantitative mode). For selected macrofossil specimens the anticipated primary mineral phase was aragonite with potentially diagenetic calcite and gypsum. XRD analysis identified 2 specimens with a dominant calcitic shell material. XRD profile data were extracted from the Bruker RAW powder diffraction data files using PowDLL Converter (Version 2.33) (Kourkoumelis, 2013) before being plotted using Excel. Individual XRD profiles for analysed specimens are provided in Appendix C.

The XRD profiles (Figures 3-1(a and b) and 3-2(a) represent the standard aragonite, calcite and gypsum profiles against which all specimen profiles were compared, Figure B-6(b) illustrates the likely peak overlaps for a composite profile for aragonite, calcite and gypsum. Specimen data were extracted from the Bruker RAW powder diffraction data files with PowDLL Converter (Version 2.33) (see Kourkoumelis, 2013). Raw XRD profile data by permission of RRUFF Project (Lafuente *et al*., 2015).

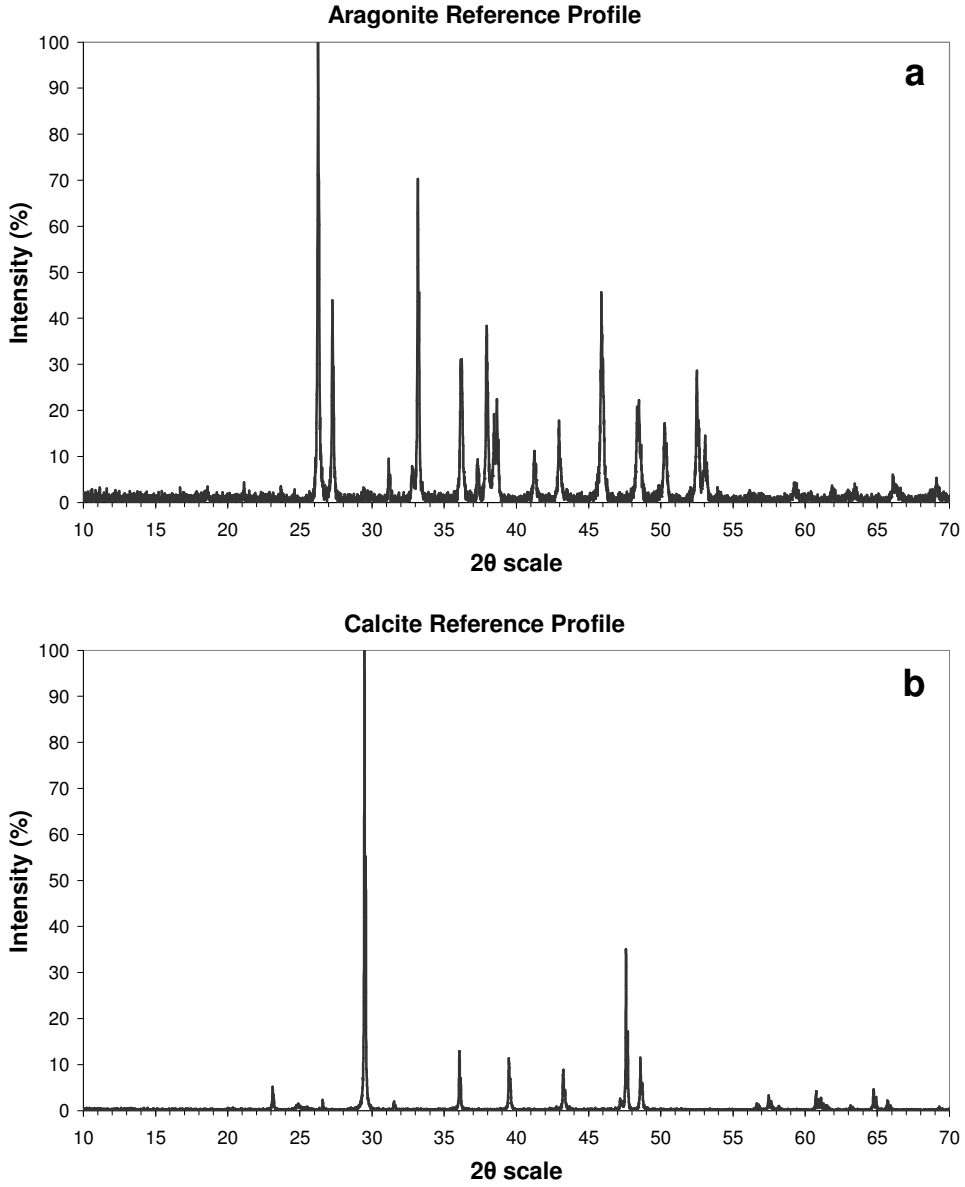

Figure 3-1 Standard XRD diffraction peak profiles for aragonite and calcite. Raw XRD profile data by permission of RRUFF Project (Lafuente *et al.*, 2015). Refer to Table 3-4 for details of equipment operating parameters.
(http://rruff.info/repository/sample_child_record_powder/by_minerals/Aragonite__R040078-1__Powder__Xray_Data_XY_RAW__211.txt,
http://rruff.info/repository/sample_child_record_powder/by_minerals/Calcite__R040070-1__Powder__Xray_Data_XY_RAW__190.txt,

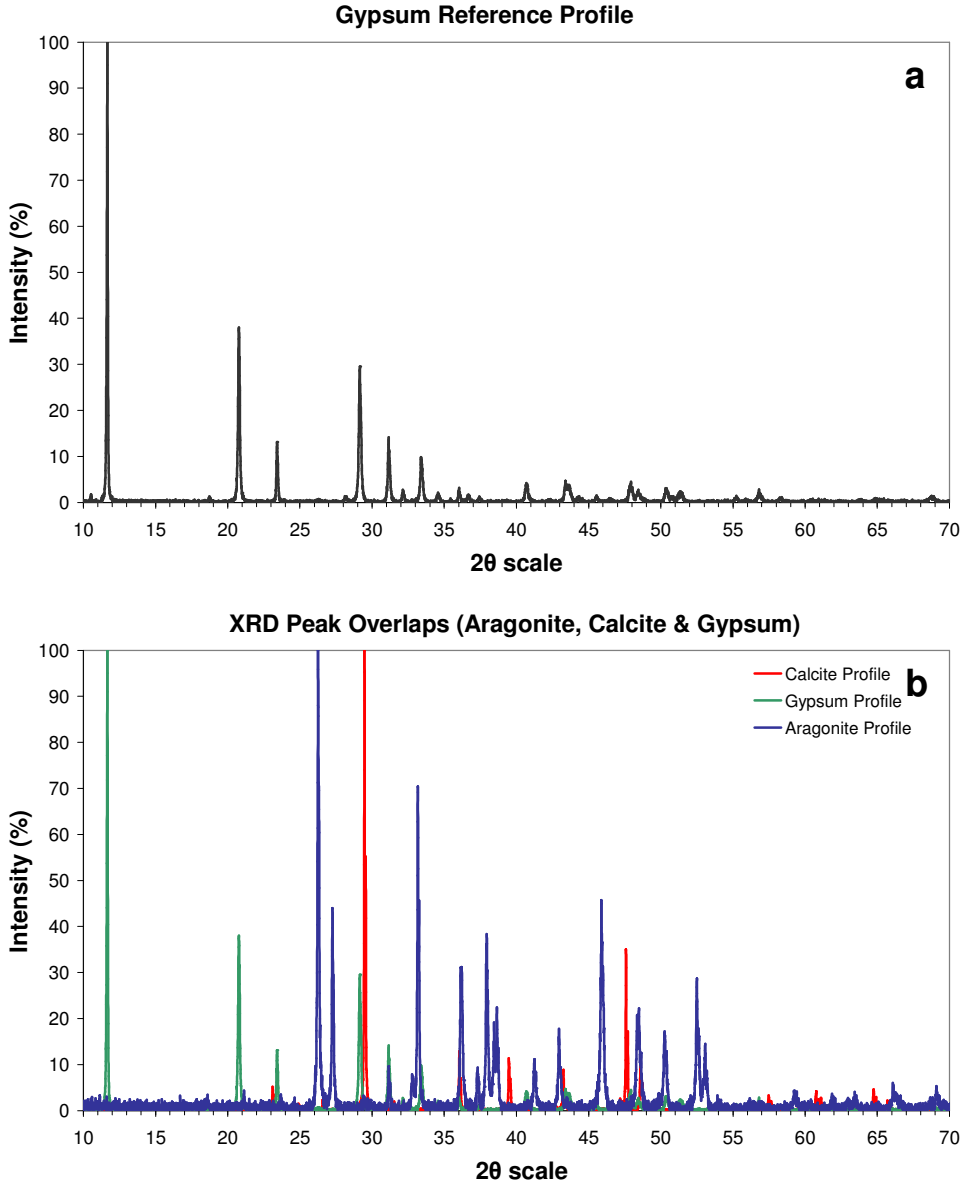

Figure 3-2. Standard XRD diffraction peak profiles for gypsum and composite profile of aragonite + calcite + gypsum. Raw XRD profile data by permission of RRUFF Project (Lafuente *et al.*, 2015). Refer to Table 3-4 for details of equipment operating parameters. http://rruff.info/repository/sample_child_record_powder/by_minerals/Gypsum__R040029-1__Powder__Xray_Data_XY_RAW__67.txt

In the case of specimens with small quantities of sample powder the XRD profile was generally noisy but the profile typically retained the relative peak spacing seen from specimens with ample powders. Figures 3-3 and 3-4 show the XRD profiles recorded for four specimens, namely D5.219.1185.2/C, D5.212.865.3/E, D5.222.1257.2/A and D5.215.216.5/A with actual sample peaks superimposed upon peaks exhibited from an aragonite standard[1], where the raw standard reference data was downloaded and used by permission of the RRUFF Project (Lafuente *et al.*, 2015). The four profiles illustrate

[1] http://rruff.info/repository/sample_child_record_powder/by_minerals/Aragonite__R040078-1__Powder__Xray_Data_XY_RAW__211.txt

quality for the XRD scoring with a range of 5 to 2, where 5 represents the highest score, note that like the SEM preservation index this mineral scoring is subjective and is based upon an assessment of the mineralogy as determined by semi-quantitative XRD. No aragonite specimens with XRD screening scored lower than 3 in the XRD diagenetic assessment, see Appendix B, Table B-3 for the full diagenetic scoring data.

The XRD profile coloured grey (Figures 3-3 and 3-4) represents the standard aragonite profile against which all specimen profiles were compared, Table 3-2 lists the XRD scoring characteristics. Specimen data were extracted from the Bruker RAW powder diffraction data files with PowDLL Converter (Version 2.33) (see Kourkoumelis 2013). Raw XRD profile data used by permission of RRUFF Project (Lafuente *et al*., 2015). Figure B-3(a) illustrates a noisy XRD profile for specimen D5.219.1185.2/C (ammonite genus – *Maorites* a nektonic carnivore) matching aragonite and possible gypsum, typical style of profile associated with specimens that yielded small quantities of sample powders. Figure B-3(b) illustrates a better quality XRD profile, but with low counts, for specimen D5.212.865.3/E (bivalve genus – unidentified) matching standard aragonite profile peaks. Figure B-4(a and b) illustrate examples of good to excellent XRD profiles with high count levels and clear matching of the standard aragonite profile peaks for specimens D5.222.1257.2/A (nautiloid genus – unidentified carnivore) and D5.215.216.5/A (gastropod genus – *Pleurotomaria* an epifaunal carnivore/scavenger). In all four specimens the profiles clearly match the aragonite peaks from the standard profile.

Table 3-2 Definition of XRD Mineralogy Index scale. See Figures 3-3 and 3-4 for images of shell material which match the criteria listed. See Appendix C, Figure C-34 for an example of a specimen that was classified as exhibiting a MI = 0.

MI	Descriptor	Characteristic features of shell surface
5	Excellent	Good clear profile with regular peak positions, high count rate and no contaminant mineral phases present
4	Good	Good clear profile with regular peak positions, medium count rate and no contaminant mineral phases present
3	Moderate	Reduced count rate with a moderate s/n ratio or with gypsum as a contaminant mineral phase
2	Fair	Reduced count rate, lower s/n ratio and with contaminant mineral phases
1	Poor	No aragonite present, low count rate with low s/n ratio and presence of contaminant mineral phases (principally calcite)

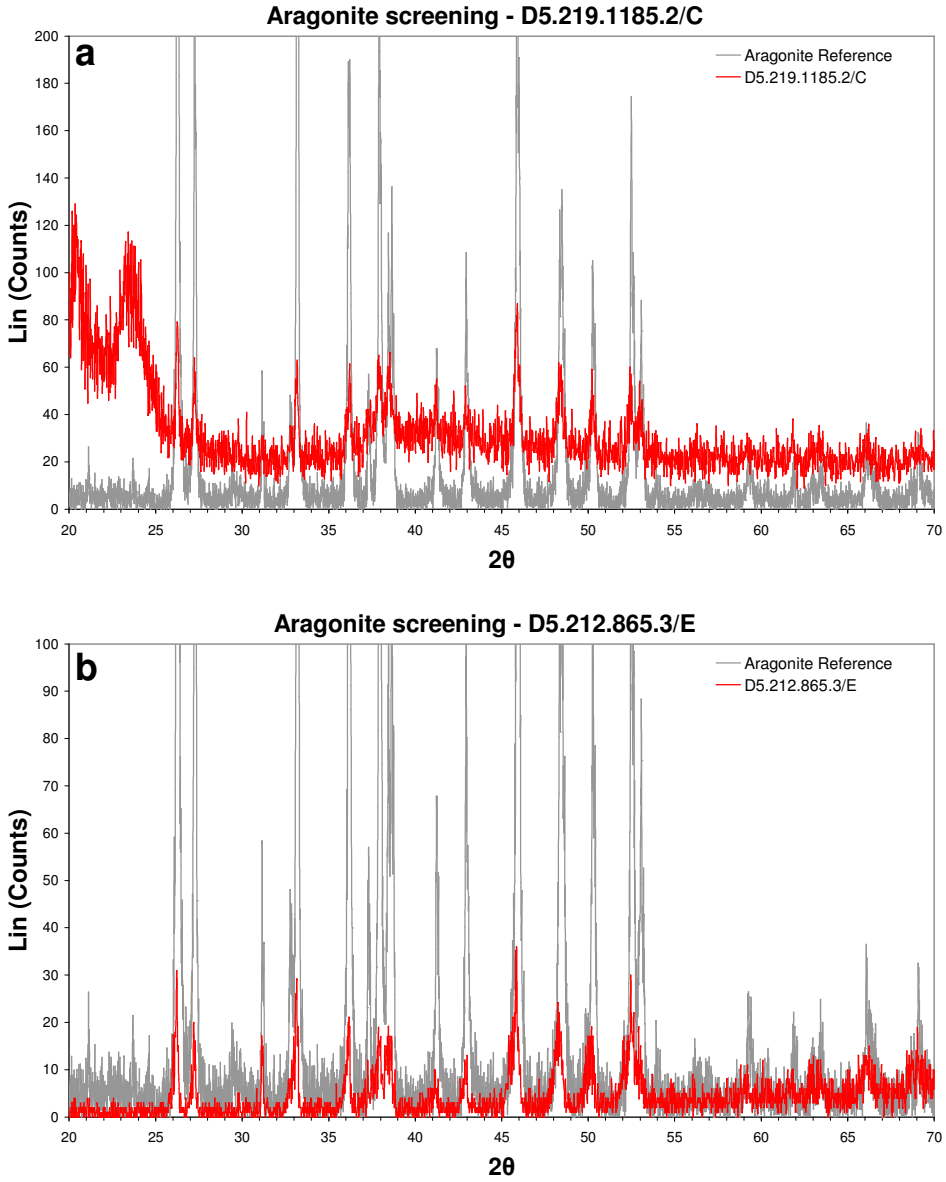

Figure 3-3. XRD diffraction peak profiles for the biogenic mineral aragonite ($CaCO_3$) taken from specimens D5.219.1185.2/C and D5.212.865.3/E and superimposed upon a standard aragonite profile[2], in both cases the peaks are strong and well defined and clearly match the standard profile. (a) D5.219.1185.2/C Ammonite genus – *Maorites* a nektonic carnivore (XRD score = 2). Typical profile associated with specimens that yielded small quantities of sample powders. (b) D5.212.865.3/E Bivalve genus – unidentified (XRD score = 3). Profile illustrates a better quality XRD profile, but with low counts.Specimen data extracted from the Bruker RAW powder diffraction data file with PowDLL Converter (Version 2.33) (See Kourkoumelis 2013). Raw XRD profile data by permission of RRUFF Project (Lafuente *et al.*, 2015).

[2] (http://rruff.info/repository/sample_child_record_powder/by_minerals/Aragonite__R040078-1__Powder__Xray_Data_XY_RAW__211.txt)

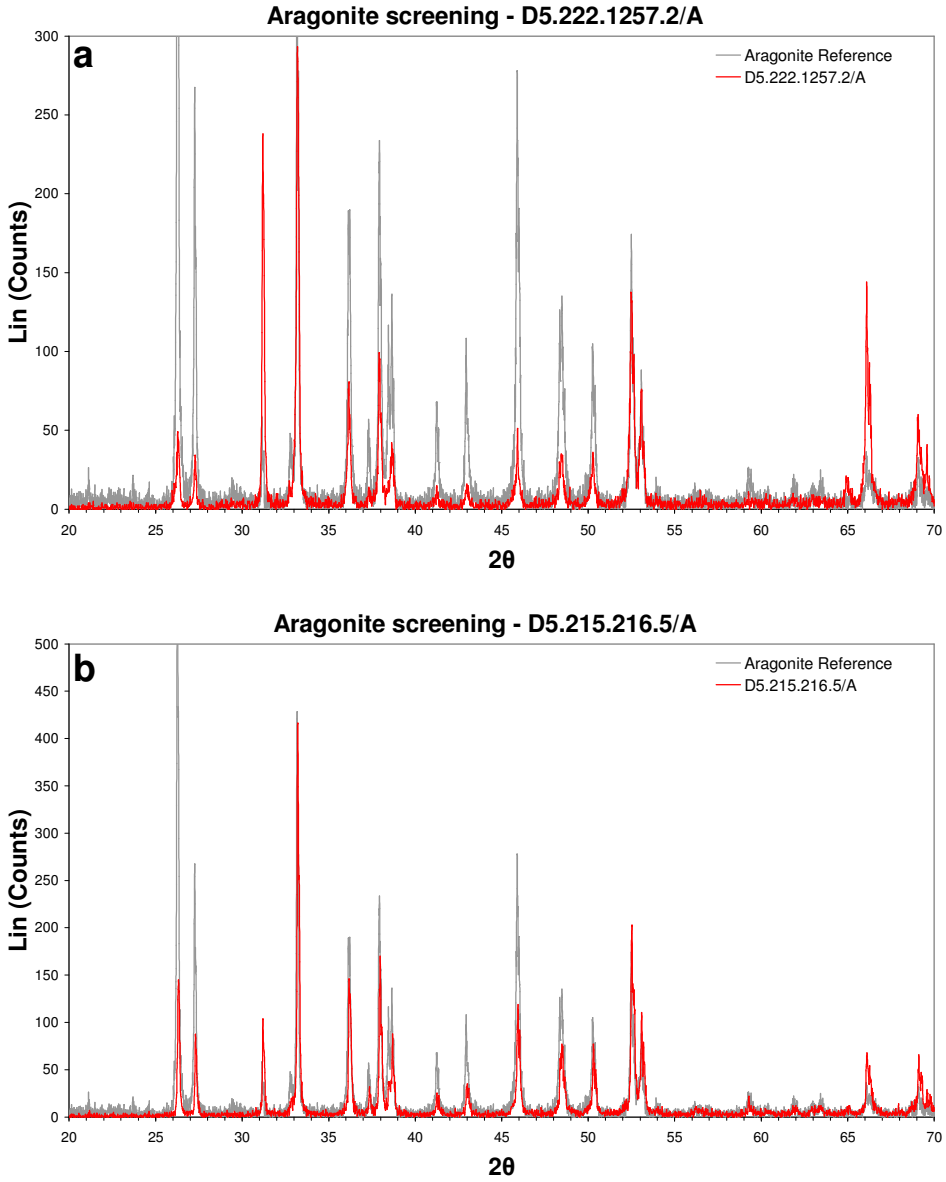

Figure 3-4. XRD diffraction peak profile for the biogenic mineral aragonite ($CaCO_3$) taken from specimens D5.222.1257.2/A and D5.215.216.5/A and superimposed upon a standard aragonite profile[3], in both cases the peaks are strong and well defined and clearly match the standard profile. (a) D5.222.1257.2/A Nautiloid genus – Unidentified carnivore (XRD score = 5). (b) D5.215.216.5/A Gastropod genus – *Pleurotomaria* an epifaunal carnivore/scavenger (XRD score = 5). Specimen data extracted from the Bruker RAW powder diffraction data file with PowDLL Converter (Version 2.33) (See Kourkoumelis 2013). Raw XRD profile data by permission of RRUFF Project (Lafuente *et al.*, 2015).

[3] (http://rruff.info/repository/sample_child_record_powder/by_minerals/Aragonite__R040078-1__Powder__Xray_Data_XY_RAW__211.txt)

3.3 ICP trace element screening

Diagenetic screening based upon an investigation of the remaining shell ultrastructure remains an important tool in the determination of the degree of diagenesis that may have affected a macrofossil specimen. Likewise screening of shell mineralogy through XRD analysis had proved a significant technique for the determination of potentially altered specimens but with the proviso that only mineral phases with an abundance of >5% were accurately reported. The limitation was due to the detection limit of the instrument when operated in a semi-quantitative mode.

Trace element composition further complemented the SEM and XRD diagenetic screening and scoring with shell preservation assessed using ICP-OES data. A small number of samples retained insufficient sample powder after stable isotope analysis for subsequent ICP-OES analyses and consequently there were 35 specimens for which no trace element geochemistry data were recorded. The total number of actual samples processed was in excess of 500. Aliquots for analysis were prepared in batches of 24 that included blank and replicate samples (see Appendix D for a description of the methodology). Measurement of the concentrations of selected elements in blank samples enabled the correlation of instrument detection limits which in turn provided a measure of confidence for the results generated by the ICP-OES instrument; see Appendix D, Table D-1 for the relevant data.

One oversight in the design of the ICP-OES analysis methodology was the omission of an external certified standard, thus there was no check on the accuracy of the ICP-OES instrument. Yttrium was included as an internal calibration standard at a concentration of 1 ppm. As a further measure of data quality standard calibration solutions were also included within each run of the ICP-OES instrument as unknown samples in order to determine the precision of the data. The operating procedure specified that a standard solution be included for measurement every 10^{th} sample.

3.3.1 Ocean Geochemistry

Archer *et al*. (2004) describe variations in the mean temperature of the ocean that operate at a number of time scales, including millennial to millions of years that are large enough to impact the geochemistry of the carbon, oxygen and methane geochemical systems. The time scale of the temperature perturbation is key; on time frames of 1–100 ky atmospheric CO_2 is controlled by the ocean. CO_2 temperature-dependent solubility and greenhouse forcing combine to create an amplifying feedback with ocean temperature; the $CaCO_3$ cycle increases this effect somewhat on time scales longer than ~5–10 ky. Timing is important for oxygen, the atmosphere controls the ocean on short time scales, but ocean anoxia controls atmospheric pO_2 on million-

year time scales and longer. An ocean warmed to Cretaceous temperatures might, in the absence of other perturbations, increase pO_2 by approximately 25% above present day levels. Because residence times of Sr, Mg and Ca are on the order of 10^6 yr and complete ocean mixing occurs approximately every 10^3 yr, only small shifts in the global seawater Mg/Ca ratio are expected for time scales on the order of 10^5 yr.

3.3.2 Mg/Ca ratio

Skeletal Mg/Ca ratios show little sensitivity to environmental conditions other than an exponential increase with temperature (Archer *et al*., 2004), probably thermodynamic but also controlled by species dependent characteristics. Covariance of Mg/Ca and temperature can be represented by the following expression:

$$T = 2.50_{(\pm 0.36)} \times [(Mg/Ca) \times 1000] - 2.07_{(\pm 2.35)}$$

Where T is estimated temperature (°C) with 95% confidence limits (Klein *et al*., 1996).

Study of trace elements in extant aragonite bivalves suggested that incorporation of Mg into aragonite was subject to control by the organism (a 'vital effect') and did not fully reflect any environmental control (Poulain *et al*., 2014). The authors also proposed that a portion of the Mg was hosted by proteins present within the shell structure.

The Mg/Ca ratio of seawater is little changed by fresh-water dilution from a salinity of 35‰ down to 18‰; this reduction in salinity changes the Mg/Ca ratio from 5.2 to 5.0, based on global means for seawater (Klein *et al*., 1996) and corresponds to less than a 4% change in the Mg/Ca ratio of the seawater mixture. Currently, it is not possible to solve uniquely for salinity by using skeletal Mg/Ca and $^{18}O/^{16}O$ ratios. Finally, for the case where ^{18}O and Mg palaeotemperature estimates do not overlap, the difference in estimated temperatures most likely results from salinity fluctuations caused by freshwater input. Application of combined isotopic and chemical proxies to studies of molluscan macrofossils may provide powerful constraints for reconstructing palaeoclimate and palaeosalinity for coastal marine settings.

3.3.3 Mn/Ca ratio

Mn/Ca records derived from biogenic carbonate provides a proxy for dissolved Mn concentrations and thereby reflects those redox processes that control the concentration of this element in seawater (Freitas *et al*., 2006). Dissolved Mn is delivered to the oceans by riverine input and is slowly removed from solution by oxidation to Mn^{4+}, whilst reducing conditions in sediments and also in certain situations in the water column can recycle Mn back into solution (Freitas *et al*., 2006). Mn solubility is determined by the redox state of the element, it is most soluble in its reduced Mn state and will precipitate oxyhydroxides from its oxidised Mn^{4+} state

(Freitas *et al*., 2006). The presence of elevated levels of Mn in analyses of carbonate geochemistry are used as a screening methodology (Morrison and Brand, 1988; Brand, 1991) for determining the degree to which biogenic carbonates have been affected by diagenesis. The presence of elevated levels of Mn (> 50 ppm) actively promotes cathodoluminescence in biogenic carbonates. Ideally the level of Mn in a biogenic carbonate should not exceed 100 ppm for inclusion of the carbonate in stable isotope studies.

3.3.4 Sr/Ca ratio

The Sr concentration in biogenic carbonate reflects the Sr/Ca ratio in the water in which the carbonate formed as well as the physiological factors involved in biomineralisation (Lowenstam and Weiner, 1989), the latter are dependent upon water temperature, salinity and organism growth rate (Cochran *et al*., 2003). Factors such as water temperature and growth rate also may be interdependent. Study of trace elements in extant aragonite bivalves suggested that incorporation of Sr into the aragonite was subject to a 'vital effect' and not environmental control (Poulain *et al*., 2014). With respect to the variability in the Sr/Ca ratio of the water, the present-day ocean shows a difference between the value in the open ocean and in world-mean river water, with the former being approximately three times greater than the latter. Variability of the Sr/Ca ratio in the water is not the first-order control on Sr/Ca in the carbonate shell material. Although the exact fractionation of Sr/Ca in the shell vs. water will vary among species, fundamental differences in biomineralisation (Lowenstam and Weiner, 1989) related to environmental factors such as temperature, salinity and pCO_2 are responsible for the trends. The effects of temperature and other factors on the Sr/Ca ratio of biogenic carbonates have been documented for both macrofossils, microfossils (Cochran *et al*., 2003) and extant bivalve species (Freitas *et al*., 2006; Poulain *et al*., 2014)).

The Sr/Ca ratio can be employed in evaluating the degree to which oxygen isotope values may have been affected by the preservation of biogenic carbonate shell fragments and the significance of any diagenesis effects present. Generally, diagenetic processes reduce Sr concentrations in aragonite because of the similar chemistry of Sr and Ca (Li and Keller, 1999). Strong diagenetic effects result in a good correlation between Sr/Ca ratios and $\delta^{18}O$ values due to the loss of Sr. Thus, a low correlation coefficient (e.g. $R^2 = 0.02$) between the Sr/Ca ratio for screened $\delta^{18}O$ values, would indicate that there was no significant evidence for diagenetic effects (Li and Keller, 1999). Note also that Sr is generally enriched in aragonite with respect to calcite. Sr and Mn covary as a result of diagenesis

3.3.5 Sr/Na ratio

Biogenic aragonite precipitated in normal salinity seawater contains on average ~6,000 ppm Na (Brand, 1986). Previous studies of geochemical trace element analysis of molluscan fauna have indicated that a relationship exists between Na and salinity; Brand (1986) stated that this relationship was best shown by calculating the Sr/Na ratio, where the covariance was expressed as a salinity equation:

Salinity (ppt, ± 0.5) = -5.769 Ln (A) + 28.380 (1)

where Ln (A) is the natural log of the geometric mean of the Sr/Na ratio calculated for molluscan aragonite (Brand, 1984).

3.4 Trace element analysis

Aliquots of dissolved sample powders were analysed for major and trace element chemistry using a Varian 725-ES-ICP-OES at the School of Environmental Chemistry, University of Plymouth, Plymouth, UK. There were 35 specimens with insufficient sample powders following the stable isotope analyses, for which as a consequence no trace element chemistry data were generated. For these specimens diagenetic screening was completed by a subjective comparison with specimens of the same taxon using the stable isotope data.

The presence of elevated or reduced levels of trace elements (Mg, Sr, Na, Fe and Mn) must also be considered when assessing the diagenetic history of a specimen. For example in Table B-4(i) ('PI' – 1) specimen Id D5.215.347.2/I shows extensive neomorphism of the aragonite nacre plates but exhibited a trace element geochemistry that still retained low levels of Fe and Mn (Fe = 59 ppm and Mn = 174 ppm). This suggested that the prevailing redox conditions were incompatible with the precipitation of Fe or Mn from the pore fluids and thus were unlikely to have altered the original shell geochemistry. Alternatively it was possible that pore fluids carried low levels of Fe and Mn or that conditions within the James Ross Basin may have inhibited the diagenesis of the aragonite nacre shell material. Petersen *et al*. (2016) discussed the screening by cathodoluminescence (CL) of bivalve specimens collected on Seymour Island and noted that only cracks, infilled with a carbonate cement, actively luminesced under CL. This indicated that whilst there may have been reducing Mn rich pore fluids there was no evidence for diagenesis of the shell material.

As previously discussed only 2 specimens were identified as calcite by XRD analysis but a further 32 specimens were also rejected due to the presence of elevated Mg levels following classification from ICP-OES trace element analyses (see Appendix D; Brand, 1991). All 34 macrofossil specimens exhibited elevated levels of both Fe and

Mn except for a small number of cases (e.g. Fe < 500 ppm, n=4) and Mn < 200 ppm, n=1).

The principal indicators of diagenesis used were the divalent cations of iron (Fe) and manganese (Mn) which typically should have low values in pristine primary skeletal carbonates, ideally <100 ppm (Morrison and Brand, 1988). Specimens with a geochemistry that exhibited concentrations of Mn < 190 ppm and Mg <900 ppm correspond to the expected data typical of either an extant mollusc or an unaltered fossil mollusc (Morrison and Brand,1988; Brand, 1991). Brand (1991) also defined the natural limit of magnesium (Mg) in biogenic aragonite at a concentration of < 1000 ppm. Note that Mn < 1200 ppm and Mg < 900 ppm correspond to the range expected from a macrofossil with well preserved aragonite, samples with Mn > 1200 ppm represent specimens with a potential diagenetic signature (Brand, 1991).

Figure 3-5 illustrates a series of covariance plots of Mg vs. Mn (for method see Morrison and Brand, 1988; Brand, 1991) for all specimens with ICP trace element data (n=169) with the data categorised as follows.

- Unscreened data set of all aragonite specimens plus LMC specimens identified by red diamonds.
- Screened aragonite data set (n=116) with all LMC specimens removed and with orange diamonds representing specimens with elevated Fe or Mn (n=53).
- Screened aragonite data sets for bivalves, cephalopods, gastropods and specimens with an uncertain classification and with orange diamonds representing specimens with elevated Fe or Mn.

Acceptable levels of Fe and Mn for well preserved aragonite nacre shell material have been published by a number of different authors (Morrison and Brand, 1988; Anderson *et al*., 1994; Ditchfield *et al*., 1994; Petersen *et al*., 2016). Specimens with Fe < 500 and Mn < 200 ppm (Anderson *et al*., 1994; Ditchfield *et al*., 1994; Petersen *et al*., 2016) and Mg < 900 ppm correspond to the expected data for extant molluscan aragonite (Morrison and Brand, 1988).

Removing all specimens with Mg > 1000 ppm had a marked effect on the levels recorded for Mn (see Figure 3-5), there was a strong covariance between elevated levels of Mg and Mn. In the reduced data set the mean Mn level for bivalves = 184 ppm, ammonites = 226 ppm, gastropods = 114 ppm, nautiloids = 172 ppm and for specimens of uncertain affinity the level = 11 ppm. Note that based on mean geochemical data all ammonite specimens exceeded the Mn threshold (200 ppm) and should be deemed unsuitable for palaeotemperature determination.

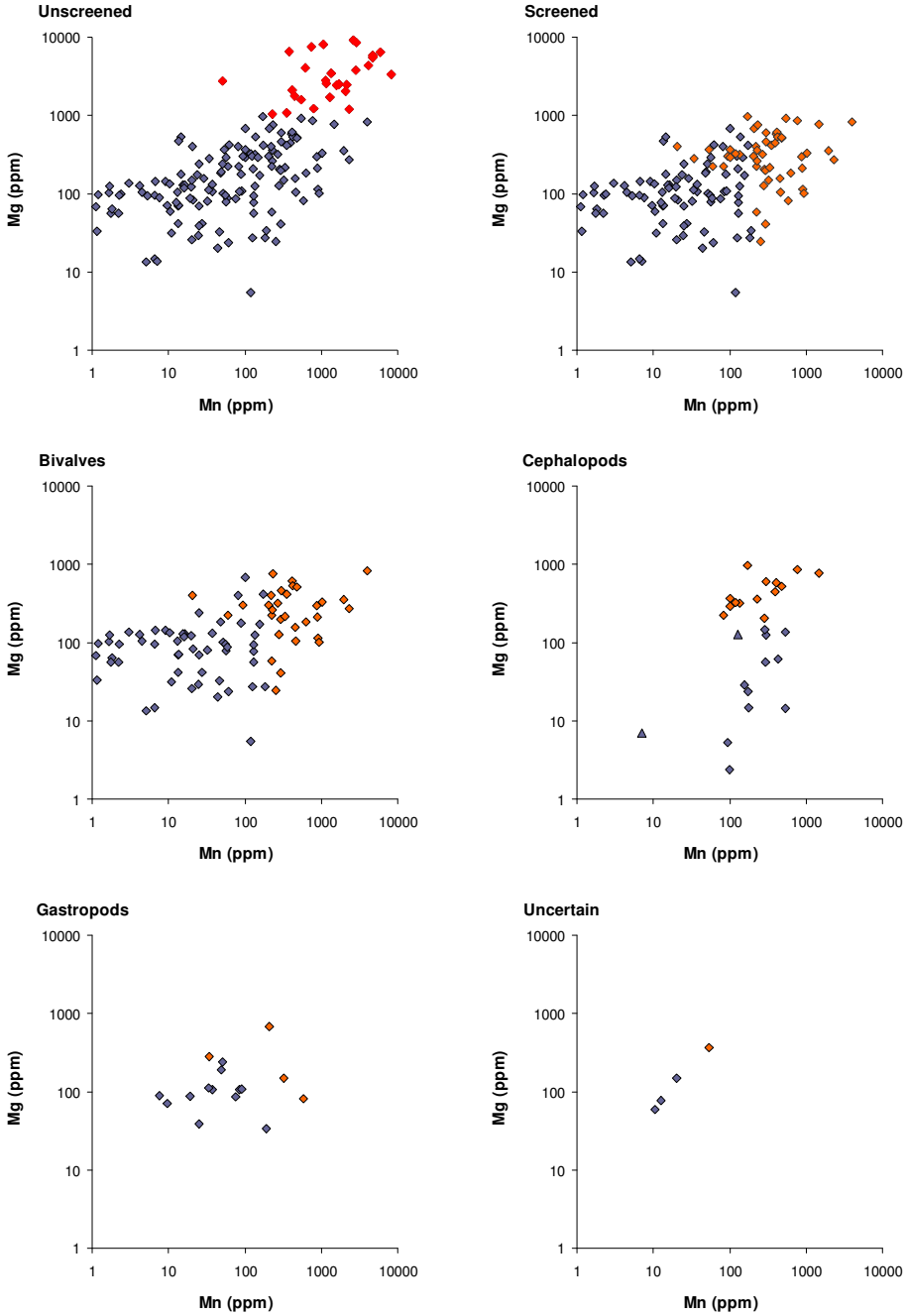

Figure 3-5. Covariance plot of Mg vs. Mn for all specimens with ICP trace element data, categorised as follows:- 1) Unscreened data set of aragonite specimens (n=169) plus LMC specimens (n=34) identified by red diamonds, 2) Screened aragonite data set (n=116) with all LMC specimens removed and with orange diamonds representing specimens with elevated Fe or Mn (n=53). 3) Screened aragonite data sets for **bivalves**, **cephalopods**, **gastropods** and specimens with an **uncertain** classification and with orange diamonds representing specimens with elevated Fe or Mn. Specimens with Fe > 500 ppm or Mn > 200 ppm (Ditchfield *et al.*, 1994; Petersen *et al.*, 2016) are deemed to be potentially subject to diagenesis. Specimens with Mg < 900 ppm, Fe and Mn < ~200 ppm correspond to the expected data for extant molluscan aragonite (Morrison and Brand, 1988). Note that the maximum Mg content of biogenic aragonite is set at 1000 ppm (Brand, 1991). Specimens with Mn < 1200 ppm and Mg < 900 ppm correspond to the range expected from a macrofossil with well preserved aragonite. All points with Mn > 1200 represent specimens with a potential diagenetic signature. Methods after Morrison and Brand (1988) and Brand (1991) and Ditchfield *et al.* (1994).

Figure 3-6 illustrates a series of covariance plots of Sr/Ca vs Mg, Fe and Mn that show the relationship of Sr/Ca and the principal diagenetic indicator elements. Blue symbols represent specimens taken from the initial aragonite data that have been subject to further screening to remove specimens that exhibited elevated levels of Fe or Mn (Fe > 500 ppm and Mn > 200 ppm). Removal of those data points with elevated Fe and Mn yielded a considerably reduced spread in the overall data. During the course of carbonate diagenesis there is a reduction of Sr whilst dissolution takes place and a covarying precipitation of Mn during neomorphism or calcitisation with the development of diagenetic calcite cements or the wholesale recrystallisation of calcite.

The reduction of Sr concentrations in aragonite occurs because of the similar chemistry of Sr and Ca (Brand and Veizer 1988; Li and Keller 1999; Ullmann *et al*., 2013). Note that aragonite is enriched in Sr with respect to calcite. Significant diagenetic alteration will result in a good correlation between Sr/Ca ratios and Mn values due to the Sr and Mn covarying. A simple linear trend line was applied to the Fe and Mn covariance graphs (see Figure 3-6(b and c) and the resulting correlation coefficient (R^2) values were included for each plot, note that in neither case did the value approximate to unity (strong correlation). In this case neither Mn (R^2 = 0.1605) or Fe (R^2 = 0.0431) covaried with the concentration of Sr in the aragonite and consequently there was little evidence for diagenesis having altered the specimens. However, diagenesis could have affected individual samples to a greater or lesser extent.

Based upon previously published data on diagenetic trace element indicators a substantial portion of the data set would be rejected because of the high Fe and Mn levels (e.g. Morrison and Brand, 1988; Brand, 1991; Anderson *et al*., 1994; Ditchfield *et al*., 1994; Tobin *et al*., 2012; Petersen *et al*., 2016). Similar stable isotope studies (e.g. Anderson *et al*., 1994; Ditchfield *et al*., 1994) and recent studies from Seymour Island (Tobin *et al*., 2012; Tobin and Ward 2015; Petersen *et al*., 2016) discussed the question of screening specimens for elevated levels of either Fe or Mn and the limits that should be adopted. In this study it was decided to adopt previously published figures of 500 ppm for Fe and 200 ppm for Mn (Anderson *et al*., 1994; Ditchfield *et al*., 1994; Petersen *et al*., 2016). Tobin *et al*. (2012) indicated that although a portion of their data set could be rejected under the same rationale the overall effect upon the variability of the stable isotope data set was insignificant. A similar approach was adopted for this study and where trace element and stable isotope data are presented in graphs those specimens with elevated Fe and Mn are plotted in a contrasting colour to the screened aragonite data. However, data from specimens potentially subject to diagenesis were also included for further screening of the stable isotope data.

Geochemical variables are to a certain extent independent (Marshall 1992) and low concentrations of trace elements do not necessarily indicate the preservation of primary isotopic values. Even where trace element values are high, marine isotopic values can be preserved where recrystallisation or cementation took place in a relatively closed environment (Marshall 1992).

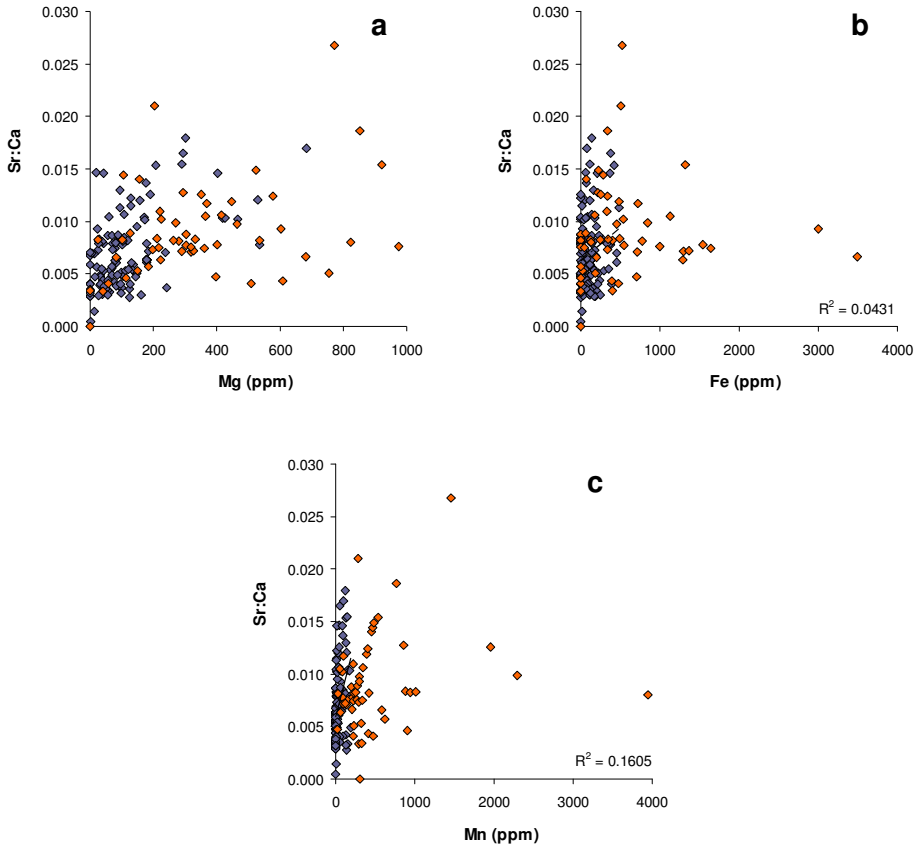

Figure 3-6. Covariance plots of Sr/Ca vs Mg, Fe and Mn. Blue symbols represent specimens taken from the initial aragonite data that have been subject to further screening to remove specimens that exhibited elevated levels of Fe or Mn (Fe > 500 ppm and Mn > 200 ppm). Removal of those data points with elevated Fe and Mn yield a considerably reduced spread in the overall data. Carbonate diagenesis leads to a reduction in Sr and a corresponding increase in Mn. A simple linear trendline was applied to the plots (b and c) and the resulting R^2 values were included in each plot, note that in neither case did the value approximate close to unity (strong covariance). In this case neither Mn or Fe covaried with the concentration of Sr in the aragonite.

3.4.1 LMC - Trace elements

As previously discussed a number of specimens (n=32) that exhibited Mg concentrations > 1000 ppm were deemed as unsuitable for palaeotemperature determination according to the method of Brand (1991) and were consequently rejected. Note that for these specimens and the small number (n=2) of specimens that following XRD and ICP-OES analysis were categorised as LMC there was a strong correlation (see Appendix D Tables D-3, 4, 5 and 6) with elevated Fe and Mn levels in

the geochemical data; the presence of which can be indicative of diagenesis (Morrison and Brand, 1986). These specimens would have been rejected regardless of the mineralogical classification of the shell material due to the highly elevated levels present, for example **ammonites** (mean values of Fe = 3735 ppm and Mn = 2283 ppm), **bivalves** (mean values of Fe = 16193 ppm and Mn = 259 ppm) and specimens of **uncertain** affinity (mean values of Fe = 4785 and Mn = 2231 ppm). Categorising the trace element data by genus shows a high Fe concentration for each genus except ***Pycnodonte*** and a high Mn concentration for each genus except ***Nucula***. In both cases the data represent a single specimen. For example **unclassified ammonites** ($_{n=5}$) (mean values of Fe = 3505 ppm and Mn = 3332 ppm), ***Anagaudryceras*** ($_{n=1}$) (mean values of Fe = 5536 ppm and Mn = 2822 ppm), **unclassified bivalve** ($_{n=1}$) (mean values of Fe = 41069 ppm and Mn = 378 ppm), ***Kitchinites*** ($_{n=1}$) (mean values of Fe = 2350 ppm and Mn = 380 ppm), ***Maorites*** ($_{n=14}$) (mean values of Fe = 3788 ppm and Mn = 2006 ppm), ***Nucula*** ($_{n=1}$) (mean values of Fe = 7261 ppm and Mn = 51 ppm), ***Pycnodonte*** ($_{n=1}$) (mean values of Fe = 249 ppm and Mn = 349 ppm) specimens of **uncertain affinity** ($_{n=9}$) (mean values of Fe = 4785 ppm and Mn = 2231 ppm).
The corresponding trace element data for habitat show a high Fe concentration in all categories and the high Mn concentration in all categories except for infaunal specimens. In both cases the data represent a single specimen. Note the high Fe concentration in all categories except epifaunal and the high Mn concentration in all categories except infaunal. In both cases the data represent a single specimen. The corresponding trace element data for the measured stratigraphy show a high Fe concentration at all stratigraphic positions except 925 m and a high Mn concentration at all stratigraphic positions except 682 m and 642 m.

It is apparent from the categorisation of the trace element data for those specimens classified as either low magnesium calcite or having Mg > 1000 ppm (Brand, 1991) that all specimens with a small number of exceptions have elevated Fe and Mn levels. All of these specimens were rejected for use as sources of stable isotope data suitable for palaeotemperature determination.

3.4.2 Aragonite – Trace elements

Mean trace element data categorised by stratigraphy for partially screened aragonite specimens with Mg < 1000 ppm are presented in Figure 3-7. Vertical dashed lines for Fe and Mn indicate thresholds for elevated values possibly as a result of diagenesis. Orange highlight represents Fe ≥ 500 ppm or Mn ≥ 200 ppm. The presence of elevated Fe and Mn levels may be linked to specific stratigraphic horizons but there is an apparent correlation with the highest populations of selected specimens.

The trace element data (mean ppm) presented in Appendix D, Table D-7 are categorised by fossil type for specimens determined as being aragonite based upon an Mg concentration < 1000 ppm (Brand, 1991). All categories with the exception of ammonites (Fe = 775 ppm) have diagenetic indicator elements (Fe or Mn) at levels below the selected threshold values. The corresponding data categorised by genus (mean ppm) are presented in Appendix D, Table D-8. For example, ***Amberlaya*** $_{(n=13)}$ (mean values of Fe = 390 ppm and Mn = 135 ppm), **Ammonite** $_{(n=9)}$ (mean values of Fe = 775 ppm and Mn = 93 ppm), **Bivalve** $_{(n=21)}$ (mean values of Fe = 142 ppm and Mn = 63 ppm), ***Diplomoceras*** $_{(n=1)}$ (mean values of Fe = 179 ppm and Mn = 61 ppm), ***Eselaevitrigonia*** $_{(n=34)}$ (mean values of Fe = 136 ppm and Mn = 155 ppm), **Gastropod** $_{(n=1)}$ (mean values of Fe = 0 ppm and Mn = 19 ppm), ***Grossouvrites*** $_{(n=1)}$ (mean values of Fe = 369 ppm and Mn = 15 ppm), ***Lahillia*** $_{(n=1)}$ (mean values of Fe = 137 ppm and Mn = 28 ppm), ***Maorites*** $_{(n=14)}$ (mean values of Fe = 534 ppm and Mn = 338 ppm), **Nautiloid** $_{(n=4)}$ (mean values of Fe = 439 ppm and Mn = 172 ppm), ***Nucula*** $_{(n=29)}$ (mean values of Fe = 235 ppm and Mn = 481 ppm), ***Oistotrigonia*** $_{(n=26)}$ (mean values of Fe = 76 ppm and Mn = 84 ppm), ***Pinna*** $_{(n=3)}$ (mean values of Fe = 672 ppm and Mn = 51 ppm), ***Pleurotomaria*** $_{(n=2)}$ (mean values of Fe = 70 ppm and Mn = 24 ppm), ***Solemya*** $_{(n=1)}$ (mean values of Fe = 78 ppm and Mn = 100 ppm) and **Unidentified** $_{(n=9)}$ (mean values of Fe = 216 ppm and Mn = 11). Note that for Fe only *Maorites*, unidentified Ammonites and *Pinna* exceed the threshold of 500 ppm and that for Mn both *Maorites* and *Nucula* exceed the 200 ppm threshold. The corresponding data categorised by habitat (mean ppm) are presented in Appendix D, Table D-9. Note that for Fe only nektonic taxa exceed the 500 ppm threshold and that for Mn both infaunal and nektonic taxa exceed the 200 ppm threshold. For example, **Epifaunal** $_{(n=16)}$ (mean values of Fe = 326 ppm and Mn = 114 ppm), **Infaunal** $_{(n=104)}$ (mean values of Fe = 163 ppm and Mn = 208 ppm), **Nektonic** $_{(n=28)}$ (mean values of Fe = 592 ppm and Mn = 224 ppm), **Planktonic** $_{(n=1)}$ (mean values of Fe = 179 ppm and Mn = 61 ppm) and **Uncertain** $_{(n=30)}$ (mean values of Fe = 164 ppm and Mn = 47 ppm). The corresponding trace element data for the measured stratigraphy are presented in Appendix D, Table D-10 and show a high Fe concentration at stratigraphic positions 1084 m, 1068 m, 943 m, 851 m, 632 m, 627 m, 622 m, 443 m and 438 m, and a high Mn concentration at stratigraphic positions 1084 m, 1068 m, 1028 m, 943 m, 857 m, 851 m, 632 m, 627 m, 622 m, 443 m and 438 m.

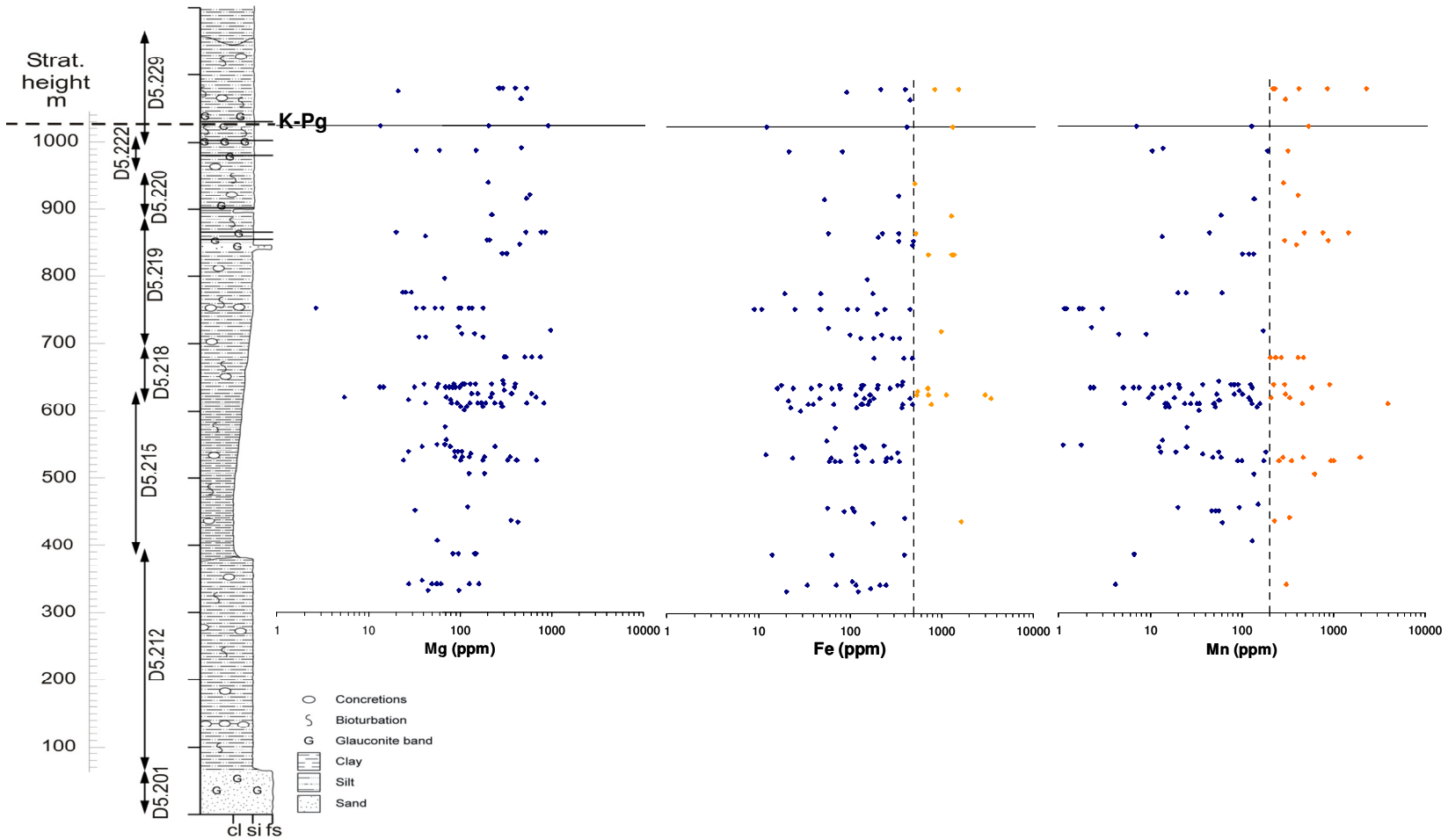

Figure 3-7. Mean trace element data categorised by stratigraphy for partially screened aragonite specimens with Mg < 1000 ppm. Vertical dashed line for Fe and Mn indicate thresholds for elevated values possibly as a result of diagenesis. Orange highlight represents Fe ≥ 500 ppm or Mn ≥ 200 ppm. The presence of elevated Fe and Mn levels may be linked to specific stratigraphic horizons but there is an apparent correlation with the highest populations of selected specimens.

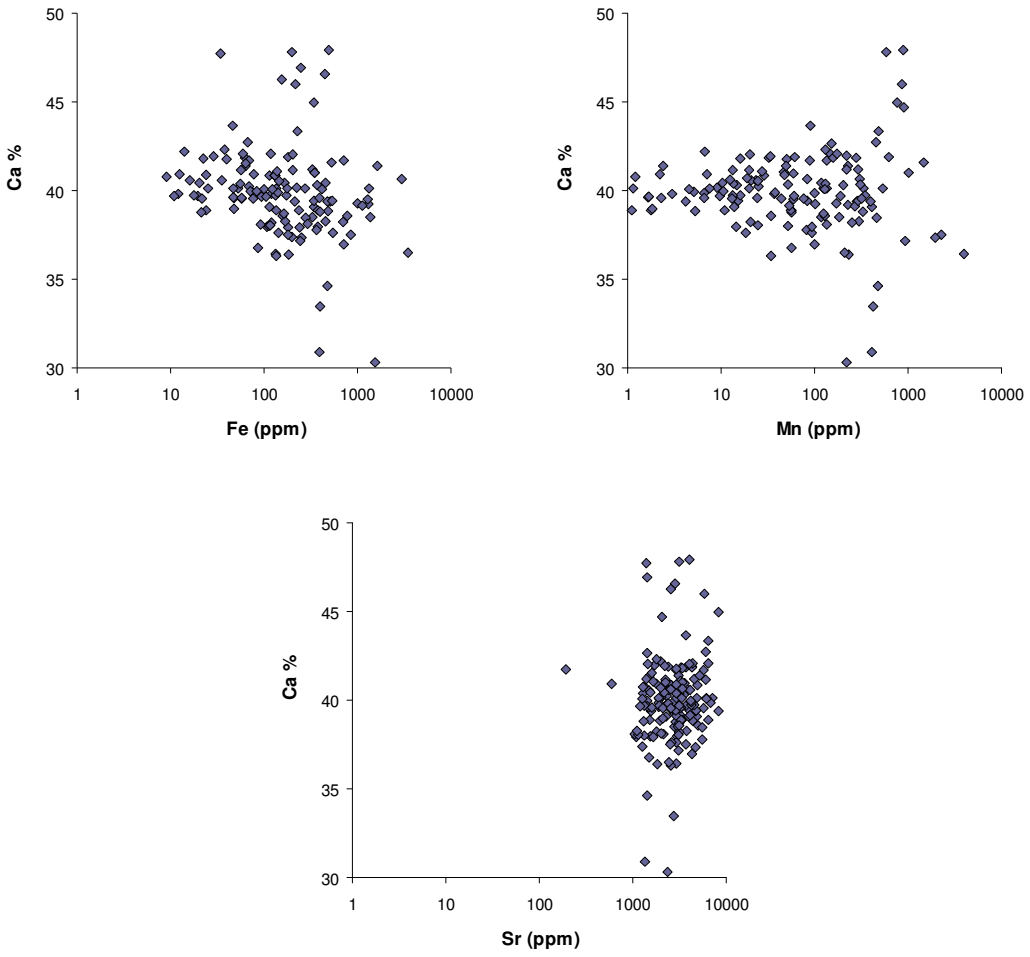

Figure 3-8. Covariance plots of screened trace element geochemical data for Ca (%) vs selected elements. (n=179). The inclusion of specimens with elevated levels of either Fe or Mn shows no apparent covariance with the Ca %. There is also no obvious covariance between Sr and Ca.

3.5 Criteria for the recognition of primary carbonates

Ideally in a palaeoclimate study the shell material for analysis must be as near pristine as possible, although within the geological record all shell material comprising carbonate whether calcite or aragonite, will exhibit some evidence of diagenetic alteration of the original primary carbonate. This alteration may result from endolithic microbial activity that occurred prior to burial during life or post-mortem, in addition post burial diagenesis may be due to marine or meteoric fluid flow or thermal alteration. Little previous evidence for temperature related thermal alteration of carbonate shell material present in the Late Maastrichtian section of the James Ross Basin has been reported (Macdonald *et al*., 1988; Pirrie *et al*., 1994;Tobin *et al*., 2012, Little *et al*., 2015; Petersen *et al*., 2016). The majority of the selected molluscan macrofossils retained original aragonite shell material, indicated by the presence of iridescent nacre

resulting from a diffraction grating effect controlled by the presence of protein layers within the nacre (Lowenstam and Weiner 1989).

The presence of aragonite nacre indicated that specimens were subject to a relatively shallow burial history and low temperature diagenesis (Pirrie *et al*., 1994; Tobin *et al*., 2012). A limited number of specimens (n=34) exhibited evidence of either unsuitable mineralogy or significant diagenetic overprinting of the trace element geochemistry and were rejected for further analyses. The remainder of the specimens were deemed suitable for stable isotope analysis even though some also showed a range of insignificant diagenetic effects, most notably elevated levels of Fe and Mn.

3.6 Cathodoluminescence, carbonate staining and QEMSCAN

Cathodoluminescence (CL) petrography, in particular cold cathodoluminescence, has been widely used as an essential tool for characterising and highlighting discreet geochemical events both during carbonate cement development and during diagenesis of biogenic carbonates. CL can highlight characteristic zoning present within a carbonate material that is invisible to standard optical microscopy. It can detect elevated levels of activator cations incorporated in diagenetic carbonate due to post depositional water rock interaction (Marshall 1998; Budd *et al*., 2000; Fouke *et al*., 2002; Gaft *et al*., 2005; Rausch *et al*., 2013). The main activator elements of luminescence in carbonates are Mn, Pb, Sb, Cr, Sm, important quencher elements are Fe and Ni. Luminescence in natural carbonates is mainly controlled by the concentration of ferrous iron and manganese. The minimum concentration of Mn for luminescence in calcite and dolomite is 20-40 ppm (Richter and Zinkernagel 1980). Luminescence caused by transition elements, such as Mn or Cr is due to electron transitions of the outer, partially filled 3d shell. Energy levels are influenced by the crystal field and the CL emission is a property of the material (Marshall 1988).

For a small subset of the research samples it was decided that thin section analysis using both a Cambridge Image Technology CL MK3A system linked to a JVC digital camera and standard carbonate staining techniques after the method of Dickson (1966) would complement the other analytical screening methodologies. Cathodoluminescence analysis of preserved biogenic carbonate samples has generally been associated with calcite shell material (Marshall 1988, Tobin *et al*., 2012) rather than aragonite (although in contrast see Petersen *et al*., 2016) and routine carbonate staining after the method of Dickson (1966) fails to distinguish between calcite and aragonite. Since aragonite was the primary constituent of the shell material present for specimens selected for this study the use of CL and staining seems inappropriate. However, for a number of reasons it was decided to employ this technique:

1. Specimens of *Rotularia spp* were ubiquitous within the López de Bertodano Fm. and have previously formed the basis of biostratigraphic zonation (Macellari, 1984) and as a possible source of carbonate for the analysis of oxygen and carbon stable isotopes plus strontium isotope analyses (McArthur *et al*., 1998, 2000; Tobin *et al*., 2012; Tobin and Ward 2015). With a vertical sampling resolution of ~5 m *Rotularia* potentially offered a source of carbonate powders for both high resolution stable isotope analysis and subsequent $^{87}Sr/^{86}Sr$ isotope analysis. Selection of *Rotularia* carbonate material from Seymour Island for $^{87}Sr/^{86}Sr$ isotope analysis was described by McArthur *et al*., 1988). CL analysis and carbonate staining techniques enabled an assessment of the level of diagenesis affecting the worm tubes. Note that if *Rotularia* were found to be suitable for analysis the decision to analyse only aragonitic material would have required further justification.
2. A large Pachydiscid ammonite was selected for sequential ontogenetic sampling from both external shell material and from discrete septal walls, as described by Lukeneder *et al*. (2010). The specimen was sectioned longitudinally and the carbonate cemented infill of the camerae and individual septal walls were investigated using CL analysis and carbonate staining techniques to enable an assessment of the level of diagenesis affecting the internal structure of the specimen.

Once the thin sections were prepared for optical examination both techniques were quick to implement but qualitative in nature. They provided an initial assessment of the potential suitability of the specific specimens for further analysis.

3.6.1 *Rotularia* diagenetic screening

Within the measured stratigraphic section specimens of *Rotularia* were ubiquitous and potentially presented an ideal source of biogenic carbonate for stable isotope analysis subject to satisfactory diagenetic screening. A number of polished thin sections were prepared from specimens of *Rotularia* selected from specific positions within the succession. Figure 3-9 shows wide field photomicrographs of a transverse section through a *Rotularia* worm tube, (a) under PPL and (b) after carbonate staining following the method of Dickson (1966). The presence of a pink colouration and the corresponding absence of a characteristic indigo blue colouration in the stained section indicated that a ferroan calcite cement was not present in the carbonate infill (Dickson, 1966). Photomicrographs of a thin section under PPL and CL are shown, see Figure 3-10. Note the extensive orange luminescence present in the carbonate that forms the worm tube, typical of Mn activation following diagenetic alteration of the original LMC

by pore fluids (Marshall 1988). The carbonate cemented infill of the worm tube and the prominent fracture cutting across the tube wall were non luminescent.

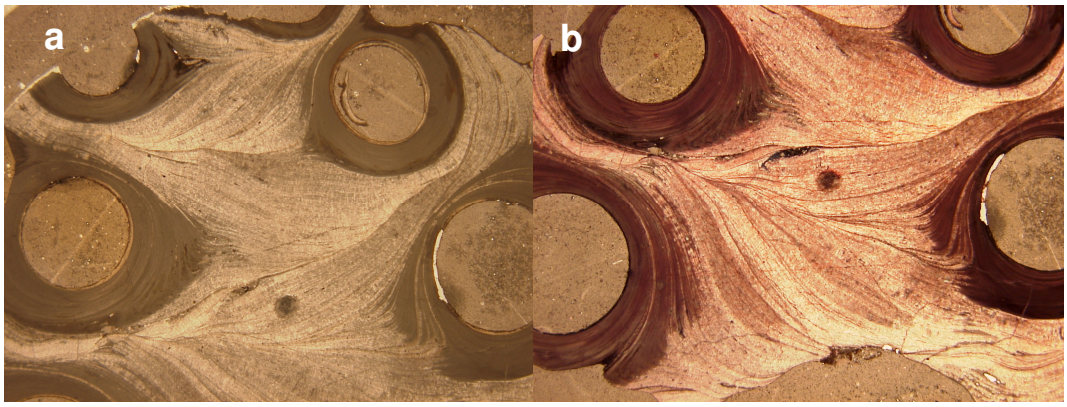

Figure 3-9. PPL and stained wide field photomicrographs of a transverse section through *Rotularia* worm tube to illustrate internal structure. (a) PPL and (b) Standard carbonate staining after the method of Dickson (1966). The presence of a pink colouration and the corresponding absence of an indigo blue colouration indicated that the infill did not comprise ferroan carbonate (Dickson, 1966). Specimen Id D5.218.1028.2/A. Fields of view ~13 mm.

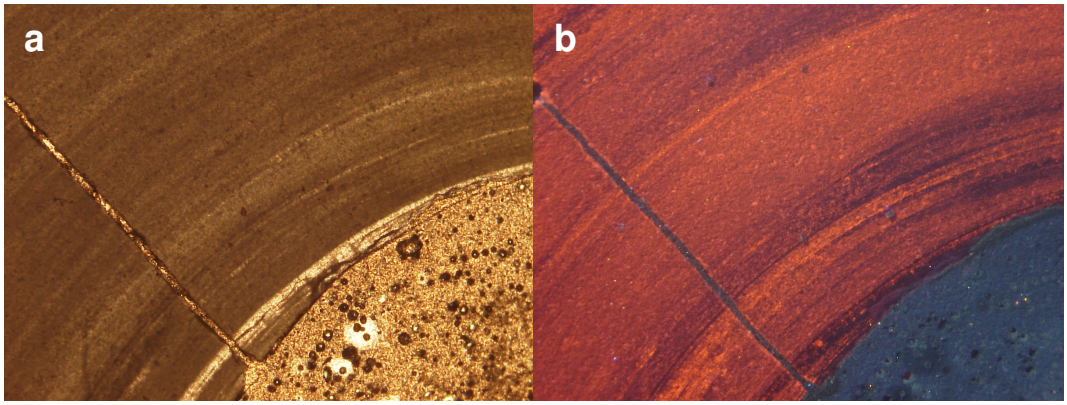

Figure 3-10. PPL and CL images of a transverse section through a *Rotularia* worm tube. Note that the carbonate wall of the worm tube exhibits a typical Mn activated luminescence, whereas the carbonate cemented infill of the worm tube and the prominent fracture exhibit no luminescence. Standard carbonate staining exhibited no blue colouration indicating that the infill did not comprise ferroan carbonate. Specimen Id D5.218.1028.2/A. Fields of view ~2.5 mm.

All specimens of *Rotularia* imaged under CL, see Figure 3-10(b), gave a similar orange luminescence, the colour was consistent with the Mn activation of diagenetically altered carbonate (Marshall 1988). As a consequence no specimens of *Rotularia* were selected for either further diagenetic screening or stable isotope analysis. Note that Tobin *et al*. (2012) used *Rotularia* worm tubes as a source of carbonate powders for stable isotope analyses. McArthur *et al*. (1998) also considered *Rotularia* suitable for inclusion in determining the $^{87}Sr/^{86}Sr$ ratio of Late Maastrichtian macrofossils from Seymour Island, analyses that subsequently provided data for inclusion in the Late Maastrichtian section of the global marine Strontium Isotope Stratigraphy SIS curve (McArthur *et al*., 1998, 2001).

3.6.2 Ammonite ontogenetic analysis

An additional research aim was to test whether inter/intra-annual variability was detectable in the stable isotope data recorded from a single macrofossil specimen; such data might reflect variation of the $\delta^{18}O$ and $\delta^{13}C$ during the ontogeny of the organism. For an ammonite this variability might represent changes in the water depth during the life of the organism; a similar ammonite study was described by Lukeneder *et al*. (2010). Cephalopod shells are generally precipitated in oxygen isotope equilibrium with ambient seawater, do not exhibit any 'vital effects' and represent good palaeoenvironmental proxies. Similar studies have been carried out on both extant species (Barrera *et al*., 1994; Dettman *et al*., 1999; Goodwin *et al*., 2003; Ivany *et al*., 2003) and fossil species (Jones and Quitmyer 1996; Dutton *et al*., 2007; Lukeneder *et al*., 2010).

A large (200 mm) specimen of a pachydiscid ammonite (Specimen Id D5.222.1248.2/K) was selected as the initial specimen for sequential ontogenetic sampling from both external shell material and discrete septal walls. The specimen was sectioned and thin sections were prepared from the carbonate cemented infill of the camerae and from individual septal walls, see Figure 3-11.

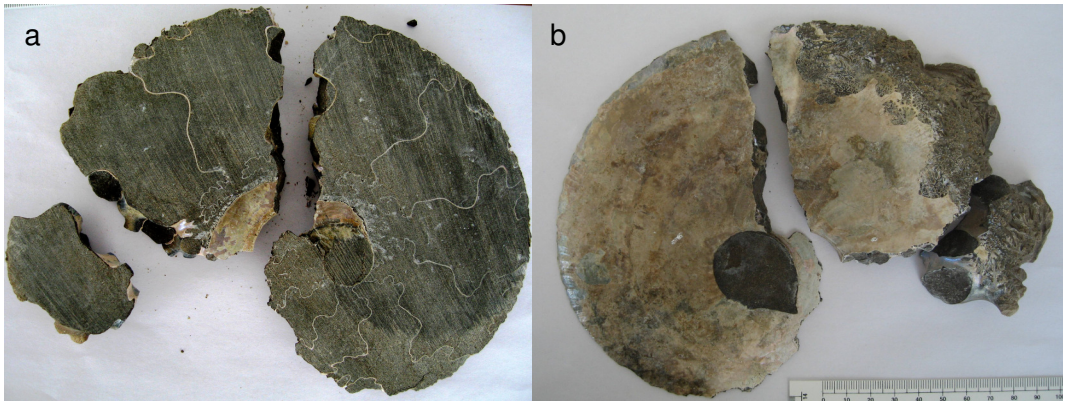

Figure 3-11 (a) Internal view showing the nature of infilled camerae and septal walls and (b) external view of pachydiscid ammonite after making a median cut prior to carrying out multiple sampling on individual septa. Ammonite genus – *Pachydiscus* a nektonic carnivore. Specimen Id - D5.222.1248.2/K. Field of view ~200 mm.

The thin sections were investigated using CL and carbonate staining (Dickson, 1966) to enable an assessment of the level of diagenesis affecting the internal structure of the ammonite.Figure 3-12 shows photomicrographs of an internal septal wall in Plain Polarised Light (PPL) and CL. The septal wall contained small areas that luminesced orange, the typical colour (Marshall 1988) for Mn hosted luminescence. The overall lack of Mn hosted luminescence within the septal wall and the pervasive luminescence of the infill indicated that whilst the Late Maastrichtian pore fluids were enriched with Mn there was minimal diagenesis of the shell material. The majority of the septal wall was non- luminescent and was deemed suitable for stable isotope analysis. However,

the pervasive luminescence of the infill from the camerae indicated that basin pore fluids were enriched with Mn.

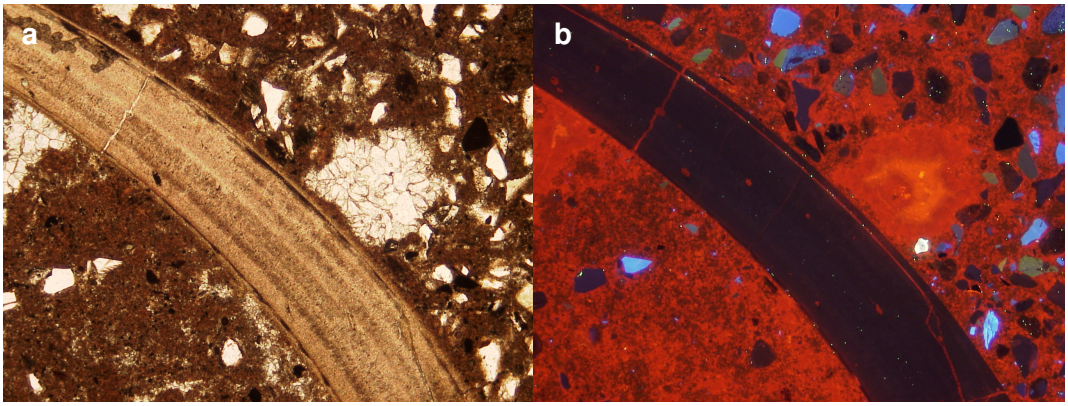

Figure 3-12. Corresponding photomicrographs in (a) PPL and (b) CL from a thin section of a septal wall from a *Pachydiscus* ammonite. The orange luminescence response of the carbonate cements suggests that alteration by Mn-rich pore fluids was confined to fractures and small discrete areas within the septal material. Note also the strong zoned luminescence of the area of sparry calcite and the blue colouration of the quartz grains present within the clastic infilling sediment. The overall lack of Mn hosted luminescence within the septal wall and the pervasive luminescence of the infill indicated that whilst the pore fluids were reducing enriched with Mn there was minimal diagenesis of the shell material. Specimen Id D5.222.1248.2/K-14. Fields of view ~2.5 mm.

Whilst the accumulation of possible ontogenetic stable isotope data was deemed valuable for correlation with similar data from other studies (E.g. Lukeneder *et al*., 2010; Petersen *et al*., 2016) the execution of this technique was subject to delay in sampling and was dropped due to a lack of data.

3.6.3 QEMSCAN diagenetic screening

To complement the existing diagenetic analyses in particular as a potential replacement for carbonate staining of calcite macrofossils a single specimen of *Rotularia* was analysed using QEMSCAN. The specimen was prepared as a stained polished thin section (Dickson, 1966), examined optically under both plain polarised light and cold CL and finally carbon coated. The mineralogy and textures present within the specimen were quantified using automated SEM-EDS and back scattered electron (BSE) analysis using QEMSCAN technology (Pirrie *et al*., 2004; Haberlah *et al*., 2011; Pirrie *et al*., 2014). The thin section was scanned using a 5 µm beam stepping interval. The actual area analysed was optimised by defining a 'best fit' rectangle that maximised the coverage of the *Rotularia* specimen but also sought to minimise the overall area of glass that would be measured. The instrument was operated in fieldscan mode with the measurement area divided into a pre-defined number of square fields as determined by the operator. Each field was then further broken down into a pre-defined grid of pixel squares with each pixel having an X-ray analysis point and a pixel spacing, in this case of 5 µm with identical vertical and horizontal spacing.

The resin mount of the thin section was ignored due to being below a pre-set BSE threshold. After processing, the resultant fields were recombined to give an overall image. Fieldscan mode measured the entire area of the sample and generated 5,796,572 X-ray analysis points. Once collected the data were processed and the interpreted mineralogy reported (see Figure 3-13).

The application of QEMSCAN technology to the indication of the presence or otherwise of diagenetic alteration of biogenic carbonates intended for stable isotope analysis is an unusual application of an instrument that may now be considered a mature technology (Pirrie *et al*., 2004; Haberlah *et al*., 2011; Pirrie *et al*., 2014; Little *et al*., 2015). With reference to Figure 3-13(b) it can be seen that the majority of the *Rotularia* specimen consists of non-ferroan calcium carbonate, note also that the QEMSCAN is unable to distinguish polymorphs and that for the purposes of analysis and reporting all calcium carbonate is reported as calcite (Pirrie *et al*., 2004). There are certain areas of the specimen that have been identified as ferroan carbonate, for comparison see Figure 3-10(b) where no obvious blue colouration developed in the stained thin section, indicating that no optically detectable ferroan carbonate was present in the *Rotularia* specimen. The QEMSCAN colour classification indicated that calcite was the predominant phase, but the quantitative modal data confirmed that ferroan calcite had a larger modal percentage (calcite (vol %) = 33.51, ferroan calcite (vol %) = 61.20, Mg calcite (vol %) = 2.50). A separate modified colour classification (see Figure 3-13(c) provides contrasting colours for calcite and ferroan calcite.

No specimens of *Rotularia* were selected for further diagenetic characterisation or for subsequent stable isotope analysis following the CL and QEMSCAN analyses. However, stable isotope data based on analysis of sample powders from specimens of *Rotularia* have been included in strontium isotope and palaeotemperature studies (McArthur *et al*., 1998; Tobin *et al*., 2012).

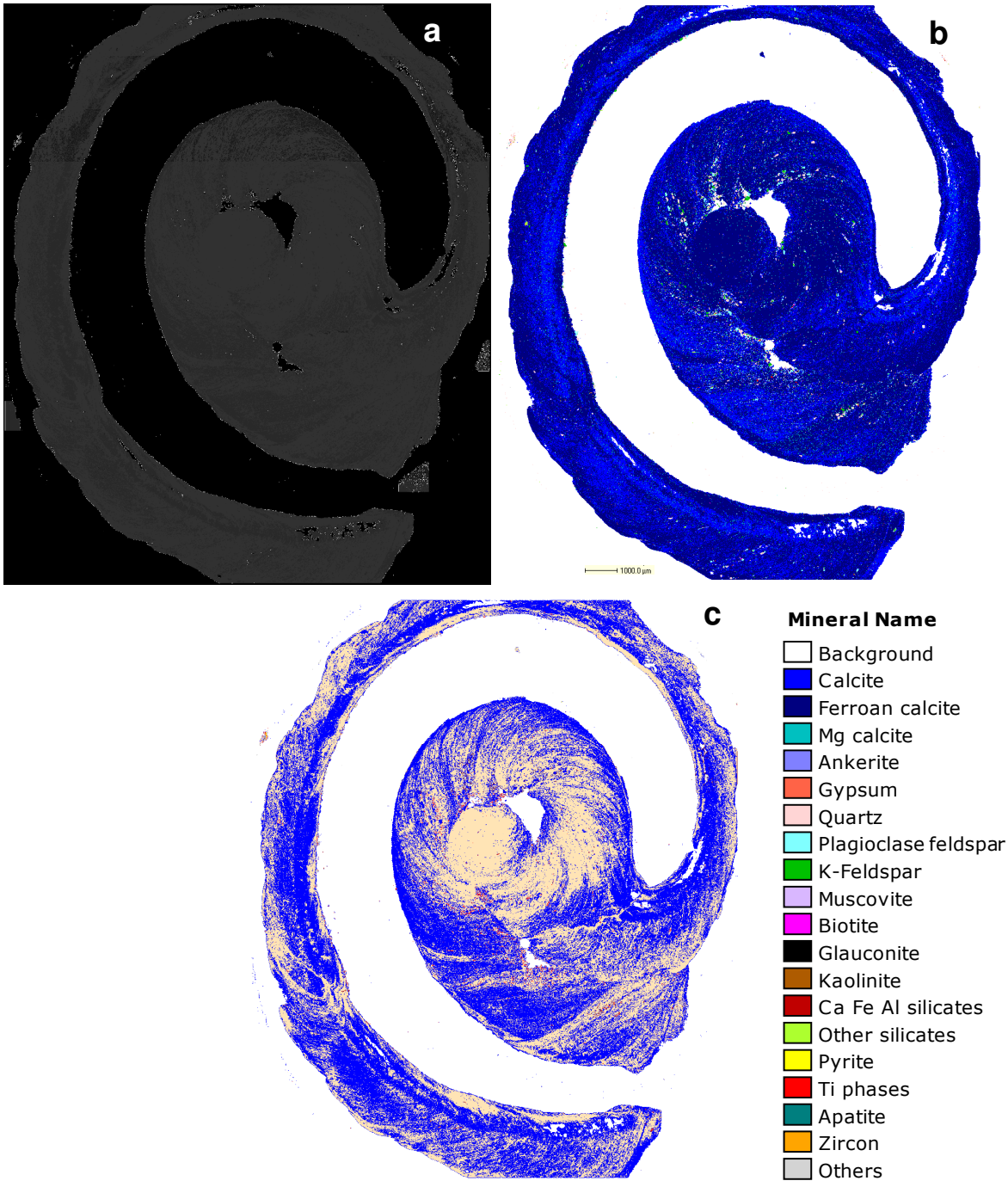

Figure 3-13. QEMSCAN BSE and false colour mineral classifications of a transverse section through a specimen of *Rotularia*, specimen id D5.212.855.2/A. Pixel spacing 5 µm, total number of X-Ray analysis points = 5,796,572. BSE mode (a) illustrates structure present within the calcareous worm tube. Colour classification (b) suggested that calcite was the predominant phase, but quantitative modal data showed that ferroan calcite had a larger modal percentage (calcite (vol %) = 33.51, ferroan calcite (vol %) = 61.20, Mg calcite (vol %) = 2.50). Modified colour classification (c) illustrates relative proportions of calcite and ferroan calcite. Note that with QEMSCAN data it is not possible to distinguish polymorphs and that for the purposes of analysis and reporting all calcium carbonate is treated as calcite. Scale bar 1 mm.

3.7 Conclusions

This chapter has presented the diagenetic screening methods that enabled an assessment of the overall suitability of individual specimens for inclusion in stable isotope analysis. Subsequent palaeotemperature determination was completed for those specimens deemed to be least altered after the completion of diagenetic evaluation. A key decision in the research planning for this study was that only specimens with aragonite skeletal carbonate would be selected for stable isotope analyses. As previously mentioned all of the macrofossil specimens selected for this study from the British Antarctic Survey (BAS) collection have been subject to a certain degree of diagenetic alteration (Marshall 1992). Diagenetic screening was intended to identify those specimens that show the least altered characteristics.

Three principal methods were used for the diagenetic screening of skeletal carbonate shell material namely; image analysis (SEM), mineralogical analysis by X-ray diffraction (XRD) and determination of trace element concentration by ICP-OES. Additional minor techniques included cold cathodoluminescence (CL), carbonate staining and automated SEM-EDS analysis using QEMSCAN technology. No single method can confidently identify those least altered specimens that were deemed suitable for stable isotope analyses. It is apparent that an over reliance on any single one of the three methods may lead to either the rejection of specimens that would have been suitable for further analysis or perhaps worse still the introduction of flawed analyses. Thus imaging of skeletal carbonate ultrastructure can identify the presence of neomorphic features in a specimen but cannot indicate the presence of diagenetic trace element indicators at below threshold concentrations. Likewise mineralogical analysis by XRD can identify the primary mineral phases present but will be unable to confirm the presence diagenetic features affecting the physical structure of the skeletal carbonate. The best and most reliable overall diagenetic screening methodology comprised the adoption of a combination of these three principal methods, each of which was scored or assessed before arriving at an overall suitability score for each individual specimen. However, within this study not all of the techniques were employed for each of the specimens; for example there were specimens with insufficient sample powders available for trace element analysis and others without SEM imaging. Consequently there are 117 specimens with no SEM images, 27 specimens with no XRD analysis and 44 specimens with no ICP-OES trace element screening. With these gaps in the diagenetic screening it was unfeasible to apply a single approach to diagenetic scoring of the specimens. Given the outstanding quality of the macrofossils from Seymour

Island and the good preservation state of the aragonitic specimens it seemed inappropriate to reject those specimens where the scoring process was incomplete.

Reviewing the diagenetic scoring data (see Appendix B, Table B-3) it was apparent that without ICP-OES trace element data it would be impossible to confirm whether diagenetic indicator elements (Fe and Mn) had elevated concentrations and whether Mg was present at a concentration in excess of the threshold of 1000 ppm for biogenic aragonite (Brand, 1991). Thus, where there was no XRD scoring it was possible to screen for aragonite by inspection of trace element data. Finally the lack of SEM imaging meant that it would be impossible to determine the presence of diagenetic features unless trace element analyses indicated elevated Fe or Mn levels.

For a fully effective and reliable diagenetic screening of skeletal material comprised of aragonite nacre all three principal techniques are required. Note that there was a fourth screening technique employed in this study through a comparison between the stable isotope data from screened specimens and partially screened specimens that lacked ICP-OES trace element data. This option was available due to the completion of the majority of stable isotope analyses prior to the commencement of trace element analyses. The primary outcome of this approach was that the majority of specimens were sampled, partially screened for diagenesis (SEM and XRD), analysed for stable isotopes and following subsequent ICP-OES trace element analysis were then found to be unsuitable for inclusion in both the stable isotope measurement data and the determination of palaeotemperatures.

The diagenetic screening indicates that 34 specimens were found to have a wholly unsuitable shell mineralogy for inclusion in further analyses. The remaining 213 specimens were all deemed to be suitable for stable isotope analysis but only 116 fully satisfied all of the screening requirements. From the remainder, 53 specimens showed Fe or Mn concentrations above the selected threshold levels (e.g. Fe ≥ 500 ppm and Mn ≥ 200 ppm) and the final 44 specimens recorded no trace element data. Further comparative screening of stable isotope data from screened and partially screened specimens will be further discussed in Appendix E.

3.7.1 Aragonite skeletal preservation

One obvious question that remains is why the preservation of the skeletal carbonates, in particular aragonite, is so good in the James Ross Basin. It is apparent that the basin underwent rapid infilling with a range of infill rates (for example ~270, 175 and 100 to 200 m/Ma^{-1} (MacDonald *et al*., 1988; McArthur *et al*., 1988; Dutton *et al*., 2007; Tobin *et al*., 2012). Based upon the section stratigraphy and GSSP ages an average rate of ~160 m/Ma^{-1} was calculated for this study (Gradstein *et al*., 2012).

Although the basin infill rate was rapid the presence of well preserved macrofossils with abundant aragonite nacre indicated a shallow burial depth (1 to 2 km) and an associated low temperature (~30 to <60°C) limited diagenesis (Svojtka *et al*., 2009; Tobin *et al*., 2012). The low burial temperature must have had a significant influence on restricting the diagenetic alteration of the skeletal carbonates. The lack of persistent diagenesis in aragonite nacre specimens suggests that conditions within the basin limited both the dissolution of primary aragonite and the subsequent precipitation of diagenetic cements (see Boggs, 2009; Petersen *et al*., 2016). The evidence of luminescence under CL for fractures infills in bivalves as reported by Petersen *et al*. (2016) but with no corresponding luminescence of the skeletal carbonate also indicated that limited diagenesis had occurred. Jordan *et al*. (2015) discussed the nature of aragonite preservation and reported that approximately 50% of carbonate sediments are preserved but this drops to 10% for aragonite. Dissolution of aragonite is inhibited where the sediment water interface is depleted in O_2, aragonite also undergoes dissolution at a higher pH (7.8) than calcite. The preservation of aragonite may be linked to buffering by sediment which inhibited dissolution by limiting change of pH. This scenario may reflect what occurred with the rapid infilling of the James Ross Basin limiting the rate of aragonite dissolution. Schoepfer *et al*. (2017) discussed the development of cyclic anoxic to euxinic conditions in the Late Maastrichtian to Early Danian James Ross Basin based upon the analysis of major and minor trace elements.

As previously described the presence of primary skeletal aragonite is rare in the Phanerozoic fossil record due to the metastable nature of the mineral, when present it provides a direct geochemical link to the palaeoenvironment in which the macrofauna flourished. The López de Bertodano Fm. contains a relatively low diversity but abundant invertebrate and vertebrate macrofauna and appears to be dominated by taxa with aragonite skeletal carbonate. Other studies have reported stable isotope and trace element data from taxa utilising just calcite skeletal carbonate, notably foraminifera, oysters and belemnites. But as this study has shown there appeared to be a strong basis for a correlation between calcitic shell material and evidence of extensive diagenesis, most notably within the trace element data.

However, due consideration must be be given for the style of shell material selected for stable isotope analysis. Whilst Tobin *et al*. (2012) and Tobin and Ward (2015) analysed both calcitic and aragonitic macrofossils the decision in this study to carry out stable isotope analyses on only aragonitic specimens will, in all certainty, have introduced a preservational bias.

4 Oxygen and carbon stable isotope analysis

4.1 Synopsis/Summary

In this chapter the nature and usage of the aragonite palaeothermometer is discussed and comparisons are made of palaeotemperatures calculated for differing levels of $\delta^{18}O_{water}$ in the Cretaceous ocean. Together with a further discussion of the significance of the stable isotope and palaeotemperature data generated. A comparison of these stable isotope and palaeotemperature data with that from recently published studies of macrofossil specimens from Seymour Island is also discussed. The nature and significance of the $\delta^{13}C$ record is also discussed and a comparison made with other recently published studies of late Cretaceous $\delta^{13}C$.

Details of the taxa selected for analysis are presented together with the analytical methods adopted for the stable isotope analyses. The suitability of the individual diagenetic screening methodologies are further described and discussed with reference to the stable isotope data. Whilst all carbonates are suitable for stable isotope analysis the intended outcome of the screening process (see Chapter 3) was to identify those specimens that were the least altered and retained a reliable palaeoclimate signal. It was anticipated that a further phase of the selection and screening process would take place after the measurement and correlation of oxygen and carbon stable isotopes from the diagenetically unaltered aragonite nacre shell material selected.

4.2 Palaeotemperature determination

Calcite and aragonite derived palaeotemperatures may be determined from fossil skeletal material provided no significant diagenetic changes have occurred. A comparison of the relative concentrations of Fe and Mn from fossil shell material with values from extant organisms where Mn (< 100 ppm) and Fe (< 250 ppm) provides an indication of whether samples have been subject to diagenesis (Morrison and Brand, 1988; Marshall 1992; Crame *et al*., 1999; Tobin *et al*., 2012). The possibility of Fe and Mn surface contamination of the carbonate shell material must also be considered. The Fe and Mn may only be loosely bound to the carbonate and may not be accommodated within the aragonite lattice. Thus high Fe or Mn concentrations may not necessarily indicate the presence of excessive diagenetic change to the skeletal carbonate shell material (see Chapter 3). The presence of elevated Fe and Mn levels in trace element analyses from Seymour Island as well as the selection of threshold levels for Fe and Mn was discussed in Tobin *et al*. (2012) and Petersen *et al*. (2016).

There was also an assumption that the organisms secreted their shell material in isotopic and chemical equilibrium with the seawater in which they lived. In which case there was no 'vital effect' in place whilst the shell was being grown and the oxygen stable isotope record derived from the bicarbonate taken up by the organism represented an accurate record of the $\delta^{13}C$ and $\delta^{18}O$ in the seawater. However, it was also noted in studies of extant species of bivalves and cephalopods that there was evidence which indicated that the carbonate shell material was subject, in certain cases, to a 'vital effect' during the formation of the shell material (Marshall *et al*., 1996; Tripati *et al*., 2010; Schöne *et al*., 2011; Lécuyer *et al*., 2012, 2013). For example, Lécuyer *et al*. (2012) reported that the oxygen isotope composition of biogenic aragonite might not reflect the mean annual seawater temperature but rather a mean temperature from the warm season. The authors also suggested that $\delta^{18}O$ values from molluscs were only reliable palaeotemperature proxies for low-mid latitudes, although this view was at odds with the significant body of high palaeolatitude studies (for example Tobin *et al*., 2012; Petersen *et al*., 2016). Indeed for high palaeolatitude sites this may be more difficult to reconcile due to the marked seasonality of specimen growth, Petersen *et al*. (2016) described the wide variability of the stable isotope range of Maastrichtian bivalves which they considered a combination of ontogenetic growth linked to distinct seasonality and modification of $\delta^{18}O_{water}$ by seasonal run off from the proximal landmass.

Lécuyer *et al*. (2012) also reported an isotopic enrichment for biogenic aragonite that affected both carbon and oxygen relative to biogenic calcite; $\delta^{13}C$ was enriched by +0.95±0.81‰ and $\delta^{18}O$ was enriched by +0.37±0.65‰. These results suggested precipitation of aragonite close to, but not in oxygen isotope equilibrium. Carbon isotope composition may be affected by non-equilibrium fractionation with higher $\delta^{13}C$ values expected from aragonitic shell material due to the enrichment of $\delta^{13}C$ by +1.7‰ in comparison with LMC (Romanek *et al*., 1992).

4.3 Macrofossil Types

See Table 4-1 for a summary of suitable macrofossil types selected for inclusion in the stable isotope analysis. Note that specimens identified as 'Ammonite', 'Bivalve', 'Gastropod' or 'Nautiloid' were not identifiable to genus level. There were 213 specimens selected after the completion of the initial diagenetic screening. Summary screened data for the macrofossil types selected for stable isotope analysis are presented in Appendix E, Tables E-2, 3, 4, 5 and 6. The corresponding trace element geochemical data are presented in Appendix d and Table D-7, 8, 9 and 10. A series of covariance plots of screened $\delta^{13}C$ and $\delta^{18}O$ data from aragonite macrofossils are

displayed with categorised data points, see Appendix E, Figures E-1, 2, 3, 4, 5, 6 and 7. A further series of plots that show the covariance between screened aragonite stable isotope date versus trace element data concentrations (ppm) are presented in Appendix E, Figures E-8, 9 and 10.

Table 4-1. Summary identification of specimens with genus selected for stable isotope analysis. A = ammonites, B = bivalves, G = gastropods, N = nautiloids and U = unclassified specimens.

Genus	**No.**	**Type**	**Genus**	**No.**	**Type**
Amberlaya	14	G	*Maorites*	17	A
Ammonite	9	A	Nautiloid	4	N
Bivalve	22	B	*Nucula*	49	B
Diplomoceras	1	A	*Oistotrigonia*	28	B
Eselaevitrigonia	43	B	*Pinna*	5	B
Gastropod	4	G	*Pleurotomaria*	2	G
Grossouvrites	1	A	*Solemya*	3	B
Lahillia	1	B	Unidentified	10	U

4.3.1 Habitat and fossil type

The data summarised in Table 4-2 illustrate the range of stable isotope values for identified molluscs categorised by habitat, the entries titled ‘Uncertain’ reflect those specimens where it was not possible to reliably identified the actual fossil type. Following the removal of specimens that were identified as having suffered from diagenesis the number of epifaunal and infaunal specimens was subject to a minimal change but nektonic specimens were significantly reduced in number. As a result the stratigraphic distribution of epifaunal and infaunal specimens was extensive and correspondingly of significant overall importance. Figures E-1 and 2 present a comparison of the stable isotope data for specimens classified by habitat and fossil type respectively. With a large number of specimens and a wide stratigraphic distribution the epifaunal and infaunal specimens (bivalves and gastropods) form the most important and influential part of the stable isotope dataset. Unfortunately there was found to be a paucity of suitable specimens in the stratigraphy from 900 m to 1084 m, this section also included the position of the K-Pg boundary.

4.3.2 Bivalves

The data summarised in Table 4-3 illustrate the range of stable isotope values for identified bivalve molluscs, the entries titled ‘Bivalve’ reflect those specimens that were correctly identified as bivalves but for which no genus was identified. Following the removal of specimens that were identified as having suffered from diagenesis the number of bivalves was subject to minimal change. As a result their stratigraphic distribution was extensive and correspondingly of significant overall importance. Figures E-3 and 4 present a comparison of the stable isotope data for bivalves. The

$\delta^{13}C$ data for *Solemya* indicates that the specimens were either subject to post-mortem early stage diagenesis or that the bicarbonate was depleted in ^{13}C.

Table 4-2. Summary screened stable isotope trace element geochemical data classified by habitat selected for analysis. Stable isotope data reported as standard per mil (‰ VPDB) and trace element analyses (ppm) below detection limits = b/d.

Epifaunal	**$\delta^{13}C$**	**$\delta^{18}O$**	**Mg**	**Sr**	**Na**	**Fe**	**Mn**	**T (°C)**
Mean	1.99	1.12	154	3037	6119	325	114	11.4
Minima	-0.19	0.72						
Maxima	3.33	1.42						
Std Err	0.96	0.17						
Std Dev	0.94	0.17						
Count	20	20						
Conf Level (95%)	1.89	0.34						
Infaunal	**$\delta^{13}C$**	**$\delta^{18}O$**	**Mg**	**Sr**	**Na**	**Fe**	**Mn**	**T (°C)**
Mean	1.43	1.24	153	2788	5778	167	230	10.9
Minima	-10.49	0.26						
Maxima	4.34	2.11						
Std Err	2.26	0.40						
Std Dev	2.26	0.41						
Count	128	128						
Conf Level (95%)	4.43	0.79						
Nektonic	**$\delta^{13}C$**	**$\delta^{18}O$**	**Mg**	**Sr**	**Na**	**Fe**	**Mn**	**T (°C)**
Mean	-1.62	0.99	396	4766	4530	592	224	12.0
Minima	-5.18	0.13						
Maxima	1.56	1.53						
Std Err	1.58	0.32						
Std Dev	1.67	0.32						
Count	31	31						
Conf Level (95%)	3.10	0.63						
Uncertain	**$\delta^{13}C$**	**$\delta^{18}O$**	**Mg**	**Sr**	**Na**	**Fe**	**Mn**	**T (°C)**
Mean	1.61	1.20	101	2273	5357	164	47	11.1
Minima	-1.51	-0.06						
Maxima	2.91	1.92						
Std Err	1.00	0.42						
Std Dev	1.09	0.43						
Count	33	33						
Conf Level (95%)	1.95	0.83						

Little *et al*. (2015) reported on the occurrence of methane seeps in the James Ross Basin. The authors identified Solemyids as a bivalve group that were actively involved in colonising methane seep environments and which had thiotrophic chemosymbionts involved in the anaerobic oxidation of methane. What was unexpected was that the range of $\delta^{13}C$ data for *Solemya* specimens was more positive than might be expected (Little *et al*., 2015). Actual $\delta^{13}C$ data (minima -10.49, maxima -5.99 and mean -8.01‰) have more in common with $\delta^{13}C$ data from Snow Hill Island although still more positive than the range reported (minima -20.4 and maxima -10.7‰) (Little *et al*., 2015).

Bivalve specimens represent ~74% of the stable isotope data and with a wide stratigraphic distribution they form the most important and influential part of the stable isotope dataset. However, there was a noticeable lack of specimens in the section between 900 m to 1084 m and this caused some difficulties in correlation of data from this study with that from other recent Seymour Island studies.

Table 4-3. Summary screened stable isotope trace element geochemical data for bivalve taxa selected for analysis. Stable isotope data reported as standard per mil (‰ VPDB) and trace element analyses (ppm) below detection limits = b/d.

Eselaevitrigonia	**$\delta^{13}C$**	**$\delta^{18}O$**	**Mg**	**Sr**	**Na**	**Fe**	**Mn**	**T (°C)**
Mean	1.71	1.28	93	2838	6062	101	42	9.8
Minima	-5.06	0.70						
Maxima	3.70	2.02						
Std Err	1.68	0.40						
Std Dev	1.69	0.39						
Count	25	25						
Lahillia	**$\delta^{13}C$**	**$\delta^{18}O$**	**Mg**	**Sr**	**Na**	**Fe**	**Mn**	**T (°C)**
D5.215.696.2/AV	3.29	1.47	42	3252	3977	137	28	9.0
Nucula	**$\delta^{13}C$**	**$\delta^{18}O$**	**Mg**	**Sr**	**Na**	**Fe**	**Mn**	**T (°C)**
Mean	2.11	1.52	116	3837	5899	95	47	8.8
Minima	-0.51	0.49						
Maxima	3.65	2.05						
Std Err	1.10	0.46						
Std Dev	1.09	0.49						
Count	13	13						
Oistotrigonia	**$\delta^{13}C$**	**$\delta^{18}O$**	**Mg**	**Sr**	**Na**	**Fe**	**Mn**	**T (°C)**
Mean	2.13	0.95	68	1565	5930	86	32	11.3
Minima	0.81	0.59						
Maxima	3.26	1.49						
Std Err	0.64	0.22						
Std Dev	0.64	0.22						
Count	23	23						
Pinna	**$\delta^{13}C$**	**$\delta^{18}O$**	**Mg**	**Sr**	**Na**	**Fe**	**Mn**	**T (°C)**
D5.215.216.2/A	2.44	0.92	b/d	2541	3417	181	b/d	11.4
Solemya	**$\delta^{13}C$**	**$\delta^{18}O$**	**Mg**	**Sr**	**Na**	**Fe**	**Mn**	**T (°C)**
Mean	-8.01	1.05	684	6768	2776	78	100	10.8
Minima	-10.49	0.99						
Maxima	-5.99	1.11						
Std Err	2.09	0.09						
Std Dev	2.29	0.06						
Count	3	3						
Bivalve	**$\delta^{13}C$**	**$\delta^{18}O$**	**Mg**	**Sr**	**Na**	**Fe**	**Mn**	**T (°C)**
Mean	2.09	1.32	63	2102	5460	121	15	9.7
Minima	-0.04	0.86						
Maxima	2.91	1.92						
Std Err	0.67	0.35						
Std Dev	0.69	0.34						
Count	18	18						

4.3.3 Cephalopods

The data summarised in Table 4-4 illustrate the range of stable isotope values for identified cephalopod molluscs, the entries titled 'Ammonite' and 'Nautiloid' reflect those specimens that were correctly identified as ammonites or nautiloids but for which no genus was identified. Following the removal of specimens that were identified as having suffered from diagenesis the number of cephalopods was significantly reduced. As a result their stratigraphic distribution was limited and correspondingly of less overall importance. Figures E-5 and 6 present a comparison of the stable isotope data for cephalopods. The $\delta^{13}C$ data for *Maorites* indicates that the specimens were either

subject to post-mortem early stage diagenesis or that the bicarbonate was depleted in ^{13}C.

Table 4-4. Summary geochemical data for stable isotopes, major element and trace elements from selected cephalopod molluscs.

Diplomoceras	**$\delta^{13}C$**	**$\delta^{18}O$**	**Mg**	**Sr**	**Na**	**Fe**	**Mn**	**T (°C)**
D5.215.955.3/A	-1.63	1.44	426	4327	6719	179	61	9.1
Grossouvrites	**$\delta^{13}C$**	**$\delta^{18}O$**	**Mg**	**Sr**	**Na**	**Fe**	**Mn**	**T (°C)**
D5.215.691.2/B	-1.32	0.53	178	3195	7506	369	15	13.1
Maorites	**$\delta^{13}C$**	**$\delta^{18}O$**	**Mg**	**Sr**	**Na**	**Fe**	**Mn**	**T (°C)**
Mean	-2.09	1.03	362	5283	4783	159	90	10.9
Minima	-5.18	0.76						
Maxima	1.18	1.33						
Std Err	2.69	0.23						
Std Dev	2.38	0.26						
Count	5	5						
Ammonite	**$\delta^{13}C$**	**$\delta^{18}O$**	**Mg**	**Sr**	**Na**	**Fe**	**Mn**	**T (°C)**
Mean	-1.48	1.04	165	4107	4106	240	22	10.9
Minima	-3.96	0.88						
Maxima	0.54	1.27						
Std Err	0.15	0.20						
Std Dev	2.22	0.17						
Count	4	4						
Nautiloid	**$\delta^{13}C$**	**$\delta^{18}O$**	**Mg**	**Sr**	**Na**	**Fe**	**Mn**	**T (°C)**
Mean	-2.09	0.69	229	3572	4332	144	49	12.4
Minima	-3.47	0.56						
Maxima	0.06	0.77						
Std Err	0.43	0.13						
Std Dev	1.89	0.12						
Count	3	3						

4.3.4 Gastropods

The data summarised in Table 4-5 illustrate the range of stable isotope values for identified gastropod molluscs, the entries titled 'Gastropod' reflect those specimens that were correctly identified as gastropods but for which no genus was identified. Following the removal of specimens that were identified as having suffered from diagenesis the number of gastropods was subject to a minimal change. With few specimens their stratigraphic distribution was restricted. Figure E-7presents a comparison of the stable isotope data for gastropods which form an important part of the stable isotope dataset.

Table 4-5. Summary geochemical data for stable isotopes and trace elements from selected gastropod molluscs.

Amberlaya	**$\delta^{13}C$**	**$\delta^{18}O$**	**Mg**	**Sr**	**Na**	**Fe**	**Mn**	**T (°C)**
Mean	2.38	1.15	111	3154	6403	64	67	10.4
Minima	0.51	0.72						
Maxima	3.28	1.42						
Std Err	0.85	0.23						
Std Dev	0.81	0.22						
Count	9	9						
Pleurotomaria	**$\delta^{13}C$**	**$\delta^{18}O$**	**Mg**	**Sr**	**Na**	**Fe**	**Mn**	**T (°C)**
Mean	0.92	1.00	89	3692	6467	70	24	11.1
Minima	-0.19	0.97						
Maxima	2.02	1.03						
Count	2	2						

Gastropod	$\delta^{13}C$	$\delta^{18}O$	Mg	Sr	Na	Fe	Mn	T (°C)
D5.215.361.2/A	2.40	1.04	87	2001	4491	b/d	19	10.9

4.3.5 Unidentified molluscs

The data summarised in Table 4-6 illustrate the range of stable isotope values for unidentified molluscs and reflects those specimens for which no genus was identified. Following the removal of specimens that were identified as having suffered from diagenesis the number of unidentified specimens was subject to a minimal change. With few specimens their stratigraphic distribution was restricted. Figure E-8 presents a comparison of the stable isotope data for unidentified specimens which form part of the stable isotope dataset.

Table 4-6. Summary geochemical data for stable isotopes and trace elements from unidentified molluscs.

Unidentified	$\delta^{13}C$	$\delta^{18}O$	Mg	Sr	Na	Fe	Mn	T (°C)
Mean	1.15	0.94	61	2374	4509	102	5	11.3
Minima	-1.51	-0.06						
Maxima	2.64	1.55						
Std Err	1.28	0.40						
Std Dev	1.35	0.49						
Count	8	8						

4.4 Stable isotope variability

The stable isotope data presented in Tables 4-2, 3, 4, 5 and 6 showed that at individual stratigraphic levels, the ranges of measured $\delta^{18}O$ exhibited significant variability i.e. +0.9 to +1.1‰ at 343 m, +0.8 to +2.1‰ at 613 m, +0.8 to +1.7‰ at 712 m and +1.3 to +1.7‰ at 1084 m (K-Pg boundary located at 1029 m above datum) (Thorn *et al*., 2009). It seemed improbable that all of this variability was ascribed to the operation of environmental change. It has been shown in previous studies that stable isotope variability within stratigraphy may result from the operation of inequilibrium growth of shell material with respect to the $\delta^{18}O_{water}$, and that species specific 'vital effects' may be more common than expected (Morrison and Brand, 1988; Marshall *et al*., 1996; Voigt *et al*., 2003; Weiner and Dove 2003; Eiler 2011; Schöne *et al*., 2011; Lecuyer *et al*. (2012); Tobin *et al*., 2012; Grauel *et al*., 2013; Petersen *et al*., 2016).

Marshall *et al*. (1996) discussed the carbon and oxygen stable isotope composition of skeletal aragonite from extant Antarctic marine invertebrates; the oxygen isotopic values exhibited a considerable overall range from +0.8 to +3.8‰ and by 2‰ parts within individual specimens. The authors reported that the most positive values were compatible with equilibrium precipitation from ambient seawater but the range of measured values was difficult to reconcile with equilibrium precipitation given the narrow annual range of environmental temperatures and measured water compositions, even assuming a bias toward shell precipitation during the austral

summer. Vital effects cannot therefore be ruled out. Carbon isotopic values range from -0.2‰ to +2.2‰ VPDB and show an overall pattern of covariance with the oxygen data. They concluded that most of the variation was from seasonal changes in food supply and dissolved bicarbonate composition, although vital effects might also be involved. The range and variability of isotopic composition in samples collected from an environmentally stable site demonstrates the potential for inherent inhomogeneity in the isotopic record and provides a cautionary tale for those attempting to interpret similar data sets from the fossil record (Marshall *et al*., 1996).

Petersen *et al*. (2016) reported on the possible effects of localised continental run-off and sampling from seasonal growth when considering the range of $\delta^{18}O$ values in their dataset. If 'vital effects' were in operation then this has a potentially significant impact on the selection of macrofossil specimens and sample data for palaeoenvironmental purposes.

Despite screening the $\delta^{18}O$ data there still remains the question of the isotopically lighter $\delta^{13}C$ values in some samples suggesting that significant diagenetic alteration may have occurred (Marshall 1992). Low carbon values associated with 'marine' oxygen probably indicated contamination by early diagenetic carbonate related to organic degradation (Marshall 1992). Data have also been published that described Late Cretaceous (Maastrichtian) shallow water hydrocarbon seeps from Snow Hill and Seymour Islands (for example Little *et al*., 2015). The carbon isotopic composition of marine carbonates reflects the isotopic composition of dissolved inorganic carbon; carbon isotopic fractionation between $CaCO_3$ and the dissolved carbon is generally independent of temperature in sedimentary environments (Grossman and Ku 1986; Romanek *et al*., 1992). For a stratified seawater column the $^{13}C/^{12}C$ ratio of the dissolved inorganic carbon in surface waters will be higher than that in deep waters due to oxidation of ^{13}C depleted particulate organic matter by microorganisms in deep waters and in sediments (Kroopnick 1985). The vertical profile of $^{13}C/^{12}C$ should thus reflect the extent of biological cycling of carbon in the water column. Significant differences in stable isotope compositions may exist between organisms that lived at differing depths in a stratified seawater column. For a well mixed water column, these differences would be obliterated. However, the extensive variability observed in this study for $\delta^{13}C$ at specific stratigraphic positions and for a benthic fauna suggests that other mechanisms were responsible. Possibly through the development of early stage diagenetic carbonate contamination (Boggs, 2009).

Previous studies of the Latest Maastrichtian – Early Palaeocene section from Seymour Island had also considered the covariance between levels of Fe and Mn and the degree of diagenesis (Tobin *et al*., 2012; Petersen *et al*., 2016) and addressed the

issue in the following manner. Filtering the stable isotope data set at differing levels of the two primary diagenetic markers, Fe and Mn, and comparing the overall impact upon the remainder of the stable isotope data. In the case of this study screening of the data reduced the overall data set but made little overall difference to the variability exhibited by the stable isotope data. Care must be taken when reviewing the significance of trace element diagenetic indicators since the presence of medium-high trace element concentrations does not necessarily indicate that the cations of interest were present in the carbonate lattice. It seemed probable that a proportion of the apparent Fe and Mn diagenetic signature may only represent surface contamination by oxyhydroxide minerals together with the presence of microscopic grains of framboidal pyrite (Schoepfer *et al*., 2017).

Based upon previous work (Morrison and Brand, 1988; Brand, 1991) a substantial portion of the data set would be rejected because of the high Fe and Mn levels, however the range of $\delta^{18}O$ values were well constrained and indicated that the data were acceptable for inclusion in the final data set. Recent published works relating to Late Maastrichtian stable isotope studies (Tobin *et al*., 2012; Petersen *et al*., 2016) also discussed the nature of the potential impact of trace element geochemistry with concentrations above recommended guidelines (Morrison and Brand, 1988; Brand, 1991; Anderson *et al*., 1994; Ditchfield *et al*., 1994; Petersen *et al*., 2016). Discriminating within their data set such that only specimens with trace element levels below guidelines were included, their conclusion was that 'culling the data by removing shells outside the limits for each trace element did not alter the overall $\delta^{18}O$ pattern' (Tobin *et al*., 2012).

Large variations in $\delta^{13}C$ were also observed for ammonites (this study; Tobin *et al*., 2012; Tobin and Ward 2015), removal of specimens with isotopically light $\delta^{13}C$ values had little overall effect on the oxygen isotope data set but obviously had a larger impact on the observed range of $\delta^{13}C$. However, comparison of the $\delta^{13}C$ ranges observed in the rejected specimens (see Figure D-1(a) - LMC and high Mg data set) exhibited a $\delta^{13}C$ range ~25‰, the majority of these specimens were ammonites with the remainder representing bivalves. The corresponding $\delta^{13}C$ range for the screened aragonite specimens (see Figure D -1(b)) was ~12‰, where the lightest value was from a specimen of *Solemya rossiana*. The corresponding $\delta^{13}C$ range for the expanded grouping of aragonite specimens (see Figure D -1(c)) was ~16‰, where the lightest values were from a specimens of *Solemya rossiana*. If the data associated with specimens of *Solemya rossiana* in Figure D -1(b and c) are ignored then no discernible difference existed in the $\delta^{13}C$ range.

A further comparison of screened $\delta^{13}C$ and $\delta^{18}O$ data versus key diagenetic trace elements (Mg, Fe, Mn, Sr and Na) are presented in Figures E-8 and 9. In each covariance plot blue symbols represent specimens exhibiting Mg < 1000 ppm, Fe < 500 ppm and Mn < 200 ppm and orange symbols represent specimens with Fe or Mn concentrations that exceeded the diagenetic threshold (Fe > 500 ppm and Mn > 200 ppm). It can be seen that in no case does the inclusion of specimens that exhibited elevated levels of either Fe or Mn result in an expansion of the overall range of the stable isotope data. This further confirmed the view put forward by Tobin *et al*. (2012) with regard to the inclusion of specimens that exhibited elevated Fe and Mn levels.

Covariance plots of Ca vs. $\delta^{13}C$ and Ca vs. $\delta^{18}O$ are also presented, see Figure E-10. There is a close clustering of the $\delta^{18}O$ (-0.06 – +2.2‰) data with respect to the Ca (37 – 42%) where the Ca values reflect a normal range for biogenic aragonite. A similar, but tighter, cluster exists for the $\delta^{13}C$ data. Figure E-11 presents an initial correlation of the partially screened stable isotope versus the stratigraphy of the Latest Maastrichtian López de Bertodano Fm. section on Seymour Island, Antarctica showing the position of unscreened $\delta^{18}O$ data categorised by habitat. Data coverage is generally good but there are gaps in the data for sections D5.201, D5.212 and D5.229 which reflect a lack of suitable macrofossil specimens. The position of the K-Pg boundary at 1029 m above section base was defined by palynological analysis (Thorn *et al*., 2009). (Ivany *et al*., 2008) quote a similar variability for stable isotope data in the Eocene La Meseta Fm. from Seymour Island. Whilst (Latal *et al*., 2006) quote a similar $\delta^{18}O$ variability for gastropods from the Central Paratethys (Europe) around the Lower/Middle Miocene transition.

A comparison of stratigraphy vs partially screened aragonite $\delta^{13}C$ and $\delta^{18}O$ data categorised by habitat is presented (see Figure E-12) with the K-Pg boundary inferred from palynology (Thorn *et al*., 2009). Note the wide variability in data exhibited by the infaunal samples. The ‘Uncertain’ category represents specimens where it was not possible to identify a specific fossil type and habitat but where the fragmentary shell material was of sufficient quality to pass diagenetic screening. Note that with the exception of a single value in the ‘Uncertain’ category (-0.06‰) all $\delta^{18}O$ data were > 0.0‰. The 3 lightest infaunal $\delta^{13}C$ values represent specimens of the bivalve *Solemya rossiana* that have thiotrophic chemosymbionts involved in the anaerobic oxidation of methane (Little *et al*., 2015). A similar plot compares the stratigraphy vs fossil type (see Figure E-13) note the wide variability in $\delta^{13}C$ exhibited by the bivalve category.

4.5 James Ross Basin - Water stratification

An intended objective for this research was to compare the oxygen stable isotope data derived from stratigraphically paired benthic – pelagic taxa in order to determine

whether any evidence of water stratification existed. With an extensive data set there should have been no problem with this approach with the pelagic data provided from the analysis of shell material from cephalopod molluscs, namely ammonites and nautiloids. However, the viability of this particular analytical approach was questioned in Lukeneder *et al*. (2010), they stated that stable isotope analyses ($\delta^{18}O$, $\delta^{13}C$) on ammonoids are numerous but typically data were obtained as single-point measurements and combined with other taxa of coeval stratigraphic positions. These studies were typically designed to reveal ocean water temperatures at distinct time slices, neglecting the enormous effect on the isotope composition due to migration and habitat change (Lukeneder *et al*., 2010). As $\delta^{18}O$ data from single cephalopod shells can range around 2.00‰, spanning a temperature range of almost 8–10°C, these "one-measurement per shell-data" are inappropriate for palaeotemperature estimations (Lukeneder *et al*., 2010). The ranges are ontogenetically induced and single point measurements will snap-shot ocean water temperatures at a very specific point of development only (Lukeneder *et al*., 2010). Note that (Lukeneder *et al*., 2010) are commenting with reference to reconstructing the ontogenetic development of a suitable taxon based upon stable isotope analyses but the criticism also remains true, perhaps with more significance, for the comparison of data derived from paired benthic – pelagic taxa.

Previous authors have published data indicating that present day cephalopods occupy differing depths during life as determined by stable isotope analysis (Cochran *et al*., 1981; Auclair *et al*., 2004; Lukeneder *et al*., 2010) these studies related to the ontogenetic stable isotope record of *Nautilus pompilius* (Cochran *et al*., 1981) and *Nautilus macromphalus* (Auclair *et al*., 2004). The extant cephalopod mollusc *Nautilus* has an overall mode of life that differs from that of nektonic Mesozoic cephalopoda but it does provide an analogous proxy with some similarities. Thus it is reasonable to consider that specific stages of the ammonite life cycle took place at differing depths within the water column. Without a rigorous control over the specific stage of the ammonite life cycle from which the sample powder was collected it would be difficult to draw conclusions about water stratification based purely upon spot stable isotope data. In which case determining any correlation between a sessile benthic taxon and an active nektonic taxon would only be successful if the nektonic taxon was either confined at a specific waterdepth or the shell material being analysed was sampled from a portion of the shell at a known point during the ontogenetic development of an individual specimen.

A comparison of $\delta^{18}O$ data from a limited set of stratigraphically paired benthic – nektonic taxa is presented in Figure 4-1, the plot illustrates the only suitable

stratigraphic positions at which there were benthic and nektonic taxa following diagenetic screening. Nektonic taxa show the lightest (warmer temperatures) $\delta^{18}O$ values (~0.5 to ~1.3‰) and benthic taxa show either heavier (cooler temperatures) $\delta^{18}O$ values (~0.5 to ~2.15‰) or a wider overall spread of $\delta^{18}O$ values. Conversely the benthic taxa at 636 m and 642 m also show a range of lighter (warmer temperatures) $\delta^{18}O$ values. Whilst some indication of possible temperature stratification exists the available data are stratigraphically limited in extent.

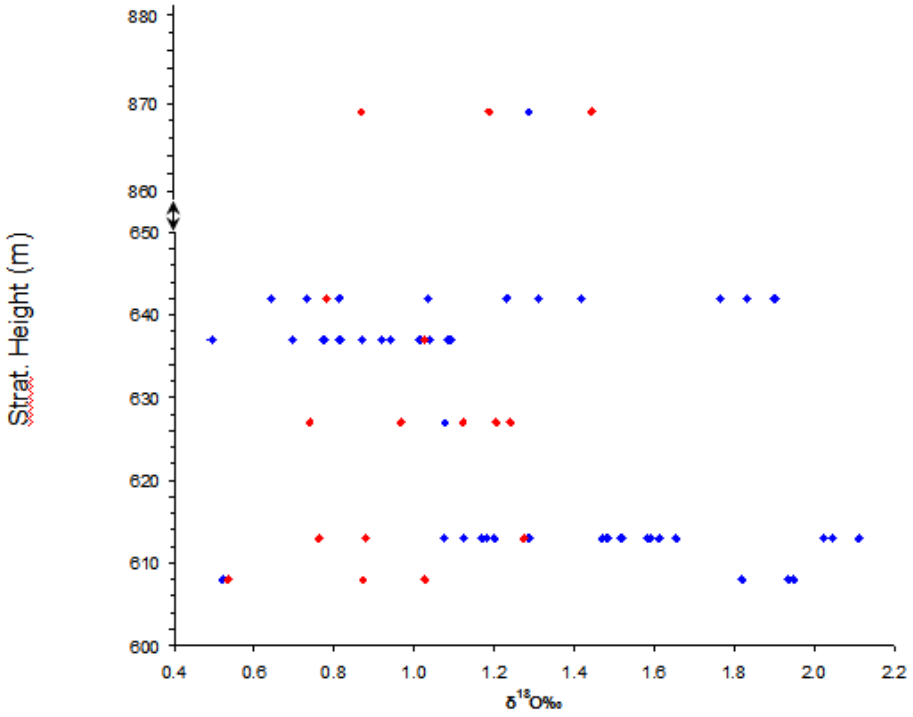

Figure 4-1. Comparison of screened $\delta^{18}O$ data from stratigraphically paired benthic – nektonic taxa, Note that following diagenetic screening the only available candidate pairs were at the stratigraphic positions plotted. Nektonic taxa show the lightest $\delta^{18}O$ values (~0.5 to 1.3‰) which correlate with warmer temperatures and benthic taxa show either heavier (cooler temperatures) $\delta^{18}O$ values (~0.5 to 2.15‰) or a wider spread of $\delta^{18}O$ values. Conversely the benthic taxa at 636 m and 642 m also show a range of lighter $\delta^{18}O$ values. Whilst some indication of possible temperature stratification exists the available data are stratigraphically limited in extent.

4.6 Stable isotope record - Discussion

Screened stable isotope data for primary aragonite from bivalves, cephalopods and gastropods exhibited a range of -0.06 to +2.1‰ for $\delta^{18}O$ and -10.49 to +4.34‰ for $\delta^{13}C$. Note that the range of $\delta^{13}C$ is considerably expanded by the presence of 3 specimens of *Solemya rossiana*, which have thiotrophic chemosymbionts involved in the anaerobic oxidation of methane (Little *et al.*, 2015). Screened stable isotope data show that at individual stratigraphic levels the range in screened $\delta^{18}O$ exhibits significant variability i.e. +0.9 to +1.1‰ at 343 m, +0.8 to +2.1‰ at 613 m, +0.8 to +1.7‰ at 712 m and +1.3 to +1.7‰ at 1084 m all with respect to the K-Pg boundary (1029 m above datum, as defined by palynology (Thorn *et al.*, 2009). Organisms

generally deposit biogenic carbonates (e.g. calcite and aragonite) under equilibrium conditions with respect to seawater (Weiner and Dove 2003). Bivalve molluscs with a benthic mode of life exhibited the widest range of $\delta^{18}O$ and $\delta^{13}C$ values, in the latter case it should be noted that the $\delta^{13}C$ range was enhanced by the presence of 3 isotopically light specimens of *Solemya rossiana*.

The variability seen in the $\delta^{18}O$ stable isotope data in this study was similar to that exhibited by a high latitude present day shallow marine molluscan assemblage from Antarctica (Marshall *et al*., 1996). Comparison of the stable isotope data from this study with recently published results (Tobin *et al*., 2012; Tobin and Ward, 2015; Petersen *et al*., 2016) from Seymour Island, Antarctica showed that a similar level of stable isotope variability was also present. A similar $\delta^{18}O$ variability was noted for Eocene macrofossils from the La Meseta Fm. on Seymour Island (Gaździcki *et al*., 1992; Ivany *et al*., 2003) and a similar $\delta^{18}O$ variability was also recorded for gastropods (Latal *et al*., 2006) from the Central Paratethys (Europe) around the Lower/Middle Miocene transition.

Relative palaeotemperatures (°C) were calculated for screened $\delta^{18}O$ values for a constant seawater composition of -1.0‰ (SMOW), representing ice free ocean water (Shackleton and Kennett 1975). The value of SMOW may require modification for parts of the succession since there is evidence that a lowering of sea level, as a result of glacioeustasy, occurred during the Latest Maastrichtian (Miller *et al*., 2005; Haq, 2014). In which case a value of -0.9‰ (SMOW) may better reflect the $\delta^{18}O$ state of the seawater (Price, 1999). Alternatively, if there was substantial mixing with freshwater run-off then a value of -1.5‰ (SMOW) may be more appropriate (Price, 1999). Stable isotope data show that individual stratigraphic levels can exhibit significant variability for $\delta^{18}O$ and $\delta^{13}C$ and that as a result analysis of single samples at discrete stratigraphic levels may provide an erroneous interpretation of climate change. Previous studies using single results at discrete stratigraphic levels, a common approach may suggest climate was much more variable. This high resolution data set with multiple analyses at discrete stratigraphic levels was intended to provide an opportunity to compare stable isotope data from both benthic and pelagic macrofossils at corresponding levels. The data set also enables an investigation of water stratification within the Latest Maastrichtian James Ross Basin. Key events recognised from palynology (Thorn *et al*., 2009; Bowman *et al*., 2012; Bowman *et al*., 2013) appear to be associated with low oxygen isotope values and may reflect periods of warmer climate; higher oxygen isotope values were seen mid-section and may reflect periods of cooler climate.

The extensive ~1100 m thick Latest Maastrichtian – Earliest Danian section on Seymour Island generated a high resolution oxygen and carbon stable isotope record. The data set enabled the comparison of the stable isotope data from benthic and pelagic macrofossils at corresponding levels within the measured succession. There was good overall coverage of stable isotope data in the succession within the measured stratigraphy that included measurements to within 1 m of the K-PG boundary. There were fewer macrofossils deemed suitable for isotopic analysis at the top of the section and this was most noticeable in the upper 280 m of the section. Unusually for this data set the majority of the specimens selected from this section of the stratigraphy were ammonites. This paucity of of suitable specimens in the upper portion of the section was in marked contrast to the number of specimens selected by Tobin *et al*. (2012) and Petersen *et al*. (2016).

The study has provided a high resolution stable isotope data set for the interval studied, with a range of -0.06 to +2.1‰ for $\delta^{18}O$ derived from screened data. Data indicated that individual stratigraphic levels exhibited significant variability for $\delta^{18}O$ and $\delta^{13}C$ and that as a consequence analysis of single samples at discrete stratigraphic levels might provide an erroneous interpretation of climate change. Samples with Mg, Fe and Mn trace element concentrations above published guidelines (Morrison and Brand, 1988; Brand, 1991) were excluded from the data set but the presence of surface contamination of the aragonite nacre shell material may have caused the trace element data to highlight potential diagenetic issues without actually representing the true cation levels present within the aragonite lattice, see Chapter 3 and Appendix D for a more detailed explanation. Screened oxygen isotope values range from -0.06 to +2.1‰ $\delta^{18}O$ and corresponding carbon isotope values range from -10.8 to +4.3‰ $\delta^{13}C$.

Isotope data were not recorded below 311 m above datum, due to a lack of suitably preserved macrofossil specimens. Highest oxygen isotope values are in mid section and may be associated with periods of cooler climate. However, the wide variability of the stable isotope values, in particular that for $\delta^{18}O$, suggests that the interpretation of warmer or cooler climatic conditions may be problematic.

4.6.1 Oxygen isotope variability

The wide variability in the $\delta^{18}O$ data within the measured stratigraphy and at specific stratigraphic levels cannot be entirely dependent upon diagenetic alteration. Diagenesis of the skeletal aragonite has been discussed in this chapter as well as in Chapter 3 and it was shown that even specimens with elevated levels of Fe and Mn had a minimal effect on the overall variability of the stable isotope data. It seems unlikely that diagenesis was wholly responsible for the variability of the stable isotope

data. Similar variability was quoted for stable isotope data from extant shallow marine invertebrates from Antarctica (Marshall *et al*., 1996) and in the Eocene La Meseta Fm. from Seymour Island, Antarctica (Ivany *et al*., 2008). Whilst Latal *et al*. (2006) quote a similar $\delta^{18}O$ variability for gastropods from the Central Paratethys (Europe) around the Lower/Middle Miocene transition. Further recent stable isotope data from Seymour Island also show a similar variability (Tobin *et al*., 2012; Tobin and Ward, 2015; Petersen *et al*., 2016). Isotopic mixing caused by the runoff of fresh water was proposed as a mechanism for the observed variability by Petersen *et al*. (2016). Whilst it is plausible that the variability resulted from isotopic mixing at discrete positions within the stratigraphy it seems less likely that the overall variability at stratigraphic levels reflect mixing.

4.7 Palaeotemperature determination

Temperatures were calculated using a range of values for the $\delta^{18}O$ seawater composition with respect to the SMOW standard, values adopted were -0.8, -1.0, -1.2 and -1.5‰, with the range of calculated palaeotemperatures presented in Table 4-7. The range of palaeotemperatures for gastropods are 9.2 to 12.3 (℃), for cephalopods 8.8 to 14.8 (℃), for bivalves 6.2 to 14.3 (℃) and for specimens of an uncertain classification 8.7 to 15.7 (℃). The gastropods exhibit a smaller temperature range than the bivalves but both are benthic, it is probable that the difference reflects a difference between epifaunal and infaunal modes of life. The relatively cool temperatures are generally consistent but with a reduced overall range of temperatures in comparison with data from previous studies (Tobin *et al*., 2012; Petersen *et al*., 2016). Temperatures indicated that at altitude ice may have been present at the pole.

4.7.1 Seymour Island palaeotemperatures

The stable isotope data indicated cool and relatively stable benthic temperatures of ~10℃ for the measured section, see Table 4-7. A significant variability also exists within the $\delta^{13}C$ isotope data. The overall variability in the isotope data complicated any attempt to generate an accurate stable isotope or temperature trend from the data. A correlation of palaeotemperature versus the López De Bertodano Fm. stratigraphy is presented in Figure 4-2 that illustrates the range of calculated palaeotemperatures derived from the $\delta^{18}O$ data. Note that the entire screened stable isotope data set is presented in Figure 4-2.

Table 4-7. Range of palaeotemperatures calculated from the $\delta^{18}O$ stable isotope data for a range of constant seawater compositions with respect to the SMOW standard.

	$\delta^{18}O$‰			Temperature (°C) [SMOW]							
Type	**Avg**	**Min**	**Max**	**-0.8**		**-1.0**		**-1.2**		**-1.5**	
Bivalve	1.25	0.26	2.11	7.1	15.1	6.2	14.3	5.4	13.4	4.1	12.1
Cephalopod	1.00	0.13	1.53	9.6	15.7	8.8	14.8	7.9	14.0	6.6	12.7
Gastropod	1.12	0.72	1.42	10.1	13.2	9.2	12.3	8.4	11.4	7.1	10.1
Uncertain	0.96	-0.06	1.55	9.5	16.5	8.7	15.7	7.8	14.8	6.5	13.5
Habitat											
Epifaunal	1.12	0.72	1.42	10.1	13.2	9.2	12.3	8.4	11.4	7.1	10.1
Infaunal	1.24	0.26	2.11	7.1	15.1	6.2	14.3	5.4	13.4	4.1	12.1
Nektonic	0.99	0.13	1.53	9.6	15.7	8.8	14.8	7.9	14.0	6.6	12.7
Planktonic	1.44	1.44	1.44	10.0	10.0	9.1	9.1	8.3	8.3	7.0	7.0
Uncertain	1.20	-0.06	1.92	7.9	16.5	7.0	15.7	6.2	14.8	4.9	13.5
Mode of life											
Browser	1.00	0.97	1.03	11.8	12.0	10.9	11.2	10.0	10.3	8.7	9.0
Carnivore	1.00	0.13	1.53	9.6	15.7	8.8	14.8	7.9	14.0	6.6	12.7
Scavenger	1.14	0.72	1.42	10.1	13.2	9.2	12.3	8.4	11.4	7.1	10.1
Deposit	1.39	0.26	2.05	7.4	15.1	6.5	14.3	5.6	13.4	4.3	12.1
Suspension	1.14	0.38	2.11	7.1	14.6	6.2	13.7	5.4	12.9	4.1	11.6
Uncertain	1.19	-0.06	1.92	7.9	16.5	7.0	15.7	6.2	14.8	4.9	13.5
Genus											
Amberlaya	1.13	0.72	1.42	10.1	13.2	9.2	12.3	8.4	11.4	7.1	10.1
Ammonite	1.21	0.88	1.53	9.6	12.4	8.8	11.6	7.9	10.7	6.6	9.4
Bivalve	1.32	0.59	1.92	7.9	13.7	7.0	12.8	6.2	12.0	4.9	10.7
Diplomoceras	1.44	1.44	1.44	10.0	10.0	9.1	9.1	8.3	8.3	7.0	7.0
Eselaevitrigonia	1.28	0.38	2.11	7.1	14.6	6.2	13.7	5.4	12.9	4.1	11.6
Gastropod	1.14	1.02	1.26	10.8	11.8	9.9	11.0	9.1	10.1	7.8	8.8
Grossouvrites	0.53	0.53	0.53	13.9	13.9	13.1	13.1	12.2	12.2	10.9	10.9
Lahillia	1.47	1.47	1.47	9.9	9.9	9.0	9.0	8.1	8.1	6.8	6.8
Maorites	1.00	0.58	1.33	10.5	13.8	9.6	12.9	8.7	12.0	7.4	10.7
Nautiloid	0.55	0.13	0.77	12.9	15.7	12.1	14.8	11.2	14.0	9.9	12.7
Nucula	1.39	0.26	2.05	7.4	15.1	6.5	14.3	5.6	13.4	4.3	12.1
Oistotrigonia	0.92	0.59	1.49	9.8	13.7	8.9	12.9	8.1	12.0	6.8	10.7
Pinna	1.07	0.84	1.62	9.2	12.6	8.4	11.8	7.5	10.9	6.2	9.6
Pleurotomaria	1.00	0.97	1.03	11.8	12.0	10.9	11.2	10.0	10.3	8.7	9.0
Solemya	1.05	0.99	1.11	11.4	12.0	10.6	11.1	9.7	10.2	8.4	8.9
Unidentified	0.96	-0.06	1.55	9.5	16.5	8.7	15.7	7.8	14.8	6.5	13.5

Principal lowstands in global sea level were indicated (Haq, 2014) together with the position of the onset of Deccan Trap volcanism (Schoene *et al*., 2015). Overall variability of the $\delta^{18}O$ data was an issue possibly influenced by either the effects of fluctuating levels of $\delta^{18}O_{water}$ as a result of freshwater run-off from the proximal landmass or the sampling of specimen shell material that reflected growth during both the warm and cool seasons for particular specimens. Both possibilities are in agreement with views suggested by Petersen *at al*. (2016). The wide variability of the $\delta^{18}O$ data and the corresponding calculated palaeotemperature values suggested that the interpretation of warmer or cooler climatic conditions may be problematic. Palaeotemperatures presented in Figure 4-2 were calculated using a $\delta^{18}O_{water}$ value of -1.2‰ (equivalent to -1.0‰ SMOW).

The trend line presented in Figure 4-2 indicates a relative stability in benthic temperatures but with a cooling phase that commenced at around 450 m (~69.5 Ma) with the coolest temperature developed mid-section at around 630 m (~69 Ma). Thereafter temperatures recovered towards the K-Pg boundary before a further cooling trend developed. The cooling trends show a generally good correlation with the reported position of seawater lowstands as reported by Haq (2014). In contrast the paucity of selected specimens in the section immediately prior to and post the K-Pg event resulted in a lack of confidence in accepting the development of the Deccan Traps volcanism as a causal mechanism for the limited degree of observed warming (Schoene *et al*., 2015; Petersen *et al*., 2016). This was in contrast to a more extended data set (Petersen *et al*., 2016) which in close proximity to the K-Pg boundary event indicated a pair of distinctive phases of warming prior to the K-Pg event. There was evidence for a period of cooling post K-Pg and this also correlated well with the PaDa1 lowstand reported by Haq (2014). Sea ice was also proposed by Bowman *et al*. (2013) based upon palynological analyses and there was a good correlation with the presence of lowstands reported by Haq (2014). The presence of sub-zero sea water temperatures was reported by Petersen *et al*. (2016) based upon a subset of their clumped isotope analyses of aragonite bivalve shell material, for similar stratigraphic positions their data showed a range of temperatures that exceeded the ranges reported in this study. The extended range of the temperatures may reflect the analysis of aragonite from potentially seasonal bivalve shell material or through modification of the $\delta^{18}O_{water}$ by freshwater run off (Petersen *et al*., 2016).

Data are comparable with younger populations, suggesting that a range of factors influence the values. Palaeotemperature results were in general agreement with previous macrofossil studies on Seymour Island (Ditchfield *et al*., 1994; Elorza *et al*., 2001; Dutton *et al*., 2007; Tobin *et al*., 2012, Little *et al*., 2015; Tobin *et al*., 2015; Petersen *et al*., 2016). Warming during the last several thousand years of the Cretaceous has been recognized in deep ocean cores from benthic foraminiferal data at both mid- (Li and Keller 1998) and southern high latitudes (Barrera 1994), similar trends have also been recognised from palynology (Thorn *et al*., 2009; Bowman *et al*., 2012). Mid-latitude near-shore settings (Dennis *et al*., 2013) indicated that temperature variability at high latitudes may also have reflected change at a global level.

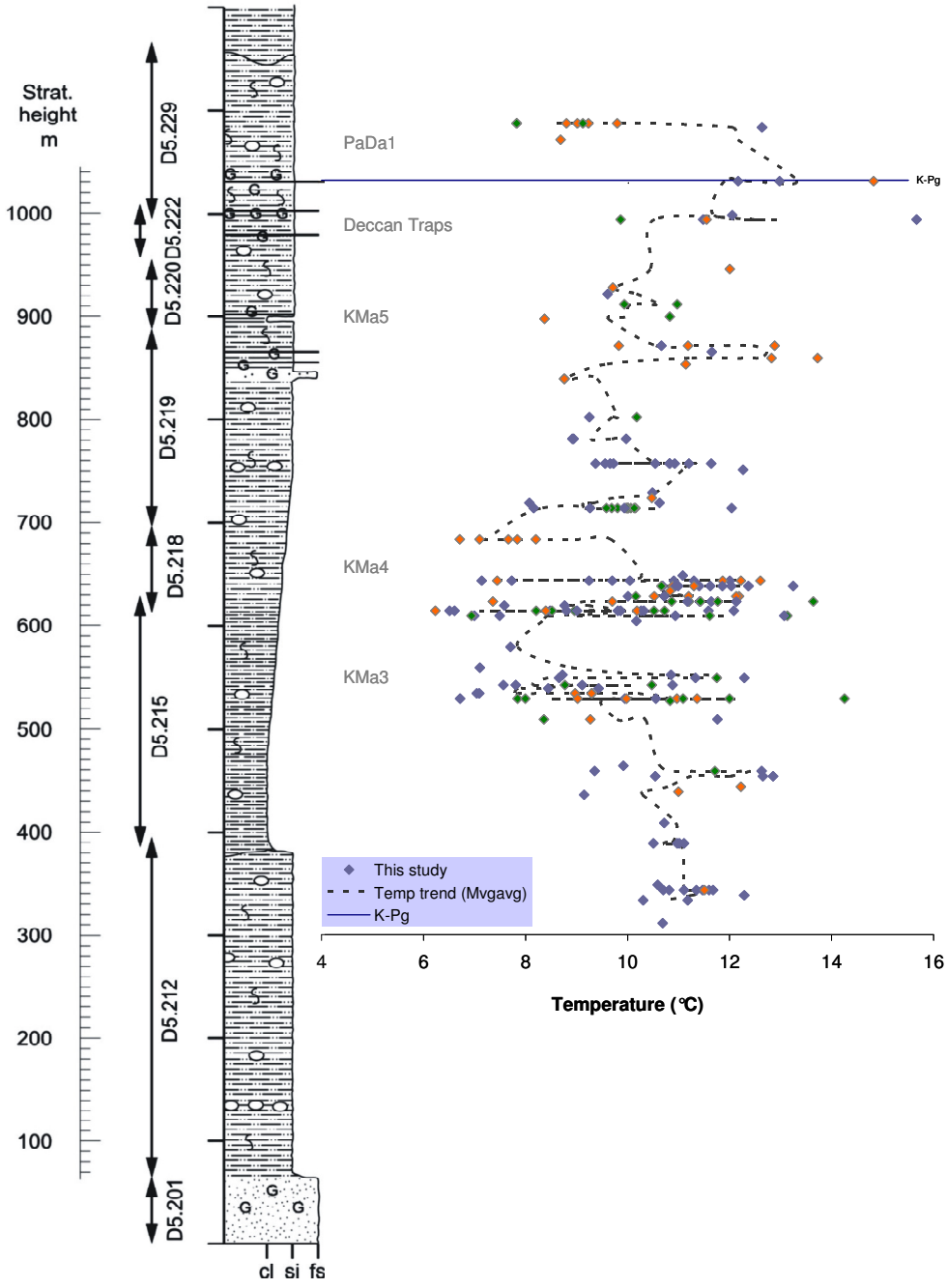

Figure 4-2. Palaeotemperature correlation with López De Bertodano Fm. stratigraphy. A smoothed temperature curve (moving average, step size = 3) indicated a cooling phase that commenced at 450 m with the coolest temperatures developed mid-section at 630 m. Thereafter temperatures recover towards the K-Pg boundary followed by a further gentle cooling trend. Principal lowstands in global sea level are also indicated (Haq, 2014) together with the position of the onset of Deccan Trap volcanism (Schoene *et al.*, 2015). The wide variability of the $\delta^{18}O$ data and the corresponding calculated palaeotemperature values suggests that the interpretation of warmer or cooler climatic conditions may be problematic. Palaeotemperatures calculated using a $\delta^{18}O_{water}$ value of -1.2‰ (equivalent to -1.0‰ SMOW). Note the wide variability in the temperatures. In both plots blue symbols represent specimens exhibiting Mg < 1000 ppm, Fe < 500 ppm and Mn < 200 ppm; green symbols represent specimens for which no trace element diagenetic screening was carried out and orange symbols represent specimens with Fe or Mn concentrations that exceeded the diagenetic threshold (Fe > 500 ppm and Mn > 200 ppm).

The data presented in Figure 4-2 comprised all of the screened $\delta^{18}O$ data. Thus the temperature trend reflects data from both benthic and nektonic taxa, although only 17% are nektonic. The same data are presented in Figure 4-3 but with separate trend lines for benthic and nektonic taxa. There is an overall similarity between both trends until approximately 780 m (68.2 Ma) at which point the nektonic data more prominently display a warming trend. One distinct problem with the upper part of the section is the relative paucity of suitable specimens and unusually for this study there are more nektonic specimens present until a number of bivalve specimens appear post K-Pg. The data presented in Figure 4-4 were categorised by fossil type and highlight the importance of the bivalve data.

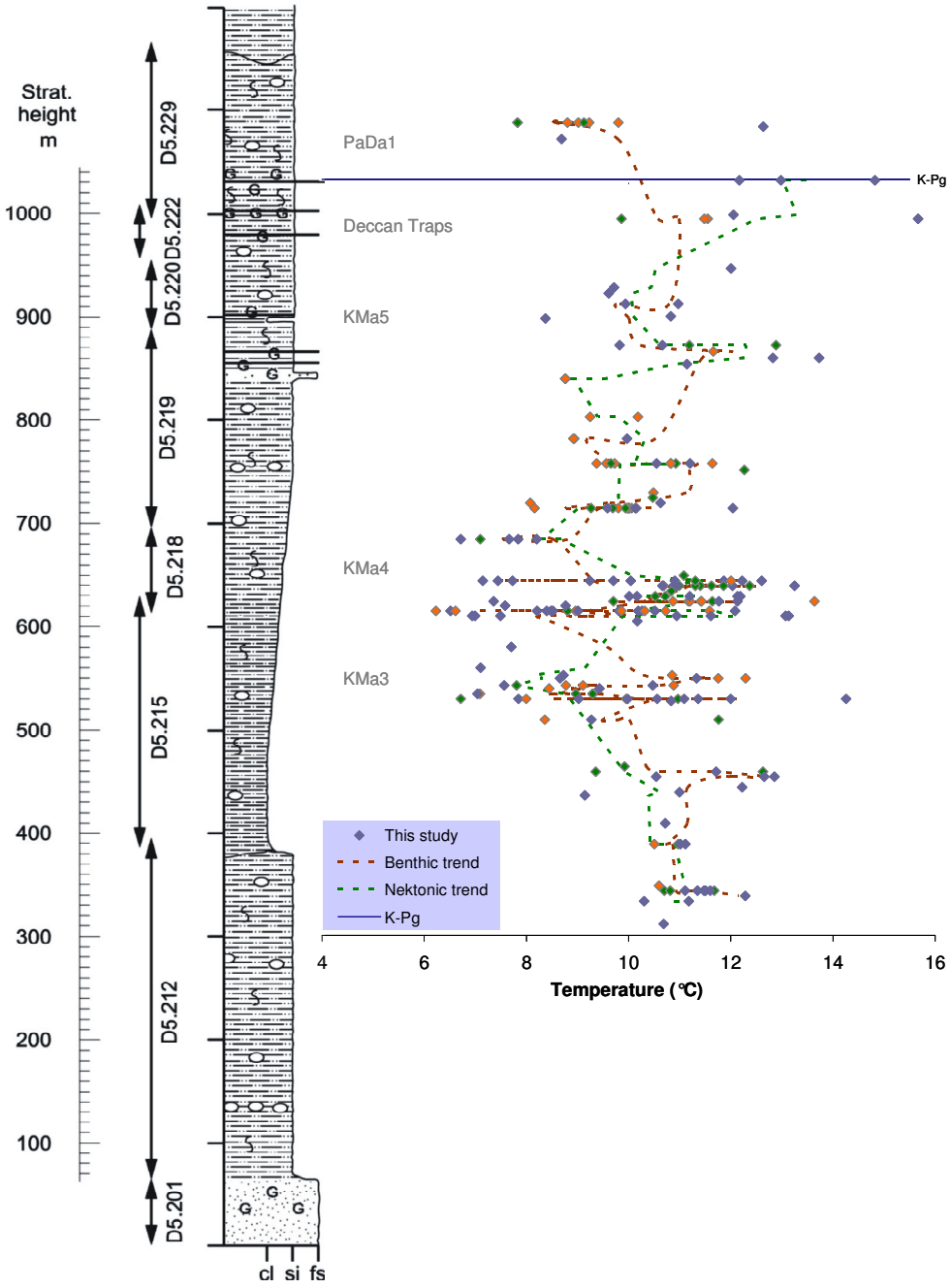

Figure 4-3. Palaeotemperature correlation with López De Bertodano Fm. stratigraphy. Smoothed temperature curves (moving average, step size = 3) for (a) benthic and (b) nektonic taxa. There is an overall similarity between both trends with a cooling phase that commenced at 450 m with the coolest temperatures developed mid-section at 630 m until approximately 780 m (68.2 Ma) at which point the nektonic data more prominently display a warming trend. See Figure 4-2 caption for information concerning colour coding of symbols.

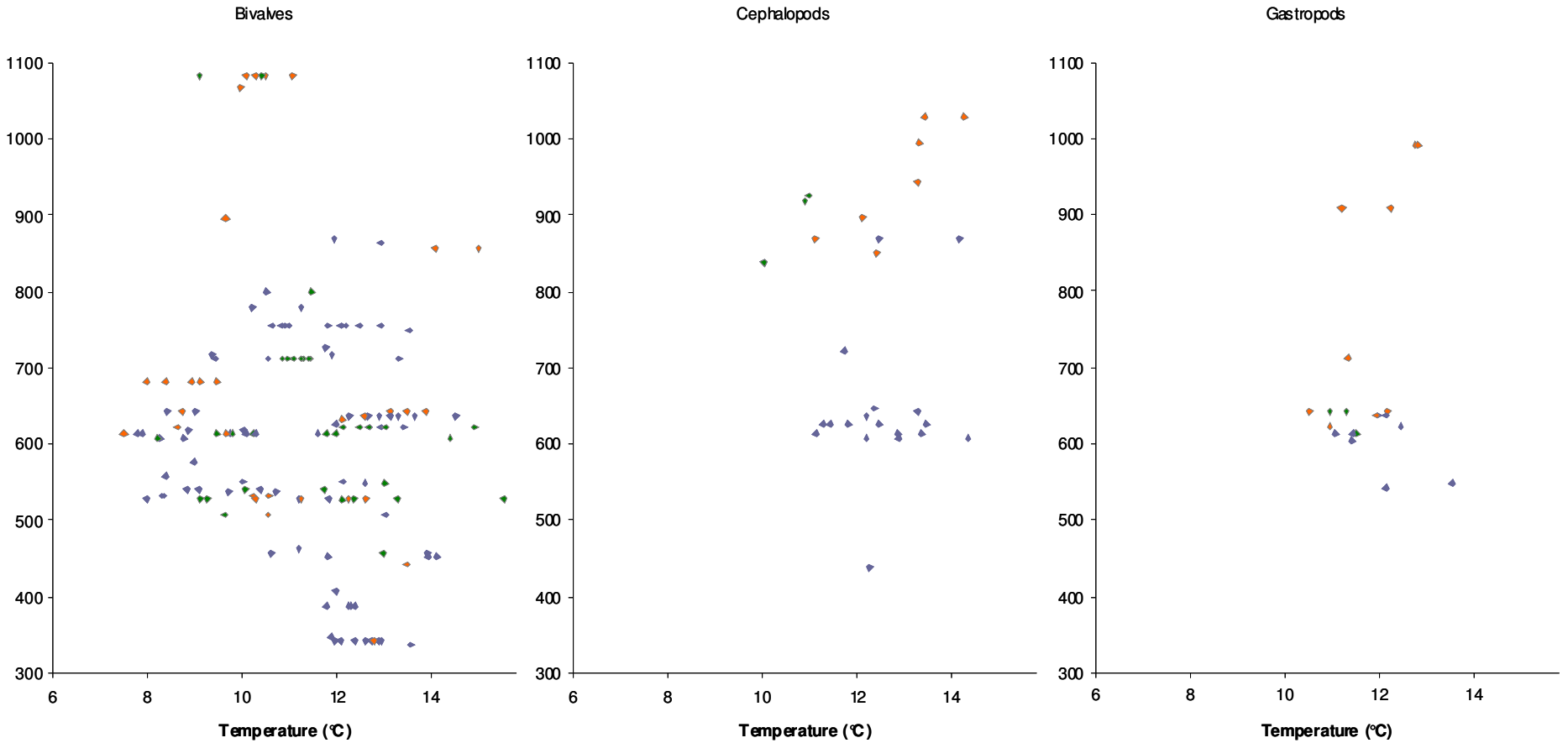

Figure 4-4. Palaeotemperature correlation with López De Bertodano Fm. stratigraphy (See Figure 4-23). The bivalve data suggest a the presence of a cooling phase that commenced at ~450 m with the coolest temperature developed mid-section at ~630 m. Data from cephalopods and gastropods add little further information about seawater temperature. The lack of benthic data for the section from 900 m to 1080 m complicates any attempt to estimate the nature of the bottom water temperatures but there does appear to be a further gentle cooling trend that develops towards the K-Pg boundary. The wide variability of the $\delta^{18}O$ data and the corresponding calculated palaeotemperature values suggest that the interpretation of warmer or cooler climatic conditions may be problematic. Calculation of palaeotemperature with $\delta^{18}O_{water}$ value of -1.2‰ (-1.0‰ SMOW) adopted.

4.8 Stable isotope studies – Seymour Island

In addition to this study a number of recent studies have also described stable isotope data ($\delta^{13}C$ and $\delta^{18}O$) derived from the analysis of molluscan macrofossils from the López de Bertodano Fm., Seymour Island (Tobin *et al*., 2012; Little *et al*., 2015; Tobin and Ward, 2015; Petersen *et al*., 2016). All studies were based upon the analysis of aragonitic shell material but Tobin *et al*. (2012) also described stable isotope date derived from the analysis of calcitic shell material, where appropriate calcite derived data are included for comparison purposes. Petersen *et al*. (2016) also selected a subset of their specimens for 'clumped isotope' analysis, unfortunately their overall stratigraphy did not cover the full stratigraphic range from this study. Their derived $\delta^{18}O_{water}$ data are also included for comparison with the default value of -1.2‰ (-1.0‰ SMOW) adopted for the palaeotemperature calculations in this study. There was significant variability within their $\delta^{18}O_{water}$ data and a lack of $\delta^{18}O_{water}$ data for the lower section of the stratigraphy was unfortunate. Note that no 'clumped isotope' analyses were carried out as part of this study and as a consequence there was no opportunity to compare $\delta^{18}O_{water}$ values with those data published by Petersen *et al*. (2016). Palaeotemperature values vs. stratigraphy are presented in Figure 4-5, note the wide temperature range and especially the presence of sub-zero values. There was a good correlation between the calculated sub-zero temperatures and the position of the KMa4 lowstand (see Figure 4-2; Haq, 2014).

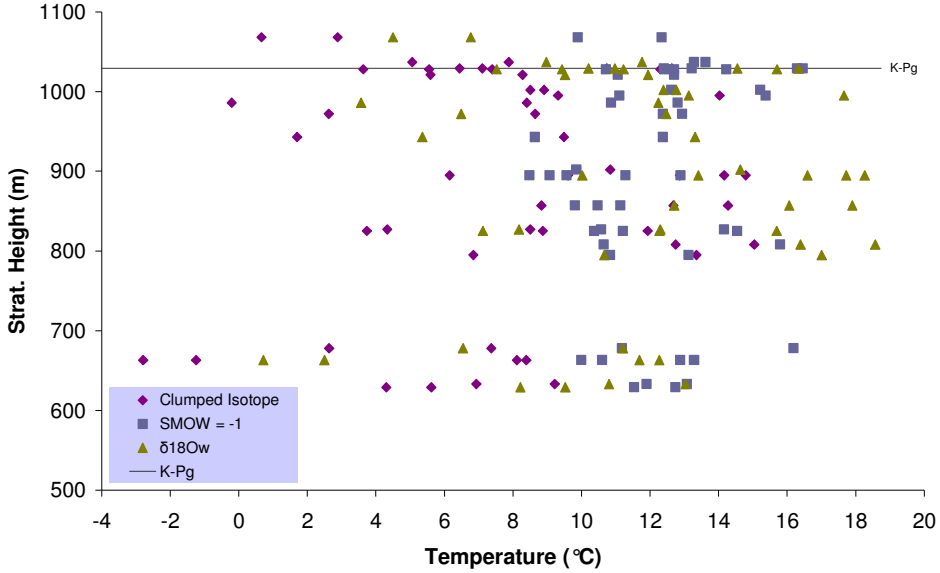

Figure 4-5. Comparison of palaeotemperatures derived from clumped isotope data and as calculated from $\delta^{18}O$ ‰ for ocean water $\delta^{18}O_{water}$ of SMOW = -1‰ and finally using clumped isotope derived values for $\delta^{18}O_{water}$. All stable isotope measurements from aragonitic bivalve shell material. Note the considerable temperature ranges reported, especially the presence of sub-zero values (All data from Petersen *et al*., 2016). Note that the stratigraphic positions represent the BAS D5 sampling scheme.

A comparison of their data and that from from this study are presented in Figures 4-5, 6, 7 and 8. All aragonite data are presented in Figure 4-6 in the form of a covariance plot. Note the extensive variability within all of the individual datasets with the largest range exhibited by Tobin *et al*. (2012). There is a good overall correlation between the data with the majority indicating a typical marine isotopic signature. The nature of the stable isotopic variability in this study has already been discussed and it was concluded that experimental error and diagenesis were not responsible for the presence of the variability. This conclusion is given further credence by the publication of similar data from two separate studies from the same locality. It seems unlikely that three separate studies would all produce potentially flawed data from Seymour Island. It also seems unlikely that the geographical location of individual sampling points on a relatively small island with a well understood geology can significantly influence the data. This suggests that the stable isotope data are genuinely reflecting the isotopic signal present within the macrofossils which in turn reflect the marine isotopic conditions in the late Maastrichtian.

A comparison of late Maastrichtian stable isotope ($\delta^{13}C$ and $\delta^{18}O$) data from Seymour Island versus stratigraphy is presented in Figures 4-7 and 8. Data from this study were derived from aragonitic macrofossils (Bivalves, Ammonites, Nautiloids and Gastropods), Tobin *et al*. (2012) (Bivalves, Ammonites and Gastropods) and Petersen *et al*. (2016) (Bivalves). Note that Tobin *et al*. (2012) also measured $\delta^{13}C$ and $\delta^{18}O$ from calcitic macrofossils and these data have also been included for consistency. Ringed data points (n=3) illustrated in Figure 4-7 represent specimens of *Solemya rossiana*. As previously discussed note the wide variability of data from all four datasets with the widest range presented in Tobin *et al*. (2012) and the narrowest range from this study.

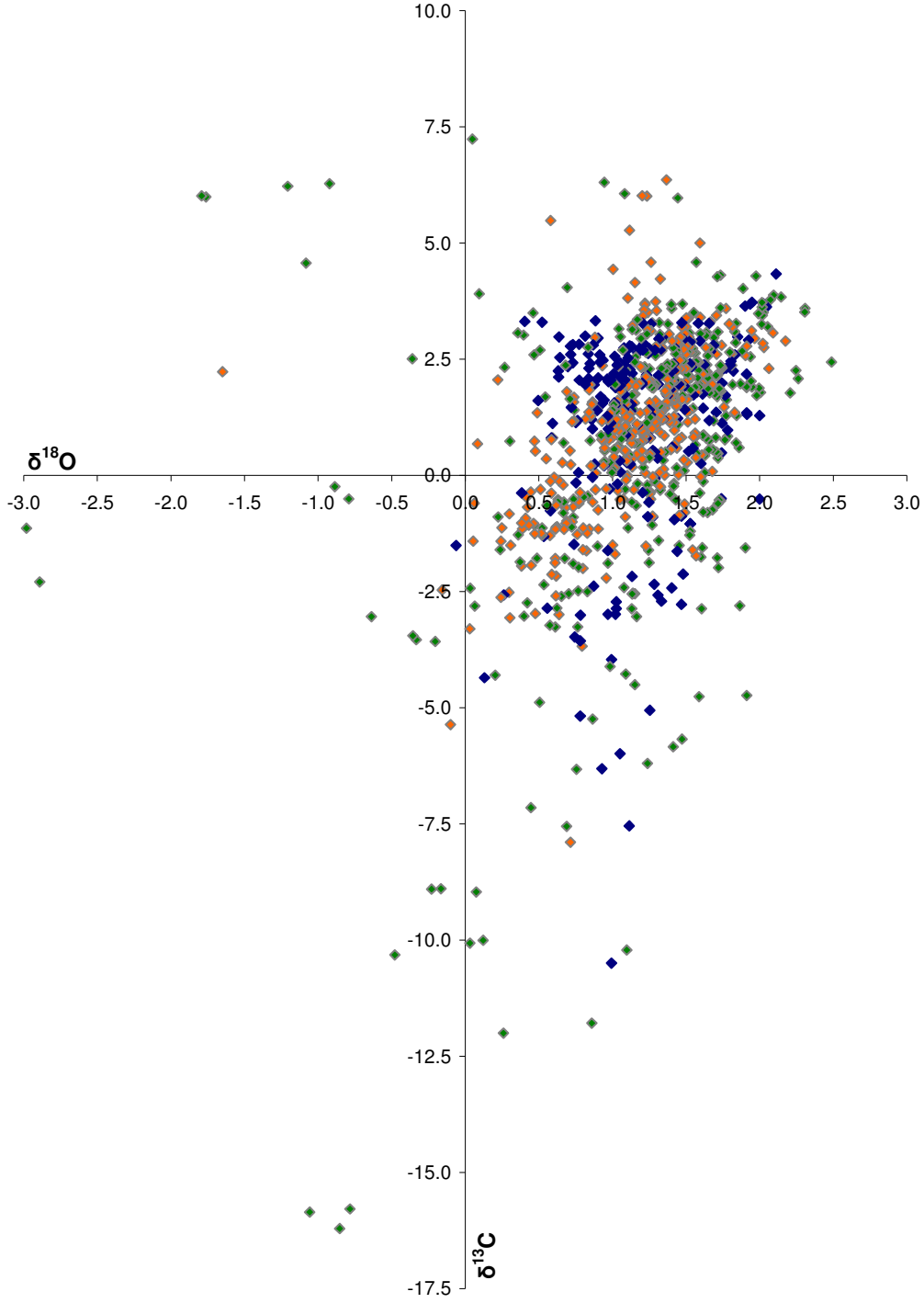

Figure 4-6. Late Maastrichtian stable isotope data from Seymour Island, Antarctica. Sources include this study (blue), Tobin *et al.* (2012) (green) and Petersen *et al.* (2016) (orange). Note the wide variability of both $\delta^{13}C$ and $\delta^{18}O$ data.

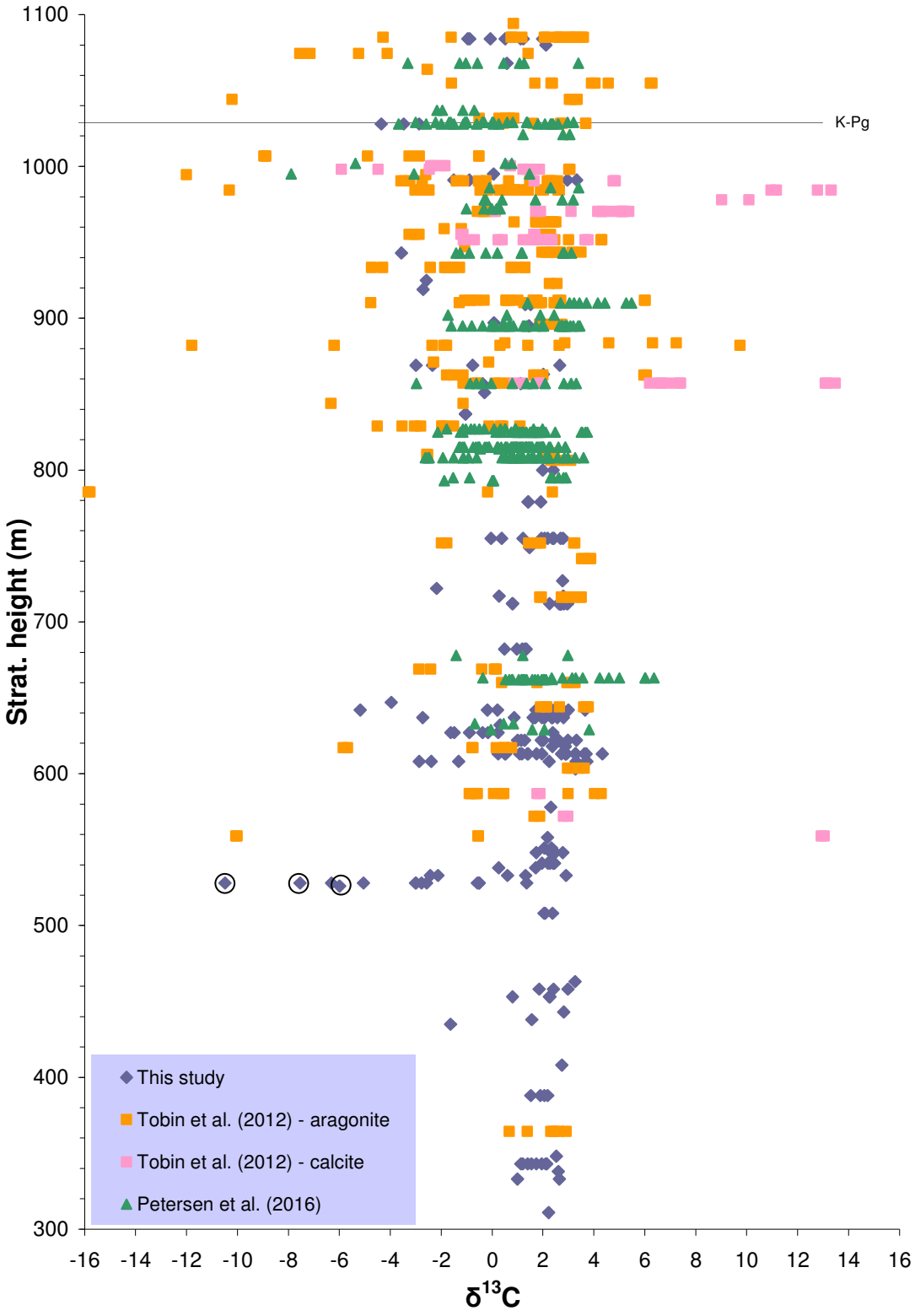

Figure 4-7. Late Maastrichtian $\delta^{13}C$ data from Seymour Island, Antarctica. Sources include this study (**Bivalves**, **Ammonites**, **Nautiloids** and **Gastropods**), Tobin *et al.* (2012) (**Bivalves**, **Ammonites** and **Gastropods**) and Petersen *et al.* (2016) (Bivalves). Note that Tobin *et al.* (2012) also measured $\delta^{13}C$ from calcite macrofossils and these data were included for consistency. Ringed data points (n=3) represent specimens of *Solemya rossiana* that have thiotrophic chemosymbionts involved in the anaerobic oxidation of methane (Little *et al.*, 2015). Note the wide variability of data from all four datasets, with the greatest range presented in Tobin *et al.* (2012). There is no apparent shift in $\delta^{13}C$ data at the K-Pg as reported by Keller (2011)

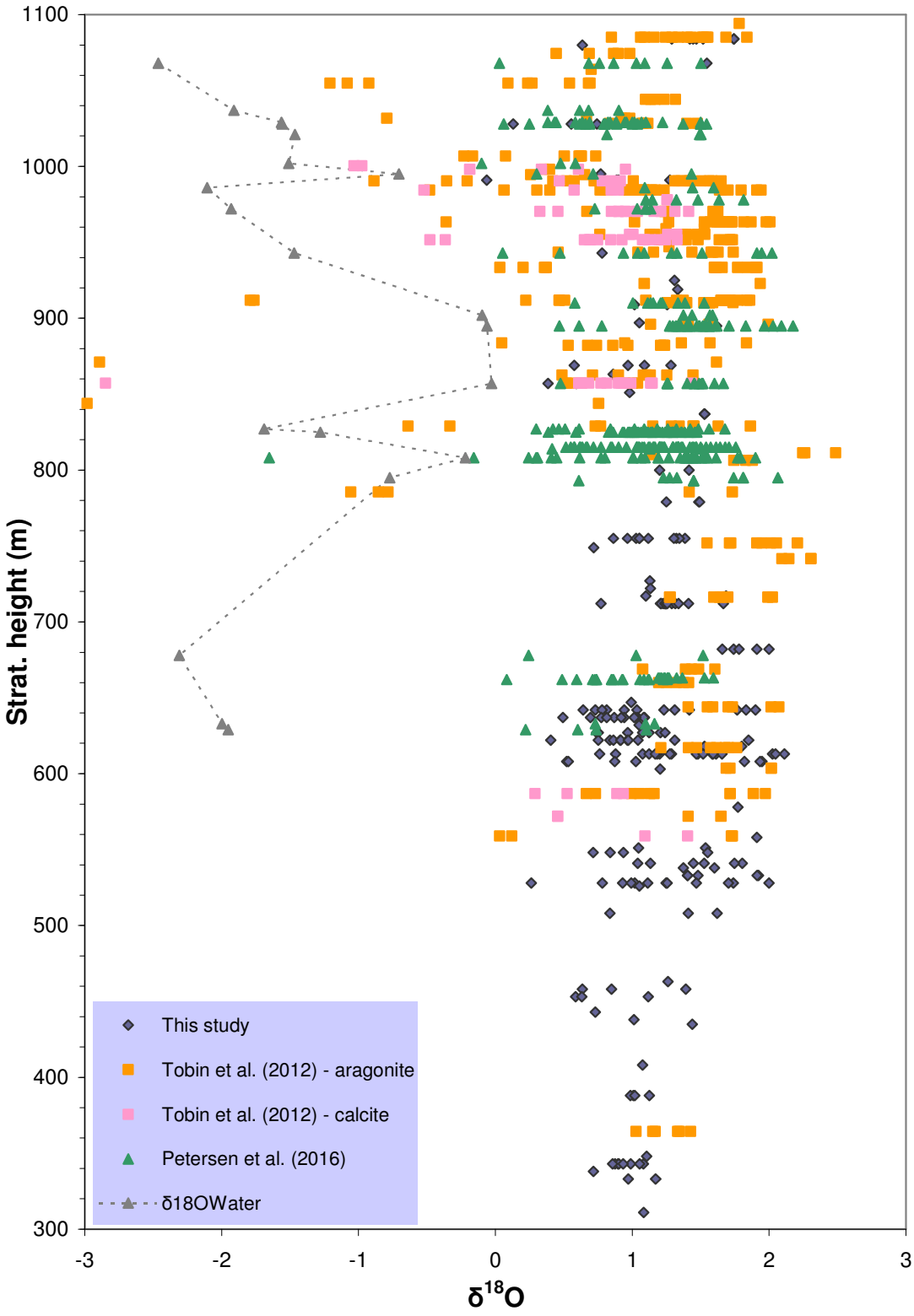

Figure 4-8. Late Maastrichtian $\delta^{18}O$ data from Seymour Island, Antarctica. Sources include this study (Bivalves, Ammonites, Nautiloids and Gastropods), Tobin *et al.* (2012) (Bivalves, Ammonites and Gastropods) and Petersen *et al.* (2016) (Bivalves). Note that Tobin *et al.* (2012) also measured $\delta^{18}O$ from calcite macrofossils and these data have also been included for consistency. Petersen *et al.* (2016) also analysed a subset of their specimens for 'clumped isotope' analysis, the mean derived $\delta^{18}O_{water}$ data are also included for comparison with the default value of -1.2‰ (-1.0‰ SMOW) adopted for the palaeotemperature calculations.

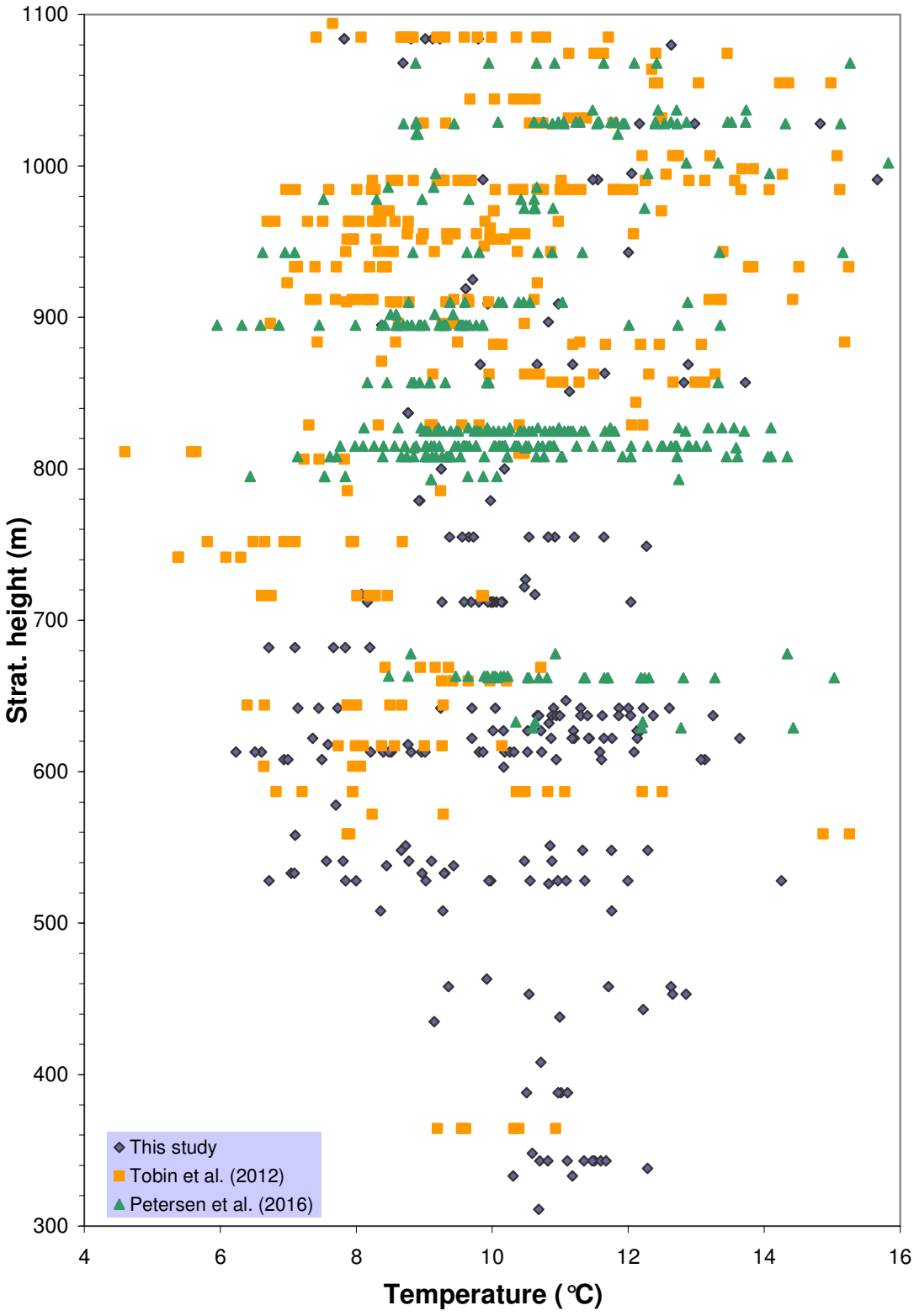

Figure 4-9. Late Maastrichtian palaeotemperature data from Seymour Island, Antarctica. Sources include this study (Bivalves, Ammonites, Nautiloids and Gastropods), Tobin *et al.* (2012) (Bivalves, Ammonites and Gastropods) and Petersen *et al.* (2016) (Bivalves). Palaeotemperatures were calculated with a $\delta^{18}O_{water}$ value of -1.2‰ (-1.0‰ SMOW).

4.9 Stable isotope synthesis

A high resolution oxygen and carbon stable isotope record through the Latest Maastrichtian – Earliest Danian was generated using diagenetically unaltered aragonite nacre shell material from a molluscan fauna collected from the López de Bertodano Fm., an extensive 1100 m thick Late Maastrichtian section from Seymour Island, Antarctica. The majority of the specimens collected exhibited good preservation of primary shell mineralogy and approximately 650 individual macrofossils were catalogued prior to selection of specimens from which sample powders were collected. Many of the specimens furnished substantial powder samples, in certain cases > 1000 mg.

Coverage of stable isotope data for the measured stratigraphy was good, with ~280 stable isotope analyses including data from specimens collected within 1 m of the K-Pg boundary, as determined by palynology. Multiple analyses at discrete stratigraphic levels enabled the comparison of stable isotope data from both benthic and pelagic macrofossils at corresponding levels. Stable isotopes exhibited unscreened ranges of -0.06 to +2.11‰ for $\delta^{18}O$ and -10.49 to +4.34‰ for $\delta^{13}C$, corresponding screened stable isotope data gave ranges of -0.06 to +2.05‰ for $\delta^{18}O$ and -7.54 to +3.7‰ for $\delta^{13}C$. Data show that at individual stratigraphic levels, the measured range of $\delta^{18}O$ exhibited significant variability e.g. +0.86 to +1.08‰ at 343 m, +0.76 to +2.11‰ at 613 m, +0.77 to 1.67‰ at 712 m and +1.29 to +1.74‰ at 1084 m, with respect to the K-Pg boundary (1029 m above datum, as defined by palynology (Thorn *et al*., 2009). Bivalve molluscs and a benthic mode of life exhibited the widest range of $\delta^{18}O$ and $\delta^{13}C$ values. The variability seen in the oxygen stable isotope data has similarities with that from a present day shallow marine molluscan assemblage (Marshall *et al*., 1996) and similar variability was also reported for the late Maastrichtian of Seymour Island in recent separate studies (Tobin *et al*., 2012; Tobin and Ward, 2015; Petersen *et al*., 2016). Ivany *et al*., 2008) also record a similar variability for Eocene macrofossils from the La Meseta Fm. on Seymour Island. This oxygen isotope variability may reflect a record of annual/intra-annual growth that for an individual taxon may indicate seasonal periods of dominant growth or a dilution of the $\delta^{18}O_{water}$ in the James Ross Basin resulting from localised continental run-off or a combination of both as reported in Petersen *et al*. (2016) The stable isotope data highlight that individual stratigraphic levels can exhibit significant variability for $\delta^{18}O$ and $\delta^{13}C$ and that analysis of single samples at discrete stratigraphic levels may provide an erroneous interpretation of climate change.

The stable isotope data generated from this research project have raised a number of questions with regard to the interpretation of climate change from high resolution stable isotope studies. In particular variability within the range of $\delta^{13}C$ and $\delta^{18}O$ isotope data

measured at specific stratigraphic positions, it has been shown that the reported ranges were not necessarily present as a result of errors introduced either during specimen selection, powder preparation, diagenetic selection or analysis of the actual specimen powders. A similar variability was also present in the stable isotope data from Seymour Island (Tobin *et al*., 2012; Tobin and Ward, 2015; Petersen *et al*., 2016). Other studies have reported similar ranges within their stable isotope data sets and it is probable that the significant variability seen within this data set may indeed reflect the norm for stable isotope palaeoenvironmental studies (Marshall *et al*., 1996; Latal *et al*., 2006; Ivany *et al*., 2008; Tobin *et al*., 2012; Petersen *et al*., 2016).

Overall the data indicate the presence of both a cooling and a subsequent increase in benthic water temperatures in the Late Maastrichtian/Early Palaeocene. A tentative moving average curve representing temperature has been superimposed upon calculated palaeotemperatures, see Figures 4-2 and 3. It must be noted that the temperature curve presented in Figure 4-2 comprised data for bivalves, gastropods and cephalopods, consequently there was a minor level of mixing between the benthic and nektonic records. However, the benthic taxa represented 83% of the screened specimens and also exhibited the widest stratigraphic range. The same data are presented in Figure 4-3 but with separate trend lines for benthic and nektonic taxa. There is an overall similarity between both trends until approximately 780 m (68.2 Ma) at which point the nektonic data more prominently display a warming trend. One distinct problem with the upper part of the section is the relative paucity of suitable specimens and unusually for this study there are more nektonic specimens present until a number of bivalve specimens post K-Pg. The data presented in Figure 4-4 were categorised by fossil type and highlight the importance of the bivalve data.

The stable isotope record from this study was correlated with corresponding data sets that described the effects of falls in sea level, the presence of reduced seawater temperatures and the corresponding elevation of sea water temperature as a result of CO_2 outgassing that resulted from Deccan Traps volcanism. Both Tobin *et al*. (2012) and Petersen *et al*. (2016) described and documented a rise of sea water temperatures that correlated well with the Deccan Traps volcanism. Indeed in the latter case evidence was presented for two separate episodes of warming during the period of the K-Pg boundary event. For this study there were data from a small number of specimens (n=11) grouped at three individual stratigraphic positions that spanned ~600 kyr, which suggested tentative evidence (See Figures 4-2 and 3) for the presence of warming phases both immediately prior to and post the K-Pg boundary. But a lack of suitable specimens coeval with the commencement of the Deccan Traps volcanism, the primary causal mechanism proposed by Petersen *et al*. (2016), made it more

difficult to accurately correlate these events for this section of the López de Bertadano Fm. stratigraphy.

5 Strontium Isotope Analysis

5.1 Introduction

As discussed in Chapter 1 no published absolute dating exists for the younger section of the succession other than the GSSP figure of 66 ± 0.043 Ma for the K-Pg boundary (Gradstein *et al*., 2012). The base of the Maastrichtian Stage in Antarctica was formally defined on the basis of a mean $^{87}Sr/^{86}Sr$ value (0.7077359) for the six best preserved samples from a bivalve-nautiloid assemblage within the *Gunnarites antarcticus* fauna from Cape Lamb, Vega Island (Crame *et al*., 1999). This occurred at a stratigraphical level 81.5 – 96.5 m above the base of the *G. antarcticus* fauna and it was assumed that the latter datum could be taken as the Campanian-Maastrichtian boundary with a date of 72.1 ± 0.2 Ma (Crame *et al*., 1999; Gradstein *et al*., 2012). On both Vega and Snow Hill islands it was noted that the distinctive *G. antarcticus* assemblage had a very sharp base (Pirrie *et al*., 1991, 1997).

The inclusion of an updated and expanded strontium isotope record for the measured section offered a valuable addition to the data set. Following a successful application for NERC funding strontium isotope analyses were carried out at the National Isotopes Geoscience Laboratory (NIGL), Kingsley Dunham Centre, British Geological Survey. The $^{87}Sr/^{86}Sr$ isotope data further enhanced the overall stable isotope ($\delta^{13}C$ and $\delta^{18}O$) data set and provided an opportunity to confirm that the strontium isotope record derived from this study correlated with the existing Late Cretaceous Strontium Isotope Stratigraphy (SIS) curve (McArthur *et al*., 2001). The availability of $^{87}Sr/^{86}Sr$ isotope data would also help constrain the dating of palaeoenvironmental events, as indicated by the stable isotope record within the James Ross Basin, with those detected by other proxies e.g. palynology (Thorn *et al*., 2009; Bowman *et al*., 2012) and magnetostratigraphy (Tobin *et al*., 2012). An age model based upon the correlation of these ages together with biostratigraphical data and magnetostratigraphy has been published (see Figure 1-5; Tobin *et al*., 2012; Witts *et al*., 2015; Petersen *et al*., 2016). A series of spot $^{87}Sr/^{86}Sr$ isotope analyses were reported by Petersen *et al*. (2016) but none of these data were used to extend their age model.

5.2 Strontium isotope stratigraphy

Strontium isotope stratigraphy (SIS) is a well established chemostratigraphic method (McArthur, 1994; McArthur and Howarth, 2004; McArthur *et al*., 2012). The use of the reference curve as a stratigraphic tool is facilitated by its conversion into a look-up table, giving the numerical ages and the 95% confidence limits for any value of $^{87}Sr/^{86}Sr$ interpolated in steps of 0.000001. The ratio of strontium isotopes ($^{87}Sr/^{86}Sr$) of

biogenic carbonates and phosphates provides a useful chemostratigraphic and chronostratigraphic tool because the ratio varies over geologic time. The original method suggested that the ratio would increase in a linear manner and that following suitable calibration of the method the ratio from any point in the Phanerozoic could provide an actual numeric age (Wickman, 1948). The residence time in the oceans for Sr (~1 Ma) exceeds the rate of ocean mixing by 3 orders of magnitude (see McArthur *et al.*, 2012). The ratio of $^{87}Sr/^{86}Sr$ derived from the weathering of continental rocks was higher than that of marine Sr derived from mid-ocean ridge sources. Strontium isotope ratios for the Maastrichtian were published by Vonhof *et al.* (2011) based on belemnites from the Maastrichtian stratotype area in the Netherlands. Their data indicated that two plateaus existed with a lower plateau of approximately 0.707750 for the lower Maastrichtian and an upper plateau of approximately 0.707820 for the upper Maastrichtian.

5.3 Materials and Methods

Calcareous fossil samples selected for analysis consisted of subsamples of aragonite nacre shell material already screened for diagenetic alteration and for which stable isotope data existed. In order to test for changes in the stable isotopic, palynological or sedimentological record powder samples were selected for $^{87}Sr/^{86}Sr$ isotope analysis from 15 separate levels in the measured succession. It was intended that the data would enable the construction of a chronostratigraphic framework together with the correlation of key events in the stable isotope and palynological records. A relatively flat seawater $^{87}Sr/^{86}Sr$ curve in the latest Cretaceous/earliest Palaeogene (Figure 5-1) required high precision $^{87}Sr/^{86}Sr$ isotope data in order to provide a suitable high resolution chronology.

Performance of the Triton mass spectrometer at NIGL was monitored using SRN987 and standard seawater this ensured consistent external reproducibility of better than 5 ppm 1 σ (i.e. ± 0.000007, 2 σ on the $^{87}Sr/^{86}Sr$ ratio) during the periods of analysis. This was achieved through the use of large (>10V ^{88}Sr) ion beams, extended counting times and baseline measurements. In order to establish the geological variability in the sample material, it was decided that three individual fossils (or sub samples thereof) would be analysed at each horizon. In practice this was not always feasible due to availability of sufficient carbonate powders (see Figure 5-2 for the location of samples).

5.4 Selected fossil types

A total of 71 separate samples were analysed including duplicates and triplicates, data reproducibility was generally good and with an average internal error for the $^{87}Sr/^{86}Sr$ data = ±0.000003. Previous Sr isotope analysis was carried out by McArthur

et al., 1998) on samples collected from Seymour Island and some of the data were incorporated into the LOWESS Smoothed Global Strontium Isotope Curve V3 (McArthur *et al.*, 2001).

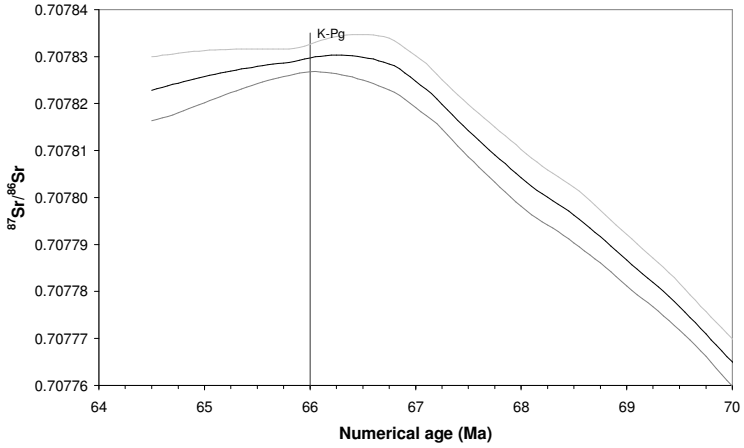

Figure 5-1. The latest Maastrichtian/earliest Palaeogene shows a relatively flat seawater $^{87}Sr/^{86}Sr$ curve from the required high precision $^{87}Sr/^{86}Sr$ isotope data in order to provide a suitable high resolution chronology.

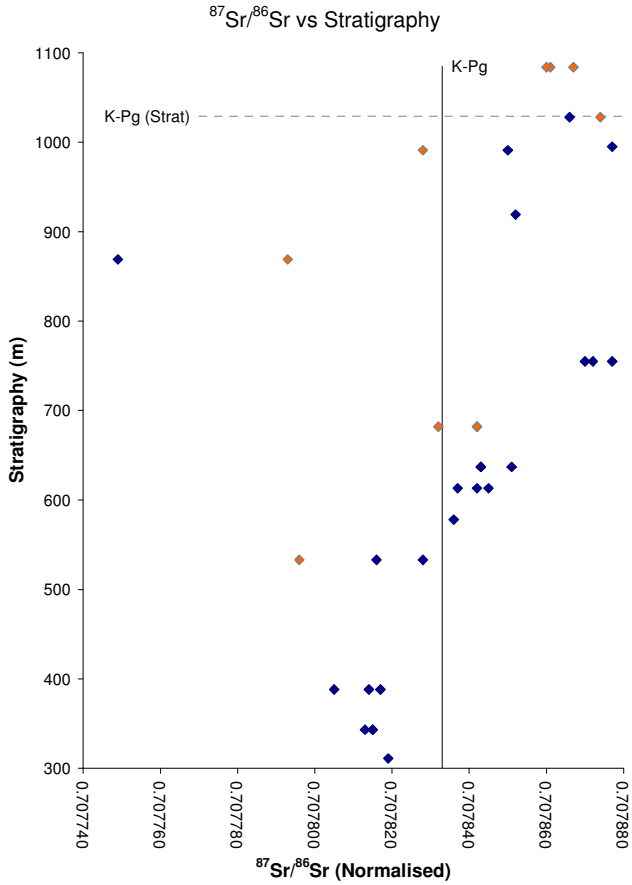

Figure 5-2. Location of specimens selected for $^{87}Sr/^{86}Sr$ isotope analysis. The absence of data below 300 m reflects a lack of suitably preserved macrofossils.

5.4.1 Analytical method

Samples were leached in 1M acetic acid at room temperature for one hour. The solutions were centrifuged and the supernatant solution was pipetted off, dried down and converted to chloride using 6M HCl. Samples were then redissolved in 2.5M HCl and Sr was separated on cation exchange columns using Dowex AG50 ion exchange resin. Samples were loaded on single Re filaments using a TaO activator and analysed using a Thermo-Electron Triton thermal ionisation mass spectrometer in dynamic multicollection mode. During the period of measurement (~18 months) performance of the instrument was monitored by multiple analyses (n=149) of the SRN987 standard analysed with the samples gave a $^{87}Sr/^{86}Sr$ ratio = 0.710254 ± 0.000005 (1 σ) with a standard error of mean = $5.18x10^{-07}$. Data presented in Table F-3 were normalised to a value of 0.710250 for this standard. Two samples of standard seawater run with the unknown samples gave $^{87}Sr/^{86}Sr$ data of 0.709171 ± 0.000003 and 0.709175 ± 0.000004 (1SE).

Details of the calculated standard error for each individual sample are presented in Table F-3. The calculated standard error of the measurement (SEm) for all $^{87}Sr/^{86}Sr$ data = ±0.000003, for Petersen *et al*. (2016) a calculated standard error of measurement = ±0.000009 and McArthur *et al*. (1998) quoted a precision of ±0.000015 (2 σ) based upon replicated sample analysis, their data have a calculated standard error of measurement = ±0.000004. Error bars are plotted for the separate data sources presented, see Figure 5-3.

5.4.2 Strontium isotope data

Due to the presence of a number of anomalous low and high data values (see Table 5-4) in the Sr isotope data set all specimens selected for $^{87}Sr/^{86}Sr$ analysis were retrospectively checked on a JEOL 5400V SEM. The instrument was operated in BSE mode in conjunction with EDS X-ray analysis and specimens were checked for the presence of any mineral phases that carried significant Sr abundances, for example strontianite ($SrCO_3$). No evidence for the presence of strontianite was found in any of the fragments of shell material checked. Gypsum was also considered as a source of contaminant Sr since it has been shown to carry Sr levels of 1550 to 1900 ppm (e.g. Matano *et al*., 2005; de Souza *et al*., 2014). The only specimens that were included for $^{87}Sr/^{86}Sr$ measurement that exhibited elevated (> 5%) levels of S (where S in the absence of elevated levels of Fe was used as an indicator of gypsum) both exhibited Sr levels lower than the mean for all skeletal aragonite analysed for trace element data (mean Sr = 3057 ppm, n=169). It was anticipated that for any gypsum hosted Sr contamination the concentration would exceed the mean value due to the presence of

Sr contributed from both gypsum and aragonite. The trace element data suggested that this was not the case.

It was shown in Chapter 3 that there was a strong correlation between diagenetic indicators and specimens of *Rotularia*, interestingly specimens of *Rotularia* from Seymour Island were selected for inclusion in $^{87}Sr/^{86}Sr$ studies (McArthur *et al*., 1998). Data generated from those analyses of macrofossils from Seymour Island were also incorporated into the LOWESS Smoothed Global Strontium Isotope curve (McArthur *et al*., 1998, 2001).

See Figure 5-3 for a comparison of Sr isotope data from this study with that from the LOWESS smoothed global Strontium Isotope Stratigraphy curve (McArthur *et al*., 2001) and data from previous Seymour Island studies (McArthur *et al*., 1998; Petersen *et al*., 2016) . The K-Pg boundary has an age of 66 Ma (Gradstein *et al*., 2012) and has a $^{87}Sr/^{86}Sr$ value of 0.707833 from the Strontium Isotope Stratigraphy curve (McArthur *et al*., 2001). Data from McArthur *et al*. (1998) represent a partial dataset of aragonitic specimens from a range of mixed aragonite and calcite macrofossils. Note the larger range of $^{87}Sr/^{86}Sr$ variability in the data from this study and Petersen *et al*. (2016) in comparison with that from McArthur *et al*. (1998). The wide variability may result from the diagenetic alteration of the skeletal carbonates but there still remains the fact that the 3rd dataset (McArthur *et al*., 1998) does not exhibit a similar variability although there is no indication of any discarded data from their study. McArthur *et al*. (1998) noted that diagenesis of skeletal carbonates in their data appeared to decrease the level of Sr in contrast to the normal expected increase. Their range of specimens included both aragonitic and calcitic shell mineralogies there was, however, no indication of which shell mineralogy was referred to in their comments. The average value of Sr from this study was 2863 ppm in comparison with a value of 2121 ppm for the aragonitic specimens reported in McArthur *et al*, (1998).

A further possibility for the variability might be reflected in the selected taxa but Petersen *et al*. (2016) only used bivalves and this study included bivalves, cephalopods and gastropods. McArthur *et al*. (1998) commented that aragonite from ammonites and bivalves was suitable for Sr isotope analysis, although no ammonite specimens were reported in their data. What was difficult to reconcile was the overall similarity of the data from this study and Petersen *et al*. (2016) in comparison with those from previously published data (McArthur *et al*., 1998, 2001). The similarity suggests that preparation or analytical procedures were not responsible for the discrepancies observed in the Sr data.

A correlation of $^{87}Sr/^{86}Sr$ data (this study) with $\delta^{18}O$ data vs. the measured stratigraphy is presented in Figure 5-4. There is a possible trend in the strontium data that parallels a similar trend in the $\delta^{18}O$ data, there is a generally good agreement between both trends until an apparent deviation that occurs at ~870 m. This position coincides with an increase in grain size from silt to fine sand, it is possible that this reflects evidence of the reworking of older fossils and sediments and the development of a diagenetic overprint. Thereafter any further correlation between both trends is limited. Inspection of the trace element data at ~870 m indicated that there was an increase in the measured concentration of Sr for the specimens with anomalous $^{87}Sr/^{86}Sr$ data, see Table F-4.

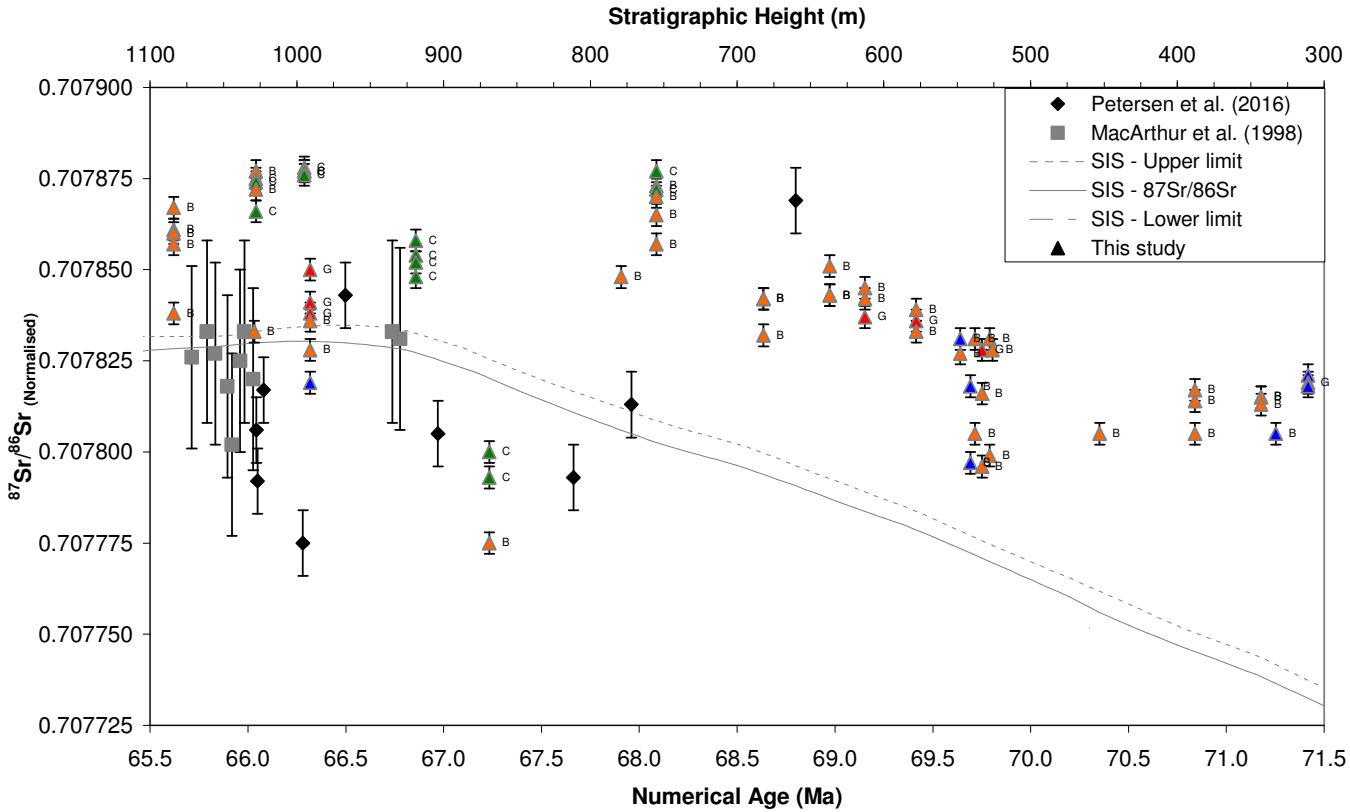

Figure 5-3. Comparison of Sr isotope data from this study with that from the LOWESS smoothed global Strontium Isotope Stratigraphy curve (McArthur *et al*., 2001), previous data from Seymour Island (McArthur *et al*., 1998; Petersen *et al*., 2016). The K-Pg boundary with an age of 66 Ma (Gradstein *et al*., 2012) has a $^{87}Sr/^{86}Sr$ value of 0.707833 from the Strontium Isotope Stratigraphy curve. Data from this study are colour coded, Bivalves = orange, Cephalopods = green, Gastropods = red and specimens of uncertain affinity = blue. Data from McArthur *et al*. (1998) represent a partial dataset of aragonitic specimens from a range of mixed aragonite and calcite macrofossils. Note the larger range of $^{87}Sr/^{86}Sr$ variability in the Sr data from this study and Petersen *et al*. (21016) in comparison with that from McArthur *et al*. (1998). Data for this study have a calculated standard error of measurement = ±0.000003, for Petersen *et al*. (2016) a calculated standard error of measurement = ±0.000009 and McArthur *et al*. (1998) quoted a precision of ±0.000015 (2 σ) based upon replicated sample analysis, their data have a calculated standard error of measurement = ±0.000004.

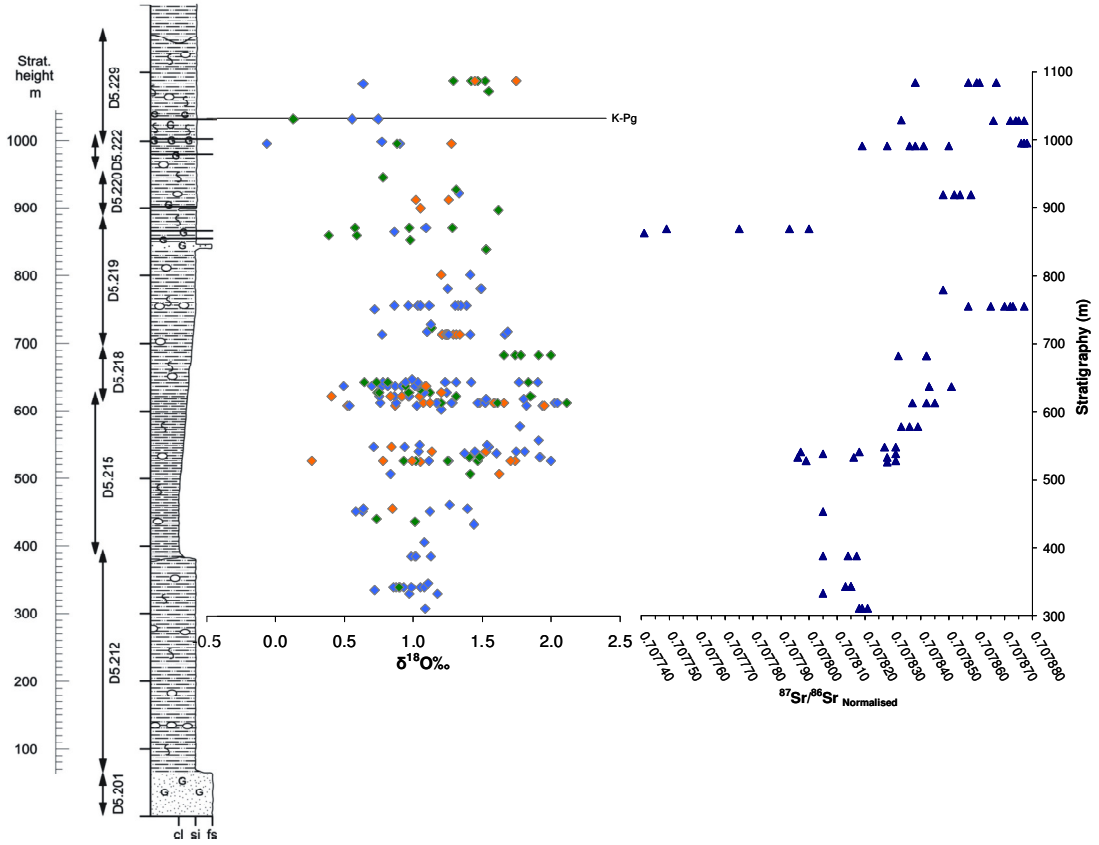

Figure 5-4. Correlation of $^{87}Sr/^{86}Sr$ data (this study) with $\delta^{18}O$ data vs. the measured stratigraphy. There is a possible trend in the strontium data that parallels a similar trend in the $\delta^{18}O$ data, there is a generally good agreement between both trends until an apparent deviation that occurs at ~870 m. This position coincides with an increase in grain size from silt to fine sand, it is possible that this reflects evidence of reworking of sediments and the development of a diagenetic overprint. . Thereafter any further correlation between both trends is limited.

5.5 Synthesis

The wide variability exhibited by the $^{87}Sr/^{86}Sr$ data may result from the diagenetic alteration of the skeletal carbonates but given the overall quality of the stable isotope data and the good correlation of the trace element chemistry with the stable isotope data this seems less likely. The similarities between this dataset and the published data from Petersen *et al*. (2016) suggest that the variability did not arise from faulty or flawed sample preparation or a flawed Sr extraction process. The standard error of measurement for the $^{87}Sr/^{86}Sr$ data was ±0.000003 which again suggests that the measurements are consistent and repeatable particularly since many of the measurements were performed on replicate samples. However, there still remains the fact that the 3rd dataset (McArthur *et al*., 1998) does not exhibit a similar variability although there is no indication of whether any data were discarded from their study. Nor is there any indication of possible outliers within their original data. Their range of specimens included both aragonitic and calcitic shell mineralogies there was, however, no indication of which shell mineralogy was referred to in their comments.

McArthur *et al*. (1998) noted that diagenesis of skeletal carbonates in their data appeared to decrease the level of Sr in contrast to the normal expected increase. Perhaps the increase in Sr concentrations in the section between 800 and 869 m and the subsequent reduction towards 900 m reflected reworking of older fossil material, perhaps with a diagenetic signature (see Table F-4). The converse is that the majority of the specimens sampled were in fact showing evidence of pervasive diagenesis. This seems highly unlikely given the intensive work undertaken to confirm the lack of diagenetic features in the selected specimens. The average value of Sr from this study was 2863 ppm in comparison with a value of 2121 ppm for the aragonitic specimens reported in McArthur *et al*, (1998). A further possibility for the variations might be reflected in the selected taxa, Petersen *et al*. (2016) only measured skeletal carbonates from bivalves but this study included bivalves, cephalopods and gastropods. McArthur *et al*. (1998) commented that aragonite from ammonites and bivalves was suitable for Sr isotope analysis, although no ammonite specimens were reported in their data.

What is difficult to reconcile is the overall similarity of the data from this study and Petersen *et al*. (2016) in comparison with those from previously published data (McArthur *et al*., 1998, 2001), especially since data were derived from aragonite shell material in all three studies. The similarity suggests that preparation or analytical procedures were not responsible for the discrepancies observed in the Sr data.

Only a minimal number of data points provided a good fit with the SIS curve and these were all in close proximity to the position of the K-Pg boundary, consequently it has not been possible to improve the chronostratigraphy of the measured section. This is a disappointing and perplexing outcome to a section of the study that, as has already been mentioned, appeared to produce good and consistent internal data. Whether the discrepancy of these data and those from Petersen *et al*. (2016) indicate a possible problem with the interpretation and usage of strontium isotope data from aragonite skeletal material stratigraphy in high palaeolatitudes remains open to question. However, comparison of the $^{87}Sr/^{86}Sr$ data from this study with the Late Cretaceous SIS curve (McArthur *et al*., 2001) was inconclusive, it has not been possible to reliably date any palaeoenvironmental events using the $^{87}Sr/^{86}Sr$ data. Further investigation of the specimens from Seymour Island and these data are required.

6 Conclusions

6.1 Introduction

The primary aim for this study was the investigation of climate change during the latest Maastrichtian – earliest Danian, aragonite molluscan shell material was analysed and generated stable isotope, trace element chemistry and shell mineralogy data. A further phase of the study also measured strontium isotopes from a subset of the diagenetically screened specimens. The decision to only analyse aragonitic material was made at the commencement of the project - AFI 6/28 titled **"Terminal Cretaceous climate change and biotic response in Antarctica".** This decision was vindicated by the apparent paucity of calcitic specimens within the measured stratigraphy and a strong correlation between extensive diagenetic alteration and molluscan specimens with a calcite shell material.

6.2 Diagenetic screening

Diagenetic screening methods enabled an assessment of the overall suitability of individual specimens for inclusion in both stable isotope analysis and for those with minimal diagenetic alteration subsequent palaeotemperature determination. A key decision in the research design for this study was that only specimens with aragonite skeletal carbonate would be selected for stable isotope analyses.

As previously mentioned all of the macrofossil specimens selected for this study from the BAS collection were subject to a certain degree of diagenetic alteration (Marshall 1992). Diagenetic screening was intended to identify those specimens that showed the least altered characteristics. Three principal methods were adopted for the diagenetic screening of skeletal carbonate shell material namely; image analysis (SEM), mineralogical analysis by X-ray diffraction (XRD) and determination of trace element concentration by ICP-OES. Minor techniques included cold cathodoluminescence (CL), carbonate staining and automated SEM-EDS analysis using QEMSCAN technology. No single method can confidently identify the least altered specimens suitable for stable isotope analyses. It was apparent that an over reliance on any single one of the three methods might lead to either flawed analysis or perhaps worse still the rejection of suitable specimens for further analysis. The diagenetic screening methodology comprised a combination of these three principal methods, each of which was scored or assessed before arriving at an overall suitability score for each individual specimen.

However, not all of the techniques were employed for each of the specimens; for example there were specimens where insufficient sample powders were available for

trace element analysis and others without SEM imaging. Consequently there were 117 specimens with no SEM images, 27 specimens with no XRD analysis and 44 specimens with no ICP-OES trace element screening. With these gaps in the diagenetic screening it was unfeasible to apply a single unified approach to diagenetic scoring of the specimens. Given the outstanding quality of the macrofossils from Seymour Island and the good preservation state of the aragonitic specimens it seemed inappropriate to reject those where the scoring process was incomplete.

Reviewing the diagenetic scoring data (see Appendix B, Table B-3) indicated that 34 specimens were found to have a wholly unsuitable shell mineralogy for inclusion in further analyses. The remaining 213 specimens were all deemed to be suitable for stable isotope analysis but only 116 fully satisfied all of the screening requirements. From the remainder, 53 specimens showed Fe or Mn concentrations above the selected threshold levels (e.g. Fe ≥ 500 ppm and Mn ≥ 200 ppm) and the final 44 specimens recorded no trace element data. Further comparative screening of stable isotope data from screened and partially screened specimens (e.g. those without trace element data) was discussed in Appendix D.

6.2.1 Aragonite skeletal preservation

One obvious question was why the preservation of the skeletal carbonates, in particular aragonite, was so good in the James Ross Basin. It was apparent that the basin underwent rapid infilling (~270 m/Ma) but with a relatively shallow burial depth and an associated low temperature, (MacArthur *et al*., 1998; Svojtka *et al*., 2009; Tobin *et al*., 2012). Temperatures < 60°C have been reported based upon vitrinite and AMS analyses and this low burial temperature must have had a significant effect on restricting the diagenetic alteration of the skeletal carbonates (Svojtka *et al*., 2009; Tobin *et al*., 2012). The lack of persistent diagenesis in aragonite specimens suggests that conditions within the basin limited the dissolution of the primary aragonite and subsequent precipitation of diagenetic cements (see Petersen *et al*., 2016). The nature of aragonite preservation was reported by Jordan *et al*. (2015), they stated that approximately 10% of aragonite was preserved in the geological record. Dissolution of aragonite was inhibited where the sediment water interface was depleted in O_2, aragonite also undergoes dissolution at a higher pH (7.8) than calcite. The preservation of aragonite may be linked to buffering by sediment which inhibits dissolution by limiting change of pH. Reducing the transport of O_2 across the seawater/sediment interface limits the activity of sulphate oxidising bacteria and the generation of H_2S, which in turn alters the pH and induces dissolution of the aragonite. This scenario may reflect what occurred with the rapid infilling of the James Ross Basin limiting the rate of aragonite

dissolution. Schoepfer *et al*. (2017) discussed the development of cyclic anoxic to euxinic conditions in the Late Maastrichtian to Early Danian James Ross Basin based upon the analysis of major and minor trace elements.

As previously described the presence of primary skeletal aragonite is rare in the Phanerozoic due to the metastable nature of the mineral, when present it provides a direct geochemical link to the palaeoenvironment in which the macrofauna flourished. The López de Bertodano Fm. contains a relatively low diversity but abundant invertebrate and vertebrate macrofauna and appears to be dominated by taxa with aragonite skeletal carbonate. Other studies have reported stable isotope and trace element data from taxa utilising just calcite skeletal carbonate, notably foraminifera, oysters and belemnites. But as this study has shown there appeared to be a strong basis for a correlation between calcitic shell material and evidence of diagenesis. This was most apparent within the trace element data.

6.3 Stable isotope analysis

A high resolution oxygen and carbon stable isotope record through the Latest Maastrichtian – Earliest Danian was generated using diagenetically unaltered aragonite nacre shell material from a molluscan fauna collected from the López de Bertodano Fm., part of the Marambio Group, which forms an extensive 1100 m thick Late Maastrichtian section from Seymour Island, Antarctica. Coverage of stable isotope data for the measured stratigraphy was good, with 247 analyses including data from within 1 m of the K-Pg boundary, although there were fewer macrofossils deemed suitable for isotopic analysis at the top of the section. No suitably preserved macrofossil specimens were found in the lower 300 m of the succession. Samples with Mg, Fe and Mn trace element concentrations above published guidelines (Morrison and Brand, 1988; Brand, 1991) were excluded from the data set but the presence of surface contamination of the aragonite nacre shell material may have caused the trace element data to highlight potential diagenetic issues without actually representing the true cation levels present within the aragonite lattice.

Stable isotope data (‰ VPDB) for primary aragonite from a molluscan fauna (bivalves, cephalopods and gastropods) exhibited unscreened ranges of -0.06 to +2.11‰ for $\delta^{18}O$ and -10.49 to +4.34‰ for $\delta^{13}C$, corresponding screened stable isotope data $_{(n=213)}$ gave ranges of -0.06 to +2.05‰ for $\delta^{18}O$ and -7.54 to +3.7‰ for $\delta^{13}C$. Data show that at individual stratigraphic levels, the range in measured $\delta^{18}O$ exhibits significant variability e.g. +0.86 to +1.08‰ at 343 m, +0.76 to +2.11‰ at 613 m, +0.77 to 1.67‰ at 712 m and +1.29 to +1.74‰ at 1084 m (K-Pg boundary located

at 1029 m above datum) (Thorn *et al*., 2009). Bivalve molluscs with a benthic mode of life exhibited the widest range of $\delta^{18}O$ and $\delta^{13}C$ values.

The variability seen in the $\delta^{18}O$ stable isotope data has similarities with that exhibited by both present day shallow marine and fossil molluscan assemblages on Seymour Island. Significant variability in $\delta^{18}O$ values at individual stratigraphic levels cannot be attributed to just diagenetic alteration, a similar variability was quoted for stable isotope data in the Eocene La Meseta Fm. from Seymour Island, Antarctica. It has been generally accepted that organisms deposit carbonate shell material under equilibrium conditions with respect to seawater, evidence from the stable isotope data from this study indicates that this may not be the case. The overall variability in the range of stable isotope values generated in this study suggest that there is a good case for the presence of species specific 'vital effects' operating whilst organisms precipitate carbonate shell material. It is probable that the implementation of 'vital effects' may not be systematic for an individual genus and that some variation in the stable isotope data will reflect variability generated by a specific individual organism.

6.3.1 $\delta^{18}O_{water}$ selection

Relative palaeotemperatures (°C) were calculated for screened $\delta^{18}O$ values for a constant seawater composition of -1.0‰ (SMOW), representing ice free ocean water. The value of SMOW may require modification for parts of the succession since there is evidence that a lowering of sea level, as a result of glacioeustasy, occurred during the Latest Maastrichtian. The adoption of a fixed value for $\delta^{18}O_{water}$ was restrictive and significantly underestimated the range of temperatures for a single specimen in comparison with the temperatures generated by clumped isotope analysis, see Petersen *et al*. (2016). The ability to generate a value of $\delta^{18}O_{water}$ direct from a $\delta^{18}O$ value and a clumped isotope temperature is a highly valuable technique but with attendant issues regarding variability. The technique was unfortunately of only marginal use for this study for a number of reasons:

- Stratigraphic coverage was limited to the upper 500 m of the stratigraphic section
- Derived $\delta^{18}O_{water}$ values exhibited extensive ranges, as reflected in the $\delta^{18}O$ values, at the same stratigraphic positions (see Table F-4). For example the data presented in Table 6-1 illustrate the effect of differing values of $\delta^{18}O_{water}$ for an identical $\delta^{18}O$ value, note the variability in temperature.

The range of calculated temperatures at any stratigraphic position will reflect both differences in the $\delta^{18}O_{water}$ and selection of seasonal shell material. The former may

reflect the waxing and waning of localised ice sheets and how much surface freshwater runoff was depleted in $\delta^{18}O$.

Table 6-1. Comparison of temperatures determined with different values of $\delta^{18}O_{Water}$ for the same $\delta^{18}O$ value

Depth(m)	$\delta^{18}O_{Water}$	$\delta^{18}O$	Temp (℃)
1029	-2.6	1	5.0
1029	-2.46	1	5.6
1029	-0.71	1	13.2
1029	-0.48	1	14.2
1028	-1.93	1	7.9
1028	-1.9	1	8.0
1028	-1.89	1	8.1
1028	-0.51	1	14.0
895	-1.49	1	9.8
895	-0.2	1	15.4
895	-0.09	1	15.9
895	1.05	1	20.8

Many bivalves exhibit seasonal growth patterns, for example with shell growth slowing or even ceasing during the winter. Petersen *et al*. (2016) argued that this was one reason for the variability in the temperatures generated from their clumped isotope work. Their material for analysis was prepared from specific known positions on individual specimens, the material sampling for this study was considerably more random because in many cases the fossil specimens were providing loose aragonite nacre. This limited the ability to determine from where fragments of nacre had originated for a particular specimen and may be a reason for the wide variability seen in the $\delta^{18}O$ in this study, with fluctuation in the value of $\delta^{18}O_{water}$ also being responsible for variability in calculated temperatures.

6.3.2 Palaeotemperature synthesis

Relative palaeotemperatures were calculated for the 3 fossil types with ranges of 6 to 14℃ for bivalves, 9 to 12℃ for gastropods and 9 to 15℃ for cephalopods. Palaeotemperatures indicate the presence of a cooling trend in the Latest Maastrichtian followed by a small recovery prior to the K-Pg boundary and subsequently followed by a further phase of cooling. These trends reflect global changes to the Late Maastrichtian as published by other authors. For example Linnert *et al*. (2014) reported on the Late Cretaceous climate using TEX_{86} analysis of sediments from the western North Atlantic at 35 °N, which indicated significant cooling (~7 ℃) to <~28 ℃ during the Maastrichtian. They noted that the overall stratigraphic trend was similar to other records of high latitude SSTs and bottom water temperatures.

Stable isotope data show that individual stratigraphic levels can exhibit significant variability for $\delta^{18}O$ and $\delta^{13}C$ and that as a result analysis of single samples at discrete stratigraphic levels may provide an erroneous interpretation of climate change. Previous studies using single results at discrete stratigraphic levels may suggest climate was more variable.

Highest oxygen isotope values are evident in mid section and may be associated with periods of cooler climate. However, the wide variability of the stable isotope values, in particular that for $\delta^{18}O$, suggests that the interpretation of warmer or cooler climatic conditions may be problematic. The relatively cool temperatures are consistent with data from previous studies and indicate that ice may have been present at the pole. There is evidence of both warm and cool events. The stable isotope data indicate cool and relatively stable benthic temperatures of ~10°C for the section.

Overall the data indicate the presence of both a cooling and a subsequent modest increase in benthic water temperatures in the Late Maastrichtian/Early Palaeocene. A tentative moving average curve representing temperature has been superimposed upon calculated palaeotemperatures, see Figures 4-2 and 3. It must be noted that the temperature curve presented in Figure 4-2 comprised data for bivalves, gastropods and cephalopods, consequently there was a minor level of mixing between the benthic and nektonic records. However, the benthic taxa represented 83% of the screened specimens and also exhibited the widest stratigraphic range. The same data are presented in Figure 4-3 but with separate trend lines for benthic and nektonic taxa. There is an overall similarity between both trends until approximately 780 m (68.2 Ma) at which point the nektonic data more prominently display a warming trend. One distinct problem with the upper part of the section is the relative paucity of suitable specimens and unusually for this study there are more nektonic specimens present until a number of bivalve specimens post K-Pg. The data presented in Figure 4-4 were categorised by fossil type and highlight the importance of the bivalve data. However, the overall variability in the data complicates any attempt to generate an accurate stable isotope or temperature trend. Data are comparable with younger populations, suggesting that a range of factors influence the values. Palaeotemperature results were in general agreement with previous macrofossil studies on Seymour Island.

6.3.3 Winter sea ice?

It seems likely that Seymour Island was subject to winter sea ice, temperatures from this study indicate cool conditions for benthic organisms. Although temperatures were warmer than some of the data reported by Petersen *et al*. (2016) where temperatures derived from clumped isotope analyses indicate benthic temperatures of ~3 - 5°C and

in some cases sub-zero temperatures. However, without the benefit of variable $\delta^{18}O_{water}$ values provided from clumped isotope analyses all temperatures were determined using a fixed value of -1.0‰ (SMOW). As previously discussed and based on the data reported by Petersen *et al*. (2016) this reduces the overall range of temperatures at any particular stratigraphic position. Bowman *et al*. (2013) proposed the development of winter sea ice determined from the palynomorph record of Seymour Island, Antarctica. The authors reported the dominance of the dinoflagellate cyst *Impletosphaeridium clavus* caused by the presence of cysts from dinoflagellate blooms associated with the decay of winter sea ice. They also reported that peaks and lows of *Impletosphaeridium clavus* abundance marked cold temporary stratification of polar waters, interposed with warmer periods when the ocean was well-mixed. Prior to the K-Pg boundary *Impletosphaeridium clavus* decreased dramatically in abundance possibly due to the onset of warming associated with Deccan Traps volcanism.

The stable isotope data generated from this study have raised a number of questions with regard to the interpretation of climate change from high resolution stable isotope studies. In particular variability within the range of $\delta^{13}C$ and $\delta^{18}O$ isotope data measured at specific stratigraphic positions, it has been shown that the reported ranges were not necessarily present as a result of errors introduced either during specimen selection, powder preparation, diagenetic selection or analysis of the actual specimen powders.

Other studies have reported similar ranges within their stable isotope data sets and it is probable that the significant variability seen within this data set may indeed be more common than expected for stable isotope palaeoenvironmental studies. It is also possible that the variability seen in the stable isotope data may be attributable to the effects of fresh water run-off from the proximal landmass modifying the $\delta^{18}O_{water}$ by mixing.

6.4 Strontium isotope analysis

A total of 71 separate samples were analysed including duplicates and triplicates. The wide variability exhibited by the $^{87}Sr/^{86}Sr$ data may result from the diagenetic alteration of the skeletal carbonates but given the overall quality of the stable isotope data and the good correlation of the trace element chemistry with the stable isotope data this seems less likely. The similarities between this dataset and the published data from Petersen *et al*. (2016) suggest that the variability did not arise from faulty or flawed sample preparation or a flawed Sr extraction process. The standard error of measurement for the $^{87}Sr/^{86}Sr$ data was ±0.000003, which suggests that the measurements are consistent and repeatable particularly since many of the

measurements were performed on replicate samples. However, there still remains the fact that the 3rd dataset (McArthur *et al*., 1998) did not exhibit a similar variability although there is no indication of whether any data were discarded from their study. Nor is there any indication of possible outliers within their original data. Their range of specimens included both aragonitic and calcitic shell mineralogies there was, however, no indication of which shell mineralogy was referred to in their comments.

McArthur *et al*. (1998) noted that diagenesis of skeletal carbonates in their data appeared to decrease the level of Sr in contrast to the normal expected increase. Perhaps the increase in Sr concentrations in the stratigraphy between 800 and 869 m and the subsequent reduction towards 900 m reflected reworking of older fossil material, perhaps with a diagenetic signature (see Table F-4). The converse is that the majority of the specimens sampled were in fact showing evidence of pervasive diagenesis. This seems highly unlikely given the intensive work undertaken to confirm the lack of diagenetic features in the selected specimens. The average value of Sr from this study was 2863 ppm in comparison with a value of 2121 ppm for the aragonitic specimens reported in McArthur *et al*, (1998). A further possibility for the variations might be reflected in the selected taxa, Petersen *et al*. (2016) only measured skeletal carbonates from bivalves but this study included bivalves, cephalopods and gastropods. McArthur *et al*. (1998) commented that aragonite from ammonites and bivalves was suitable for Sr isotope analysis, although no ammonite specimens were reported in their data.

What is difficult to reconcile is the overall similarity of the data from this study and Petersen *et al*. (2016) in comparison with those from previously published data (McArthur *et al*., 1998, 2001), especially since data were derived from aragonite shell material in all three studies. The similarity suggests that preparation or analytical procedures were not responsible for the discrepancies observed in the Sr data.

Only a minimal number of data points provided a good fit with the SIS curve and these were all in close proximity to the position of the K-Pg boundary, consequently it has not been possible to improve the chronostratigraphy of the measured section. This is a disappointing and perplexing outcome to a section of the study that, as has already been mentioned, appeared to produce good and consistent internal data. Whether the discrepancy of these data and those from Petersen *et al*. (2016) indicate a possible problem with the interpretation and usage of strontium isotope data from aragonite skeletal material stratigraphy in high palaeolatitudes remains open to question. However, comparison of the $^{87}Sr/^{86}Sr$ data from this study with the Late Cretaceous SIS curve (McArthur *et al*., 2001) was inconclusive, it was not possible to reliably date any palaeoenvironmental events using the $^{87}Sr/^{86}Sr$ data. Only a small portion of the

dataset lie within the 95% confidence range for the published SIS curve and these values are all clustered around the position of the K-Pg boundary.

Previous Sr isotope analysis was carried out on samples collected from Seymour Island and some of those data were incorporated into the LOESS Smoothed Global Strontium Isotope Curve. The lack of dateable ash layers in the succession and the endemism present within the Austral Late Cretaceous mollusca makes the provision of accurate absolute dates a matter of some importance. Further investigation of these data are required.

6.5 Further work

Since the project data set conveniently splits into a number of discrete areas actual results may be published as a series of manuscripts for publication. Topics to be covered will include:

1. An overall discussion of the oxygen and carbon stable isotope data and interpreted palaeoclimate.
2. A discussion of the wide variability seen in the oxygen and carbon stable isotope data at certain stratigraphic positions in comparison with the overall variability seen for the full succession.
3. A discussion of the preservation of molluscan aragonite nacre from Seymour Island.
4. A discussion of the $^{87}Sr/^{86}Sr$ data and why their correlation with the published global marine strontium isotope curve is poor.

The following further work should also be planned:

- Investigation of differences in the stable isotope data derived from specimens with a calcite shell mineralogy versus that derived from aragonite nacre shell mineralogy.
- Investigation of differences that may exist in the $^{87}Sr/^{86}Sr$ isotope data derived from aragonite and calcite from Seymour Island.

6.6 Epilogue

As a closing statement at the end of this period of research, which for numerous reasons took 12 years to reach completion, I offer the following quotation:

> '*Far from static, Antarctica has travelled long distances, in both space and time. The most ancient fragments once basked beneath a tropical Precambrian sun, in communion with cratonic West Australia and enveloped in a loosely defined supercontinent, Rodinia. Playing an active role in Rodinia breakup and Gondwana assembly at the dawn of the Palaeozoic, Antarctica commenced a*

long southward drift in Late Ordovician time. During the transit to its present polar position, Antarctica participated in the assembly of yet another supercontinent, Pangea. Jurassic and subsequent divorces left Antarctica surrounded by spreading ridges and marine circum-Antarctic gateways at the beginning of the Oligocene. Once the queen of the continental cotillion, Antarctica has danced away from the heart of it all to a splendid, ice-bound isolation at the bottom of the world—truly the Last Place on Earth.' (Torsvik *et al*., 2008).

7 Acknowledgements

I wish to take this opportunity to thank the following people who provided invaluable help during my period of research and offered helpful and pertinent advice; Dr. Duncan Pirrie, Prof. Jim Marshall, Prof. Jane Francis, Dr. Vanessa Bowman, Dr. Ian Millar, Dr. Jane Evans, Dr. Jens Andersen, Dr. Gavyn Rollinson, Dr. Andrew Fisher. I further wish to acknowledge the NERC Isotope Geoscience laboratory, Kingsley Dunham Centre, Keyworth for the use of their strontium isotope facilities.

I gratefully acknowledge the assistance that I received from other members of the 'AFI 6/28' NERC funded research project, in particular Dr. Pirrie and Prof. Marshall from the University of Liverpool who both provided considerable assistance regarding the analysis and interpretation of the stable isotope data; Prof. J. Francis and Dr. V. Bowman for their support and assistance during the project and for a number of the figures and field photographs. I also acknowledge the financial support received from the project and Dr. Pirrie that met the cost of stable isotope measurements at the University of Liverpool and my travel costs associated with project meetings and conference attendance. I also acknowledge the support provided by the University of Exeter that enabled me to carry out this research programme.

Finally I would like to thank my wife Jane who whilst living in British Columbia was always close by in my thoughts, my children Kirsen and Ben, my sister Cathy and close friends Simon, Jane, Susi and Tony for their continuing interest in my research. Without your support I could never have completed this journey.

8 References

http://rruff.info/repository/sample_child_record_powder/by_minerals/Aragonite__R040078-1__Powder__Xray_Data_XY_RAW__211.txt. Accessed 20-12-2014

http://rruff.info/repository/sample_child_record_powder/by_minerals/Calcite__R040070-1__Powder__Xray_Data_XY_RAW__190.txt. Accessed 20-12-2014

http://rruff.info/repository/sample_child_record_powder/by_minerals/Gypsum__R040029-1__Powder__Xray_Data_XY_RAW__67.txt. Accessed 20-12-2014

http://archive.org/details/voyageofhuronhun00stac.html. Accessed 12-08-2013

http://www.eoearth.org/article/antarctic_peninsula. Accessed 13-05-2013.

http://www.stratigraphy.org/ICSchart/ChronostratChart2014-02.pdf. Accessed 18-01-2015.

Dr. Pieter Tans, NOAA/ESRL (www.esrl.noaa.gov/gmd/ccgg/trends/) and Dr. Ralph Keeling, Scripps Institution of Oceanography (scrippsco2.ucsd.edu/). Date accessed: 11-02-2015.

Affek, H. P., Guo, W., Daeron, M. and Eiler, J. M., 2008. 'Clumped isotopes' in speleothem carbonate and atmospheric CO(2) - Is there a kinetic isotope effect?. *Geochimica et Cosmochimica Acta*, **72**, A6-A6.

Alley, N.F. and Frakes, L.A., 2003. First known Cretaceous glaciation: Livingston Tillite Member of the Cadna-owie Fm., South Australia. *Australian Journal of Earth Sciences*, **50**, 139-144.

Allison, N., 1996. Comparative determinations of trace and minor elements in coral aragonite by ion microprobe analysis, with preliminary results from Phuket, southern Thailand. *Geochimica et Cosmochimica Acta*, **60**, 3457-3470.

Altman, D.G. and Bland, J.M., 2005. Standard deviations and standard errors. *British Medical Journal*, **331**, 903.

Anderson, T.F., Popp, B.N., Williams, A.C., Ho, L.-Z. and Hudson, J.D., 1994. The stable isotopic records of fossils from the Peterborough Member, Oxford Clay Fm. (Jurassic), UK: palaeoenvironmental implications. *Journal of the Geological Society*, **151**, 125-138.

Archer, D., Martin, P., Buffett, B., Brovkin, V., Rahmstorf, S. and Ganopolski. A., 2004. The importance of ocean temperature to global biogeochemistry. *Earth And Planetary Science Letters*, **222**, 333-348.

Askin, R.A. and Jacobson, S.R., 1996. Palynological change over the Cretaceous–Tertiary boundary on Seymour Island, Antarctica: environmental and depositional

factors. *In*: Macleod, N., Keller, G. (Eds.), *Cretaceous–Tertiary Mass Extinctions: Biotic and Environmental Changes*. W.W. Norton and Company, New York, 7–25.

Auclair, A., Joachimskib, M.M. and Lecuyer, C., 2003. Deciphering kinetic, metabolic and environmental controls on stable isotope fractionations between seawater and the shell of *Terebratalia transversa* (Brachiopoda). *Chemical Geology*, **202**, 59– 78.

Auclair, A., Lecuyer, C., Bucher, H. and Sheppard, S.M.F., 2004. Carbon and oxygen isotope composition of Nautilus macromphalus: a record of thermocline waters off New Caledonia. *Chemical Geology*, **207**, 91-100.

Bailey, T.R., McArthur, J.M., Prince, H. and Thirlwall, M.F., 2000. Dissolution methods for strontium isotope stratigraphy: whole rock analysis. *Chemical Geology*, **167**, 313-319.

Bain, R.J., 1990, Diagenetic, nonevaporative origin for gypsum. *Geology*, **18**, 447-450.

Barrera, E., 1994. Global environmental changes preceding the Cretaceous-Tertiary boundary: Early-late Maastrichtian Transition. *Geology,* **22**, 877-880.

Barrera, E., Tevesz, M.J.S., carter, J.G., McCall, P.L., 1994. Oxygen and carbon isotopic composition and shell ultrastructure of the bivalve *Laternula elliptica* from Antarctica. *Palaios*, **9**, 275-287.

Barron, E. J., Thompson, S. L . and Schneider, S. H., 1981. An ice-free Cretaceous - results from climate model simulations. *Science*, **212**, 501-508.

Barron, E.J, Fawcett, P.J., Pollard, D., Thompson, S., 1994. Model simulations of Cretaceous climates: the role of geography and carbon dioxide. *In*: Allen, J.R.L., Hoskins, B.J., Sellwood, B.W., Spicer, R.S., Valdes, P.J. (Eds.), *Palaeoclimates and their modelling: With special reference to the Mesozoic Era*. Chapman and Hall, pp. 99–108.

Bemis, B.E., Spero, H., Bijma J. and Lea, D.W., 1998. Reevaluation of the oxygen isotopic composition of planktonic foraminifera: experimental results and revised paleotemperature equations. *Paleoceanography* **13**, 150–160.

Bennett, M.R., Doyle, P. and Mather, A.E., 1996. Dropstones: their origin and significance. *Palaeogeography, Palaeoclimatology, Palaeoecology*, **121**, 331-339.

Bernasconi, S.M., Schmid, T.W., Grauel, A.-L. and Mutterlose, J., 2011. Clumped-isotope geochemistry of carbonates: A new tool for the reconstruction of temperature and oxygen isotope composition of seawater. *Applied Geochemistry*, **26**, S279-S280.

Boggs, S., 2009. *Petrology of sedimentary rocks 2nd edition*. Cambridge University Press, The Edinburgh Building, Cambridge, UK.

Bowman, V.C., Francis, J.E., Riding, J.B., Hunter, S.J. and Haywood, A.M., 2012. A latest Cretaceous to earliest Palaeogene dinoflagellate cyst zonation from Antarctica and implications for phytoprovincialism in the high southern latitudes. *Review of Palaeobotany and Palynology*, **171**, 40–56.

Bowman, V.C., Francis, J.E. and Riding, J.B., 2013. Late Cretaceous winter sea ice in Antarctica? *Geology*, **41**, 1227-1230.

Brand, U., 1984. A salinity equation: chemical evaluation of molluscan aragonite. *Society of Economic Paleontologists and Mineralogists Mid-year Meeting*, **Book of Abstracts**, 1-16.

Brand, U., 1986. Paleoenvironmental analysis of Middle Jurassic (Callovian) ammonoids from Poland: Trace elements and stable isotopes. *Journal of Paleontology*, **60**, 293-301.

Brand, U., 1991. Strontium isotope diagenesis of biogenic aragonite and low-mg calcite. *Geochimica et Cosmochimica Acta*, **55**, 505-513.

Brentnall, S.J., Beerling, D.J., Osborne, C.P., Harland, M., Francis, J.E., Valdes, P.J. and Wittig, V.E., 2005. Climatic and ecological determinants of leaf lifespan in polar forests of the high CO_2 Cretaceous 'greenhouse' world. *Global Change Biology*, **11**, 2177–2195.

Budd, D.A., Hammes, U. and Ward, W.B., 2000. Cathodoluminescence in Calcite Cements: New Insights on Pb and Zn Sensitizing, Mn Activation, and Fe Quenching at Low Trace-Element Concentrations. *Journal of Sedimentary Research*, **70**, 217-226.

Buchardt, B., Weiner, S., 1981. Diagenesis of aragonite from Upper Cretaceous ammonites: a geochemical case study. *Sedimentology*, **28**, 423–438.

Cantrill, D.J., 2005a. Taxonomic turnover and abundance in Cretaceous to Tertiary wood floras of Antarctica: Implications for changes in forest ecology. *Palaeogeography Palaeoclimatology Palaeoecology*, **215**, 205-219.

Cantrill, D.J . and Poole, I., 2005b. A new Eocene Araucaria from Seymour Island, Antarctica: evidence from growth form and bark morphology. *Alcheringa*, **29**, 341-350.

Cao, X. and Liu, Y., 2012. Theoretical estimation of the equilibrium distribution of clumped isotopes in nature. *Geochimica et Cosmochimica Acta*, **77**, 292-303.

Chateigner, D., Hedegaardb, C. and Wenk, H.-R., 2000. Mollusc shell ultrastructures and crystallographic textures. *Journal of Structural Geology*, **22**, 1723-1735.

Cicero, A.D., and Lohman, K.C., 2001. Sr/Mg variation during rock-water interaction: Implications for secular changes in the elemental chemistry of ancient seawater. *Geochimica et Cosmochimica Acta*, **65**, 741-761.

Cichowolski, M., Ambrosio, A. and Concheyro, A., 2005. Nautilids from the Upper Cretaceous of the James Ross Basin, Antarctic Peninsula. *Antarctic Science*, **17**, 267-280.

Cochran, J.K., Rye, D.M. and Landman, N.H., 1981. Growth Rate and Habitat of *Nautilus pompilius* Inferred from Radioactive and Stable Isotope Studies. *Paleobiology*, **7**, 469-480.

Cochran, J.K., Neil, H.L., Karl, K.T., Annie, M. and Daniel, P.S., 2003. Paleoceanography of the Late Cretaceous (Maastrichtian) Western Interior Seaway of North America: evidence from Sr and O isotopes. *Palaeogeography, Palaeoclimatology, Palaeoecology*, **191**, 45-64.

Cotton, F.A. and Wilkinson, G., 1980. *Advanced inorganic chemistry*. John Wiley and Sons, New York, USA.

Craggs, H.J., 2005. Late Cretaceous climate signal of the Northern Pekulney Range Flora of northeastern Russia. *Palaeogeography, Palaeoclimatology, Palaeoecology*, **217**, 25-46.

Craggs, H.J., Valdes, P.J. and Widdowson, M., 2012. Climate model predictions for the latest Cretaceous: An evaluation using climatically sensitive sediments as proxy indicators. *Palaeogeography, Palaeoclimatology, Palaeoecology*, **316**,12-23.

Crame, J.A., 1992. Late Cretaceous palaeoenvironment and biotas: an Antarctic perspective. *Antarctic Science*, **4**, 371-382.

Crame, J.A., Lomas, S.A., Pirrie, D. and Luther, A., 1996. Late Cretaceous extinction patterns in Antarctica. *Journal of the Geological Society, London*, **153**, 503-506.

Crame, J.A., Mcarthur, J.M., Pirrie, D. and Riding, J.B., 1999. Strontium isotope correlation of the basal Maastrichtian Stage in Antarctica to the European and US biostratigraphic schemes. *Journal of the Geological Society*, **156**, 957-964.

Crame, J.A., Francis, J.E., Cantrill, D.J. and Pirrie, D., 2004. Maastrichtian stratigraphy of Antarctica: *Cretaceous Research*, **25**, 411-423.

Crame, J.A., Beu, A.G., Ineson, J.R., Francis, J.E., Whittle, R.J. and Bowman, V.C., 2014. The early origin of the Antarctic marine fauna and its evolutionary implications. *PLoS ONE*, **9(12)**: e114743. doi:10.1371/journal.pone.0114743

de Paula, S.M. and Silveira, M., 2009. Studies on molluscan shells: Contributions from microscopic and analytical methods: *Micron*, **40**, 669-690.

de Souza, K.K.D., Schaefer, C.E.G.R., Simas, F.N.B., Spinola, D.N. and de Paula, M.D., 2014. Soil Fm. in Seymour Island,Weddell Sea, Antarctica. G*eomorphology*, **225**, 87–99.

Dennis, K.J., Affek, H.P., Passey, B.H., Schrag, D.P. and Eiler, J.M., 2011. Defining an absolute reference frame for 'clumped' isotope studies of CO2. *Geochimica et Cosmochimica Acta*, **75**, 7117-7131.

Dennis, K.J., Cochran, J.K., Landman, N.H. and Schrag, D.P., 2013. The climate of the Late Cretaceous: New insights from the application of the carbonate clumped isotope thermometer to Western Interior Seaway macrofossil. *Earth and Planetary Science Letters*, **362**, 51-65.

Dettman, D.L, Reische, A.K and Lohmann, K.C., 1999. Controls on the stable isotope composition of seasonal growth bands in aragonitic fresh-water bivalves (unionidae). *Geochimica et Cosmochimica Acta*, **63**, 1049-1057.

Dickson, J.A.D., 1966. Carbonate identification and genesis as revealed by staining. *Journal of Sedimentary Petrology*, **36**, 491-505.

Ditchfield, P.W., Marshall, J.D. and Pirrie, D., 1994. High latitude palaeotemperature variability: New data from the Tithonian to Eocene of James Ross Island, Antarctica. *Palaeogeography, Palaeoclimatology, Palaeoecology*, **107**, 79-101.

Dutton, A., Huber, B.T., Lohmann, K.C. and Zinsmeister, W.J., 2007. High-resolution stable isotope profiles of a dimitobelid belemnite: Implications for paleodepth habitat and late maastrichtian climate seasonality. *Palaios*, **22**, 642-650.

Eglinton, T.I. and Eglinton, G., 2008. Molecular proxies for paleoclimatology: *Earth and Planetary Science Letters*, v. **275**, 1-16.

Eiler, J.M., 2006a, 'Clumped' isotope geochemistry. *Geochimica et Cosmochimica Acta*, **70**, A156-A156.

Eiler, J.M., 2006b, A practical guide to clumped isotope geochemistry. *Geochimica et Cosmochimica Acta*, **70**, A157-A157.

Eiler, J., 2007. “Clumped-isotope” geochemistry—The study of naturally-occurring, multiply-substituted isotopologues. *Earth and Planetary Science Letters*, v. **262**, 309-327.

Eiler, J.M., Affek, H., Daeron, M., Ferry, J., Guo, W.F., Huntington, K., Thiagarajan, N. and Tripati, A., 2008. Carbonate 'clumped isotope' thermometry: A status report. *Geochimica et Cosmochimica Acta*, **72**, A239-A239.

Eiler, J., Bergmann, K., Bonifaci, M., Eagle, R., Finnegan, S., Fischer, W., Passey, B., Stolper, D. and Tripati, A., 2010. Carbonate clumped isotope thermometry as a tool for paleoceanography. *Geochimica et Cosmochimica Acta*, v. **74**, A261-A261.

Eiler, J.M., 2011. Paleoclimate reconstruction using carbonate clumped isotope thermometry. *Quaternary Science Reviews*, v. **30**, 3575-3588.

Elliot, D.H., Askin, R.A., Kyte, F.T. and Zinsmeister, W.J. 1994. Iridium and dinocysts at the Cretaceous-Tertiary boundary on Seymour Island, Antarctica: Implications for the K-T event. *Geology* **22**, 675-678.

Elorza, J., Alday, J.J.G. and Olivero, E.B., 2001. Environmental stress and diagenetic modifications in inoceramids and belemnites from the Upper Cretaceous James Boss Basin, Antarctica. *Facies*, **44**, 227-242.

Epstein, S., Buchsbaum, R., Lowenstam, H.A. and Urey, H.C., 1951. Carbonate-water isotopic temperature scale. *Geol. Soc. Am. Bull.*, **62**, 417–426.

Etheridge, D.M., Steele, L.P., Langenfelds, R.L., Francey, R.J., Barnola, J.M. and V.I. Morgan, 1996. Natural and anthropogenic changes in atmospheric CO_2 over the last 1000 years from air in Antarctic ice and firn. *J. Geophys. Res.*, **101**, 4115–4128

Farrow, G.E. and Alan Fyfe, J., 1988. Bioerosion and carbonate mud production on high-latitude shelves. *Sedimentary Geology*, **60**, 281-297.

Flögel, S., Wallmann, K. and Kuhnt, W., 2011. Cool episodes in the Cretaceous — Exploring the effects of physical forcings on Antarctic snow accumulation. *Earth and Planetary Science Letters*, **307**, 279-288.

Florindo, F., Cooper, A.K. and O’Brien, P.E., 2003. Introduction to ‘Antarctic Cenozoic palaeoenvironments: geologic record and models’. *Palaeogeography, Palaeoclimatology, Palaeoecology*, **198**, 1-9.

Foster, L.C., Finch, A.A., Allison, N., Andersson, C. and Clarke, L.J., 2008. Mg in aragonitic bivalve shells: Seasonal variations and mode of incorporation in *Arctica islandica*. *Chemical Geology*, **254**, 113–119

Fouke, B.W., Zerkle, A.L., Alvarez, W., Pope, K.O., Ocampo, A.C., Wachtman, R.J., Grajales Nishimura, J.M., Claeys, P. and Fischer, A.G., 2002. Cathodoluminescence petrography and isotope geochemistry of KT impact ejecta deposited 360?km from the Chicxulub crater, at Albion Island, Belize. *Sedimentology*, **49**, 117-138.

Frakes, L.A. and Francis, J.E., 1990. Cretaceous Palaeoclimates. *In*: Ginsburg, R.N. and Beaudoin, B. (eds) Cretaceous Resources. Events and Rhythms, 273-287.

Frakes, L.A. and Krassay, A.A., 1992. Discovery of probable ice-rafting in the Late Mesozoic of the Northern Territory and Queensland. *Australian Journal of Earth Sciences*, **39**, 115-119.

Francis, J.E., 1986. Growth rings in Cretaceous and Tertiary wood from antarctica and their palaeoclimatic implications. *Palaeontology*, **29**, 665-684.

Francis, J.E. and Poole, I., 2002. Cretaceous and early Tertiary climates of Antarctica: evidence from fossil wood. *Palaeogeography, Palaeoclimatology, Palaeoecology*, **182**,47-64.

Francis, J.E., Pirrie, D. and Crame, J.A. (eds) 2006. *Cretaceous-Tertiary High-Latitude Palaeoenvironments, James Ross Basin, Antarctica*. Geological Society, London, Special Publications, **258**, 1-5.

Francis, J.E., Ashworth, A., Cantrill, D.J., Crame, J.A., Howe, J., Stephens, R., Tosolini, A.-M. and Thorn, V., 2008. 100 Million Years of Antarctic Climate Evolution: Evidence from Fossil Plants. *In*: Cooper, A.K., P.J. Barrett, H. Stagg, B. Storey, E. Stump, W. Wise, and the 10th ISAES editorial team, eds. (2008). *Antarctica: A Keystone in a Changing World.* Proceedings of the 10th International Symposium on Antarctic Earth Sciences. Washington, DC: The National Academies Press. doi:10.3133/of2007-1047.kp03

Freitas, P., Clarke, L., Kennedy, H., Richardson, C. and Abrantes, F., 2006. Environmental and biological controls on elemental (Mg/Ca, Sr/Ca and Mn/Ca) ratios in shells of the king scallop Pecten maximus. *Geochimica et Cosmochimica Acta*, **70**, 5119-5133.

Gaft, M., Reisfeld,R. and Panczer, G., 2005. *Modern luminescence spectroscopy of minerals and materials*. Springer-Verlag, Berlin, Germany.

Gallagher, S.J., Wagstaff, B.E., Baird, J.G., Wallace, M.W. and Li, C.L., 2008. Southern high latitude climate variability in the Late Cretaceous greenhouse world. *Global and Planetary Change*, **60**, 351-364.

Gazdzicki, A., Gruszczynski, M., Hoffman, A., Malkowski, K., Marenssi, S.A., Halas, S. and Tatur, A., 1992. Stable carbon and oxygen isotope record in the Palaeogene La Meseta Formation, Seymour-Island, Antarctica. *Antarctic Science*, **4**, 461-468.

Ghosh, P., Adkins, J., Affek, H., Balta, B., Guo, W., Schauble, E., Schrag, D. and Eiler, J., 2006. ^{13}C–^{18}O bonds in carbonate minerals: A new kind of paleothermometer. *Geochimica et Cosmochimica Acta*, **70**, 1439-1456.

Ghosh, P., Eiler, J., Campana, S.E. and Feeney, R.F., 2007a. Calibration of the carbonate 'clumped isotope' paleothermometer for otoliths. *Geochimica et Cosmochimica Acta*, **71**, 2736-2744.

Ghosh, P., Eiler, J. and Petersen, S., 2007b. Carbonate clumped isotope thermometry of molluscs and its applications to Pleistocene gastropod fossils from South Dakota. *Geochimica et Cosmochimica Acta*, **71**, A319-A319.

Goodwin, D.H., Schone, B.R. and Dettman, D.L., 2003. Resolution and fidelity of oxygen isotopes as paleotemperature proxies in bivalve mollusk shells: Models and observations. *Palaios*, **18**, 110-125.

Goody, R., 1980. Polar process and World climate (a brief overview). *Monthly Weather Review*, **108**, 1935-1942.

Gordon, C., Cooper, C., Senior, C.A., Banks, H., Gregory, J.M., Johns, T.C., Mitchell, J.F.B. and Wood, R.A., 2000. The simulation of SST, sea ice extents and ocean heat transports in a version of the Hadley Centre coupled model without flux adjustments. *Climate Dynamics*, **16**, 147–168.

Gradstein, F.M., Ogg, J.G., Schmitz, M.D. and Ogg, G.M., 2012. *The Geologic Time Scale 2012*. Elsevier, Oxford, UK (1144 pp.).

Grauel, A.-L., Schmid, T.W., Hu, B., Bergami, C., Capotondi, L., Zhou, L. and Bernasconi, S.M., 2013. Calibration and application of the 'clumped isotope' thermometer to foraminifera for high-resolution climate reconstructions. *Geochimica et Cosmochimica Acta*, **108**, 125-140.

Grossman, E.L. and Ku, T., 1986. Oxygen and carbon fractionation in biogenic aragonite: temperature effects. *Chemical Geology (Isotope geoscience section),* **59**, 59-74.

Haberlah, D., Strong, C., Pirrie, D., Rollinson, G.K., Gottlieb, P., Botha, P.P.W.S.K. and Butcher, A.R., 2011. Automated petrography applications in Quaternary Science. *Quaternary Australasia*, **28**, 3-12.

Habermann, D., Neuser, R.D. and Richter, D.K., 1996. REE-activated cathodoluminescence of calcite and dolomite: high-resolution spectrometric analysis of CL emission (HRS-CL). *Sedimentary Geology*, **101**, 1-7.

Hallam, A., 1985. A review of Mesozoic climates. *Journal of the Geological Society, London*, **142**, 433-445.

Haq, B.U., 2014. Cretaceous eustasy revisited. *Global and Planetary Change*, **113**, 44–58.

Hathway, B., 2000. Continental rift to back-arc basin: Jurassic-Cretaceous stratigraphy and structural evolution of the Larsen Basin, Antarctic Peninsula. *Journal of the Geological Society, London*, **157**, 417-432.

Hay, W.W., 2008. Evolving ideas about the Cretaceous climate and ocean circulation. *Cretaceous Research*, **29**, 725-753.

Hay, W.W., 2011. Can humans force a return to a 'Cretaceous' climate? *Sedimentary Geology*, **235**, 5-26.

Hay, W.W., DeConto, R.M. and Wold, C.N., 1997. Climate: Is the past the key to the future?. *Geologische Rundschau*, **86**, 471-491.

Hay, W.W. and Floegel, S., 2012. New thoughts about the Cretaceous climate and oceans. *Earth-Science Reviews*, **115**, 262-272.

Hay, W.W., Migdisov, A., Balukhovsky, A. N., Wold, C. N., Flogel, S. and Soding, E., 2006. Evaporites and the salinity of the ocean during the Phanerozoic: Implications for climate, ocean circulation and life. *Palaeogeography Palaeoclimatology Palaeoecology*, **240**, 3-46.

Hayes, P.A., Francis, J.E., Cantrill, D.J. and Crame, J.A., 2006. Palaeoclimate analysis of Late Cretaceous angiosperm leaf floras, James Ross Island, Antarctica. *Geological Society, London, Special Publications*, **258**, 49-62.

Haywood, A.M., Ridgwell, A., Lunt, D.J., Hill, D.J., Pound, M.J., Dowsett, H.J., Dolan, A.M., Francis, J.E. and Williams, M., 2011. Are there pre-Quaternary geological analogues for a future greenhouse gas-induced global warming?. *Philosophical Transactions of the Royal Society of London*, **Series A**, 933-956.

Henkes, G.A., Passey, B.H., Wanamaker, A.D., Grossman, E.L., Ambrose, W.G. and Carroll, M.L., 2013. Carbonate clumped isotope compositions of modern marine mollusk and brachiopod shells. *Geochimica et Cosmochimica Acta*, **106**, 307-325.

Herfort, L., Schouten, S., Boon, J.P. and Damste, J.S.S., 2006. Application of the TEX(86) temperature proxy to the southern North Sea. *Organic Geochemistry*, **37**, 1715-1726.

Huber, B.T., 1988. Upper Campanian-Palaeogene foraminifera from the James Ross Island region, Antarctic Peninsula. *In*: Feldmann, R. M. and Woodburne, M. O. (eds.). *Geology and Paleontology of Seymour Island, Antarctic Peninsula*. The Geological Society of America, Memoir **169**, 163-252.

Huber, B.T., Hodell, D.A. and Hamilton, C.P., 1995. Mid- to Late Cretaceous climate of the southern high latitudes. Stable isotopic evidence for minimal equator-to-pole thermal gradients. *Bull. Geol. Soc. Am.*, **107**, 1164-1191.

Huber, B.T., Norris, R.D. and MacLeod, K.G., 2002. Deep-sea palaeotemperature record of extreme warmth during the Cretaceous. *Geology* **30**, 123-126.

Hunter, S.J., Valdes, P.J., Haywood, A.M. and Markwick, P.J., 2008. Modelling Maastrichtian climate: investigating the role of geography, atmospheric CO2 and vegetation. *Climate of the Past Discussions*, **4**, 1-39.

Hunter, S.J., Haywood, A.M., Valdes, P.J., Francis, J.E. and Pound, M.J., 2013. Modelling equable climates of the Late Cretaceous: Can new boundary conditions resolve data–model discrepancies? *Palaeogeography, Palaeoclimatology, Palaeoecology*, **392**, 41-51.

Huguet, C., Kim, J.H., de Lange, G.J., Damste, J.S.S. and Schouten, S., 2009. Effects of long term oxic degradation on the U-37(K '), TEX86 and BIT organic proxies. *Organic Geochemistry*, **40**, 1188-1194.

Huntington, K.W., Eiler, J.M., Affek, H.P., Guo, W., Bonifacie, M., Yeung, L.Y., Thiagarajan, N., Passey, B., Tripati, A., Daeron, M. and Came, R., 2009. Methods and limitations of 'clumped' CO(2) isotope (Delta(47)) analysis by gas-source isotope ratio mass spectrometry. *Journal of Mass Spectrometry*, **44**, 1318-1329.

Huntington, K.W., Wernicke, B.P. and Eiler, J.M., 2010. Influence of climate change and uplift on Colorado Plateau paleotemperatures from carbonate clumped isotope thermometry. *Tectonics*, **29**.

Immenhauser, A., Nägler, T.F., Steuber, T. and Hippler, D., 2005. A critical assessment of mollusk $^{18}O/^{16}O$, Mg/Ca and $^{44}Ca/^{40}Ca$ ratios as proxies for Cretaceous seawater temperature seasonality. *Palaeogeography, Palaeoclimatology, Palaeoecology*, **215**, 221-237.

Ivany, L.C., Lohmann, K.C., Hasiuk, F., Blake, D.B., Glass, A., Aronson, R.B. and Moody, R.M., 2008. Eocene climate record of a high southern latitude continental shelf: Seymour Island, Antarctica. *Geological Society of America Bulletin*, **120**, 659-678.

Ivany, L.C., Wilkinson, B.H. and Jones, D.S., 2003. Using stable isotopic data to resolve rate and duration of growth throughout ontogeny: An example from the Surf Clam, *Spisula solidissima*. *Palaios*, **18**, 126-137.

Jacob, D.E., Soldati, A.L., Wirth, R., Huth, J., Wehrmeister, U. and Hofmeister, W., 2008. Ultrastructure, composition and mechanisms of bivalve shell growth. *Geochimica et Cosmochimica Acta* **72**, 5401–5415.

Jamalian, M., and Adabi, M.H., 2015. Geochemistry, microfacies and diagenetic evidences for original aragonite mineralogy and open diagenetic system of Lower Cretaceous carbonates Fahliyan Formation (Kuh-e Siah area, Zagros Basin, South Iran). *Carbonates and Evaporites*, **30**, 77-98.

Jenkyns, H.C., Forster, A., Schouten, S. and Damste, J.S.S., 2004. High temperatures in the Late Cretaceous Arctic Ocean. *Nature*, **432**, 888-892.

Jimenez-Berrocoso, A., Olivero, E.B., and Elorza, J., 2006. New petrographic and geochemical insights on diagenesis and palaeoenvi ron mental stress in Late Cretaceous inoceramid shells from the James Ross Basin, Antarctica. *Antarctic Science*, **18**, 357-376.

Jones, D.S. and Quitmyer, I.R., 1996. Marking time with bivalve shells: Oxygen isotopes and season of annual increment Fm.. *Palaios*, **11**, 340-346.

Jordan, N., Allison, P.A., Hill, J. and Sutton, M.D., 2015. Not all aragonitic molluscs are missing: taphonomy and significance of a unique shelly lagerst€atte from the Jurassic of SW Britain. *Lethaia*, **48**, 540–548.

Joseph, C., Campbell, K.A., Torres, M.E., Martin, R.A., Pohlman, J.W., Riedel, M. and Rose, K., 2013. Methane-derived authigenic carbonates from modern and paleoseeps on the Cascadia margin : Mechanisms of formation and diagenetic signals. PALAEOGEOGRAPHY *PALAEOCLIMATOLOGY PALAEOECOLOGY* : Tracing Phanerozoic hydrocarbon seepage from local basins to the global Earth system, **390**, 52-67.

Keller, G., Barrera, E., Schmitz, B. and Mattson, E., 1993. Gradual mass extinction, species survivorship and long term environmental changes across the Cretaceous-Tertiary boundary in high latitudes. *Geological Society of America Bulletin*, **105**, 979-997.

Keller, G., 2011. The End-Cretaceous Mass Extinction and the Chicxulub Impact in Texas. *SEPM Special Publication*, **100**, 197–226.

Kemp, D.B., Robinson, S.A., Crame, J.A., Francis, J.E., Ineson, J., Whittle, R.J., Bowman, V.C. and O'Brien, C., 2014. A cool temperate climate on the Antarctic Peninsula through the latest Cretaceous to early Palaeogene. *Geology* **42**, 583–586.

Kim, J.-H., Schouten, S., Hopmans, E.C., Donner, B. and Sinninghe Damsté, J.S., 2008a. Global sediment core-top calibration of the TEX86 paleothermometer in the ocean. *Geochimica et Cosmochimica Acta*, **72**, 1154-1173.

Kim, J.-H., van der Meer, J., Schouten, S., Helmke, P., Willmott, V., Sangiorgi, F., Koç, N., Hopmans, E.C. and Damsté, J.S.S., 2010. New indices and calibrations derived from the distribution of crenarchaeal isoprenoid tetraether lipids: Implications for past sea surface temperature reconstructions. *Geochimica et Cosmochimica Acta*, **74**, 4639-4654.

Kim, J.H., Schouten, S., Hopmans, E.C., Donner, B. and Damste, J.S.S., 2008b. Global sediment core-top calibration of the TEX86 paleothermometer in the ocean. *Geochimica et Cosmochimica Acta*, **72**, 1154-1173.

Kim, S.-T., O'Neil, J.R., Hillaire-Marcel, C . and Mucci, A., 2007. Oxygen isotope fractionation between synthetic aragonite and water: Influence of temperature and Mg concentration. *Geochimica et Cosmochimica Acta*, **71**, 4704-4715.

King, A.L. and Howard, W.R., 2005. delta O-18 seasonality of planktonic foraminifera from Southern Ocean sediment traps: Latitudinal gradients and implications for paleoclimate reconstructions. *Marine Micropaleontology*, **56**, 1-24.

Klein, R.T., Lohmann, K.C. and Thayer, C.W., 1996. Bivalve skeletons record sea-surface temperature and $\delta^{18}O$ via Mg/Ca and $^{18}O/^{16}O$ ratios. *Geology*, **24**, 415-418.

Kominz, M.A., Browning, J.V., Miller, K.G., Sugarman, P.J., Mizintseva, S. and Scotese, C.R., 2008. Late Cretaceous to Miocene sea-level estimates from the New Jersey and Delaware coastal plain coreholes: an error analysis. *Basin Research*, **20**, 211-226.

Kourkoumelis, N., 2013. PowDLL: A program for the interconversion of powder diffraction data files, Version 2.33, University of Ioannina, Ioannina, Greece, 2013. http://users.uoi.gr/nkourkou/powdll.htm

Lafuente, B., Downs, R.T., Yang, H. and Stone, N., 2015. The power of databases: the RRUFF project. *In*: Armbruster, T. and Danisi, R.M., (Eds.), *Highlights in Mineralogical Crystallography*. Berlin, Germany, W. De Gruyter, pp. 1-30

Laskar, J., Robutel, P., Joutel, F., Gastineau, M., Correia, A.C.M. and Levrard, B., 2004. A long-term numerical solution for the insolation quantities of the Earth. *Astronomy and Astrophysics*, **428**, 261–285.

Latal, C., Piller, W.E. and Harzhauser, M., 2006. Shifts in oxygen and carbon isotope signals in marine molluscs from the Central Paratethys (Europe) around the Lower/Middle Miocene transition. *Palaeogeography, Palaeoclimatology, Palaeoecology*, **231**, 347-360.

Li, L. and Keller, G., 1999. Variability in Late Cretaceous climate and deep waters: evidence from stable isotopes. *Marine Geology*, **161**, 171-190.

Linnert, C., Robinson, S.A., Lees, J.A., Bown, P.R., Pérez-Rodríguez, I., Petrizzo, M.R., Falzoni, F., Littler, K., Arz, J.A. and Russell, E.E., 2014. Evidence for global cooling in the Late Cretaceous. *Nature Communications*, **5**.

Lipp, J.S. and Hinrichs, K.-U., 2009. Structural diversity and fate of intact polar lipids in marine sediments: Geochimica et Cosmochimica Acta, v. **73**, 6816-6833.

Little, C.T.S., Birgel, D., Boyce, A.J., Crame, J.A., Francis, J.E., Kiel, S., Peckmann, J., Pirrie, D., Rollinson, G.K. and Witts, J.D., 2015. Late Cretaceous (Maastrichtian) shallow water hydrocarbon seeps from Snow Hill and Seymour Islands, James Ross Basin, Antarctica. Palaeogeography*, Palaeoclimatology, Palaeoecology*, **418**, 213–228.

Lowenstam, H.A. and Weiner, S., 1989. *On Biomineralization*. Oxford University Press, New York.

Lukeneder, A., Harzhauser, M., Müllegger, S. and Piller, W.E., 2010. Ontogeny and habitat change in Mesozoic cephalopods revealed by stable isotopes ($\delta^{18}O$, $\delta^{13}C$). *Earth and Planetary Science Letters*, **296**, 103-114.

Macdonald, D.I.M., Barker, P.F., Garrett, S.W., Ineson, J.R., Pirrie, D., Storey, B.C., Whitham, A.G., Kinghorn, R.R.F. and Marshall, J.E.A., 1988. A preliminary assessment of the hydrocarbon potential of the Larsen-Basin, Antarctica. *Marine and Petroleum Geology*, **5**, 34-53.

Macellari, C.E., 1984. Revision of Serpulids of the genus Rotularia (Annelida) at Seymour Island (Antarctic Peninsula) and their value in stratigraphy. *Journal of Paleontology*, **58**, 1098-1116.

Macellari, C.E., 1988. Stratigraphy, sedimentology and paleoecology of Upper Cretaceous/Palaeogene shelf-deltaic sediments of Seymour Island. *In*: Feldmann, R.M. and Woodburne, M.O. (eds.). *Geology and Paleontology of Seymour Island, Antarctic Peninsula*. The Geological Society of America, Memoir **169**, 25-53.

Manabe, S. and Stouffer R.J., 1980. Sensitivity of a global climate model to an increase of CO_2 concentration in the atmosphere. *J. Geophys. Res.,* **85***,* 5529–5554.

Marshall, C.R., 1995. Predicting between sudden and gradational extinctions in the fossil record: Predicting the position of the Cretaceous-Tertiary iridium anomaly using the ammonite fossil record on Seymour Island, Antarctica. *Geology*, **23**, 731-734.

Marshall, D.J., 1988 *Cathodoluminescence of geological materials*. Unwin Hyman Ltd., London, UK.

Marshall, J.D., 1992. Climatic and oceanographic isotopic signals from the carbonate rock record and their preservation. *Geological Magazine*, **129**, 143-160.

Marshall, J.D., Ditchfield, P.W. and Pirrie, D., 1993. Stable isotope palaeotemperatures and the evolution of high palaeolatitude climate in the Cretaceous. *Antarctic Special Topic*, 71-79.

Marshall, J.D., Pirrie, D., Clarke, A., Nolan, C.P. and Sharman, J., 1996. Stable-isotopic composition of skeletal carbonates from living Antarctic marine invertebrates: *Lethaia*, **29**, 203-212.

Marwick, P.J. and Valdes, P.J., 2004. Palaeo-digital elevation models for use as boundary conditions in coupled ocean–atmosphere GCM experiments: a Maastrichtian (late Cretaceous) example. *Palaeogeography, Palaeoclimatology, Palaeoecology*, **213**, 37–63.

McArthur, J.M., Kennedy, W.J., Chen, M., Thirlwall, M.F. and Gale, A.S., 1994. Strontium isotope stratigraphy for Late Cretaceous time: Direct numerical calibration of the Sr isotope curve based on the US Western Interior. *Palaeogeography, Palaeoclimatology, Palaeoecology*, **108**, 95-119.

McArthur, J.M., Thirlwall, M.F., Engkilde, M., Zinsmeister, W.J. and Howarth, R.J., 1998. Strontium isotope profiles across K-Pg boundary sequences in Denmark and Antarctica. *Earth and Planetary Science Letters*, **160**, 179-192.

McArthur, J.M., Crame, J.A. and Thirlwall, M.F., 2000. Definition of Late Cretaceous stage boundaries in Antarctica using strontium isotope stratigraphy. *Journal of Geology*, **108**, 623-640.

McArthur, J.M., Howarth, R.J. and Bailey, T.R., 2001. Strontium isotope stratigraphy: LOWESS version 3: Best fit to the marine Sr-isotope curve for 0-509 Ma and accompanying look-up table for deriving numerical age. *Journal of Geology*, **109**, 155-170.

McArthur, J.M., Janssen, N.M.M., Reboulet, S., Leng, M.J., Thirlwall, M.F. and van de Schootbrugge, B., 2007. Palaeotemperatures, polar ice-volume, and isotope stratigraphy (Mg/Ca, $\delta^{18}O$, $\delta^{13}C$, $^{87}Sr/^{86}Sr$): The Early Cretaceous (Berriasian, Valanginian, Hauterivian). *Palaeogeography, Palaeoclimatology, Palaeoecology*, **248**, 391-430.

McRae, S.G., 1972. Glauconite. *Earth-Science Reviews*, **8**, 397-440.

Miller, D.J. and Mitchell, S.F., 2003. Palaeokarstic surfaces in the Upper Cretaceous limestones of central Jamaica. *Cretaceous Research*, **24**, 119-128.

Miller, K.G., Barrera, E., Olsson, R. K., Sugarman, P. J. and Savin, S. M., 1999. Does ice drive early Maastrichtian eustasy? *Geology*, **27**, 783-786.

Miller, K.G., Sugarman, P.J., Browning, J.V., Kominz, M.A., Hernández, J.C., Olsson, R.C., Wright, J.D., Feigenson, M.D. and Van Sickel, W., 2003. Late Cretaceous chronology of large, rapid sea-level changes: Glacioeustasy during the greenhouse world. *Geology,* **31**, 585-588.

Miller, K.G., Sugarman, P.J., Browning, J.V., Kominz, M.A., Olsson, R.K., Feigenson, M.D. and Hernandez, J.C., 2004. Upper Cretaceous sequences and sea-level history, New Jersey Coastal Plain. *Geological Society of America Bulletin*, **116**, 368-393.

Miller, K.G., Kominz, M.A., Browning, J.V., Wright, J.D., Mountain, G.S., Katz, M.E., Sugarman, P.J., Cramer, B.S., Christie-Blick, N. and Pekar, S.F., 2005a. The phanerozoic record of global sea-level change. *Science*, **310**, 1293-1298.

Miller, K.G., Wright, J.D. and Browning, J.V., 2005b. Visions of ice sheets in a greenhouse world. *Marine Geology*, **217**, 215-231.

Miller, K.G., 2009. Broken greenhouse windows. *Nature Geoscience*, **2**, 465-466.

Miller, K.G., Mountain, G.S., Wright, J.D. and Browning, J.V., 2011. A 180-Million-Year Record of Sea Level and Ice Volume Variations from Continental Margin and Deep-Sea Isotopic Records. *Oceanography*, **24**, 40-53.

Morrison, J., Brand, U., 1986. Geochemistry of Recent Marine Invertebrates. *Geoscience Canada*, **13**, 237-254

Morrison, J.O. and Brand, U., 1988. An evaluation of diagenesis and chemostratrigraphy of Upper Cretaceous molluscs from the Canadian Interior Seaway. *In*: A.R. Chivas (Guest Editor), *Isotopes in Palaeoenvironments.* Chemical Geology (Isotope geoscience section), **72**, 235-248.

Mutterlose, J., Malkoc, M., Schouten, S., Sinninghe Damsté, J.S. and Forster, A., 2010. TEX86 and stable [delta]^{18}O paleothermometry of early Cretaceous sediments: Implications for belemnite ecology and paleotemperature proxy application. *Earth and Planetary Science Letters*, **298**, 286-298.

Nelson, B.K., MacLeod, K.G. and Ward, P.D., 1991. Rapid change in strontium isotopic composition of sea water before the Cretaceous/Tertiary boundary. *Nature*, **351**, 644-647.

Olivero, E.B. and Zinsmeister, W.J., 1989. Large heteromorph ammonites from the Upper Cretaceous of Seymour Island, Antarctica. *Journal of Paleontology*, **63**, 626-636.

Olivero, E.B. and Medina, F.A., 2000. Patterns of Late Cretaceous ammonite biogeography in southern high latitudes: the family Kossmaticeratidae in Antarctica. *Cretaceous Research*, **21**, 269-279.

Olivero, E.B., Ponce, J.J. and Martinioni, D.R., 2008. Sedimentology and architecture of sharp-based tidal sandstones in the upper Marambio Group, Maastrichtian of Antarctica. *Sedimentary Geology*, **210**, 11-26.

Olivero, E.B., 2012. Sedimentary cycles, ammonite diversity and palaeoenvironmental changes in the Upper Cretaceous Marambio Group, Antarctica. *Cretaceous Research*, **34**, 348-366.

Passey, B.H. and Henkes, G.A., 2012. Carbonate clumped isotope bond reordering and geospeedometry. *Earth and Planetary Science Letters*, **352**, 223-236.

Petersen, S.V., Dutton, A., and Lohmann, K.C., 2016. End-Cretaceous extinction in Antarctica linked to both Deccan volcanism and meteorite impact via climate change. *Nat Commun*, **7**.

Pirrie, D., 1989. Sedimentology of the Marambio Group, Larsen Basin, Antarctica (unpubl. Ph.D. dissert.). Council for National Academic Awards, 334 pp.

Pirrie, D. and Marshall, J.D., 1990. High palaeolatitude Late Cretaceous palaeotemperatures: New data from James Ross Island, Antarctica. *Geology*, **18**, 31-34.

Pirrie, D. and Marshall, J.D., 1991. Field relatonships and stable isotope geochemistry of concretions from James Ross Island, Antarctica. *Sediment. Geol.*, **71**, 137-150.

Pirrie, D., Whitham, A.G. and Ineson, J.R., 1991. The role of tectonics and eustacy in the evolution of a marginal basin: Cretaceous-Tertiary Basin, Antarctica. *Spec. Publs. Int Ass. Sediment.*, **12**, 293-305.

Pirrie, D., Ditchfield, P.W., Marshall, J.D., 1994. Burial diagenesis and pore-fluid evolution in a Mesozoic back-arc basin: the Marambio Group, Vega Island, Antarctica. *J. Sediment. Res.*, **64**, 541–552.

Pirrie, D., Doyle, P., Marshall, J.D. and Ellis, G., 1995. Cool Cretaceous climates: new data from the Albian of Western Australia. *Journal of the Geological Society, London*, **152**, 739-742.

Pirrie, D., Crame, J.A., Lomas, S.A. and Riding, J.B., 1997. Late Cretaceous stratigraphy of the Admirality Sound Region, James Ross Basin, Antarctica. *Cretaceous Research*, **18**, 109-137.

Pirrie, D., Butcher, A.R., Power, M.R., Gottlieb, P., Miller, G.L., 2004. Rapid quantitative mineral and phase analysis using automated scanning electron microscopy (QemSCAN); potential applications in forensic geoscience. *In*: Pye, K., Croft, D.J. (Eds.), *Forensic Geoscience: Principles, Techniques and Applications*. Geological Society, London, Special Publication **232**, 123–136.

Pirrie, D., Rollinson, G.K. and Power, M.R., 2009. Role of automated mineral analysis in the characterisation of mining-related contaminated land. *Geoscience in South-West England*, **12**, 162-170.

Pojeta, J . and Sohl, N. F., 1987. Ascaulocardium-armatum (morton, 1833), new genus (late Cretaceous) - the ultimate variability on the bivalve paradigm. *Journal of Paleontology*, **61**, 1-77.

Poole, I., Cantrill, D . and Utescher, T., 2005. A multi-proxy approach to determine Antarctic terrestrial palaeoclimate during the Late Cretaceous and Early Tertiary. *Palaeogeography Palaeoclimatology Palaeoecology*, **222**, 95-121.

Pope, V.D., Gallani, M.L., Rowntree, P.R . and Stratton, R.A., 2000. The impact of new physical parametrizations in the Hadley Centre climate model: HadAM3. *Climate Dynamics*, **16**, 123-146.

Poulain, C., Gillikin, D.P., Thebault, J., Munaron, J.M., Bohn, M., Robert, R., Paulet, Y.M. and Lorrain, A., 2015. An evaluation of Mg/Ca, Sr/Ca, and Ba/Ca ratios as environmental proxies in aragonite bivalve shells. *Chemical Geology*, **396**, 42-50.

Powers, L.A., Werne, J.P., Johnson, T.C., Hopmans, E.C., Damste, J.S.S. and Schouten, S., 2004. Crenarchaeotal membrane lipids in lake sediments: A new paleotemperature proxy for continental paleoclimate reconstruction? *Geology*, **32**, 613-616.

Powers, L.A., Werne, J.P., Johnson, T.C., Hopmans, E.C., Damste, J.S.S. and Schouten, S, 2005. The development of TEX86 for continental paleotemperature reconstruction: Problems and promise. *Geochimica et Cosmochimica Acta*, **69**, A78-A78.

Price, G.D., Valdes, P.J. and Sellwood, B.W., 1997. Quantitative palaeoclimate GCM validation: Late Jurassic and mid-Cretaceous case studies. *Journal of the Geological Society, London*, **154**, 769-772.

Price, G.D., Sellwood, B.W., Corfield, R.M., Clarke, I. and Cartlidge, J.E., 1998. Isotopic evidence for palaeotemperatures and depth stratification of Middle Cretaceous planktonic foraminifera from the Pacific Ocean. *Geol. Mag.* **135,** 183–191.

Price, G.D., Ruffell, A.H., Jones, C.E., Kalin, M.R. and Mutterlose, J., 2000. Isotopic evidence for temperature variability during the early Cretaceous (late Ryazanian-mid-Hauterivian). *Journal of the Geological Society, London*, **157**, 335-343.

Price, G.D. and Passey, B.H., 2010. Carbonate clumped-isotope paleothermometry of sub-Arctic early Cretaceous fossils. *Geochimica et Cosmochimica Acta*, **74**, A832-A832.

Prokoph, A., Shields, G.A. and Veizer, J., 2008. Compilation and time-series analysis of a marine carbonate $\delta^{18}O$, $\delta^{13}C$, $^{87}Sr/^{86}Sr$ and $\delta^{34}S$ database through Earth history. *Earth-Science Reviews*, **87**, 113-133.

Randall, D.A., Wood, R.A., Bony, S., Colman, R., Fichefet, T., Fyfe, J., Kattsov, V., Pitman, A., Shukla, J., Srinivasan, J., Stouffer, R.J., Sumi, A. and Taylor, K.E., 2007. Climate Models and Their Evaluation. In: *Climate Change 2007: The Physical Science Basis. Contribution of Working Group I to the Fourth Assessment Report of the Intergovernmental Panel on Climate Change* [Solomon, S., Qin, D., Manning, M., Chen, Z., Marquis, M., Averyt, K.B., Tignor, M. and Miller, H.L. (eds.)]. Cambridge University Press, Cambridge, United Kingdom and New York, NY, USA.

Rausch, S., Böhm, F., Bach, W., Klügel, A. and Eisenhauer, A., 2013. Calcium carbonate veins in ocean crust record a threefold increase of seawater Mg/Ca in the past 30 million years. *Earth and Planetary Science Letters*, **362**, 215-224.

Reuning, L., Reijmer, J.J., and Mattioli, E., 2006. Aragonite cycles : diagenesis caught in the act. *Sedimentology*, **53**, 849-866.

Rexfort, A. and J. Mutterlose, 2006. Stable isotope records from *Sepia officinalis*—a key to understanding the ecology of belemnites? *Earth and Planetary Science Letters* **247,**212-221.

Rollinson, H.R., 1983. *Using geochemical data: Evaluation, Presentation, Interpretation*. Pearson Education Limited, Harlow, Essex, CM20 2JE, England.

Romanek, C.S., Grossman, E.L., and Morse, J.W., 1992. Carbon isotopic fractionation in synthetic aragonite and calcite: Effects of temperature and precipitation rate. *Geochimica et Cosmochimica Acta*, **56**, 419-430.

Russell, A.D., Hönisch, B., Spero, H.J. and Lea, D.W., 2004. Effects of seawater carbonate ion concentration and temperature on shell U, Mg and Sr in cultured planktonic foraminifera. *Geochimica et Cosmochimica Acta*, **68**, 4347-4361.

Schauble, E., Ghosh, P. and Eiler, J., 2006. Preferential Fm. of $^{13}C–^{18}O$ bonds in carbonate minerals, estimated using first-principles lattice dynamics. *Geochimica et Cosmochimica Acta*, **70**, 2510-2529.

Schöne, B.R., Zhang, Z., Radermacher, P., Thébault, J., Jacob, D.E., Nunn, E.V . and Maurer, A.-F., 2011. Sr/Ca and Mg/Ca ratios of ontogenetically old, long-lived bivalve shells (Arctica islandica) and their function as paleotemperature proxies. *Palaeogeography, Palaeoclimatology, Palaeoecology*, **302**, 52-64.

Schoene, B., Samperton, K.M., Eddy, M.P., Keller, G., Adatte, T., Bowring, S.A., Khadri, S.F.R. and Gertsch, B., 2015. U-Pb geochronology of the Deccan Traps and relation to the end-Cretaceous mass extinction. *Science*, **347**, 182–184.

Schoepfer, S.D., Tobin, T.S., Witts, J.D., and Newton, R.J., 2017. Intermittent euxinia in the high-latitude James Ross Basin during the latest Cretaceous and earliest Paleocene. *Palaeogeography, Palaeoclimatology, Palaeoecology*, **477**, 40-54.

Schouten, S., Forster, A., Panoto, F.E. and Sinninghe Damsté, J.S., 2007. Towards calibration of the TEX^{86} palaeothermometer for tropical sea surface temperatures in ancient greenhouse worlds. *Organic Geochemistry*, **38**, 1537-1546.

Sellwood, B.W. and Valdes, P.J., 2006. Mesozoic climates: General circulation models and the rock record. *Sedimentary Geology* **190**, 269-287.

Sellwood, B.W. and Valdes, P.J., 2007. Mesozoic climates. *In:* Williams, M. Haywood, A.M., Gregory, F.J. and Schmidt, D.N. (eds.). *Deep-Time Perspectives on Climate Change: Marrying the Signal from Computer Models and Biological Proxies*. The Micropalaeontological Society, Special Publications. The Geological Society, London, 201-224.

Shackleton, N.J., Kennett, J.P., 1975. Late Cenozoic oxygen and carbon isotopic changes at DSPDP Site 284: implications for glacial history of the Northern Hemisphere and Antarctica. *Initial Reports of the Deep Sea Drilling Project*, **29**, 801–807.

Sial, A.N., Ferreira, V.P., Toselli, A.J., Parada, M.A., Acenolaza, F.G., Pimentel, M.M. and Alonso, R.N., 2001. Carbon and oxygen isotope compositions of some upper Cretaceous-Paleocene sequences in Argentina and Chile. *International Geology Review*, **43**, 892-909.

Skelton, P.W., 2003. Introduction to the Cretaceous. *In:* Skelton, P.W. (ed.) *The Cretaceous World*. Cambridge University Press, Cambridge, UK.

Smith, A.M. and Key Jr. M.M., 2004. Controls, variability, and a record of climate change in detailed stable isotope record in a single bryozoan skeleton. *Quaternary Research*, **61**, 123– 133.

Sohl, N.F., 1987. Cretaceous gastropods - contrasts between Tethys and the temperate provinces. *Journal of Paleontology*, **61**, 1085-1111.

Spicer, R.A. and Parrish, J.T., 1990a. Late Cretaceous-early Palaeogene palaeoclimates of northern high latitudes: a quantitative view. *Journal of the Geological Society, London*, **147**, 329-341.

Spicer, R.A. and Parrish, J.T., 1990b. Latest Cretaceous woods of the central North Slope, Alaska. *Palaeontology*, **33**, 225-242.

Spicer, R.A., Valdes, P.J., Spicer, T.E.V., Craggs, H.J., Srivastava, G., Mehrotra, R.C. and Yang, J., 2009. New developments in CLAMP: Calibration using global gridded meteorological data. *Palaeogeography Palaeoclimatology Palaeoecology*, **283**, 91-98.

Spicer, R.A., and Herman, A.B., 2010. The Late Cretaceous environment of the Arctic: A quantitative reassessment based on plant fossils. *Palaeogeography, Palaeoclimatology, Palaeoecology*, **295**, 423-442.

Steuber, T. and Buhl, D., 2006. Calcium-isotope fractionation in selected modern and ancient marine carbonates. *Geochimica et Cosmochimica Acta*, **70**, 5507-5521.

Steuber, T. and Rauch, M., 2005. Evolution of the Mg/Ca ratio of Cretaceous seawater: Implications from the composition of biological low-Mg calcite. *Marine Geology*, **217**, 199-213.

Stevens, K., Mutterlose, J., and Wiedenroth, K., 2015. Stable isotope data (δ18O, δ13C) of the ammonite genus Simbirskites — implications for habitat reconstructions of extinct cephalopods. *Palaeogeography, Palaeoclimatology, Palaeoecology*, **417**, 164-175.

Stevenson, E.I., Hermoso, M., Rickaby, R.E.M., Tyler, J.J., Minoletti, F., Parkinson, I. J., Mokadem, F. and Burton, K.W., 2014. Controls on stable strontium isotope fractionation in coccolithophores with implications for the marine Sr cycle. *Geochimica et Cosmochimica Acta*, **128**, 225-235.

Stilwell, J.D., 2003. Patterns of biodiversity and faunal rebound following the K-T boundary extinction event in Austral Palaeocene molluscan faunas. *Palaeogeography, Palaeoclimatology, Palaeoecology*, **195**, 319-356.

Stoll, H.M. and Schrag, D.P., 1996. Evidence for glacial control of rapid sea level changes in the early cretaceous: *Science*, v. **272**, 5269, -1774.

Stoll, H.M. and Schrag, D.P., 2000. High-resolution stable isotope records from the Upper Cretaceous rocks of Italy and Spain: Glacial episodes in a greenhouse planet?. *Geological Society of America Bulletin*, **112**, 308-319.

Stoll, H.M. and Schrag, D.P., 2001. Sr/Ca variations in Cretaceous carbonates: relation to productivity and sea level changes. *Palaeogeography, Palaeoclimatology, Palaeoecology*, **168**, 311-336.

Strahler, A. and Archibold, O.W., 2011. *Physical geography: science and systems of the human environment*. John Wiley and Sons Canada Ltd, Ontario L5R 4J3, Canada.

Svojtka, M., Nývlt, D., Murakami, M., Vávrová, J., Filip, J. and Mixa, P., 2009. Provenance and post-depositional low-temperature evolution of the James Ross Basin sedimentary rocks (Antarctic Peninsula) based on fission track analysis. *Antarctic Science*, **21**, 593–607.

Taylor, J.D., Glover, E.A. and Williams, S.T., 2008. Ancient shallow water chemosynthetic bivalves: systematics of Solemyidae from eastern and southern Australia (Mollusca, Bivalvia). *Queensland Mus. Mem*. **54**, 75–104.

Thomas, S., Tvrtko, K., Vladimir, J. and Ivan, G., 2005. Strontium-isotope stratigraphy of Upper Cretaceous platform carbonates of the island of Brac (Adriatic Sea, Croatia): implications for global correlation of platform evolution and biostratigraphy. *Cretaceous Research*, **26**, 741-756.

Thompson, S.L . and Barron, E.J., 1981. Comparison of Cretaceous and present earth albedos - implications for the causes of paleoclimates. *Journal of Geology*, **89**, 143-167.

Thorn, V.C., Francis, J.E., Riding, J.B., Raiswell, R.W., Pirrie, D., Haywood, A.M., Crame, J.A. and Marshall, J.M., 2007. Terminal Cretaceous climate change and biotic response in Antarctica. *In*: Cooper, A., Raymond, C. and the 10th ISAES Editorial Team (Eds.), *Antarctica; A Keystone in a Changing World—Online Proceedings for the 10th International Symposium on Antarctic Earth Sciences*. U.S. Geological Survey Open-File Report 2007-1047. http://pubs.usgs.gov/of/2007/1047/.

Thorn, V.C., Francis, J.E. and Riding, J.B., 2008. Terminal Cretaceous climate change and biotic response in Antarctica. *Palynology*, **32**, 271-271.

Thorn, V.C., Riding, J.B., Francis, J.E., 2009. The Late Cretaceous dinoflagellate cyst Manumiella - Biostratigraphy, systematics and palaeoecological signals in Antarctica. *Review of Palaeobotany and Palynology,* **156**, 436-448.

Tobin, T.S., Ward, P.D., Steig, E.J., Olivero, E.B., Hilburn, I.A., Mitchell, R.N., Diamond, M.R., Raub, T.D. and Kirschvink, J.L., 2012. Extinction patterns, $\delta^{18}O$ trends and magnetostratigraphy from a southern high-latitude Cretaceous–Palaeogene section: Links with Deccan volcanism. *Palaeogeography, Palaeoclimatology, Palaeoecology*, **350–352**, 180-188.

Tobin, T.S. and Ward, P.D., 2015. Carbon isotope (δ13C) differences between Late Cretaceous ammonites and benthic mollusks from Antarctica. *Palaeogeography, Palaeoclimatology, Palaeoecology*, **428**, 50-57.

Tomsich, C.S., McCarthy, P.J., Fowell, S.J. and Sunderlin, D., 2010. Paleofloristic and paleoenvironmental information from a Late Cretaceous (Maastrichtian) flora of the lower Cantwell Formation near Sable Mountain, Denali National Park, Alaska. *Palaeogeography Palaeoclimatology Palaeoecology*, **295**, 389-408.

Torsvik, T.H., Gaina, C. and Redfield, T.F., 2008. Antarctica and Global Paleogeography: From Rodinia, Through Gondwanaland and Pangea, to the Birth of the Southern Ocean and the Opening of Gateways. *In*: Cooper, A., Raymond, C. and the 10th ISAES Editorial Team (Eds.), *Antarctica; A Keystone in a Changing World—*

Online Proceedings for the 10th International Symposium on Antarctic Earth Sciences. U.S. Geological Survey Open-File Report 2007-1047. http://pubs.usgs.gov/of/2007/1047/.

Tripati, A.K., Eagle, R.A., Thiagarajan, N., Gagnon, A.C., Bauch, H., Halloran, P.R. and Eiler, J.M., 2010. (13)C-(18)O isotope signatures and 'clumped isotope' thermometry in foraminifera and coccoliths. *Geochimica et Cosmochimica Acta*, **74**, 5697-5717.

Tucker, M.E., 2001. *Sedimentary petrology: an introduction to the origin of sedimentary rocks*. Blackwell Science Ltd., Osney Mead, Oxford OX2 0EL, UK.

Ubukata, T., 1994. Architectural constraints on the morphogenesis of prismatic structure in Bivalvia. *Palaeontology*, **37**, 241–261.

Urey, H.C., 1947. The thermodynamic properties of isotopic substances. *J. Chem. Soc.,* **47**, 562-581.

Urey, H.C., Lowenstam, H.A., Epstein, S., McKinney, C.R. 1951. Measurement of paleotemperatures and temperatures of the Upper Cretaceous of England, Denmark and the southeastern United States. *Geol. Soc. Am. Bull.,* **62**, 399–416.

Veizer, J. and Prokoph, A., 2015. Temperatures and oxygen isotopic composition of Phanerozoic oceans. *Earth-Science Reviews*, **146**, **Supplement C**, 92-104.

Voight, S. and Wiese, F., 2000. Evidence for late Cretaceous (Late Turonian) climate cooling from oxygen isotope variations and palaeobiogeographic changes in Western and Central Europe. *Journal of the Geological Society, London*, **157**, 737-743.

Vonhof, H.B. and Smit, J., 1997. High-resolution late Maastrichtian early Danian oceanic Sr-87/Sr-86 record: Implications for Cretaceous-Tertiary boundary events. *Geology*, **25**, 347-350.

Ward, P.D., 1990. The Cretaceous/Tertiary extinctions in the marine realm; A 1990 perspective. *In*: Sharpton, V.L. and Ward, P.D. (Eds.) *Global catastrophes in Earth History; An interdisciplinary conference on impacts, volcanism and mass mortality*. Geological Society of America Special Paper 247.

Weijers, J.W.H., Schouten, S., Spaargaren, O.C. and Damste, J.S.S., 2006. Occurrence and distribution of tetraether membrane lipids in soils: Implications for the use of the TEX(86) proxy and the BIT index. *Organic Geochemistry*, **37**, 1680-1693.

Weiner, S. and Dove, P.M., 2003. *An overview of biomineralization processes and the problem of the vital effect*. Reviews in Mineralogy and Geochemistry **54**, 1.

Wendt, J., 1977, Aragonite in Permian Reefs. *Nature*, **267**, 335-337.

Witts, J.D., Bowman, V.C., Wignall, P.B., Alistair Crame, J., Francis, J.E. and Newton, R.J., 2015. Evolution and extinction of Maastrichtian (Late Cretaceous) cephalopods from the López de Bertodano Fm., Seymour Island, Antarctica. *Palaeogeography, Palaeoclimatology, Palaeoecology*, **418**, 193-212.

Witts, J.D., Whittle, R.J., Wignall, P.B., Crame, J.A., Francis, J.E., Newton, R.J. and Bowman, V.C., 2016. Macrofossil evidence for a rapid and severe Cretaceous–Palaeogene mass extinction in Antarctica. *Nature Communications*, **7**, 11738-11738.

Wuchter, C., Schouten, S., Wakeham, S.G., and Damste, J.S.S., 2005. Temporal and spatial variation in tetraether membrane lipids of marine Crenarchaeota in particulate organic matter: Implications for TEX86 paleothermometry. *Paleoceanography*, **20**.

Young, H.R. and Nelson, C.S., 1988. Endolithic biodegradation of cool-water skeletal carbonates on Scott shelf, northwestern Vancouver Island, Canada. *Sedimentary Geology*, **60**, 251-267.

Zakharov, Y.D., Shigeta, Y., Nagendra, R., Safronov, P.P., Smyshlyaeva, O.P., Popov, A.M., Velivetskaya, T A. and Afanasyeva, T.B., 2011. Cretaceous climate oscillations in the southern palaeolatitudes: New stable isotope evidence from India and Madagascar. *Cretaceous Research*, **32**, 623-645.

Ziegler, A.M., Parrish, J.M., Jiping, Y., Gyllenhaal, E.D., Rowley,D.B., Parrish, J.T., Shangyou, N., Behher, A. and Hulver, M.L., 1994. Early Mesozoic phytogeography and climate. *In*: Allen, J.R.L., Hoskins, B.J., Sellwood, B.W., Spicer, R.S., Valdes, P.J. (Eds.), *Palaeoclimates and their Modelling: With Special Reference to the Mesozoic Era*. Chapman and Hall, pp. 89–97.

Zinsmeister, W.J., 1982. Review of the Upper Cretaceous-Lower Tertiary sequence on Seymour Island, Antarctica. *J. geol.* Soc. *London,* **139,** 779-785.

Zinsmeister, W.J., 1984. Geology and palaeontology of Seymour Island, Antarctic Peninsula. *Antarctic Journal of the United States*, **19**, 1-5.

Zinsmeister, W.J. and Macellari, C.E., 1989a. Bivalvia (Mollusca) from Seymour Island, Antarctic Peninsula. *In*: Feldmann, R. M. and Woodburne, M. O. (Eds.), *Geology and Paleontology of Seymour Island, Antarctic Peninsula*. The Geological Society of America, Memoir **169**, 25-53.

Zinsmeister, W.J., Feldmann, R.M., Woodburne, M.O. and Elliot, D.H., 1989b, Latest Cretaceous Earliest Tertiary Transition on Seymour-Island, Antarctica. *Journal of Paleontology*, **63**, 731-738.

Zinsmeister, W.J and Feldman, R.M., 1996. Late Cretaceous Faunal Changes in the High Southern Latitudes: A Harbinger of Global Biotic Catastrophe? *In*: MacLeod, N. and Keller, G. (Eds.), *Cretaceous tertiary mass extinction: biotic and environmental changes*.

Appendices

Appendix A. Specimen selection and screening

A.1 Methodology

Sample selection commenced following the collection of suitable fossil specimens from the AFI project material stored at the School of Earth and Environment, University of Leeds in January 2007. Further material was collected in Jan 2008 and June 2009. Selection of samples that were deemed suitable for isotopic analysis comprised a number of separate and discrete stages.

All specimen bags were laid out and an initial entry was logged into the research database for each individual specimen bag. The information recorded on each bag included the Collecting Station Id, Sample Number and vertical position above datum for the particular Station Id. For example the following information applied to a single specimen bag, **Collecting Station Id D5.220**, **Sample Number 1217.2** and **Depth 48 - 54 (m)**. The '**D5'** component of the Collecting Station Id follows a convention adopted by the British Antarctic Survey (BAS) that specifies the year of collection. Following the initial completion of the logging procedure it was noted that further information would be necessary since many of the specimen bags contained numerous palaeontological specimens some of which were from different taxa. It was also noted that there were multiple bags each with the same identification data, so a further **Sub Code** was added to the sample number. Thus each entry in the database referred to either a single palaeontological specimen or bulk sample of shell material. E.g. The original identification of the sample bag was **D5.220.1217.2** and the unique specimen identification became **D5. 220.1217.2/C** as further specimens for **D5.220.1217.2** were logged the sub code letter was incremented and for those sample numbers that exceeded 26 specimens then the sub code progressed to **AA …. AZ**. The highest allocated sub code used was **AV** for Sample Number **D5.215.696.2**. See Figure A-1 for an example of a completed sample bag with an ammonite specimen, genus *Anagaudryceras,* allocated a Sub-code of 'C'.

A further level of division was also introduced for individual specimens that afforded a number of discrete samples, for example in the case of sequential sampling from the septal walls of a large ammonite. By this stage of the screening process there were a considerable number of individual sample bags, each with a unique specimen id and an entry in the database. The mineralogy of the shell material for all candidate specimens had been identified by visual inspection and the appropriate fields updated in the database.

Figure A-1. Example sample bag identification. Note that the ammonite specimen, genus – *Anagaudryceras,* has been allocated the sub-code 'C'

Details of the identified macrofossils screened for possible inclusion in the stable isotope study may be found in Table A-1 and for those deemed suitable for stable isotope analysis see Table A-2. Further data relating to the palaeontology of selected macrofossils may be found in Appendix G. Specimens categorised as having 'Unidentified affinity' or for example, 'Unidentified gastropod', represent shell matter deemed suitable for study as bulk samples and comprise loose aragonite nacre shell material present within a small proportion of original specimen bags.

Table A-1. Details of individual macrofossil types included in research database. Specimens categorised as having 'Unidentified affinity' represent shell material deemed suitable for inclusion in the study as bulk samples and comprise loose aragonite material present in a small proportion of specimen bags.

Macrofossil Types	**Specimens**
Ammonoidea	79
Nautiloidea	5
Bivalvia	337
Gastropoda	73
Unidentified affinity	30
Rotularia	48
Total specimens	**572**

All bulk materials were subject to an identical suite of diagenetic tests as employed for identified macrofossils (See Appendix B for an in-depth explanation of the procedure). Identification of specimens was carried out with reference to (Macellari, 1984,1986) [Ammonoidea, *Rotularia*], (Cichowolski *et al.,* 2005) [Nautiloidea] and (Zinsmeister and Macellari, 1988) [Bivalvia].

Table A-2. Macrofossil taxa selected for stable isotope analysis. Note that due to diagenetic alteration, sediment contamination, insufficient shell material and other factors not all identified specimens were deemed suitable for further analysis

Taxa	Fossil type	Habitat	Count
Amberlaya	Gastropod	Benthic	14
Diplomoceras lambii	Ammonite	Planktonic	1
Eselaevitrigonia	Bivalve	Benthic	43
Eutrephoceras	Nautiloid	Nektonic	4
Grossouvrites	Ammonite	Nektonic	1
Lahillia	Bivalve	Benthic	1
Maorites	Ammonite	Nektonic	17
Nucula	Bivalve	Benthic	49
Oistotrigonia	Bivalve	Benthic	28
Pinna	Bivalve	Benthic	5
Pleurotomaria	Gastropod	Benthic	2
Solemya rossiana	Bivalve	Benthic	3
Unidentified	Uncertain	Uncertain	10
Unidentified - Ammonite	Ammonite	Nektonic	9
Unidentified - Bivalve	Bivalve	Benthic	22
Unidentified - Gastropod	Gastropod	Benthic	4
Total specimens selected			213

A.2 Selected taxa

In total 618 separate macrofossil specimens were initially selected from the complete sample set collected from Seymour Island as potential sources of shell material for subsequent diagenetic screening and isotopic analysis. Following initial inspection 280 specimens from the following taxa were selected for diagenetic screening and possible stable isotope analysis.

- Bivalves: *Eselaevitrigonia, Lahillia, Nucula, Oistotrigonia, Pinna, Pycnodonte* and *Solemya*.
- Cephalopods: [Ammonites] *Anagaudryceras, Diplomoceras, Grossouvrites, Kitchinites* and *Maorites*.
- Cephalopods: [Nautiloids] *Eutrephoceras*
- Gastropods: *Amberlaya, Pleurotomaria*.
- Serpulid: *Rotularia*.

In addition, shell material from unidentified ammonites and nautiloids, bivalves and gastropods was also selected. This shell material was fragmentary with actual identification of individual molluscan types unreliable but it was selected for analysis as 'bulk' samples. Previous studies within the Cretaceous of the James Ross Basin have been based upon the use of molluscan specimens and report the use of similar groups of taxa for palaeoenvironmental research employing stable isotope analyses, e.g. [**Bivalves**] (See Kelly and Moncrieff, 1992; Crame *et al*., 1996; McArthur *et al*., 1998; Crame *et al*., 1999; Doyle and Pirrie, 1999; Elorza *et al*., 2001; Javier *et al*., 2001; Tobin *et al*., 2012; Little *et al*., 2015; Tobin and Ward, 2015; Witts *et al*., 2015; Petersen *et al*., 2016) [**Ammonites**] (See Kelly and Moncrieff, 1992; Crame *et al*., 1996;

McArthur *et al*., 1998; Crame *et al*., 1999; Doyle and Pirrie, 1999; Elorza *et al*., 2001; Javier *et al*., 2001; Dutton *et al*., 2007; Tobin *et al*., 2012; Tobin and Ward, 2015; Witts *et al*., 2015), [**Nautiloids**] (see Cichowolski *et al*., 2005) [**Belemnites**] (See McArthur *et al*., 1998); Dutton *et al*., 2007). The use of gastropod specimens for palaeoenvironmental studies within the Cretaceous of the James Ross Basin were not as common as studies of cephalopods and bivalves (see Gazdzicki *et al*., 1992; Marshall *et al*., 1996, Stilwell *et al*., 2003; Tobin *et al*., 2012). Figure A-2 illustrates a specimen of gastropod genus *Amberlaya* exhibiting a good state of preservation with abundant aragonite nacre.

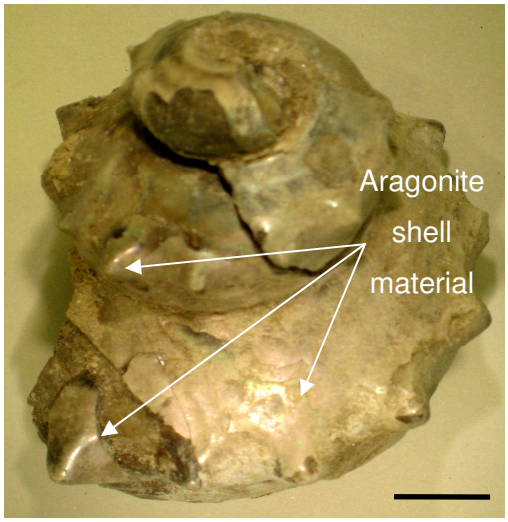

Figure A-2. Photograph of gastropod exhibiting a good state of preservation with abundant aragonite nacre. Gastropod genus - *Amberlaya* an epifaunal carnivore/scavenger. Specimen Id D5.215.696.2/AU. Scale bar 10 mm.

Whilst the overall remit of this study was to incorporate stable isotope data from shell fragments composed of aragonite it was anticipated that taxa with shell material comprising low Mg calcite would also be present within the entire macrofossil collection. With the exception of the serpulid *Rotularia*, specimens of which were ubiquitous and comprised a calcite mineralogy, only a small number of *Pycnodonte* oysters were identified amongst the selected specimens. However, there were two notable exceptions with only a single specimen each of a foraminifera and a belemnite identified as being present within the sampled material. The paucity of suitable low Mg calcite but corresponding abundance of aragonite bioclasts for analysis is an unusual feature of the basin studied. There has been a considerable body of stable isotope research carried out using Cretaceous belemnites (Pirrie and Marshall, 1990; Ditchfield *et al*., 1993; Marshall *et al*., 1994); Doyle and Pirrie, 1999; Elorza *et al*., 2001a,b; Dutton *et al*., 2007) and foraminifera (Huber, 1988) and the apparent lack of either types of fossil raised questions about sampling and preservation of material. The lack of foraminifera was particularly unexpected since (Huber, 1988) described the Upper

Campanian-Palaeogene foraminiferal assemblages from the James Ross Island region and in particular from sites on Seymour Island. Previous research described a belemnite (*Dimitobelus (Dimitobelus) seymouriensis*) collected to the north of the D5 section lines at 636 m below the K–Pg boundary and this specimen was dated at 67.5 Ma using strontium isotope stratigraphy (McArthur *et al*., 1998).

Appendix B. Diagenetic screening

B.1 Initial preparation methodology

The initial stage of the diagenetic screening procedure involved examination and selection of samples using a low power binocular microscope, followed by the removal of suitable fragments of aragonitic shell material from individual macrofossil specimens using either tweezers or for those cases where the shell material was more intact a scalpel blade. In a small number of cases the shell material was removed using a small cold chisel and hammer. In some sample bags the shell material was more fragmentary and dissociated from particular fossil specimens, in these cases shell material was still sampled but with the intention of providing bulk samples for analysis. Whilst the actual provenance of the shell material was in the majority of these cases unknown the screening followed an identical procedure to that used for material removed from identified specimens. Shell fragments were placed in small plastic specimen bags with an identical specimen id to that specified on the original specimen bag, thus ensuring that there was a one to one relationship between the actual palaeontological specimens and the shell material selected for analysis. At this stage of the screening the database contained 558 entries of which 284 were categorised as specimens with primary aragonitic shell material.

Samples of shell material for each specimen were rinsed in de-ionised water for 3 minutes, and then air dried on filter paper in a fume cupboard overnight or until dry. The omission of ultrasonic cleaning during the powder preparation will have introduced a certain level of uncertainty, although it was anticipated that a similar level of uncertainty would be inherited by all powders.Once dry the sample shell material was sub-sampled for a suite of analytical techniques. Photomicrographs of the shell material were taken prior to the grinding stage so that the original physical appearance of the shell fragments was still available at later stages of the analytical process, see Figure B-1.

Figure B-1. Nacreous aragonite. Shell fragments exhibiting a characteristic colouration. Image (a) gastropod genus *Amberlaya* - Sample Id D5.215.216.4/A-1. Image (b) fragments of ammonite shell illustrating internal morphology of sutures. Field of view ~12 mm.

1. A small (~0.5 to 1.0 mm) fragment of representative shell material was attached to a sticky carbon tab mounted on a 10 mm aluminium stub and carbon coated ready for imaging of shell ultrastructure with a scanning electron microscope (SEM).
2. A portion of the shell material was ground by hand, using an agate pestle and mortar and the subsequent powders transferred to a weighed 1.5 ml Eppendorf tube, reweighed and the mass of powder recorded. The pestle and mortar were first rinsed with 1M HCl and then with de-ionised water and subsequently dried, in readiness for the next specimen.
3. A quantity of the sample powder was transferred to an XRD sample holder in preparation for carrying out semi-quantitative X-ray diffraction analysis. Upon completion of the XRD analysis the sample powders were recovered, reweighed and stored for subsequent analytical procedures.
4. A small portion (~10 mg) of the sample powder was retained for the preparation of aliquots suitable for trace element analysis on a Varian 725-ES-ICP-OES at the School of Environmental Chemistry, University of Plymouth, Plymouth, UK. Blank and replicate samples were also included in each batch of solutions prepared.
5. A total of 85 powder samples, including replicates and triplicates were also selected for subsequent $^{87}Sr/^{86}Sr$ isotope analyses.
6. The remainder of the sample powder was sent to the Jane Herdmann Laboratory at the University of Liverpool for analysis of $\delta^{13}C$ and $\delta^{18}O$. Replicate samples and control samples were included in each batch submitted to the isotope laboratory.
7. Additionally for certain specimens (In particular *Rotularia* and internal septal wall material taken from an ammonite - specimen D5.222.1248.2/K) thin-sections were also prepared in readiness for cold cathodoluminescence and carbonate staining after the method of Dickson (1966). Thin-sections were produced with a thickness of ~100 µm, rather than the standard thickness of 30 µm used for optical microscopy. This approach ensured that there was sufficient shell material present for any further lapping, polishing and carbonate staining, according to the method of (Dickson, 1966) if the cathodoluminescence analysis indicated that either diagenetic features were present or that carbonate staining was required.

B.2 Analytical methods

A number of different techniques were employed in order to assess the degree of diagenesis affecting the skeletal carbonates. Results of the diagenetic screening techniques described in this chapter determined whether individual specimens were considered suitable for $\delta^{18}O$ and $\delta^{13}C$ stable isotope analysis and for those considered as being diagenetically least altered subsequent palaeotemperature determination. Carbonate staining was considered less appropriate for specimens that comprised original aragonite due to the inability of the standard staining methodology (Dickson, 1966) to distinguish between calcite and aragonite. Consequently except for a small number of individual specimens prepared as polished thin sections staining techniques were not employed. Through the use of a number of different techniques the overall aim was to identify those specimens that were either unaltered or perhaps more realistically had been subject to a minimum of alteration.

The macrofossil specimens collected from Seymour Island that were included in this study had all been subject to a certain level of weathering indicated by the lack of the outer sections of the shell due to either chemical or mechanical removal of the shell material. All material sampled from either individual macrofossils or 'bulk' shell fragments comprised loose, loosely attached or detached nacreous shell material and in many of the specimens only nacreous shell material was present.

Sampled macrofossil specimens were from either bivalves, cephalopods or gastropods, all of which exhibited differing shell ultrastructures (Chateigner *et al*., 2000; Jacob *et al*., 2008). A number of shell ultrastructures have been described, based on SEM imaging, by Chateigner *et al*. (2000) for extant species of bivalves, cephalopods and gastropods; a series of general structure styles were recognised and described (e.g. Simple prismatic, spherulitic prismatic ultrastructure, nacreous ultrastructures, simple crossed lamellar ultrastructures, complex crossed lamellar ultrastructures and homogeneous). Ultrastructures observed included:

ICN	Inside Columnar Nacre	ISN	Inside Sheet Nacre
ICL	Inside Comarginal Crossed Lamellar	ICCL	Inner Complex Crossed Lamellar
IICCL	Inner Irregular Complex Crossed Lamellar	IRCL	Inner Radial Crossed Lamellar
ISP	Inner Simple Prismatic	OCL	Outer Comarginal Crossed Lamellar
OFSP	Outer Fibrous Simple Prismatic	ORCL	Outer Radial Crossed Lamellar
OSP	Outer Simple Prismatic	OSpP	Outer Spherulitic Prismatic
OH	Outer Homogeneous	OICP	Outer Intersected Crossed Platy

Specimens in this study showed ICN, ISN and minor ISP, no evidence was observed of the more complex cross lamellar structures described by Chateigner *et al*. (2000).

Figure B-2 illustrates the idealised structure of a bivalve shell and the orientation of the aragonite crystals present within the nacre layer (Jacob *et al.*, 2008). Note that this layer forms the innermost layer present in molluscan shells and for this study represents the source of all sampled shell material.

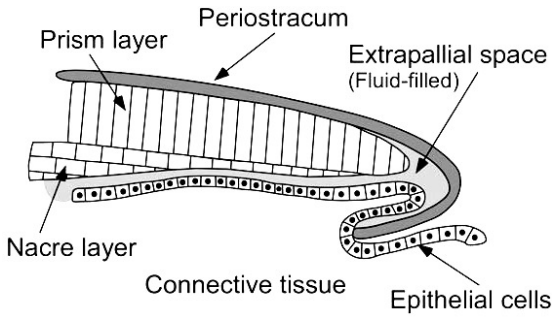

Figure B-2. Bivalve shell illustrating structural units, diagram not to scale. Shell growth is achieved by the cells of the outer mantle epithelium. Growth starts with a thick organic layer, the periostracum. The second layer is formed by prism-shaped $CaCO_3$ crystals followed by a layer of pseudo-hexagonal platelet-shaped crystals, the actual nacre or 'mother-of-pearl'. This layer is the innermost layer present in molluscan shells and for this study represents the majority of the sampled material. (After Jacob *et al.*, 2008).

B.3 Diagenetic overview

An increasing level of diagenesis will be indicated by a number of factors influenced by changes that occurred during life, post-mortem and post deposition (Brand and Veizer, 1980, 1981; Morrison and Brand, 1983; Farrow and Fyfe, 1988; Morrison and Brand, 1988; Young and Nelson, 1988; Brand, 1991; Pirrie *et al.*, 1994). Changes will include physical/textural change, geochemical changes to the original shell material and increases and corresponding decreases of trace element concentrations; the scale of change will be dependent upon factors including the $CO_3^{=}$ stability of the original shell material, openness of the diagenetic system, the isotopic composition of the seawater and the degree of isotopic fractionation (see Brand and Veizer, 1980, 1981; Morrison and Brand, 1983, 1988; Brand, 1991; Pirrie *et al.*, 1994; Brachert and Dullo, 2000; [secular seawater change] Jimenez-Berrocoso *et al.*, 2006; Reuning *et al.*, 2006; Cochran *et al.*, 2010; Joseph *et al.*, 2013; Jamalian and Adabi, 2015). Textural changes will lead to the development of textural maturity (Brand and Veizer, 1981) and may involve damage/alteration resulting from the action of endolithic bacteria (e.g. Farrow and Fyfe, 1988; Young and Nelson, 1988), dissolution features, and neomorphism of the shell carbonate together with the development of replacement carbonate cements. Geochemical changes may include increases and decreases in the proportion of certain cations (Fe, Mn, Sr and Na) and changes to the stable isotope composition of the shell material (see Brand and Veizer, 1980, 1981; Morrison and Brand, 1983, 1988; Brand, 1991). In summary, post depositional changes tend to result

in an increase of Fe and Mn with a corresponding decrease in Sr, Na and $\delta^{18}O$, and possibly $\delta^{13}C$ (Brand and Veizer, 1980, 1981; Morrison and Brand, 1983, 1988; Brand, 1991). In the case of $\delta^{18}O$, factors affecting the final isotopic value include temperature and salinity of the seawater, latitude and seasonal variations together with secular changes (Cicero, 2001) to the $\delta^{18}O$ and $\delta^{13}C$ seawater conditions and the outcome of any biological isotopic fractionation ('Vital effects').

B.4 Determination of diagenetic alteration

Previous methodologies (for example McArthur *et al*., 1994; Cochran *et al*., 2010; Stevens *et al*., 2015) that described the selection of suitable skeletal carbonates for palaeoclimate studies adopted a number of different techniques to assess the preservation state of selected shell material (e.g. ICP analysis for trace elements, SEM imaging of shell ultrastructure and XRD analysis of shell mineralogy) either singly or in combination. Each technique offers benefits but with limitations thus whilst ICP-OES trace element analysis provides elemental proportions it fails to indicate the source of significant trace elements, in this case Mg, Sr, Na, Fe and Mn.

In order to attribute the scale of diagenesis affecting individual specimens a preservation scheme was introduced to categorise the state of preservation exhibited by individual specimens. The scheme was based upon a combination of SEM imaging of skeletal carbonate, determination of shell mineralogy by XRD and ICP-OES trace element analysis The preservation index as implemented provides an extension to the methodology of existing schemes (for example Cochran *et al*., 2010; Stevens *et al*., 2015) that were based upon the assessed quality of SEM images to address the suitability of skeletal carbonate for use in palaeoclimate and palaeotemperature determination. This scheme incorporates scoring from SEM images together with semi-quantitative XRD scoring and quantitative trace element analysis of Mg, Fe and Mn concentrations. It offers benefits in the case of specimens where the diagenetic screening record is incomplete (for example the lack of an SEM image for a particular specimen) or where an assessed score is at odds with the other methods (for example where the SEM image suggests a low preservation index due to significant fusing of the nacre but both the XRD and trace element scoring indicate a good to excellent score).

B.5 SEM Textural analysis

SEM investigation of shell material from bivalve and gastropod specimens showed that they predominantly comprised an arrangement of nacre sheets and tablets in a 'brick wall' structure. Individual nacre sheets were larger than the corresponding

lenticular tablets observed in selected ammonite taxa that exhibited individual nacre tablets 2-3 µm across arranged in vertical columns. In a number of specimens layers of prismatic aragonite were also observed, see Figure B-4 for an example of a section of ammonite shell which that clearly exhibited a zone of prismatic aragonite. A number of the photomicrographs of ammonite shell fragments clearly showed the presence of external morphological features, in this case ribbing. It should be noted that although the nacreous layers were relatively thick the abundance of potential sample material depended upon the sampling strategy employed for each individual specimen.

Visually well preserved shell material with an initial state of preservation determined by the presence of an iridescent lustre (Cochran *et al*., 2010) was selected in preparation for imaging with a scanning electron microscope (SEM) to assess the state of preservation of the shell structure. Both external surfaces and internal structures of the shell material were examined at a range of magnifications (35 to 2,000X) and specimens were assigned a “Preservation Index” (PI) based on higher magnification images taken of cross sections of the shell structure (see Cochran *et al*., 2010; Stevens *et al*., 2015). Due to the operating characteristics of the SEM instrument the actual magnification used was generally limited to a maximum of 2,000X and although this upper limit was considerably lower than that described by either Cochran *et al*. (2010) or Stevens *et al*. (2015), the available range was found to yield satisfactory results.

The preservation index was ranked from 5 (excellent preservation) to 1 (poor preservation) based on a comparison of the shell ultra-structure with that from an extant cephalopod (*Nautilus macromphalus*) using images of freshly fractured nacreous shell material, (see Figure B-3). The ranking of the preservation index was based on an assessment of the nature of the aragonite nacre plates; namely morphology, contact relationship with surrounding nacre and the nature of any dissolution textures present.

‘Excellent’ The nacre is well defined and distinct from surrounding layers with clean edges and no obvious indication of any etching of the nacreous plates. Samples of the skeletal aragonite are indistinguishable from the nacreous shell structure in a modern mollusc (e.g. a control sample taken from a specimen of *Nautilus macromphalus*).

‘Good’ The nacre is well defined and generally distinct from surrounding layers but surfaces of the nacreous plates are slightly irregular and boundaries between adjacent tablets are less distinct than in excellent preservation but without any obvious fusion. Nacre shows clean edges and no obvious indication of any etching of the nacreous plates.

‘Moderate’ The nacre is visible but with some etching and fusion with the surrounding layers. The surfaces of the nacreous plates are irregular and for a single macrofossil specimen the SEM images may show some variation in preservation depending on the shell material selected.

‘Fair’ The nacre is visible but there is etching present; nacreous tablets are discernible, but show increasing fusion with adjacent layers.

‘Poor’ There is significant etching of the nacre; nacreous tablets are indistinct and fused with adjacent layers. Development of carbonate neomorphism.

All SEM images were examined and ranked according to the preservation index criteria, see preceding text for a description of the preservation indices and Table B-1 for an illustration of the corresponding actual preservation states. Note that the categorisation and scoring of a preservation index is subjective and may vary from author to author. None of the imaged specimens from this study scored a PI lower than 3 when compared with published preservation indices (Cochran *et al*., 2010; Stevens *et al*., 2015).

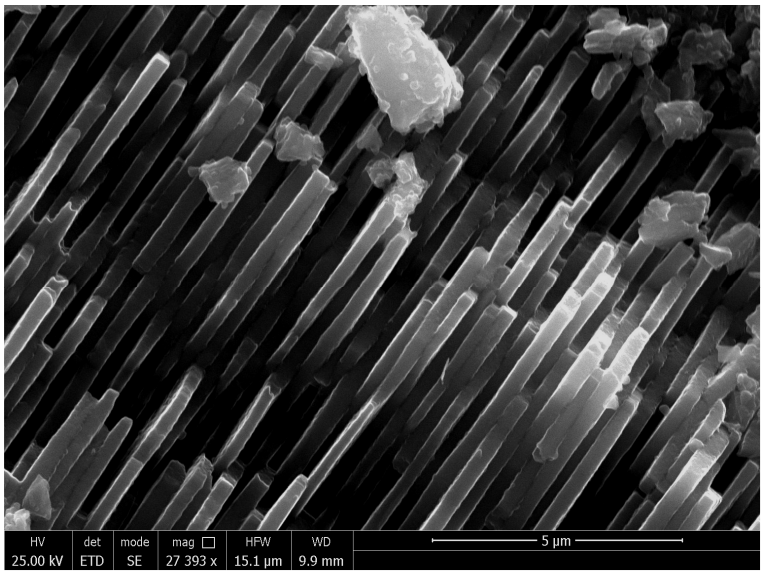

Figure B-3. Preservation index control sample showing cross sectional view of aragonite nacre imaged from an extant specimen of *Nautilus macromphalus*. Note the well defined individual nacre plates (~ 0.4 µm thick). Scale bar 5 µm.

Whilst the primary method (Preservation Index ‘PI’) for detecting the presence of diagenetic alteration was based upon a qualitative inspection of SEM images there were 137 specimens for which no SEM images were generated. Since a lack of SEM images negated the application of the described Preservation Index (‘PI’) further selection and screening methods were also employed.

Table B-1. Definition of preservation index scale as determined from SEM imaging of cross sections of specimen shell fragments. See Table B-4 for images of shell material which match the criteria listed. Modified from methods described in Cochran *et al*. (2010) and Stevens *et al*. (2015).

PI	Descriptor	Characteristic features of shell surface
5	Excellent	Clean and unetched. Internal nacreous tablets distinct from adjacent layers and well-defined. Samples indistinguishable from nacreous shell structure in modern molluscs (e.g. *Nautilus macromphalus*).
4	Good	Clean and unetched; nacreous tablets well defined, but surfaces are slightly irregular and boundaries between adjacent tablets are less distinct than in excellent preservation.
3	Moderate	Some signs of etching; nacreous tablets are visible, but with onset of fusion with adjacent tablets. For a single specimen the images may show variation in preservation depending on the shell material selected.
2	Fair	Etching present; nacreous tablets are discernible, but show fusion with adjacent layers.
1	Poor	Significant etching; nacreous tablets are indistinct and fused with adjacent layers. Development of carbonate neomorphism

In one case the shell material exhibited small spherical structures on the margin of the shell fragment (Figure B-5(a)), with an approximate size of 5-10 µm. Spherulites may indicate sites of aragonite dissolution and the development of neomorphic carbonate. Ubukata (1994) offers an alternative explanation in which the spherulites represent the interaction of prismatic crystals in the shell material. However, a comparison of Figures B-5(a and b) illustrates the development of extensive carbonate neomorphism. The most extreme case observed was from a bivalve of genus *Eselaevitrigonia* (Specimen Id D5.215.347.2/I) that exhibited well defined stacked plates of aragonite nacre but with the presence of extensive neomorphism of the original aragonite. A number of samples exhibited pyrite framboids, with a typical size of ~10 µm, (see Figure B-5(c)). Wignall and Newton (1998) describe how the size of pyrite framboids may be used to indicate the presence of dysoxic and anoxic conditions. Finally, in a number of cases the shell material exhibited small pits with a circular – lenticular shape and an approximate size of 0.5 - 1 µm arranged orthogonal to the shell margin (Figure B-5(d)). These pits may reflect the site of protein strands that mediated the crystallisation of aragonite nacre (Jacob *et al*., 2008) or may either indicate sites of carbonate dissolution or result from the activities of endolithic bacteria (Farrow and Fyfe, 1988; Young and Nelson, 1988). Examination of the images indicated that dissolution was less likely due to the overall uniformity of the pits.

Figure B-6 illustrates a more complex ammonite shell structure, consisting of two well defined layers of nacre plates of aragonite separating a layer of prismatic aragonite crystals. There remains the possibility that the feature identified as a prismatic layer

may be a diagenetic vein but there appears to be little evidence for fusing or neomorphism of the surrounding nacre. The highlighted section (Figure B-6(a)) clearly shows the presence of external ribbing, note that Figures B-6(b and c) also retain the same overall morphology at a reduced scale.

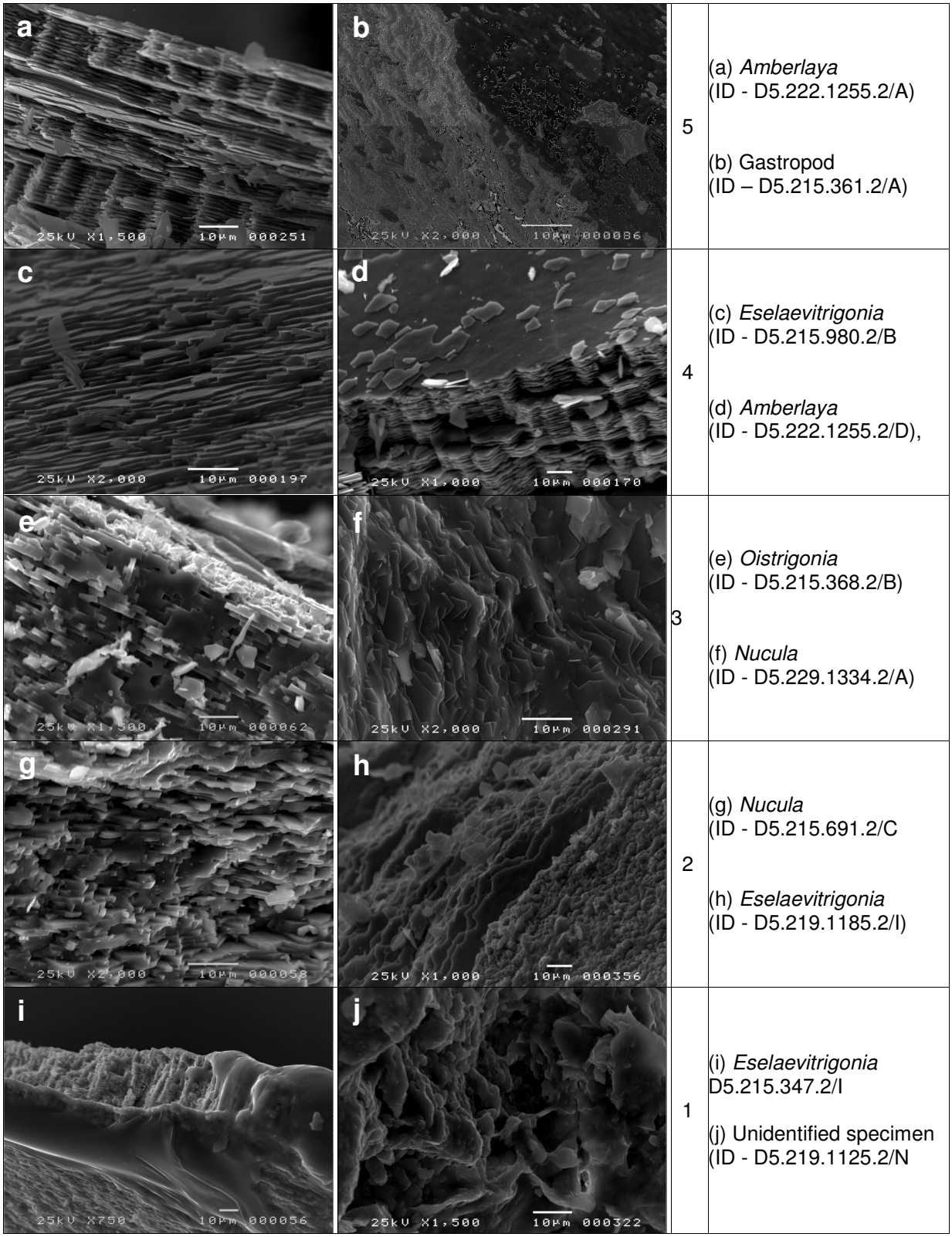

5	(a) *Amberlaya* (ID - D5.222.1255.2/A) (b) Gastropod (ID – D5.215.361.2/A)
4	(c) *Eselaevitrigonia* (ID - D5.215.980.2/B (d) *Amberlaya* (ID - D5.222.1255.2/D),
3	(e) *Oistrigonia* (ID - D5.215.368.2/B) (f) *Nucula* (ID - D5.229.1334.2/A)
2	(g) *Nucula* (ID - D5.215.691.2/C (h) *Eselaevitrigonia* (ID - D5.219.1185.2/I)
1	(i) *Eselaevitrigonia* D5.215.347.2/I (j) Unidentified specimen (ID - D5.219.1125.2/N

Figure B-4. SEM images representing differing categories of the Preservation Index (PI) scale as defined for aragonite nacre shell material included in this study. A and B “Excellent” preservation (5), C and D “Very Good” preservation (4), E and F—“Good” preservation (3), G and H—“Fair” preservation (2), I and J—“Poor” preservation (1). See Table B-1 for a definition of the characteristics associated with each level of PI.

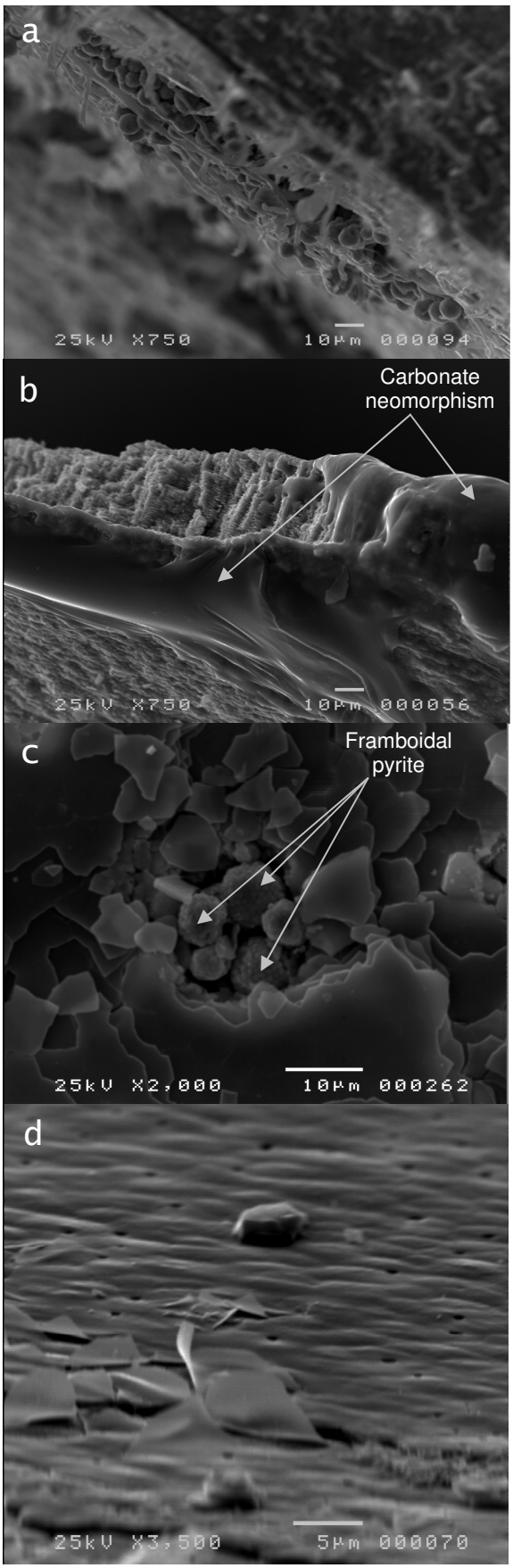

SEM image showing the development of extensive 5-10 µm 'spherules' on aragonite nacre plates. Bivalve genus - *Nucula* an infaunal deposit feeder. Specimen Id D5.215.396.2/A. Scale bar 10 µm.

SEM image of shell material exhibiting diagenetic neomorphism of aragonite nacre. Note the presence of stacked nacre plates parallel to shell margin. Bivalve genus - *Eselaevitrigonia* an infaunal suspension feeder. Specimen Id D5.215.347.2/I. Scale bar 10 µm.

SEM image of aragonitic nacre shell material, note the presence of framboidal pyrite. Bivalve genus - *Nucula* an infaunal deposit feeder. Specimen Id D5.229.1361.2/A. Scale bar 10 µm.

SEM image showing the presence of 0.5 µm pits in aragonite nacre. Pits may reflect the site of protein strands that mediated the crystallisation of aragonite nacre (Jacob *et al*., 2008), sites of carbonate dissolution or sites of activity by endolithic bacteria (Farrow and Fyfe 1988; Young and Nelson 1988). Bivalve genus - *Nucula* an infaunal deposit feeder. Specimen Id D5.215.696.2/AK. Scale bar 5 µm.

Figure B-5. Examples of diagenetic alteration exhibited by aragonite nacre shell material.

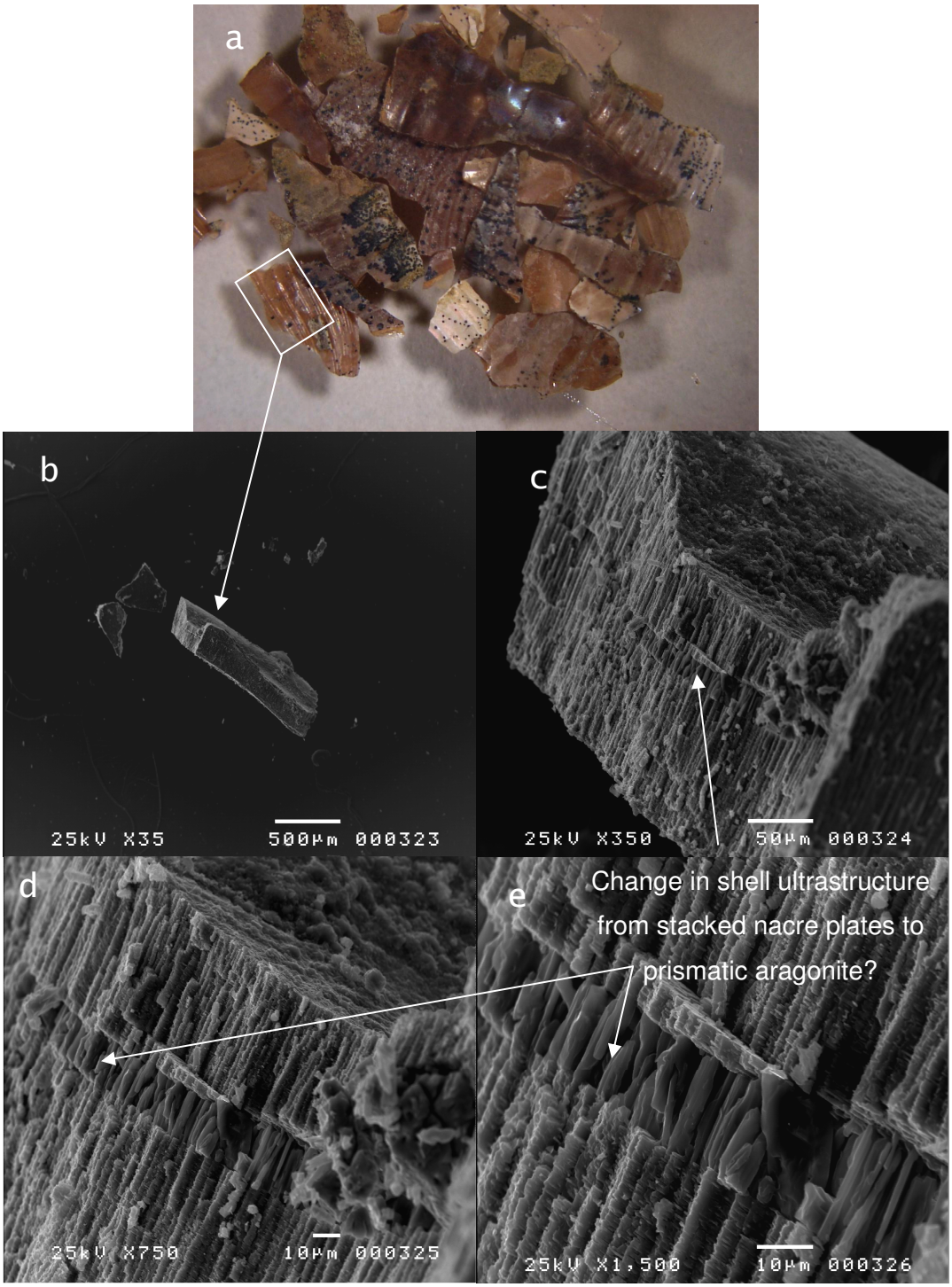

Figure B-6. Optical photomicrograph and SEM images of stacked plates of aragonite nacre shell material separated by a layer of prismatic aragonite. It is possible the feature identified as a prismatic layer is a diagenetic vein but there appears to be little evidence for neomorphism of the surrounding nacre. The highlighted section in image (a) clearly shows the presence of external ribbing, image (b) retains the same overall morphology at a reduced scale. Ammonite genus - *Maorites* a nektonic carnivore. Specimen Id D5.219.1185.2/C. Field of view ~13 mm and scale bars respectively 500, 50, 10 and 10 µm.

B.3 Diagenetic scoring

Table B-3. Diagenetic scoring based upon SEM imaging, qualitative XRD and trace element geochemistry.
Data are presented in stratigraphic order. Highlighted cells indicate specimens that fall outside the expected range for the element concerned. Primary diagenetic trace element indicators used are Fe (Threshold < 500 ppm) and Mn (Threshold <200 ppm) (Morrison and Brand, 1988; Anderson *et al.*, Petersen *et al.*, 2016). Low magnesium calcite (LMC) defined by the natural limit for Mg in biogenic aragonite at > 1000 ppm (Brand, 1991).

Depth (m)	Specimen Id	Mg	Sr	Na	Fe	Mn	Type	Genus	Habitat	Mode of life	Min'lgy	SEM Score	SEM Mag.	SEM Quality	XRD Score	XRD Quality
1084	D5.229.1361.2/A	264	3216	4616	0	229	B	Nucula	I	D	A	4	1500	Minimal fusing of nacre? and pyrite framboids	4	Moderate - low count
1084	D5.229.1361.2/B	271	3705	7447	844	2295	B	Nucula	I	D	A	0		No image	3	Gypsum present
1084	D5.229.1361.2/C	536	2744	7423	399	421	B	Nucula	I	D	A	0		No image	3	Gypsum present
1084	D5.229.1361.2/D	401	2359	4713	1542	219	B	Nucula	I	D	A	0		No image	3	Gypsum present
1084	D5.229.1361.2/E		No trace element data				B	Nucula	I	D	A	4	1500	Minimal fusing of nacre	2	Poor signal - low count
1084	D5.229.1361.2/F	295	5871	4829	217	863	B	Nucula	I	D	A	0		No image	2	Poor signal - low count
1084	D5.229.1361.2/H		No trace element data				B	Nucula	I	D	A	0		No image	2	Poor - low count
1080	D5.229.1353.2/C	21	2142	3932	92	0	U	Unidentified	?	?	A	4	2000	Minimal fusing of nacre	5	Excellent
1068	D5.229.1334.2/A	464	3741	3529	450	299	B	Nucula	I	D	A	3	1500	Dissolution pits/endolithic bacteria?	5	Excellent
1028	D5.229.1292.2/A-1	921	6179	3216	1324	538	N	Nautiloid	N	C	A	3	1500	Fused plates?	4	Good
1028	D5.229.1292.2/A-1	207	6139	3675	419	128	N	Nautiloid	N	C	A	3	1500	Partially fused plates	4	Good
1028	D5.229.1292.2/A-2	14	594	377	12	7	N	Nautiloid	N	C	A	3	1000	Fused plates?	5	Excellent
995	D5.222.1257.2/A	466	3982	8943	0	14	N	Nautiloid	N	C	A	0		No image	5	Excellent
991	D5.222.1254.1/A	60	4170	4479	83	11	U	Unidentified	?	?	A	0	350	Low resolution	5	Excellent
991	D5.222.1255.2/A	34	1940	10760	0	190	G	Amberlaya	E	S	A	5	1500	Good	5	Excellent
991	D5.222.1255.2/D	149	2108	4331	22	320	G	Amberlaya	E	S	A	4	1000	Minimal fusing of nacre	5	Excellent
943	D5.220.1226.2/A	204	8279	3529	506	286	A	Maorites	N	C	A	0		No image	1	LMC
925	D5.220.1217.2/A	577	4839	3801	340	410	A	Maorites	N	C	A	0		No image	3	S/N ratio
919	D5.220.1214.2/A	529	4842	3660	52	136	A	Maorites	N	C	A	0		No image	5	Excellent
909	D5.220.1209.3/A-1		No trace element data				G	Gastropod	E	S	?	0		No image	0	No profile
909	D5.220.1209.3/A-2		No trace element data				G	Gastropod	E	S	?	0		No image	0	No profile
897	D5.220.1202.2/B-4		No trace element data				A	Maorites	N	C	C	2	2000	Fused plates?	1	S/N ratio
895	D5.220.1200.2/A	223	2514	4641	1286	59	B	Pinna	I	P	A	3	1500	Dissolution pits?	2	S/N ratio and peaks missing

Depth (m)	Specimen Id	Mg	Sr	Na	Fe	Mn	Type	Genus	Habitat	Mode of life	Min'lgy	SEM Score	SEM Mag.	SEM Quality	XRD Score	XRD Quality
869	D5.219.1185.2/C	771	11129	4740	526	1462	A	Maorites	N	C	A	4	750	Minimal fusing of nacre	1	S/N ratio
869	D5.219.1185.2/D	524	6459	5430	226	482	A	Maorites	N	C	A	0	350	Low resolution	1	S/N ratio
869	D5.219.1185.2/G-1	853	8381	4196	340	769	A	Maorites	N	C	A	0		No image	5	Excellent
869	D5.219.1185.2/I	20	5783	7945	58	44	B	Eselaevitrigonia	I	P	A	2	1000	Neomorphism?	5	Excellent
863	D5.219.1182.2/A	42	5997	8276	204	13	B	Nucula	I	D	A	3	1500	Fused plates?	5	Excellent
857	D5.219.1179.2/A-1	198	2884	5065	340	294	B	Bivalve	?	?	A	0		No image	5	Excellent
857	D5.219.1179.2/A-2	211	4008	4155	493	882	B	Eselaevitrigonia	I	P	A	0		No image	4	Good - S/N ratio
851	D5.219.1176.2/A	447	4680	3588	481	394	A	Maorites	N	C	A	0		No image	4	Good
837	D5.219.1168.2/B	319	2952	6567	717	134	A	Ammonite	N	C	A	0		No image	0	No profile
837	D5.219.1168.2/B	326	2777	3976	1366	119	A	Ammonite	N	C	A	0		No image	5	Excellent
837	D5.219.1168.2/B	289	2800	4515	1299	102	A	Ammonite	N	C	A	0		No image	0	No profile
800	D5.219.1149.1/A-1		No trace element data				B	Bivalve	?	?	A	0		No image	5	Excellent
800	D5.219.1149.1/A-2	68	2567	5215	155	0	B	Bivalve	?	?	A	5	1500	Fused plates?	2	S/N ratio and peaks missing
779	D5.219.1138.3/A	26	2916	4116	177	20	B	Bivalve	?	?	A	0		No image	5	Excellent
779	D5.219.1138.3/B	29	3276	4251	48	25	B	Oistotrigonia	I	P	A	0		No image	5	Excellent
779	D5.219.1138.3/C	24	3681	3712	19	61	B	Eselaevitrigonia	I	P	A	3	2000	Fused plates	5	Excellent
755	D5.219.1125.2/C-1	179	2856	5194	450	0	B	Eselaevitrigonia	I	P	A	0		No image	4	Good - S/N ratio
755	D5.219.1125.2/C-2	136	2353	8919	120	3	B	Eselaevitrigonia	I	P	A	0		No image	4	Good
755	D5.219.1125.2/D	103	1900	11234	47	2	B	Oistotrigonia	I	P	A	0		No image	5	Excellent
755	D5.219.1125.2/E	98	2088	9197	9	1	B	Oistotrigonia	I	P	A	0		No image	5	Excellent
755	D5.219.1125.2/G-1	3	192	695	0	0	B	Bivalve	?	?	A	3	2000	Fused plates	5	Excellent
755	D5.219.1125.2/G-2	33	1890	6637	25	1	B	Bivalve	?	?	A	3	2000	Fused plates	5	Excellent
755	D5.219.1125.2/L	40	1662	3567	240	0	B	Bivalve	?	?	A	2	1500	Fused plates	4	Good - S/N ratio
755	D5.219.1125.2/L	53	1340	8365	11	0	B	Bivalve	?	?	A	2	1500	Fused plates	5	Separate analysis
755	D5.219.1125.2/M	63	2098	9489	48	2	B	Bivalve	?	?	A	0		No image	5	Excellent
755	D5.219.1125.2/N	125	1428	6664	94	2	B	Bivalve	?	?	A	1	1500	Nacre fused + neomorphism	5	Excellent
749	D5.219.1122.2/D	0	1270	3582	198	0	B	Oistotrigonia	I	P	A	4	1500	Dissolution pits/endolithic bacteria damage. Minimal fusing of nacre	4	S/N ratio
727	D5.219.1106.2/C	96	1460	4357	58	2	B	Oistotrigonia	I	P	A	4	350	Low resolution	5	Excellent
722	D5.219.1101.2/D	974	2987	3744	996	171	A	Ammonite	N	C	A	0		No image	4	Good - peaks shifted

Depth (m)	Specimen Id	Mg	Sr	Na	Fe	Mn	Type	Genus	Habitat	Mode of life	Min'lgy	SEM Score	SEM Mag.	SEM Quality	XRD Score	XRD Quality
717	D5.219.1096.3/H	105	1923	8207	101	5	B	Eselaevitrigonia	I	P	A	0		No image	0	No profile
717	D5.219.1096.3/I	144	2030	6247	222	9	B	Eselaevitrigonia	I	P	A	0		No image	5	Excellent
712	D5.219.1091.2/A-2		No trace element data				G	Gastropod	E	S	?	0		No image	0	No profile
712	D5.219.1091.2/F	178	2582	9797	131	0	B	Nucula	I	D	A	4	3500	Fusing of nacre	5	Excellent
712	D5.219.1091.2/G	42	2024	3505	295	0	U	Unidentified	?	?	A	4	1500	Minimal fusing of nacre	4	Missing peaks
712	D5.219.1091.2/H	36	2251	3680	350	0	B	Bivalve	?	?	A	5	1500	Good	5	Excellent
712	D5.219.1091.2/I-2	0	1083	3715	181	0	B	Oistotrigonia	I	P	A	4	1500	Minimal fusing of nacre	4	Missing peaks
682	D5.218.1061.2/B	608	1345	3038	389	411	B	Eselaevitrigonia	I	P	A	0		No image	4	Good + minor gypsum
682	D5.218.1061.2/C	304	3540	10203	0	203	B	Eselaevitrigonia	I	P	A	0		No image	5	Excellent
682	D5.218.1061.2/D	755	1842	4025	184	233	B	Eselaevitrigonia	I	P	A	3	3500	Fusing of nacre	4	Good + minor gypsum
682	D5.218.1061.2/F	318	2946	12384	0	269	B	Bivalve	?	?	A	4	2000	Minimal fusing of nacre	5	Excellent
682	D5.218.1061.2/H	509	1425	5621	476	474	B	Bivalve	?	?	A	0		No image	4	Good + minor gypsum
647	D5.218.1027.2/A		No trace element data				B	Pycnodonte	E	P	C	0		No image	1	Calcite
647	D5.218.1027.2/B	293	6412	3993	377	56	A	Ammonite	N	C	A	0		No image	5	Excellent
642	D5.218.1021.2/A-1	108	3710	5440	47	91	G	Amberlaya	E	S	A	0		No image	5	Excellent
642	D5.218.1021.2/A-2	107	3403	4622	0	84	G	Amberlaya	E	S	A	0		No image	5	Excellent
642	D5.218.1021.2/B	107	4256	8695	140	37	G	Pleurotomaria	E	B	A	3	1500	Fusing of nacre	5	Excellent
642	D5.218.1021.2/C	85	2543	8544	76	76	G	Amberlaya	E	S	A	0		No image	5	Excellent
642	D5.218.1021.2/D	222	4513	6676	333	222	B	Nucula	I	D	A	0		No image	5	Excellent
642	D5.218.1021.2/E	129	4553	8214	18	16	B	Nucula	I	D	A	3	2000	Neomorphism on surface, nacre (score 4)	5	Excellent
642	D5.218.1021.2/G	402	5522	5997	368	81	B	Nucula	I	D	A	0		No image	4	Good + minor gypsum
642	D5.218.1021.2/H	58	1725	5114	0	222	B	Oistotrigonia	I	P	A	0		No image	5	Excellent
642	D5.218.1021.2/I	41	1390	4657	0	294	B	Nucula	I	D	A	0		No image	5	Excellent
642	D5.218.1021.2/J	113	2062	5577	0	905	B	Oistotrigonia	I	P	A	0		No image	5	Excellent
642	D5.218.1021.2/V	301	7202	3856	135	124	A	Maorites	N	C	A	0		No image	5	Excellent
642	D5.218.1021.2/W	148	4008	4594	201	20	U	Unidentified	?	?	A	2	1500	Fused nacre + neomorphism	4	Missing peaks
637	D5.218.1016.2/B	77	1790	6967	38	130	B	Nucula	I	D	A	0		No image	5	Excellent
637	D5.218.1016.2/C	13	2758	4538	0	5	B	Nucula	I	D	A	0		No image	5	Excellent
637	D5.218.1016.2/D	89	3334	4989	273	8	G	Amberlaya	E	S	A	0		No image	5	Excellent
637	D5.218.1016.2/E		No trace element data				G	Amberlaya	E	S	?	0		No image	5	Excellent

Depth (m)	Specimen Id	Mg	Sr	Na	Fe	Mn	Type	Genus	Habitat	Mode of life	Min'lgy	SEM Score	SEM Mag.	SEM Quality	XRD Score	XRD Quality
637	D5.218.1016.2/G	82	3157	6114	199	587	G	Amberlaya	E	S	A	0		No image	5	Excellent
637	D5.218.1016.2/J	15	1881	4504	0	7	B	Eselaevitrigonia	I	P	A	4	1500	Minimal fusing of nacre	5	Excellent
637	D5.218.1016.2/K	56	1793	6551	78	2	B	Eselaevitrigonia	I	P	A	0		No image	5	Excellent
637	D5.218.1016.2/L-1	70	1956	9603	133	13	B	Eselaevitrigonia	I	P	A	4	1500	Minimal fusing of nacre	5	Excellent
637	D5.218.1016.2/L-2	32	1530	10044	24	11	B	Eselaevitrigonia	I	P	A	0		No image	5	Excellent
637	D5.218.1016.2/M	397	1802	8150	707	21	B	Nucula	I	D	A	0		No image	4	Good
637	D5.218.1016.2/N	83	2450	4058	16	21	B	Eselaevitrigonia	I	P	A	0		No image	5	Excellent
637	D5.218.1016.2/O	100	1524	4933	63	2	A	Ammonite	N	C	A	2	1500	Fused nacre + neomorphism	5	Excellent
632	D5.218.1011.2/A	304	2913	4094	549	94	B	Pinna	I	P	A	0		No image	5	Excellent
627	D5.218.1006.2/A	224	4019	4076	538	83	A	Maorites	N	C	A	0		No image	5	Excellent
627	D5.218.1006.2/B	602	3787	4926	2999	301	A	Maorites	N	C	A	0	35	Insufficient resolution	5	Excellent
627	D5.218.1006.2/C	368	4337	3925	720	101	A	Maorites	N	C	A	0		No image	4	Good + minor gypsum
627	D5.218.1006.2/I	157	4911	6432	115	29	A	Maorites	N	C	A	0		No image	5	Excellent
627	D5.218.1006.2/O	134	2160	10856	165	10	B	Oistotrigonia	I	P	A	0		No image	5	Excellent
627	D5.218.1006.2/P	366	4114	3294	1128	53	U	Unidentified	?	?	A	0		No image	4	Good + minor gypsum
622	D5.215.216.2/A	0	2541	3417	181	0	B	Pinna	I	P	A	0		No image	5	Excellent
622	D5.215.216.2/A		No trace element data				B	Pinna	I	P	A	0		No image	0	No profile
622	D5.215.216.2/A		No trace element data				B	Pinna	I	P	A	0		No image	0	No profile
622	D5.215.216.3/A-1	0	2609	3506	143	18	B	Eselaevitrigonia	I	P	A	0		No image	5	Excellent
622	D5.215.216.3/A-10		No trace element data				B	Eselaevitrigonia	I	P	A	0		No image	0	No profile
622	D5.215.216.3/A-11		No trace element data				B	Eselaevitrigonia	I	P	A	0		No image	0	No profile
622	D5.215.216.3/A-2	5	2825	3873	453	119	B	Eselaevitrigonia	I	P	A	0		No image	5	Excellent
622	D5.215.216.4/A	681	2422	4111	3494	208	G	Amberlaya	E	S	A	4	1000	Surface debris, some fused nacre	5	Excellent
622	D5.215.216.5/A	71	3128	4238	0	10	G	Pleurotomaria	E	B	A	3	1000	Focus poor and fused nacre	5	Excellent
622	D5.215.705.2/H	218	3011	5182	47	335	B	Eselaevitrigonia	I	P	A	0		No image	4	Good + minor gypsum
618	D5.215.701.2/A	79	2885	4120	21	56	B	Nucula	I	D	A	2	1000	Focus poor and fused nacre	5	Excellent
618	D5.215.701.2/B	27	3157	3794	164	125	B	Bivalve	?	?	A	0		No image	5	Excellent
613	D5.215.696.2/AA	0	2559	3834	136	34	B	Nucula	I	D	A	0		No image	5	Excellent
613	D5.215.696.2/AI		No trace element data				B	Nucula	I	D	A	0		No image	2	Poor - low count
613	D5.215.696.2/AK	129	4810	3576	0	15	B	Nucula	I	D	A	5	2000	Good nacre + some dissolution/endolithic boring	5	Excellent

Depth (m)	Specimen Id	Mg	Sr	Na	Fe	Mn	Type	Genus	Habitat	Mode of life	Min'lgy	SEM Score	SEM Mag.	SEM Quality	XRD Score	XRD Quality
613	D5.215.696.2/AL	93	5005	3571	158	129	B	Nucula	I	D	A	0		No image	5	Excellent
613	D5.215.696.2/AM	156	5995	6076	67	454	B	Eselaevitrigonia	I	P	A	0	35	Low resolution image	5	Excellent
613	D5.215.696.2/AN	80	3325	6260	0	32	B	Eselaevitrigonia	I	P	A	4	2000	Surface debris, some fused nacre(?)	5	Excellent
613	D5.215.696.2/AN		No trace element data				B	Eselaevitrigonia	I	P	A	0		No image	0	No profile
613	D5.215.696.2/AN		No trace element data				B	Eselaevitrigonia	I	P	A	0		No image	0	No profile
613	D5.215.696.2/AN-2		No trace element data				B	Eselaevitrigonia	I	P	A	0		No image	0	No profile
613	D5.215.696.2/AO	824	2914	6846	132	3945	B	Nucula	I	D	A	2	2000	Poor focus + fused nacre	5	Excellent
613	D5.215.696.2/AQ	171	4341	8443	0	157	B	Eselaevitrigonia	I	P	A	0		No image	5	Excellent
613	D5.215.696.2/AR	174	4110	4298	35	24	A	Ammonite	N	C	A	0	350	Low resolution	5	Excellent
613	D5.215.696.2/AT	93	4382	3199	483	5	A	Ammonite	N	C	A	0		No image	5	Excellent
613	D5.215.696.2/AU	190	5213	4548	0	49	G	Amberlaya	E	S	A	4	1500	Surface debris, some fused nacre	0	No profile
613	D5.215.696.2/AV	42	3252	3977	137	28	B	Lahillia	I	P	A	0		No image	5	Excellent
613	D5.215.696.2/N	279	3131	8298	773	34	G	Amberlaya	E	S	A	4	2000	Good nacre	5	Excellent
613	D5.215.696.2/P	239	2949	7159	40	50	G	Amberlaya	E	S	A	0		No image	5	Excellent
613	D5.215.696.2/Q	535	2964	3895	375	15	A	Maorites	N	C	A	0		No image	3	Noisy profile
613	D5.215.696.2/W		No trace element data				B	Eselaevitrigonia	I	P	?	0		No image	0	No profile
608	D5.215.691.2/A	289	6496	6074	117	146	A	Maorites	N	C	A	3	2000	Minimal fusing of nacre	4	Good
608	D5.215.691.2/B	178	3195	7506	369	15	A	Grossouvrites	N	C	A	4	2000	Good nacre	5	Excellent
608	D5.215.691.2/C	119	3414	7290	23	16	B	Nucula	I	D	A	3	2000	Minimal fusing of nacre	5	Excellent
608	D5.215.691.2/D-1	101	3150	7236	0	52	B	Eselaevitrigonia	I	P	A	5	1500	Good nacre + some dissolution/endolithic boring	5	Excellent
603	D5.215.686.2/A	112	2219	7735	29	34	G	Amberlaya	E	S	A	4	2000	Good nacre	5	Excellent
578	D5.215.396.2/A	69	2308	4786	69	25	B	Nucula	I	D	A	1	750	Neomorphism?	5	Excellent
558	D5.215.378.2/A	71	2953	4732	56	14	B	Bivalve	?	?	A	4	1000	Good nacre	5	Excellent
551	D5.215.371.2/A	68	3366	3786	234	1	B	Bivalve	?	?	A	0		No image	5	Excellent
551	D5.215.371.2/B	56	3363	3723	135	2	B	Eselaevitrigonia	I	P	A	0		No image	5	Excellent
548	D5.215.368.2/A	78	2550	5080	0	12	U	Unidentified	?	?	A	3	2000	Minimal fusing of nacre	5	Excellent
548	D5.215.368.2/B	241	1494	4639	144	25	B	Oistotrigonia	I	P	A	3	1500	Localised fusing of nacre, primary structure present	5	Excellent
548	D5.215.368.2/B		No trace element data				B	Oistotrigonia	I	P	A	0		No image	0	No profile
548	D5.215.368.2/C	39	3074	3834	115	25	G	Amberlaya	E	S	A	0		No image	0	No profile

Depth (m)	Specimen Id	Mg	Sr	Na	Fe	Mn	Type	Genus	Habitat	Mode of life	Min'lgy	SEM Score	SEM Mag.	SEM Quality	XRD Score	XRD Quality
541	D5.215.361.2/A	87	2001	4491	0	19	G	Gastropod	E	?	A	5	2000	Good nacre + some dissolution/endolithic boring	5	Excellent
541	D5.215.361.2/B	95	3271	3970	0	56	B	Bivalve	?	?	A	4	1500	Minimal fusing of nacre	5	Excellent
541	D5.215.361.2/C	105	3215	4432	0	13	B	Eselaevitrigonia	I	P	A	3	1500	Focus poor and localised fusing of nacre	5	Excellent
541	D5.215.361.2/D	27	3049	3680	332	183	B	Eselaevitrigonia	I	P	A	0		No image	5	Excellent
541	D5.215.361.2/E		No trace element data				B	Nucula	I	D	A	4	1500	Out of focus, nacre good	4	Good
541	D5.215.361.2/E		No trace element data				B	Nucula	I	D	A	4	1500	Good nacre	4	Good
538	D5.215.357.2/A	0	2296	4197	115	0	B	Eselaevitrigonia	I	P	A	0		No image	5	Excellent
538	D5.215.357.2/B	131	2415	4797	12	37	B	Eselaevitrigonia	I	P	A	3	1500	Focus poor and some fusing of nacre	5	Excellent
533	D5.215.352.2/A	88	3563	6919	0	59	B	Eselaevitrigonia	I	P	A	2	350	Low resolution	5	Excellent
533	D5.215.352.2/B	185	2925	6597	24	48	B	Bivalve	?	?	A	4	1000	Minimal fusing of nacre	5	Excellent
533	D5.215.352.2/C	105	5545	3390	281	465	B	Nucula	I	D	A	0		No image	3	Moderate - low count
533	D5.215.352.2/D	127	3728	7350	63	280	B	Nucula	I	D	A	3	1000	Fusing of nacre	4	Noisy pattern
533	D5.215.352.2/E	352	4692	3372	253	1961	B	Nucula	I	D	A	0		No image	3	Moderate - low count
528	D5.215.347.2/A	176	5700	5726	69	90	B	Nucula	I	D	A	3	2000	Fusing of nacre	5	Excellent
528	D5.215.347.2/A-2		No trace element data				B	Nucula	I	D	A	0		No image	5	Excellent
528	D5.215.347.2/D	332	3402	6713	345	1017	B	Eselaevitrigonia	I	P	A	4	3500	Good nacre	4	Noisy pattern
528	D5.215.347.2/E		No trace element data				B	Nucula	I	D	A	0		No image	0	No profile
528	D5.215.347.2/F		No trace element data				B	Nucula	I	D	A	0		No image	0	No profile
528	D5.215.347.2/G	414	4216	6314	175	349	B	Eselaevitrigonia	I	P	A	3	2000	Fusing of nacre	4	Good
528	D5.215.347.2/I	418	4355	5726	59	174	B	Eselaevitrigonia	I	P	A	1	750	Poor -	4	Good - low count
528	D5.215.347.2/J	24	3159	3795	120	254	B	Nucula	I	D	A	0		No image	5	Excellent
528	D5.215.347.2/K		No trace element data				B	Nucula	I	D	A	0		No image	0	No profile
528	D5.215.347.2/L	101	3060	3631	244	941	B	Nucula	I	D	A	0		No image	4	Good
528	D5.215.347.2/M	684	6768	2776	78	100	B	Solemya	I	P	A	0		No image	5	Excellent
528	D5.215.347.2/N		No trace element data				B	Solemya	I	P	A	0		No image	0	No profile
526	D5.215.345.2/A-1		No trace element data				B	Solemya	I	P	A	0		No image	0	No profile
508	D5.215.327.2/A		No trace element data				B	Nucula	I	D	A	5	1000	Good nacre + some dissolution/endolithic boring	5	Excellent
508	D5.215.327.2/A-1	184	2388	9111	0	624	B	Nucula	I	D	A	4	1000	Good nacre	5	Excellent
508	D5.215.327.2/A-2	125	1058	3995	0	135	B	Oistotrigonia	I	P	A	0		No image	4	Good + minor gypsum

Depth (m)	Specimen Id	Mg	Sr	Na	Fe	Mn	Type	Genus	Habitat	Mode of life	Min'lgy	SEM Score	SEM Mag.	SEM Quality	XRD Score	XRD Quality
463	D5.215.985.2/B	0	1431	6615	0	151	B	Oistotrigonia	I	P	A	0		No image	5	Excellent
458	D5.215.980.2/A	0	1546	3662	106	94	B	Oistotrigonia	I	P	A	4	2000	Dissolution/endolithic boring	0	No profile
458	D5.215.980.2/A		No trace element data				B	Oistotrigonia	?	?	A	3	2000	Fusing of nacre	4	Good - minor peak offset
458	D5.215.980.2/B	122	2236	3917	57	20	B	Eselaevitrigonia	I	P	A	4	2000	Minimal fusing of nacre	5	Excellent
453	D5.215.975.2/A	32	1646	4329	0	47	B	Oistotrigonia	I	P	A	4	2000	Minimal fusing of nacre	5	Excellent
453	D5.215.975.2/B	0	1495	3464	86	56	B	Oistotrigonia	I	P	A	0		No image	4	Good + minor gypsum
453	D5.215.975.2/C	0	1339	3687	112	52	B	Oistotrigonia	I	P	A	0		No image	4	Good
443	D5.215.965.2/A	0	1316	3839	398	332	B	Eselaevitrigonia	I	P	A	0		No image	5	Excellent
438	D5.215.960.3/B	361	3090	5780	1640	226	A	Ammonite	N	C	A	4	2000	Minimal fusing of nacre	3	Noisy profile
435	D5.215.955.3/A	426	4327	6719	179	61	A	Diplomoceras	P	C	A	3	2000	Fusing of nacre	5	Excellent
408	D5.215.930.2/A	56	1296	4323	0	130	B	Oistotrigonia	I	P	A	0		No image	5	Excellent
388	D5.212.909.2/A	144	2000	4709	14	7	B	Oistotrigonia	I	P	A	0		No image	5	Excellent
388	D5.212.909.2/B	83	1604	4436	64	0	B	Bivalve	?	?	A	0		No image	4	Good - low count
388	D5.212.909.2/C	96	1609	7914	391	7	B	Bivalve	?	?	A	0		No image	4	Good, minor gypsum?
388	D5.215.910.1/A	149	1969	9846	0	0	B	Eselaevitrigonia	I	P	A	3	1500	Fusing of nacre	5	Excellent
348	D5.212.870.2/A	38	1210	9178	106	0	B	Bivalve	?	?	A	0		No image	5	Excellent
343	D5.212.865.3/A-1	56	1456	5613	0	0	B	Oistotrigonia	I	P	A	2	1500	Out of focus, fused nacre	4	Good, low count
343	D5.212.865.3/A-2	62	1345	4570	0	0	B	Oistotrigonia	I	P	A	2	1500	Poor focus + fused nacre	5	Excellent
343	D5.212.865.3/B	127	1582	8921	213	4	B	Oistotrigonia	I	P	A	5	1500	Excellent	5	Excellent
343	D5.212.865.3/C	160	1136	12321	117	0	B	Oistotrigonia	I	P	A	0		No image	5	Excellent
343	D5.212.865.3/D	0	0	9854	0	307	B	Oistotrigonia	I	P	A	0		No image	4	Good
343	D5.212.865.3/E	28	1395	5437	34	0	B	Bivalve	?	?	A	0		No image	3	Low count
343	D5.212.865.3/F	55	1412	5418	248	0	B	Oistotrigonia	I	P	A	0		No image	4	Good - low count
343	D5.212.865.3/G	49	1421	9235	71	0	B	Oistotrigonia	I	P	A	4	3500	Good nacre	5	Excellent
338	D5.212.860.2/A	0	1099	3697	168	0	B	Oistotrigonia	I	P	A	0		No image	5	Excellent
333	D5.212.855.2/B	45	1541	4986	20	0	U	Unidentified	?	?	A	3	1500	Some fusing of nacre	5	Excellent
333	D5.212.855.2/C	97	1272	4216	123	0	U	Unidentified	?	?	A	4	1000	Good nacre	5	Excellent
311	D5.212.833.2/A	0	1287	5283	0	0	U	Unidentified	?	?	A	0		No image	3	Peak offset + low count
1001	D5.229.1264.2/A	5843	2172	3085	3499	4699	A	Ammonite	N	C	C	3	1000	Fused plates?	1	Excellent (LMC)
1001	D5.229.1264.2/B	5635	2247	2644	12313	4757	U	Unidentified	?	?	C	0		No image	1	Poor signal - low count

Depth (m)	Specimen Id	Mg	Sr	Na	Fe	Mn	Type	Genus	Habitat	Mode of life	Min'lgy	SEM Score	SEM Mag.	SEM Quality	XRD Score	XRD Quality
991	D5.222.1254.1/A	2451	4002	4369	3829	1580	U	Unidentified	?	?	C	0		No image	5	Excellent
991	D5.222.1254.1/A-1	5490	2193	2403	9696	4662	U	Unidentified	?	?	C	4	1500	Minimal fusing of nacre	5	Excellent
991	D5.222.1254.1/A-2	2469	3046	2777	3485	2139	U	Unidentified	?	?	C	4	1500	Well defined nacre	0	No profile
991	D5.222.1254.1/A-2	2530	2981	6230	2051	1692	U	Unidentified	?	?	C	3	1500	Fused nacre?	1	Moderate - low count + gypsum?
991	D5.222.1254.1/A-2	2493	2986	7397	2012	1671	U	Unidentified	?	?	C	3	3500	Fused nacre?	5	Excellent
991	D5.222.1255.2/B	6572	1846	2818	2350	380	A	Kitchinites	N	C	C	0	350	Low resolution	1	Moderate - low count
979	D5.222.1248.2/E	9099	2395	2444	3151	2634	A	Ammonite	N	C	C	2	1500	Fused nacre?	1	S/N ratio - LMC
979	D5.222.1248.2/G	15263	1205	2022	2996	5106	A	Maorites	N	C	C	0		No image	1	LMC
979	D5.222.1248.2/H	6479	2245	3224	4792	5942	A	Ammonite	N	C	C	0		No image	1	LMC
961	D5.222.1238.2/A	4365	1900	3813	5070	4110	A	Maorites	N	C	C	0		No image	1	LMC
961	D5.222.1238.2/F	8545	2045	5001	20708	2868	A	Maorites	N	C	C	2	1500	Fused nacre?	1	LMC
955	D5.222.1234.2/A	1696	1696	3951	4842	1296	U	Unidentified	?	?	C	0	350	Low resolution	1	S/N ratio- LMC
955	D5.222.1234.2/B	2039	1751	8620	3790	2058	U	Unidentified	?	?	C	0		No image	1	LMC
955	D5.222.1234.2/K	3810	1503	8007	5536	2822	A	Anagaudryceras	N	C	C	3	1500	Fused nacre? + gypsum	1	Gypsum? (LMC)
949	D5.220.1229.2/A	4050	3249	3048	3147	614	A	Maorites	N	C	C	0		No image	1	LMC
949	D5.220.1229.2/B	7507	3024	3527	332	740	A	Maorites	N	C	C	0		No image	1	LMC
937	D5.220.1223.2/F	3343	2420	3059	6627	8207	A	Maorites	N	C	C	0		No image	1	LMC
925	D5.220.1217.2/B	10277	2312	6309	143	580	A	Maorites	N	C	C	0		No image	1	LMC
897	D5.220.1202.2/A-1	2115	2599	8329	4053	413	A	Maorites	N	C	C	0		No image	1	LMC
897	D5.220.1202.2/A-2	14180	1644	7004	41069	378	B	Bivalve	?	?	C	0		No image	1	LMC
897	D5.220.1202.2/B-3	1220	2880	3750	4604	800	A	Maorites	N	C	C	3	1500	Fused nacre?	4	Minor LMC
869	D5.219.1185.2/F-1	3442	4498	6786	580	1341	A	Maorites	N	C	C	0		No image	1	LMC
869	D5.219.1185.2/F-2	2824	5062	4691	803	1147	A	Maorites	N	C	C	0		No image	1	LMC
869	D5.219.1185.2/H	1582	5175	3303	264	540	A	Maorites	N	C	C	0		No image	1	LMC
837	D5.219.1168.2/A	1197	3400	5800	2494	2316	A	Ammonite	N	C	C	3	1500	Fused nacre?	1	S/N ratio - minor LMC
682	D5.218.1061.2/J	1033	1406	5275	1047	229	U	Unidentified	?	?	C	4	1500	Minimal fusing of nacre	2	Gypsum?
642	D5.218.1021.2/F	2734	2723	6554	7261	50	B	Nucula	I	D	C	0		No image	5	Excellent
642	D5.218.1021.2/Q	1074	702	3874	249	349	B	Pycnodonte	E	P	C	0		No image	1	Calcite
637	D5.218.1016.2/A	2562	8332	6026	2529	1169	A	Maorites	N	C	C	0		No image	1	LMC
627	D5.218.1006.2/G	1754	3680	6120	1178	449	A	Maorites	N	C	C	2	1000	Fusing of nacre + neomorphism	1	Aragonite + LMC

Depth (m)	Specimen Id	Mg	Sr	Na	Fe	Mn	Type	Genus	Habitat	Mode of life	Min'lgy	SEM Score	SEM Mag.	SEM Quality	XRD Score	XRD Quality
627	D5.218.1006.2/N	8039	3583	4855	3586	1067	A	Ammonite	N	C	C	0		No image	1	LMC

B.4 Scanning Electron Microscopy

The Low Vacuum (JEOL JSM-5400LV) Scanning Electron Microscope (SEM) was used to carry out an initial investigation of the shell morphology of samples selected together with screening of samples for the presence of significant diagenetic features. Note that a certain degreee of diagenetic alteration must have occurred since the shell material from the specimens had already de-laminated to form fragments and thin sheets of aragonite nacre (Marshall, 1992). Samples were investigated at a series of scales that ranged from a field of view of ~3.5mm to ~35µm with a respective range of magnification that spanned x35 – x3500. The equipment was operated with a 25kv accelerating voltage and a typical filament load current of ~89 µA. In order to reduce the frequency of sample changeover a new design of sample holder was manufactured with a capacity of 9 x 10mm aluminium stubs in an orientated grid pattern that saved a considerable amount of time during the SEM imaging phase of the project, see Figure B-7.

Figure B-7. SEM sample holder with 3 stubs holding shell fragments.

The instrument was initially operated in low vacuum mode in order to avoid the necessity for carbon coating. However, it was found that the image quality was inferior to that afforded by using Secondary Electron (SEI) mode under high vacuum; consequently all subsequent imaging was carried out using carbon coated samples under high vacuum. Figure B-8 illustrates three images of the same specimen at different magnification that illustrate the good level of preservation of the nacreous aragonite plates.

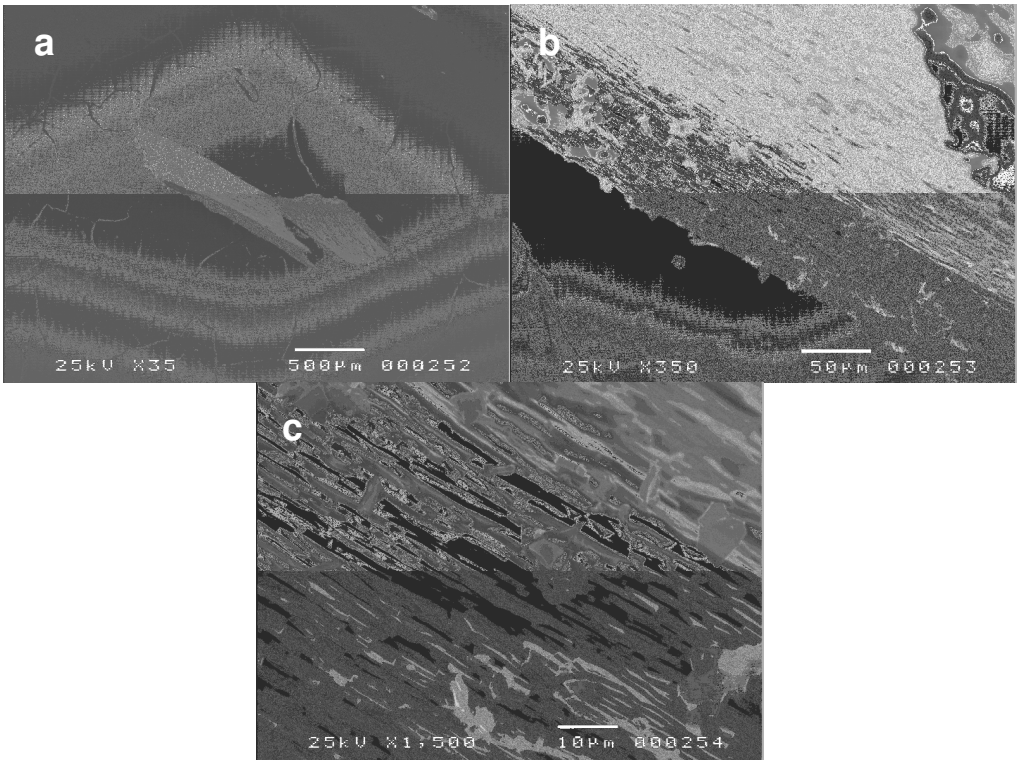

Figure B-8. SEM photomicrographs at x35, x350 and x1500.
Bivalve genus – *Oistotrigonia* an infaunal suspension feeder. Specimen Id D5.212.865.3/B.
Scale bar respectively 500, 50 and 10 µm.

The only exception to this methodology was that adopted for additional diagenetic screening of specimens selected for $^{87}Sr/^{86}Sr$ isotopic analysis, in which an additional check was included using Back Scatter Electron (BSE) mode under low vacuum for the presence of strontianite ($SrCO_3$). No specimens analysed using BSE tested positive for the presence of strontianite.

B.5 SEM images – Bivalves

This section shows high magnification SEM photomicrographs of aragonite nacre shell material for the bivalve genus *Nucula*, an infaunal deposit feeder.

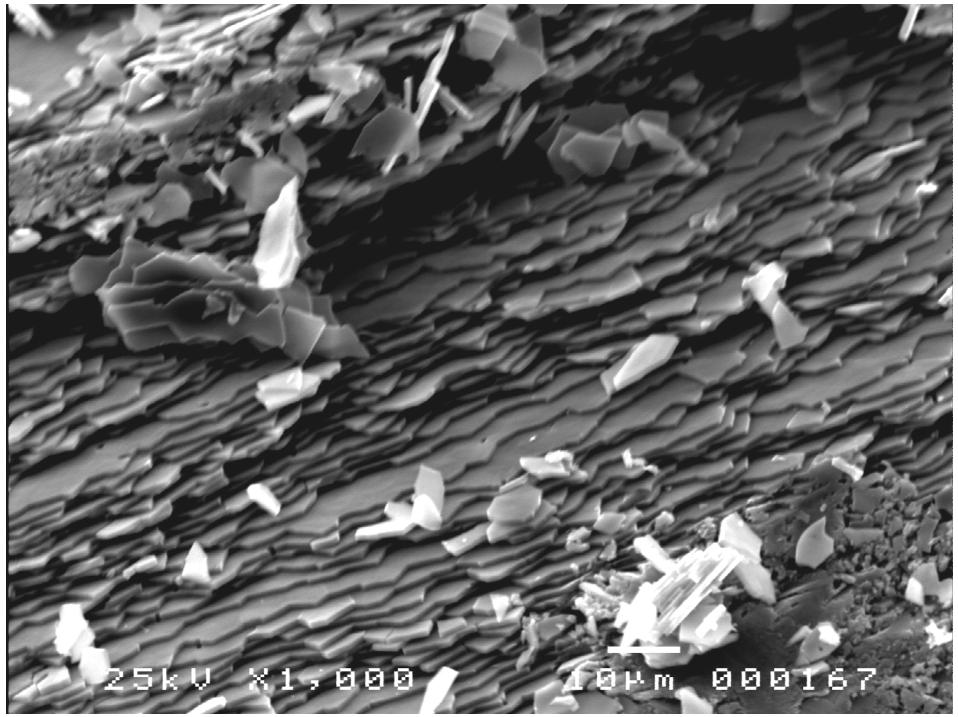

Figure B-9. Specimen Id D5.215.327.2/A
Bivalve genus *Nucula*, an infaunal deposit feeder. Nacreous aragonite shell material, note the presence of well defined layers of nacre with loose fragments of shell material on the surface. Scale bar 10 µm.

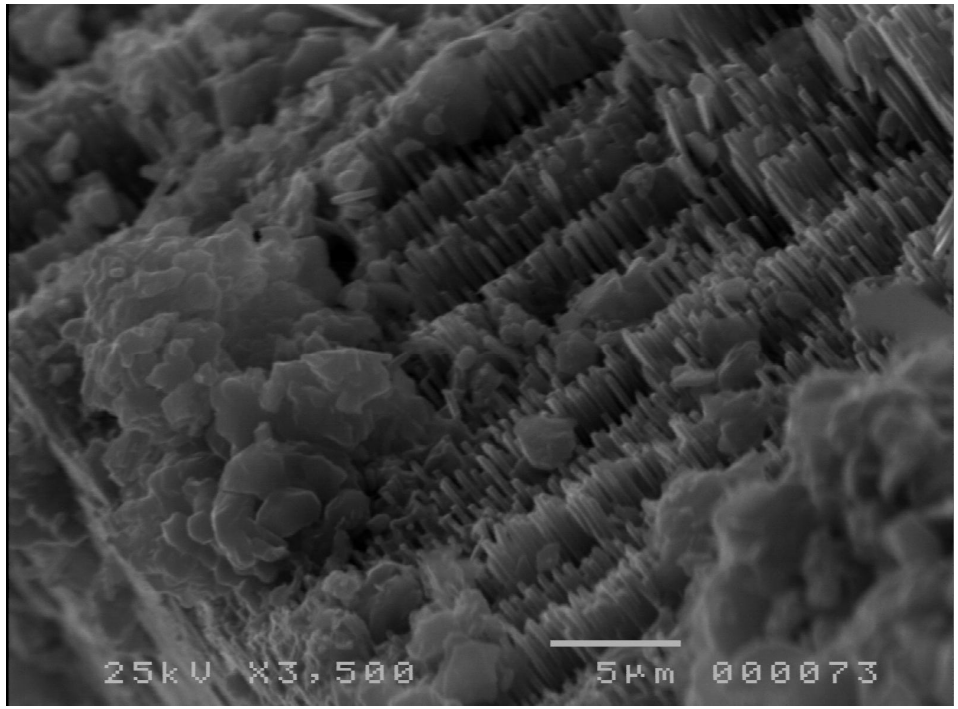

Figure B-10. Specimen Id D5.219.1091.2/F
Bivalve genus *Nucula*, an infaunal deposit feeder. Nacreous aragonite shell material,note the presence of well defined layers of nacre together with loose fragments of shell material on the surface. Scale bar 5 µm.

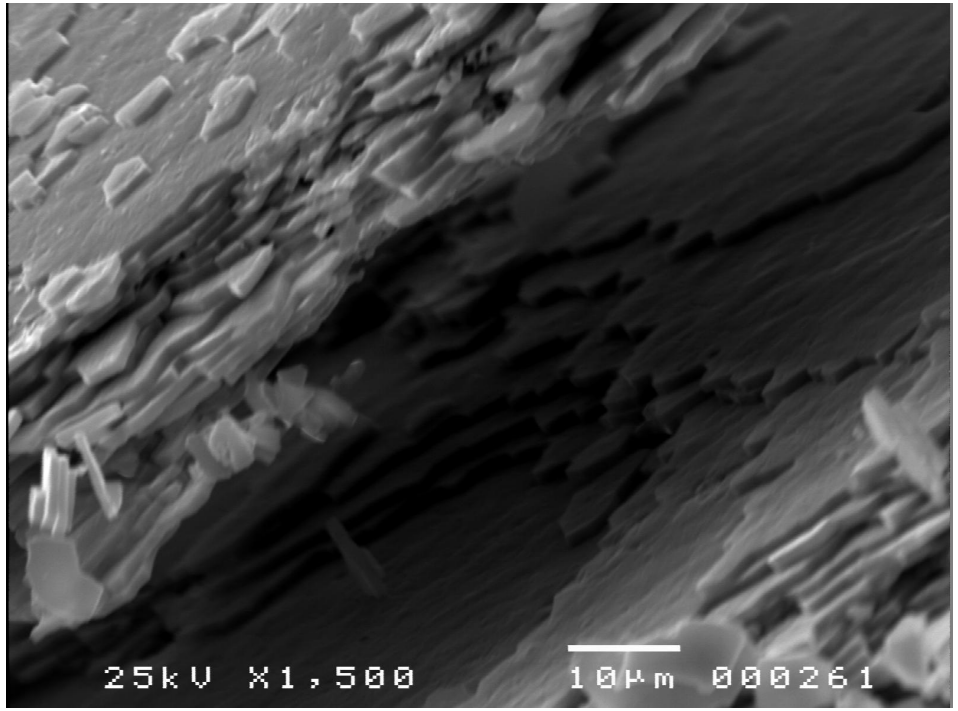

Figure B-11. Specimen Id D5.229.1361.2/A
Bivalve genus *Nucula*, an infaunal deposit feeder. Nacreous aragonite shell material, note the presence of well defined layers of nacre with loose fragments of shell material on the surface. Scale bar 10 µm.

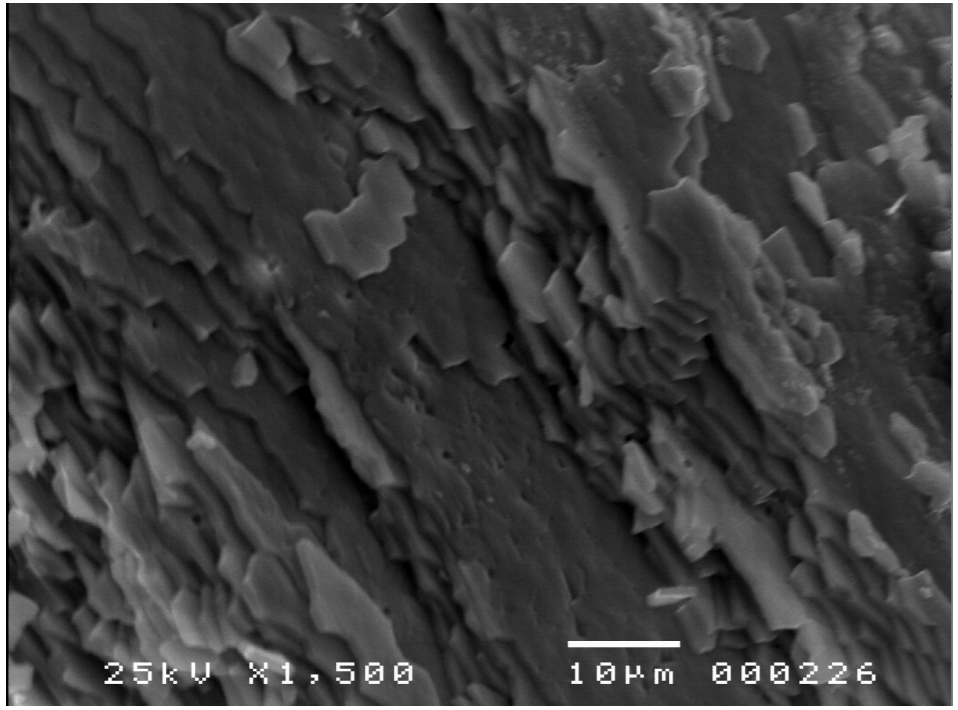

Figure B-12. Specimen Id D5.229.1361.2/E
Bivalve genus *Nucula*, an infaunal deposit feeder. Aragonite nacre, note the presence of well defined layers of nacre together with loose fragments of shell material on the surface. Scale bar 10 µm.

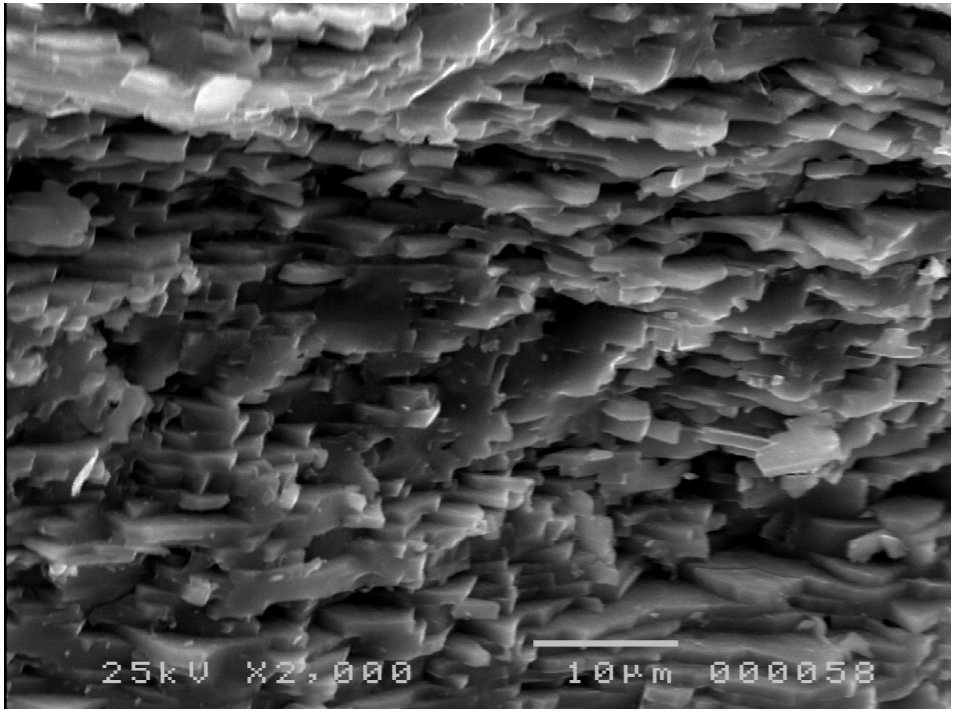

Figure B-13. Specimen Id D5.215.361.2/C
Bivalve genus *Nucula*, an infaunal deposit feeder. Aragonite nacre, note the presence of well defined layers of nacre together with loose fragments of shell material on the surface. Scale bar 10 µm.

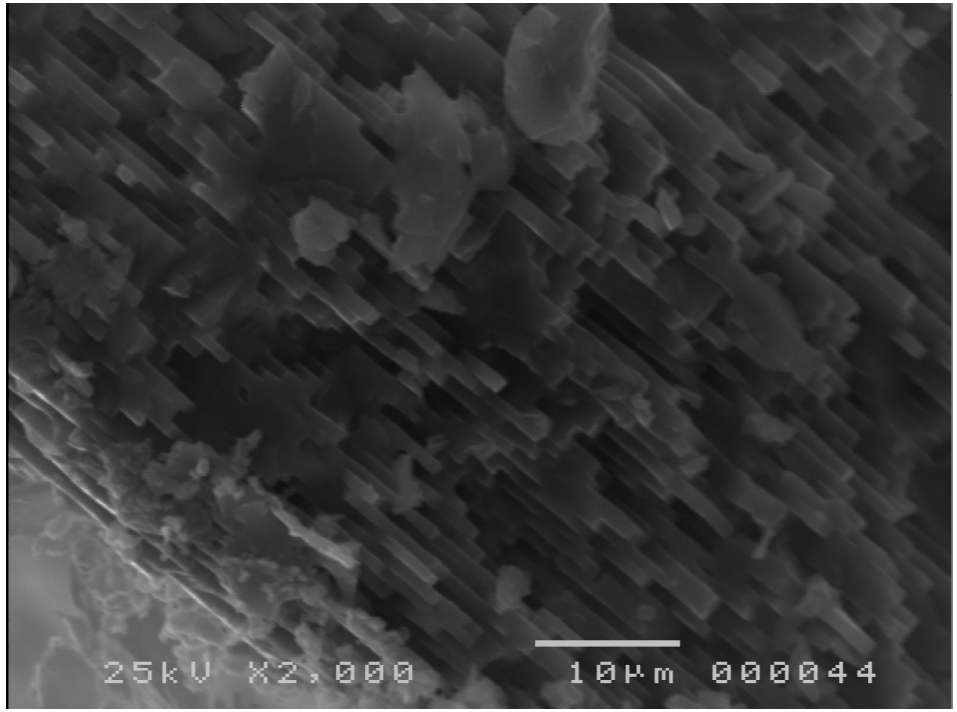

Figure B-14. Specimen Id D5.215.347.2/A
Bivalve genus *Nucula*, an infaunal deposit feeder. Aragonite nacre, note the presence of well defined layers of nacre together with loose fragments of shell material on the surface. Scale bar 10 µm.

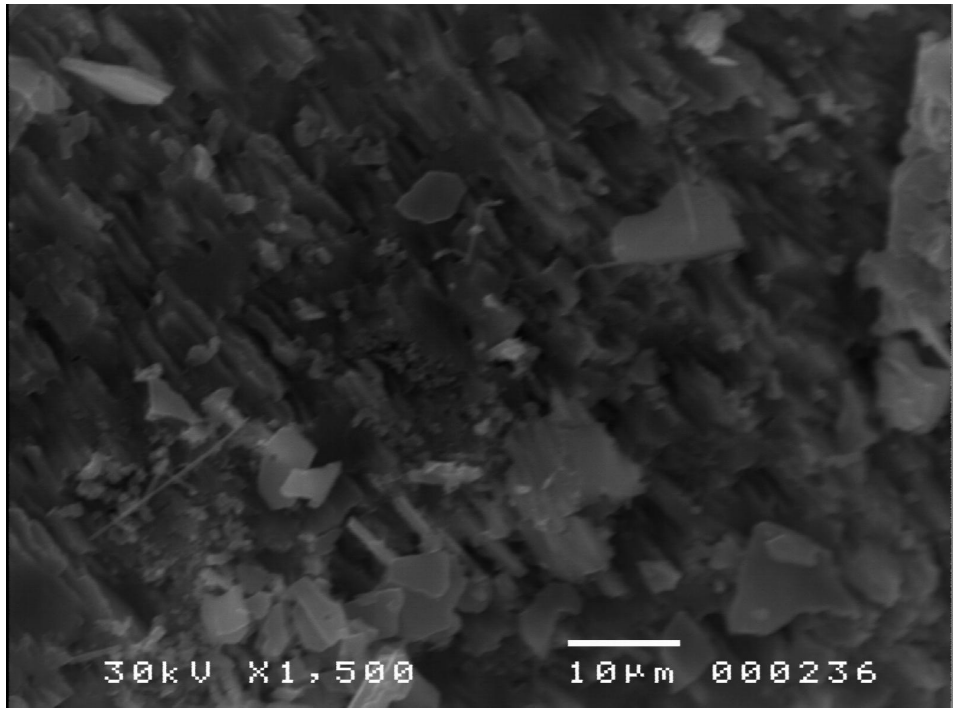

Figure B-15. Specimen Id D5.212.865.3/A
Aragonite nacre, Bivalve genus - *Oistotrigonia* an infaunal suspension feeder.
Scale bar 10 µm.

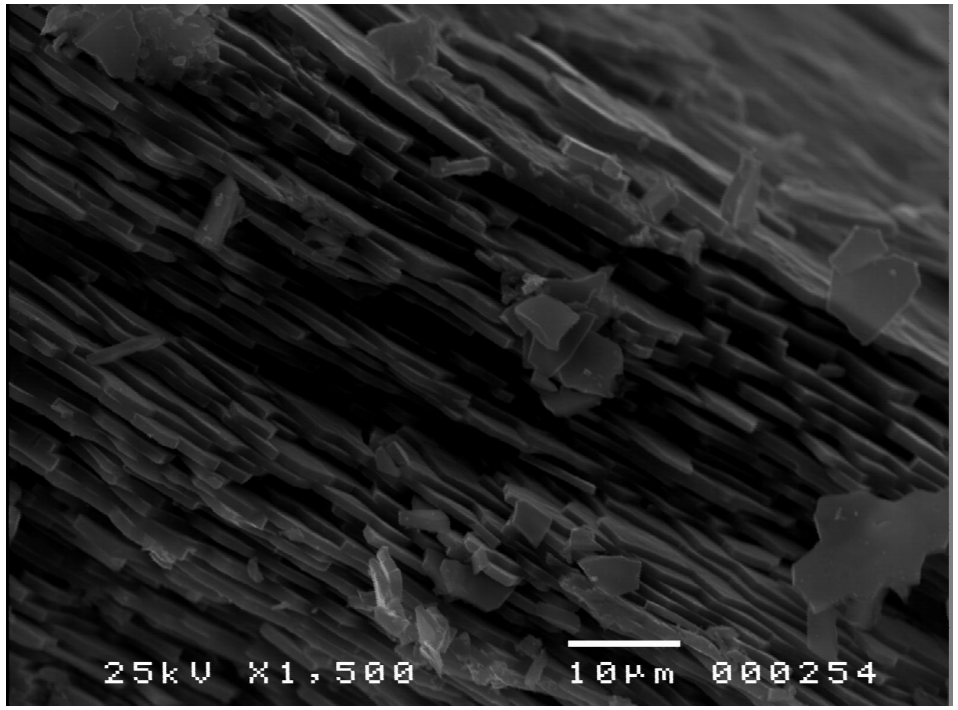

Figure B-16. Specimen Id D5.212.865.3/B
Aragonite nacre, Bivalve genus - *Oistotrigonia* an infaunal suspension feeder.
Scale bar 10 µm.

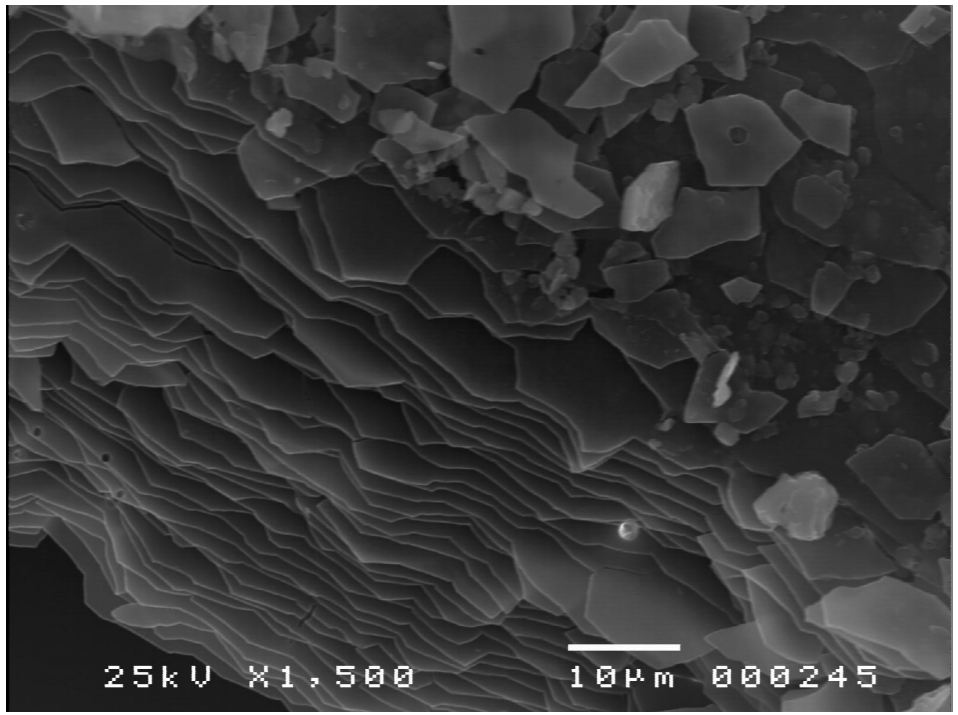

Figure B-17. Specimen Id D5.212.865.3/G
Aragonite nacre, Bivalve genus - *Oistotrigonia* an infaunal suspension feeder.
Scale bar 10 µm.

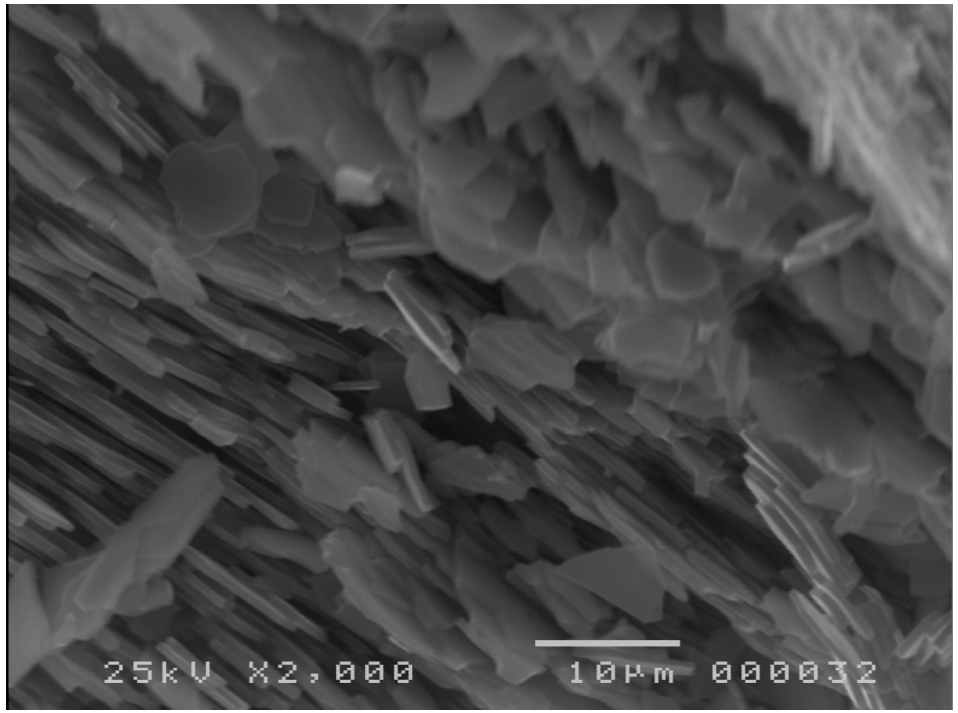

Figure B-18. Specimen Id D5.215.696.2/AN
Aragonite nacre, Bivalve genus - *Eselaevitrigonia* an infaunal suspension feeder. Scale bar 10 µm.

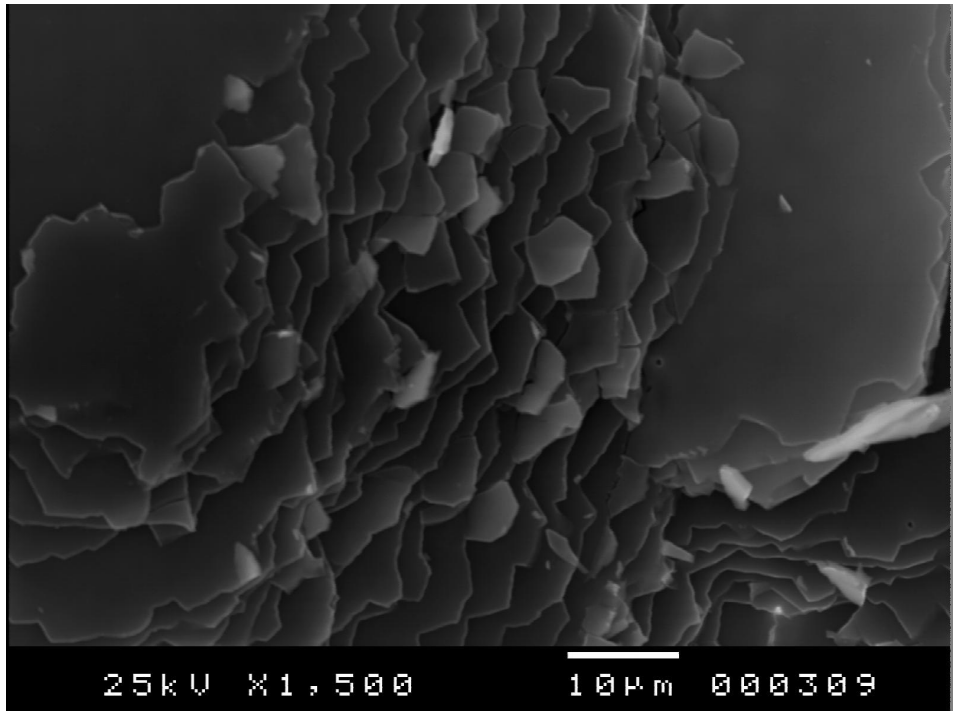

Figure B-19. Specimen Id D5.219.1096.3/H
Aragonite nacre, Bivalve genus – *Eselaevitrigonia* an infaunal suspension feeder. Scale bar 10 µm.

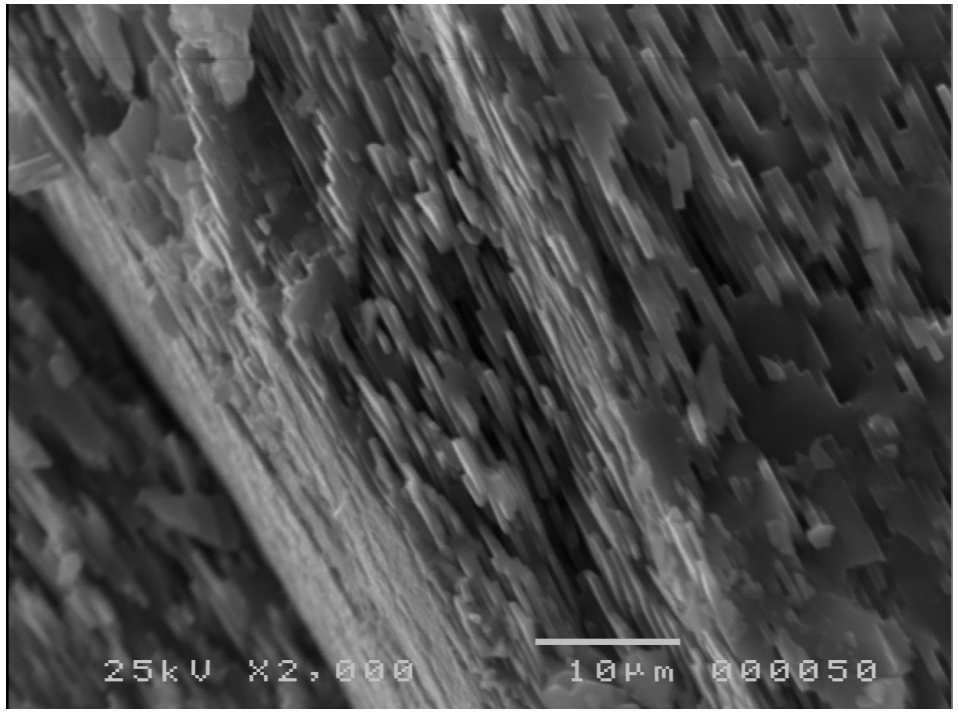

Figure B-20. Specimen Id D5.215.352.2/A
Aragonite nacre, Bivalve genus – *Eselaevitrigonia* an infaunal suspension feeder. Scale bar 10 µm.

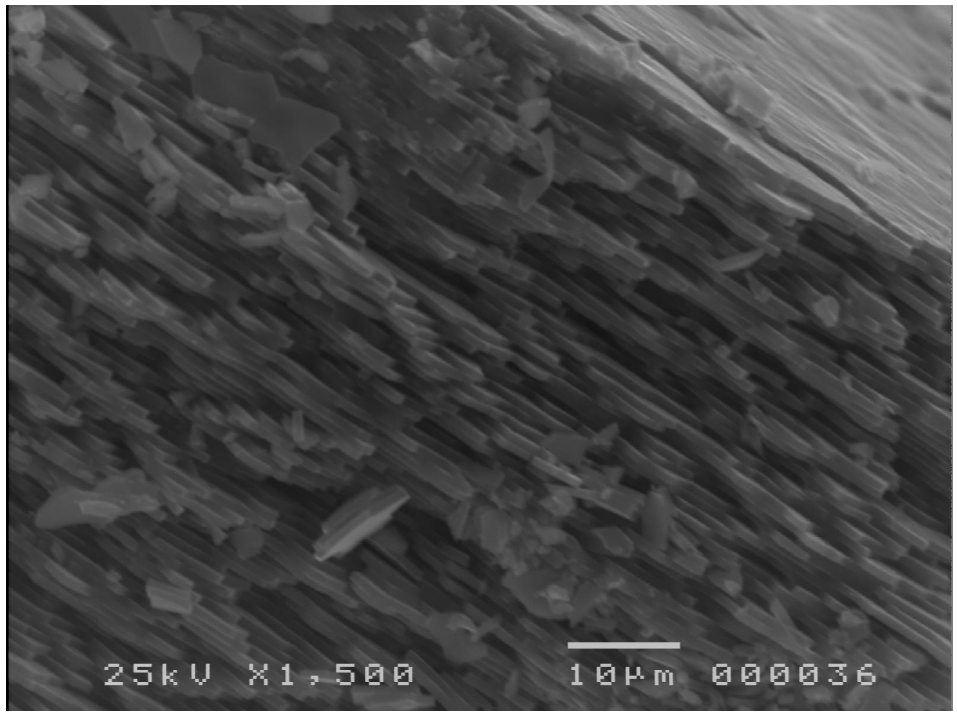

Figure B-21. Specimen Id D5.215.691.2/D-1
Aragonite nacre, Bivalve genus – *Eselaevitrigonia* an infaunal suspension feeder. Scale bar 10 µm.

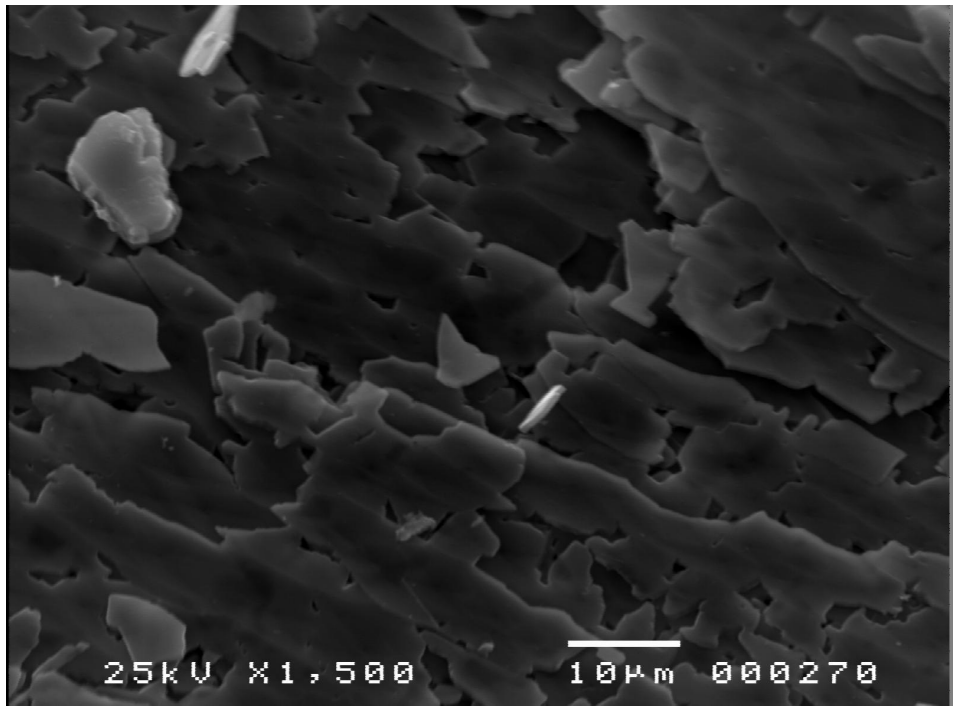

Figure B-22. Specimen Id D5.220.1200.2/A
Aragonite nacre, Bivalve genus – *Pinna* an infaunal suspension feeder. Scale bar 10 µm.

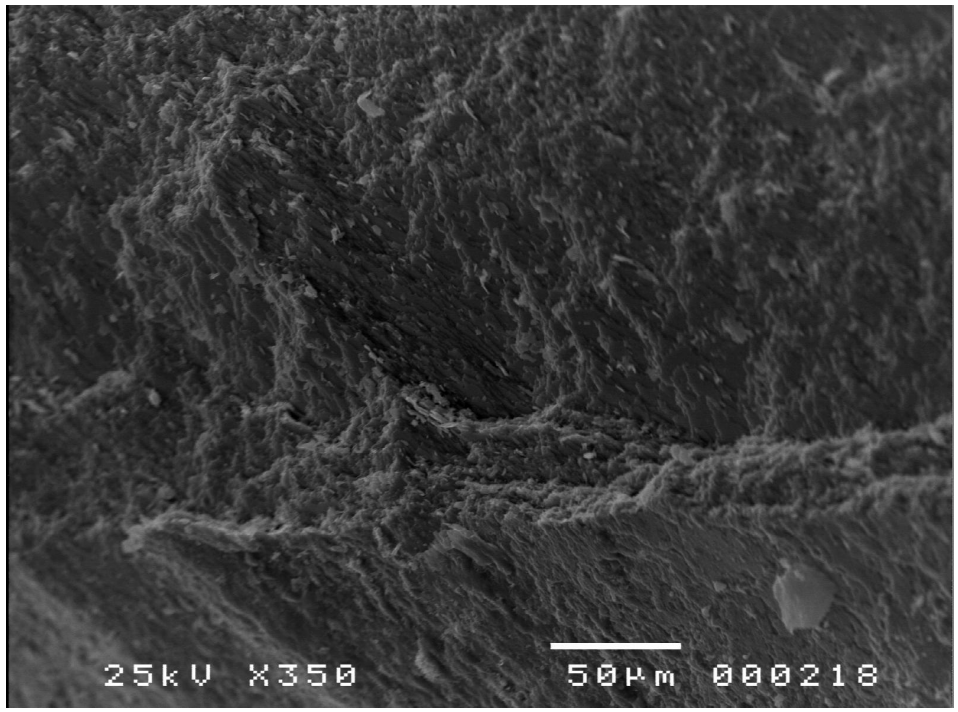

Figure B-23. Specimen Id D5.222.1234.2/A
Aragonite nacre, Aragonite shell material, genus – unidentified. Scale bar 50 µm.

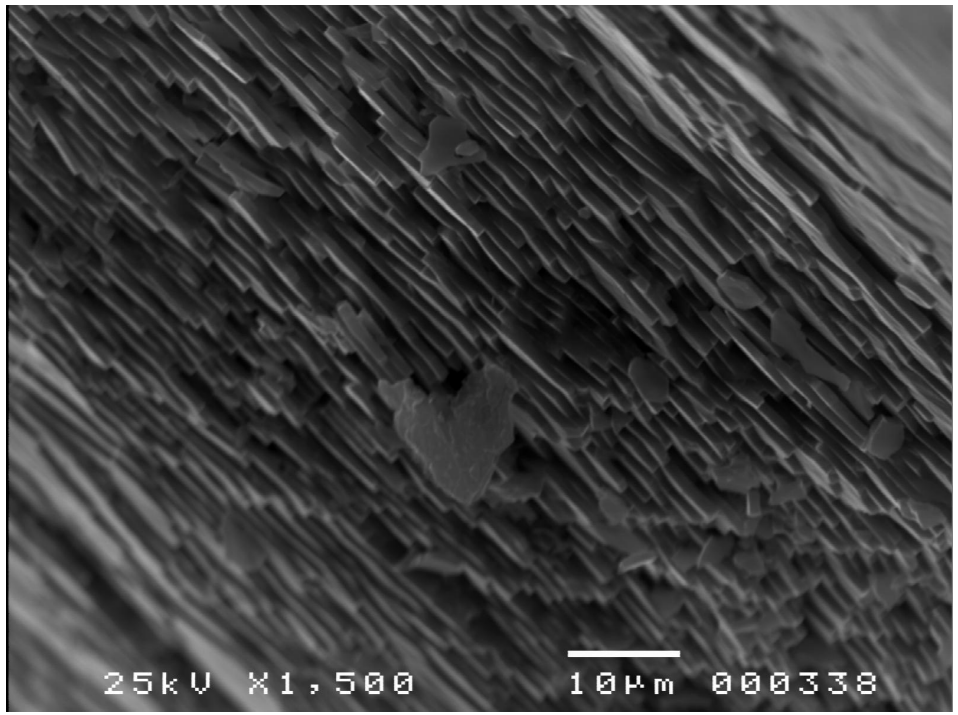

Figure B-24. Specimen Id D5.219.1149.1/A
Aragonite nacre, Bivalve of unidentified genus. Scale bar 10 µm.

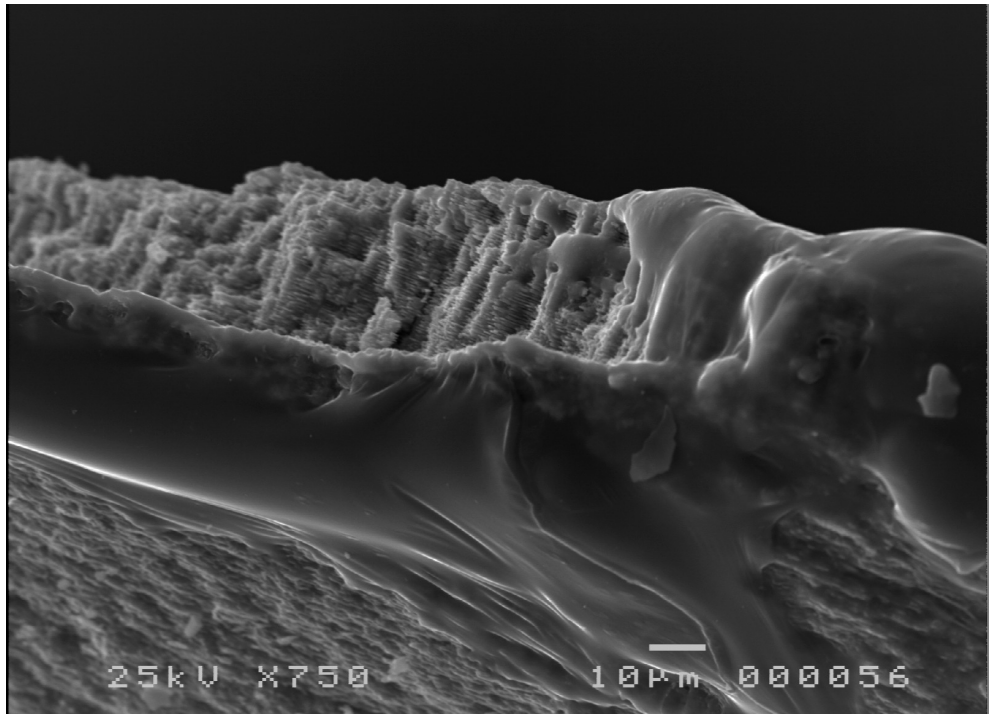

Figure B-25. Specimen Id D5.215.347.2/I
Aragonitic shell material exhibiting diagenetic neomorphism . Note the presence of stacked aragonite nacre plates. Bivalve genus - *Eselaevitrigonia* an infaunal suspension feeder. Scale bar 10 µm.

B.6 Diagenetic screening - Cephalopoda – Ammonoidea

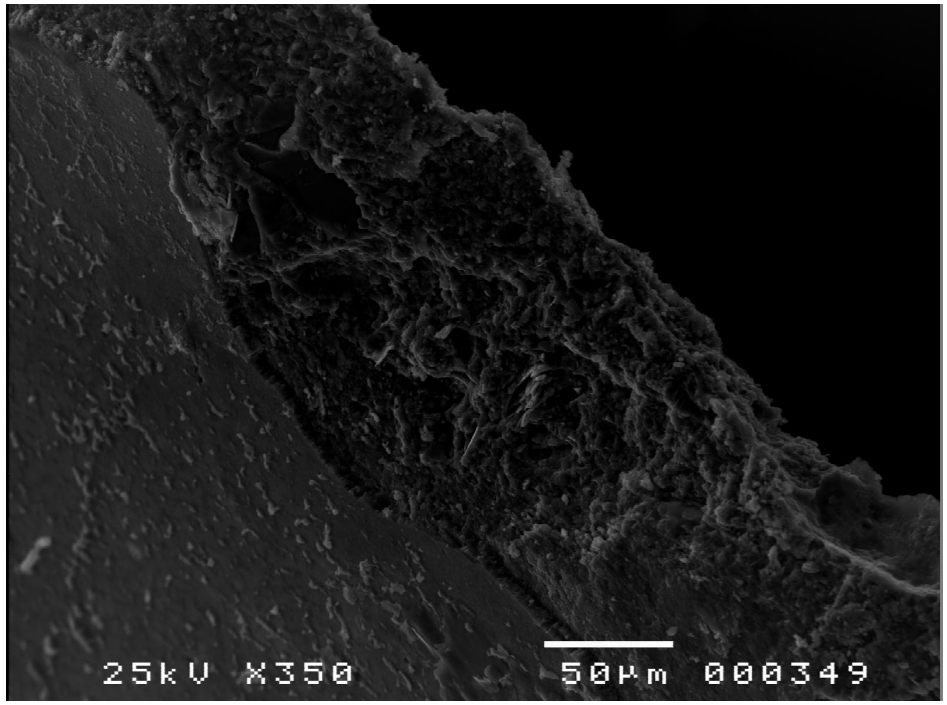

Figure B-26. Specimen Id D5.219.1185.2/D
Aragonite nacre . Ammonite genus – *Maorites* a nektonic carnivore. Scale bar 50 µm.

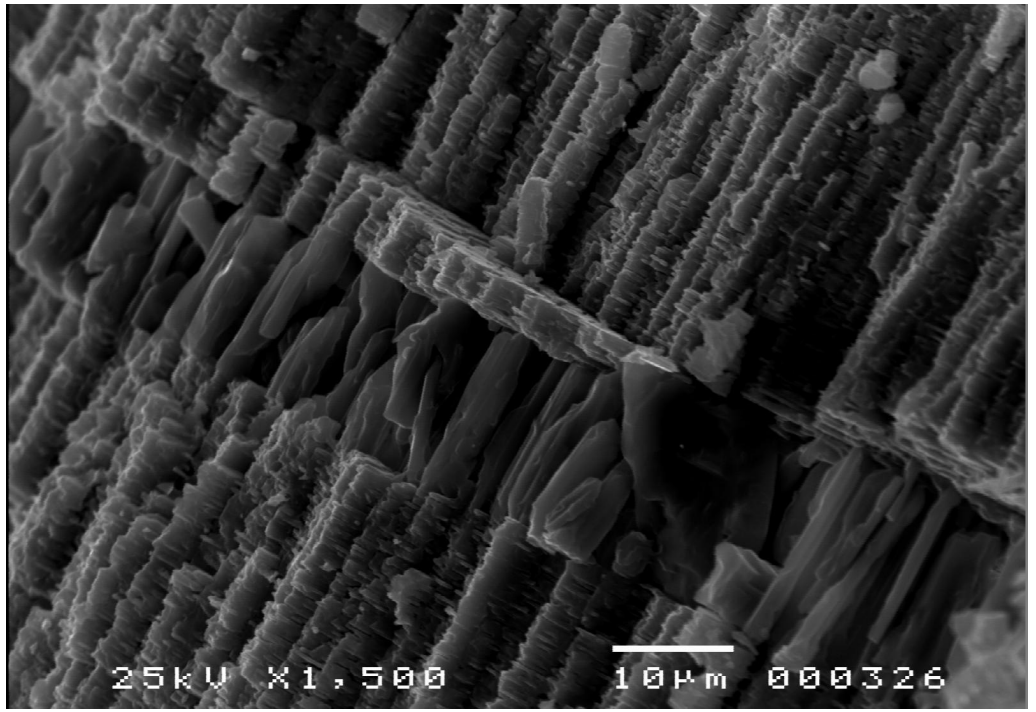

Figure B-27. Specimen Id D5.219.1185.2/C
Stacked plates of aragonite nacre shell material separated by a layer of prismatic aragonite. Ammonite genus - *Maorites* a nektonic, carnivore. Scale bar 10 µm.

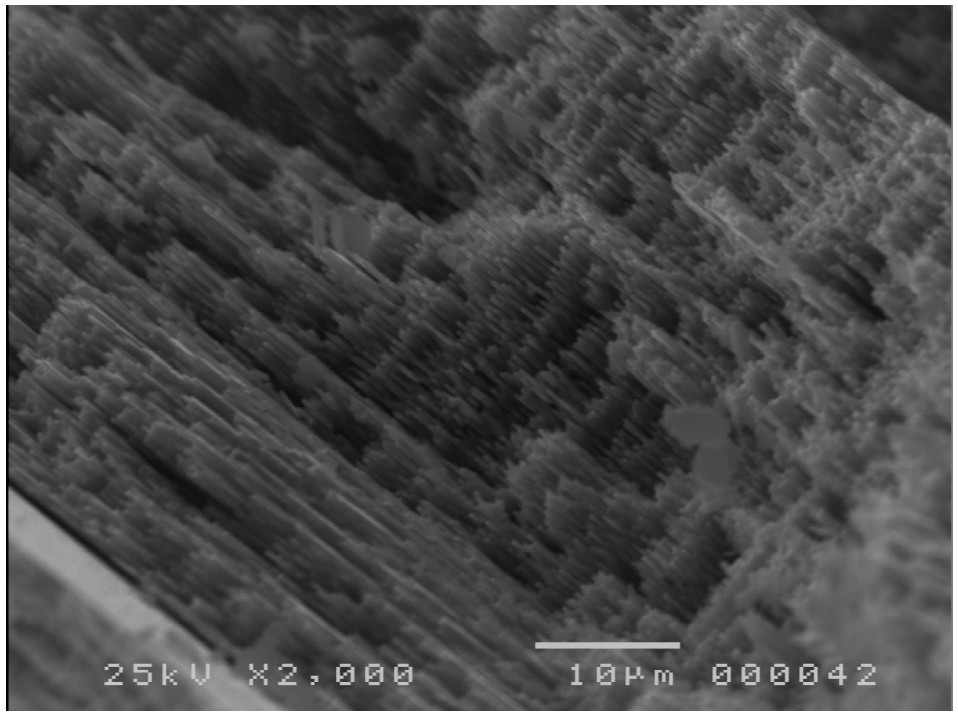

Figure B-28. Specimen Id D5.215.960.3/B
Aragonite nacre, Ammonite genus – Unidentified, a nektonic carnivore. Scale bar 10 µm.

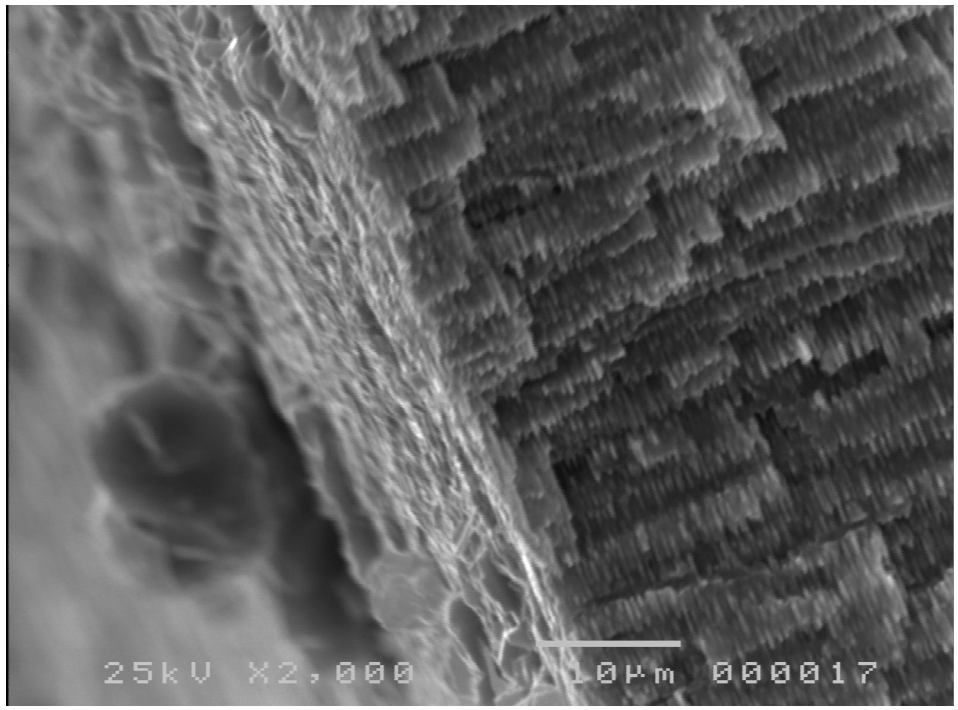

Figure B-29. Specimen Id D5.215.691.2/A
Aragonite nacre, Ammonite genus – *Maorites* a nektonic carnivore. Scale bar 10 µm.

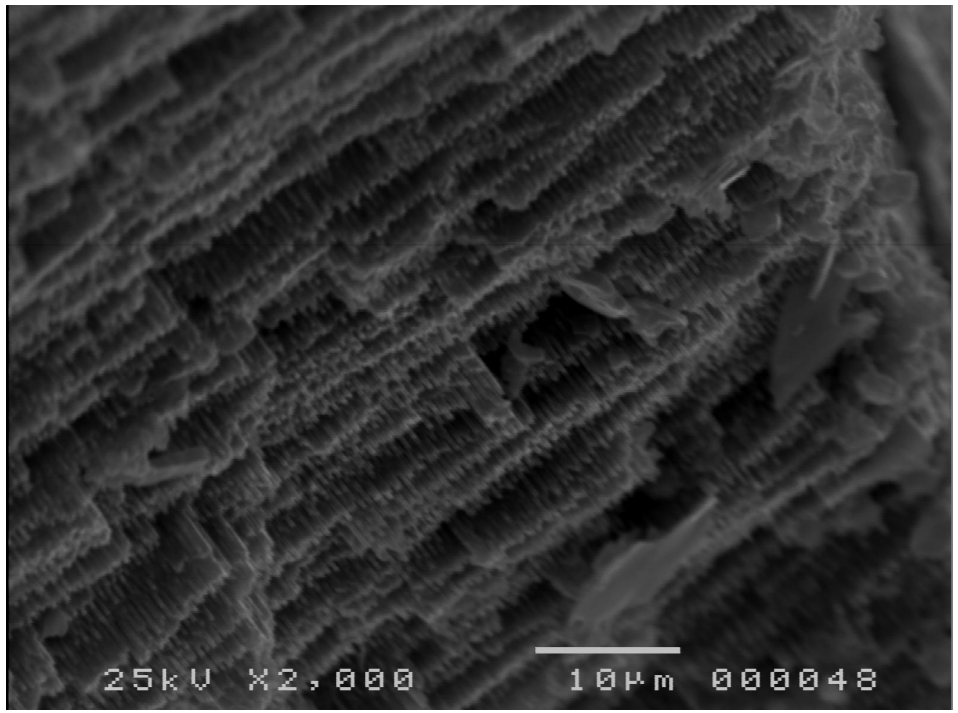

Figure B-30. Specimen Id D5.215.691.2/B
Aragonite nacre, Ammonite genus – *Grossouvrites* a nektonic carnivore. Scale bar 10 µm.

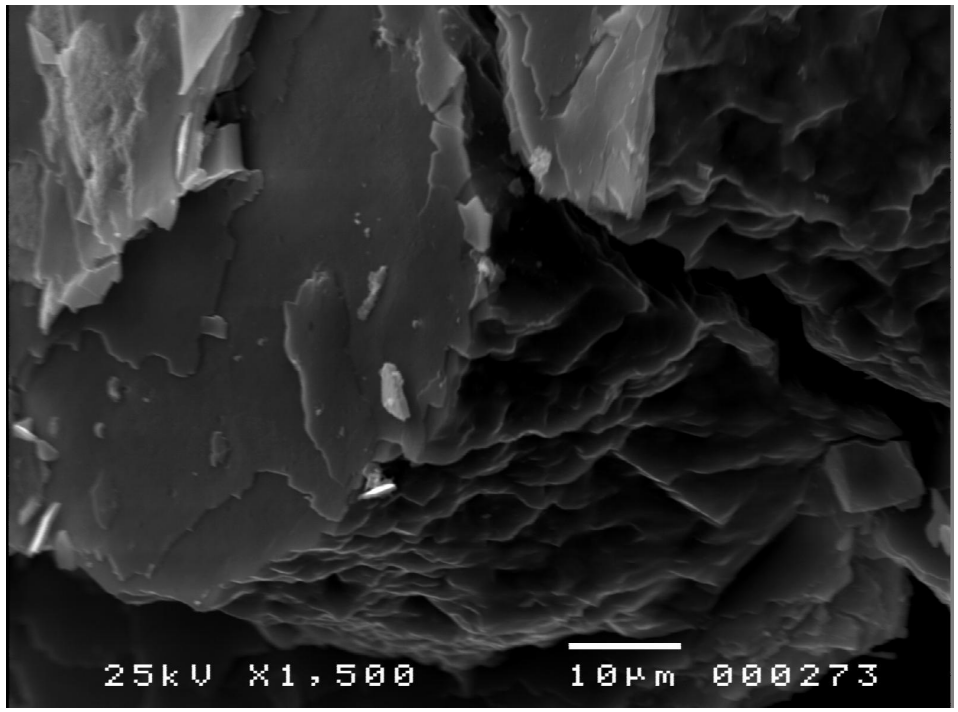

Figure B-31. Specimen Id D5.222.1234.2/K
Aragonite nacre, Ammonite genus – *Anagaudryceras* a nektonic carnivore. Scale bar 10 µm.

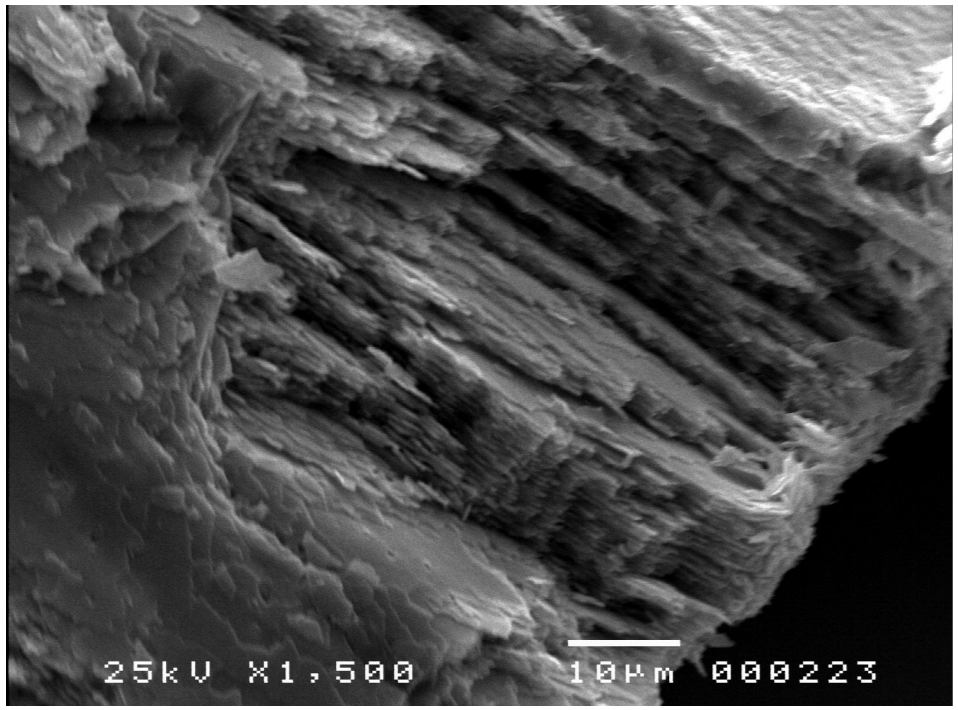

Figure B-32. Specimen Id D5.222.1238.2/F
Aragonite nacre, Ammonite genus – *Maorites* a nektonic carnivore. Scale bar 10 µm.

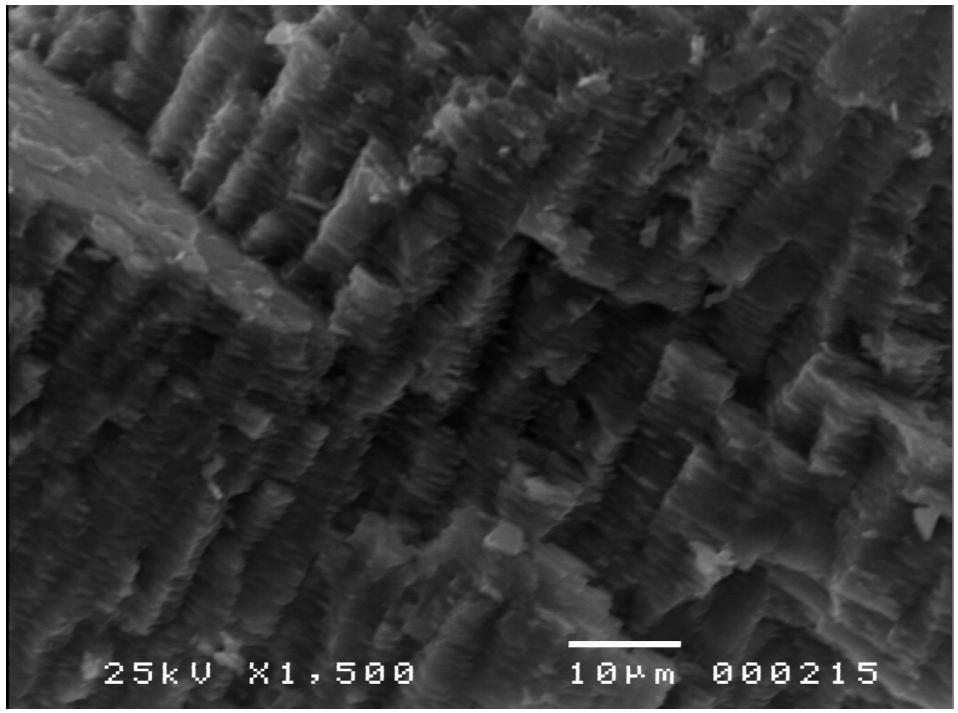

Figure B-33. Specimen Id D5.222.1248.2/E
Aragonite nacre, Ammonite genus – unidentified. Scale bar 10 µm.

B.7 Diagenetic screening – Gastropoda

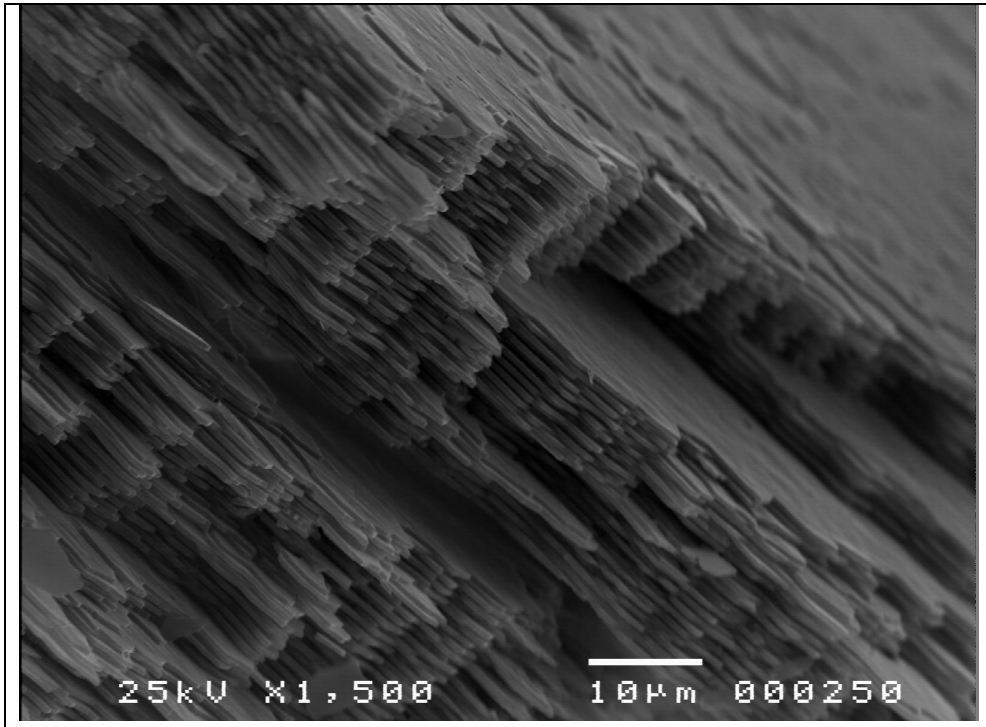

Figure B-34. Specimen Id D5.222.1255.2/A
Aragonite nacre, Gastropod genus – *Amberlaya* an epifaunal carnivore/scavenger. Scale bar 10 µm.

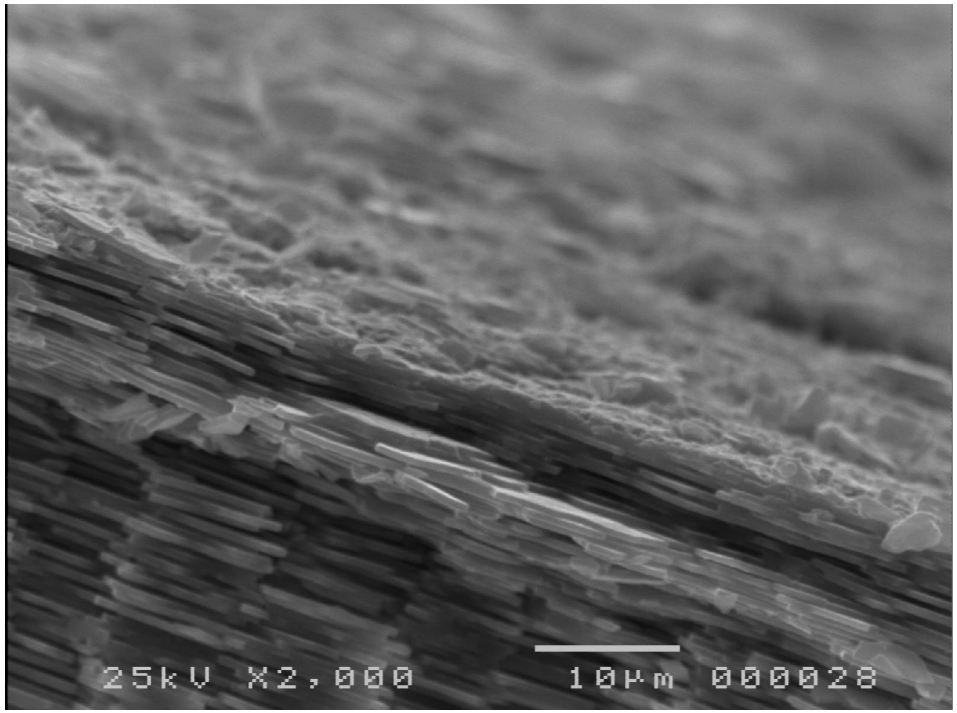

Figure B-35. Specimen Id D5.215.686.2/A
Aragonite nacre, Gastropod genus – *Amberlaya* an epifaunal carnivore/scavenger. Scale bar 10 µm.

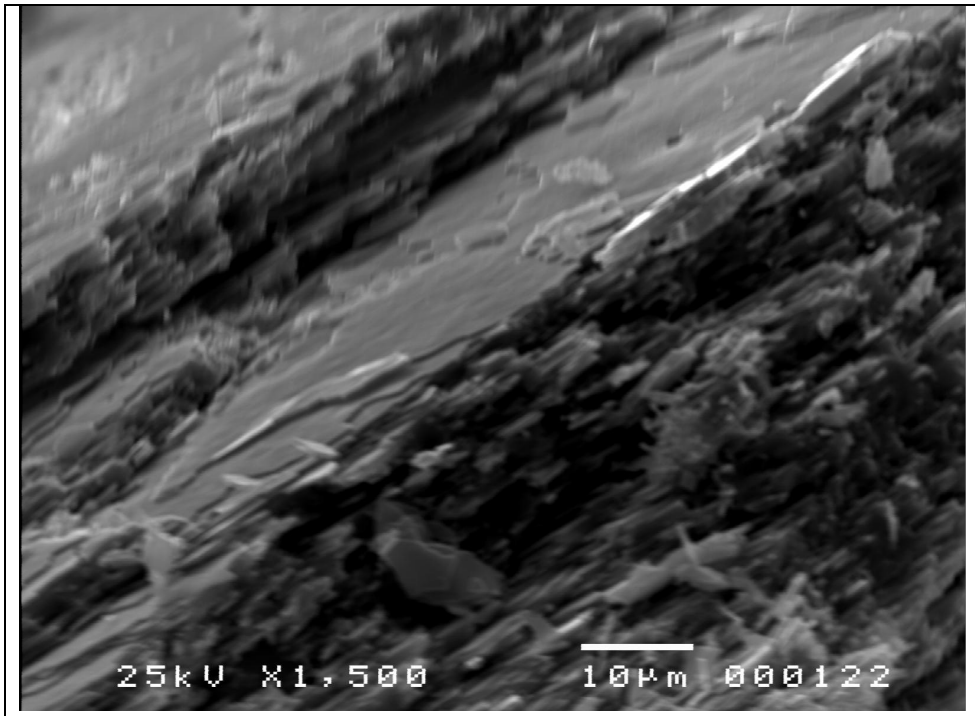

Figure B-36. Specimen Id D5.215.216.5/A
Aragonite nacre, Gastropod genus – *Pleurotomaria* an epifaunal carnivore/scavenger. Scale bar 10 µm.

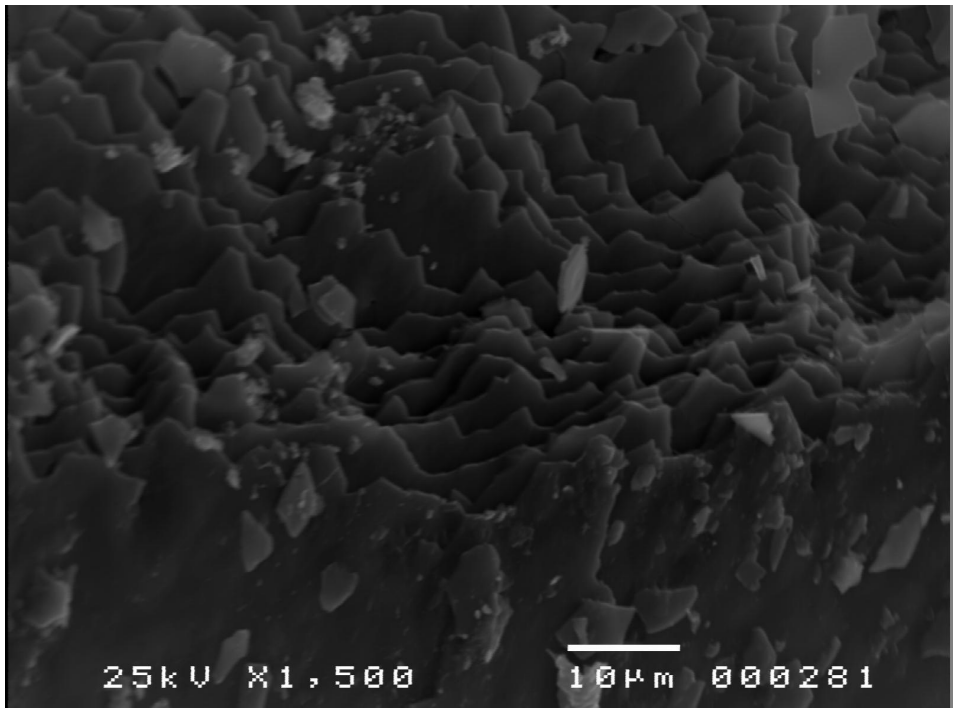

Figure B-37. Specimen Id D5.220.1200.2/A
Aragonite nacre, shell material from an unidentified genus. Scale bar 10 µm.

Appendix C. X-ray Diffraction (XRD)

Prior to all stable isotope analyses each powder sample was analysed for major mineralogical phases using a Siemens D5000 X-ray Diffractometer. In the qualitative operational mode the equipment had a detection limit of approximately 5%, thus any mineral phase present below this level was not reported. Principal minerals of interest were aragonite, calcite (both HMC and LMC), dolomite, gypsum, pyrite and strontianite. Operational setup parameters for the analysis of carbonate shell material using the XRD instrument are specified in Table C-1. Initially the instrument was run with a 2θ range of 2-70 but it was noted that significant aragonite peaks did not appear until 2θ reached a value of 25. As a result the 2θ range was reduced to 20-70 with a corresponding reduction in run time. The equipment was fitted with an automated sample holder with a capacity for 40 specimens, for this study no more than 20 specimens were processed in any single run and steps were taken to reduce the danger of cross-contamination by only using even numbered positions in the sample holder magazine.

Table C-1. Finalised operational setup parameters for the X-ray Diffractometer used during analysis of carbonate shell material.

Estimated scan time	41 mins
Scan mode	Continous scan
Start position (2θ)	20
Increment	0.02
No of steps	2500
Time per step (s)	1
Synchronous rotation	On
Generator voltage	40 kV
Generator current	30 mA

Sample powders prepared for stable isotope analysis were sub-sampled for XRD analysis, although in certain cases where the volume of sample was small the entire sample was used. Under normal operating procedures powders analysed on the XRD instrument are treated as disposable items and are discarded at the end of the analysis. However, in this study sample powders rarely exceeded 1g and in most cases the mass of available powders was between 35 - 300 mg. Thus the sample powders were analysed using the XRD, recovered and subsequently re-used for the stable isotope and trace element analyses.

C.1 XRD profiles – Bivalves

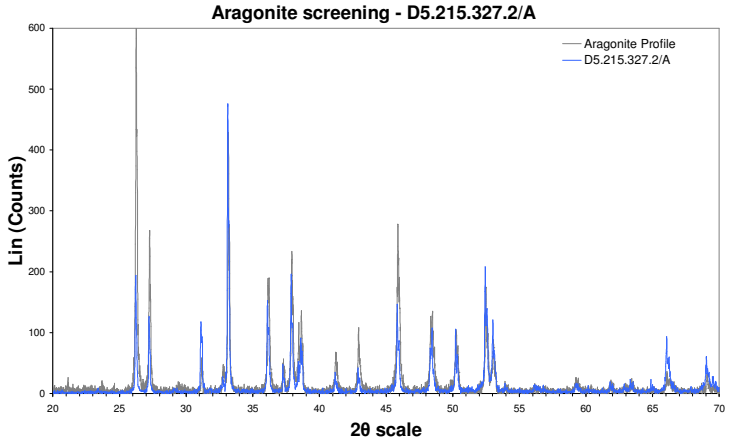

Figure C-1. XRD profile for specimen D5.215.327.2/A. Bivalve genus – Nucula an infaunal deposit feeder.

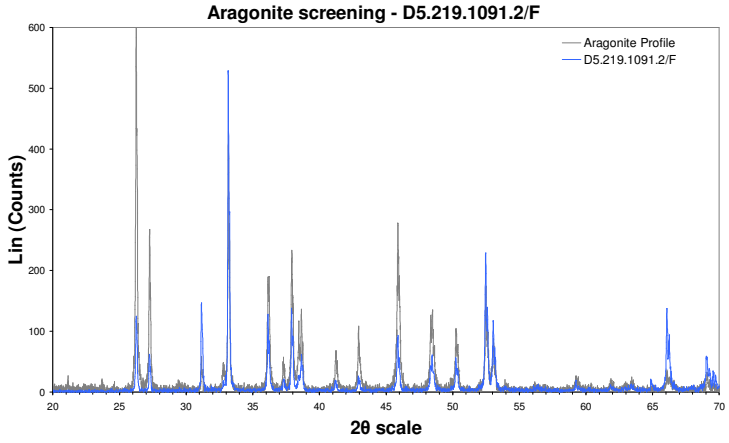

Figure C-2. XRD profile for specimen D5.219.1091.2/F. Bivalve genus – *Nucula* an infaunal deposit feeder.

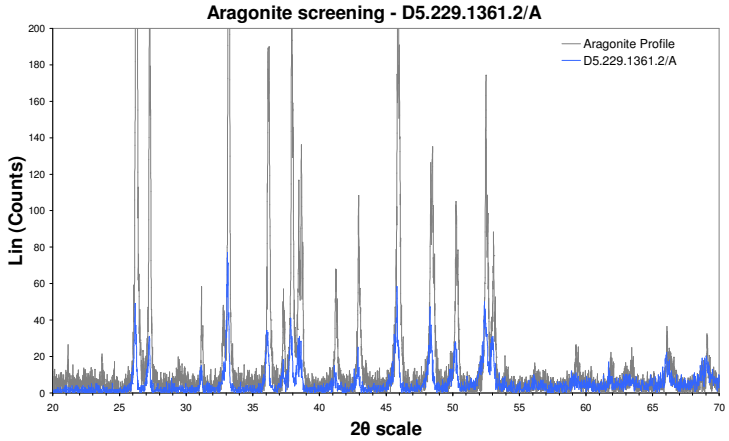

Figure C-3. XRD profile for specimen D5.229.1361.2/A. Bivalve genus – *Nucula* an infaunal deposit feeder.

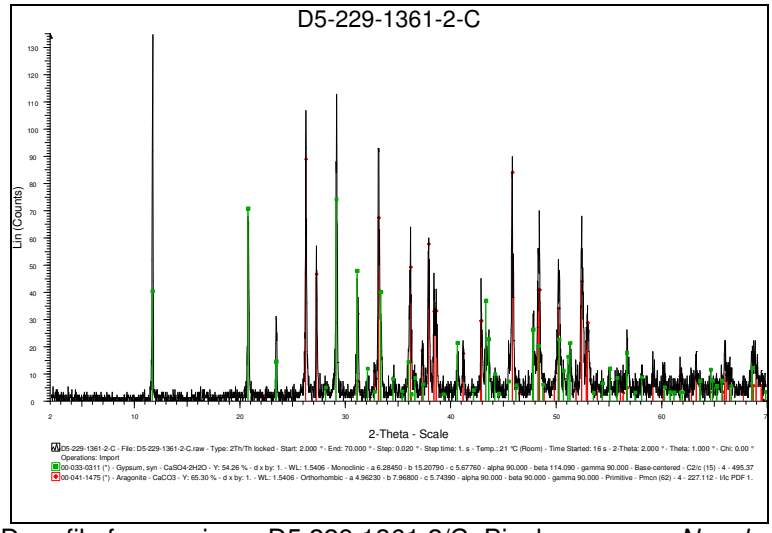

Figure C-4. XRD profile for specimen D5.229.1361.2/C. Bivalve genus – *Nucula* an infaunal deposit feeder. The relative aragonite peak positions are well defined but there is also gypsum present.

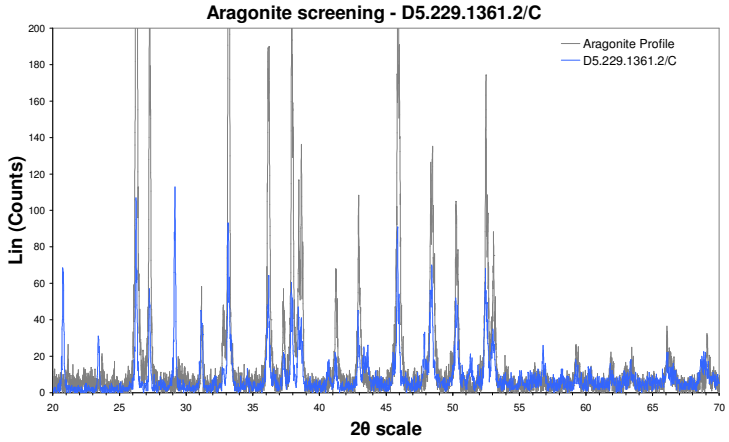

Figure C-5. XRD profile for specimen D5.229.1361.2/C. Bivalve genus – *Nucula* an infaunal deposit feeder.

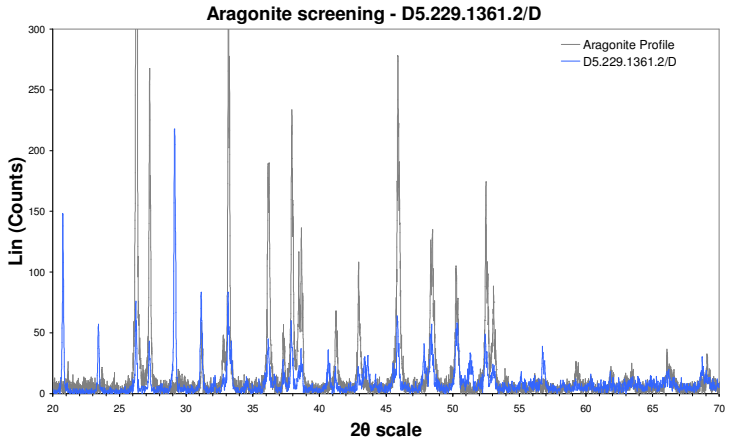

Figure C-6. XRD profile for specimen D5.229.1361.2/D. Profiles match aragonite and gypsum. Bivalve genus – *Nucula* an infaunal deposit feeder.

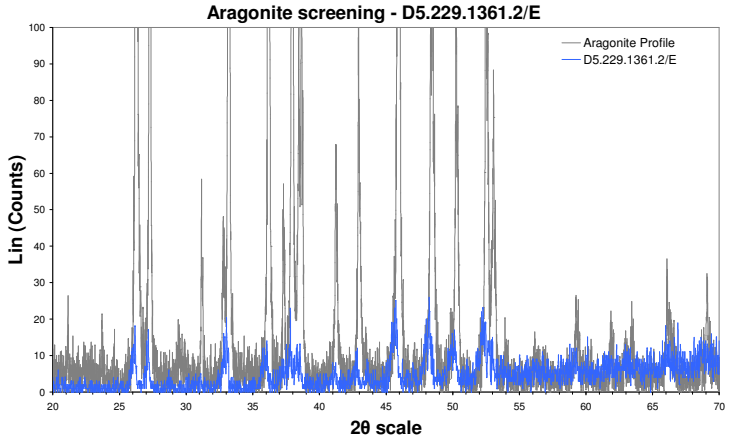

Figure C-7. Noisy XRD profile for specimen D5.229.1361.2/E. Bivalve genus – *Nucula* an infaunal deposit feeder. Typical profile associated with specimens that yielded small quantities of sample powders. The relative aragonite peak positions are well defined but minor gypsum may also be present.

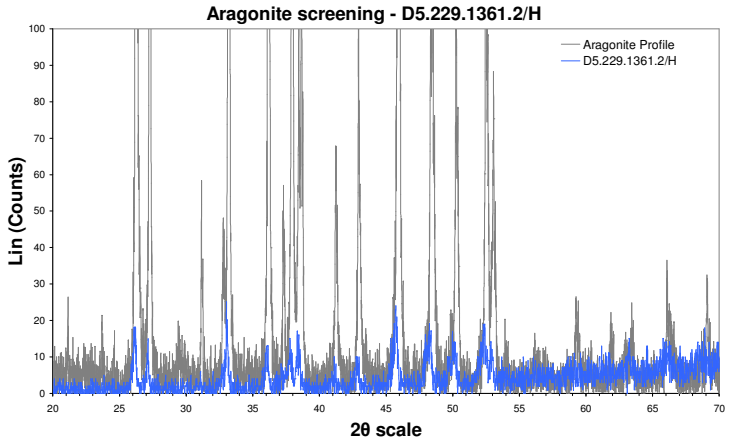

Figure C-8. Noisy XRD profile for specimen D5.229.1361.2/H. Matching aragonite peaks from the PDF database, minor gypsum is also present. Bivalve genus – *Nucula* an infaunal deposit feeder. Typical profile associated with specimens that yielded small quantities of sample powders.

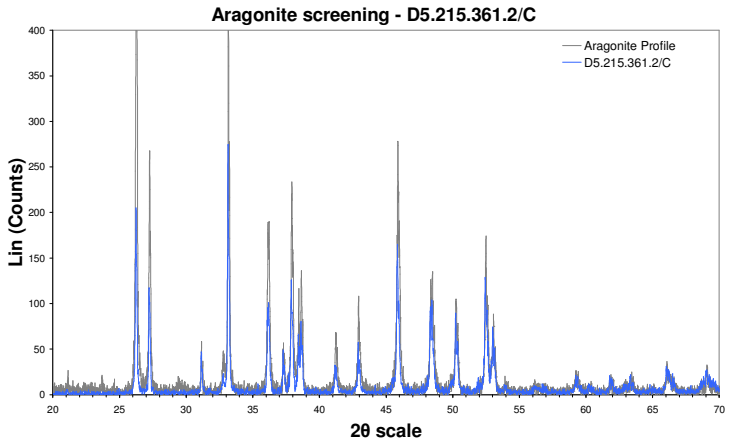

Figure C-9. XRD profile for specimen D5.215.361.2/C. Bivalve genus – *Nucula* an infaunal deposit feeder.

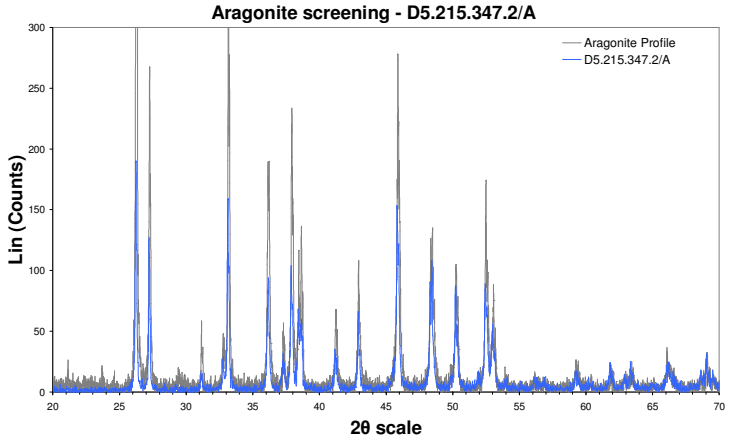

Figure C-10. XRD profile for specimen D5.215.347.2/A. Bivalve genus – *Nucula* an infaunal deposit feeder.

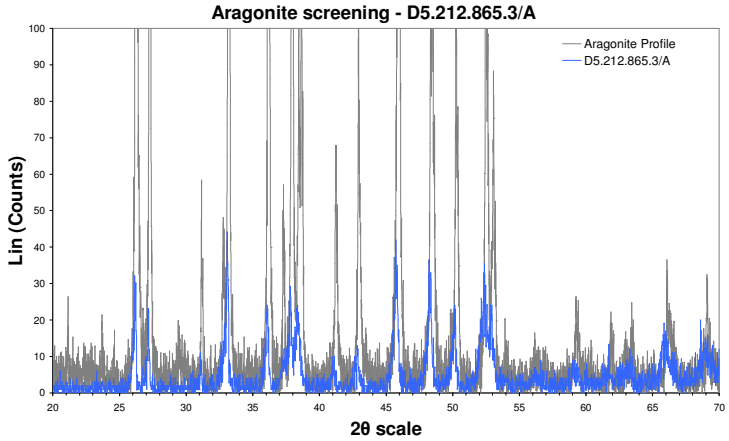

Figure C-11. Noisy XRD profile for specimen D5.212.865.3/A. Bivalve genus – *Oistotrigonia* an infaunal suspension feeder. Typical profile associated with specimens that yielded small quantities of sample powders, the relative aragonite peak positions are well defined.

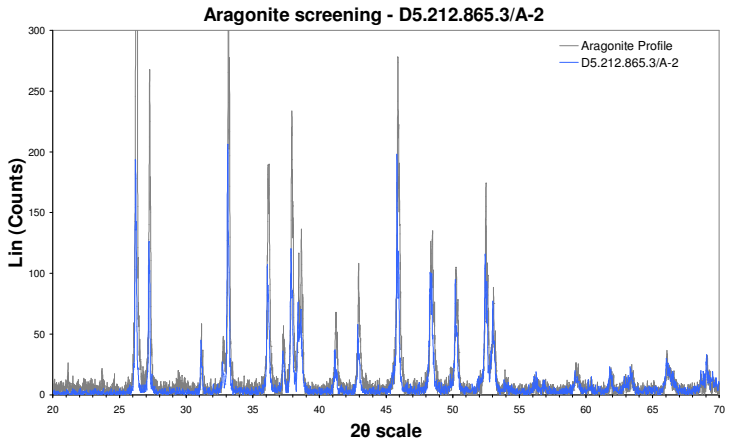

Figure C-12. XRD profile for specimen D5.212.865.3/A. Bivalve genus – *Oistotrigonia* an infaunal suspension feeder.

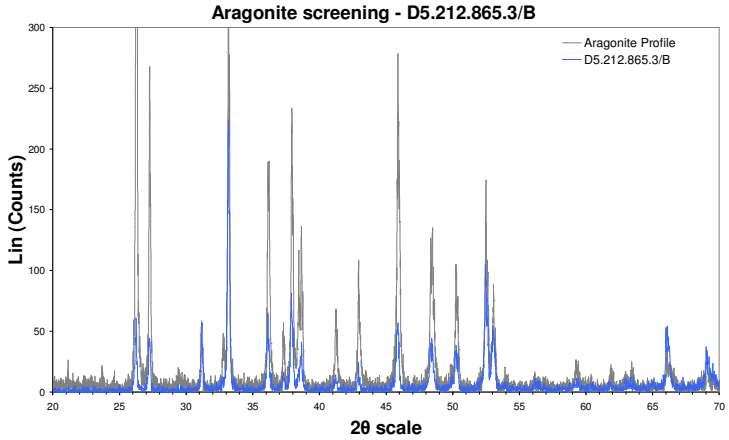

Figure C-13. XRD profile for specimen D5.212.865.3/B. Bivalve genus – *Oistotrigonia* an infaunal suspension feeder.

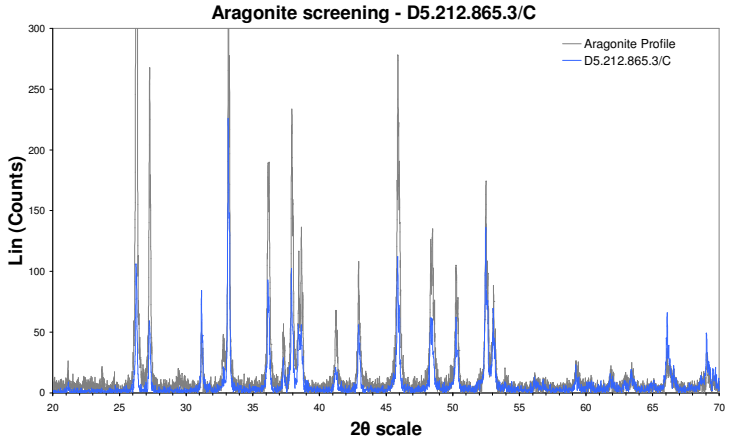

Figure C-14. XRD profile for specimen D5.212.865.3/C. Bivalve genus – *Oistotrigonia* an infaunal suspension feeder.

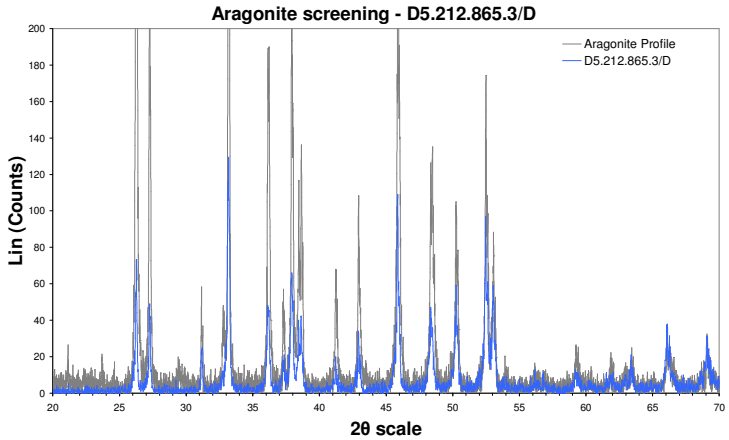

Figure C-15. XRD profile for specimen D5.212.865.3/D. Matching aragonite peaks and possibly minor gypsum from the PDF database. Bivalve genus – *Oistotrigonia* an infaunal suspension feeder.

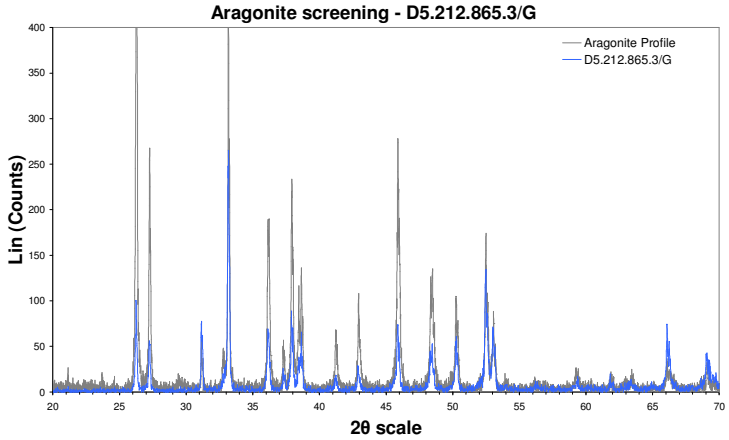

Figure C-16. XRD profile for specimen D5.212.865.3/G. Bivalve genus – *Oistotrigonia* an infaunal suspension feeder.

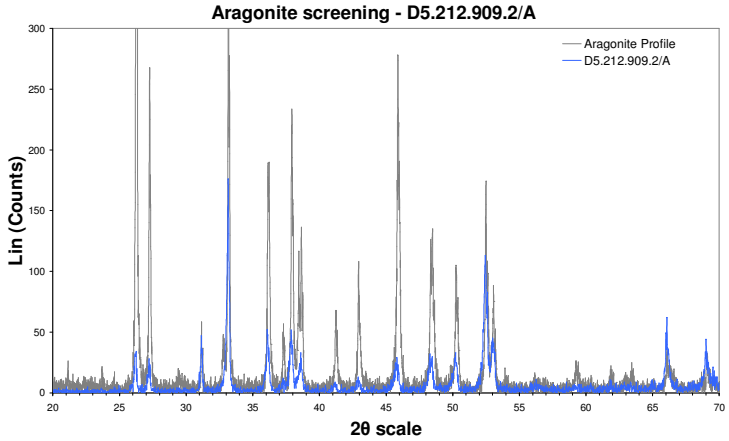

Figure C-17. XRD profile for specimen D5.212.909.2/A. Bivalve genus – *Oistotrigonia* an infaunal suspension feeder.

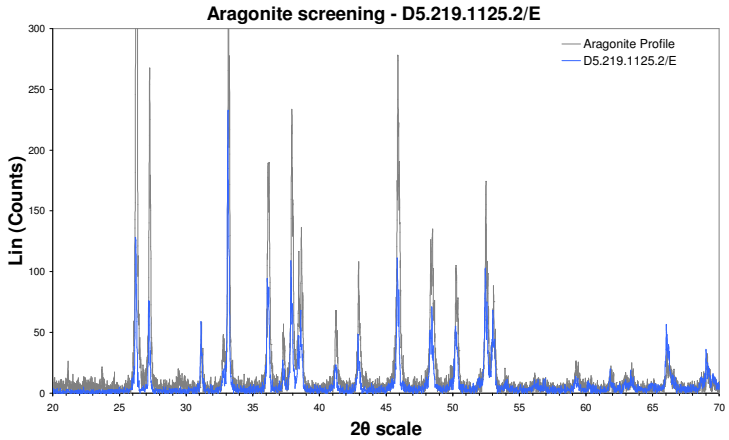

Figure C-18. XRD profile for specimen D5.219.1125.2/E. Bivalve genus – *Oistotrigonia* an infaunal suspension feeder.

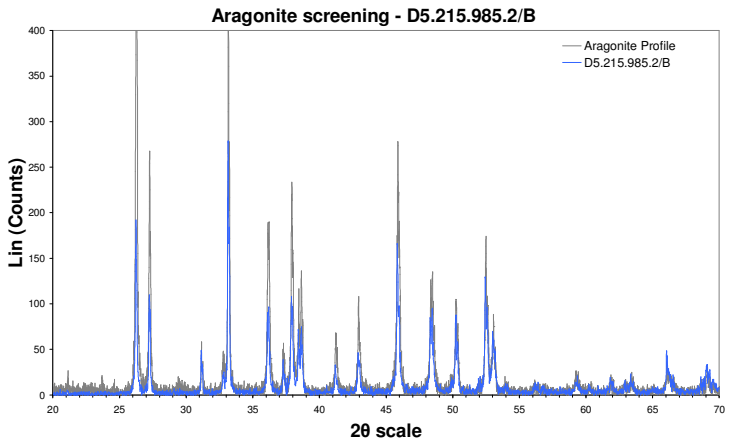

Figure C-19. XRD profile for specimen D5.215.985.2/B. Bivalve genus – *Oistotrigonia* an infaunal suspension feeder.

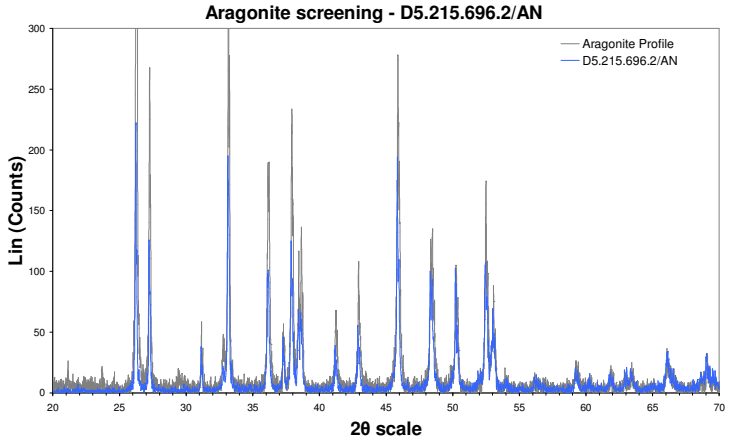

Figure C-20. XRD profile for specimen D5.215.696.2/AN. Bivalve genus – *Eselaevitrigonia* an infaunal suspension feeder.

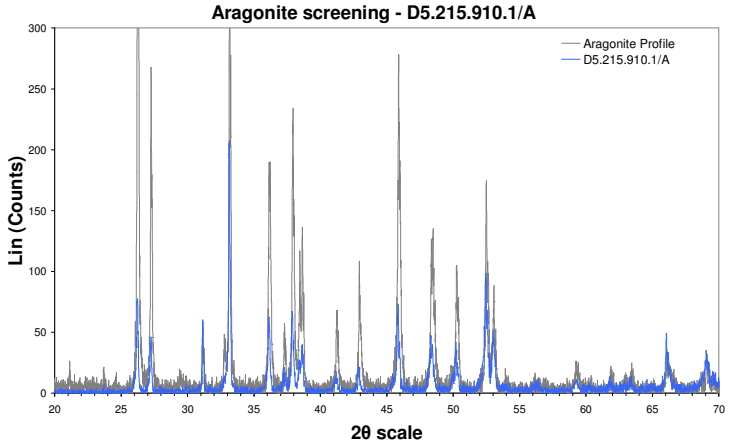

Figure C-21. XRD profile for specimen D5.215.910.1/A. Bivalve genus – *Eselaevitrigonia* an infaunal suspension feeder.

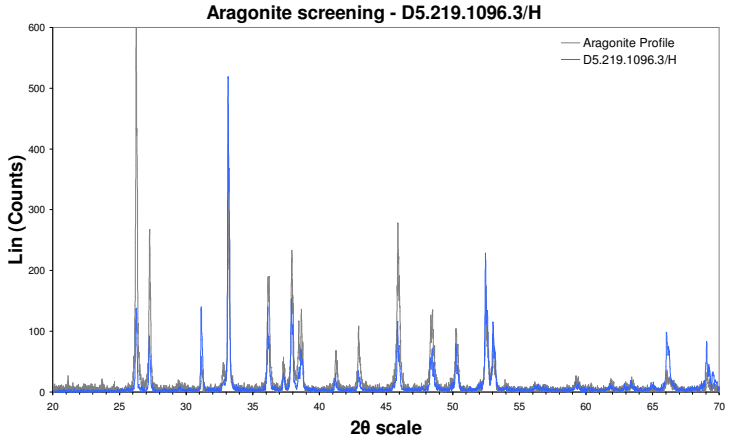

Figure C-22. XRD profile for specimen D5.219.1096.3/H. Bivalve genus – *Eselaevitrigonia* an infaunal suspension feeder.

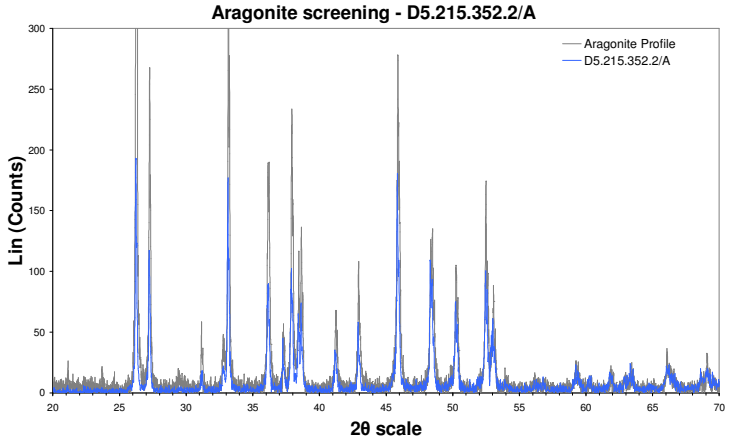

Figure C-23. XRD profile for specimen D5.215.352.2/A. Bivalve genus – *Eselaevitrigonia* an infaunal suspension feeder.

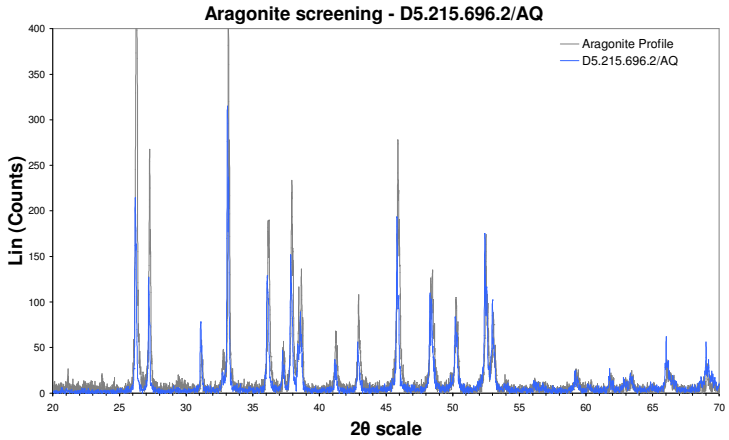

Figure C-24. XRD profile for specimen D5.215.696.2/AQ. Bivalve genus – *Eselaevitrigonia* an infaunal suspension feeder.

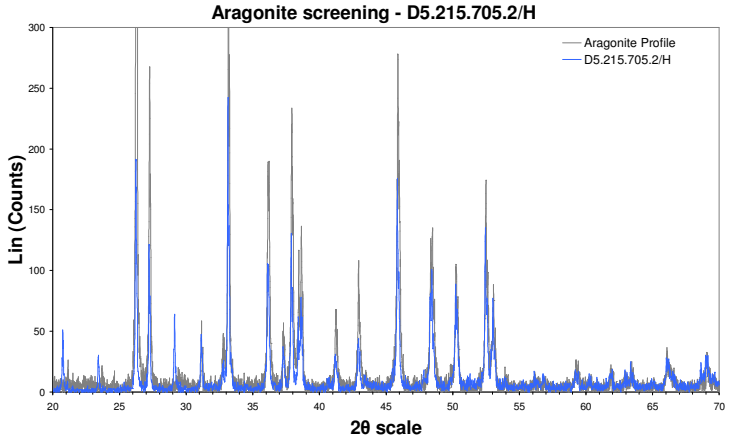

Figure C-25. XRD profile for specimen D5.215.705.2/H. Bivalve genus – *Eselaevitrigonia* an infaunal suspension feeder.

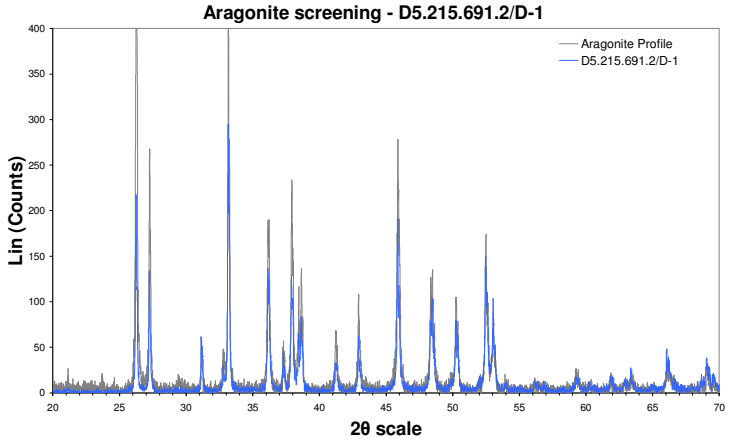

Figure C-26. XRD profile for specimen D5.215.691.2/D-1. Bivalve genus – *Eselaevitrigonia* an infaunal suspension feeder.

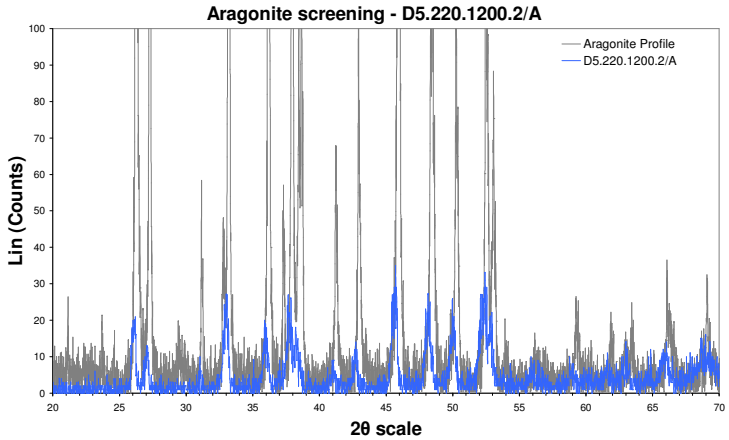

Figure C-27. Noisy XRD profile for specimen D5.220.1200.2/A. Bivalve genus – *Pinna* an infaunal suspension feeder. Typical profile associated with specimens that yielded small quantities of sample powders, the relative aragonite peak positions are well defined.

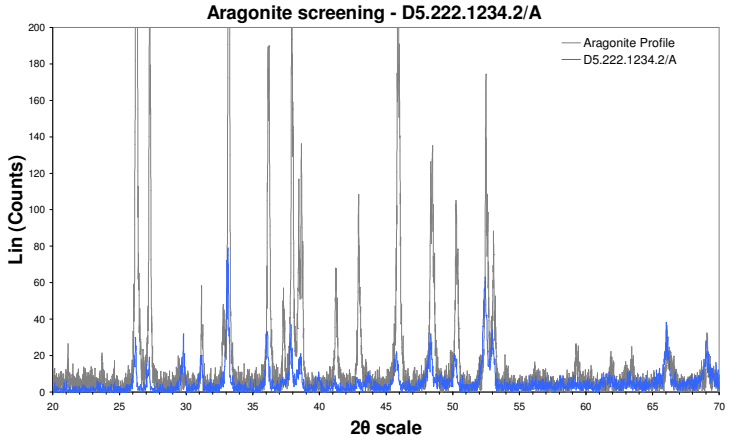

Figure C-28. Noisy XRD profile for specimen D5.222.1234.2/A. Matching aragonite and calcite peaks from the PDF database. Aragonite shell material, genus – unidentified.

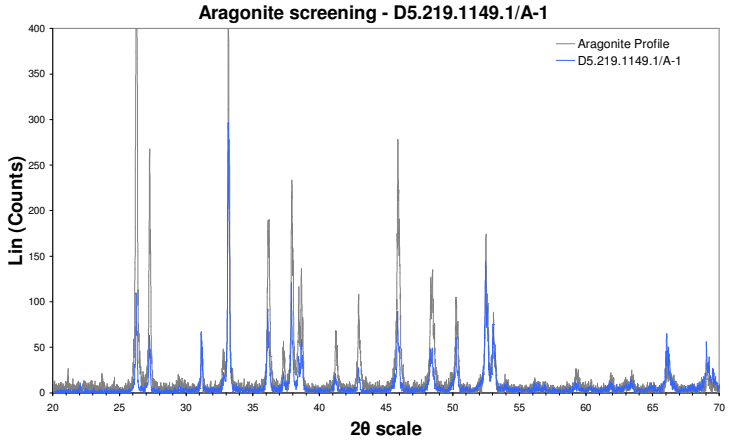

Figure C-29. XRD profile for specimen D5.219.1149.1/A-1. Bivalve of unidentified genus.

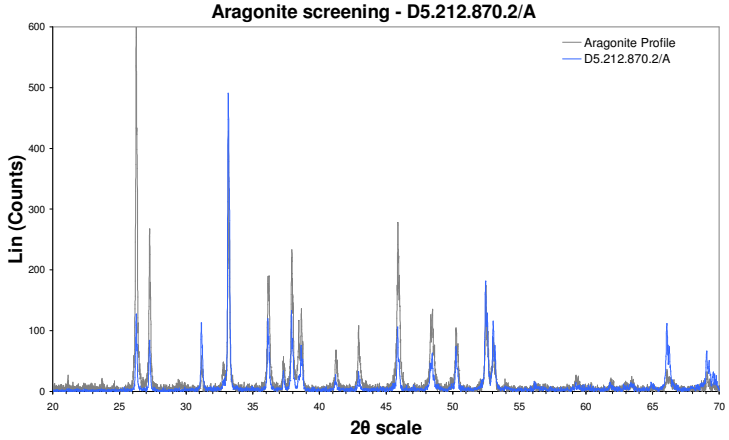

Figure C-30. XRD profile for specimen D5.212.870.2/A. Bivalve of unidentified genus.

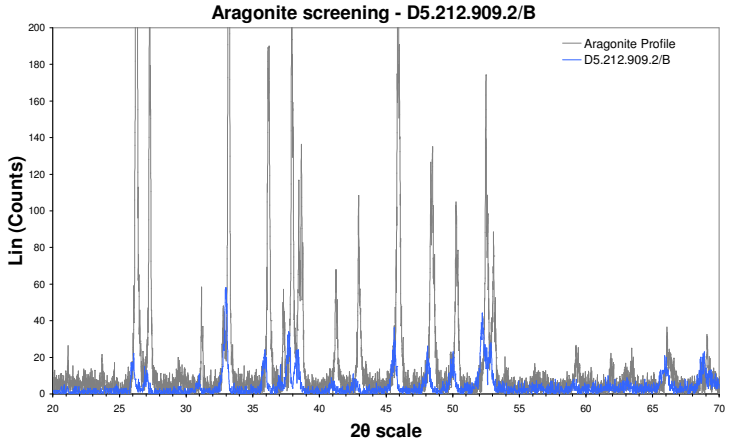

Figure C-31. XRD profile for specimen D5.212.909.2/B. Bivalve of unidentified genus.

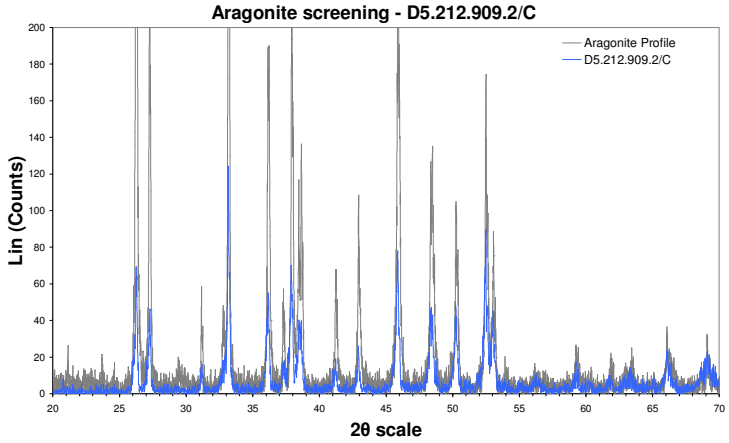

Figure C-32. XRD profile for specimen D5.212.909.2/C. Bivalve of unidentified genus.

C.2 XRD profiles – Bivalves – Rejected specimens

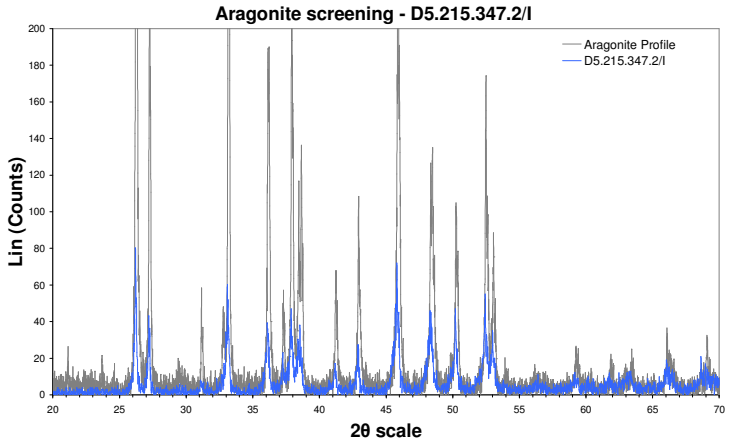

Figure C-33. XRD profile for specimen D5.215.347.2/I. Bivalve genus – *Eselaevitrigonia* an infaunal suspension feeder.

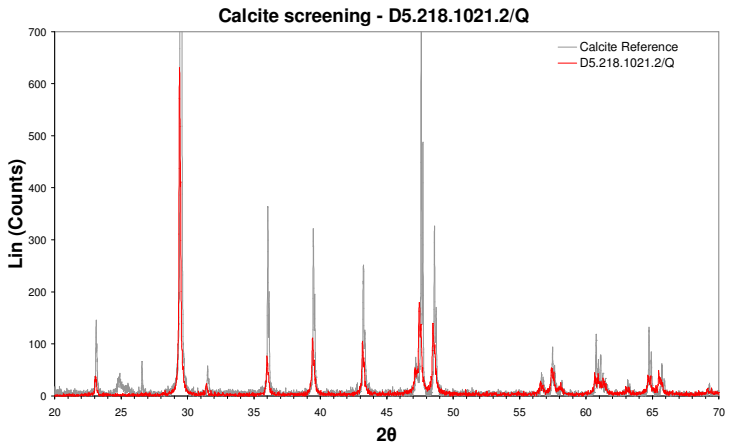

Figure C-34. XRD profile (calcite) for specimen D5.218.1021.2/Q. Bivalve genus – *Pycnodonte* an epifaunal suspension feeder.

C.3 XRD profiles – Cephalopoda – Ammonoidea

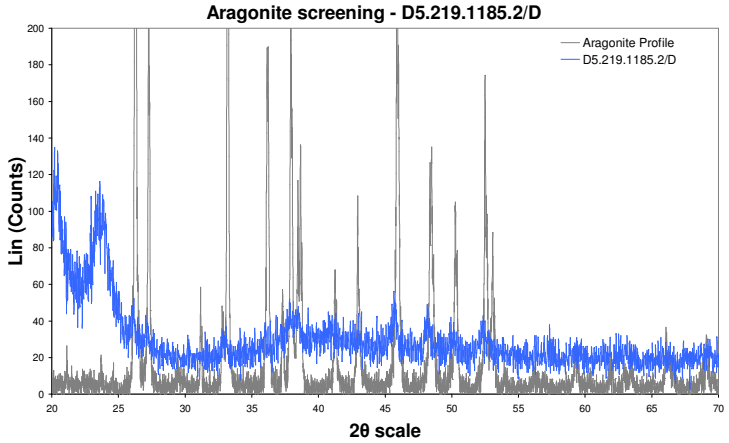

Figure C-35. Noisy XRD profile for specimen D5.219.1185.2/D. Ammonite genus – *Maorites* a nektonic carnivore. Typical noisy profile associated with specimens that yielded small quantities of sample powders, the relative aragonite peak positions are well defined.

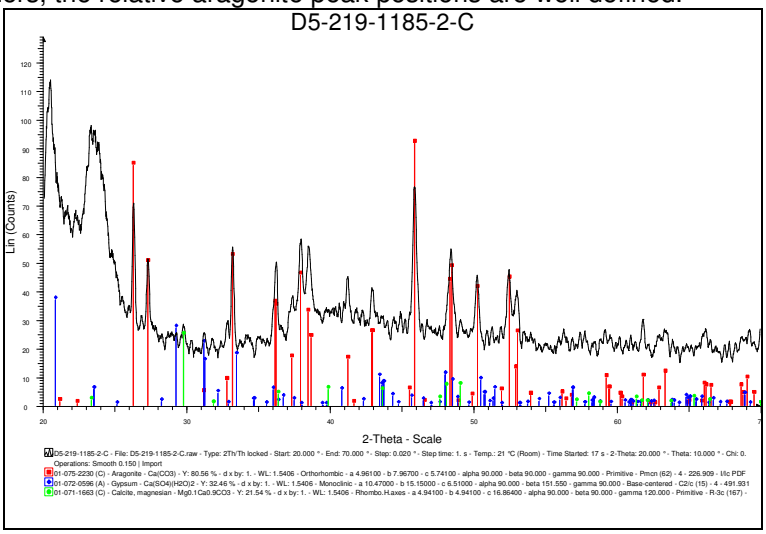

Figure C-36. Noisy XRD profile for specimen D5.219.1185.2/C. Matching aragonite, gypsum and possible calcite from the PDF database. Ammonite genus – *Maorites* a nektonic carnivore. Typical profile associated with specimens that yielded small quantities of sample powders, the relative aragonite peaks positions are well defined.

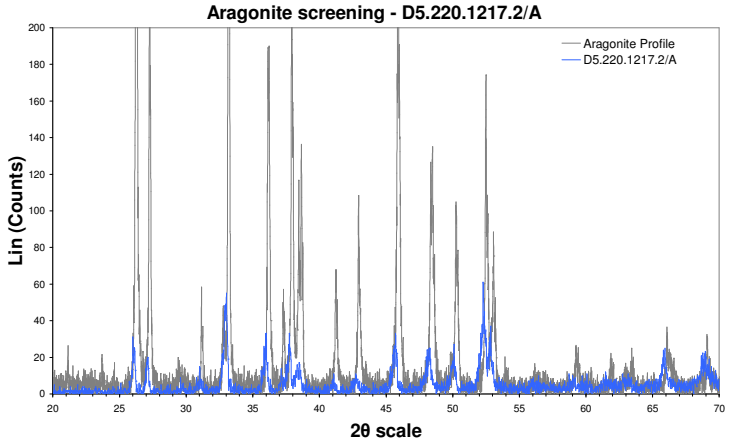

Figure C-37. Noisy XRD profile for specimen D5.220.1217.2/A. Ammonite genus – *Maorites* a nektonic carnivore. Typical profile associated with specimens that yielded small quantities of sample powders, the relative aragonite peak positions are well defined.

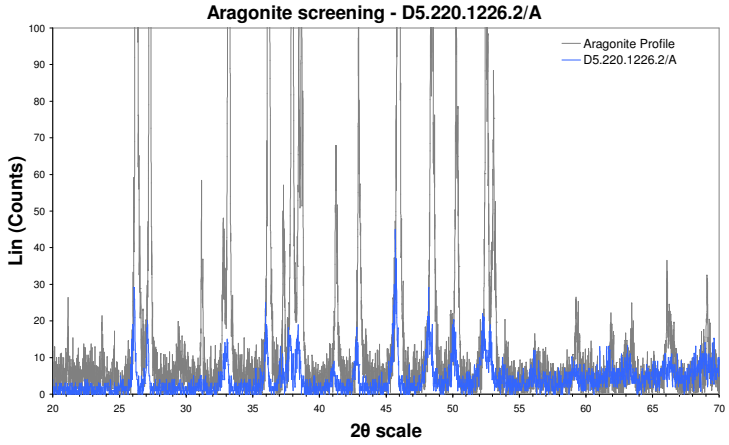

Figure C-38. Noisy XRD profile for specimen D5.220.1226.2/A. Ammonite genus – *Maorites* a nektonic carnivore. Typical profile associated with specimens that yielded small quantities of sample powders, the relative aragonite peak positions are well defined.

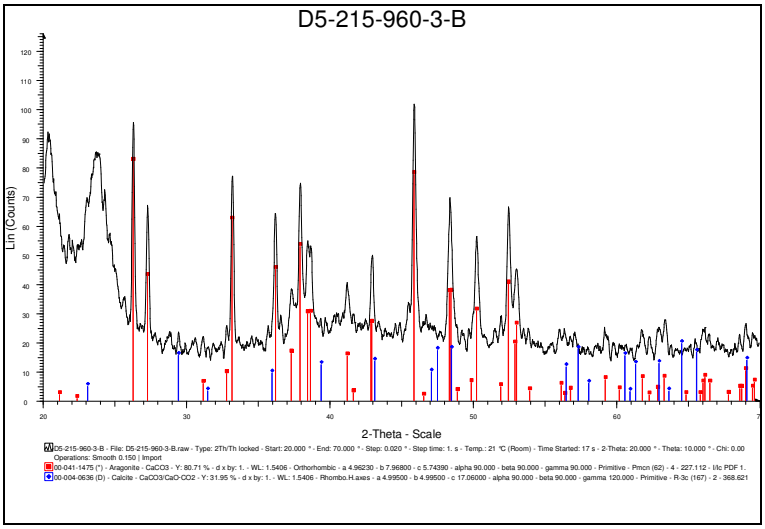

Figure C-39. Noisy XRD profile for specimen D5.215.960.3/B. Ammonite genus – Unidentified, a nektonic carnivore. Typical profile associated with specimens that yielded small quantities of sample powders. The relative aragonite peak positions are well defined but calcite is also present.

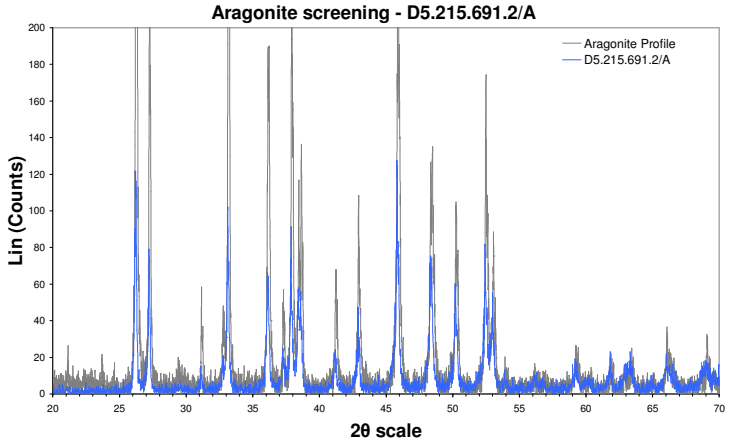

Figure C-40. XRD profile for specimen D5.215.691.2/A. Ammonite genus – Maorites a nektonic carnivore.

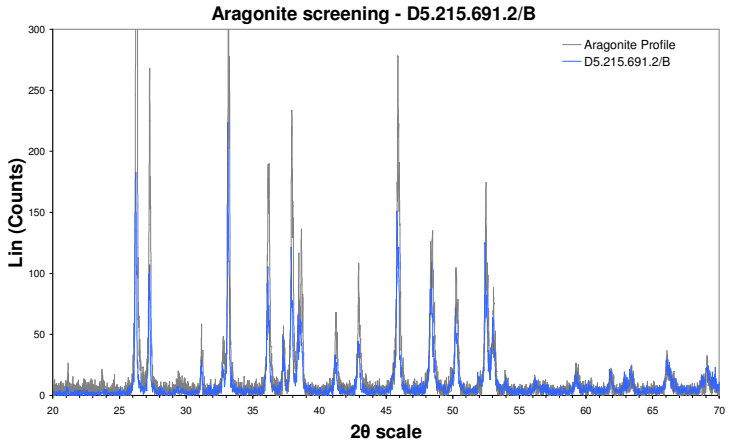

Figure C-41. XRD profile for specimen D5.215.691.2/B. Ammonite genus – *Grossouvrites* a nektonic carnivore.

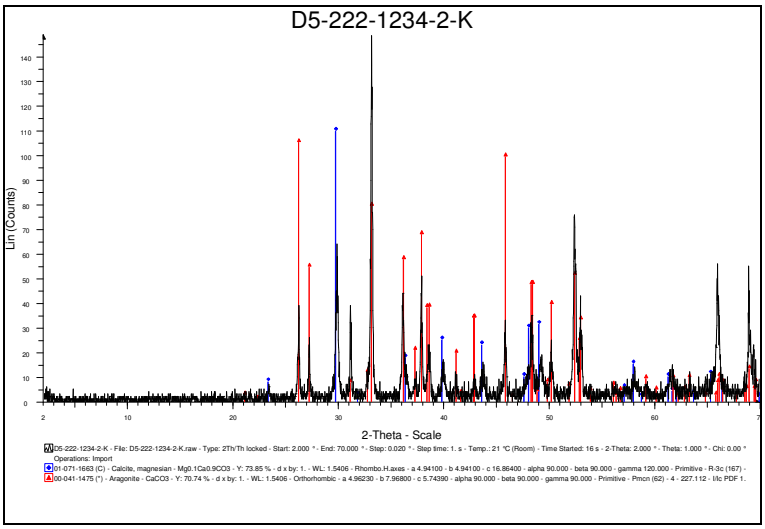

Figure C-42. XRD profile for specimen D5.222.1234.2/K. Matching aragonite peaks (red) and minor LMC calcite (blue)from the PDF database. Ammonite genus – *Anagaudryceras* a nektonic carnivore.

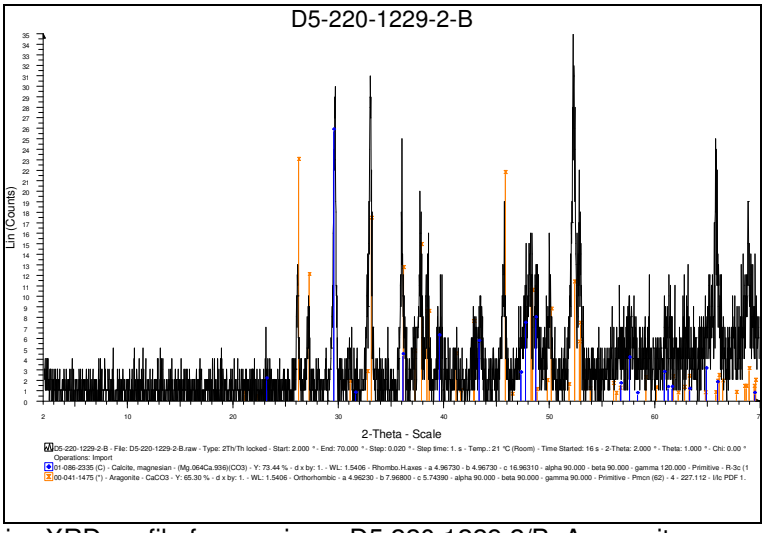

Figure C-43. Noisy XRD profile for specimen D5.220.1229.2/B. Ammonite genus – *Maorites* a nektonic carnivore. Typical profile associated with specimens that yielded small quantities of sample powders, the relative aragonite peak positions are well defined.

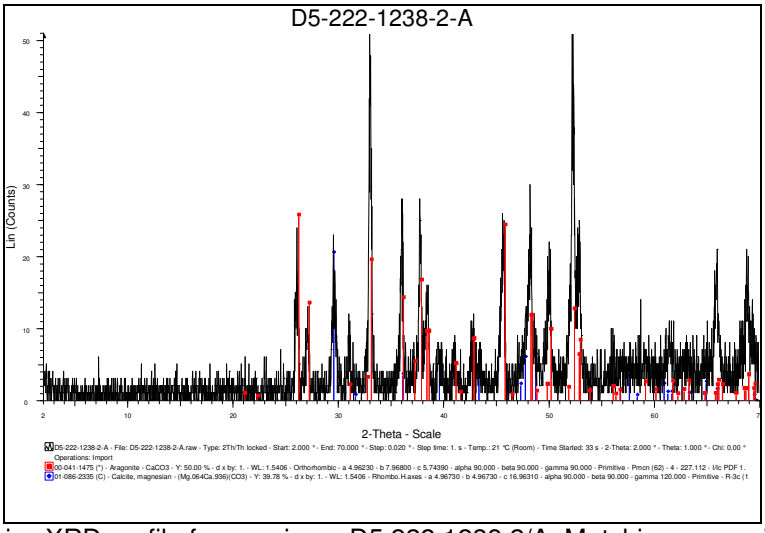

Figure C-44. Noisy XRD profile for specimen D5.222.1238.2/A. Matching aragonite peaks (red) and minor LMC calcite (blue) peaks from the PDF database. Ammonite genus – *Maorites* a nektonic carnivore. Typical profile associated with specimens that yielded small quantities of sample powders. The relative aragonite peak positions are well defined.

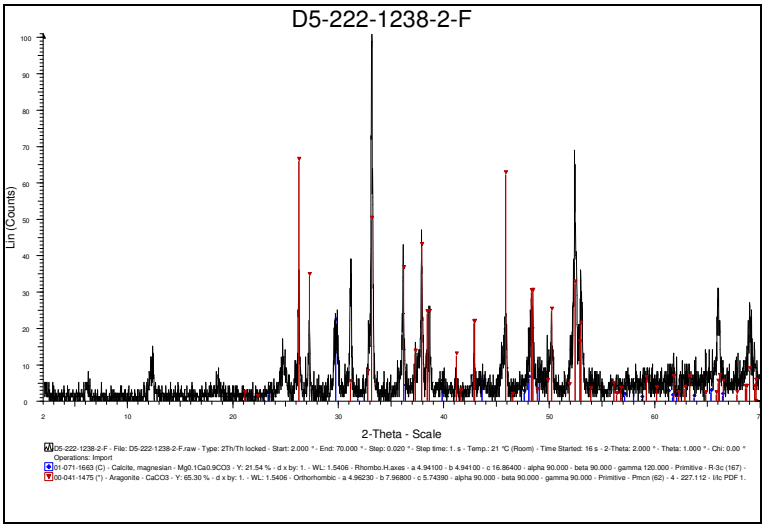

Figure C-45. Noisy XRD profile for specimen D5.222.1238.2/F. Matching aragonite (red) and LMC calcite (blue) peaks from the PDF database. Ammonite genus – *Maorites* a nektonic carnivore. Typical profile associated with specimens that yielded small quantities of sample powders. The relative aragonite peak positions are well defined.

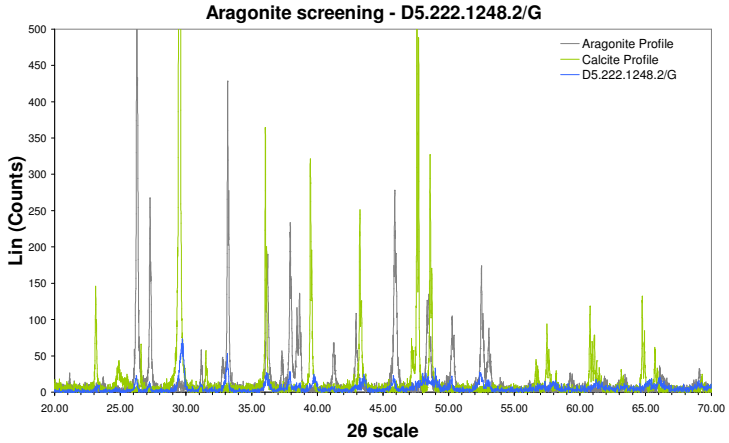

Figure C-46. Noisy XRD profile for specimen D5.222.1248.2/G. Ammonite genus – *Maorites* a nektonic carnivore. Typical profile associated with specimens that yielded small quantities of sample powders. The relative aragonite peak positions are well defined but there is also calcite present.

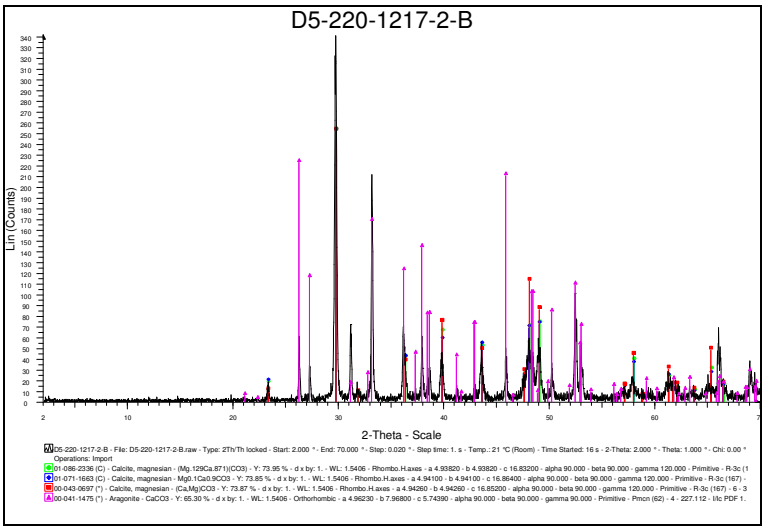

Figure C-47. XRD profile for specimen D5.220.1217.2/B. Ammonite genus – *Maorites* a nektonic carnivore. Complex profile associated with specimens contaminated with calcite, relative aragonite peak positions are well defined.

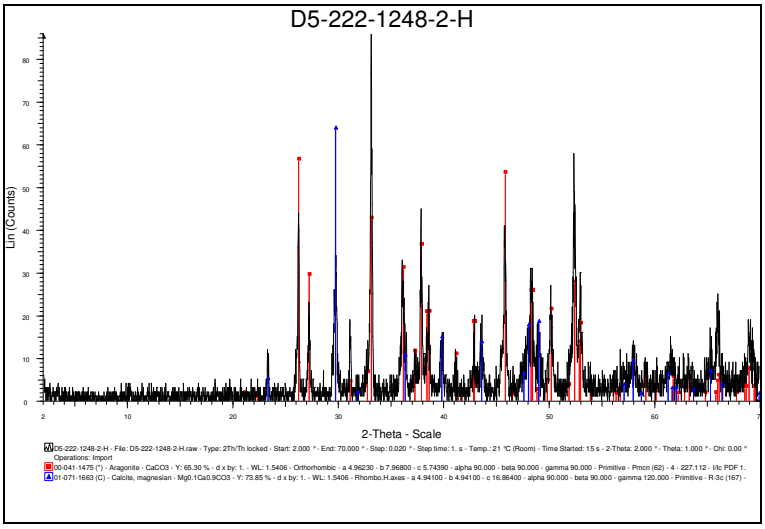

Figure C-48. Noisy XRD profile for specimen D5.222.1248.2/H. Ammonite genus – Unidentified. Typical profile associated with specimens that yielded small quantities of sample powders. The relative aragonite peak positions are well defined but there is also calcite present.

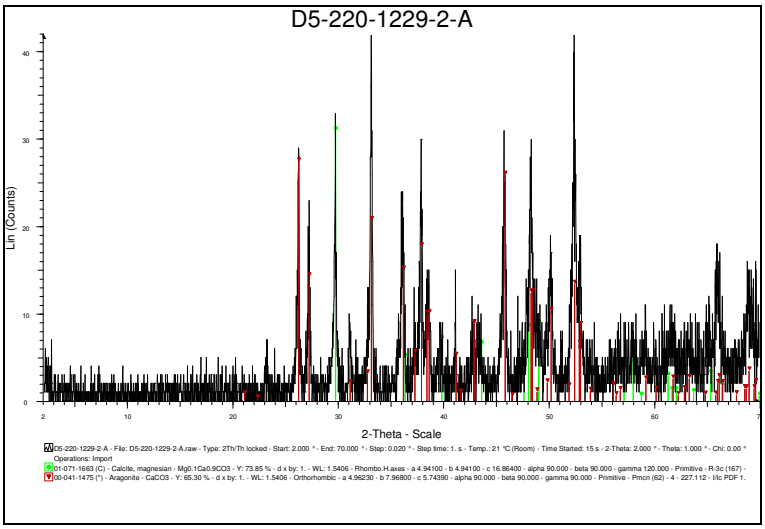

Figure C-49. Noisy XRD profile for specimen D5.220.1229.2/A. Matching calcite and aragonite peaks from the PDF database. Ammonite genus – *Maorites* a nektonic carnivore. Typical profile associated with specimens that yielded small quantities of sample powders. The relative aragonite peak positions are well defined but there is also calcite present..

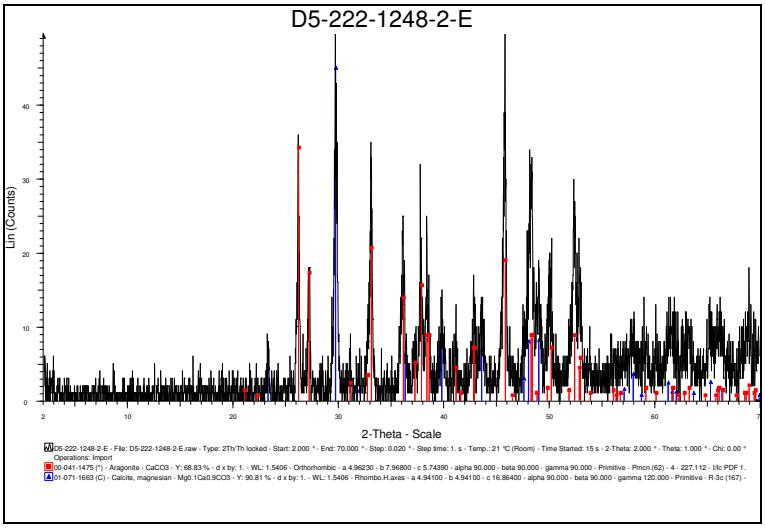

Figure C-50. Noisy XRD profile for specimen D5.222.1248.2/E. Ammonite genus – unidentified. Typical profile associated with specimens that yielded small quantities of sample powders. The relative aragonite peak positions are well defined but there is also calcite present..

C.4 XRD profiles – Cephalopoda – Nautiloidea

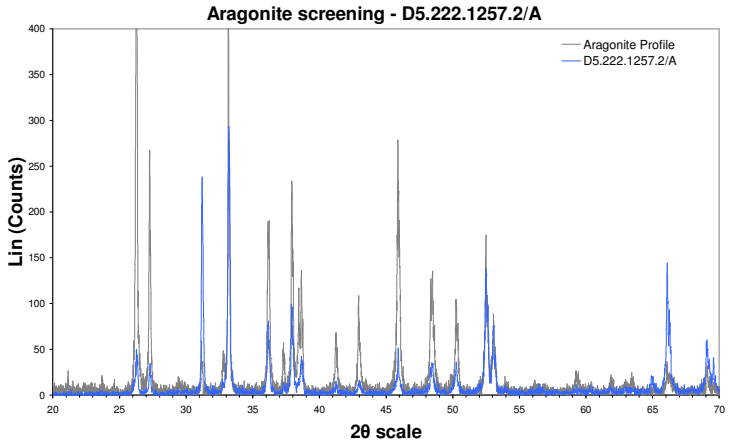

Figure C-51. XRD profile for specimen D5.222.1257.2/A. Nautiloid genus – Unidentified carnivore.

C.5 XRD profiles – Gastropoda

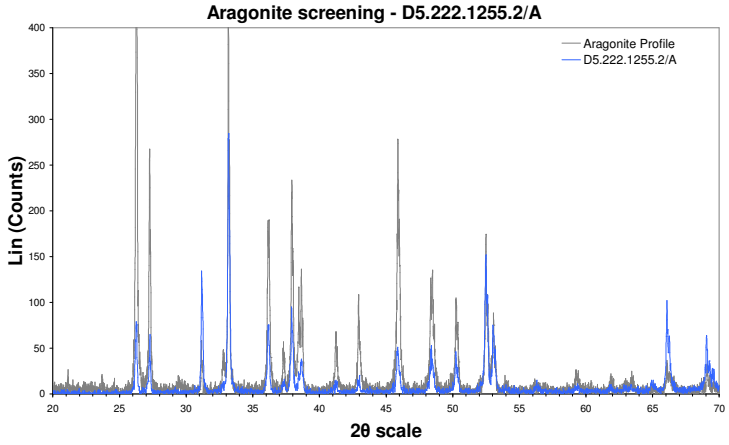

Figure C-52. XRD profile for specimen D5.222.1255.2/A. Gastropod genus – *Amberlaya* an epifaunal carnivore/scavenger.

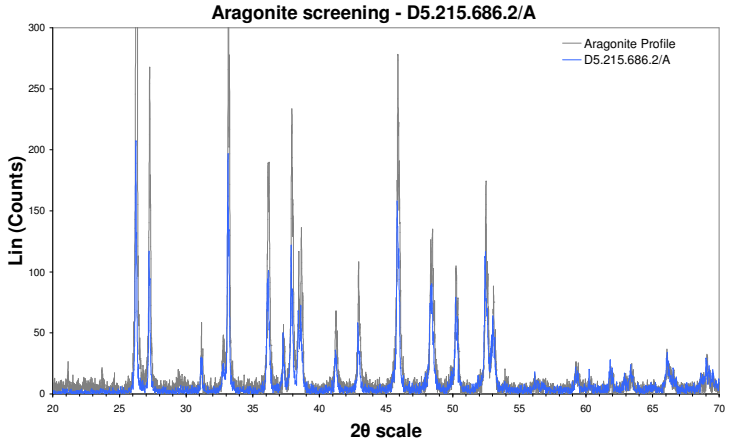

Figure C-53. XRD profile for specimen D5.215.686.2/A. Gastropod genus – *Amberlaya* an epifaunal carnivore/scavenger.

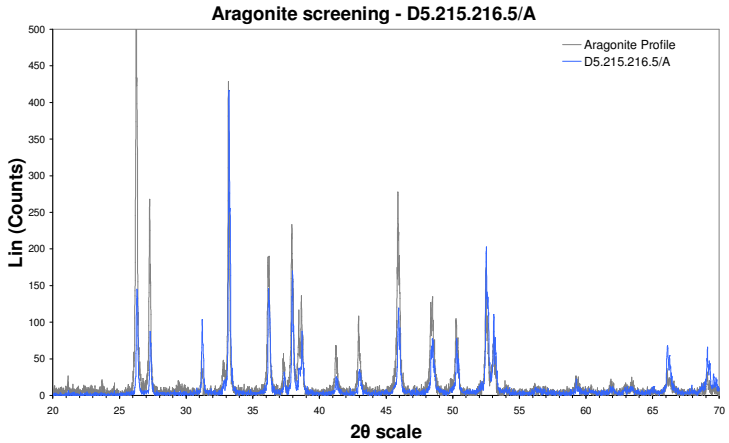

Figure C-54. XRD profile for specimen D5.215.216.5/A. Gastropod genus – *Pleurotomaria* an epifaunal carnivore/scavenger.

C.6 XRD profiles – Unidentified specimens

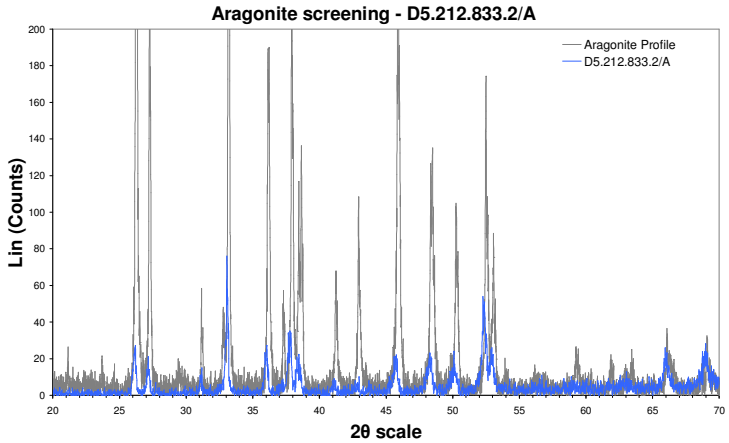

Figure C-55. Noisy XRD profile for specimen D5.212.833.2/A. Shell fragments from an unidentified genus. Typical profile associated with specimens that yielded small quantities of sample powders, the aragonite peaks are well defined.

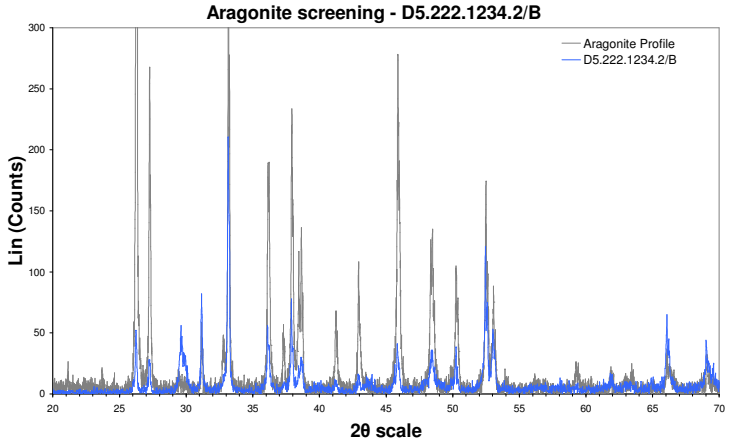

Figure C-56. XRD profile for specimen D5.222.1234.2/B. Shell fragments from an unidentified genus.

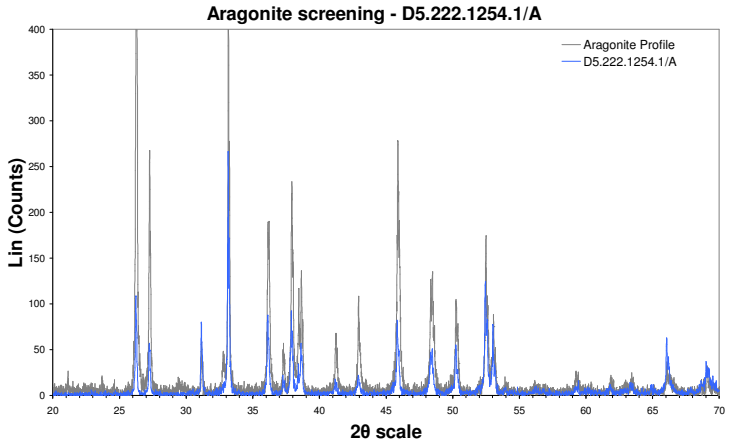

Figure C-57. XRD profile for specimen D5.222.1254.1/A. Shell material genus – Unidentified.

Appendix D. ICP-OES Trace Element Geochemistry

D.1 Introduction

A standard suite of elements (Ca, Mg, Sr, Fe and Mn) were checked together with the inclusion of a number of other elements (S, Na and initially Ba and U), blanks and replicates were also included within each batch of samples. All samples submitted for ICP analysis were 'spiked' with a 1 ppm concentration of yttrium, which provided an internal lab standard as recommended by the analytical laboratory staff in the Department of Environmental Chemistry, University of Plymouth. The non-standard elements included within the analysis were included for the following reasons:

1. The sediments that comprise the López de Bertodano Fm. commonly contain gypsum ($CaSO_4.2H_2O$) (de Souza *et al.*, 2014), which was observed in many of the bulk samples taken from specimen bags whilst carrying out initial sampling of shell material. Gypsum was also identified in a number of the XRD analyses and from experimentation it was also found that gypsum was readily soluble in both distilled water and 1M HCl. It was decided that analysis for sulphur would provide a simple indication of the presence of gypsum (de Souza *et al.*, 2014) providing that the iron levels were low (< 1000 ppm).
2. One of the key hypotheses to be tested was whether there was any evidence for stable isotope variation resulting from water stratification within the Latest Maastrichtian James Ross Basin. Brand (1986) indicated that Na could provide a useful proxy for variation in salinity by calculating Sr/Na ratios, which might also provide evidence of water stratification.
3. Allison, (1996) indicated that the presence of barium and uranium within the aragonite lattice, into which both elements will readily partition, might also provide a suitable palaeotemperature proxy. (Russell *et al.*, 2004) also discussed the suitability of U/Ca as a proxy for the carbonate concentration of the ocean.

D.2 Preparation methodology

1. All glassware, including glass weighing boat, was washed in warm water and rinsed with de-ionised water, followed by an overnight soak in a 1M HCl acid bath.
2. Sample tubes were once again rinsed with de-ionised water and placed in a drying oven overnight at 50°C. The 10 ml measuring flasks were also rinsed with de-ionised water and left to dry in a fume cupboard until required.

3. Approximately 10 mg of sample powder was accurately weighed into a glass boat and transferred to a 10ml measuring flask. In the case of samples processed as 'blanks' no powders were added.
4. 100 µl of a yttrium standard solution, Y_2O_3 dissolved in nitric acid, was also added to provide a 1 ppm 'spike' for internal calibration purposes. Sufficient 1M HCL was then added to the measuring flask to bring it up to the required volume (10 ml).
5. No steps were taken to buffer the pH of the resulting solutions since the dissolution was rapid and with the exception of a small number of samples (< 10) there was no obvious particulate matter visible once any effervescence had ceased. In the case of samples that showed an insoluble residue the resulting solution was vacuum filtered using a glass fibre filter and the residue retained for further analysis.
6. Once each batch (n=24) was complete the solutions were transferred to labelled sample tubes and stored ready for analysis.
7. All glassware was then re-washed in preparation for the next cycle.

Following the processing of an initial batch of test samples the concentration of the required trace elements were finally set at the levels listed in Table D-1, also detailed are the selected ICP-OES detection wavelengths for each element (see Table D-2).

Table D-1. ICP-OES Standard trace element concentrations and detection wavelengths (nm).

Element	Standards (µg/ml)					Wavelength (nm)
	1	2	3	4	Blank	
Ca	50	100	200	400		317.933 and 422.673
Mg	2	5	10	15		280.270 and 285.213
Sr	0.5	1	2	5		407.771 and 421.552
Fe	0.1	0.5	1	2		238.204
Mn	0.05	0.1	0.2	0.5		257.610
Ba	0.01	0.02	0.05	0.1		455.403 and 493.408
S	50	100	200	500		181.972
Na	1	2	5	10		588.995 and 589.592
Y	1	1	1	1	1	360.074 and 371.029

Table D-2. ICP-OES calibration data for trace element standards listed in Table D-1.

Ca 317.933	Correlation Coefficient: 0.999954					
	Label	Int. (c/s)	Std Conc.	Calc Conc.	Error	%Error
	Blank	235.001	0	0	-	-
	Std. 1	95625.2	50	50.0374	0.037399	0.1
	Std. 2	192549	100	100.879	0.879303	0.9
	Std. 3	386789	200	202.769	2.76894	1.4
	Std. 4	759719	400	398.391	-1.60901	-0.4
		Equation: y = 1906.4 x + 235.0				
Ca 422.673	Correlation Coefficient: 0.999968					
	Label	Int. (c/s)	Std Conc.	Calc Conc.	Error	%Error
	Blank	168.94	0	0	-	-
	Std. 1	98727	50	49.5448	-0.455215	-0.9
	Std. 2	199710	100	100.309	0.308502	0.3
	Std. 3	402507	200	202.254	2.25394	1.1

	Std. 4	793596	400	398.853	-1.14722	-0.3
		Equation: y = 1989.3 x + 168.9				
Fe 238.204	Correlation Coefficient: 0.997614					
	Label	Int. (c/s)	Std Conc.	Calc Conc.	Error	%Error
	Blank	496.855	0	0	-	-
	Std. 1	0	0.1	-0.089733	-0.189733	-189.7
	Std. 2	3524.64	0.5	0.546823	0.046823	9.4
	Std. 3	5904.28	1	0.976589	-0.023411	-2.3
	Std. 4	0	2	0	-2	-100
		Equation: y = 5537.1 x + 496.9				
Mg 280.270	Correlation Coefficient: 0.999903					
	Label	Int. (c/s)	Std Conc.	Calc Conc.	Error	%Error
	Blank	374.512	0	0	-	-
	Std. 1	38593.7	2	2.20847	0.20847	10.4
	Std. 2	87263.7	5	5.02083	0.020825	0.4
	Std. 3	172998	10	9.9749	-0.025098	-0.3
	Std. 4	259649	15	14.982	-0.018006	-0.1
		Equation: y = 17305.8 x + 374.5				
Mg 285.213	Correlation Coefficient: 0.999886					
	Label	Int. (c/s)	Std Conc.	Calc Conc.	Error	%Error
	Blank	76.7693	0	0	-	-
	Std. 1	6852.4	2	2.15668	0.156675	7.8
	Std. 2	15627.8	5	4.94986	-0.050138	-1
	Std. 3	31235.7	10	9.91786	-0.082139	-0.8
	Std. 4	47361.2	15	15.0506	0.05058	0.3
		Equation: y = 3141.7 x + 76.8				
Mn 257.610	Correlation Coefficient: 0.999700					
	Label	Int. (c/s)	Std Conc.	Calc Conc.	Error	%Error
	Blank	197.864	0	0	-	-
	Std. 1	1075.44	0.05	0.05396	0.00396	7.9
	Std. 2	1691.29	0.1	0.091827	-0.008173	-8.2
	Std. 3	3384.61	0.2	0.195944	-0.004056	-2
	Std. 4	8376.16	0.5	0.502861	0.002861	0.6
		Equation: y = 16263.5 x + 197.9				
S 181.972	Correlation Coefficient: 0.999986					
	Label	Int. (c/s)	Std Conc.	Calc Conc.	Error	%Error
	Blank	7.59512	0	0	-	-
	Std. 1	2557.78	50	50.0531	0.053101	0.1
	Std. 2	5054.54	100	99.0577	-0.942291	-0.9
	Std. 3	10181.9	200	199.694	-0.306458	-0.2
	Std. 4	12776.1	250	250.611	0.61145	0.2
		Equation: y = 50.9 x + 7.6				
Sr 407.771	Correlation Coefficient: 0.998044					
	Label	Int. (c/s)	Std Conc.	Calc Conc.	Error	%Error
	Blank	216.409	0	0	-	-
	Std. 1	198477	0.5	0.743856	0.243856	48.8
	Std. 2	284529	1	1.06672	0.066716	6.7
	Std. 3	504313	2	1.89133	-0.108674	-5.4
	Std. 4	1334401	5	5.00574	0.005741	0.1
		Equation: y = 266530.9 x + 216.4				

D.3 Trace element data – LMC

In Tables D-3, 4, 5 and 6 grey highlighting represents mean values exceeding the Fe 500 ppm and Mn 200 ppm diagenetic thresholds. Specimens determined as low magnesium calcite or having Mg ≥ 1000 ppm (Brand, 1991).

Table D-3. Trace element data categorised by fossil type (mean ppm) for LMC specimens. Note the high Fe and Mn concentrations in all categories.

Type	Mg	Sr	Na	Fe	Mn
Ammonite (n=21)	5233	3120	4572	3735	2283
Bivalve (n=4)	5996	1690	5810	16193	259
Uncertain (n=9)	2871	2479	4852	4785	2231

Table D-4. Trace element data categorised by genus (mean ppm) for LMC specimens. Note the high Fe concentration in all categories except *Pycnodonte* and the high Mn concentration in all categories except *Nucula*.

Genus	Mg	Sr	Na	Fe	Mn
Ammonite (n=5)	6131	2759	3882	3505	3332
Anagaudryceras (n=1)	3810	1504	8007	5536	2822
Bivalve (n=1)	14180	1644	7004	41069	378
Kitchinites (n=1)	6572	1846	2818	2350	380
Maorites (n=14)	4918	3456	4699	3788	2006
Nucula (n=1)	2734	2723	6554	7261	51
Pycnodonte (n=1)	1074	702	3874	249	349
Unidentified (n=9)	2871	2479	4852	4785	2231

Table D-5. Mean trace element data categorised by habitat for LMC specimens. Note the high Fe concentration in all habitats and the high Mn concentration in all habitats except the infaunal category. In both cases the data represent a single specimen.

Habitat	Mg	Sr	Na	Fe	Mn
Epifaunal (n=1)	1074	702	3874	249	349
Infaunal (n=1)	2734	2723	6554	7261	51
Nektonic (n=21)	5233	3120	4572	3735	2283
Uncertain (n=10)	4002	2395	5067	8413	2046

Table D-6. Mean trace element data categorised by stratigraphy for LMC specimens. Note the high Fe concentration at all stratigraphic positions except 925 m and the high Mn concentration at all stratigraphic positions except 682 m and 642 m.

Depth	Mg	Sr	Na	Fe	Mn
1001 (n=2)	5739	2209	2865	7906	4728
991 (n=6)	3668	2842	4332	3904	2021
979 (n=3)	10280	1948	2564	3646	4561
961 (n=2)	6455	1973	4407	12889	3489
955 (n=3)	2515	1650	6859	4723	2059
949 (n=2)	5779	3137	3288	1739	677
937 (n=1)	3343	2420	3060	6627	8207
925 (n=1)	10277	2312	6309	143	580
897 (n=3)	5838	2374	6361	16575	531
869 (n=3)	2616	4912	4927	549	1009
837 (n=1)	1197	3400	5800	2494	2316
682 (n=1)	1033	1406	5275	1047	229
642 (n=2)	1904	1713	5214	3755	200
637 (n=1)	2562	8332	6026	2529	1169
627 (n=2)	4896	3632	5487	2382	758

D.4 Trace element data - Aragonite

In Tables D-7, 8, 9 and 10 grey highlighting represents mean values exceeding the Fe 500 ppm and Mn 200 ppm diagenetic thresholds. Specimens determined as aragonite based upon an Mg concentration < 1000 ppm (Brand, 1991).

Table D-7. Trace element data categorised by fossil type (Mean ppm) for aragonite specimens.

Type	Mg	Sr	Na	Fe	Mn
Ammonite (n=25)	397	4835	4694	600	226
Bivalve (n=125)	147	2664	6100	160	184
Gastropod (n=16)	154	3037	6119	326	114
Nautiloid (n=4)	402	4224	4053	439	172
Uncertain (n=9)	95	2568	4375	216	11

Table D-8. Trace element data categorised by genus (Mean ppm) for aragonite specimens. Note that for Fe only *Maorites*, unidentified Ammonites and *Pinna* exceed the threshold of 500 ppm and that for Mn both *Maorites* and *Nucula* exceed the 200 ppm threshold.

Genus	Mg	Sr	Na	Fe	Mn
Amberlaya (n=13)	169	3016	6191	390	135
Ammonite (n=9)	326	3448	4556	775	93
Bivalve (n=21)	103	2147	5778	142	63
Diplomoceras (n=1)	426	4327	6719	179	61
Eselaevitrigonia (n=34)	156	2930	5914	136	155
Gastropod (n=1)	87	2001	4491	0	19
Grossouvrites (n=1)	178	3195	7506	369	15
Lahillia (n=1)	42	3252	3977	137	28
Maorites (n=14)	456	5880	4438	534	338
Nautiloid (n=4)	402	4224	4053	439	172
Nucula (n=29)	211	3611	5732	235	481
Oistotrigonia (n=26)	67	1530	6036	76	84
Pinna (n=3)	176	2656	4051	672	51
Pleurotomaria (n=2)	89	3692	6467	70	24
Solemya (n=1)	684	6768	2776	78	100
Unidentified (n=9)	95	2568	4375	216	11

Table D-9. Trace element data categorised by habitat/mode of life (Mean ppm) for aragonite specimens. Note that for Fe only nektonic taxa exceed the 500 ppm threshold and that for Mn both infaunal and nektonic taxa exceed the 200 ppm threshold.

Habitat	Mg	Sr	Na	Fe	Mn
Epifaunal (n=16)	154	3037	6119	326	114
Infaunal (n=104)	156	2769	6165	163	208
Nektonic (n=28)	396	4766	4530	592	224
Planktonic (n=1)	426	4327	6719	179	61
Uncertain (n=30)	101	2273	5357	164	47

Table D-10. Trace element data categorised by stratigraphy (Mean ppm) for aragonite specimens. No Fe or Mn screening.

Depth	Mg	Sr	Na	Fe	Mn
1084 (n=5)	353	3579	5806	600	806
1080 (n=1)	21	2142	3932	92	0
1068 (n=1)	464	3741	3529	451	299
1028 (n=3)	380	4304	2423	585	224
995 (n=1)	467	3982	8943	0	14
991 (n=3)	81	2739	6524	35	174
943 (n=1)	204	8280	3529	506	286
925 (n=1)	577	4840	3801	340	410
919 (n=1)	529	4842	3660	52	136
895 (n=1)	223	2514	4641	1286	59
869 (n=4)	542	7938	5578	288	689
863 (n=1)	42	5997	8276	204	13
857 (n=2)	204	3446	4610	417	588
851 (n=1)	447	4680	3588	481	394
837 (n=3)	311	2843	5020	1127	119
800 (n=1)	68	2567	5215	155	0
779 (n=3)	26	3291	4027	81	35
755 (n=10)	83	1781	6996	104	1
749 (n=1)	0	1270	3583	198	0
727 (n=1)	97	1460	4357	58	2
722 (n=1)	974	2988	3744	996	171
717 (n=2)	125	1977	7227	162	7
712 (n=14)	146	2411	8476	162	0
682 (n=5)	499	2220	7054	210	318
647 (n=1)	293	6412	3993	378	56
642 (n=12)	152	3741	5999	110	181
637 (n=11)	92	2180	6405	139	73
632 (n=1)	304	2913	4094	549	94
627 (n=6)	309	3888	5585	944	96
622 (n=6)	163	2756	4055	720	115
618 (n=2)	53	3021	3957	93	91
613 (n=14)	215	3925	5284	167	355
608 (n=4)	172	4064	7027	127	57
603 (n=1)	112	2219	7735	29	34
578 (n=1)	69	2308	4786	69	25
558 (n=1)	71	2953	4732	56	14
551 (n=2)	62	3365	3755	184	1
548 (n=3)	119	2373	4518	87	21
541 (n=4)	79	2884	4143	83	68
538 (n=2)	66	2356	4497	63	19
533 (n=5)	172	4091	5526	124	563
528 (n=7)	307	4380	4954	156	418
508 (n=2)	155	1723	6553	0	380
463 (n=1)	0	1431	6615	0	151
458 (n=2)	61	1891	3789	82	57
453 (n=3)	11	1493	3827	66	52
443 (n=1)	0	1316	3839	398	332
438 (n=1)	361	3090	5781	1640	226
435 (n=1)	426	4327	6719	179	61
408 (n=1)	56	1296	4323	0	131
388 (n=4)	118	1796	6726	117	3
348 (n=1)	38	1210	9178	106	0
343 (n=8)	67	1218	7671	86	39
338 (n=1)	0	1099	3697	168	0
333 (n=2)	71	1407	4601	72	0
311 (n=1)	0	1287	5283	0	0

D.5 Diagenetic evaluation of stable isotope data

This section describes the additional diagenetic screening of stable isotope data measured from screened aragonite macrofossils, the methodology and analysis carried out at the stable isotope laboratory at the Jane Herdman Laboratory, School of Earth and Ocean Sciences, University of Liverpool. A further discussion of the initial selection process that determined whether individual $\delta^{18}O$ and $\delta^{13}C$ pairs from the stable isotope data set were considered as diagenetically least altered and therefore suitable for palaeotemperature determination. Chapter 3 assessed the diagenetic suitability of specimens for stable isotope analysis and subsequent palaeotemperature determination. The ICP-OES trace element diagenetic screening of selected shell material did not commence until after the majority of the stable isotope analyses were completed. As a result the stable isotope data set contained data for specimens subsequently determined as being diagenetically unsuitable for further palaeotemperature determination either due to the presence of either LMC or where Mg concentrations were in excess of screening guidelines (Brand, 1991). The availability of the extended stable isotope data set provided an opportunity to test whether a combination of trace element and stable isotope data could also be employed as a method for evaluating diagenesis of skeletal aragonite. An assessment was made as to whether the outcome of the diagenetic screening of samples that were deemed to be altered, based on criteria discussed in Chapter 3, was matched by the quality of the stable isotope data. The question of applying a specific threshold value for an individual trace element raised certain concerns, the adoption of a ‘tapered’ filter was also considered to reject specimens as altered if the trace element data was within a specified range (for example +5%) of the threshold level. After inspection of diagenetic scoring it was decided that ’tapered’ thresholds were not required.

Removal of specimens that exhibited the presence of LMC or those with Mg above the adopted threshold level reduced the entire data set by 34 measurements, the majority of which were from ammonites or unidentified aragonite nacre shell material most probably derived from ammonites. The majority of these rejected specimens also exhibited high levels of either Fe or Mn indicating a strong likelihood of diagenesis. The full variability of the stable isotope data are presented in Table D-11.

Stable isotope and trace element geochemical data were assessed using covariance plots that combined stable isotope and ICP-OES data for evidence of diagenesis. Initial analysis (see Figure D-1) plotted $\delta^{18}O$ versus $\delta^{13}C$ and provides a comparison of the stable isotope data from LMC and aragonite nacre shell material (n=247).

Table D-11. Comparison of stable isotope data sets following diagenetic screening. The aragonite category includes all specimens with mineralogy confirmed by XRD, SEM preservation index and trace elements below defined thresholds (Mg < 1000 ppm, Fe < 500 ppm and Mn < 200 ppm (Brand, 1991; Morrison and Brand, 1988; Anderson *et al*., 1994; Ditchfield *et al*., 1994; Petersen *et al*., 2016)

	Aragonite		**High Fe/Mn**		**No trace element**		**LMC and high Mg**	
	$\delta^{13}C$	**$\delta^{18}O$**	**$\delta^{13}C$**	**$\delta^{18}O$**	**$\delta^{13}C$**	**$\delta^{18}O$**	**$\delta^{13}C$**	**$\delta^{18}O$**
Minima (‰)	-7.54	-0.06	-6.31	0.13	-10.49	0.26	-20.71	-2.94
Maxima (‰)	3.70	2.05	4.34	2.11	3.73	1.95	9.60	1.70
Range (‰)	11.24	2.11	10.65	1.98	14.22	1.69	30.31	4.64

The LMC and high Mg data, Figure D-1(a), exhibited a much wider spread of isotopic values than those presented in Figure D-1(b and c). With the elevated levels of Fe and Mn within this subset of the data there was good cause to remove those specimens from the final stable isotope data set. All specimens classified as LMC or high Mg were removed from the final stable isotope data set. Removal of these specimens left the remaining stable isotope data set with a considerably reduced variability for the $\delta^{13}C$ and $\delta^{18}O$ data. Note that only a small subset of the data was deemed to represent specimens that exhibited either LMC or elevated Mg levels.

One key issue with the filtering of the stable isotope data was to ensure that the diagenetic selection had correctly removed unsuitable specimens and data from the analysed data set. Particularly any specimens showing elevated levels of Fe and Mn, recognised indicators of diagenesis (Morrison and Brand, 1988; Brand, 1991; Marshall 1992) were not included in the final data set. As previously discussed in Chapter 3 the question of whether fossil specimens had been subject to diagenetic change was partly based upon the presence of intact original shell ultrastructure, reliably identified mineralogy and the presence of low levels of the diagenetic trace element indicators Fe and Mn. Also commented upon was specimen Id D5.215.347.2/I, which despite exhibiting extensive neomorphism of the aragonite nacre had concentrations of Fe (59 ppm) and Mn (174 ppm) that were below the threshold values (Morrison and Brand, 1988; Brand, 1991) with the trace element geochemistry indicating that it was unlikely that diagenesis had altered the original shell geochemistry. This suggested that the prevailing redox conditions were incompatible with the precipitation of Fe or Mn from pore fluids. It was also possible that pore fluids either carried low levels of Fe and Mn, or that conditions within the James Ross Basin may have inhibited the diagenesis of the aragonite nacre shell material (see Petersen *et al*., 2016).

A comparison of the stable isotope data from LMC and aragonite nacre shell material (n=247) is presented in Figure 4-1. The widest variability within the stable isotope data can be seen in Figure D-1 (a) which illustrates the rejected LMC data set (n=2) and specimens (n=32) with Mg > 1000 ppm (see Brand, 1991). The removal of these data produced a significantly more compact stable isotope data set which can be seen in

Figure D-1(b) that represents screened aragonite specimens (n=116). Finally Figure D-1(c) represents an expanded screened aragonite data set where green symbols represent specimens for which no trace element diagenetic screening (n=44) was carried out and the orange symbols represent specimens (n=53) with Fe or Mn concentrations that exceeded the diagenetic threshold (Fe > 500 ppm and Mn > 200 ppm). Note that the most negative $\delta^{18}O$ value for the screened data = -0.06‰ and that the 3 most negative $\delta^{13}C$ values represent specimens of the bivalve *Solemya rossiana* which have thiotrophic chemosymbionts involved in the anaerobic oxidation of methane (Little *et al*., 2015).

The inclusion of data for specimens with elevated Fe or Mn and specimens with no trace element screening had a minimal effect on the overall stable isotope population. Whilst it would be normal practice to reject specimens from these categories it can be seen from the stable isotope data summarised in Table D-1 that no increase in the range of $\delta^{18}O$ resulted from inclusion of these data. For the $\delta^{13}C$ data there was an increase in the overall range with the inclusion of specimens without trace element screening but the increase results from the inclusion of data from a single isotopically light specimen of the bivalve *Solemya rossiana*.

There were also specimens that had no trace element screening and as a consequence the diagenetic screening was incomplete, especially regarding LMC. For specimens with no trace element data it was decided that screening would be carried out by a comparison of the screened and unscreened stable isotope data. Whilst this approach carried certain limitations it was deemed suitable because the unscreened specimens had been identified and the stable isotope data could thus be compared with other stable isotope data from screened specimens from the same taxa.

The methodology for assessing aragonitic shell material is straightforward, for details of the diagenetic screening methodology see Chapter 3. The initial diagenetic screening will normally be completed prior to runnng the stable isotope analyses. However, in this study the majority of the stable isotope measurements were completed before any any ICP-OES analyses of major and trace elements (Ca and Mg, Sr, Na, Fe and Mn) had been carried out. This sequence of analysis occurred because of a combination of organisational and financial factors. Tables 4-4 and 4-5 illustrate the effect of trace element screening on the stable isotope data which were categorised by fossil type, habitat, genus and stratigraphy.

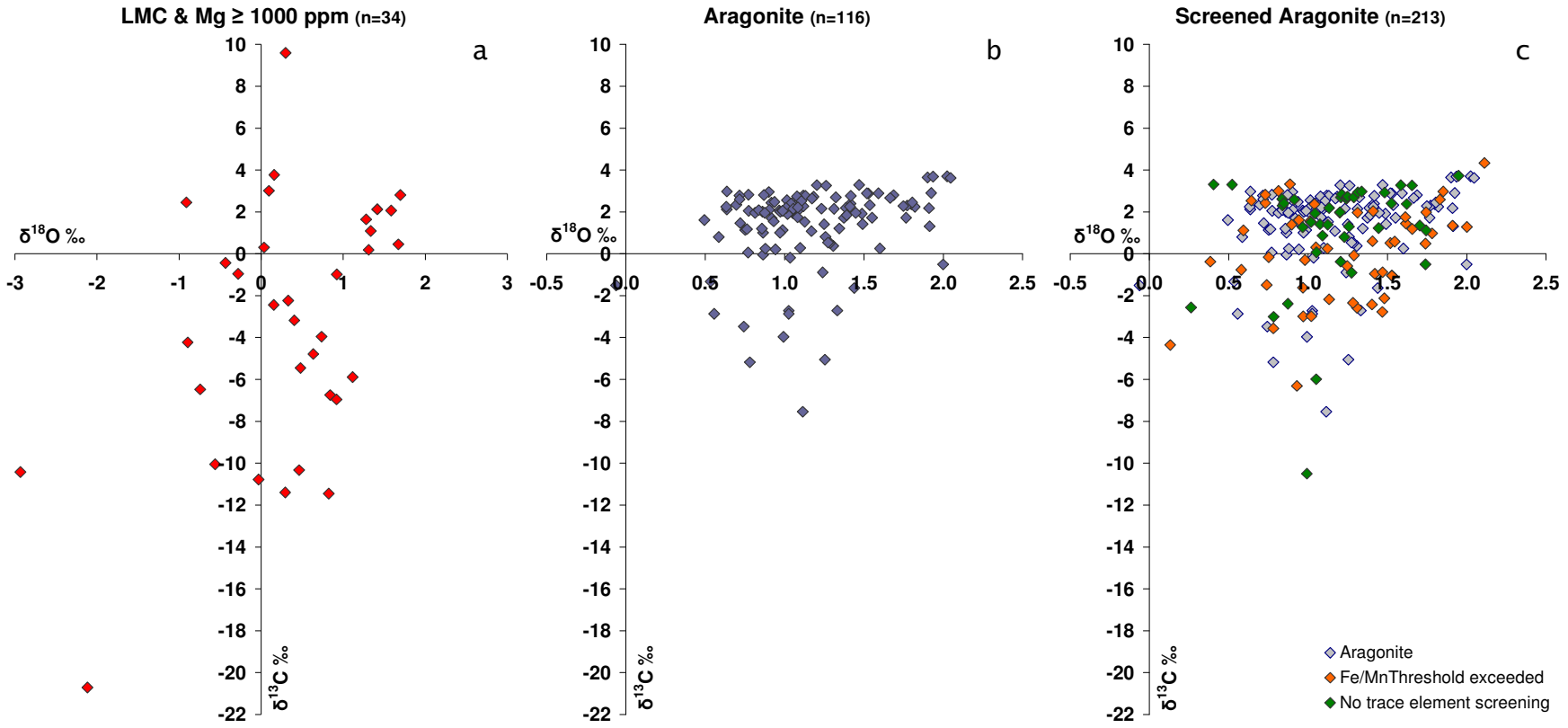

Figure D-1. Comparison of stable isotope data (n=247) from LMC and aragonite nacre shell material. Plot (a) illustrates the rejected LMC data set (n=2) and specimens (n=32) with Mg ≥ 1000 ppm (see Brand, 1991), plot (b) represents screened aragonite specimens (n=116) and plot c) represents an expanded screened aragonite data set where green symbols represent specimens for which no trace element diagenetic screening (n=44) was carried out and the orange symbols represent specimens (n=53) with Fe or Mn concentrations that exceeded the diagenetic threshold (Fe > 500 ppm and Mn > 200 ppm). Note that the most negative $\delta^{18}O$ value for the screened data = -0.06‰ and for $\delta^{13}C$ the 3 lightest values represent specimens of the bivalve *Solemya rossiana* which have thiotrophic chemosymbionts involved in the anaerobic oxidation of methane (Little *et al.*, 2015)

Table D-12. Screened aragonite stable isotope data (mean) categorised by genus, mode of life and stratigraphy.

Genus	$\delta^{13}C$‰	$\delta^{18}O$‰
Amberlaya (n=13)	2.39	1.14
Ammonite (n=9)	-1.07	1.21
Bivalve (n=21)	1.93	1.33
Diplomoceras (n=1)	-1.63	1.44
Eselaevitrigonia (n=34)	1.38	1.31
Gastropod (n=1)	2.40	1.04
Grossouvrites (n=1)	-1.32	0.53
Lahillia (n=1)	3.29	1.47
Maorites (n=14)	-1.84	0.99
Nautiloid (n=4)	-2.66	0.55
Nucula (n=39)	1.53	1.41
Oistotrigonia (n=26)	2.13	0.93
Pinna (n=3)	1.40	1.19
Pleurotomaria (n=2)	0.92	1.00
Solemya (n=1)	-7.54	1.11
Unidentified (n=9)	1.01	0.92
Mode of life	**$\delta^{13}C$‰**	**$\delta^{18}O$‰**
Epifaunal (n=16)	2.20	1.11
Infaunal (n=104)	1.56	1.25
Nektonic (n=28)	-1.69	0.98
Planktonic (n=1)	-1.63	1.44
Uncertain (n=30)	1.65	1.21

Depth (m)	$\delta^{13}C$‰	$\delta^{18}O$‰
1084 (n=5)	0.12	1.49
1080 (n=1)	2.12	0.64
1068 (n=1)	0.58	1.55
1028 (n=3)	-3.56	0.48
995 (n=1)	0.06	0.77
991 (n=3)	1.59	0.57
943 (n=1)	-3.56	0.78
925 (n=1)	-2.58	1.31
919 (n=1)	-2.71	1.33
895 (n=1)	1.45	1.62
869 (n=4)	-0.86	0.98
863 (n=1)	2.01	0.86
857 (n=2)	0.37	0.49
851 (n=1)	-0.29	0.98
837 (n=3)	-1.04	1.53
800 (n=1)	2.40	1.42
779 (n=3)	1.58	1.41
755 (n=10)	1.80	1.14
749 (n=1)	1.47	0.72
727 (n=1)	2.77	1.13
722 (n=1)	-2.18	1.13
717 (n=2)	1.54	1.39

Depth (m)	$\delta^{13}C$‰	$\delta^{18}O$‰
712 (n=14)	2.58	1.26
682 (n=5)	1.06	1.82
647 (n=1)	-3.96	0.99
642 (n=12)	1.49	1.20
637 (n=11)	1.67	0.88
632 (n=1)	0.32	1.05
627 (n=6)	-0.25	0.98
622 (n=6)	1.92	1.11
618 (n=2)	2.63	1.66
613 (n=14)	2.19	1.44
608 (n=4)	0.44	1.33
603 (n=1)	3.28	1.20
578 (n=1)	2.31	1.77
558 (n=1)	2.18	1.91
551 (n=2)	2.19	1.29
548 (n=3)	2.33	1.07
541 (n=4)	2.27	1.51
538 (n=2)	0.98	1.49
533 (n=5)	0.06	1.63
528 (n=7)	-3.68	1.29
508 (n=2)	2.06	1.12
463 (n=1)	3.26	1.26

Depth (m)	$\delta^{13}C$‰	$\delta^{18}O$‰
458 (n=2)	2.41	1.01
453 (n=3)	1.78	0.78
443 (n=1)	2.82	0.73
438 (n=1)	1.56	1.01
435 (n=1)	-1.63	1.44
408 (n=1)	2.74	1.08
388 (n=4)	1.92	1.04
348 (n=1)	2.52	1.11
343 (n=8)	1.65	0.95
338 (n=1)	2.60	0.72
333 (n=2)	1.82	1.07
311 (n=1)	2.22	1.08
333 (n=2)	1.82	1.07
311 (n=1)	2.22	1.08

Table D-13. Aragonite stable isotope data categorised by stratigraphy, fossil type, mode of life and genus. Ranges marked 'n/a' represent categories containing a single specimen.

Depth (m)	No.	$\delta^{13}C$ Mean	$\delta^{13}C$ Min	$\delta^{13}C$ Max	$\delta^{13}C$ Range	$\delta^{18}O$ Mean	$\delta^{18}O$ Min	$\delta^{18}O$ Max	$\delta^{18}O$ Range
1084	7	0.42	-0.95	1.99	2.94	1.52	1.29	1.74	0.46
1080	1	2.12	2.12	2.12	n/a	0.64	0.64	0.64	n/a
1068	1	0.58	0.58	0.58	n/a	1.55	1.55	1.55	n/a
1028	3	-3.56	-4.35	-2.86	1.49	0.48	0.13	0.74	0.61
995	1	0.06	0.06	0.06	n/a	0.77	0.77	0.77	n/a
991	4	0.97	-1.51	3.33	4.83	0.75	-0.06	1.27	1.34
943	1	-3.56	-3.56	-3.56	n/a	0.78	0.78	0.78	n/a
925	1	-2.58	-2.58	-2.58	n/a	1.31	1.31	1.31	n/a
919	1	-2.71	-2.71	-2.71	n/a	1.33	1.33	1.33	n/a
909	2	1.41	1.30	1.51	0.21	1.14	1.02	1.26	0.24
897	1	0.08	0.08	0.08	n/a	1.05	1.05	1.05	n/a
895	1	1.45	1.45	1.45	n/a	1.62	1.62	1.62	n/a
869	4	-0.86	-2.99	2.66	5.65	0.98	0.58	1.28	0.71
863	1	2.01	2.01	2.01	n/a	0.86	0.86	0.86	n/a
857	2	0.37	-0.38	1.12	1.50	0.49	0.38	0.59	0.21
851	1	-0.29	-0.29	-0.29	n/a	0.98	0.98	0.98	n/a
837	3	-1.04	-1.04	-1.04	n/a	1.53	1.53	1.53	n/a
800	2	2.20	1.99	2.40	0.41	1.31	1.20	1.42	0.21
779	3	1.58	1.41	1.92	0.51	1.41	1.25	1.49	0.24
755	10	1.80	-0.04	2.79	2.83	1.14	0.86	1.39	0.52
749	1	1.47	1.47	1.47	n/a	0.72	0.72	0.72	n/a
727	1	2.77	2.77	2.77	n/a	1.13	1.13	1.13	n/a
722	1	-2.18	-2.18	-2.18	n/a	1.13	1.13	1.13	n/a
717	2	1.54	0.28	2.80	2.53	1.39	1.10	1.69	0.59
712	15	2.46	0.80	2.97	2.18	1.26	0.77	1.67	0.89
682	5	1.06	0.49	1.34	0.86	1.82	1.66	2.00	0.34
647	1	-3.96	-3.96	-3.96	n/a	0.99	0.99	0.99	n/a
642	12	1.49	-5.18	3.65	8.82	1.20	0.64	1.90	1.26
637	12	1.60	-2.72	2.81	5.53	0.90	0.49	1.09	0.60
632	1	0.32	0.32	0.32	n/a	1.05	1.05	1.05	n/a
627	7	-0.27	-1.62	2.39	4.00	1.01	0.74	1.24	0.50
622	11	2.12	1.00	3.31	2.31	0.98	0.40	1.85	1.45
618	2	2.63	2.37	2.88	0.50	1.66	1.53	1.80	0.27
613	19	2.26	0.24	4.34	4.09	1.42	0.76	2.11	1.35
608	7	0.91	-2.86	3.73	6.59	1.24	0.52	1.95	1.43
603	1	3.28	3.28	3.28	n/a	1.20	1.20	1.20	n/a
578	1	2.31	2.31	2.31	n/a	1.77	1.77	1.77	n/a
558	1	2.18	2.18	2.18	n/a	1.91	1.91	1.91	n/a
551	2	2.19	2.06	2.33	0.27	1.29	1.05	1.54	0.49
548	4	2.32	1.73	2.78	1.05	1.01	0.72	1.55	0.84
541	6	2.28	1.96	2.45	0.49	1.45	1.04	1.80	0.76
538	2	0.98	0.26	1.71	1.46	1.49	1.37	1.60	0.23
533	5	0.06	-2.42	2.91	5.33	1.63	1.40	1.92	0.52
528	12	-3.41	-10.49	1.36	11.85	1.21	0.26	2.00	1.74
526	1	-5.99	-5.99	-5.99	n/a	1.05	1.05	1.05	n/a
508	3	2.17	2.04	2.38	0.34	1.29	0.84	1.62	0.78
463	1	3.26	3.26	3.26	n/a	1.26	1.26	1.26	n/a
458	3	2.41	1.85	2.98	1.14	0.96	0.64	1.39	0.76
453	3	1.78	0.81	2.27	1.47	0.78	0.59	1.12	0.53
443	1	2.82	2.82	2.82	n/a	0.73	0.73	0.73	n/a
438	1	1.56	1.56	1.56	n/a	1.01	1.01	1.01	n/a
435	1	-1.63	-1.63	-1.63	n/a	1.44	1.44	1.44	n/a
408	1	2.74	2.74	2.74	n/a	1.08	1.08	1.08	n/a
388	4	1.92	1.53	2.19	0.67	1.04	0.99	1.13	0.14
348	1	2.52	2.52	2.52	n/a	1.11	1.11	1.11	n/a
343	8	1.65	1.13	2.15	1.02	0.95	0.86	1.08	0.22
338	1	2.60	2.60	2.60	n/a	0.72	0.72	0.72	n/a
333	2	1.82	1.00	2.64	1.64	1.07	0.97	1.17	0.20

Depth (m)	No.	$\delta^{13}C$ Mean	$\delta^{13}C$ Min	$\delta^{13}C$ Max	$\delta^{13}C$ Range	$\delta^{18}O$ Mean	$\delta^{18}O$ Min	$\delta^{18}O$ Max	$\delta^{18}O$ Range
311	1	2.22	2.22	2.22	n/a	1.08	1.08	1.08	n/a

Type	No.	$\delta^{13}C$ Mean	$\delta^{13}C$ Min	$\delta^{13}C$ Max	$\delta^{13}C$ Range	$\delta^{18}O$ Mean	$\delta^{18}O$ Min	$\delta^{18}O$ Max	$\delta^{18}O$ Range
Bivalve	151	1.51	-10.49	4.34	14.83	1.25	0.26	2.11	1.85
Cephalopod	32	-1.62	-5.18	1.56	6.74	1.00	0.13	1.53	1.40
Gastropod	20	1.99	-0.19	3.33	3.51	1.12	0.72	1.42	0.70
Uncertain	10	0.82	-1.51	2.64	4.15	0.96	-0.06	1.55	1.61

Habitat	No.	$\delta^{13}C$ Mean	$\delta^{13}C$ Min	$\delta^{13}C$ Max	$\delta^{13}C$ Range	$\delta^{18}O$ Mean	$\delta^{18}O$ Min	$\delta^{18}O$ Max	$\delta^{18}O$ Range
Epifaunal	20	1.99	-0.19	3.33	3.51	1.12	0.72	1.42	0.70
Infaunal	128	1.43	-10.49	4.34	14.83	1.24	0.26	2.11	1.85
Nektonic	31	-1.62	-5.18	1.56	6.74	0.99	0.13	1.53	1.40
Planktonic	1	-1.63	-1.63	-1.63	n/a	1.44	1.44	1.44	n/a
Uncertain	33	1.61	-1.51	2.91	4.41	1.20	-0.06	1.92	1.99

Mode of life	No.	$\delta^{13}C$ Mean	$\delta^{13}C$ Min	$\delta^{13}C$ Max	$\delta^{13}C$ Range	$\delta^{18}O$ Mean	$\delta^{18}O$ Min	$\delta^{18}O$ Max	$\delta^{18}O$ Range
Browser	2	0.92	-0.19	2.02	2.20	1.00	0.97	1.03	0.06
Carnivore	32	-1.62	-5.18	1.56	6.74	1.00	0.13	1.53	1.40
Scavenger	17	2.09	0.51	3.33	2.82	1.14	0.72	1.42	0.70
Deposit feeder	49	1.34	-3.01	3.65	6.65	1.39	0.26	2.05	1.78
Suspension feeder	79	1.49	-10.49	4.34	14.83	1.14	0.38	2.11	1.73
Uncertain	34	1.63	-1.51	2.91	4.41	1.19	-0.06	1.92	1.99

Genus	No.	$\delta^{13}C$ Mean	$\delta^{13}C$ Min	$\delta^{13}C$ Max	$\delta^{13}C$ Range	$\delta^{18}O$ Mean	$\delta^{18}O$ Min	$\delta^{18}O$ Max	$\delta^{18}O$ Range
Amberlaya	14	2.28	0.51	3.33	2.82	1.13	0.72	1.42	0.70
Ammonite	9	-1.07	-3.96	1.56	5.52	1.21	0.88	1.53	0.65
Bivalve	22	1.93	-0.04	2.91	2.95	1.32	0.59	1.92	1.33
Diplomoceras	1	-1.63	-1.63	-1.63	n/a	1.44	1.44	1.44	n/a
Eselaevitrigonia	43	1.66	-6.31	4.34	10.65	1.28	0.38	2.11	1.73
Gastropod	4	1.50	0.80	2.40	1.60	1.14	1.02	1.26	0.24
Grossouvrites	1	-1.32	-1.32	-1.32	n/a	0.53	0.53	0.53	n/a
Lahillia	1	3.29	3.29	3.29	n/a	1.47	1.47	1.47	n/a
Maorites	17	-1.68	-5.18	1.18	6.36	1.00	0.58	1.33	0.75
Nautiloid	4	-2.66	-4.35	0.06	4.42	0.55	0.13	0.77	0.64
Nucula	49	1.34	-3.01	3.65	6.65	1.39	0.26	2.05	1.78
Oistotrigonia	28	2.14	0.81	3.26	2.45	0.92	0.59	1.49	0.91
Pinna	5	1.88	0.32	2.62	2.30	1.07	0.84	1.62	0.78
Pleurotomaria	2	0.92	-0.19	2.02	2.20	1.00	0.97	1.03	0.06
Solemya	3	-8.01	-10.49	-5.99	4.51	1.05	0.99	1.11	0.12
Unidentified	10	0.82	-1.51	2.64	4.15	0.96	-0.06	1.55	1.61

Table D-14. Comparison of stable isotope data vs diagenetic scoring categories. Note that not all specimen categories are present for the three diagenetic scoring categories.

	Screened - Aragonite data							Screened - High Fe and/or Mn data							Screened - No trace element data						
		$\delta^{13}C‰$			$\delta^{18}O‰$				$\delta^{13}C‰$			$\delta^{18}O‰$				$\delta^{13}C‰$			$\delta^{18}O‰$		
Type	**No.**	**Mean**	**Min**	**Max**	**Mean**	**Min**	**Max**	**No.**	**Mean**	**Min**	**Max**	**Mean**	**Min**	**Max**	**No.**	**Mean**	**Min**	**Max**	**Mean**	**Min**	**Max**
Bivalve	82	1.89	-7.54	3.70	1.23	0.49	2.05	33	0.60	-6.31	4.34	1.34	0.38	2.11	36	1.48	-10.49	3.73	1.19	0.26	1.95
Cephalopod	14	-1.83	-5.18	1.18	0.95	0.53	1.44	15	-1.56	-4.35	1.56	1.04	0.13	1.53	3	-0.89	-2.38	0.08	1.04	0.87	1.21
Gastropod	12	2.13	-0.19	3.28	1.11	0.72	1.42	4	2.41	1.96	3.33	1.11	0.89	1.31	4	1.12	0.80	1.51	1.15	1.02	1.26
Uncertain	8	1.15	-1.51	2.64	0.94	-0.06	1.55	1	-0.16	-0.16	-0.16	0.75	0.75	0.75	1	-0.90	-0.90	-0.90	1.27	1.27	1.27
Habitat																					
Epifaunal	12	2.13	-0.19	3.28	1.11	0.72	1.42	4	2.41	1.96	3.33	1.11	0.89	1.31	4	1.12	0.80	1.51	1.15	1.02	1.26
Infaunal	64	1.83	-7.54	3.70	1.21	0.49	2.05	30	0.56	-6.31	4.34	1.33	0.38	2.11	34	1.44	-10.49	3.73	1.20	0.26	1.95
Nektonic	13	-1.84	-5.18	1.18	0.92	0.53	1.33	15	-1.56	-4.35	1.56	1.04	0.13	1.53	3	-0.89	-2.38	0.08	1.04	0.87	1.21
Planktonic	1	-1.63	-1.63	-1.63	1.44	1.44	1.44				No data							No data			
Uncertain	26	1.80	-1.51	2.91	1.20	-0.06	1.92	4	0.70	-0.16	1.34	1.25	0.59	1.91	3	1.17	-0.90	2.41	1.11	0.85	1.27
Genus																					
Amberlaya	9	2.38	0.51	3.28	1.15	0.72	1.42	4	2.41	1.96	3.33	1.11	0.89	1.31	1	0.86	0.86	0.86	1.09	1.09	1.09
Ammonite	4	-1.48	-3.96	0.54	1.04	0.88	1.27	5	-0.75	-2.18	1.56	1.35	1.01	1.53	1	1.99	1.99	1.99	1.20	1.20	1.20
Bivalve	18	2.09	-0.04	2.91	1.32	0.86	1.92	3	0.98	0.49	1.34	1.41	0.59	1.91				No data			
Diplomoceras	1	-1.63	-1.63	-1.63	1.44	1.44	1.44				No data							No data			
Eselaevitrigonia	25	1.71	-5.06	3.70	1.28	0.70	2.02	9	0.43	-6.31	4.34	1.38	0.38	2.11	9	2.71	1.27	3.73	1.19	0.40	1.95
Gastropod	1	2.40	2.40	2.40	1.04	1.04	1.04				No data				3	1.20	0.80	1.51	1.17	1.02	1.26
Grossouvrites	1	-1.32	-1.32	-1.32	0.53	0.53	0.53				No data							No data			
Lahillia	1	3.29	3.29	3.29	1.47	1.47	1.47				No data							No data			
Maorites	5	-2.09	-5.18	1.18	1.03	0.76	1.33	9	-1.71	-3.56	0.25	0.97	0.58	1.31	3	-0.89	-2.38	0.08	1.04	0.87	1.21
Nautiloid	3	-2.09	-3.47	0.06	0.69	0.56	0.77	1	-4.35	-4.35	-4.35	0.13	0.13	0.13							
Nucula	13	2.11	-0.51	3.65	1.52	0.49	2.05	16	0.31	-2.77	3.00	1.41	0.81	1.83	20	1.68	-3.01	2.97	1.28	0.26	1.74
Oistotrigonia	23	2.13	0.81	3.26	0.95	0.59	1.49	3	2.12	1.40	2.54	0.76	0.64	0.90	2	2.36	2.30	2.41	0.84	0.84	0.85
Pinna	1	2.44	2.44	2.44	0.92	0.92	0.92	2	0.88	0.32	1.45	1.33	1.05	1.62	2	2.60	2.59	2.62	0.87	0.84	0.91
Pleurotomaria	2	0.92	-0.19	2.02	1.00	0.97	1.03				No data							No data			
Solemya	1	-7.54	-7.54	-7.54	1.11	1.11	1.11				No data				2	-8.24	-10.49	-5.99	1.02	0.99	1.05
Unidentified	8	1.15	-1.51	2.64	0.94	-0.06	1.55	1	-0.16	-0.16	-0.16	0.75	0.75	0.75	1	-0.90	-0.90	-0.90	1.27	1.27	1.27

Table D-15. Comparison of stable isotope data vs diagenetic scoring categories (Aragonite, high Fe or Mn and a lack of trace element data). Note that as indicated (No data) not all specimens are present for each of the three diagenetic scoring categories.

	Screened - Aragonite data							Screened - High Fe and/or Mn data							Screened - No trace element data						
		$\delta^{13}C‰$			$\delta^{18}O‰$				$\delta^{13}C‰$			$\delta^{18}O‰$				$\delta^{13}C‰$			$\delta^{18}O‰$		
Depth (m)	No.	Mean	Min	Max	Mean	Min	Max	No.	Mean	Min	Max	Mean	Min	Max	No.	Mean	Min	Max	Mean	Min	Max
1084				No data				5	0.12	-0.95	1.99	1.49	1.29	1.74	2	1.17	1.12	1.23	1.59	1.44	1.74
1080	1	2.12	2.12	2.12	0.64	0.64	0.64				No data							No data			
1068				No data				1	0.58	0.58	0.58	1.55	1.55	1.55				No data			
1029	K-Pg Boundary																				
1028	2	-3.17	-3.47	-2.86	0.65	0.56	0.74	1	-4.35	-4.35	-4.35	0.13	0.13	0.13				No data			
995	1	0.06	0.06	0.06	0.77	0.77	0.77				No data							No data			
991	2	0.73	-1.51	2.96	0.42	-0.06	0.90	1	3.33	3.33	3.33	0.89	0.89	0.89	1	-0.90	-0.90	-0.90	1.27	1.27	1.27
943				No data				1	-3.56	-3.56	-3.56	0.78	0.78	0.78				No data			
925				No data				1	-2.58	-2.58	-2.58	1.31	1.31	1.31				No data			
895				No data				1	1.45	1.45	1.45	1.62	1.62	1.62				No data			
919	1	-2.71	-2.71	-2.71	1.33	1.33	1.33				No data							No data			
909				No data							No data				2	1.41	1.30	1.51	1.14	1.02	1.26
897				No data							No data				1	0.08	0.08	0.08	1.05	1.05	1.05
869	1	2.66	2.66	2.66	1.09	1.09	1.09	3	-2.03	-2.99	-0.76	0.94	0.58	1.28				No data			
863	1	2.01	2.01	2.01	0.86	0.86	0.86				No data							No data			
857				No data				2	0.37	-0.38	1.12	0.49	0.38	0.59				No data			
851				No data				1	-0.29	-0.29	-0.29	0.98	0.98	0.98				No data			
837				No data				3	-1.04	-1.04	-1.04	1.53	1.53	1.53				No data			
800	1	2.40	2.40	2.40	1.42	1.42	1.42				No data				1	1.99	1.99	1.99	1.20	1.20	1.20
779	3	1.58	1.41	1.92	1.41	1.25	1.49				No data							No data			
755	10	1.80	-0.04	2.79	1.14	0.86	1.39				No data							No data			
749	1	1.47	1.47	1.47	0.72	0.72	0.72				No data							No data			
727	1	2.77	2.77	2.77	1.13	1.13	1.13				No data							No data			
722				No data				1	-2.18	-2.18	-2.18	1.13	1.13	1.13				No data			
717	2	1.54	0.28	2.80	1.39	1.10	1.69				No data							No data			
712	4	2.14	0.81	2.82	1.28	0.77	1.67				No data				11	2.58	0.80	2.97	1.25	1.21	1.34
682				No data				5	1.06	0.49	1.34	1.82	1.66	2.00				No data			
647	1	-3.96	-3.96	-3.96	0.99	0.99	0.99				No data							No data			
642	8	0.91	-5.18	3.65	1.30	0.78	1.90	4	2.64	2.42	3.00	1.00	0.64	1.83				No data			
637	9	1.60	-2.72	2.81	0.85	0.49	1.08	2	2.00	1.62	2.37	0.99	0.94	1.04	1	0.86	0.86	0.86	1.09	1.09	1.09
632				No data				1	0.32	0.32	0.32	1.05	1.05	1.05				No data			
627	2	0.75	-0.89	2.39	1.16	1.08	1.24	4	-0.75	-1.62	0.25	0.90	0.74	1.12	1	-0.37	-0.37	-0.37	1.21	1.21	1.21
622	4	1.65	1.00	2.44	0.88	0.75	0.97	2	2.47	1.96	2.98	1.58	1.31	1.85	5	2.35	1.27	3.31	0.83	0.40	1.04
618	2	2.63	2.37	2.88	1.66	1.53	1.80				No data							No data			
613	11	2.06	0.24	3.70	1.38	0.76	2.05	3	2.69	1.76	4.34	1.64	1.20	2.11	5	2.45	1.39	3.27	1.38	1.08	1.66
608	4	0.44	-2.86	3.68	1.33	0.53	1.94				No data				3	1.55	-2.38	3.73	1.11	0.52	1.95
603	1	3.28	3.28	3.28	1.20	1.20	1.20				No data							No data			
578	1	2.31	2.31	2.31	1.77	1.77	1.77				No data							No data			
558	1	2.18	2.18	2.18	1.91	1.91	1.91				No data							No data			
551	2	2.19	2.06	2.33	1.29	1.05	1.54				No data							No data			
548	3	2.33	1.73	2.78	1.07	0.72	1.55				No data				1	2.30	2.30	2.30	0.84	0.84	0.84

Table D-15 (cont.)

	Screened - Aragonite data							Screened - High Fe and/or Mn data							Screened - No trace element data						
		$\delta^{13}C$‰			$\delta^{18}O$‰				$\delta^{13}C$‰			$\delta^{18}O$‰				$\delta^{13}C$‰			$\delta^{18}O$‰		
Depth (m)	No.	Mean	Min	Max	Mean	Min	Max	No.	Mean	Min	Max	Mean	Min	Max	No.	Mean	Min	Max	Mean	Min	Max
541	4	2.27	1.96	2.45	1.51	1.04	1.80				No data				2	2.30	2.20	2.41	1.33	1.13	1.53
538	2	0.98	0.26	1.71	1.49	1.37	1.60				No data							No data			
533	2	2.11	1.31	2.91	1.92	1.91	1.92	3	-1.31	-2.42	0.61	1.43	1.40	1.48				No data			
528	3	-4.37	-7.54	-0.51	1.46	1.11	2.00	4	-3.16	-6.31	-0.58	1.17	0.93	1.47	5	-3.04	-10.49	1.36	1.10	0.26	1.74
526				No data											1	-5.99	-5.99	-5.99	1.05	1.05	1.05
508	1	2.09	2.09	2.09	0.84	0.84	0.84	1	2.04	2.04	2.04	1.41	1.41	1.41	1	2.38	2.38	2.38	1.62	1.62	1.62
463	1	3.26	3.26	3.26	1.26	1.26	1.26				No data							No data			
458	2	2.41	1.85	2.98	1.01	0.64	1.39				No data				1	2.41	2.41	2.41	0.85	0.85	0.85
453	3	1.78	0.81	2.27	0.78	0.59	1.12				No data							No data			
443				No data				1	2.82	2.82	2.82	0.73	0.73	0.73				No data			
438				No data				1	1.56	1.56	1.56	1.01	1.01	1.01				No data			
435	1	-1.63	-1.63	-1.63	1.44	1.44	1.44				No data							No data			
408	1	2.74	2.74	2.74	1.08	1.08	1.08				No data							No data			
388	4	1.92	1.53	2.19	1.04	0.99	1.13				No data							No data			
348	1	2.52	2.52	2.52	1.11	1.11	1.11				No data							No data			
343	7	1.69	1.13	2.15	0.96	0.86	1.08	1	1.40	1.40	1.40	0.90	0.90	0.90				No data			
338	1	2.60	2.60	2.60	0.72	0.72	0.72				No data							No data			
333	2	1.82	1.00	2.64	1.07	0.97	1.17				No data							No data			
311	1	2.22	2.22	2.22	1.08	1.08	1.08				No data							No data			

D.6 Screened Stable Isotope Data

A number of key requirements exist for an accurate interpretation of extant palaeoenvironmental and palaeoclimate conditions using stable isotopes of carbon and oxygen from the fossil record. The degree to which oxygen isotope values may have been affected by the preservation of the original aragonite nacre shell fragments and any associated diagenetic alteration must be evaluated. A number of analytical tests can be carried out to determine whether recrystallisation had occurred including SEM investigation of shell fragments and covariance plots of $\delta^{18}O$ vs. Sr/Ca ratios. In the latter case diagenetic processes generally reduce Sr concentrations in aragonite because of the similar chemistry of Sr and Ca (Brand and Veizer 1981; Li and Keller 1999; Ullmann *et al.*, 2013). Strong diagenetic effects result in a good correlation between Sr/Ca ratios and $\delta^{18}O$ values due to the loss of Sr.

These oxygen isotope data show a low correlation coefficient (R^2 = 0.01) between the Sr/Ca ratio for all screened $\delta^{18}O$ values, which indicated that there were no major diagenetic effects, see Figure D-2. However, the overall variability in the $\delta^{18}O$ data was large and diagenesis could have affected individual samples to a greater or lesser extent.

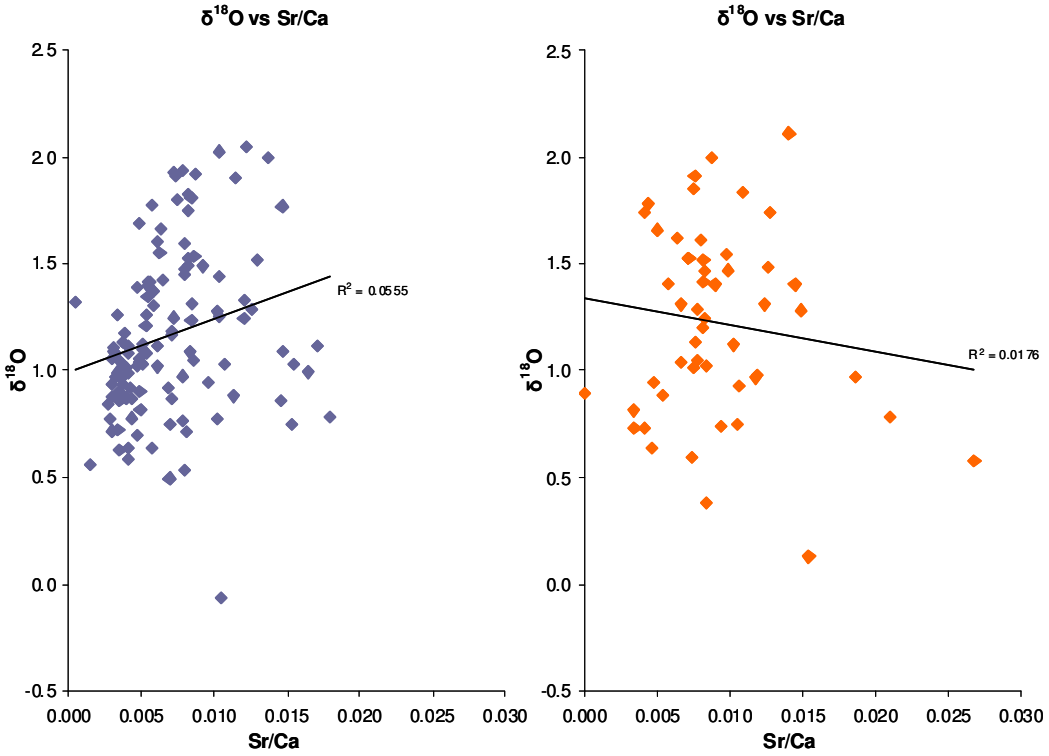

Figure D-2. Oxygen isotope data show a low correlation coefficients (R^2 = 0.0555 and 0.0176) with the Sr/Ca ratio for all screened $\delta^{18}O$ values, which indicated that there were no major diagenetic effects. Orange symbols represent specimens (n=53) with Fe or Mn concentrations that exceeded the diagenetic threshold (Fe > 500 ppm and Mn > 200 ppm). Note that overall variability in the $\delta^{18}O$ data was large and diagenesis may have affected samples to a greater or lesser extent.

Appendix E. Stable isotope methods and data

E.1 Isotope measurement

Sample carbonate powders were ground by hand using an agate pestle and mortar to < 53 µm prior to diagentic screening. For each sample a small quantity (~10 mg) of the powder was placed in a low temperature oxygen plasma for a minimum of 2 hours to ensure the oxidation of any organic carbon present. Stable isotope data for carbon and oxygen were determined using a SIRA Series II mass spectrometer located at the Jane Herdman Laboratory, Department of Earth and Ocean Sciences, University of Liverpool by the analysis of CO_2 generated from the reaction of the carbonate powder with 100% H_3PO_4 at a temperature of 25°C in a common bath setup. All values were reported in the standard (δ) notation in per mil (‰) relative to the Vienna Peedee belemnite (VPDB) standard, where:

$$\delta^{18}O = [(^{l8}O/^{16}O)_{sample}/(^{18}O/^{16}O)_{standard} - 1] \times 10^3 \text{ per mil (‰).} \quad \textbf{Eqn (3)}$$

Fractionation factors were applied for calcite (1.01025) and aragonite (1.01034), a correction for ^{17}O was also applied (Craig, 1957). Quoted laboratory reproducibility for $\delta^{13}C$ and $\delta^{18}O$ was better than ±0.1‰ determined by repeated analyses of aragonite standards (Marshall pers. comm., 2007). Replicate samples were analysed to check for measurement consistency, Table E-1 shows replicate stable isotope data analysed for a single macrofossil specimen.

Table E-1. Stable isotope replicate analyses for sample powders from specimen Id D5.219.1091.2/F. All aragonite stable isotope compositions are reported as standard per mil relative to the Vienna Peedee Belemnite (‰ VPDB).

	$\delta^{13}C$‰	$\delta^{18}O$‰
Replicate Samples	2.94	1.31
	2.73	1.25
	2.62	1.24
	2.67	1.24
	2.84	1.21
	2.72	1.25
	2.67	1.67
	2.66	1.24
	2.70	1.29
	2.70	1.21
	2.97	1.34
	2.94	1.31
Mean	2.748	1.295
Standard Error	0.035	0.039
Standard Deviation	0.117	0.130
Sample Variance	0.014	0.017
Count	11	11
Confidence Level (95.0%)	0.079	0.087

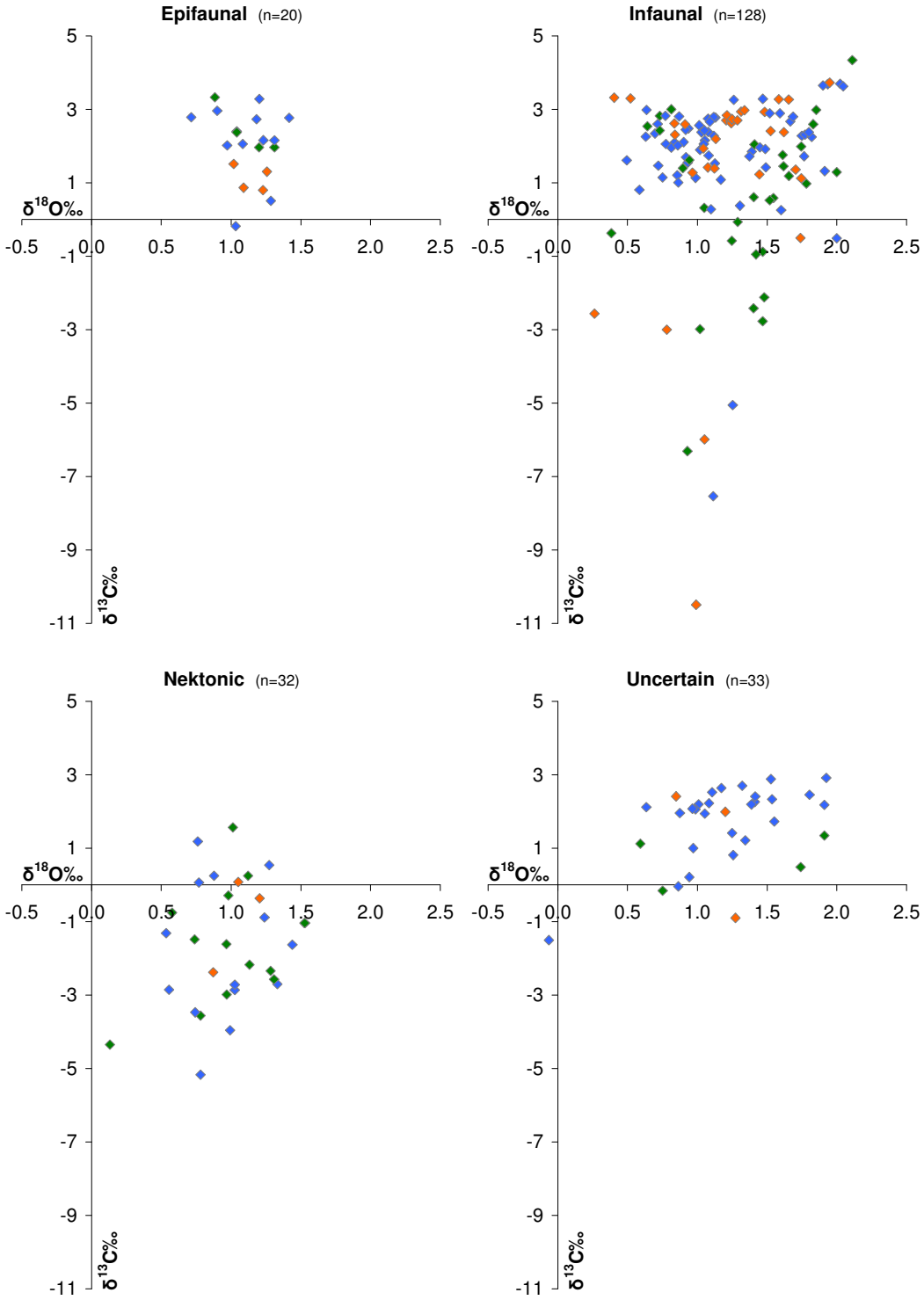

Figure E-1. Comparison of aragonite stable isotope data categorised by mode of life. The 'Uncertain' category represents specimens where it was not possible to identify to either a specific fossil type or taxon but where the fragmentary shell material was of sufficient quality to pass diagenetic screening. Note that with the exception of a single datapoint in the 'Uncertain' category (-0.06‰) all $\delta^{18}O$ data were > 0.0‰. In all plots green symbols represent specimens for which no trace element diagenetic screening was carried out and the orange symbols represent specimens with Fe or Mn concentrations that exceeded the diagenetic threshold (Fe > 500 ppm and Mn > 200 ppm).

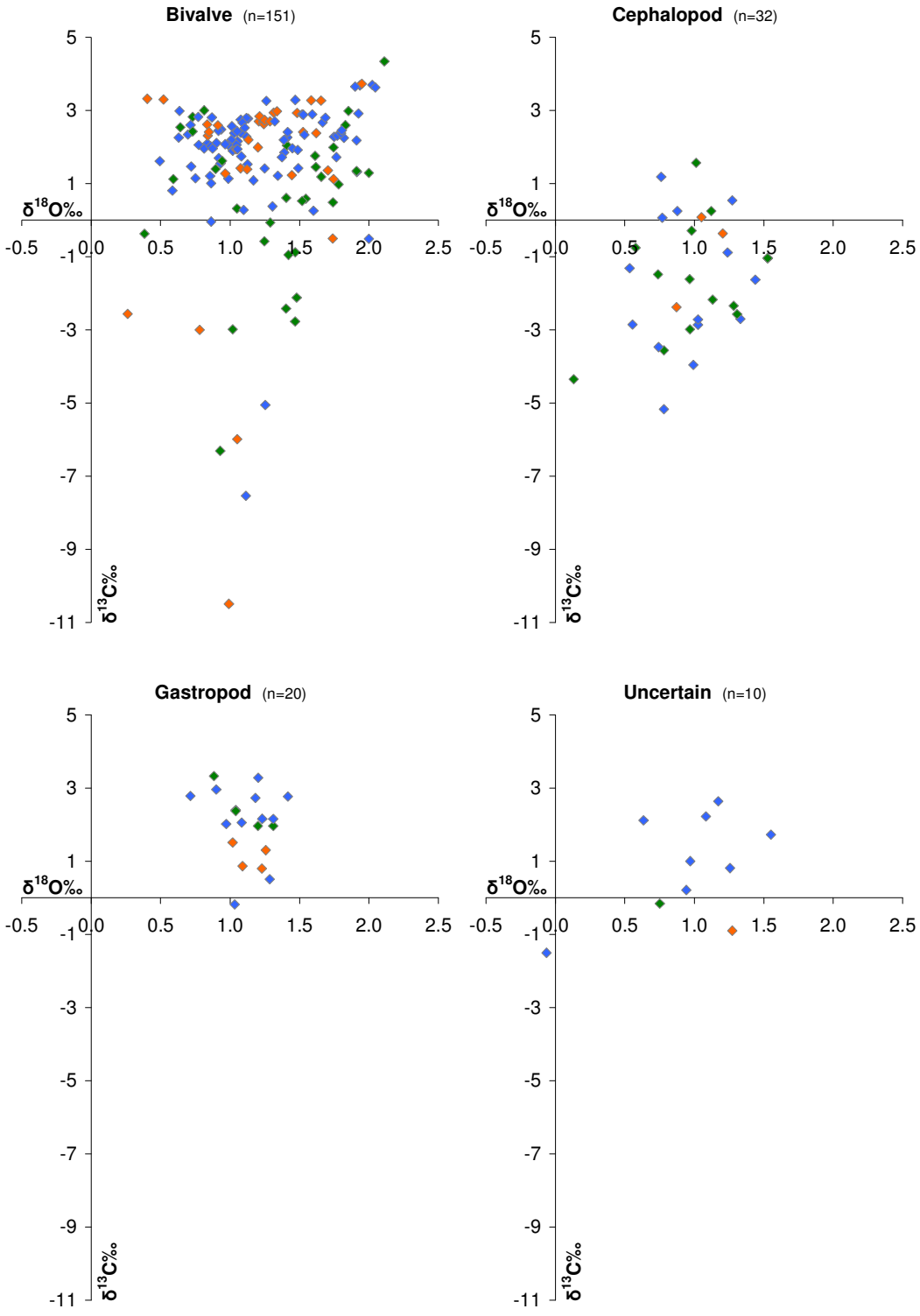

Figure E-2. Comparison of aragonite stable isotope data categorised by fossil type.
The 'Uncertain' category represents specimens where it was not possible to identify to either a specific fossil type but where the fragmentary shell material was of sufficient quality to pass diagenetic screening. Note that with the exception of a single datapoint in the 'Uncertain' category (-0.06‰) all $\delta^{18}O$ data were > 0.0‰. In all plots green symbols represent specimens for which no trace element diagenetic screening was carried out and the orange symbols represent specimens with Fe or Mn concentrations that exceeded the diagenetic threshold (Fe > 500 ppm and Mn > 200 ppm).

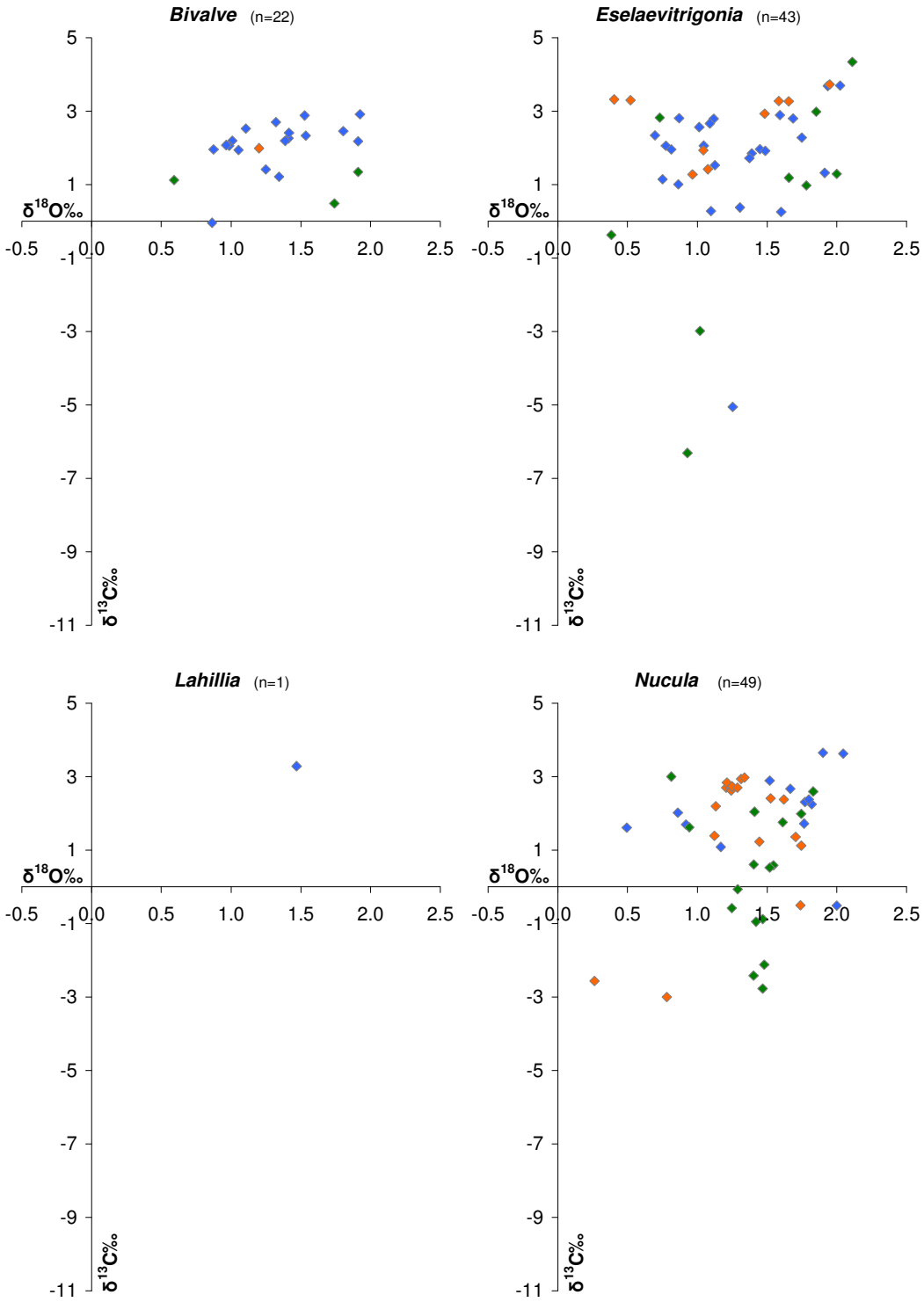

Figure E-3. Comparison of bivalve aragonite nacre shell material stable isotope data categorised by taxa. The 'Bivalve' category represents specimens where it was not possible to identify to a specific taxon but where the fragmentary shell material was of sufficient quality to pass diagenetic screening. Note that all $\delta^{18}O$ data were > 0.0‰. In all plots green symbols represent specimens for which no trace element diagenetic screening was carried out and the orange symbols represent specimens with Fe or Mn concentrations that exceeded the diagenetic threshold (Fe > 500 ppm and Mn > 200 ppm).

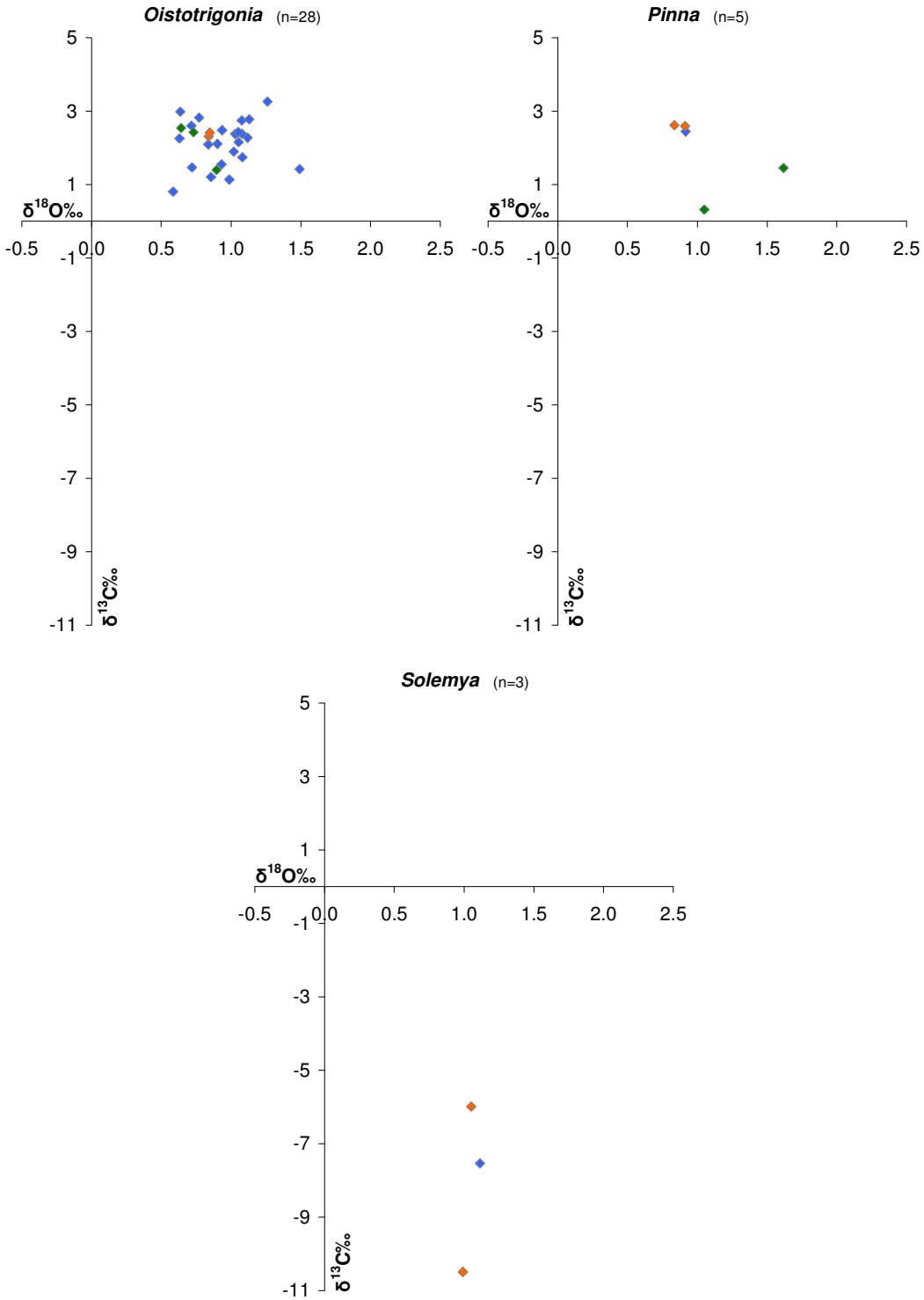

Figure E-4. Comparison of bivalve aragonite nacre shell material stable isotope data categorised by taxa. The 'Bivalve' category represents specimens where it was not possible to identify to a specific taxon but where the fragmentary shell material was of sufficient quality to pass diagenetic screening. Note that all $\delta^{18}O$ data were > 0.0‰. In all plots red symbols represent specimens for which no trace element diagenetic screening was carried out and the orange symbols represent specimens with Fe or Mn concentrations that exceeded the diagenetic threshold (Fe > 500 ppm and Mn > 200 ppm).

E.2 Bivalves

Table E-2. Screened stable isotope and trace element data for bivalve taxa. Stable isotope data reported as standard per mil (‰ VPDB) and trace element analyses (ppm) below detection limits = b/d. Temperature calculated using $\delta^{18}O_{Water}$ value of -1.2‰ (-1.0‰ SMOW).

Eselaevitrigonia	**$\delta^{13}C$**	**$\delta^{18}O$**	**Mg**	**Sr**	**Na**	**Fe**	**Mn**	**Temp (℃)**
D5.219.1185.2/I	2.66	1.09	20	5783	7945	58	44	10.7
D5.219.1138.3/C	1.92	1.49	24	3681	3712	19	61	8.9
D5.219.1125.2/C-2	0.37	1.31	136	2353	8919	120	3	9.7
D5.219.1125.2/C-1	2.79	1.12	179	2856	5194	450	b/d	10.5
D5.219.1096.3/H	2.80	1.69	105	1923	8207	101	5	8.1
D5.219.1096.3/I	0.28	1.10	144	2030	6247	222	9	10.6
D5.218.1016.2/J	2.34	0.70	15	1881	4504	b/d	7	12.4
D5.218.1016.2/N	2.56	1.01	83	2450	4058	16	21	11.0
D5.218.1016.2/L-2	2.81	0.87	32	1530	10044	24	11	11.6
D5.218.1016.2/K	2.05	0.77	56	1793	6551	78	2	12.0
D5.218.1016.2/L-1	1.96	0.81	70	1956	9603	133	13	11.9
D5.215.216.3/A-1	1.14	0.75	b/d	2609	3506	143	18	12.1
D5.215.216.3/A-2	1.00	0.86	5	2825	3873	453	119	11.6
D5.215.696.2/AN	2.89	1.59	80	3325	6260	b/d	32	8.5
D5.215.696.2/AQ	3.70	2.02	171	4341	8443	b/d	157	6.6
D5.215.691.2/D-1	3.68	1.94	101	3150	7236	b/d	52	7.0
D5.215.371.2/B	2.06	1.05	56	3363	3723	135	2	10.9
D5.215.361.2/C	2.28	1.75	105	3215	4432	b/d	13	7.8
D5.215.361.2/D	1.96	1.45	27	3049	3680	332	183	9.1
D5.215.357.2/B	0.26	1.60	131	2415	4797	12	37	8.4
D5.215.357.2/A	1.71	1.37	b/d	2296	4197	115	b/d	9.4
D5.215.352.2/A	1.31	1.91	88	3563	6919	b/d	59	7.1
D5.215.347.2/I	-5.06	1.25	418	4355	5726	59	174	9.9
D5.215.980.2/B	1.85	1.39	122	2236	3917	57	20	9.4
D5.215.910.1/A	1.53	1.13	149	1969	9846	b/d	b/d	10.5
Mean	1.71	1.28	93	2838	6062	101	42	9.8
Minima	-5.06	0.70						
Maxima	3.70	2.02						
Std Err	1.68	0.40						
Std Dev	1.69	0.39						
Count	25	25						
Confidence Level (95%)	3.30	0.78						

Lahillia	**$\delta^{13}C$**	**$\delta^{18}O$**	**Mg**	**Sr**	**Na**	**Fe**	**Mn**	**Temp (℃)**
D5.215.696.2/AV	3.29	1.47	42	3252	3977	137	28	9.0

Nucula	**$\delta^{13}C$**	**$\delta^{18}O$**	**Mg**	**Sr**	**Na**	**Fe**	**Mn**	**Temp (℃)**
D5.219.1182.2/A	2.01	0.86	42	5997	8276	204	13	11.7
D5.219.1091.2/F	2.67	1.67	178	2582	9797	131	b/d	8.2
D5.218.1021.2/E	3.65	1.90	129	4553	8214	18	16	7.1
D5.218.1021.2/G	1.72	1.77	402	5522	5997	368	81	7.7
D5.218.1016.2/C	1.61	0.49	13	2758	4538	b/d	5	13.2
D5.218.1016.2/B	1.70	0.92	77	1790	6967	38	130	11.4
D5.215.701.2/A	2.37	1.80	79	2885	4120	21	56	7.6
D5.215.696.2/AK	3.63	2.05	129	4810	3576	b/d	15	6.5
D5.215.696.2/AA	1.08	1.17	b/d	2559	3834	136	34	10.3
D5.215.696.2/AL	2.89	1.52	93	5005	3571	158	129	8.8
D5.215.691.2/C	2.25	1.82	119	3414	7290	23	16	7.5
D5.215.396.2/A	2.31	1.77	69	2308	4786	69	25	7.7
D5.215.347.2/A	-0.51	2.00	176	5700	5726	69	90	6.7
Mean	2.11	1.52	116	3837	5899	95	47	8.8

Nucula	**$\delta^{13}C$**	**$\delta^{18}O$**	**Mg**	**Sr**	**Na**	**Fe**	**Mn**	**Temp (°C)**
Minima	-0.51	0.49						
Maxima	3.65	2.05						
Std Err	1.10	0.46						
Std Dev	1.09	0.49						
Count	13	13						
Confidence Level (95%)	2.16	0.89						

Oistotrigonia	**$\delta^{13}C$**	**$\delta^{18}O$**	**Mg**	**Sr**	**Na**	**Fe**	**Mn**	**Temp (°C)**
D5.219.1138.3/B	1.42	1.49	29	3276	4251	48	25	8.9
D5.219.1125.2/E	2.37	1.03	98	2088	9197	9	1	10.9
D5.219.1125.2/D	2.43	1.05	103	1900	11234	47	2	10.8
D5.219.1122.2/D	1.47	0.72	b/d	1270	3582	198	b/d	12.3
D5.219.1106.2/C	2.77	1.13	96	1460	4357	58	2	10.5
D5.219.1091.2/I-2	2.82	0.77	b/d	1083	3715	181	b/d	12.0
D5.218.1006.2/O	2.39	1.08	134	2160	10856	165	10	10.7
D5.215.368.2/B	2.48	0.94	241	1494	4639	144	25	11.3
D5.215.327.2/A-2	2.09	0.84	125	1058	3995	b/d	135	11.8
D5.215.985.2/B	3.26	1.26	b/d	1431	6615	b/d	151	9.9
D5.215.980.2/A	2.98	0.64	b/d	1546	3662	106	94	12.6
D5.215.975.2/A	2.27	1.12	32	1646	4329	b/d	47	10.5
D5.215.975.2/B	0.81	0.59	b/d	1495	3464	86	56	12.9
D5.215.975.2/C	2.25	0.63	b/d	1339	3687	112	52	12.7
D5.215.930.2/A	2.74	1.08	56	1296	4323	b/d	130	10.7
D5.212.909.2/A	1.89	1.02	144	2000	4709	14	7	11.0
D5.212.865.3/A-1	2.10	0.90	56	1456	5613	b/d	b/d	11.5
D5.212.865.3/A-2	1.13	0.99	62	1345	4570	b/d	b/d	11.1
D5.212.865.3/G	1.20	0.86	49	1421	9235	71	b/d	11.7
D5.212.865.3/C	1.55	0.93	160	1136	12321	117	b/d	11.3
D5.212.865.3/B	1.74	1.08	127	1582	8921	213	4	10.7
D5.212.865.3/F	2.15	1.05	55	1412	5418	248	b/d	10.8
D5.212.860.2/A	2.60	0.72	b/d	1099	3697	168	b/d	12.3
Mean	2.13	0.95	68	1565	5930	86	32	11.3
Minima	0.81	0.59						
Maxima	3.26	1.49						
Std Err	0.64	0.22						
Std Dev	0.64	0.22						
Count	23	23						
Confidence Level (95%)	1.26	0.42						

Pinna	**$\delta^{13}C$**	**$\delta^{18}O$**	**Mg**	**Sr**	**Na**	**Fe**	**Mn**	**Temp (°C)**
D5.215.216.2/A	2.44	0.92	b/d	2541	3417	181	b/d	11.4

Solemya	**$\delta^{13}C$**	**$\delta^{18}O$**	**Mg**	**Sr**	**Na**	**Fe**	**Mn**	**Temp (°C)**
D5.215.347.2/M	-7.5	1.1	684	6768	2776	78	100	11

Bivalve	**$\delta^{13}C$**	**$\delta^{18}O$**	**Mg**	**Sr**	**Na**	**Fe**	**Mn**	**Temp (°C)**
D5.219.1149.1/A-2	2.40	1.42	68	2567	5215	155	b/d	9.3
D5.219.1138.3/A	1.41	1.25	26	2916	4116	177	20	10.0
D5.219.1125.2/G-1	2.70	1.32	3	192	695	b/d	b/d	9.7
D5.219.1125.2/L	1.94	1.05	53	1340	8365	11	b/d	10.8
D5.219.1125.2/G-2	2.19	1.39	33	1890	6637	25	1	9.4
D5.219.1125.2/M	1.21	1.34	63	2098	9489	48	2	9.6

High palaeolatitude record of Late Maastrichtian – Early Danian climate change, Seymour Island, Antarctica

Bivalve	$\delta^{13}C$	$\delta^{18}O$	Mg	Sr	Na	Fe	Mn	Temp (°C)
D5.219.1125.2/N	2.07	0.97	125	1428	6664	94	2	11.2
D5.219.1125.2/L	-0.04	0.86	40	1662	3567	240	b/d	11.6
D5.219.1091.2/H	2.26	1.41	36	2251	3680	350	b/d	9.3
D5.215.701.2/B	2.88	1.53	27	3157	3794	164	125	8.8
D5.215.378.2/A	2.18	1.91	71	2953	4732	56	14	7.1
D5.215.371.2/A	2.33	1.54	68	3366	3786	234	1	8.7
D5.215.361.2/B	2.45	1.80	95	3271	3970	b/d	56	7.6
D5.215.352.2/B	2.91	1.92	185	2925	6597	24	48	7.0
D5.212.909.2/B	2.19	1.01	83	1604	4436	64	b/d	11.0
D5.212.909.2/C	2.05	0.99	96	1609	7914	391	7	11.1
D5.212.870.2/A	2.52	1.11	38	1210	9178	106	b/d	10.6
D5.212.865.3/E	1.95	0.88	28	1395	5437	34	b/d	11.6
Mean	2.09	1.32	63	2102	5460	121	15	9.7
Minima	-0.04	0.86						
Maxima	2.91	1.92						
Std Err	0.67	0.35						
Std Dev	0.69	0.34						
Count	18	18						
Confidence Level (95%)	1.32	0.68						

E.3 Ammonites and nautiloids

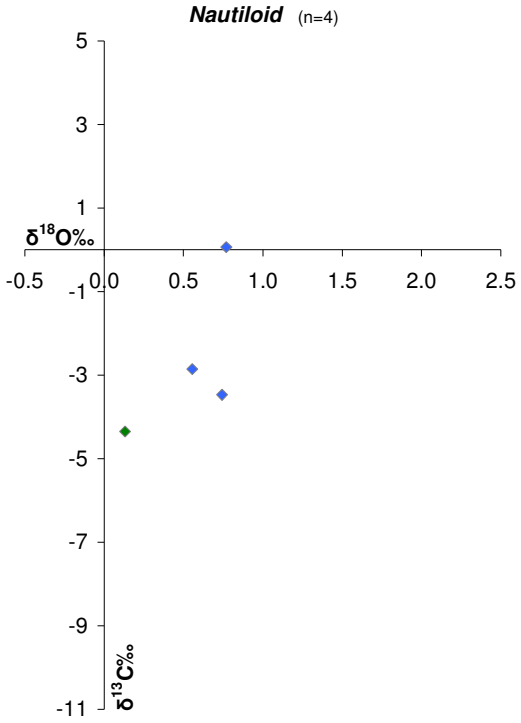

Figure E-5. Comparison of 'Nautiloid' aragonite nacre shell material stable isotope data represents specimens where it was not possible to identify to a specific taxon but where the fragmentary shell material was of sufficient quality to pass diagenetic screening. Note that all $\delta^{18}O$ data were > 0.0‰. In plot green symbols represent specimens for which no trace element diagenetic screening was carried out.

Table E-3. Screened stable isotope and trace element data for cephalopod taxa. Stable isotope data reported as standard per mil (‰ VPDB) and trace element analyses (ppm) below detection limits = b/d.

Diplomoceras	**$\delta^{13}C$**	**$\delta^{18}O$**	**Mg**	**Sr**	**Na**	**Fe**	**Mn**	**Temp (°C)**
D5.215.955.3/A	-1.63	1.44	426	4327	6719	179	61	9.1

Grossouvrites	**$\delta^{13}C$**	**$\delta^{18}O$**	**Mg**	**Sr**	**Na**	**Fe**	**Mn**	**Temp (°C)**
D5.215.691.2/B	-1.32	0.53	178	3195	7506	369	15	13.1

Maorites	**$\delta^{13}C$**	**$\delta^{18}O$**	**Mg**	**Sr**	**Na**	**Fe**	**Mn**	**Temp (°C)**
D5.220.1214.2/A	-2.71	1.33	529	4842	3660	52	136	9.6
D5.218.1021.2/V	-5.18	0.78	301	7202	3856	135	124	12.0
D5.218.1006.2/I	-0.89	1.24	157	4911	6432	115	29	10.0
D5.215.696.2/Q	1.18	0.76	535	2964	3895	375	15	12.1
D5.215.691.2/A	-2.86	1.03	289	6496	6074	117	146	10.9
Mean	-2.09	1.03	362	5283	4783	159	90	10.9
Minima	-5.18	0.76						
Maxima	1.18	1.33						
Std Err	2.69	0.23						
Std Dev	2.38	0.26						
Count	5	5						
Confidence Level (95%)	5.27	0.45						

Ammonite	**$\delta^{13}C$**	**$\delta^{18}O$**	**Mg**	**Sr**	**Na**	**Fe**	**Mn**	**Temp (°C)**
D5.218.1027.2/B	-3.96	0.99	293	6412	3993	377	56	11.1
D5.218.1016.2/O	-2.72	1.03	100	1524	4933	63	2	10.9
D5.215.696.2/AR	0.54	1.27	174	4110	4298	35	24	9.9
D5.215.696.2/AT	0.24	0.88	93	4382	3199	483	5	11.6
Mean	-1.48	1.04	165	4107	4106	240	22	10.9
Minima	-3.96	0.88						
Maxima	0.54	1.27						
Std Err	0.15	0.20						
Std Dev	2.22	0.17						
Count	4	4						
Confidence Level (95%)	0.29	0.39						

Nautiloid	**$\delta^{13}C$**	**$\delta^{18}O$**	**Mg**	**Sr**	**Na**	**Fe**	**Mn**	**Temp (°C)**
D5.229.1292.2/A-2	-2.86	0.56	14	594	377	12	7	13.0
D5.229.1292.2/A-1	-3.47	0.74	207	6139	3675	419	128	12.2
D5.222.1257.2/A	0.06	0.77	466	3982	8943	b/d	14	12.1
Mean	-2.09	0.69	229	3572	4332	144	49	12.4
Minima	-3.47	0.56						
Maxima	0.06	0.77						
Std Err	0.43	0.13						
Std Dev	1.89	0.12						
Count	3	3						
Confidence Level (95%)	0.85	0.26						

E.4 Gastropods

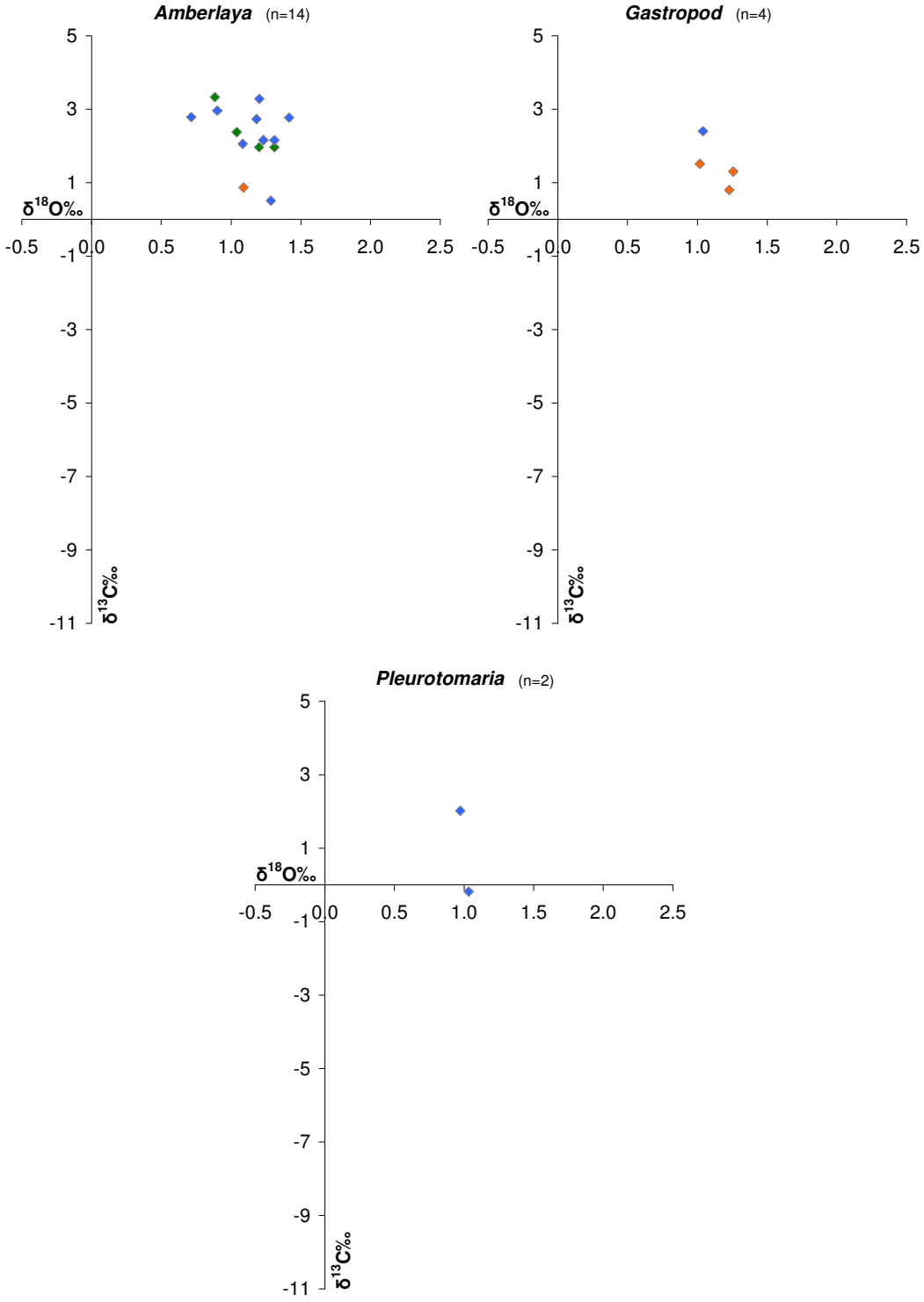

Figure E-6. Comparison of gastropod aragonite stable isotope data categorised by taxa. The 'Gastropod' category represents specimens where it was not possible to identify to a specific taxon but where the fragmentary shell material was of sufficient quality to pass diagenetic screening. Note that all $\delta^{18}O$ data were > 0.0‰. In all plots green symbols represent specimens for which no trace element diagenetic screening was carried out and the orange symbols represent specimens with Fe or Mn concentrations that exceeded the diagenetic threshold (Fe > 500 ppm and Mn > 200 ppm).

Table E-4. Screened stable isotope and trace element data for gastropod taxa. Stable isotope data reported as standard per mil (‰ VPDB) and trace element analyses (ppm) below detection limits = b/d.

Amberlaya	**$\delta^{13}C$**	**$\delta^{18}O$**	**Mg**	**Sr**	**Na**	**Fe**	**Mn**	**Temp (℃)**
D5.222.1255.2/A	2.96	0.90	34	1940	10760	b/d	190	11.5
D5.218.1021.2/A-2	2.16	1.23	107	3403	4622	b/d	84	10.0
D5.218.1021.2/A-1	2.15	1.31	108	3710	5440	47	91	9.7
D5.218.1021.2/C	2.77	1.42	85	2543	8544	76	76	9.2
D5.218.1016.2/D	2.06	1.08	89	3334	4989	273	8	10.7
D5.215.696.2/AU	0.51	1.29	190	5213	4548	b/d	49	9.8
D5.215.696.2/P	2.73	1.18	239	2949	7159	40	50	10.3
D5.215.686.2/A	3.28	1.20	112	2219	7735	29	34	10.2
D5.215.368.2/C	2.78	0.72	39	3074	3834	115	25	12.3
Mean	2.38	1.15	111	3154	6403	64	67	10.4
Minima	0.51	0.72						
Maxima	3.28	1.42						
Std Err	0.85	0.23						
Std Dev	0.81	0.22						
Count	9	9						
Confidence Level (95%)	1.67	0.45						

Pleurotomaria	**$\delta^{13}C$**	**$\delta^{18}O$**	**Mg**	**Sr**	**Na**	**Fe**	**Mn**	**Temp (℃)**
D5.218.1021.2/B	-0.19	1.03	107	4256	8695	140	37	10.9
D5.215.216.5/A	2.02	0.97	71	3128	4238	b/d	10	11.2
Mean	0.92	1.00	89	3692	6467	70	24	11.1
Minima	-0.19	0.97						
Maxima	2.02	1.03						
Count	2	2						

Gastropod	**$\delta^{13}C$**	**$\delta^{18}O$**	**Mg**	**Sr**	**Na**	**Fe**	**Mn**	**Temp (℃)**
D5.215.361.2/A	2.40	1.04	87	2001	4491	b/d	19	10.9

E.5 Unidentified fossil types

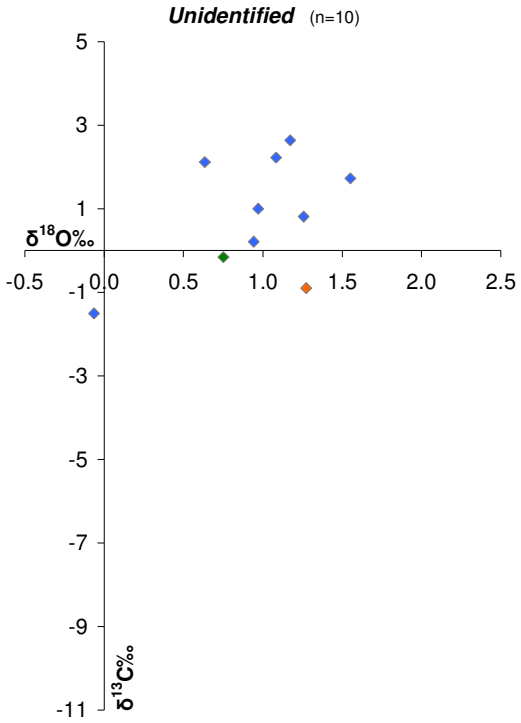

Figure E-7. Comparison of screened stable isotope data from unidentified aragonite nacre shell material. This category represents specimens where it was not possible to identify a specific taxon or fossil type but where the fragmentary shell material was of sufficient quality to pass diagenetic screening. Note that all screened $\delta^{18}O$ data were > -0.06‰. In all plots green symbols represent specimens for which no trace element diagenetic screening was carried out and the orange symbols represent specimens with Fe or Mn concentrations that exceeded the diagenetic threshold (Fe > 500 ppm and Mn > 200 ppm).

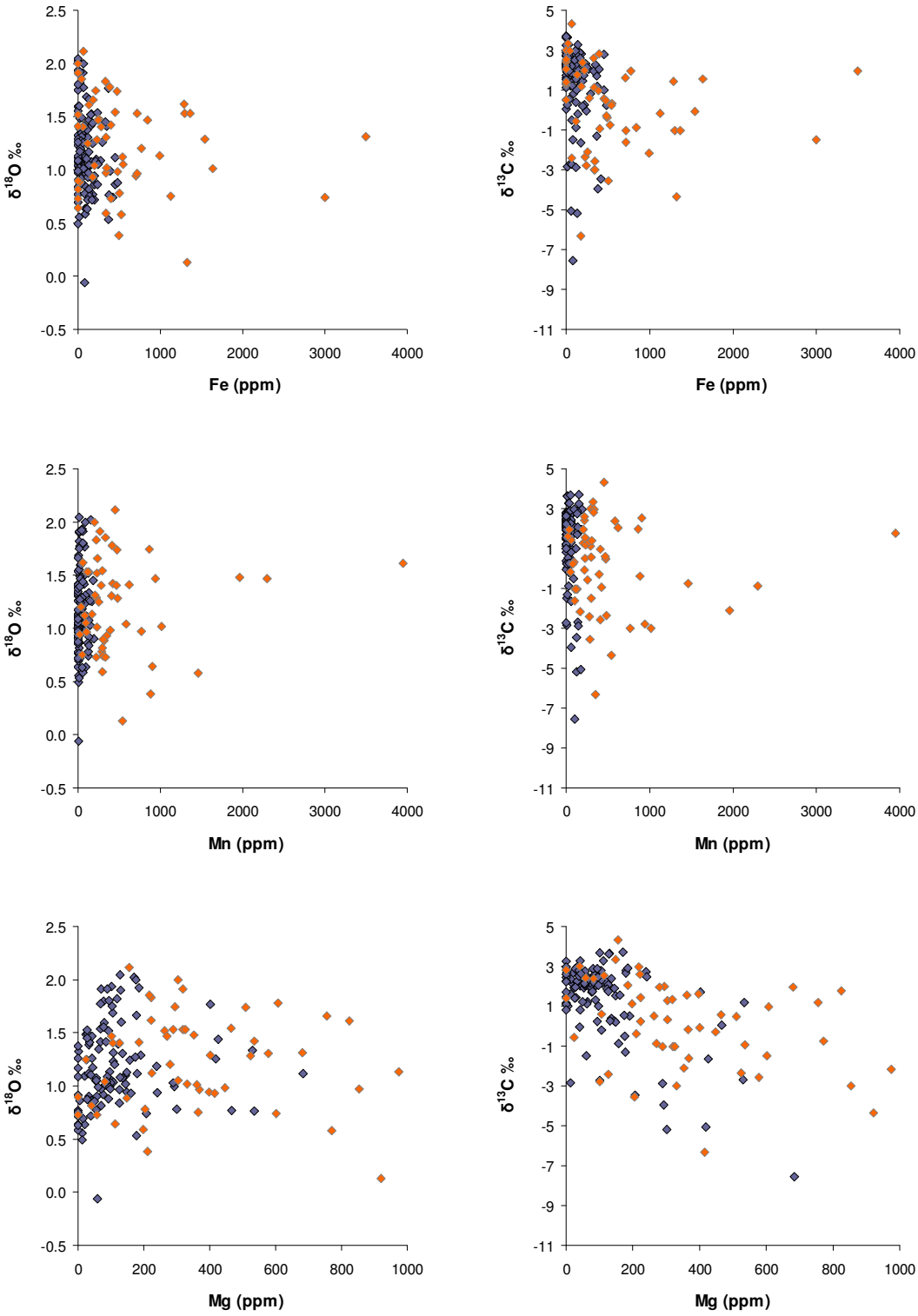

Figure E-8. Covariance plots of screened $\delta^{18}O$ and $\delta^{13}C$ vs screened trace element concentrations (Fe, Mn and Mg all ppm) as determined by ICP-OES analysis. In both plots blue symbols represent specimens exhibiting Mg < 1000 ppm, Fe < 500 ppm and Mn < 200 ppm and orange symbols represent specimens with Fe or Mn concentrations that exceeded the diagenetic threshold (Fe > 500 ppm and Mn > 200 ppm). In no case does the inclusion of specimens with elevated levels of either Fe or Mn result in an expansion of the overall range of the stable isotope data.

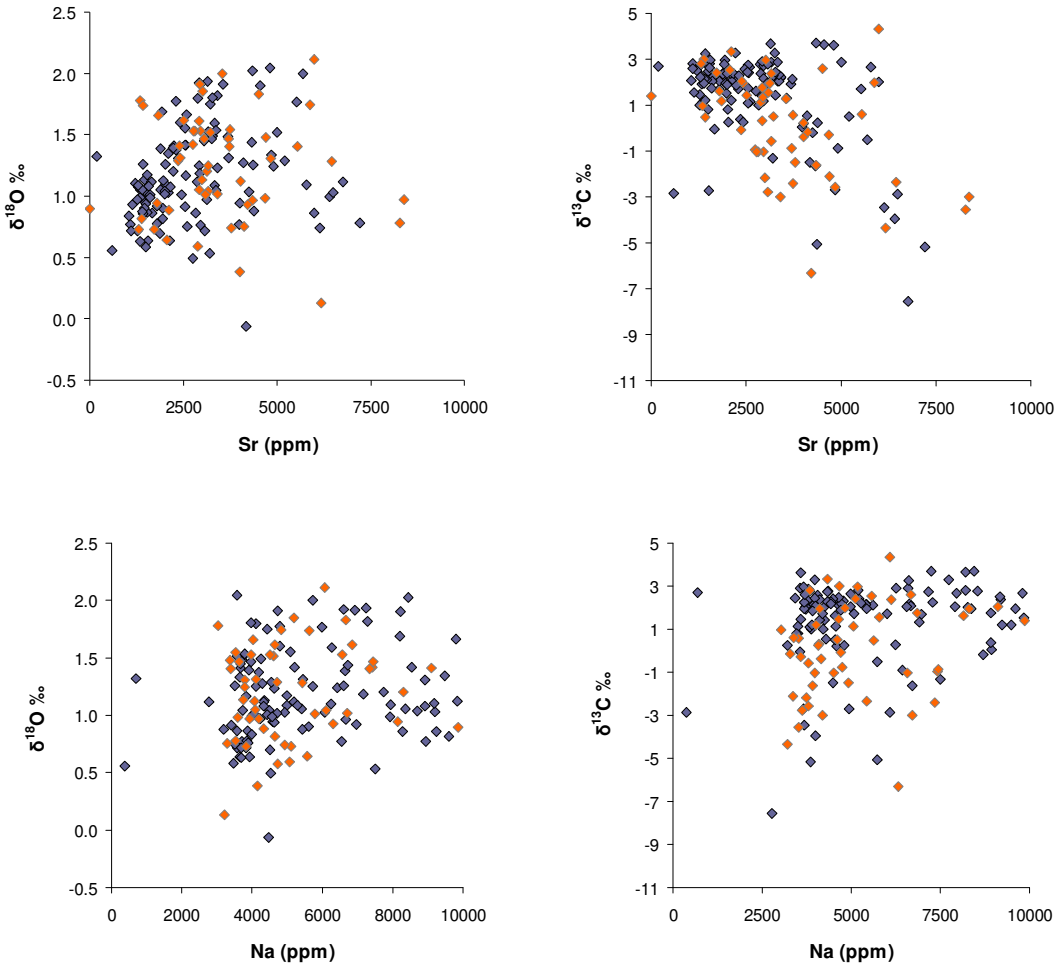

Figure E-9. Covariance plots of partially screened $\delta^{18}O$ and $\delta^{13}C$ vs trace element concentrations (Sr and Na all ppm) as determined by ICP-OES analysis. In both plots blue symbols represent specimens exhibiting Mg < 1000 ppm, Fe < 500 ppm and Mn < 200 ppm and orange symbols represent specimens with Fe or Mn concentrations that exceeded the diagenetic threshold (Fe > 500 ppm and Mn > 200 ppm). In neither case does the stable isotope data covary with the respective trace element.

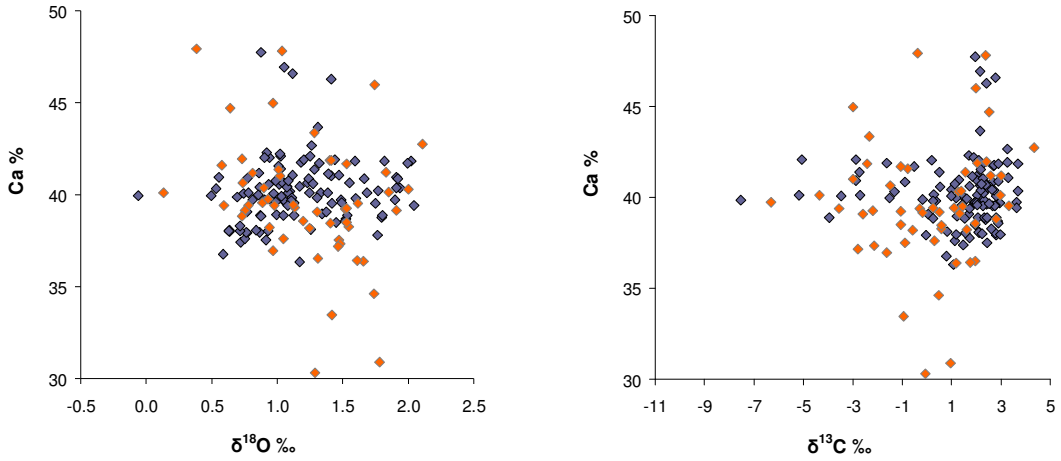

Figure E-10. Covariance plots of partially screened data for Ca (%) vs $\delta^{18}O$ and $\delta^{13}C$. In both plots blue symbols represent specimens exhibiting Mg < 1000 ppm, Fe < 500 ppm and Mn < 200 ppm and orange symbols represent specimens with Fe or Mn concentrations that exceeded the diagenetic threshold (Fe > 500 ppm and Mn > 200 ppm). In neither case does the stable isotope data covary with the Ca content of the analysed shell material.

Table E-5. Screened stable isotope and trace element data from unidentified fossil types. Stable isotope data reported as standard per mil (‰ VPDB) and trace element analyses (ppm) below detection limits = b/d.

Unidentified	$\delta^{13}C$	$\delta^{18}O$	Mg	Sr	Na	Fe	Mn	Temp (℃)
D5.229.1353.2/C	2.12	0.64	21	2142	3932	92	b/d	12.6
D5.222.1254.1/A	-1.51	-0.06	60	4170	4479	83	11	15.7
D5.219.1091.2/G	0.81	1.26	42	2024	3505	295	b/d	9.9
D5.218.1021.2/W	0.21	0.94	148	4008	4594	201	20	11.3
D5.215.368.2/A	1.73	1.55	78	2550	5080	b/d	12	8.7
D5.212.855.2/B	2.64	1.17	45	1541	4986	20	b/d	10.3
D5.212.855.2/C	1.00	0.97	97	1272	4216	123	b/d	11.2
D5.212.833.2/A	2.22	1.08	b/d	1287	5283	b/d	b/d	10.7
Mean	1.15	0.94	61	2374	4509	102	5	11.3
Minima	-1.51	-0.06						
Maxima	2.64	1.55						
Std Err	1.28	0.40						
Std Dev	1.35	0.49						
Count	8	8						
Confidence Level (95%)	2.50	0.79						

E.6 Clumped isotope $\delta^{18}O_{Water}$ values

Table E-6. Values of $\delta^{18}O_{Water}$ calculated from clumped isotope temperature data reported by Petersen *et al*. (2016). Data derived from the analysis of late Maastrichtian bivalves collected on Seymour Island. Stratigraphic height adjusted to reflect the BAS D5 stratigraphy (where D5 depth (m) = Petersen *et al*. (2016) depth – 30 m).

Depth (m)	Age (Ma)	$\delta^{18}O_{Water}$	Depth (m)	Age (Ma)	$\delta^{18}O_{Water}$
1068	65.808	-3.01	895	66.971	-0.09
1068	65.808	-1.92	895	66.971	-1.49
1037	65.995	-2.19	895	66.971	-0.20
1037	65.995	-1.63	895	66.971	1.05
1029	66.043	-2.60	857	67.346	0.67
1029	66.043	-2.46	857	67.346	-0.68
1029	66.043	-0.48	857	67.346	-0.06
1029	66.043	-0.71	827	67.643	-0.80
1028	66.048	-0.51	827	67.643	-2.58
1028	66.048	-1.89	825	67.663	-0.95
1028	66.048	-1.90	825	67.663	-2.91
1028	66.048	-1.93	825	67.663	0.03
1021	66.080	-1.93	808	67.830	0.63
1021	66.080	-1.00	808	67.830	-1.06
1002	66.169	-1.17	795	67.959	-1.77
1002	66.169	-1.85	795	67.959	0.22
995	66.202	-0.73	678	68.728	-1.19
995	66.202	-0.67	678	68.728	-3.42
986	66.244	-3.33	663	68.800	-3.34
986	66.244	-0.88	663	68.800	-3.07
972	66.309	-2.55	663	68.800	-1.47
972	66.309	-1.31	663	68.800	-1.43
943	66.497	-2.82	633	68.943	-1.45
943	66.497	-0.12	633	68.943	-1.21
902	66.902	-0.10	629	68.963	-1.96
895	66.971	0.42	629	68.963	-1.94

E.6 Clumped isotope derived temperatures

Table E-7. Palaeotemperatures derived from clumped isotope data, calculated from clumped isotope derived values for $\delta^{18}O_{water}$ and from $\delta^{18}O$ with ocean water ($\delta^{18}O_{water}$) = -1.2‰ (SMOW = -1‰). All stable isotope measurements generated from aragonitic bivalve shell material. Note the considerable temperature ranges reported, especially the presence of sub-zero values (All data from Petersen *et al*., 2016). Stratigraphic positions represent the BAS D5 sampling scheme.

Strat. Ht. (m)	Age (Ma)	$\delta^{18}O$	$\delta^{18}O_{water}$	Temperature (°C)		
				Cl. Isotope	$\delta^{18}O_{water}$	SMOW = -1.0‰
1068	65.808	0.704	-3.01	0.7	4.5	12.3
1068	65.808	1.268	-1.92	2.9	6.8	9.9
1037	65.995	0.487	-2.19	5.1	9.0	13.3
1037	65.995	0.408	-1.63	7.9	11.8	13.6
1029	66.043	-0.205	-2.60	6.4	10.2	16.3
1029	66.043	-0.244	-2.46	7.1	11.0	16.5
1029	66.043	0.502	-0.48	12.6	16.3	13.2
1029	66.043	0.689	-0.71	10.7	14.5	12.4
1028	66.048	0.620	-0.51	12.3	15.7	12.7
1028	66.048	0.269	-1.89	7.4	11.2	14.2
1028	66.048	0.678	-1.90	5.6	9.4	12.4
1028	66.048	1.079	-1.93	3.6	7.5	10.7
1021	66.080	0.621	-1.93	5.6	9.5	12.7

High palaeolatitude record of Late Maastrichtian – Early Danian climate change, Seymour Island, Antarctica

Strat. Ht. (m)	Age (Ma)	$\delta^{18}O$	$\delta^{18}O_{water}$	Temperature (°C)		
				Cl. Isotope	$\delta^{18}O_{water}$	SMOW = -1.0‰
1021	66.080	0.998	-1.00	8.3	11.9	11.1
1002	66.169	0.640	-1.17	8.9	12.8	12.6
1002	66.169	0.042	-1.85	8.5	12.4	15.2
995	66.202	0.988	-0.73	9.3	13.1	11.1
995	66.202	0.004	-0.67	14.0	17.7	15.4
986	66.244	0.596	-3.33	-0.2	3.6	12.8
986	66.244	1.043	-0.88	8.4	12.2	10.9
972	66.309	0.696	-2.55	2.6	6.5	12.4
972	66.309	0.566	-1.31	8.6	12.5	12.9
943	66.497	0.697	-2.82	1.7	5.4	12.4
943	66.497	1.557	-0.12	9.5	13.3	8.6
902	66.902	1.278	-0.10	10.8	14.6	9.8
895	66.971	1.343	0.42	12.9	16.6	9.6
895	66.971	0.577	-0.09	14.2	17.7	12.9
895	66.971	0.948	-1.49	6.2	10.0	11.3
895	66.971	1.457	-0.20	9.6	13.4	9.1
895	66.971	1.592	1.05	14.8	18.3	8.5
857	67.346	1.288	0.67	14.3	17.9	9.8
857	67.346	1.135	-0.68	8.8	12.7	10.5
857	67.346	0.982	-0.06	12.7	16.1	11.1
827	67.643	1.110	-0.80	8.5	12.3	10.6
827	67.643	0.285	-2.58	4.3	8.2	14.2
825	67.663	0.964	-0.95	8.9	12.3	11.2
825	67.663	0.197	-2.91	3.7	7.1	14.5
825	67.663	1.159	0.03	11.9	15.7	10.4
808	67.830	1.094	0.63	15.0	18.6	10.6
808	67.830	-0.091	-1.06	12.7	16.4	15.8
795	67.959	0.523	-1.77	6.8	10.7	13.1
795	67.959	1.051	0.22	13.4	17.0	10.8
678	68.728	0.971	-1.19	7.4	11.2	11.2
678	68.728	-0.184	-3.42	2.6	6.5	16.2
663	68.800	1.245	-3.34	-2.8	0.7	10.0
663	68.800	1.105	-3.07	-1.2	2.5	10.6
663	68.800	0.579	-1.47	8.1	11.7	12.9
663	68.800	0.485	-1.43	8.4	12.3	13.3
633	68.943	0.804	-1.45	6.9	10.8	11.9
633	68.943	0.534	-1.21	9.2	13.0	13.1
629	68.963	0.890	-1.96	4.3	8.2	11.5
629	68.963	0.610	-1.94	5.6	9.5	12.7

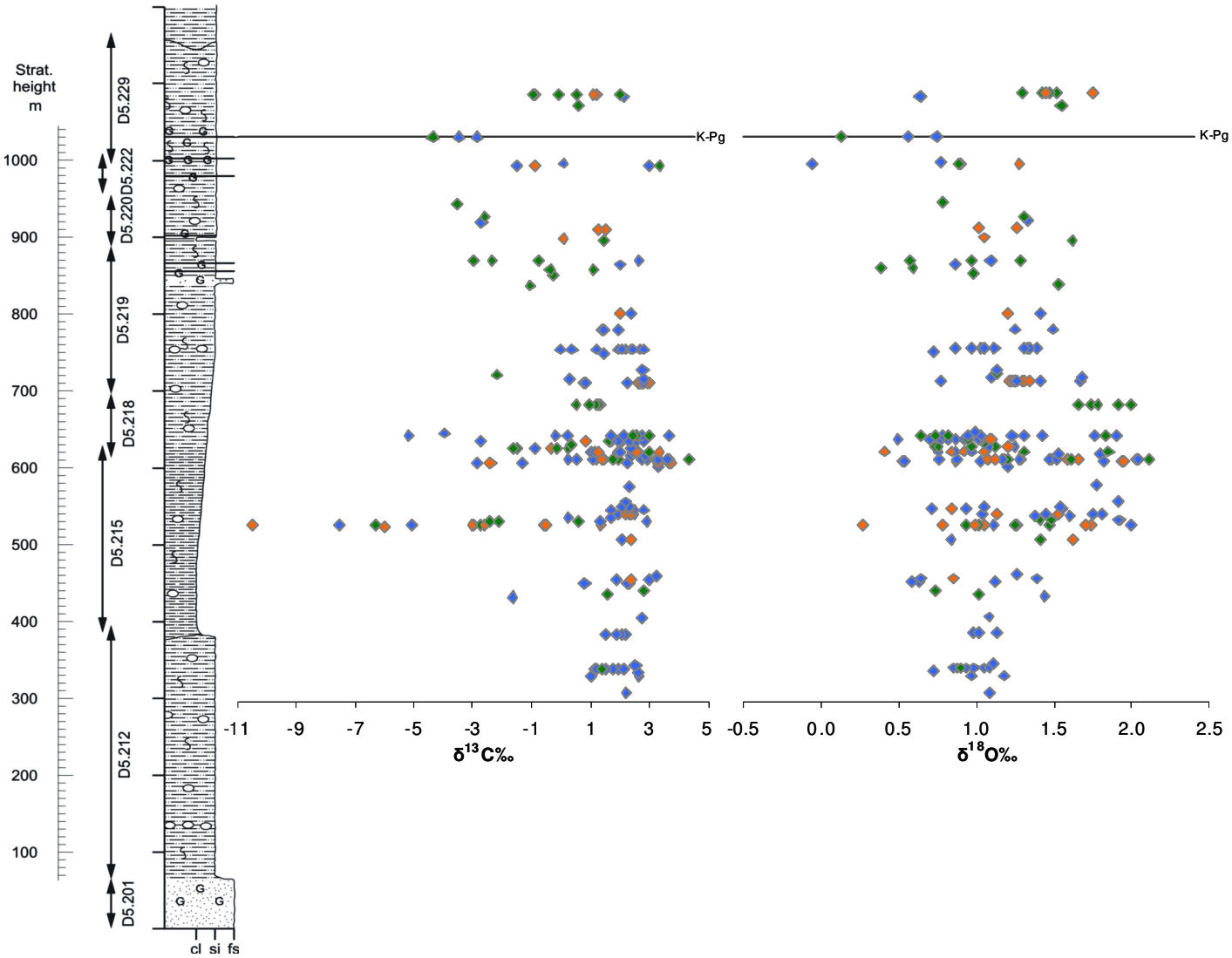

Figure E-11. Latest Maastrichtian section on Seymour Island, Antarctica showing position of screened aragonite $\delta^{13}C$ and $\delta^{18}O$ data (n=213).
Position of the K-Pg boundary (1029 m above section base) defined by palynological analysis (Thorn *et al.*, 2009). Note the good data coverage above 300 m except in section D5.229 where gaps reflect a lack of suitable macrofossil specimens. No specimens were deemed suitable for isotopic analysis at stratigraphic positions below 300 m. In both plots blue symbols represent specimens exhibiting Mg < 1000 ppm, Fe < 500 ppm and Mn < 200 ppm; green symbols represent specimens for which no trace element diagenetic screening was carried out and orange symbols represent specimens with Fe or Mn concentrations that exceeded the diagenetic threshold (Fe > 500 ppm and Mn > 200 ppm). The 3 most negative $\delta^{13}C$ values represent specimens of the bivalve *Solemya rossiana* that have thiotrophic chemosymbionts involved in the anaerobic oxidation of methane (Little *et al.*, 2015).

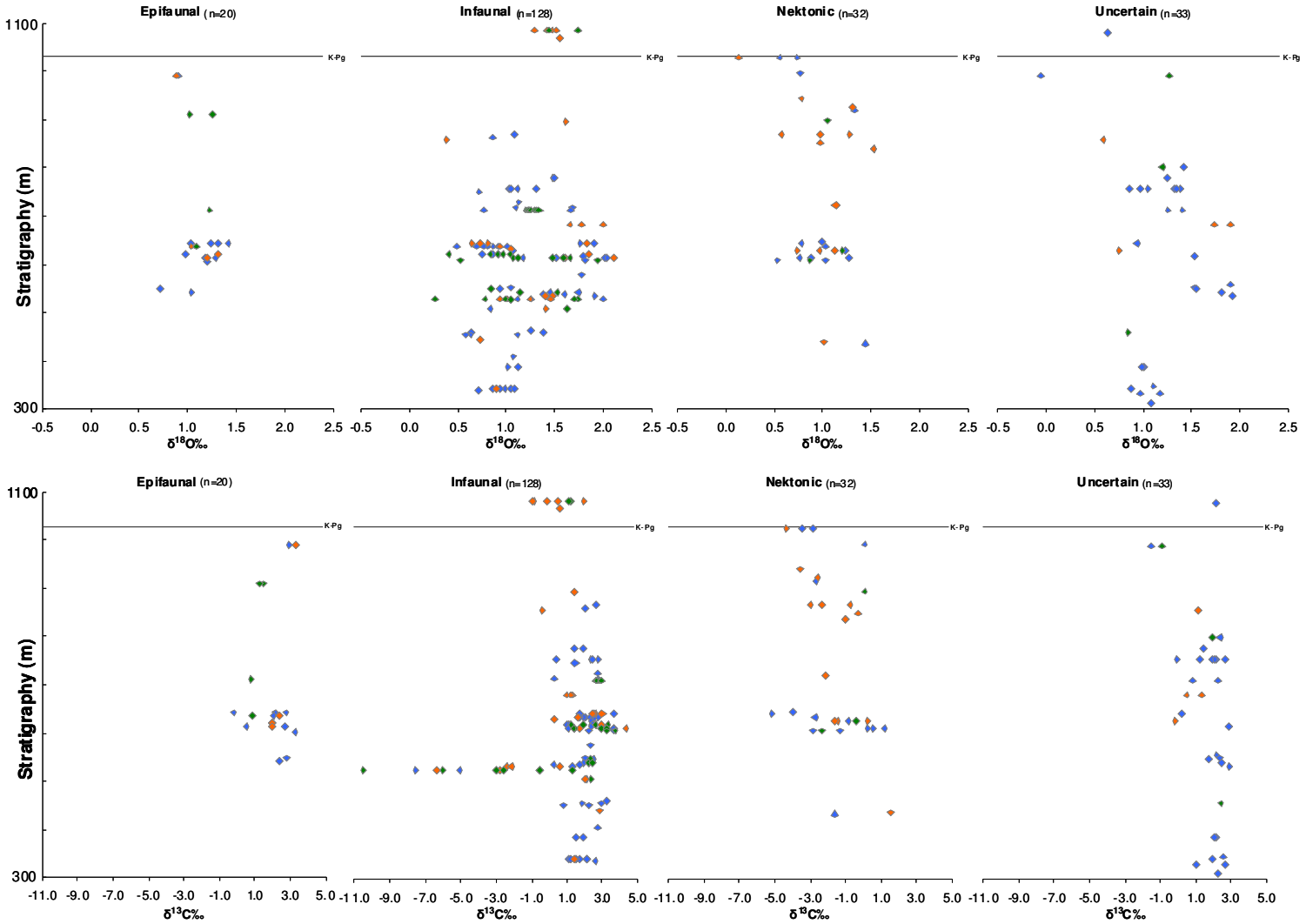

Figure E-12. Stratigraphy vs. $\delta^{13}C$ and $\delta^{18}O$ data derived from screened aragonite categorised by habitat. K-Pg boundary inferred from palynology (Thorn *et al.*, 2009). Note the wide variability in data exhibited by the bivalve samples. The 'Uncertain' category represents specimens where it was not possible to identify to either a specific fossil type or taxon but where the fragmentary shell material was of sufficient quality to pass diagenetic screening. Note that with the exception of a single datapoint in the 'Uncertain' category (-0.06‰) all $\delta^{18}O$ data were > 0.0‰. In both plots blue symbols represent specimens exhibiting Mg < 1000 ppm, Fe < 500 ppm and Mn < 200 ppm; green symbols represent specimens for which no trace element diagenetic screening was carried out and orange symbols represent specimens with Fe or Mn concentrations that exceeded the diagenetic threshold (Fe > 500 ppm and Mn > 200 ppm).

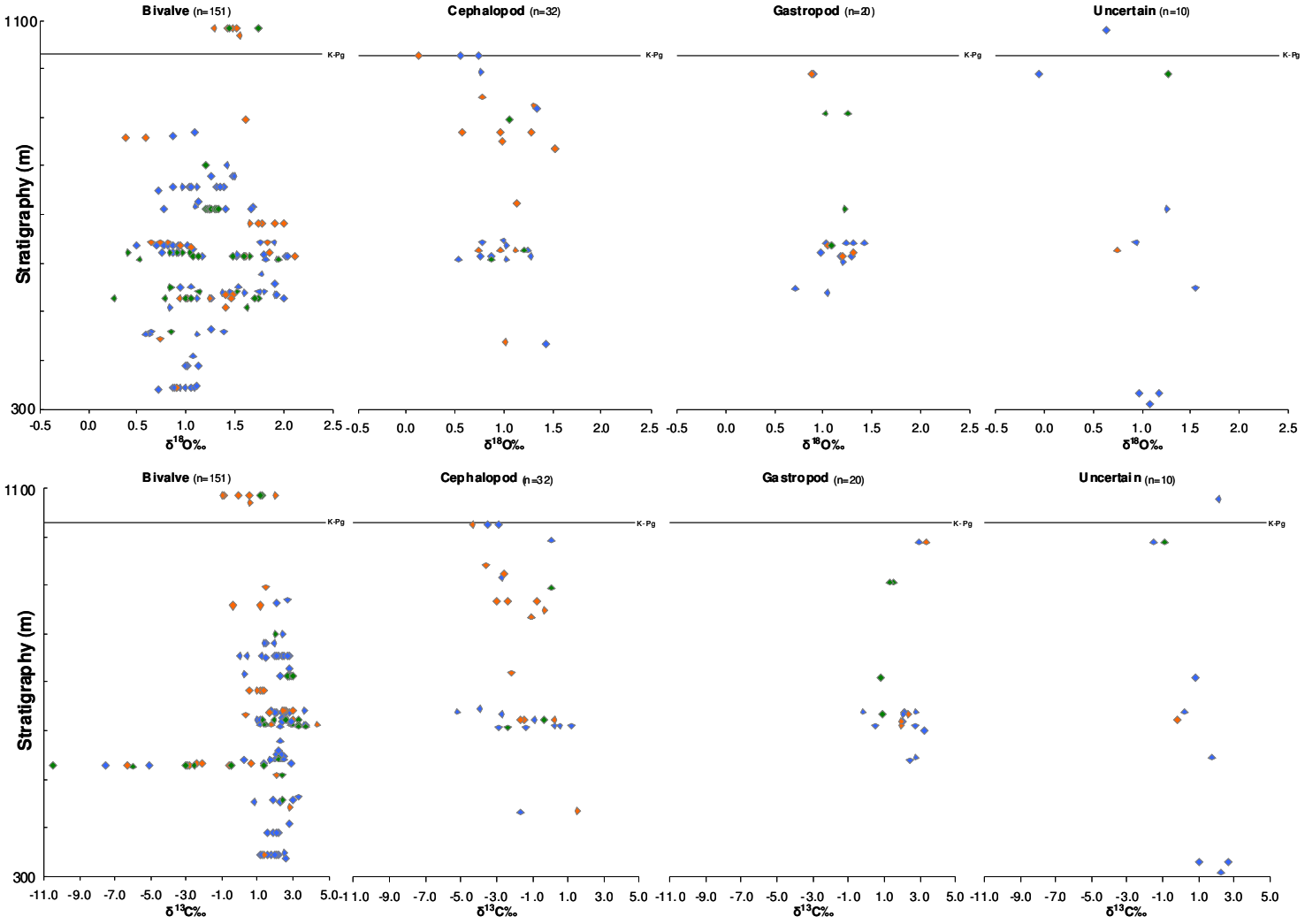

Figure E-13. Stratigraphy vs. partially screened aragonite $\delta^{13}C$ and $\delta^{18}O$ data categorised by fossil type. K-Pg boundary inferred from palynology (Thorn *et al.*, 2009). Note the wide variability in data exhibited by the bivalve samples. The $\delta^{13}C$ and $\delta^{18}O$ data have respective ranges of ~16‰ and ~1.95‰. The 3 lightest $\delta^{13}C$ values represent specimens of the bivalve *Solemya rossiana* that have thiotrophic chemosymbionts involved in the anaerobic oxidation of methane (Little *et al.*, 2015). The 'Uncertain' category represents specimens where it was not possible to identify either a specific fossil type or taxon but the shell material passed diagenetic screening. Note that with the exception of a single value in the 'Uncertain' category (-0.06‰) all $\delta^{18}O$ data were > 0.0‰. Blue symbols represent specimens exhibiting Mg < 1000 ppm, Fe < 500 ppm and Mn < 200 ppm; green symbols represent specimens for which no trace element diagenetic screening was carried out and orange symbols represent specimens with Fe or Mn concentrations that exceeded the diagenetic threshold (Fe > 500 ppm and Mn > 200 ppm).

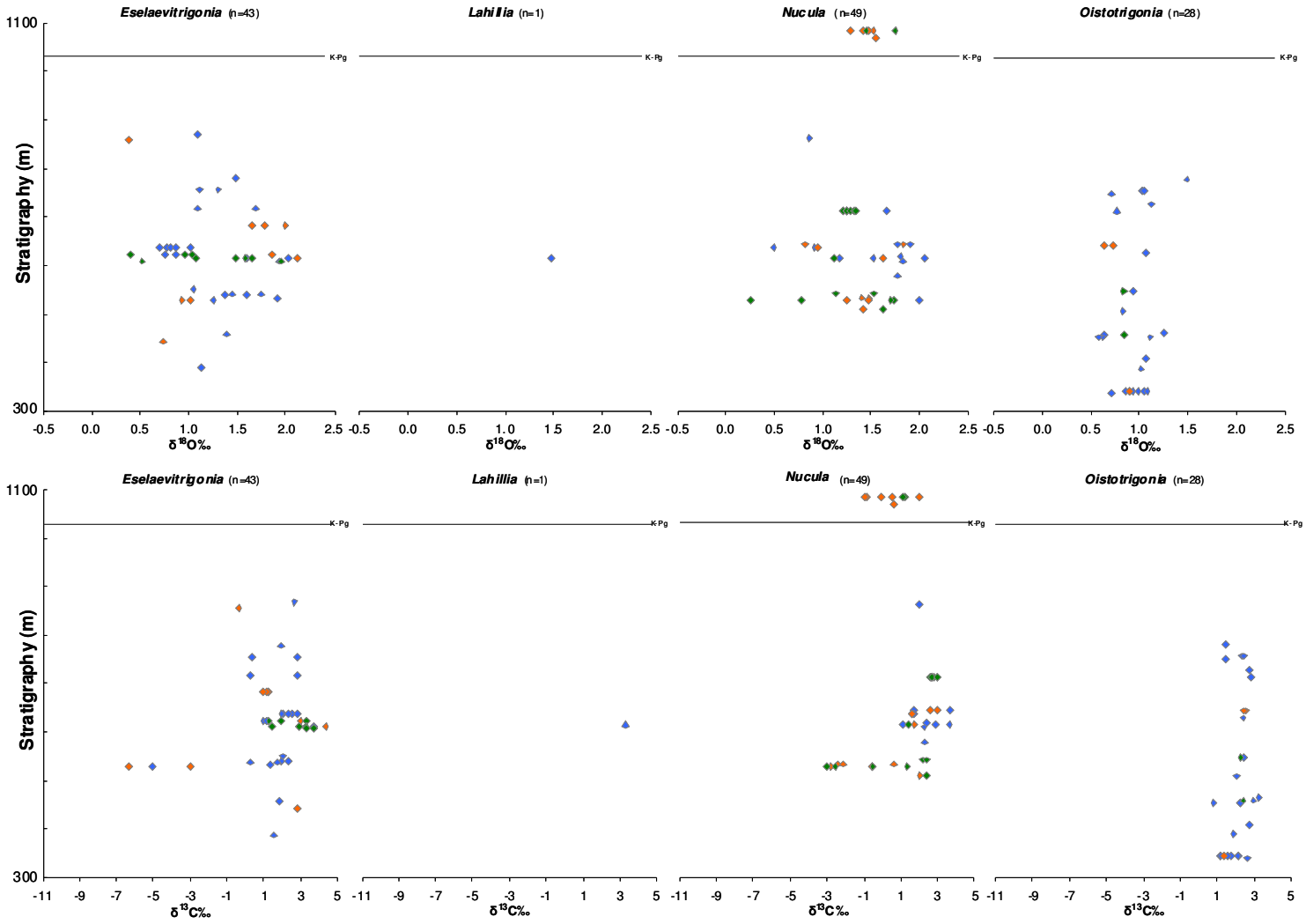

Figure E-14. Stratigraphy vs. partially screened aragonite $\delta^{13}C$ and $\delta^{18}O$ data categorised by bivalve genus. K-Pg boundary inferred from palynology (Thorn *et al.*, 2009). Note the wide variability in data exhibited by the bivalve samples. The 'Uncertain' category represents specimens where it was not possible to identify to either a specific fossil type or taxon but where the fragmentary shell material was of sufficient quality to pass diagenetic screening. Note that with the exception of a single datapoint in the 'Uncertain' category (-0.06‰) all $\delta^{18}O$ data were > 0.0‰. In both plots blue symbols represent specimens exhibiting Mg < 1000 ppm, Fe < 500 ppm and Mn < 200 ppm; green symbols represent specimens for which no trace element diagenetic screening was carried out and orange symbols represent specimens with Fe or Mn concentrations that exceeded the diagenetic threshold (Fe > 500 ppm and Mn > 200 ppm).

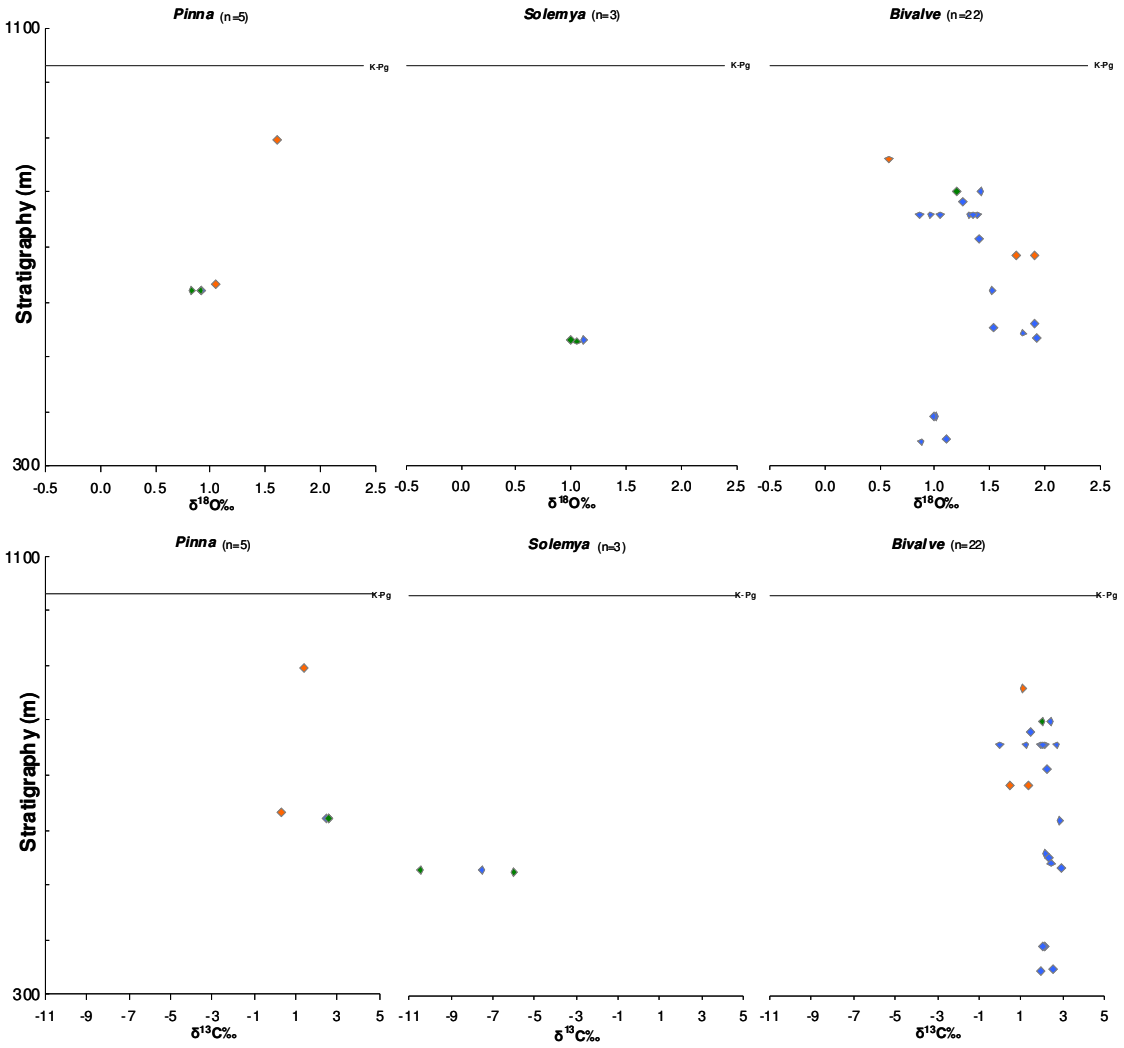

Figure E-15. Stratigraphy vs. partially screened aragonite $\delta^{13}C$ and $\delta^{18}O$ data categorised by gastropod genus. K-Pg boundary inferred from palynology (Thorn *et al.*, 2009). Note the wide variability in data exhibited by the bivalve samples. The 'Uncertain' category represents specimens where it was not possible to identify to either a specific fossil type or taxon but where the fragmentary shell material was of sufficient quality to pass diagenetic screening. Note that with the exception of a single datapoint in the 'Uncertain' category (-0.06‰) all $\delta^{18}O$ data were > 0.0‰. In both plots blue symbols represent specimens exhibiting Mg < 1000 ppm, Fe < 500 ppm and Mn < 200 ppm; green symbols represent specimens for which no trace element diagenetic screening was carried out and orange symbols represent specimens with Fe or Mn concentrations that exceeded the diagenetic threshold (Fe > 500 ppm and Mn > 200 ppm).

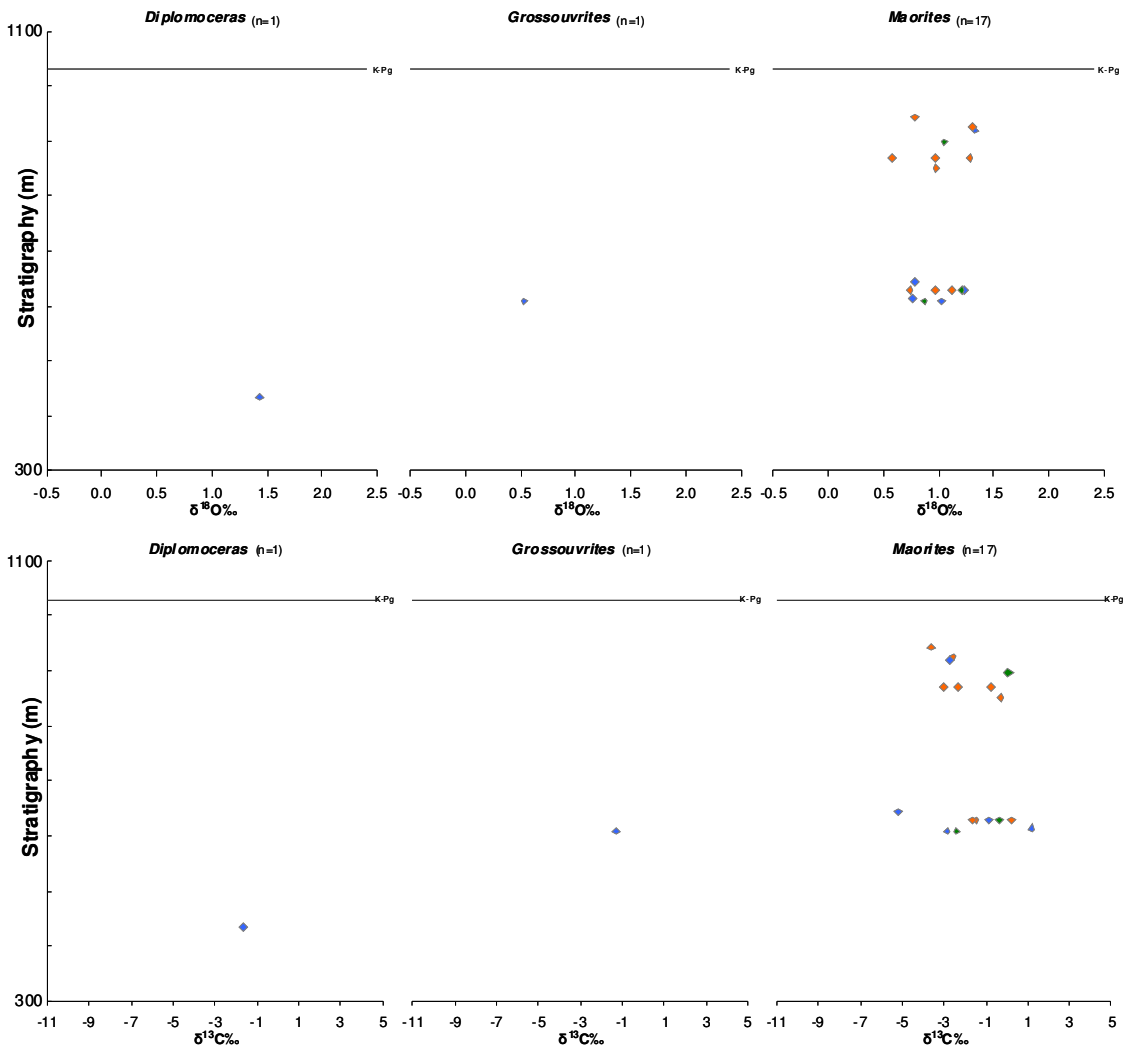

Figure E-16. Stratigraphy vs. partially screened aragonite $\delta^{13}C$ and $\delta^{18}O$ ammonite data categorised by genus. K-Pg boundary inferred from palynology (Thorn *et al.*, 2009). Note the wide variability in data exhibited by the bivalve samples. The 'Uncertain' category represents specimens where it was not possible to identify to either a specific fossil type or taxon but where the fragmentary shell material was of sufficient quality to pass diagenetic screening. Note that with the exception of a single datapoint in the 'Uncertain' category (-0.06‰) all $\delta^{18}O$ data were > 0.0‰. In both plots blue symbols represent specimens exhibiting Mg < 1000 ppm, Fe < 500 ppm and Mn < 200 ppm; green symbols represent specimens for which no trace element diagenetic screening was carried out and orange symbols represent specimens with Fe or Mn concentrations that exceeded the diagenetic threshold (Fe > 500 ppm and Mn > 200 ppm).

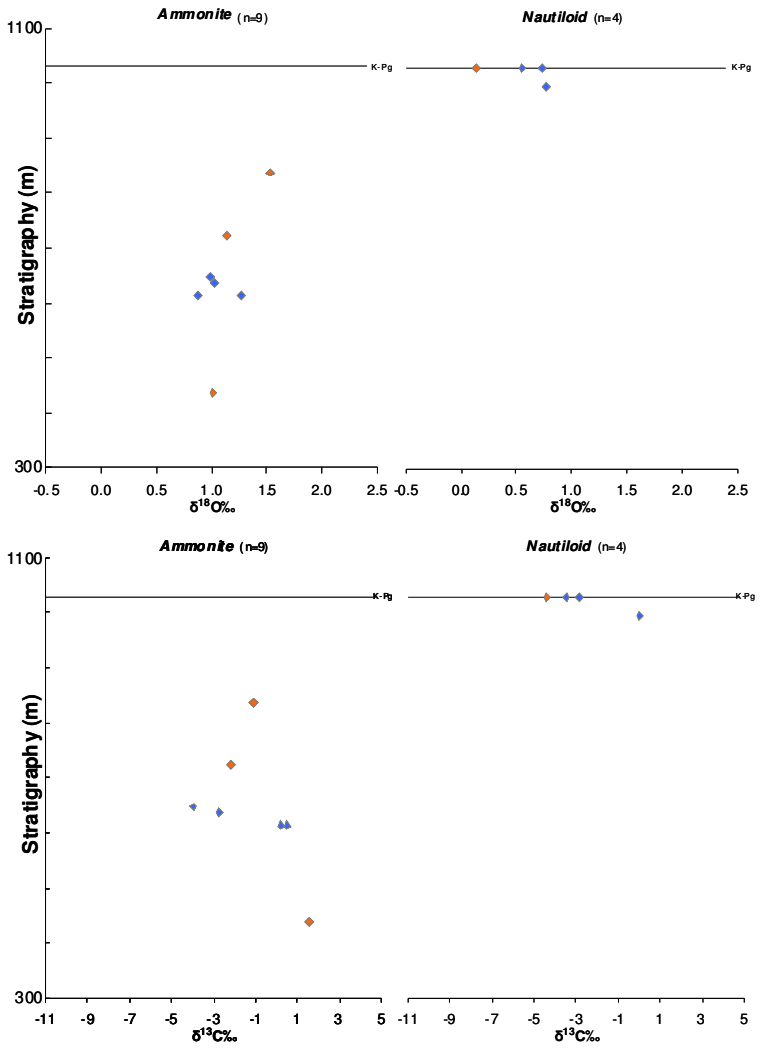

Figure E-17. Stratigraphy vs. partially screened aragonite $\delta^{13}C$ and $\delta^{18}O$ data categorised for ammonites and nautiloids where genus was unidentified. K-Pg boundary inferred from palynology (Thorn *et al.*, 2009). Note the wide variability in data exhibited by the bivalve samples. The 'Uncertain' category represents specimens where it was not possible to identify to either a specific fossil type or taxon but where the fragmentary shell material was of sufficient quality to pass diagenetic screening. Note that with the exception of a single datapoint in the 'Uncertain' category (-0.06‰) all $\delta^{18}O$ data were > 0.0‰. In both plots blue symbols represent specimens exhibiting Mg < 1000 ppm, Fe < 500 ppm and Mn < 200 ppm; green symbols represent specimens for which no trace element diagenetic screening was carried out and orange symbols represent specimens with Fe or Mn concentrations that exceeded the diagenetic threshold (Fe > 500 ppm and Mn > 200 ppm).

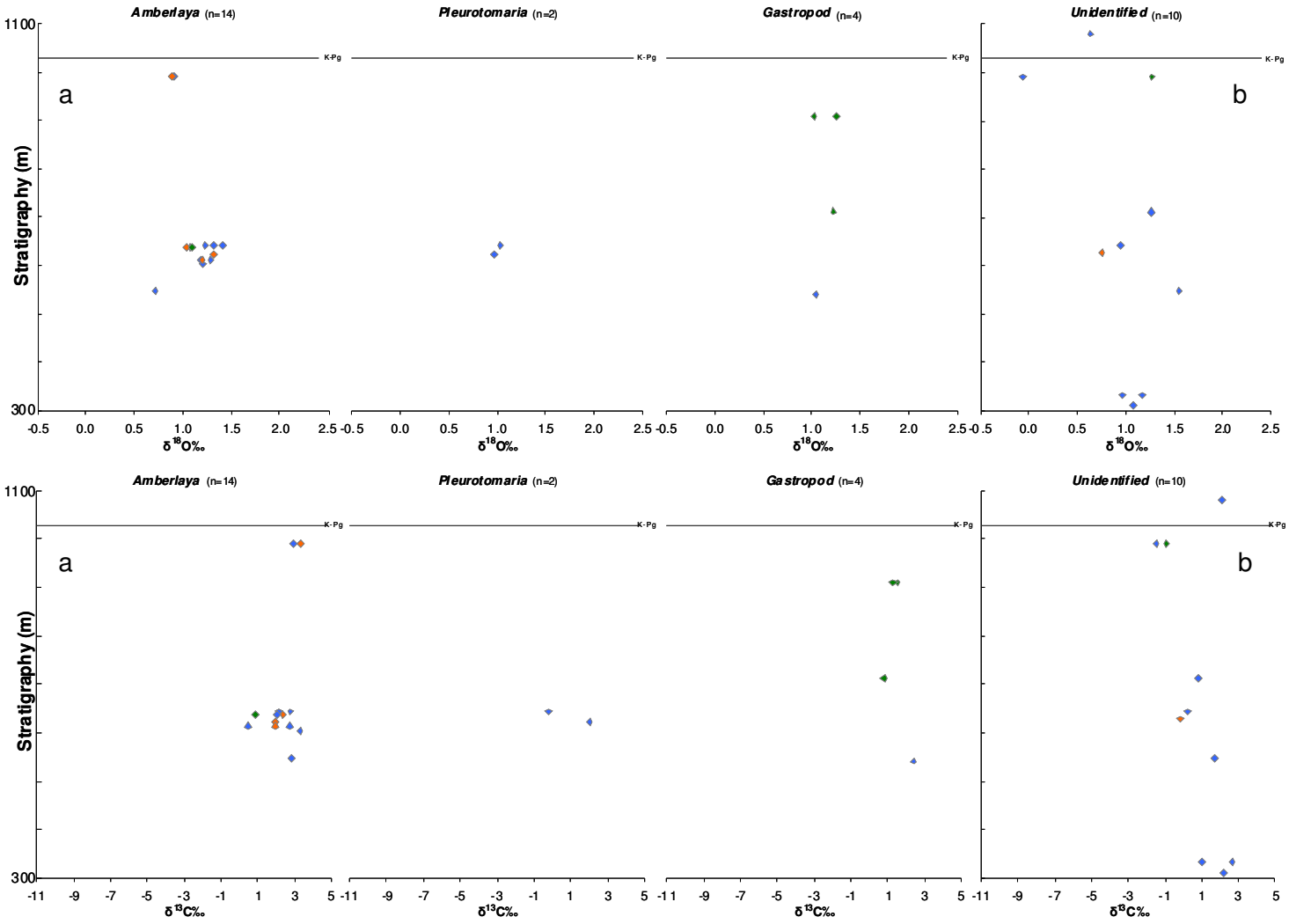

Figure E-18. Stratigraphy vs. partially screened aragonite $\delta^{13}C$ and $\delta^{18}O$ data categorised by gastropod genus (a) and unidentified shell material (b). K-Pg boundary inferred from palynology (Thorn *et al.*, 2009). Note the wide variability in data exhibited by the bivalve samples. The 'Uncertain' category represents specimens where it was not possible to identify to either a specific fossil type or taxon but where the fragmentary shell material was of sufficient quality to pass diagenetic screening. Note that with the exception of a single datapoint in the 'Uncertain' category (-0.06‰) all $\delta^{18}O$ data were > 0.0‰. In both plots blue symbols represent specimens exhibiting Mg < 1000 ppm, Fe < 500 ppm and Mn < 200 ppm; green symbols represent specimens for which no trace element diagenetic screening was carried out and orange symbols represent specimens with Fe or Mn concentrations that exceeded the diagenetic threshold (Fe > 500 ppm and Mn > 200 ppm).

Table E-7. Stable isotope and calculated palaeotemperature coverage for the measured stratigraphy.

Depth (m)	No	$\delta^{13}C$‰			$\delta^{18}O$‰			SMOW = -0.8‰		SMOW = -1.0‰		SMOW = -1.2‰		SMOW = -1.5‰		$\delta^{13}C$‰ Range	$\delta^{18}O$‰ Range
		Mean	Min	Max	Mean	Min	Max	Min (℃)	Max (℃)	Min (℃)	Max (℃)	Min (℃)	Max (℃)	Min (℃)	Max (℃)		
1084	7	0.42	-0.95	1.99	1.52	1.29	1.74	8.7	10.7	7.8	9.8	7.0	8.9	5.7	7.6	2.94	0.46
1080	1	2.12	2.12	2.12	0.64	0.64	0.64	13.5	13.5	12.6	12.6	11.8	11.8	10.5	10.5	0.00	0.00
1068	1	0.58	0.58	0.58	1.55	1.55	1.55	9.6	9.6	8.7	8.7	7.8	7.8	6.5	6.5	0.00	0.00
1029										**K-Pg boundary**							
1028	3	-3.56	-4.35	-2.86	0.48	0.13	0.74	13.0	15.7	12.2	14.8	11.3	14.0	10.0	12.7	1.49	0.61
995	1	0.06	0.06	0.06	0.77	0.77	0.77	12.9	12.9	12.1	12.1	11.2	11.2	9.9	9.9	0.00	0.00
991	4	0.97	-1.51	3.33	0.75	-0.06	1.27	10.7	16.5	9.9	15.7	9.0	14.8	7.7	13.5	4.83	1.34
943	1	-3.56	-3.56	-3.56	0.78	0.78	0.78	12.9	12.9	12.0	12.0	11.1	11.1	9.8	9.8	0.00	0.00
925	1	-2.58	-2.58	-2.58	1.31	1.31	1.31	10.6	10.6	9.7	9.7	8.8	8.8	7.5	7.5	0.00	0.00
919	1	-2.71	-2.71	-2.71	1.33	1.33	1.33	10.5	10.5	9.6	9.6	8.7	8.7	7.4	7.4	0.00	0.00
909	2	1.41	1.30	1.51	1.14	1.02	1.26	10.8	11.8	9.9	11.0	9.1	10.1	7.8	8.8	0.21	0.24
897	1	0.08	0.08	0.08	1.05	1.05	1.05	11.7	11.7	10.8	10.8	10.0	10.0	8.7	8.7	0.00	0.00
895	1	1.45	1.45	1.45	1.62	1.62	1.62	9.2	9.2	8.4	8.4	7.5	7.5	6.2	6.2	0.00	0.00
869	4	-0.86	-2.99	2.66	0.98	0.58	1.28	10.7	13.8	9.8	12.9	9.0	12.0	7.7	10.7	5.65	0.71
863	1	2.01	2.01	2.01	0.86	0.86	0.86	12.5	12.5	11.7	11.7	10.8	10.8	9.5	9.5	0.00	0.00
857	2	0.37	-0.38	1.12	0.49	0.38	0.59	13.7	14.6	12.8	13.7	12.0	12.9	10.7	11.6	1.50	0.21
851	1	-0.29	-0.29	-0.29	0.98	0.98	0.98	12.0	12.0	11.1	11.1	10.3	10.3	9.0	9.0	0.00	0.00
837	3	-1.04	-1.04	-1.04	1.53	1.53	1.53	9.6	9.6	8.8	8.8	7.9	7.9	6.6	6.6	0.00	0.00
800	2	2.20	1.99	2.40	1.31	1.20	1.42	10.1	11.0	9.3	10.2	8.4	9.3	7.1	8.0	0.41	0.21
779	3	1.58	1.41	1.92	1.41	1.25	1.49	9.8	10.8	8.9	10.0	8.1	9.1	6.8	7.8	0.51	0.24
755	10	1.80	-0.04	2.79	1.14	0.86	1.39	10.2	12.5	9.4	11.6	8.5	10.8	7.2	9.5	2.83	0.52
749	1	1.47	1.47	1.47	0.72	0.72	0.72	13.1	13.1	12.3	12.3	11.4	11.4	10.1	10.1	0.00	0.00
727	1	2.77	2.77	2.77	1.13	1.13	1.13	11.4	11.4	10.5	10.5	9.6	9.6	8.3	8.3	0.00	0.00
722	1	-2.18	-2.18	-2.18	1.13	1.13	1.13	11.3	11.3	10.5	10.5	9.6	9.6	8.3	8.3	0.00	0.00
717	2	1.54	0.28	2.80	1.39	1.10	1.69	8.9	11.5	8.1	10.6	7.2	9.8	5.9	8.5	2.53	0.59
712	15	2.46	0.80	2.97	1.26	0.77	1.67	9.0	12.9	8.2	12.0	7.3	11.2	6.0	9.9	2.18	0.89
682	5	1.06	0.49	1.34	1.82	1.66	2.00	7.6	9.1	6.7	8.2	5.8	7.3	4.5	6.0	0.86	0.34
647	1	-3.96	-3.96	-3.96	0.99	0.99	0.99	12.0	12.0	11.1	11.1	10.2	10.2	8.9	8.9	0.00	0.00
642	12	1.49	-5.18	3.65	1.20	0.64	1.90	8.0	13.5	7.1	12.6	6.3	11.7	5.0	10.4	8.82	1.26
637	12	1.60	-2.72	2.81	0.90	0.49	1.09	11.5	14.1	10.7	13.2	9.8	12.4	8.5	11.1	5.53	0.60

Depth (m)	No	$\delta^{13}C$‰			$\delta^{18}O$‰			SMOW = -0.8‰		SMOW = -1.0‰		SMOW = -1.2‰		SMOW = -1.5‰		$\delta^{13}C$‰ Range	$\delta^{18}O$‰ Range
		Mean	Min	Max	Mean	Min	Max	Min (℃)	Max (℃)	Min (℃)	Max (℃)	Min (℃)	Max (℃)	Min (℃)	Max (℃)		
632	1	0.32	0.32	0.32	1.05	1.05	1.05	11.7	11.7	10.8	10.8	10.0	10.0	8.7	8.7	0.00	0.00
627	7	-0.27	-1.62	2.39	1.01	0.74	1.24	10.9	13.1	10.0	12.2	9.1	11.3	7.8	10.0	4.00	0.50
622	11	2.12	1.00	3.31	0.98	0.40	1.85	8.2	14.5	7.4	13.6	6.5	12.8	5.2	11.5	2.31	1.45
618	2	2.63	2.37	2.88	1.66	1.53	1.80	8.5	9.6	7.6	8.8	6.7	7.9	5.4	6.6	0.50	0.27
613	19	2.26	0.24	4.34	1.42	0.76	2.11	7.1	13.0	6.2	12.1	5.4	11.2	4.1	9.9	4.09	1.35
608	7	0.91	-2.86	3.73	1.24	0.52	1.95	7.8	14.0	6.9	13.1	6.1	12.3	4.8	11.0	6.59	1.43
603	1	3.28	3.28	3.28	1.20	1.20	1.20	11.0	11.0	10.2	10.2	9.3	9.3	8.0	8.0	0.00	0.00
578	1	2.31	2.31	2.31	1.77	1.77	1.77	8.6	8.6	7.7	7.7	6.8	6.8	5.5	5.5	0.00	0.00
558	1	2.18	2.18	2.18	1.91	1.91	1.91	8.0	8.0	7.1	7.1	6.2	6.2	4.9	4.9	0.00	0.00
551	2	2.19	2.06	2.33	1.29	1.05	1.54	9.6	11.7	8.7	10.9	7.9	10.0	6.6	8.7	0.27	0.49
548	4	2.32	1.73	2.78	1.01	0.72	1.55	9.5	13.2	8.7	12.3	7.8	11.4	6.5	10.1	1.05	0.84
541	6	2.28	1.96	2.45	1.45	1.04	1.80	8.4	11.7	7.6	10.9	6.7	10.0	5.4	8.7	0.49	0.76
538	2	0.98	0.26	1.71	1.49	1.37	1.60	9.3	10.3	8.4	9.4	7.6	8.6	6.3	7.3	1.46	0.23
533	5	0.06	-2.42	2.91	1.63	1.40	1.92	7.9	10.2	7.0	9.3	6.2	8.4	4.9	7.1	5.33	0.52
528	12	-3.41	-10.49	1.36	1.21	0.26	2.00	7.6	15.1	6.7	14.3	5.8	13.4	4.5	12.1	11.85	1.74
526	1	-5.99	-5.99	-5.99	1.05	1.05	1.05	11.7	11.7	10.8	10.8	10.0	10.0	8.7	8.7	0.00	0.00
508	3	2.17	2.04	2.38	1.29	0.84	1.62	9.2	12.6	8.4	11.8	7.5	10.9	6.2	9.6	0.34	0.78
463	1	3.26	3.26	3.26	1.26	1.26	1.26	10.8	10.8	9.9	9.9	9.1	9.1	7.7	7.7	0.00	0.00
458	3	2.41	1.85	2.98	0.96	0.64	1.39	10.2	13.5	9.4	12.6	8.5	11.8	7.2	10.5	1.14	0.76
453	3	1.78	0.81	2.27	0.78	0.59	1.12	11.4	13.7	10.5	12.9	9.7	12.0	8.4	10.7	1.47	0.53
443	1	2.82	2.82	2.82	0.73	0.73	0.73	13.1	13.1	12.2	12.2	11.4	11.4	10.0	10.0	0.00	0.00
438	1	1.56	1.56	1.56	1.01	1.01	1.01	11.9	11.9	11.0	11.0	10.1	10.1	8.8	8.8	0.00	0.00
435	1	-1.63	-1.63	-1.63	1.44	1.44	1.44	10.0	10.0	9.1	9.1	8.3	8.3	7.0	7.0	0.00	0.00
408	1	2.74	2.74	2.74	1.08	1.08	1.08	11.6	11.6	10.7	10.7	9.8	9.8	8.5	8.5	0.00	0.00
388	4	1.92	1.53	2.19	1.04	0.99	1.13	11.4	12.0	10.5	11.1	9.6	10.2	8.3	8.9	0.67	0.14
348	1	2.52	2.52	2.52	1.11	1.11	1.11	11.5	11.5	10.6	10.6	9.7	9.7	8.4	8.4	0.00	0.00
343	8	1.65	1.13	2.15	0.95	0.86	1.08	11.6	12.5	10.7	11.7	9.8	10.8	8.5	9.5	1.02	0.22
338	1	2.60	2.60	2.60	0.72	0.72	0.72	13.2	13.2	12.3	12.3	11.4	11.4	10.1	10.1	0.00	0.00
333	2	1.82	1.00	2.64	1.07	0.97	1.17	11.2	12.0	10.3	11.2	9.4	10.3	8.1	9.0	1.64	0.20
311	1	2.22	2.22	2.22	1.08	1.08	1.08	11.6	11.6	10.7	10.7	9.8	9.8	8.5	8.5	0.00	0.00

Table E-8. Stable isotope and calculated palaeotemperature coverage categorised by fossil type, habitat, mode of life and genus.

Category	No	$\delta^{13}C$‰			$\delta^{18}O$‰			SMOW = -0.8‰		SMOW = -1.0‰		SMOW = -1.2‰		SMOW = -1.5‰		$\delta^{13}C$‰ Range	$\delta^{18}O$‰ Range
		Mean	Min	Max	Mean	Min	Max	Min (℃)	Max (℃)	Min (℃)	Max (℃)	Min (℃)	Max (℃)	Min (℃)	Max (℃)		
Bivalve	151	1.51	-10.49	4.34	1.25	0.26	2.11	7.1	15.1	6.2	14.3	5.4	13.4	4.1	12.1	14.83	1.85
Cephalopod	32	-1.62	-5.18	1.56	1.00	0.13	1.53	9.6	15.7	8.8	14.8	7.9	14.0	6.6	12.7	6.74	1.40
Gastropod	20	1.99	-0.19	3.33	1.12	0.72	1.42	10.1	13.2	9.2	12.3	8.4	11.4	7.1	10.1	3.51	0.70
Uncertain	10	0.82	-1.51	2.64	0.96	-0.06	1.55	9.5	16.5	8.7	15.7	7.8	14.8	6.5	13.5	4.15	1.61
Habitat																	
Epifaunal	20	1.99	-0.19	3.33	1.12	0.72	1.42	10.1	13.2	9.2	12.3	8.4	11.4	7.1	10.1	3.51	0.70
Infaunal	128	1.43	-10.49	4.34	1.24	0.26	2.11	7.1	15.1	6.2	14.3	5.4	13.4	4.1	12.1	14.83	1.85
Nektonic	31	-1.62	-5.18	1.56	0.99	0.13	1.53	9.6	15.7	8.8	14.8	7.9	14.0	6.6	12.7	6.74	1.40
Planktonic	1	-1.63	-1.63	-1.63	1.44	1.44	1.44	10.0	10.0	9.1	9.1	8.3	8.3	7.0	7.0	N/A	N/A
Uncertain	33	1.61	-1.51	2.91	1.20	-0.06	1.92	7.9	16.5	7.0	15.7	6.2	14.8	4.9	13.5	4.41	1.99
Mode of life																	
Browser	2	0.92	-0.19	2.02	1.00	0.97	1.03	11.8	12.0	10.9	11.2	10.0	10.3	8.7	9.0	2.20	0.06
Carnivore	32	-1.62	-5.18	1.56	1.00	0.13	1.53	9.6	15.7	8.8	14.8	7.9	14.0	6.6	12.7	6.74	1.40
Carn/scavenger	17	2.09	0.51	3.33	1.14	0.72	1.42	10.1	13.2	9.2	12.3	8.4	11.4	7.1	10.1	2.82	0.70
Deposit	49	1.34	-3.01	3.65	1.39	0.26	2.05	7.4	15.1	6.5	14.3	5.6	13.4	4.3	12.1	6.65	1.78
Suspension	79	1.49	-10.49	4.34	1.14	0.38	2.11	7.1	14.6	6.2	13.7	5.4	12.9	4.1	11.6	14.83	1.73
Uncertain	34	1.63	-1.51	2.91	1.19	-0.06	1.92	7.9	16.5	7.0	15.7	6.2	14.8	4.9	13.5	4.41	1.99
Genus																	
Amberlaya	14	2.28	0.51	3.33	1.13	0.72	1.42	10.1	13.2	9.2	12.3	8.4	11.4	7.1	10.1	2.82	0.70
Ammonite	9	-1.07	-3.96	1.56	1.21	0.88	1.53	9.6	12.4	8.8	11.6	7.9	10.7	6.6	9.4	5.52	0.65
Bivalve	22	1.93	-0.04	2.91	1.32	0.59	1.92	7.9	13.7	7.0	12.8	6.2	12.0	4.9	10.7	2.95	1.33
Diplomoceras	1	-1.63	-1.63	-1.63	1.44	1.44	1.44	10.0	10.0	9.1	9.1	8.3	8.3	7.0	7.0	N/A	N/A
Eselaevitrigonia	43	1.66	-6.31	4.34	1.28	0.38	2.11	7.1	14.6	6.2	13.7	5.4	12.9	4.1	11.6	10.65	1.73
Gastropod	4	1.50	0.80	2.40	1.14	1.02	1.26	10.8	11.8	9.9	11.0	9.1	10.1	7.8	8.8	1.60	0.24
Grossouvrites	1	-1.32	-1.32	-1.32	0.53	0.53	0.53	13.9	13.9	13.1	13.1	12.2	12.2	10.9	10.9	N/A	N/A
Lahillia	1	3.29	3.29	3.29	1.47	1.47	1.47	9.9	9.9	9.0	9.0	8.1	8.1	6.8	6.8	N/A	N/A
Maorites	17	-1.68	-5.18	1.18	1.00	0.58	1.33	10.5	13.8	9.6	12.9	8.7	12.0	7.4	10.7	6.36	0.75
Nautiloid	4	-2.66	-4.35	0.06	0.55	0.13	0.77	12.9	15.7	12.1	14.8	11.2	14.0	9.9	12.7	4.42	0.64
Nucula	49	1.34	-3.01	3.65	1.39	0.26	2.05	7.4	15.1	6.5	14.3	5.6	13.4	4.3	12.1	6.65	1.78
Oistotrigonia	28	2.14	0.81	3.26	0.92	0.59	1.49	9.8	13.7	8.9	12.9	8.1	12.0	6.8	10.7	2.45	0.91

Category	No	$\delta^{13}C$‰			$\delta^{18}O$‰			SMOW = -0.8‰		SMOW = -1.0‰		SMOW = -1.2‰		SMOW = -1.5‰		$\delta^{13}C$‰ Range	$\delta^{18}O$‰ Range
		Mean	Min	Max	Mean	Min	Max	Min (℃)	Max (℃)	Min (℃)	Max (℃)	Min (℃)	Max (℃)	Min (℃)	Max (℃)		
Pinna	5	1.88	0.32	2.62	1.07	0.84	1.62	9.2	12.6	8.4	11.8	7.5	10.9	6.2	9.6	2.30	0.78
Pleurotomaria	2	0.92	-0.19	2.02	1.00	0.97	1.03	11.8	12.0	10.9	11.2	10.0	10.3	8.7	9.0	2.20	0.06
Solemya	3	-8.01	-10.49	-5.99	1.05	0.99	1.11	11.4	12.0	10.6	11.1	9.7	10.2	8.4	8.9	4.51	0.12
Unidentified	10	0.82	-1.51	2.64	0.96	-0.06	1.55	9.5	16.5	8.7	15.7	7.8	14.8	6.5	13.5	4.15	1.61

Table E-9. Variability of oxygen and carbon stable isotope data categorised by fossil type and diagenetic screening. The 'Uncertain' category describes aragonite shell material of uncertain fossil type.

	No.	$\delta^{13}C$	Min	Max	$\delta^{18}O$	Min	Max
Fossil Type	**Screened Aragonite**						
Bivalve	82	1.89	-7.54	3.70	1.23	0.49	2.05
Cephalopod	14	-1.83	-5.18	1.18	0.95	0.53	1.44
Gastropod	12	2.13	-0.19	3.28	1.11	0.72	1.42
Uncertain	8	1.15	-1.51	2.64	0.94	-0.06	1.55
	Screened aragonite (Fe or Mn > threshold)						
Bivalve	115	1.52	-7.54	4.34	1.26	0.38	2.11
Cephalopod	29	-1.69	-5.18	1.56	1.00	0.13	1.53
Gastropod	16	2.20	-0.19	3.33	1.11	0.72	1.42
Uncertain	9	1.01	-1.51	2.64	0.92	-0.06	1.55
	Screened aragonite (No trace element screening)						
Bivalve	151	1.51	-10.49	4.34	1.25	0.26	2.11
Cephalopod	32	-1.62	-5.18	1.56	1.00	0.13	1.53
Gastropod	20	1.99	-0.19	3.33	1.12	0.72	1.42
Uncertain	10	0.82	-1.51	2.64	0.96	-0.06	1.55

Table E-10. Variability of oxygen and carbon stable isotope data categorised by habitat and diagenetic screening. The 'Unidentified' category describes aragonite shell material of uncertain type.

	No.	$\delta^{13}C$	Min	Max	$\delta^{18}O$	Min	Max
Mode of life	**Screened Aragonite**						
Infaunal	1	2.66	2.66	2.66	1.09	1.09	1.09
Epifaunal	12	2.13	-0.19	3.28	1.11	0.72	1.42
Infaunal	63	1.82	-7.54	3.70	1.21	0.49	2.05
Nektonic	13	-1.84	-5.18	1.18	0.92	0.53	1.33
Planktonic	1	-1.63	-1.63	-1.63	1.44	1.44	1.44
Uncertain	26	1.80	-1.51	2.91	1.20	-0.06	1.92
	Screened aragonite (Fe or Mn > threshold)						
Infaunal	1	2.66	2.66	2.66	1.09	1.09	1.09
Epifaunal	16	2.20	-0.19	3.33	1.11	0.72	1.42
Infaunal	93	1.41	-7.54	4.34	1.25	0.38	2.11
Nektonic	28	-1.69	-5.18	1.56	0.98	0.13	1.53
Planktonic	1	-1.63	-1.63	-1.63	1.44	1.44	1.44
Uncertain	30	1.65	-1.51	2.91	1.21	-0.06	1.92
	Screened aragonite (No trace element screening)						
Epifaunal	20	1.99	-0.19	3.33	1.12	0.72	1.42
Infaunal	128	1.43	-10.49	4.34	1.24	0.26	2.11
Nektonic	31	-1.62	-5.18	1.56	0.99	0.13	1.53
Planktonic	1	-1.63	-1.63	-1.63	1.44	1.44	1.44
Uncertain	33	1.61	-1.51	2.91	1.20	-0.06	1.92

Table E-11. Variability of oxygen and carbon stable isotope data categorised by genus. The 'Uncertain' category describes aragonite shell material of uncertain fossil type.

Genus	No.	$\delta^{13}C‰$	Min	Max	$\delta^{18}O‰$	Min	Max
Eselaevitrigonia	1	2.66	2.66	2.66	1.09	1.09	1.09
Amberlaya	9	2.38	0.51	3.28	1.15	0.72	1.42
Ammonite	4	-1.48	-3.96	0.54	1.04	0.88	1.27
Bivalve	18	2.09	-0.04	2.91	1.32	0.86	1.92
Diplomoceras	1	-1.63	-1.63	-1.63	1.44	1.44	1.44
Eselaevitrigonia	24	1.67	-5.06	3.70	1.29	0.70	2.02
Gastropod	1	2.40	2.40	2.40	1.04	1.04	1.04
Grossouvrites	1	-1.32	-1.32	-1.32	0.53	0.53	0.53
Lahillia	1	3.29	3.29	3.29	1.47	1.47	1.47
Maorites	5	-2.09	-5.18	1.18	1.03	0.76	1.33
Nautiloid	3	-2.09	-3.47	0.06	0.69	0.56	0.77
Nucula	13	2.11	-0.51	3.65	1.52	0.49	2.05
Oistotrigonia	23	2.13	0.81	3.26	0.95	0.59	1.49
Pinna	1	2.44	2.44	2.44	0.92	0.92	0.92
Pleurotomaria	2	0.92	-0.19	2.02	1.00	0.97	1.03
Solemya	1	-7.54	-7.54	-7.54	1.11	1.11	1.11
Unidentified	8	1.15	-1.51	2.64	0.94	-0.06	1.55

Appendix F. Strontium isotope data

Table F-1. $^{87}Sr/^{86}Sr$ isotope data for present day seawater, run as an internal standard

Seawater	0.709175	0.709171	0.000003
	0.709179	0.709175	0.000004

Table F-2. $^{87}Sr/^{86}Sr$ isotope results derived from NIGL NBS987 standard

Run	Batch	Sample	$^{87}Sr/^{86}Sr$	± 1SE
Triton1-553	NBS987	Sr standard	0.710253	0.000005
Triton1-553	NBS987	Sr standard	0.710250	0.000004
Triton1-554	NBS987	Sr standard	0.710258	0.000003
Triton1-554	NBS987	Sr standard	0.710251	0.000003
Triton1-553	NBS987	Sr standard	0.710244	0.000003
Triton1-554	NBS987	Sr standard	0.710245	0.000002
Triton1-564	NBS987	Sr standard	0.710251	0.000002
Triton1-564	NBS987	Sr standard	0.710252	0.000003
Triton1-564	NBS987	Sr standard	0.710255	0.000002
Triton1-564	NBS987	Sr standard	0.710257	0.000001
Triton1-564	NBS987	Sr standard	0.710258	0.000002
Triton1-565	NBS987	Sr standard	0.710255	0.000002
Triton1-565	NBS987	Sr standard	0.710259	0.000002
Triton1-565	NBS987	Sr standard	0.710257	0.000001
Triton1-573	NBS987	Sr standard	0.710253	0.000004
Triton1-575	NBS987	Sr standard	0.710256	0.000002
Triton1-575	NBS987	Sr standard	0.710256	0.000002
Triton1-575	NBS987	Sr standard	0.710253	0.000002
			0.710254	
			0.000004	
			5.9	

Table F-3. $^{87}Sr/^{86}Sr$ isotope data analysed from late Maastrichtian aragonite nacre shell material for Batches 1 and 2 of powder samples from Seymour Island. Lookup age data from the LOWESS Smoothed Global Strontium Isotope Curve (McArthur *et al*., 2001) are inconsistent with $^{87}Sr/^{86}Sr$ data from this study, further investigation continues. K-Pg boundary at 1029 m above datum as defined by palynology (Bowman *et al*., 2012), $^{87}Sr/^{86}Sr$ isotope value = 0.707833 as derived from the global Strontium Isotope Stratigraphy (SIS) curve (McArthur *et al*., 2001).

Depth (m)	Age (Ma)	Specimen ID	$^{87}Sr/^{86}Sr$	± 2SE	Fossil Type	Genus
1084	65.5	D5.229.1361.2/C	0.707864	0.000005	Bivalve	Nucula
1084	65.5	D5.229.1361.2/C	0.707838	0.000010	Bivalve	Nucula
1084	65.5	D5.229.1361.2/A	0.707861	0.000004	Bivalve	Nucula
1084	65.5	D5.229.1361.2/A	0.707867	0.000004	Bivalve	Nucula
1084	65.5	D5.229.1361.2/F	0.707871	0.000004	Bivalve	Nucula
1084	65.5	D5.229.1361.2/F	0.707851	0.000006	Bivalve	Nucula
1028	66.0	D5.229.1292.2/A-3	0.707878	0.000004	Nautiloid	Nautiloid
1028	66.0	D5.229.1292.2/A-3	0.707877	0.000011	Nautiloid	Nautiloid
1028	66.0	D5.229.1292.2/A-4	0.707872	0.000006	Nautiloid	Nautiloid
1028	66.0	D5.229.1292.2/A-4	0.707878	0.000004	Nautiloid	Nautiloid
1028	66.0	D5.229.1292.2/A-4	0.707860	0.000005	Nautiloid	Nautiloid
995	66.3	D5.222.1257.2/A	0.707877	0.000004	Nautiloid	Nautiloid
995	66.3	D5.222.1257.2/A	0.707881	0.000002	Nautiloid	Nautiloid
995	66.3	D5.222.1257.2/A	0.707882	0.000005	Nautiloid	Nautiloid
995	66.3	D5.222.1257.2/A	0.707879	0.000003	Nautiloid	Nautiloid
991	66.3	D5.222.1255.2/A	0.707855	0.000004	Gastropod	Amberlaya
991	66.3	D5.222.1255.2/A	0.707838	0.000011	Gastropod	Amberlaya
991	66.3	D5.222.1255.2/D	0.707841	0.000005	Gastropod	Amberlaya
991	66.3	D5.222.1255.2/D	0.707840	0.000003	Gastropod	Amberlaya
991	66.3	D5.222.1255.2/D	0.707823	0.000005	Gastropod	Amberlaya
919	66.9	D5.220.1214.2/A	0.707858	0.000007	Ammonite	Maorites
919	66.9	D5.220.1214.2/A	0.707852	0.000004	Ammonite	Maorites
919	66.9	D5.220.1214.2/A	0.707857	0.000004	Ammonite	Maorites
919	66.9	D5.220.1214.2/A	0.707857	0.000004	Ammonite	Maorites
869	67.3	D5.219.1185.2/G-1	0.707800	0.000004	Ammonite	Maorites
869	67.3	D5.219.1185.2/G-1	0.707866	0.000004	Ammonite	Maorites
869	67.3	D5.219.1185.2/G-1	0.707872	0.000006	Ammonite	Maorites
869	67.3	D5.219.1185.2/I	0.707753	0.000005	Bivalve	Eselaevitrigonia
869	67.3	D5.219.1185.2/I	0.707775	0.000007	Bivalve	Eselaevitrigonia
869	67.3	D5.219.1185.2/D	0.707797	0.000005	Ammonite	Maorites
863	67.4	D5.219.1182.2/A	0.707741	0.000008	Bivalve	Nucula
779	68.1	D5.219.1138.3/A	0.707848	0.000009	Ammonite	Maorites
755	68.3	D5.219.1125.2/L	0.707874	0.000006	Bivalve	Bivalve
755	68.3	D5.219.1125.2/L	0.707867	0.000010	Bivalve	Bivalve
755	68.3	D5.219.1125.2/L	0.707863	0.000013	Bivalve	Bivalve
755	68.3	D5.219.1125.2/M	0.707876	0.000004	Bivalve	Bivalve
755	68.3	D5.219.1125.2/M	0.707857	0.000006	Bivalve	Bivalve
755	68.3	D5.219.1125.2/N	0.707881	0.000004	Bivalve	Bivalve
755	68.3	D5.219.1125.2/N	0.707873	0.000005	Bivalve	Bivalve
712	68.5	D5.219.1091.2/F	0.707853	0.000004	Bivalve	Nucula
712	68.5	D5.219.1091.2/F	0.707847	0.000004	Bivalve	Nucula
682	68.7	D5.218.1061.2/C	0.707837	0.000003	Bivalve	Eselaevitrigonia
682	68.7	D5.218.1061.2/F	0.707845	0.000002	Bivalve	Bivalve
682	68.7	D5.218.1061.2/H	0.707845	0.000003	Bivalve	Bivalve
637	68.9	D5.218.1016.2/C	0.707854	0.000003	Bivalve	Nucula
637	68.9	D5.218.1016.2/L-2	0.707848	0.000005	Bivalve	Eselaevitrigonia
637	68.9	D5.218.1016.2/K	0.707846	0.000003	Bivalve	Eselaevitrigonia
613	69.0	D5.215.696.2/P	0.707841	0.000004	Gastropod	Amberlaya
613	69.0	D5.215.696.2/AN	0.707850	0.000005	Bivalve	Eselaevitrigonia
613	69.0	D5.215.696.2/AK	0.707847	0.000004	Bivalve	Nucula
578	69.2	D5.215.396.2/A	0.707840	0.000003	Bivalve	Nucula
578	69.2	D5.215.396.2/A	0.707843	0.000003	Bivalve	Nucula

Depth (m)	Age (Ma)	Specimen ID	$^{87}Sr/^{86}Sr$	± 2SE	Fossil Type	Genus
578	69.2	D5.215.396.2/A	0.707837	0.000003	Bivalve	Nucula
548	69.4	D5.215.368.2/B	0.707827	0.000008	Bivalve	Oistotrigonia
548	69.4	D5.215.368.2/A	0.707831	0.000009	Unidentified	Unidentified
541	69.4	D5.215.361.2/A	0.707818	0.000007	Gastropod	Gastropod
541	69.4	D5.215.361.2/B	0.707797	0.000004	Bivalve	Bivalve
538	69.4	D5.215.357.2/A	0.707831	0.000007	Bivalve	Eselaevitrigonia
538	69.4	D5.215.357.2/B	0.707805	0.000007	Bivalve	Eselaevitrigonia
533	69.4	D5.215.352.2/D	0.707800	0.000003	Bivalve	Nucula
533	69.4	D5.215.352.2/B	0.707832	0.000003	Bivalve	Bivalve
533	69.4	D5.215.352.2/A	0.707822	0.000006	Bivalve	Eselaevitrigonia
528	69.5	D5.215.347.2/E	0.707799	0.000009	Bivalve	Nucula
528	69.5	D5.215.347.2/F	0.707831	0.000012	Bivalve	Nucula
526	69.5	D5.215.345.2/A-1	0.707828	0.000005	Bivalve	Solemya
453	69.8	D5.215.975.2/A	0.707805	0.000005	Bivalve	Oistotrigonia
388	70.2	D5.212.909.2/A	0.707810	0.000003	Bivalve	Oistotrigonia
388	70.2	D5.212.909.2/B	0.707821	0.000003	Bivalve	Bivalve
388	70.2	D5.212.909.2/A	0.707817	0.000003	Bivalve	Oistotrigonia
343	70.4	D5.212.865.3/B	0.707819	0.000004	Bivalve	Oistotrigonia
343	70.4	D5.212.865.3/E	0.707817	0.000004	Bivalve	Bivalve
343	70.4	D5.212.865.3/A-2	0.707819	0.000004	Bivalve	Oistotrigonia
333	70.5	D5.212.855.2/C	0.707816	0.000038	Unidentified	Unidentified
333	70.5	D5.212.855.2/C	0.707791	0.000030	Unidentified	Unidentified
311	70.6	D5.212.833.2/A	0.707822	0.000003	Unidentified	Unidentified
311	70.6	D5.212.833.2/A	0.707825	0.000003	Unidentified	Unidentified

Table F-4. Correlation of Sr concentration with specimens exhibiting anomalous $^{87}Sr/^{86}Sr$ data. There is a definite change in the levels of Sr measured between 837 and 895 m, with a distinct peak between 863 and 869 m.

Height	Specimen Id	$\delta^{13}C‰$	$\delta^{18}O‰$	$^{87}Sr/^{86}Sr$	± 2SE ($x10^{-6}$)	Sr (ppm)	Fossil Type
897	D5.220.1202.2/B-4	0.08	1.05				C
895	D5.220.1200.2/A	1.45	1.62			2514	B
869	D5.219.1185.2/G-2			0.707800	6		C
869	D5.219.1185.2/G-1	-2.99	0.97			8381	C
869	D5.219.1185.2/I	2.66	1.09	0.707749	2	5783	B
869	D5.219.1185.2/I			0.707775	7		B
869	D5.219.1185.2/I			0.707851	6		
869	D5.219.1185.2/C	-0.76	0.58			11129	C
869	D5.219.1185.2/D	-2.34	1.28	0.707793	2	6459	C
863	D5.219.1182.2/A			0.707741	8		B
863	D5.219.1182.2/A			0.707851	6		B
863	D5.219.1182.2/A	2.01	0.86			5997	B
857	D5.219.1179.2/A-1	1.12	0.59			2884	B
857	D5.219.1179.2/A-2	-0.38	0.38			4008	B
851	D5.219.1176.2/A	-0.29	0.98			4680	C
837	D5.219.1168.2/B	-1.04	1.53			2777	C
837	D5.219.1168.2/B	-1.04	1.53			2800	C
837	D5.219.1168.2/B	-1.04	1.53			2952	C

Appendix G. Palaeontology

Table G-1. Distribution of identified macrofossils from the Latest Maastrichtian López de Bertodano Fm., Seymour Island succession. Note that the table does not represent the full range of identified individual specimens because for clarity duplicate entries were removed. Where formal identification of genus was not possible material was classified as either Unidentified Ammonite/Bivalve/Gastropod/Nautiloid or shell material.

	Genus																				Unidentified				Habitat		
Position (m)	*Amberlaya*	*Anagaudryceras*	*Cassidaria*	*Cryptorhytis*	*Diplomoceras*	*Eselaevitrigonia*	*Eunaticina*	*Grossouvrites*	*Kitchinites*	*Lahillia*	*Maorites*	*Nucula*	*Oistotrigonia*	*Pachydiscus*	*Pinna*	*Pleurotomaria*	*Pulvinites*	*Pycnodonte*	*Solemya*	Shell material	Ammonite	Bivalve	Gastropod	Nautiloid	Infaunal	Epifaunal	Nektonic
1084											x																x
1084												x													x		
1080																			x						x		
1068												x													x		
1068																		x								x	
1028																							x			x	
1028																								x			x
1001																				x							
995																								x			x
991	x																									x	
991								x																			x
991										x																	
991																				x							
981													x												x		
979											x										x						x
973																		x								x	
961											x																x
955	x																									x	
955																				x							
949											x																x
943											x																x
937											x																x
925		x									x																x
919											x																x
897											x										x						x
897																						x					

	Genus																				Unidentified				Habitat		
Position (m)	*Amberlaya*	*Anagaudryceras*	*Cassidaria*	*Cryptorhytis*	*Diplomoceras*	*Eselaevitrigonia*	*Eunaticina*	*Grossouvrites*	*Kitchinites*	*Lahillia*	*Maorites*	*Nucula*	*Oistotrigonia*	*Pachydiscus*	*Pinna*	*Pleurotomaria*	*Pulvinites*	*Pycnodonte*	*Solemya*	Shell material	Ammonite	Bivalve	Gastropod	Nautiloid	Infaunal	Epifaunal	Nektonic
895														x													x
895															x										x		
869					x						x																x
863												x													x		
857						x																			x		
857																						x					
851											x																x
837																					x						x
800																						x					
779						x						x													x		
779																						x					
767													x												x		
755						x							x												x		
755																				x							
755																						x					
749													x												x		
727													x												x		
722																					x						x
717						x																			x		
712						x						x	x												x		
712																				x							
712																						x					
682						x						x													x		
682																				x							
682																						x					
647																	x										
647																					x						x
642	x															x										x	
642											x																x
642												x	x		x										x		
642																		x									
642																				x							
642																						x					

	Genus																				Unidentified				Habitat		
Position (m)	*Amberlaya*	*Anagaudryceras*	*Cassidaria*	*Cryptorhytis*	*Diplomoceras*	*Eselaevitrigonia*	*Eunaticina*	*Grossouvrites*	*Kitchinites*	*Lahillia*	*Maorites*	*Nucula*	*Oistotrigonia*	*Pachydiscus*	*Pinna*	*Pleurotomaria*	*Pulvinites*	*Pycnodonte*	*Solemya*	Shell material	Ammonite	Bivalve	Gastropod	Nautiloid	Infaunal	Epifaunal	Nektonic
637	x																									x	
637						x						x													x		
637											x										x						x
632															x										x		
627											x																x
627													x												x		
627																				x							
627																					x						x
622	x															x		x								x	
622						x									x										x		
622																	x										
618												x													x		
618																						x					
613	x		x	x			x																			x	
613		x							x		x										x						x
613						x						x													x		
613										x																	
613																		x									
608						x						x													x		
608							x																			x	
608											x																x
603	x																									x	
603																					x						x
578												x													x		
558																						x					
551						x																			x		
551																						x					
548	x																									x	
548													x												x		
548																				x							
541						x						x													x		
541																						x					
538						x																			x		

	Genus																				Unidentified				Habitat		
Position (m)	*Amberlaya*	*Anagaudryceras*	*Cassidaria*	*Cryptorhytis*	*Diplomoceras*	*Eselaevitrigonia*	*Eunaticina*	*Grossouvrites*	*Kitchinites*	*Lahillia*	*Maorites*	*Nucula*	*Oistotrigonia*	*Pachydiscus*	*Pinna*	*Pleurotomaria*	*Pulvinites*	*Pycnodonte*	*Solemya*	Shell material	Ammonite	Bivalve	Gastropod	Nautiloid	Infaunal	Epifaunal	Nektonic
533						x						x													x		
533																						x					
528	x																									x	
528						x						x							x						x		
528																					x						x
526																			x						x		
508												x	x												x		
463													x												x		
463													x												x		
458						x							x							x					x		
453													x												x		
443						x																			x		
438											x										x						x
435				x																						x	
408													x												x		
388						x							x												x		
388																						x					
388																						x					
348																						x					
343													x												x		
343																						x					
338													x												x		
333																				x							
311																				x							

Appendix H. Specimen data

Table H-1. Specimen identification, geochemistry, diagenetic screening and stable isotope data. Entries coloured orange exhibited elevated Fe or Mn levels, those coloured green had no trace element screening and finally, entries coloured blue were classified as either calcite or having elevated Mg levels (> 1,000 ppm).

Depth	Prefix	δ13C‰	δ18O‰	Ca	Mg	Sr	Na	Fe	Mn	Type	Genus	Habitat	Mode of life	SEM Score	SEM Mag.	SEM Quality	XRD Score	XRD Quality	$^{87}Sr/^{86}Sr$	$^{87}Sr/^{86}Sr$ (N)	SMOW = -0.8	SMOW = -1.0	SMOW = -1.2	SMOW = -1.5
1080	D5.229.1353.2/C	2.12	0.64	380734	21	2142	3932	92	0	U	Unidentified	Uncertain	Uncertain	4	2000	Minimal fusing of nacre	5	Excellent			13.5	12.6	11.8	10.5
1028	D5.229.1292.2/A-1	-3.47	0.74	400725	207	6139	3675	419	128	C	Nautiloid	Nektonic	Carnivore	3	1500	Partially fused plates	4	Good			13.0	12.2	11.3	10.0
1028	D5.229.1292.2/A-2	-2.86	0.56	409321	14	594	377	12	7	C	Nautiloid	Nektonic	Carnivore	3	1000	Fused plates??	5	Excellent	0.707870	0.707866	13.8	13.0	12.1	10.8
995	D5.222.1257.2/A	0.06	0.77	390683	466	3982	8943	0	14	C	Nautiloid	Nektonic	Carnivore	0		No image	5	Excellent	0.707881	0.707877	12.9	12.1	11.2	9.9
991	D5.222.1254.1/A	-1.51	-0.06	399463	60	4170	4479	83	11	U	Unidentified	Uncertain	Uncertain	0	350	Low resolution	5	Excellent			16.5	15.7	14.8	13.5
991	D5.222.1255.2/A	2.96	0.90	397009	34	1940	10760	0	190	G	Amberlaya	Epifaunal	Carnivore/sc	5	1500	Good	5	Excellent	0.707854	0.707850	12.3	11.5	10.6	9.3
919	D5.220.1214.2/A	-2.71	1.33	401044	529	4842	3660	52	136	C	Maorites	Nektonic	Carnivore	0		No image	5	Excellent	0.707856	0.707852	10.5	9.6	8.7	7.4
869	D5.219.1185.2/I	2.66	1.09	395254	20	5783	7945	58	44	B	Eselaevitrigonia	Infaunal	Suspension	2	1000	Neomorphism??	5	Excellent	0.707753	0.707749	11.5	10.7	9.8	8.5
863	D5.219.1182.2/A	2.01	0.86	411521	42	5997	8276	204	13	B	Nucula	Infaunal	Deposit	3	1500	Fused plates??	5	Excellent			12.5	11.7	10.8	9.5
800	D5.219.1149.1/A-2	2.40	1.42	462684	68	2567	5215	155	0	B	Bivalve	Uncertain	Uncertain	5	1500	Fused plates??	2	S/N ratio & peaks missing			10.1	9.3	8.4	7.1
779	D5.219.1138.3/A	1.41	1.25	401027	26	2916	4116	177	20	B	Bivalve	Uncertain	Uncertain	0		No image	5	Excellent			10.8	10.0	9.1	7.8
779	D5.219.1138.3/B	1.42	1.49	395698	29	3276	4251	48	25	B	Oistotrigonia	Infaunal	Suspension	0		No image	5	Excellent			9.8	8.9	8.1	6.8
779	D5.219.1138.3/C	1.92	1.49	396978	24	3681	3712	19	61	B	Eselaevitrigonia	Infaunal	Suspension	3	2000	Fused plates??	5	Excellent			9.8	8.9	8.1	6.8
755	D5.219.1125.2/C-1	2.79	1.12	465932	179	2856	5194	450	0	B	Eselaevitrigonia	Infaunal	Suspension	0		No image	4	Good - S/N ratio			11.4	10.5	9.7	8.4
755	D5.219.1125.2/C-2	0.37	1.31	398125	136	2353	8919	120	3	B	Eselaevitrigonia	Infaunal	Suspension	0		No image	4	Good			10.6	9.7	8.9	7.6
755	D5.219.1125.2/D	2.43	1.05	396162	103	1900	11234	47	2	B	Oistotrigonia	Infaunal	Suspension	0		No image	5	Excellent			11.7	10.8	10.0	8.7
755	D5.219.1125.2/E	2.37	1.03	407841	98	2088	9197	9	1	B	Oistotrigonia	Infaunal	Suspension	0		No image	5	Excellent			11.8	10.9	10.1	8.8
755	D5.219.1125.2/G-1	2.70	1.32	417140	3	192	695	0	0	B	Bivalve	Uncertain	Uncertain	3	2000	Fused plates	5	Excellent			10.5	9.7	8.8	7.5
755	D5.219.1125.2/G-2	2.19	1.39	401002	33	1890	6637	25	1	B	Bivalve	Uncertain	Uncertain	3	2000	Fused plates	5	Excellent			10.2	9.4	8.5	7.2
755	D5.219.1125.2/L	1.94	1.05	396745	53	1340	8365	11	0	B	Bivalve	Uncertain	Uncertain	2	1500	Fused plates ++	5	Separate analysis	0.707874	0.707870	11.7	10.8	10.0	8.7
755	D5.219.1125.2/L	-0.04	0.86	379421	40	1662	3567	240	0	B	Bivalve	Uncertain	Uncertain	2	1500	Fused plates	4	Good - S/N ratio			12.5	11.6	10.8	9.5
755	D5.219.1125.2/M	1.21	1.34	389493	63	2098	9489	48	2	B	Bivalve	Uncertain	Uncertain	0		No image	5	Excellent	0.707876	0.707872	10.4	9.6	8.7	7.4
755	D5.219.1125.2/N	2.07	0.97	396498	125	1428	6664	94	2	B	Bivalve	Uncertain	Uncertain	1	1500	Nacre fused + neomorp	5	Excellent	0.707881	0.707877	12.1	11.2	10.3	9.0
749	D5.219.1122.2/D	1.47	0.72	373977	0	1270	3582	198	0	B	Oistotrigonia	Infaunal	Suspension	4	1500	Dissolution pits/endolith	4	S/N ratio			13.1	12.3	11.4	10.1
727	D5.219.1106.2/C	2.77	1.13	395727	96	1460	4357	58	2	B	Oistotrigonia	Infaunal	Suspension	4	350	Low resolution, higher r	5	Excellent			11.4	10.5	9.6	8.3
717	D5.219.1096.3/H	2.80	1.69	400851	105	1923	8207	101	5	B	Eselaevitrigonia	Infaunal	Suspension	0		No image	0	No profile			8.9	8.1	7.2	5.9
717	D5.219.1096.3/I	0.28	1.10	401605	144	2030	6247	222	9	B	Eselaevitrigonia	Infaunal	Suspension	0		No image	5	Excellent			11.5	10.6	9.8	8.5
712	D5.219.1091.2/F	2.67	1.67	408617	178	2582	9797	131	0	B	Nucula	Infaunal	Deposit	4	3500	Fusing of nacre	5	Excellent			9.0	8.2	7.3	6.0
712	D5.219.1091.2/G	0.81	1.26	381096	42	2024	3505	295	0	U	Unidentified	Uncertain	Uncertain	4	1500	Minimal fusing of nacre	4	Missing peaks			10.8	9.9	9.1	7.8
712	D5.219.1091.2/H	2.26	1.41	410019	36	2251	3680	350	0	B	Bivalve	Uncertain	Uncertain	5	1500	Good	5	Excellent			10.1	9.3	8.4	7.1
712	D5.219.1091.2/I-2	2.82	0.77	379089	0	1083	3715	181	0	B	Oistotrigonia	Infaunal	Suspension	4	1500	Minimal fusing of nacre	4	Missing peaks			12.9	12.0	11.2	9.9
647	D5.218.1027.2/B	-3.96	0.99	388961	293	6412	3993	377	56	C	Ammonite	Nektonic	Carnivore	0		No image	5	Excellent			12.0	11.1	10.2	8.9
642	D5.218.1021.2/A-1	2.15	1.31	436717	108	3710	5440	47	91	G	Amberlaya	Epifaunal	Carnivore/sc	0		No image	5	Excellent			10.6	9.7	8.8	7.5
642	D5.218.1021.2/A-2	2.16	1.23	406520	107	3403	4622	0	84	G	Amberlaya	Epifaunal	Carnivore/sc	0		No image	5	Excellent			10.9	10.0	9.2	7.9
642	D5.218.1021.2/B	-0.19	1.03	399035	107	4256	8695	140	37	G	Pleurotomaria	Epifaunal	Browser	3	1500	Fusing of nacre	5	Excellent			11.8	10.9	10.0	8.7
642	D5.218.1021.2/C	2.77	1.42	395255	85	2543	8544	76	76	G	Amberlaya	Epifaunal	Carnivore/sc	0		No image	5	Excellent			10.1	9.2	8.4	7.1
642	D5.218.1021.2/E	3.65	1.90	397134	129	4553	8214	18	16	B	Nucula	Infaunal	Deposit	3	2000	Neomorphism on surfa	5	Excellent			8.0	7.1	6.3	5.0
642	D5.218.1021.2/G	1.72	1.77	377781	402	5522	5997	368	81	B	Nucula	Infaunal	Deposit	0		No image	4	Good + minor gypsum			8.6	7.7	6.9	5.6
642	D5.218.1021.2/V	-5.18	0.78	401142	301	7202	3856	135	124	C	Maorites	Nektonic	Carnivore	0		No image	5	Excellent			12.9	12.0	11.1	9.8
642	D5.218.1021.2/W	0.21	0.94	420262	148	4008	4594	201	20	U	Unidentified	Uncertain	Uncertain	2	1500	Fusing of nacre + neom	4	Missing peaks			12.2	11.3	10.4	9.1
637	D5.218.1016.2/B	1.70	0.92	423011	77	1790	6967	38	130	B	Nucula	Infaunal	Deposit	0		No image	5	Excellent			12.3	11.4	10.5	9.2
637	D5.218.1016.2/C	1.61	0.49	399302	13	2758	4538	0	5	B	Nucula	Infaunal	Deposit	0		No image	5	Excellent	0.707855	0.707851	14.1	13.2	12.4	11.1
637	D5.218.1016.2/D	2.06	1.08	401034	89	3334	4989	273	8	G	Amberlaya	Epifaunal	Carnivore/sc	0		No image	5	Excellent			11.6	10.7	9.8	8.5
637	D5.218.1016.2/J	2.34	0.70	398527	15	1881	4504	0	7	B	Eselaevitrigonia	Infaunal	Suspension	4	1500	Minimal fusing of nacre	5	Excellent			13.2	12.4	11.5	10.2
637	D5.218.1016.2/K	2.05	0.77	409060	56	1793	6551	78	2	B	Eselaevitrigonia	Infaunal	Suspension	0		No image	5	Excellent	0.707847	0.707843	12.9	12.0	11.2	9.9
637	D5.218.1016.2/L-1	1.96	0.81	397119	70	1956	9603	133	13	B	Eselaevitrigonia	Infaunal	Suspension	4	1500	Minimal fusing of nacre	5	Excellent			12.7	11.9	11.0	9.7
637	D5.218.1016.2/L-2	2.81	0.87	388810	32	1530	10044	24	11	B	Eselaevitrigonia	Infaunal	Suspension	0		No image	5	Excellent	0.707847	0.707843	12.5	11.6	10.8	9.5
637	D5.218.1016.2/N	2.56	1.01	405702	83	2450	4058	16	21	B	Eselaevitrigonia	Infaunal	Suspension	0		No image	5	Excellent			11.9	11.0	10.1	8.8
637	D5.218.1016.2/O	-2.72	1.03	413959	100	1524	4933	63	2	C	Ammonite	Nektonic	Carnivore	2	1500	Fusing of nacre + neom	5	Excellent			11.8	10.9	10.1	8.8
627	D5.218.1006.2/I	-0.89	1.24	408471	157	4911	6432	115	29	C	Maorites	Nektonic	Carnivore	0		No image	5	Excellent			10.9	10.0	9.1	7.8
627	D5.218.1006.2/O	2.39	1.08	404224	134	2160	10856	165	10	B	Oistotrigonia	Infaunal	Suspension	0		No image	5	Excellent			11.6	10.7	9.8	8.5

622	D5.215.216.2/A	2.44	0.92	375090	0	2541	3417	181	0	B	Pinna	Infaunal	Suspension	0		No image	5	Excellent			12.3	11.4	10.5	9.2
622	D5.215.216.3/A-1	1.14	0.75	376061	0	2609	3506	143	18	B	Eselaevitrigonia	Infaunal	Suspension	0		No image	5	Excellent			13.0	12.1	11.3	10.0
622	D5.215.216.3/A-2	1.00	0.86	404178	5	2825	3873	453	119	B	Eselaevitrigonia	Infaunal	Suspension	0		No image	5	Excellent			12.5	11.6	10.8	9.5
622	D5.215.216.5/A	2.02	0.97	396754	71	3128	4238	0	10	G	Pleurotomaria	Epifaunal	Browser	3	1000	Focus poor & some fus	5	Excellent			12.0	11.2	10.3	9.0
618	D5.215.701.2/A	2.37	1.80	387530	79	2885	4120	21	56	B	Nucula	Infaunal	Deposit	2	1000	Focus poor & fused nac	5	Excellent			8.5	7.6	6.7	5.4
618	D5.215.701.2/B	2.88	1.53	386874	27	3157	3794	164	125	B	Bivalve	Uncertain	Uncertain	0		No image	5	Excellent			9.6	8.8	7.9	6.6
613	D5.215.696.2/AA	1.08	1.17	363184	0	2559	3834	136	34	B	Nucula	Infaunal	Deposit	0		No image	5	Excellent			11.2	10.3	9.5	8.1
613	D5.215.696.2/AK	3.63	2.05	394180	129	4810	3576	0	15	B	Nucula	Infaunal	Deposit	5	2000	Good nacre + some dis	5	Excellent	0.707846	0.707842	7.4	6.5	5.6	4.3
613	D5.215.696.2/AL	2.89	1.52	385590	93	5005	3571	158	129	B	Nucula	Infaunal	Deposit	0		No image	5	Excellent			9.7	8.8	7.9	6.6
613	D5.215.696.2/AN	2.89	1.59	418403	80	3325	6260	0	32	B	Eselaevitrigonia	Infaunal	Suspension	4	2000	Surface debris, some fu	5	Excellent	0.707849	0.707845	9.4	8.5	7.6	6.3
613	D5.215.696.2/AQ	3.70	2.02	418297	171	4341	8443	0	157	B	Eselaevitrigonia	Infaunal	Suspension	0		No image	5	Excellent			7.5	6.6	5.7	4.4
613	D5.215.696.2/AR	0.54	1.27	405873	174	4110	4298	35	24	C	Ammonite	Nektonic	Carnivore	0	350	Low resolution	5	Excellent			10.7	9.9	9.0	7.7
613	D5.215.696.2/AT	0.24	0.88	388283	93	4382	3199	483	5	C	Ammonite	Nektonic	Carnivore	0		No image	5	Excellent			12.4	11.6	10.7	9.4
613	D5.215.696.2/AU	0.51	1.29	413816	190	5213	4548	0	49	G	Amberlaya	Epifaunal	Carnivore/sc	4	1500	Surface debris, some fu	0	No profile			10.7	9.8	8.9	7.6
613	D5.215.696.2/AV	3.29	1.47	410700	42	3252	3977	137	28	B	Lahillia	Infaunal	Suspension	0		No image	5	Excellent			9.9	9.0	8.1	6.8
613	D5.215.696.2/P	2.73	1.18	417601	239	2949	7159	40	50	G	Amberlaya	Epifaunal	Carnivore/sc	0		No image	5	Excellent	0.707841	0.707837	11.1	10.3	9.4	8.1
613	D5.215.696.2/Q	1.18	0.76	379456	535	2964	3895	375	15	C	Maorites	Nektonic	Carnivore	0		No image	3	Noisy profile			13.0	12.1	11.2	9.9
608	D5.215.691.2/A	-2.86	1.03	420903	289	6496	6074	117	146	C	Maorites	Nektonic	Carnivore	3	2000	Minimal fusing of nacre	4	Good			11.8	10.9	10.1	8.8
608	D5.215.691.2/B	-1.32	0.53	403126	178	3195	7506	369	15	C	Grossouvrites	Nektonic	Carnivore	4	2000	Good nacre	5	Excellent			13.9	13.1	12.2	10.9
608	D5.215.691.2/C	2.25	1.82	418128	119	3414	7290	23	16	B	Nucula	Infaunal	Deposit	3	2000	Minimal fusing of nacre	5	Excellent			8.4	7.5	6.6	5.3
608	D5.215.691.2/D-1	3.68	1.94	403506	101	3150	7236	0	52	B	Eselaevitrigonia	Infaunal	Suspension	5	1500	Good nacre + some dis	5	Excellent			7.9	7.0	6.1	4.8
603	D5.215.686.2/A	3.28	1.20	419109	112	2219	7735	29	34	G	Amberlaya	Epifaunal	Carnivore/sc	4	2000	Good nacre	5	Excellent			11.0	10.2	9.3	8.0
578	D5.215.396.2/A	2.31	1.77	402167	69	2308	4786	69	25	B	Nucula	Infaunal	Deposit	1	750	Neomorphism?	5	Excellent	0.707840	0.707836	8.6	7.7	6.8	5.5
558	D5.215.378.2/A	2.18	1.91	403765	71	2953	4732	56	14	B	Bivalve	Uncertain	Uncertain	4	1000	Good nacre	5	Excellent			8.0	7.1	6.2	4.9
551	D5.215.371.2/A	2.33	1.54	388731	68	3366	3786	234	1	B	Bivalve	Uncertain	Uncertain	0		No image	5	Excellent			9.6	8.7	7.9	6.6
551	D5.215.371.2/B	2.06	1.05	388696	56	3363	3723	135	2	B	Eselaevitrigonia	Infaunal	Suspension	0		No image	5	Excellent			11.7	10.9	10.0	8.7
548	D5.215.368.2/A	1.73	1.55	406251	78	2550	5080	0	12	U	Unidentified	Uncertain	Uncertain	3	2000	Minimal fusing of nacre	5	Excellent			9.5	8.7	7.8	6.5
548	D5.215.368.2/B	2.48	0.94	405530	241	1494	4639	144	25	B	Oistotrigonia	Infaunal	Suspension	3	1500	Localised fusing of nacı	5	Excellent			12.2	11.3	10.5	9.2
548	D5.215.368.2/C	2.78	0.72	380259	39	3074	3834	115	25	G	Amberlaya	Epifaunal	Carnivore/sc	0		No image	0	No profile			13.2	12.3	11.4	10.1
541	D5.215.361.2/A	2.40	1.04	406792	87	2001	4491	0	19	G	Gastropod	Epifaunal	Uncertain	5	2000	Good nacre + some dis	5	Excellent			11.7	10.9	10.0	8.7
541	D5.215.361.2/B	2.45	1.80	388673	95	3271	3970	0	56	B	Bivalve	Uncertain	Uncertain	4	1500	Minimal fusing of nacre	5	Excellent			8.4	7.6	6.7	5.4
541	D5.215.361.2/C	2.28	1.75	395210	105	3215	4432	0	13	B	Eselaevitrigonia	Infaunal	Suspension	3	1500	Focus poor & localised	5	Excellent			8.7	7.8	6.9	5.6
541	D5.215.361.2/D	1.96	1.45	384957	27	3049	3680	332	183	B	Eselaevitrigonia	Infaunal	Suspension	0		No image	5	Excellent			10.0	9.1	8.2	6.9
538	D5.215.357.2/A	1.71	1.37	390679	0	2296	4197	115	0	B	Eselaevitrigonia	Infaunal	Suspension	0		No image	5	Excellent			10.3	9.4	8.6	7.3
538	D5.215.357.2/B	0.26	1.60	398003	131	2415	4797	12	37	B	Eselaevitrigonia	Infaunal	Suspension	3	1500	Focus poor & some fus	5	Excellent			9.3	8.4	7.6	6.3
533	D5.215.352.2/A	1.31	1.91	409555	88	3563	6919	0	59	B	Eselaevitrigonia	Infaunal	Suspension	2	350	Low resolution	5	Excellent	0.707820	0.707816	8.0	7.1	6.2	4.9
533	D5.215.352.2/B	2.91	1.92	408822	185	2925	6597	24	48	B	Bivalve	Uncertain	Uncertain	4	1000	Minimal fusing of nacre	5	Excellent	0.707832	0.707828	7.9	7.0	6.2	4.9
528	D5.215.347.2/A	-0.51	2.00	417069	176	5700	5726	69	90	B	Nucula	Infaunal	Deposit	3	2000	Fusing of nacre	5	Excellent			7.6	6.7	5.8	4.5
528	D5.215.347.2/I	-5.06	1.25	420848	418	4355	5726	59	174	B	Eselaevitrigonia	Infaunal	Suspension	1	750	Poor -	4	Good - low count			10.8	9.9	9.1	7.8
528	D5.215.347.2/M	-7.54	1.11	398382	684	6768	2776	78	100	B	Solemya	Infaunal	Suspension	0		No image	5	Excellent			11.4	10.6	9.7	8.4
508	D5.215.327.2/A-2	2.09	0.84	380658	125	1058	3995	0	135	B	Oistotrigonia	Infaunal	Suspension	0		No image	4	Good + minor gypsum			12.6	11.8	10.9	9.6
463	D5.215.985.2/B	3.26	1.26	426573	0	1431	6615	0	151	B	Oistotrigonia	Infaunal	Suspension	0		No image	5	Excellent			10.8	9.9	9.1	7.7
458	D5.215.980.2/A	2.98	0.64	379708	0	1546	3662	106	94	B	Oistotrigonia	Infaunal	Suspension	4	2000	Dissolution/endolithic b	0	No profile			13.5	12.6	11.8	10.5
458	D5.215.980.2/B	1.85	1.39	411452	122	2236	3917	57	20	B	Eselaevitrigonia	Infaunal	Suspension	4	2000	Minimal fusing of nacre	5	Excellent			10.2	9.4	8.5	7.2
453	D5.215.975.2/A	2.27	1.12	410450	32	1646	4329	0	47	B	Oistotrigonia	Infaunal	Suspension	4	2000	Minimal fusing of nacre	5	Excellent			11.4	10.5	9.7	8.4
453	D5.215.975.2/B	0.81	0.59	367532	0	1495	3464	86	56	B	Oistotrigonia	Infaunal	Suspension	0		No image	4	Good + minor gypsum			13.7	12.9	12.0	10.7
453	D5.215.975.2/C	2.25	0.63	380039	0	1339	3687	112	52	B	Oistotrigonia	Infaunal	Suspension	0		No image	4	Good			13.5	12.7	11.8	10.5
435	D5.215.955.3/A	-1.63	1.44	418957	426	4327	6719	179	61	C	Diplomoceras	Planktonic	Carnivore	3	2000	Fusing of nacre	5	Excellent			10.0	9.1	8.3	7.0
408	D5.215.930.2/A	2.74	1.08	403847	56	1296	4323	0	130	B	Oistotrigonia	Infaunal	Suspension	0		No image	5	Excellent			11.6	10.7	9.8	8.5
388	D5.212.909.2/A	1.89	1.02	421887	144	2000	4709	14	7	B	Oistotrigonia	Infaunal	Suspension	0		No image	5	Excellent	0.707818	0.707814	11.8	11.0	10.1	8.8
388	D5.212.909.2/B	2.19	1.01	415468	83	1604	4436	64	0	B	Bivalve	Uncertain	Uncertain	0		No image	4	Good - low count	0.707821	0.707817	11.9	11.0	10.1	8.8
388	D5.212.909.2/C	2.05	0.99	395948	96	1609	7914	391	7	B	Bivalve	Uncertain	Uncertain	0		No image	4	Good, minor gypsum?			12.0	11.1	10.2	8.9
388	D5.215.910.1/A	1.53	1.13	388598	149	1969	9846	0	0	B	Eselaevitrigonia	Infaunal	Suspension	3	1500	Fusing of nacre	5	Excellent	0.707809	0.707805	11.4	10.5	9.6	8.3
348	D5.212.870.2/A	2.52	1.11	396678	38	1210	9178	106	0	B	Bivalve	Uncertain	Uncertain	0		No image	5	Excellent			11.5	10.6	9.7	8.4
343	D5.212.865.3/A-1	2.10	0.90	420258	56	1456	5613	0	0	B	Oistotrigonia	Infaunal	Suspension	2	1500	Out of focus, fused plat	4	Good, low count			12.3	11.5	10.6	9.3

343	D5.212.865.3/A-2	1.13	0.99	407388	62	1345	4570	0	0	B	Oistotrigonia	Infaunal	Suspension	2	1500	Poor focus + fused plat	5	Excellent	0.707819	0.707815	12.0	11.1	10.2	8.9
343	D5.212.865.3/B	1.74	1.08	393919	127	1582	8921	213	4	B	Oistotrigonia	Infaunal	Suspension	5	1500	Excellent	5	Excellent	0.707819	0.707815	11.6	10.7	9.8	8.5
343	D5.212.865.3/C	1.55	0.93	380290	160	1136	12321	117	0	B	Oistotrigonia	Infaunal	Suspension	0		No image	5	Excellent			12.2	11.3	10.5	9.2
343	D5.212.865.3/E	1.95	0.88	477385	28	1395	5437	34	0	B	Bivalve	Uncertain	Uncertain	0		No image	3	Low count	0.707817	0.707813	12.5	11.6	10.7	9.4
343	D5.212.865.3/F	2.15	1.05	469267	55	1412	5418	248	0	B	Oistotrigonia	Infaunal	Suspension	0		No image	4	Good - low count			11.7	10.8	9.9	8.6
343	D5.212.865.3/G	1.20	0.86	399768	49	1421	9235	71	0	B	Oistotrigonia	Infaunal	Suspension	4	3500	Good nacre	5	Excellent			12.5	11.7	10.8	9.5
338	D5.212.860.2/A	2.60	0.72	382742	0	1099	3697	168	0	B	Oistotrigonia	Infaunal	Suspension	0		No image	5	Excellent			13.2	12.3	11.4	10.1
333	D5.212.855.2/B	2.64	1.17	404371	45	1541	4986	20	0	U	Unidentified	Uncertain	Uncertain	3	1500	Some fusing of nacre	5	Excellent			11.2	10.3	9.4	8.1
333	D5.212.855.2/C	1.00	0.97	400685	97	1272	4216	123	0	U	Unidentified	Uncertain	Uncertain	4	1000	Good nacre	5	Excellent			12.0	11.2	10.3	9.0
311	D5.212.833.2/A	2.22	1.08	407342	0	1287	5283	0	0	U	Unidentified	Uncertain	Uncertain	0		No image	3	Peak offset + low count	0.707823	0.707819	11.6	10.7	9.8	8.5
1084	D5.229.1361.2/A	0.52	1.52	392013	264	3216	4616	0	229	B	Nucula	Infaunal	Deposit	4	1500	Minimal fusing of nacre	4	Moderate - low count	0.707864	0.707860	9.7	8.8	7.9	6.6
1084	D5.229.1361.2/B	-0.88	1.47	375173	271	3705	7447	844	2295	B	Nucula	Infaunal	Deposit	0		No image	3	Gypsum present			9.9	9.0	8.1	6.8
1084	D5.229.1361.2/C	-0.95	1.42	334434	536	2744	7423	399	421	B	Nucula	Infaunal	Deposit	0		No image	3	Gypsum present	0.707865	0.707861	10.1	9.2	8.4	7.1
1084	D5.229.1361.2/D	-0.07	1.29	302899	401	2359	4713	1542	219	B	Nucula	Infaunal	Deposit	0		No image	3	Gypsum present			10.7	9.8	8.9	7.6
1084	D5.229.1361.2/F	1.99	1.74	459871	295	5871	4829	217	863	B	Nucula	Infaunal	Deposit	0		No image	2	Poor signal - low count	0.707871	0.707867	8.7	7.8	7.0	5.7
1068	D5.229.1334.2/A	0.58	1.55	382589	464	3741	3529	450	299	B	Nucula	Infaunal	Deposit	3	1500	Dissolution pits/endolith	5	Excellent			9.6	8.7	7.8	6.5
1028	D5.229.1292.2/A-1	-4.35	0.13	401016	921	6179	3216	1324	538	C	Nautiloid	Nektonic	Carnivore	3	1500	Fused plates??	4	Good	0.707878	0.707874	15.7	14.8	14.0	12.7
991	D5.222.1255.2/D	3.33	0.89	395433	149	2108	4331	22	320	G	Amberlaya	Epifaunal	Carnivore/sc	4	1000	Minimal fusing of nacre	5	Excellent	0.707832	0.707828	12.4	11.6	10.7	9.4
943	D5.220.1226.2/A	-3.56	0.78	394015	204	8279	3529	506	286	C	Maorites	Nektonic	Carnivore	0		No image	1	LMC			12.9	12.0	11.1	9.8
925	D5.220.1217.2/A	-2.58	1.31	390641	577	4839	3801	340	410	C	Maorites	Nektonic	Carnivore	0		No image	3	S/N ratio			10.6	9.7	8.8	7.5
895	D5.220.1200.2/A	1.45	1.62	395113	223	2514	4641	1286	59	B	Pinna	Infaunal	Suspension	3	1500	Dissolution pits?? Imag	2	S/N ratio & peaks missing			9.2	8.4	7.5	6.2
869	D5.219.1185.2/C	-0.76	0.58	415936	771	11129	4740	526	1462	C	Maorites	Nektonic	Carnivore	4	750	Minimal fusing of nacre	1	S/N ratio			13.8	12.9	12.0	10.7
869	D5.219.1185.2/D	-2.34	1.28	433565	524	6459	5430	226	482	C	Maorites	Nektonic	Carnivore	0	350	Low resolution	1	S/N ratio	0.707797	0.707793	10.7	9.8	9.0	7.7
869	D5.219.1185.2/G-1	-2.99	0.97	449557	853	8381	4196	340	769	C	Maorites	Nektonic	Carnivore	0		No image	5	Excellent			12.1	11.2	10.3	9.0
857	D5.219.1179.2/A-1	1.12	0.59	394125	198	2884	5065	340	294	B	Bivalve	Uncertain	Uncertain	0		No image	5	Excellent			13.7	12.8	12.0	10.7
857	D5.219.1179.2/A-2	-0.38	0.38	479278	211	4008	4155	493	882	B	Eselaevitrigonia	Infaunal	Suspension	0		No image	4	Good - S/N ratio			14.6	13.7	12.9	11.6
851	D5.219.1176.2/A	-0.29	0.98	393901	447	4680	3588	481	394	C	Maorites	Nektonic	Carnivore	0		No image	4	Good			12.0	11.1	10.3	9.0
837	D5.219.1168.2/B	-1.04	1.53	416847	319	2952	6567	717	134	C	Ammonite	Nektonic	Carnivore	0		No image	0	No profile			9.6	8.8	7.9	6.6
837	D5.219.1168.2/B	-1.04	1.53	392478	289	2800	4515	1299	102	C	Ammonite	Nektonic	Carnivore	0		No image	0	No profile			9.6	8.8	7.9	6.6
837	D5.219.1168.2/B	-1.04	1.53	384844	326	2777	3976	1366	119	C	Ammonite	Nektonic	Carnivore	0		No image	5	Excellent			9.6	8.8	7.9	6.6
722	D5.219.1101.2/D	-2.18	1.13	392717	974	2987	3744	996	171	C	Ammonite	Nektonic	Carnivore	0		No image	4	Good - peaks shifted			11.3	10.5	9.6	8.3
682	D5.218.1061.2/B	0.98	1.78	308873	608	1345	3038	389	411	B	Eselaevitrigonia	Infaunal	Suspension	0		No image	4	Good + minor gypsum			8.5	7.7	6.8	5.5
682	D5.218.1061.2/C	1.29	2.00	402962	304	3540	10203	0	203	B	Eselaevitrigonia	Infaunal	Suspension	0		No image	5	Excellent	0.707836	0.707832	7.6	6.7	5.8	4.5
682	D5.218.1061.2/D	1.18	1.66	363693	755	1842	4025	184	233	B	Eselaevitrigonia	Infaunal	Suspension	3	3500	Fusing of nacre	4	Good + minor gypsum			9.1	8.2	7.3	6.0
682	D5.218.1061.2/F	1.34	1.91	391269	318	2946	12384	0	269	B	Bivalve	Uncertain	Uncertain	4	2000	Minimal fusing of nacre	5	Excellent	0.707846	0.707842	8.0	7.1	6.2	4.9
682	D5.218.1061.2/H	0.49	1.74	346052	509	1425	5621	476	474	B	Bivalve	Uncertain	Uncertain	0		No image	4	Good + minor gypsum	0.707846	0.707842	8.7	7.8	7.0	5.7
642	D5.218.1021.2/D	2.59	1.83	412086	222	4513	6676	333	222	B	Nucula	Infaunal	Deposit	0		No image	5	Excellent			8.3	7.4	6.6	5.3
642	D5.218.1021.2/H	2.42	0.73	419512	58	1725	5114	0	222	B	Oistotrigonia	Infaunal	Suspension	0		No image	5	Excellent			13.1	12.2	11.4	10.0
642	D5.218.1021.2/I	3.00	0.81	411783	41	1390	4657	0	294	B	Nucula	Infaunal	Deposit	0		No image	5	Excellent			12.7	11.9	11.0	9.7
642	D5.218.1021.2/J	2.54	0.64	447051	113	2062	5577	0	905	B	Oistotrigonia	Infaunal	Suspension	0		No image	5	Excellent			13.5	12.6	11.7	10.4
637	D5.218.1016.2/G	2.37	1.04	478153	82	3157	6114	199	587	G	Amberlaya	Epifaunal	Carnivore/sc	0		No image	5	Excellent			11.7	10.9	10.0	8.7
637	D5.218.1016.2/M	1.62	0.94	382172	397	1802	8150	707	21	B	Nucula	Infaunal	Deposit	0		No image	4	Good			12.2	11.3	10.4	9.1
632	D5.218.1011.2/A	0.32	1.05	376079	304	2913	4094	549	94	B	Pinna	Infaunal	Suspension	0		No image	5	Excellent			11.7	10.8	10.0	8.7
627	D5.218.1006.2/A	0.25	1.12	394336	224	4019	4076	538	83	C	Maorites	Nektonic	Carnivore	0		No image	5	Excellent			11.4	10.5	9.7	8.4
627	D5.218.1006.2/B	-1.48	0.74	406475	602	3787	4926	2999	301	C	Maorites	Nektonic	Carnivore	0	35	Insufficient resolution	5	Excellent			13.1	12.2	11.3	10.0
627	D5.218.1006.2/C	-1.62	0.97	369566	368	4337	3925	720	101	C	Maorites	Nektonic	Carnivore	0		No image	4	Good + minor gypsum			12.1	11.2	10.3	9.0
627	D5.218.1006.2/P	-0.16	0.75	391552	366	4114	3294	1128	53	U	Unidentified	Uncertain	Uncertain	0		No image	4	Good + minor gypsum			13.0	12.1	11.3	10.0
622	D5.215.216.4/A	1.96	1.31	365079	681	2422	4111	3494	208	G	Amberlaya	Epifaunal	Carnivore/sc	4	1000	Surface debris, some fu	5	Excellent			10.6	9.7	8.8	7.5
622	D5.215.705.2/H	2.98	1.85	401311	218	3011	5182	47	335	B	Eselaevitrigonia	Infaunal	Suspension	0		No image	0	No profile			8.2	7.4	6.5	5.2
613	D5.215.696.2/AM	4.34	2.11	427445	156	5995	6076	67	454	B	Eselaevitrigonia	Infaunal	Suspension	0	35	Low resolution image	5	Excellent			7.1	6.2	5.4	4.1
613	D5.215.696.2/AO	1.76	1.61	364206	824	2914	6846	132	3945	B	Nucula	Infaunal	Deposit	2	2000	Poor focus + fused plat	5	Excellent			9.3	8.4	7.5	6.2
613	D5.215.696.2/N	1.96	1.20	385728	279	3131	8298	773	34	G	Amberlaya	Epifaunal	Carnivore/sc	4	2000	Good nacre	5	Excellent			11.1	10.2	9.3	8.0
533	D5.215.352.2/C	0.61	1.41	384594	105	5545	3390	281	465	B	Nucula	Infaunal	Deposit	0		No image	3	Moderate - low count			10.2	9.3	8.4	7.1
533	D5.215.352.2/D	-2.42	1.40	418583	127	3728	7350	63	280	B	Nucula	Infaunal	Deposit	3	1000	Fusing of nacre	4	Noisy pattern	0.707800	0.707796	10.2	9.3	8.4	7.1
533	D5.215.352.2/E	-2.12	1.48	373346	352	4692	3372	253	1961	B	Nucula	Infaunal	Deposit	0		No image	3	Moderate - low count			9.8	9.0	8.1	6.8

528	D5.215.347.2/J	-0.58	1.25	381900	24	3159	3795	120	254	B	Nucula	Infaunal	Deposit	0		No image	5	Excellent	10.8	10.0	9.1	7.8
528	D5.215.347.2/L	-2.77	1.47	371708	101	3060	3631	244	941	B	Nucula	Infaunal	Deposit	0		No image	4	Good	9.9	9.0	8.2	6.9
508	D5.215.327.2/A-1	2.04	1.41	418660	184	2388	9111	0	624	B	Nucula	Infaunal	Deposit	4	1000	Good nacre	5	Excellent	10.1	9.3	8.4	7.1
443	D5.215.965.2/A	2.82	0.73	388113	0	1316	3839	398	332	B	Eselaevitrigonia	Infaunal	Suspension	0		No image	5	Excellent	13.1	12.2	11.4	10.0
438	D5.215.960.3/B	1.56	1.01	413687	361	3090	5780	1640	226	C	Ammonite	Nektonic	Carnivore	4	2000	Minimal fusing of nacre	3	Noisy profile	11.9	11.0	10.1	8.8
343	D5.212.865.3/D	1.40	0.90	403556	0	0	9854	0	307	B	Oistotrigonia	Infaunal	Suspension	0		No image	4	Good	12.4	11.5	10.6	9.3
1084	D5.229.1361.2/E	1.12	1.74							B	Nucula	Infaunal	Deposit	4	1500	Minimal fusing of nacre	2	Poor signal - low count	8.7	7.8	7.0	5.7
1084	D5.229.1361.2/H	1.23	1.44							B	Nucula	Infaunal	Deposit	0		No image	2	Poor - low count	10.0	9.1	8.3	7.0
991	D5.222.1254.1/A	-0.90	1.27							U	Unidentified	Uncertain	Uncertain	0		No image	0	No profile	10.7	9.9	9.0	7.7
909	D5.220.1209.3/A-1	1.30	1.26							G	Gastropod	Epifaunal	Carnivore/sc	0		No image	0	No profile	10.8	9.9	9.1	7.8
909	D5.220.1209.3/A-2	1.51	1.02							G	Gastropod	Epifaunal	Carnivore/sc	0		No image	0	No profile	11.8	11.0	10.1	8.8
897	D5.220.1202.2/B-4	0.08	1.05							C	Maorites	Nektonic	Carnivore	2	2000	Fused plates??	1	S/N ratio	11.7	10.8	10.0	8.7
800	D5.219.1149.1/A-1	1.99	1.20							B	Bivalve	Uncertain	Uncertain	0		No image	5	Excellent	11.0	10.2	9.3	8.0
712	D5.219.1091.2/A-2	0.80	1.23							G	Gastropod	Epifaunal	Carnivore/s cavenger	0		No image	0	No profile	10.9	10.1	9.2	7.9
712	D5.219.1091.2/F	2.62	1.24							B	Nucula	Infaunal	Deposit	4	3500	Fusing of nacre	5	Excellent	10.9	10.0	9.1	7.8
712	D5.219.1091.2/F	2.66	1.24							B	Nucula	Infaunal	Deposit	4	3500	Fusing of nacre	5	Excellent	10.9	10.0	9.1	7.8
712	D5.219.1091.2/F	2.67	1.24							B	Nucula	Infaunal	Deposit	4	3500	Fusing of nacre	5	Excellent	10.9	10.0	9.1	7.8
712	D5.219.1091.2/F	2.70	1.29							B	Nucula	Infaunal	Deposit	4	3500	Fusing of nacre	5	Excellent	10.7	9.8	8.9	7.6
712	D5.219.1091.2/F	2.70	1.21							B	Nucula	Infaunal	Deposit	4	3500	Fusing of nacre	5	Excellent	11.0	10.2	9.3	8.0
712	D5.219.1091.2/F	2.72	1.25							B	Nucula	Infaunal	Deposit	4	3500	Fusing of nacre	5	Excellent	10.8	10.0	9.1	7.8
712	D5.219.1091.2/F	2.73	1.25							B	Nucula	Infaunal	Deposit	4	3500	Fusing of nacre	5	Excellent	10.8	10.0	9.1	7.8
712	D5.219.1091.2/F	2.84	1.21							B	Nucula	Infaunal	Deposit	4	3500	Fusing of nacre	5	Excellent	11.0	10.1	9.3	8.0
712	D5.219.1091.2/F	2.94	1.31							B	Nucula	Infaunal	Deposit	4	3500	Fusing of nacre	5	Excellent	10.6	9.7	8.8	7.5
712	D5.219.1091.2/F	2.97	1.34							B	Nucula	Infaunal	Deposit	4	3500	Fusing of nacre	5	Excellent	10.5	9.6	8.7	7.4
637	D5.218.1016.2/E	0.86	1.09							G	Amberlaya	Epifaunal	Carnivore/sc	0		No image	5	Excellent	11.5	10.7	9.8	8.5
627	D5.218.1006.2/I	-0.37	1.21							C	Maorites	Nektonic	Carnivore	0		No image	0	No profile	11.0	10.2	9.3	8.0
622	D5.215.216.2/A	2.59	0.91							B	Pinna	Infaunal	Suspension	0		No image	0	No profile	12.3	11.4	10.6	9.3
622	D5.215.216.2/A	2.62	0.84							B	Pinna	Infaunal	Suspension	0		No image	0	No profile	12.6	11.8	10.9	9.6
622	D5.215.216.3/A-10	1.93	1.04							B	Eselaevitrigonia	Infaunal	Suspension	0		No image	0	No profile	11.7	10.9	10.0	8.7
622	D5.215.216.3/A-11	1.27	0.97							B	Eselaevitrigonia	Infaunal	Suspension	0		No image	0	No profile	12.1	11.2	10.3	9.0
622	D5.215.705.2/H	3.31	0.40							B	Eselaevitrigonia	Infaunal	Suspension	0		No image	4	Good + minor gypsum	14.5	13.6	12.8	11.5
613	D5.215.696.2/AI	1.39	1.12							B	Nucula	Infaunal	Deposit	0		No image	2	Poor - low count	11.4	10.5	9.7	8.3
613	D5.215.696.2/AN	3.27	1.66							B	Eselaevitrigonia	Infaunal	Suspension	0		No image	0	No profile	9.1	8.2	7.3	6.0
613	D5.215.696.2/AN	3.27	1.58							B	Eselaevitrigonia	Infaunal	Suspension	0		No image	0	No profile	9.4	8.5	7.6	6.3
613	D5.215.696.2/AN-2	2.93	1.48							B	Eselaevitrigonia	Infaunal	Suspension	0		No image	0	No profile	9.8	9.0	8.1	6.8
613	D5.215.696.2/W	1.41	1.08							B	Eselaevitrigonia	Infaunal	Suspension	0		No image	0	No profile	11.6	10.7	9.9	8.6
608	D5.215.691.2/A	-2.38	0.87							C	Maorites	Nektonic	Carnivore	0		No image	0	No profile	12.5	11.6	10.7	9.4
608	D5.215.691.2/D-1	3.30	0.52							B	Eselaevitrigonia	Infaunal	Suspension	0		No image	5	Excellent	14.0	13.1	12.3	11.0
608	D5.215.691.2/D-1	3.73	1.95							B	Eselaevitrigonia	Infaunal	Suspension	4	1500	Good nacre + some dis	5	Excellent	7.8	6.9	6.1	4.8
548	D5.215.368.2/B	2.30	0.84							B	Oistotrigonia	Infaunal	Suspension	0		No image	0	No profile	12.6	11.8	10.9	9.6
541	D5.215.361.2/E	2.20	1.13							B	Nucula	Infaunal	Deposit	4	1500	Out of focus, nacre goo	4	Good	11.3	10.5	9.6	8.3
541	D5.215.361.2/E	2.41	1.53							B	Nucula	Infaunal	Deposit	4	1500	Good nacre	4	Good	9.6	8.8	7.9	6.6
528	D5.215.347.2/A-2	-3.01	0.78							B	Nucula	Infaunal	Deposit	0		No image	5	Excellent	12.9	12.0	11.1	9.8
528	D5.215.347.2/E	1.36	1.70							B	Nucula	Infaunal	Deposit	0		No image	0	No profile	8.9	8.0	7.1	5.8
528	D5.215.347.2/F	-0.50	1.74							B	Nucula	Infaunal	Deposit	0		No image	0	No profile	8.7	7.8	7.0	5.7
528	D5.215.347.2/K	-2.57	0.26							B	Nucula	Infaunal	Deposit	0		No image	0	No profile	15.1	14.3	13.4	12.1
528	D5.215.347.2/N	-10.49	0.99							B	Solemya	Infaunal	Suspension	0		No image	0	No profile	12.0	11.1	10.2	8.9
526	D5.215.345.2/A-1	-5.99	1.05							B	Solemya	Infaunal	Suspension	0		No image	0	No profile	11.7	10.8	10.0	8.7
508	D5.215.327.2/A	2.38	1.62							B	Nucula	Infaunal	Deposit	5	1000	Good nacre + some dis	5	Excellent	9.2	8.4	7.5	6.2
458	D5.215.980.2/A	2.41	0.85							B	Oistotrigonia	Uncertain	Uncertain	3	2000	Fusing of nacre	4	Good - minor peak offset	12.6	11.7	10.8	9.5

1001	D5.229.1264.2/A	-6.47	-0.74	392535	5843	2172	3085	3499	4699	A	Ammonite [lmc]	Nektonic	Carnivore	3	1000	Fused plates??	1	Excellent (LMC)		
1001	D5.229.1264.2/B	-4.23	-0.90	367880	5635	2247	2644	12313	4757	U	Unidentified [lmc]	Uncertain	Uncertain	0		No image	1	Poor signal - low count (LMC)		
991	D5.222.1255.2/B	-5.45	0.48	369258	6572	1846	2818	2350	380	A	Kitchinites [lmc]	Nektonic	Carnivore	0	350	Low resolution	1	Moderate - low count (LMC)		
991	D5.222.1254.1/A-1	2.46	-0.91	363860	5490	2193	2403	9696	4662	U	Unidentified [lmc]	Uncertain	Uncertain	4	1500	Minimal fusing of nacre	5	Excellent		
991	D5.222.1254.1/A-2	2.13	1.42	385457	2530	2981	6230	2051	1692	U	Unidentified [lmc]	Uncertain	Uncertain	3	1500	Fused plates??	1	Moderate - low count + gypsum?		
991	D5.222.1254.1/A-2	2.13	1.42	382520	2493	2986	7397	2012	1671	U	Unidentified [lmc]	Uncertain	Uncertain	3	3500	Fused plates??	5	Excellent		
991	D5.222.1254.1/A-2	-0.44	-0.44	386462	2469	3046	2777	3485	2139	U	Unidentified [lmc]	Uncertain	Uncertain	4	1500	Well defined plates	0	No profile		
991	D5.222.1254.1/A	-2.44	0.15	464243	2451	4002	4369	3829	1580	U	Unidentified [lmc]	Uncertain	Uncertain	0		No image	5	Excellent		
979	D5.222.1248.2/E	-10.42	-2.94	403826	9099	2395	2444	3151	2634	A	Ammonite [lmc]	Nektonic	Carnivore	2	1500	Fused plates??	1	S/N ratio - LMC		
979	D5.222.1248.2/H	-10.05	-0.56	415264	6479	2245	3224	4792	5942	A	Ammonite [lmc]	Nektonic	Carnivore	0		No image	1	LMC		
979	D5.222.1248.2/G	-20.71	-2.12	382907	15263	1205	2022	2996	5106	A	Maorites [lmc]	Nektonic	Carnivore	0		No image	1	LMC		
961	D5.222.1238.2/F	-3.18	0.40	410174	8545	2045	5001	20708	2868	A	Maorites [lmc]	Nektonic	Carnivore	2	1500	Fused plates??	1	LMC		
961	D5.222.1238.2/A	-11.40	0.29	373909	4365	1900	3813	5070	4110	A	Maorites [lmc]	Nektonic	Carnivore	0		No image	1	LMC		
955	D5.222.1234.2/K	-0.96	-0.28	376060	3810	1503	8007	5536	2822	A	Anagaudryceras [	Nektonic	Carnivore	3	1500	Fused plates?? + gypsu	1	Gypsum?? (LMC)		
955	D5.222.1234.2/B	-2.24	0.33	378791	2039	1751	8620	3790	2058	U	Unidentified [lmc]	Uncertain	Uncertain	0		No image	1	LMC		
955	D5.222.1234.2/A	0.30	0.03	399750	1696	1696	3951	4842	1296	U	Unidentified [lmc]	Uncertain	Uncertain	0	350	Low resolution	1	S/N ratio- LMC		
949	D5.220.1229.2/B	-10.33	0.46	402339	7507	3024	3527	332	740	A	Maorites [lmc]	Nektonic	Carnivore	0		No image	1	LMC	0.707851	0.707847
949	D5.220.1229.2/A	-4.78	0.64	374036	4050	3249	3048	3147	614	A	Maorites [lmc]	Nektonic	Carnivore	0		No image	1	LMC		
937	D5.220.1223.2/F	9.60	0.30	447130	3343	2420	3059	6627	8207	A	Maorites [lmc]	Nektonic	Carnivore	0		No image	1	LMC		
925	D5.220.1217.2/B	-10.78	-0.03	390859	10277	2312	6309	143	580	A	Maorites [lmc]	Nektonic	Carnivore	0		No image	1	LMC		
897	D5.220.1202.2/A-1	0.19	1.31	372482	2115	2599	8329	4053	413	A	Maorites [lmc]	Nektonic	Carnivore	0		No image	1	LMC		
897	D5.220.1202.2/B-3	1.09	1.34	385535	1220	2880	3750	4604	800	A	Maorites [lmc]	Nektonic	Carnivore	3	1500	Fused plates??	4	Minor LMC		
897	D5.220.1202.2/A-2	2.06	1.58	333678	14180	1644	7004	41069	378	B	Bivalve [lmc]	Uncertain	Uncertain	0		No image	1	LMC		
869	D5.219.1185.2/F-1	-6.75	0.84	414033	3442	4498	6786	580	1341	A	Maorites [lmc]	Nektonic	Carnivore	0		No image	1	LMC		
869	D5.219.1185.2/F-2	-5.89	1.12	459226	2824	5062	4691	803	1147	A	Maorites [lmc]	Nektonic	Carnivore	0		No image	1	LMC		
869	D5.219.1185.2/H	-6.95	0.92	398046	1582	5175	3303	264	540	A	Maorites [lmc]	Nektonic	Carnivore	0		No image	1	LMC	0.707865	0.707861
837	D5.219.1168.2/A	1.65	1.28	419292	1197	3400	5800	2494	2316	A	Ammonite [lmc]	Nektonic	Carnivore	3	1500	Fused plates??	1	S/N ratio - minor LMC		
682	D5.218.1061.2/J	0.45	1.67	291991	1033	1406	5275	1047	229	U	Unidentified [lmc]	Uncertain	Uncertain	4	1500	Minimal fusing of nacre	2	Gypsum?		
647	D5.218.1027.2/A	3.01	0.10							B	Pycnodonte	Epifaunal	Suspension	0		No image	1	Calcite		
642	D5.218.1021.2/F	2.81	1.70	396972	2734	2723	6554	7261	50	B	Nucula [lmc]	Infaunal	Deposit	0		No image	5	Excellent		
642	D5.218.1021.2/Q	3.77	0.16	430946	1074	702	3874	249	349	B	Pycnodonte [lmc]	Epifaunal	Suspension	0		No image	1	Calcite		
637	D5.218.1016.2/A	-11.45	0.82	361295	2562	8332	6026	2529	1169	A	Maorites [lmc]	Nektonic	Carnivore	0		No image	1	LMC		
627	D5.218.1006.2/N	-3.96	0.74	404980	8039	3583	4855	3586	1067	A	Ammonite [lmc]	Nektonic	Carnivore	0		No image	1	LMC		
627	D5.218.1006.2/G	-0.99	0.92	454445	1754	3680	6120	1178	449	A	Maorites [lmc]	Nektonic	Carnivore	2	1000	Fusing of nacre + neom	1	Aragonite + LMC		